Det Kongelige Danske Videnskabernes Selskab
Matematisk-fysiske Meddelelser, bind **30**, nr. 1

Dan. Mat. Fys. Medd. **30**, no. 1 (1955)

DEDICATED TO PROFESSOR NIELS BOHR ON THE OCCASION OF HIS 70TH BIRTHDAY

MOMENTS OF INERTIA OF ROTATING NUCLEI

BY

AAGE BOHR AND BEN MOTTELSON

København 1955
i kommission hos Ejnar Munksgaard

CONTENTS

Printed in Denmark.
Bianco Lunos Bogtrykkeri A-S.

I. Introduction.

Collective nuclear excitations of rotational and vibrational character have been observed to occur systematically throughout most of the periodic table. Such states are populated in radioactive decay processes, and are also produced in inelastic scattering reactions. In particular, the Coulomb excitation process, which has been developed in recent years, has proved a powerful tool in the study of low-lying collective excitations in nuclei.

It has been possible to interpret many of the observed features of the collective spectra by comparing the collective modes of motion of the nucleus with the oscillations of an irrotational fluid* (A. Bohr, 1952; K. Ford, 1953; A. Bohr and B. R. Mottelson, 1953). In such a model, the excitation spectrum depends essentially on the nuclear equilibrium shape; it is thus of decisive importance that, in contrast to the case of an amorphous liquid drop, nuclei may acquire large equilibrium deformations as a consequence of their shell structure (Rainwater, 1950).

The nuclear shape depends on the configuration of the nucleons. In the vicinity of closed shells, the equilibrium shape is approximately spherical, and the expected collective spectrum corresponds to a set of normal vibrations, of which the lowest energy modes will be of quadrupole type.

In regions far removed from closed shells, the nuclear equilibrium shape deviates strongly from spherical symmetry, and the oscillation spectrum can be separated into shape oscillations and a rotational type of motion. In such a description the rotational motion is of wave-like character with the moment of inertia depending essentially on the deformation.

* Collective nuclear excitations similar to the vibrations of a liquid drop were first considered by N. Bohr and F. Kalckar (1937).

The observed nuclear collective spectra are found to follow such a general pattern. Thus, rotational spectra, characterized by their numerous regularities regarding energy ratios, spin sequences, and transition intensities, are associated with nuclei which exhibit large quadrupole moments and have especially been observed in the regions $150 < A < 190$ and $A > 225$. The moments of inertia are found to be appreciably smaller than corresponding to rigid rotation and to increase markedly with the deformation.*

In other regions of elements where the nuclear equilibrium shape, especially in even-even nuclei, is more nearly spherical, the collective excitations have been found to have many of the characteristics of quadrupole vibrations about a spherical equilibrium (SCHARFF-GOLDHABER and WENESER, 1955).

In the more detailed analysis of the nuclear collective spectra, it is found that the shell structure not only determines the nuclear equilibrium shape, but also has an important influence on other aspects of the nuclear potential energy surface as well as on the character of the collective flow.

Thus, the restoring force for the vibrational motion is expected to decrease rather rapidly as one moves away from closed-shell configurations; indeed, such an effect is observed in the trends of the vibrational frequencies.

The structure of the collective flow manifests itself in the mass transport associated with this motion, which can be determined from the observed excitation energies. It is found that the rotational moments of inertia as well as the inertial parameters for the vibrational motion are considerably larger than corresponding to the model of irrotational flow.**

In the present paper, we consider the analysis of the moments of inertia for rotating nuclei in terms of the motion of the nucleons.

* For a discussion of rotational spectra and a survey of empirical data, cf., e. g., BOHR and MOTTELSON (1955); A. BOHR (1954). Cf. also ALAGA, ALDER, BOHR, and MOTTELSON (1955) and BOHR, FRÖMAN, and MOTTELSON (1955) for the intensity rules, and the forthcoming review article on Coulomb excitation by ALDER, BOHR, HUUS, MOTTELSON, WINTHER, and ZUPANČIČ.

** The detailed estimate of the moment of inertia for irrotational flow is somewhat uncertain due to the possible difference between the density distribution of neutrons and protons, as well as to the influence of higher multipoles in the nuclear shape. Estimates of these effects indicate, however (cf. GUSTAFSON, 1955), that they are too small to account for the magnitude of the observed moments.

The treatment follows the method discussed by INGLIS (1954), in which the kinetic energy of rotation is obtained by considering the motion of the nucleons in the rotating self-consistent field.

The corresponding collective Hamiltonian for a system of interacting nucleons is discussed in § 2, while the evaluation of the moments of inertia is treated in § 3. For independent particle motion in an average nuclear field, the rotational moments of inertia are found to be approximately those corresponding to rigid rotation. However, the correlations in the nucleonic motion arising from residual interactions modify this result in an essential manner, and give rise, for small deformations, to a wave-like rotational motion. The absolute value of the moments of inertia depends inversely on the strength of the residual interactions, and the moments corresponding to irrotational flow are only approached when the interactions become comparable to the effect of the average field and so destroy the entire shell structure.

The observed moments, discussed in § 4, indicate a strength of interaction about three times smaller than corresponding to this strong interaction limit. Such an estimate of the interactions appears to be consistent with that obtained from other evidence. The residual interactions are also found to be responsible for the transition from rotational to vibrational collective spectra in the even-even nuclei with the approach to closed-shell regions.

II. Relation between Collective Hamiltonian and Nucleonic Motion.

Collective nuclear excitation spectra of vibrational or rotational type are expected to occur when the corresponding collective mode of motion is slow compared to the intrinsic motion of the nucleons. When this adiabatic condition is fulfilled, the nucleus will possess, for each state of the intrinsic structure, a spectrum of collective excitations.

The collective motion is described in terms of a set of co-ordinates α which, in the case of rotations, represent the angles of orientation of the nucleus; for vibrations, the collective co-ordinates may be chosen to represent the amplitudes of normal oscillations.

The Hamiltonian for the collective motion may be obtained by considering the nucleonic motion for slowly varying α. Expanding the energy of the nucleons in powers of the time derivative $\dot{\alpha}$, one obtains to a first approximation an expression of the type

$$H_{\text{coll}} = E(\alpha) + \frac{1}{2} B(\alpha) \dot{\alpha}^2, \tag{1}$$

which thus represents the collective Hamiltonian. The first term in this expression, which is the nucleonic energy for fixed α, gives the potential energy for the collective motion, while the second term, involving an inertial coefficient $B(\alpha)$, gives the collective kinetic energy. Both the functions $E(\alpha)$ and $B(\alpha)$ may depend on the intrinsic state of the nucleonic motion.

The problem of obtaining the collective nuclear Hamiltonian is similar to the adiabatic derivation of the rotation-vibration Hamiltonian for molecules. In the molecular case, however, the inertial parameter B is to a good approximation given by the nuclear motion, while the electronic contribution to the mass transport constitutes only a small correction.

The collective nuclear co-ordinates are themselves functions of the nucleonic variables (cf. below), and the nucleonic motion for prescribed α is therefore a constrained motion. The constraints express the condition that the shape and orientation of the nucleonic system as a whole have the prescribed values. Thus, if the major part of the interactions can be represented by a self-consistent field, the constraints are approximately satisfied if one considers the motion of the nucleons in a field of the prescribed shape and orientation.

We may thus find the Hamiltonian (1) by treating the nucleonic motion in the time-dependent potential $V(\alpha(t))$ (Inglis, 1954, 1955). This motion is described by a Hamiltonian of the form

$$H = \sum_p T_p + \sum_p V(x_p, \alpha(t)) + U, \tag{2}$$

where x_p represents the co-ordinates of the p^{th} nucleon. The first term in (2) is the nucleonic kinetic energy, the second term represents the average potential which is here a function of t, while

the last term represents residual effects of the nucleonic interactions not included in the average field.

For fixed α, we denote by ψ_i and E_i the proper functions and energies of (2) obeying

$$H(\alpha)\,\psi_i = E_i(\alpha)\,\psi_i. \tag{3}$$

These energy values E_i give the potential energy functions in (1).

For slowly varying α, the solution to the Hamiltonian problem (2) may be obtained by means of a time-dependent perturbation calculation. If there is no degeneracy in the static problem, the energy increase of the system resulting from the motion of the field is proportional to $\dot{\alpha}^2$ to leading order, and for the inertial parameter in (1), appropriate to the state ψ_0, one finds (Inglis, 1955)

$$B(\alpha) = 2\hbar^2 \sum_{i \neq 0} \frac{|<0|\frac{\partial}{\partial\alpha}|i>|^2}{E_i - E_0}. \tag{4}$$

In the special case of rotations of axially symmetric nuclei, the mass parameter (4) gives the moment of inertia $\Im$ if $\frac{\partial}{\partial\alpha}$ generates a rotation about an axis perpendicular to the nuclear symmetry axis.

One thus obtains

$$\Im = 2\hbar^2 \sum_{i} \frac{|<0|J_x|i>|^2}{E_i - E_0}, \tag{5}$$

where J_x is the total angular momentum of the particles about the intrinsic x-axis, which has been chosen perpendicular to the nuclear symmetry axis z.

The solution of the time-dependent problem (2) also determines other collective properties of the system. Thus, for the gyromagnetic ratio of the rotational motion, one obtains

$$g_R = \frac{\hbar^2}{\Im} \sum_{i} \frac{1}{E_i - E_0} (<0|\mu_x|i><i|J_x|0> + \text{compl. conj.}), \tag{6}$$

where the magnetic moment operator is given by

$$\mu_x = \sum_p (g_l \, l_x + g_s \, s_x)_p \tag{7}$$

in terms of the orbital and spin contributions of the individual particles.

The simple separation between collective and intrinsic motion corresponding to the Hamiltonian (1) is possible when the time-dependence of the nuclear field implies only a small modification of the motion of the individual nucleons with respect to the field. The adiabatic treatment employed above is then appropriate, and the dynamic effect of the motion of the field can be represented by the collective kinetic energy in (1).

If, however, there are near-lying intrinsic states which are strongly coupled by the motion of the field, the perturbation treatment may break down. The nucleus must then be treated in terms of a coupled system of collective motion and the intrinsic degrees of freedom involved. This situation is, for instance, met with in the partial decoupling between the rotational motion and the spin of the last odd nucleon in rotational spectra with an angular momentum component of $K = 1/2$ along the symmetry axis (cf. references in footnote on p. 4). Indeed, the level structure in odd-A nuclei is such that the motion of the last odd nucleon may quite frequently be somewhat perturbed by the rotational motion (KERMAN, 1955; cf. also the odd-even moments of inertia differences discussed below (p. 22)).

The simple derivation of the collective Hamiltonian considered above exhibits the main physical conditions underlying the separation between collective and intrinsic motion. A more detailed treatment may be obtained in terms of a canonical transformation of the equations of motion which describe the system of interacting nucleons. In such a way one may introduce partly a set of collective co-ordinates α, and partly a set of co-ordinates q describing the intrinsic motion.

Various aspects of such a transformation have been considered in a number of recent papers (A. BOHR, 1954; SÜSSMANN, 1954; TOLHOEK, 1955; TOMONAGA, 1955; COESTER, 1955; NATAF, 1955; MARUMORI, YUKAWA, and TANAKA, 1955; VILLARS, 1955; LIPKIN, DE SHALIT, and TALMI, 1955). Without intering into a detailed discussion of this approach, we shall attempt, with the following

general remarks, to indicate its relationship to the above derivation of the collective Hamiltonian.

The transformed Hamiltonian may be written in the form

$$H = H_{\text{int}}(q, \dot{q}, \alpha) + T_{\text{coll}}(\alpha, \dot{\alpha}) + H_{\text{coupl}}(\dot{q}, q, \dot{\alpha}, \alpha), \qquad (8)$$

where the first term describes the intrinsic motion for fixed α. The second term represents the collective kinetic energy (cf. the second term in (1)), while the last term in (8) contains the couplings between the intrinsic and collective motion. These couplings partly describe the effect on the nucleonic motion of the time-dependence of the collective field, as contained in (2). In addition, the transformation introduces a second type of coupling terms associated with the fact that part of the inertial effect implied by the first type of coupling is already contained in T_{coll}. The second type of coupling thus tends to screen off the first type, and the problem is to choose the collective co-ordinates α in such a way that these two contributions approximately cancel; the major part of the dynamic effects associated with the motion of the nuclear field is then contained in T_{coll}, and the inertial parameter for the collective motion is thus expected to be given by (4).

If one can in such a manner obtain a Hamiltonian in which H_{coupl} is small, one gets approximate solutions to the wave equation of the adiabatic form

$$\Psi = \Phi_\nu(\alpha)\, \psi_i(q, \alpha), \qquad (9)$$

where $\psi_i(q, \alpha)$ represents the intrinsic motion for fixed α, while $\Phi_\nu(\alpha)$ gives the collective motion specified by the quantum numbers ν.

An especially simple class of transformations is that which introduces a collective motion of irrotational character. If we further assume incompressible flow, the collective co-ordinates are given by (cf. Bohr and Mottelson, 1953, p. 10; A. Bohr, 1954)

$$\alpha_{\lambda\mu} = \sum_p \frac{4\pi}{3A} \left(\frac{r_p}{R_0}\right)^\lambda Y^*_{\lambda\mu}(\vartheta_p, \varphi_p), \qquad (10)$$

which represent the mass multipole moments.

For a system such that a transformation of the type (10) leads to separation of the motion, the collective motion can be described in terms of an irrotational flow obeying hydrodynamical equations (A. Bohr, 1954). The moment of inertia is then directly related to the density distribution; thus, for a spheroid of constant density one obtains, for small deformations,

$$\Im_{\text{irrot}} = \frac{2}{5} AM (\Delta R)^2 \tag{11}$$

in terms of the difference ΔR between the major and minor semi-axes. The nuclear mass number and the nucleonic mass are denoted by A and M, respectively.

A closed-shell configuration in an anisotropic harmonic oscillator field would provide a very special case in which a separation between intrinsic and rotational motion is obtained by a transformation of the type (10)*. The appropriate collective angles are then defined in terms of the principal axes of the quadrupole mass tensor. It has also been verified that, in this case, the expression (5) yields the irrotational moment (11) (Inglis, 1954; cf. also p. 11 below).

For most systems, however, a transformation of the type (10) leaves important residual coupling terms, which imply a very intricate interweaving between the intrinsic motion and the collective motion associated with these particular collective co-ordinates. Still, provided the adiabatic condition is fulfilled, the system will possess simple collective modes of excitation, since the couplings may be incorporated in a modified collective motion. In order to exhibit the corresponding separation of the Hamiltonian, a co-ordinate transformation of a more general type than (10) is needed, and the collective flow is no longer of irrotational character.

III. Estimates of Rotational Moments of Inertia for the Nuclear Shell Structure.

The expression (5) for the moment of inertia depends quite sensitively on the character of the nucleonic motion.

* This case has also been noted by Lipkin, de Shalit, and Talmi (1955).

We first consider the limiting situation in which the intrinsic nuclear structure may be described in terms of the independent motion of the nucleons in the average potential. A closed expression for the sum in (5) may be obtained in the case of an anisotropic harmonic oscillator potential with no spin-orbit coupling. For a rotation about one of the principal axes, x, one obtains

$$\left.\begin{aligned}\Im_x = \frac{\hbar}{2}\frac{1}{\omega_y\,\omega_z}\Bigg[&\frac{(\omega_y-\omega_z)^2}{\omega_y+\omega_z}\sum_p (n_y+n_z+1)_p \\ &+\frac{(\omega_y+\omega_z)^2}{\omega_y-\omega_z}\sum (n_z-n_y)_p\Bigg],\end{aligned}\right\} \quad (12)$$

where ω_y and ω_z are the oscillator frequencies along the y- and z-axis, while n_y and n_z are the corresponding oscillation quantum numbers.

In the case of a single particle in the lowest state ($n_x = n_y = n_z = 0$), the moment (12) is just that corresponding to irrotational flow of the average density distribution of the particle. Indeed, this result is valid for the ground state in an arbitrary potential (Wick, 1947). Again for many-particle configurations consisting entirely of closed shells (occupation a function only of $N = n_x + n_y + n_z$), the last term in (12) vanishes and the moment has the irrotational value (11) with its characteristic dependence on the square of the eccentricity (Inglis, 1954).

For a closed-shell configuration, however, the nuclear equilibrium shape is spherical and the moment of inertia vanishes. The strongly deformed nuclei, which possess rotational spectra, have configurations deviating essentially from closed shells. The last term in (12) then gives important contributions implying considerable deviation from irrotational flow in the collective motion of the particles.*

Instead, in the limit of many nucleons, the moment of inertia tends towards that corresponding to rigid rotation of the average density distribution. Thus, the expression (12) approaches the value

* Such additional terms in the moment of inertia have also been considered by R. J. Blin-Stoyle and V. F. Weisskopf (private communication), who have treated nuclear potentials other than those of harmonic oscillator type. For such potentials, even closed-shell configurations may give moments exceeding the irrotational value.

$$\Im_{\text{rig}} = \sum_p M\overline{(y^2+z^2)}_p = \hbar \sum_p \left(\frac{n_y + 1/2}{\omega_y} + \frac{n_z + 1/2}{\omega_z} \right)_p \qquad (13)$$

in the case of the ground state configuration.

This approach to the rigid moment is independent of the potential in which the particles move, as can be seen by employing the statistical approximation. The problem is considered most simply by going over to the rotating co-ordinate system where the potential is independent of time, but where the Coriolis and centrifugal forces must be added to the kinetic energy. In the absence of rotation, the velocity distribution is isotropic at each point, and the Coriolis forces cannot alter this situation to first order in the rotational frequency. Therefore, to this order, there is no net current in the rotating co-ordinate system, and the average flow is like that of a rigid body.*

Since the first-order effects of the rotation are equivalent to the effect of a magnetic field, the absence of an induced flow in the rotating co-ordinate system corresponds to the absence of diamagnetic effects in a classical electron gas (N. Bohr, 1911).

For a finite number of independent nucleons in an average potential, there may be rather large fluctuations of the moment of inertia (5) about the value $\Im_{\text{rig}}$. Thus, if the sum (12) is evaluated for a fixed deformation as a function of the number of nucleons, one finds quite violent fluctuations even for $A \sim 250$ and deformations of the observed order of magnitude. However, the fluctuations are much smaller if one considers, for each configuration, the self-consistent deformation, obtained by minimizing the total energy as a function of the deformation subject to the constraint of constant volume. In the harmonic oscillator case, the fluctuations then disappear, and one obtains just the rigid moment independent of configuration.** For other potentials in which the level structure is less regular, there may still remain some fluctuations in the moment associated with the binding of the last few particles.

* Sessler and Foley (1954) have considered a problem which in certain respects is similar to that discussed here. They find that a Thomas-Fermi treatment of an atom with a net angular momentum leads to a collective flow corresponding to rigid rotation.

** The closed-shell configurations form a singular exception to this result, since they have spherical equilibrium shape and a vanishing moment of inertia.

Thus, if the intrinsic nuclear structure could be described in terms of undisturbed independent particle motion, one would expect essentially the rigid moment of inertia. However, the inclusion of correlations in the nucleonic motion, arising from even relatively weak interactions, has an important influence on the collective motion and the resulting moment of inertia.*

The coupling scheme for a nuclear shell structure with the inclusion of particle interactions depends on the competition between the coupling effect of these interactions and the coupling of the particles to the nuclear deformation (cf. BOHR and MOTTELSON, 1953, § IIc, and especially fig. 6). For small deformations, where the former effect dominates, the particle angular momenta are coupled together to a resultant J; for large deformations, the latter effect is dominant, and the particles are coupled independently to the nuclear axes.

For an even-even nucleus, short-range attractive forces favour a state of $J = 0$ (MAYER, 1950; EDMONDS and FLOWERS, 1952; RACAH, 1952). For small deformations, for which the ground state wave function may be expanded in powers of the deformation, one thus has

$$\psi = \psi\,(J = 0) + \beta\psi\,(J \neq 0) + \cdots, \tag{14}$$

where β is the conventional deformation parameter for ellipsoidal shapes defined by

$$\beta = \frac{4}{3}\sqrt{\frac{\pi}{5}}\frac{\Delta R}{R_0} \approx 1.06\frac{\Delta R}{R_0} \tag{15}$$

in terms of the mean nuclear radius R_0 and the difference ΔR between major and minor semi-axes. The first term in the wave function (14) does not contribute to the moment of inertia (5) and one therefore obtains

$$\Im = \text{const}\ \beta^2. \tag{16}$$

* The possible significance of the residual interactions for the nuclear moments of inertia has been suggested in a somewhat different context by FORD (1954) and INGLIS (1954). These authors anticipate an effect opposite to that obtained below, since they assume the independent particle approximation to give irrotational flow.

The proportionality constant in (16) depends inversely on the excitation energies for the admixed states in (14), and thus on the strength of the interactions.

In the other limit of large deformations, one approaches the independent particle situation with the resulting rigid moment of inertia.

Some insight into the gradual transition between the two coupling schemes may be obtained by considering a greatly simplified model, in which the whole effect of nucleons outside of closed shells is represented by two interacting nucleons in p-states. Choosing the field to be of harmonic oscillator type, the closed shells may be treated collectively in terms of their resistance to deformation and their irrotational contribution to the moment of inertia. By varying the effective number of nucleons in closed shells, one obtains a sequence of configurations with varying equilibrium deformations, for which the moment of inertia may be evaluated by means of (5). The strength of the interaction between the nucleons outside closed shells may be characterized by a parameter which measures the ratio of the interaction energy to the configuration spacing $\hbar\omega$. This interaction parameter may be taken as

$$v = \frac{U}{\hbar\omega}, \tag{17}$$

where U is the energy difference between the $J = 0$ and $J = 2$ states of the two nucleons.

Corresponding to the different values of v, one obtains from this model a family of curves for $\Im$ as a function of the equilibrium deformation (cf. Fig. 1). These curves show the qualitative features discussed above, varying rapidly for small deformations and approaching $\Im_{\text{rig}}$ for $\beta \gg v$. In the limit of $v \sim 1$, in which the shell structure is destroyed by the interaction, one approaches the irrotational flow.

The curves in Fig. 1 only cover values of β larger than about $0.6\ v$. For configurations nearer to closed shells, the model considered gives no stable equilibrium deformation, and instead yields a collective spectrum corresponding to vibrations about a spherical equilibrium shape.

Such a general behaviour is expected to be characteristic of

nuclear configurations which couple to $J = 0$ or $1/2$ in the absence of deformations, and thus in particular of the ground state configurations of even-even nuclei. In fact, for such configurations, the nuclear potential energy of deformation is proportional to β^2 for small deformations. The absence of a linear term, which is

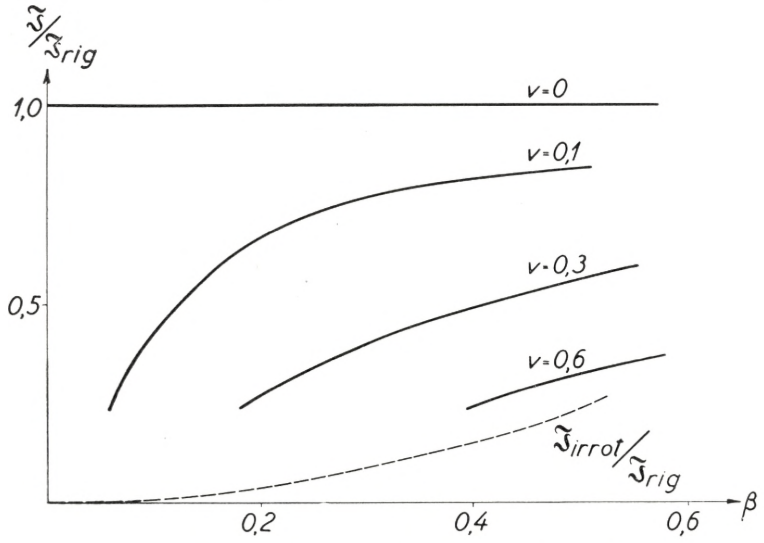

Fig. 1. Moments of Inertia for the Two-Nucleon Model.
The figure shows the dependence of the moment of inertia $\Im$ on the nuclear deformation β (cf. (15)), as estimated from the simplified two-nucleon model discussed in the text. The different curves correspond to different values of the residual interactions, as specified by the interaction parameter v (cf. (17)). For $v = 0$, the moment of inertia is equal to the value corresponding to rigid rotation, $\Im_{\text{rig}}$ (cf. (18)), independent of deformation. For $v \sim 1$, the moment approaches the value for irrotational flow, given by (11), and indicated by the dotted curve.

a consequence of the residual interactions, implies that, as one moves away from closed-shell regions, the deforming tendency of the particles in unfilled shells results at first merely in a decrease of the effective surface tension. Thus, nuclei possessing equilibrium deformations are expected to occur only in regions sufficiently far removed from closed shells, where the tendency towards deformation may overcome the effect of the interactions.

An estimate of the relative importance of the residual interactions may be obtained from the observed nuclear coupling schemes. Thus, the very occurrence of even-even nuclei with stable equilibrium deformations, as revealed by the existence of

rotational spectra, indicates that, for these nuclei, the coupling scheme is approaching that of independent particles. This conclusion is further supported by the analysis of the ground state spins and intrinsic excitation spectra for the strongly deformed nuclei (MOTTELSON and NILSSON, 1955).

Even for the largest observed deformations, there remain, however, significant effects of the interactions as revealed especially by the systematic difference in the binding energy of even-even and odd-A nuclei, amounting to about 1 MeV in the heavy nuclei (cf., e. g., MAYER and JENSEN, 1955, p. 9). A similar effect is revealed in the conspicuously different intrinsic excitation spectra exhibited by odd-A and even-even nuclei. While, in the former, the observed level spacing is a few hundred keV, corresponding to the expected spacing between single-particle levels, the first intrinsic excitation in the even-even nuclei is rarely observed to lie below an MeV.*

These differences can be interpreted in terms of a pairing effect similar to the one discussed previously (MAYER, 1950) for the coupling scheme in spherical nuclei. In deformed axially symmetric nuclei, where the particles are filled pairwise in degenerate orbits distinguished only by their sense of precession about the nuclear symmetry axis, the pairing effect can be simply accounted for in terms of the especially strong interaction between paired nucleons associated with their similar wave functions.

Such a pairing energy has the effect of increasing the energy denominators in (5), except in the contribution due to unpaired particles, and thus reducing the moment of inertia below the value for rigid rotation. In order to obtain an estimate of this effect, we have evaluated the sum (5), employing single-particle wave functions appropriate to a deformed potential with spin-orbit coupling (NILSSON, 1955). When one includes in the energy denominators a pairing energy estimated to be on the average 1.5 MeV for $A \sim 150$, the moment of inertia, for a deformation of $\beta = 0.3$, is reduced by a factor of about two. From a comparison

* A striking example of this odd-even difference is provided by the comparison between the level spectra of W^{182} and W^{183}, recently measured by MURRAY, BOEHM, MARMIER, and DUMOND (1955).

with Fig. 1 the observed pairing energies are thus seen to imply an interaction parameter v of about 0.3*.

One may employ similar methods as used in the calculation of $\Im$ to evaluate the expression (6) for the gyromagnetic ratio for the collective motion. Using the wave functions of NILSSON (1955), one obtains for even-even nuclei values for g_R which fluctuate rather little about the average value Z/A and are relatively insensitive to the strength of the pairing interaction.

IV. Discussion of Empirical Data.

The systematically occurring rotational spectra in the region $150 \leqslant A \leqslant 188$ have been especially well studied. The moments of inertia for the even-even nuclei in this region, determined from the observed rotational level spacings, are plotted in Fig. 2 as a function of the nuclear deformation. The moments are given in units of the value

$$\Im_{\text{rig}} = \frac{2}{5} MAR_0^2 (1 + 0.31\,\beta + 0.44\,\beta^2 \ldots) \tag{18}$$

associated with a rigid rotation of an ellipsoid of constant density.

The nuclear deformation is estimated from the observed electric quadrupole moment Q_0 of the nuclear shape which, for an ellipsoidal nucleus, is related to β by

$$Q_0 = \frac{3}{\sqrt{5\,\pi}} ZR_0^2 \beta (1 + 0.16\,\beta \ldots), \tag{19}$$

where Z is the nuclear charge number.

The Q_0-values are determined from the electric quadrupole transition probabilities between two members of a rotational band. The reduced transition probability for such a transition from a state I_i to a state I_f is given by

$$B(E2) = \frac{5}{16\,\pi} e^2 Q_0^2 <I_i\, 2\, K\, 0 \mid I_i\, 2\, I_f\, K>^2. \tag{20}$$

* This estimate of the residual interactions also appears compatible with the analysis of the low energy neutron scattering data in terms of the optical model (FESHBACH, PORTER, and WEISSKOPF, 1954) which yields a mean free path for nucleonic motion in the nuclear field a few times longer than the nuclear radius.

TABLE I.

Even-even nuclei				Odd-A nuclei				
Isotope	$\frac{3\hbar^2}{\Im}$ (keV)	Q_0 (10^{-24} cm^2)	Ref.	Isotope	I_0	$\frac{3\hbar^2}{\Im}$ (keV)	Q_0 (10^{-24} cm^2)	Ref.
$_{60}Nd^{150}$	131	4.8	a, b, c					
$_{62}Sm^{152}$	121	5.6	b, c, d					
Sm^{154}	82	7.5	b, c					
				$_{63}Eu^{153}$	5/2	72	7.7	b, c
$_{64}Gd^{154}$	123	6.6	b, c	Gd^{155}	(3/2)	62		b
Gd^{156}	89	8.4	b, c	Gd^{157}	(3/2)	56		b
Gd^{158}	79	9.3	b. c					
Gd^{160}	76	9.8	b. c					
				$_{65}Tb^{159}$	3/2	58	8.4	b, c
$_{66}Dy^{160}$	86	7.1	e	Dy^{161}	(5/2)	62		b
Dy^{162}	82	7.9	b, c	Dy^{163}	(5/2)			
Dy^{164}	74	9.2	b, c					
				$_{67}Ho^{165}$	7/2	63	8.6	b, c
$_{68}Er^{164}$	90	7.3	f					
Er^{166}	80	7.5	b, c, i	Er^{167}	7/2	52		b
Er^{168}								
Er^{170}								
				$_{69}Tm^{169}$	1/2	76	8.1	b, c
$_{70}Yb^{170}$	84	7.1	e, g					
Yb^{172}	78	9.2	b, c	Yb^{173}	5/2	68	8.8	b
Yb^{174}								
Yb^{176}								
				$_{71}Lu^{175}$	7/2	76	8.0	b, c, h
$_{72}Hf^{176}$	89	7.1	b, h, m	Hf^{177}	(7/2)	75	8.5	b, c, h
Hf^{178}	91	7.7	b, c, h, j	Hf^{179}	(9/2)	67		b, c, h
Hf^{180}	93	7.2	b, c, d, h, j					
				$_{73}Ta^{181}$	7/2	91	7.1	b, c, h, j, k
$_{74}W^{182}$	100	6.9	c, d, h	W^{183}	1/2	72	6.5	c, h
W^{184}	112	6.2	c, h					
W^{186}	124	6.1	c, h					
				$_{75}Re^{185}$	5/2	108		c, h, l
				Re^{187}	5/2	115		c, h, l
$_{76}Os^{186}$	137	5.6	n					
Os^{188}	155	5.2	d					

Moments of Inertia and Quadrupole Moments for Nuclei in the Region $150 \leqslant A \leqslant 188$.

References and Text to Table I.

a) SIMMONS et al. (1955).
b) HEYDENBURG and TEMMER (1955).
c) HUUS et al. (1955).
d) SUNYAR (1955).
e) MCGOWAN (1952a).
f) BROWN and BECKER (1954).
g) GRAHAM et al. (1952).
h) MCCLELLAND et al. (1955).
i) MCGOWAN (1950).
j) STELSON and MCGOWAN (1955).
k) HUUS and ZUPANČIČ (1953).
l) FAGG and WALICKI (1955).
m) MCGOWAN (1952b).
n) MCGOWAN (1951).

The table lists the available evidence on the shape and moment of inertia of nuclei in the region $150 \leqslant A \leqslant 188$. Only those nuclei have been included which appear to exhibit collective excitations of rotational character. Thus, Sm^{150} and Gd^{152} have been omitted since their low-lying collective excitations are of vibrational type, as are also observed in the even-even nuclei just outside the considered region of A.

For the even-even nuclei, column two lists the energies of the first excited $(2+)$ rotational states, while the third column gives the Q_0-values deduced from the electric quadrupole transitions between this $(2+)$ state and the $(0+)$ ground state, by means of (20). The data are obtained from Coulomb excitation experiments and lifetime measurements. The Q_0-values represent a weighted average of the available determinations. For the even isotopes of Er and Yb, only a single transition has been observed in the Coulomb excitation of the natural element. This transition is tentatively assigned to all the abundant even isotopes.

For the odd-A nuclei, the determination of the moment of inertia and the quadrupole moment depends on the ground state spin I_0. The table lists I_0-values determined from spectroscopic evidence (cf., e. g., HOLLANDER, PERLMAN, and SEABORG (1953)) and, in parenthesis, the more tentative values derived from rotational level spacings and radioactive decay schemes.

The quantum number K appearing in the vector addition coefficient represents the component of angular momentum along the nuclear axis, and is a constant for a given rotational band.

Estimates of Q_0 can also be obtained from spectroscopic determinations of the ground state quadrupole moment Q of odd-A nuclei, using the relation

$$Q = Q_0 \frac{I_0}{I_0+1} \frac{2I_0-1}{2I_0+3}, \tag{21}$$

where I_0 is the ground state spin. The Q_0-values obtained in this manner are consistent with those derived from the transition

probabilities by means of (20). (Cf. BOHR and MOTTELSON, 1955; KAMEI, 1955).

The dependence of the observed moments of inertia on the nuclear deformation, illustrated in Fig. 2, is seen to correspond to the behaviour expected for a shell structure with some residual interaction (cf. § III). The full-drawn curve in Fig. 2 which follows

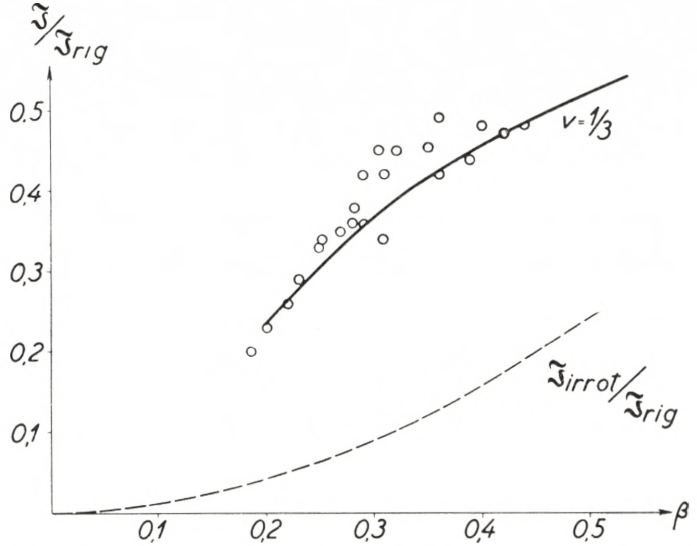

Fig. 2. Dependence of Nuclear Moments of Inertia on the Nuclear Deformation. The empirical moments of inertia for even-even nuclei in the region $150 < A < 188$ are plotted as a function of the nuclear deformation. The moments of inertia, obtained from the data in Table I, are given in units of the rigid moment (18), while the deformation parameters β are obtained from the Q_0-values in Table I by means of (19). The nuclear radius has been taken to be $R_0 = 1.2\ A^{1/3}\ 10^{-13}$ cm. The full-drawn curve represents a theoretical estimate, based on the two-nucleon model with an interaction parameter $v = 1/3$ (cf. Fig. 1). For comparison, the moment of inertia corresponding to irrotational flow is shown by the dotted curve.

the main trend of the experimental points is obtained from the simplified two-nucleon model and corresponds to an interaction parameter $v = 0.33$ (cf. (17) and Fig. 1). The scatter of the experimental points about this curve is of the order of magnitude of the estimated experimental uncertainties. However, some fluctuations about a smooth curve are to be expected, associated with specific differences of the individual nuclear configurations.

The strength of interaction ($v \sim 0.33$), revealed by the empirical moments of inertia, is just of the magnitude estimated

from the observed nuclear pairing energies (cf. pp. 16—17 above). Such residual interactions, while of major significance for the collective flow, are still a factor of about three smaller than those which would destroy the basic nuclear shell structure.

The estimated value of v refers to the nuclei in the region $150 \leqslant A \leqslant 188$; the observed variation with A of the nuclear pairing energy suggests that v varies approximately as $A^{-1/3}$.

As discussed in the previous section, one expects with the approach to closed-shell configurations a transition from rotational to vibrational collective spectra, especially in the even-even nuclei. For the two-nucleon model (cf. p. 14 above), the transition occurs when the deformation becomes comparable to $0.6\, v$. Such transitions are in fact observed to occur in the neighbourhood of Sm and Os, where the deformations are about $\beta = 0.2$.

Since the transition from vibrational to rotational spectra takes place when the nuclear coupling scheme is approaching that of independent particle motion, the transition region may be characterized, approximately independently of v, by a moment of inertia equal to a certain fraction of $\Im_{\text{rig}}$. A tentative estimate for this fraction may be obtained from the two-nucleon model, which yields $\Im_{\min} = 0.23\, \Im_{\text{rig}}$. This would imply that rotational spectra should occur in even-even nuclei only when the energy E_2 of the first excited $(2+)$ state satisfies the relation

$$E_2 < \frac{3\,\hbar^2}{0.23\,\Im_{\text{rig}}} \approx \frac{32\,\hbar^2}{MAR_0^2}. \tag{22}$$

Excitation energies appreciably smaller than this limit have been observed only in the heavy element regions ($A > 225$) and ($150 < A < 190$) and in the relatively light elements around $A = 24$ and $A = 8$ (cf., e. g., SCHARFF-GOLDHABER, 1953). The systematic occurrence of rotational spectra in the former regions is well established, and tentative evidence for a rotational spectrum in Mg^{24} is provided by the observed $4+$ state with an energy about three times that of the $2+$ state.*

* Also in Be^8 there is tentative evidence for a $4+$ state, whose energy is about 3.7 times that of the $2+$ state (cf., e. g., AJZENBERG and LAURITSEN, 1955); for this nucleus the large deformation indicated by the collective excitations may also be described as a tendency towards α-particle formation (cf. WHEELER, 1937).

In other regions of elements the condition (22) is not satisfied, and the observed collective excitation spectra in even-even nuclei exhibit the expected vibrational character (SCHARFF-GOLDHABER and WENESER, 1955).

Another feature of the nuclear moments of inertia, which may be understood in terms of the residual nucleonic interactions, is the observed difference between the moments of even-even and neighbouring odd-A nuclei. It is found that the latter are systematically larger than the former, by an amount varying from a few per cent up to as much as 40 per cent, while there appear to be no corresponding differences in the deformations (cf. Table I).* This increase in the moments of inertia for the odd-A nuclei may represent the especially large contribution to (5) of the last odd particle which, in general, possesses low-lying states of excitation. Similar odd-even differences in the gyromagnetic ratio g_R are thus also to be expected.

In such cases where an appreciable fraction of the rotational angular momentum is associated with the motion of a single nucleon, one expects significant higher-order corrections to the adiabatic treatment, implying small deviations from the simple rotational energy spectrum (cf. p. 8 above).

Perturbations of this type are revealed in the very accurately determined energy spectrum of W^{183} (MURRAY et al., 1955), and have been accounted for in terms of the non-adiabatic coupling between the two lowest intrinsic configurations (KERMAN, 1955). The detailed analysis of these perturbations permits a determination of the corresponding matrix element in (5), and it is found that the resulting contribution to $\mathfrak{I}$ is just of the magnitude of the difference between the moments of inertia for W^{183} and W^{182}.

We wish to acknowledge the stimulus we have derived from contacts with experimental physicists working in the field of nuclear spectroscopy, many of whom have kindly communicated to us results of their investigations prior to publication. We have

* The similarity of the quadrupole deformations in the even-even and odd-A nuclei has also been noted by HEYDENBURG and TEMMER (1955). Evidence for odd-even differences in the moments of inertia in the region $A > 225$ has been discussed by BOHR, FRÖMAN, and MOTTELSON (1955).

also benefited from many enlightening discussions with Professor NIELS BOHR, as well as with members of and visitors to the CERN Theoretical Division and the Institute for Theoretical Physics.

Institute for Theoretical Physics
University of Copenhagen
and
CERN (European Organization for Nuclear Research)
Theoretical Study Division, Copenhagen.

References.

F. AJZENBERG and T. LAURITSEN (1955), Rev. Mod. Phys. **27,** 77.
G. ALAGA, K. ALDER, A. BOHR, and B. R. MOTTELSON (1955), Dan. Mat. Fys. Medd. **29,** no. 9.
A. BOHR (1952), Dan. Mat. Fys. Medd. **26,** no. 14.
A. BOHR (1954), Rotational States in Atomic Nuclei. Ejnar Munksgaard, Copenhagen.
A. BOHR, P. O. FRÖMAN, and B. R. MOTTELSON (1955), Dan. Mat. Fys. Medd. **29,** no. 10.
A. BOHR and B. R. MOTTELSON (1953), Dan. Mat. Fys. Medd. **27,** no. 16.
A. BOHR and B. R. MOTTELSON (1955), Chapter 17 of "Beta- and Gamma-Ray Spectroscopy", ed. by K. SIEGBAHN, North Holland Publ. Co., Amsterdam.
N. BOHR (1911), Studier over Metallernes Elektronteori, Thanning og Appel, København.
N. BOHR and F. KALCKAR (1937), Dan. Mat. Fys. Medd. **14,** no. 10.
H. N. BROWN and R. A. BECKER (1954), Phys. Rev. **96,** 1372.
F. COESTER (1955), Phys. Rev. **99,** 170.
A. R. EDMONDS and B. H. FLOWERS (1952), Proc. Roy. Soc. A **215,** 120.
L. W. FAGG and E. WALICKI (1955), private communication.
H. FESHBACH, C. E. PORTER, and V. F. WEISSKOPF (1954), Phys. Rev. **96,** 448.
K. W. FORD (1953), Phys. Rev. **90,** 29.
K. W. FORD (1954), Phys. Rev. **95,** 1250.
R. L. GRAHAM, J. L. WOLFSON, and R. E. BELL (1952), Can. Journ. Phys. **30,** 459.
T. GUSTAFSON (1955), Dan. Mat. Fys. Medd. **30,** no. 5.
N. P. HEYDENBURG and G. M. TEMMER (1955), Phys. Rev., in press.

J. M. Hollander, I. Perlman, and G. T. Seaborg (1953), Rev. Mod. Phys. **25,** 469.
T. Huus, J. Bjerregaard, and B. Elbek (1955), private communication. In the compilation of Table I, we have employed preliminary results obtained by these authors. The more detailed evaluation of these experiments will appear in Dan. Mat. Fys. Medd.
T. Huus and C. Zupančič (1953), Dan. Mat. Fys. Medd. **28,** no. 1.
D. Inglis (1954), Phys. Rev. **96,** 1059.
D. Inglis (1955), Phys. Rev. **97,** 701.
T. Kamei (1955), to appear in Phys. Rev.
A. Kerman (1955), Dan. Mat. Fys. Medd. **30,** no. 15.
H. Lipkin, A. de Shalit, and I. Talmi (1955), to be published.
T. Marumori, J. Yukawa, and R. Tanaka (1955), submitted for publication.
M. G. Mayer (1950), Phys. Rev. **78,** 22.
M. G. Mayer and J. H. D. Jensen (1955), Elementary Theory of Nuclear Shell Structure, Wiley, New York.
C. McClelland, H. Mark, and C. Goodman (1955), Phys. Rev. **97,** 1191.
F. K. McGowan (1950), Phys. Rev. **80,** 923.
F. K. McGowan (1951), Phys. Rev. **81,** 1066.
F. K. McGowan (1952a), Phys. Rev. **85,** 151.
F. K. McGowan (1952b), Phys. Rev. **87,** 542.
B. R. Mottelson and S. G. Nilsson (1955), Phys. Rev., in press.
J. J. Murray, F. Boehm, P. Marmier, and J. W. M. DuMond (1955), Phys. Rev. **97,** 1007.
R. Nataf (1955), C. R. **240,** 2510.
S. G. Nilsson (1955), Dan. Mat. Fys. Medd. **29,** no. 16.
G. Racah (1952), Farkas Memorial Volume. Research Council of Israel, Jerusalem.
J. Rainwater (1950), Phys. Rev. **79,** 432.
G. Scharff-Goldhaber (1953), Phys. Rev. **90,** 587.
G. Scharff-Goldhaber and J. Weneser (1955), Phys. Rev. **98,** 212.
A. M. Sessler and H. M. Foley (1954), Phys. Rev. **96,** 366.
B. E. Simmons, D. M. van Patter, K. F. Famularo, and R. V. Stuart (1955), Phys. Rev. **97,** 89.
P. H. Stelson and F. K. McGowan (1955), Phys. Rev. **99,** 112.
A. W. Sunyar (1955), Phys. Rev. **98,** 653.
G. Süssman (1954), Zs. f. Phys. **139,** 543.
H. A. Tolhoek (1955), Physica XXI, 1.
S. Tomonaga (1955). Supplement to "Soryushiron-Kenkyu" **7,** 144.
F. Villars (1955), submitted for publication.
J. A. Wheeler (1937), Phys. Rev. **52,** 1083.

Indleveret til selskabet den 20. juni 1955.
Færdig fra trykkeriet den 30. september 1955.

Det Kongelige Danske Videnskabernes Selskab
Matematisk-fysiske Meddelelser, bind **30**, nr. 2

Dan. Mat. Fys. Medd. **30**, no. 2 (1955)

DEDICATED TO PROFESSOR NIELS BOHR ON THE OCCASION OF HIS 70TH BIRTHDAY

CONTINUITY, DETERMINISM, AND REALITY

BY

MAX BORN

København 1955
i kommission hos Ejnar Munksgaard

CONTENTS

Printed in Denmark
Bianco Lunos Bogtrykkeri A-S

Introduction.

The following considerations are an attempt to discuss the ancient and time honoured metaphysical concepts of continuity, determinism, and reality with the help of a simple, almost trivial example. Theoretical physics has, by its own efforts, come to a point where it had to abandon a great deal of traditional philosophical ideas and to replace them by new ones. But there are still leading physicists, amongst them EINSTEIN (1), DE BROGLIE (2), and SCHRÖDINGER (3), who have not accepted the new way of thinking. Therefore, a careful analysis of the philosophical situation in physics seems not to be superfluous. EINSTEIN himself has formulated on several occasions his objections against the current interpretation of quantum mechanics not in obscure philosophical terms, but with the help of simple models. The same method will be followed here; in fact, the model discussed is actually due to EINSTEIN (4). It makes it possible to illustrate abstract philosophical ideas by elementary geometrical considerations; these provide of course no direct answer to the metaphysical problems, but reduce them to clearly distinct alternatives and help thus to clarify the logical situation.

Part I. General Considerations.

1. Continuity.

I maintain that the mathematical concept of a point in a continuum has no direct physical significance. It has, for instance, no meaning to say the value of the coordinate x of a mass-point, or of the centre of mass of an extended body, has a value represented in a given unit by a real number (like $x = \sqrt{2}$ inch. or $x = \pi$ *cm.*).

Modern physics has achieved its greatest successes by applying the methodological principle that concepts which refer to distinctions beyond possible experience have no physical meaning and ought to be eliminated. This principle was certainly operative in many instances since Newton's time. The most glaringly successful cases are Einstein's foundation of special relativity based on the rejection of the concept of aether as a substance absolutely at rest, and Heisenberg's foundation of quantum mechanics based on the elimination of orbital radii and frequencies of electronic structures in atoms. I think that this principle should be applied also to the idea of physical continuity. Now consider, for instance, a statement like $x = \pi cm.$; if π_n is the approximation of π by its first n decimals, then the differences $\pi_n - \pi_m$ are, for sufficiently large n and m, smaller than the accuracy of any possible measurement (even if it is conceded that this accuracy may be indefinitely improved in the course of time). Hence, statements of this kind should be eliminated.

That does not mean that I reject the mathematical concept of real number. It is indispensible for applying analysis. The situation demands a description of haziness of physical quantities with the help of real numbers.

The proper tool for this is the concept of probability. It can be assumed that sentences like the following have a meaning: The probability for the value of a physical quantity to be in a given interval (represented by two real numbers) has a certain value (again a real number). Or, with other words, for any quantity x there exists a probability density $P(x)$.

This attitude is generally accepted in quantum mechanics. But it has actually a more fundamental significance and is only indirectly connected to the special features characteristic of quantum mechanics. It ought to be applied to classical mechanics as well.

2. Determinism.

Classical mechanics has its roots, since Newton's time, in astronomy where the prediction of constellations was its main aim. Thus, the deterministic character of the mechanical laws is stressed in the traditional presentations. When mechanics is applied to micro-phenomena, it is, however, necessary to analyse

the meaning of the term determinism a little deeper. The mechanical laws have the property that a precisely given initial state (configuration and velocities) determines at any time a sharp final state. There are two possibilities: Either a small change of the parameters in the initial state (small compared with the total range) produces only small changes of the final values for all times; then the orbit defined by the initial conditions is *stable.* Or this is not the case, the final deviations increase in time beyond any limit; then the orbit is *instable.*

In astronomy, much work has been done to prove the stability of the planetary system. For our purpose, the results of these investigations are irrelevant. What matters is that there exist simple mechanical systems of a type familiar in atomic physics (kinetic theory of gases) for which all orbits are instable. These systems display therefore only what I should call *weak determinism;* the future state can be predicted only if the initial state is defined absolutely sharply, in the sense of the mathematical concept of a point in a continuum; the slightest initial deviation produces an ever increasing vagueness of the final state. Thus, for systems of this kind, there is a close connection between the problems of continuity and determinism. If the point in a continuum has no physical meaning, it is impossible to maintain that systems of this type behave in a deterministically predictable way. Hence, for a wide class of mechanical systems, the traditional form of (classical) mechanics ought to be replaced by a statistical method which uses right from the beginning the notion of probability: There exists, for any coordinate x, velocity v, and any instant, a probability density $P(x, v, t)$.

The simplest example of this type of systems is the model, suggested by EINSTEIN with a very different intention, namely, to demonstrate the incompleteness of quantum mechanics (a question to which I shall return presently). It is the model of a one-dimensional one-particle gas and consists of a mass-point moving in a straight line (coordinate x) up and down between two points ($x = 0$ and $x = l$) where it is elastically reflected[1]. In a diagramme, the motion is represented by a zig-zag line

[1] If the assumption of an extensionless mass-point and perfect elasticity seems to be too unrealistic, one may take the centre of mass of a finite body running against high and steep potential walls at $x = 0$ and $x = l$.

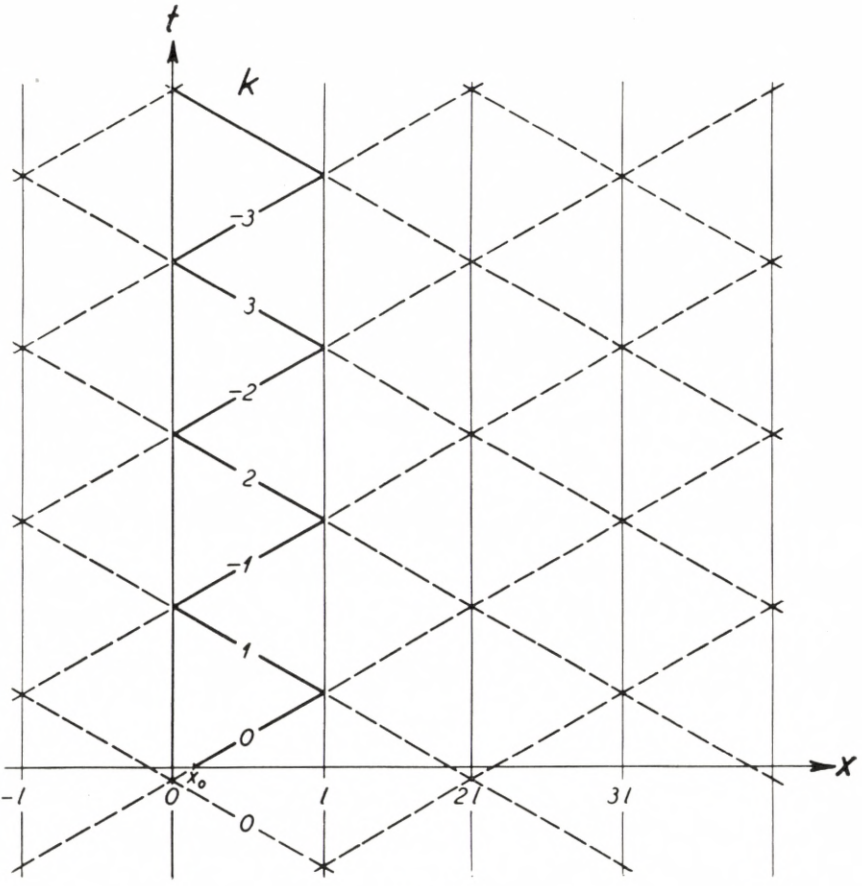

Fig. 1.

inside the strip $0 < x < l$ with alternating constant inclinations $\pm v_0$, where v_0 is the initial velocity. By taking successive images of this figure at the boundary lines of the strip, the diagramme Fig. 1 is obtained which is symmetric at vertical lines $x = kl$ ($k = 0, \pm 1, \pm 2, \ldots$) and has the period $2\,l$. The zig-zag motion is therefore equivalent to two sets of parallel, synchronized straight line motion. It is obvious that $x(t)$ is, for any t, determined by $x_0 = x(0)$ and v_0.

But, if x_0, v_0 are changed by Δx_0, Δv_0, the diagramme of Fig. 2 is obtained, which illustrates that Δx increases proportionally to $t, \Delta x = \pm t \Delta v_0$. After the time $t_c = l/\Delta v_0$, the variation of x is larger than the whole range l of x. Hence, the system is

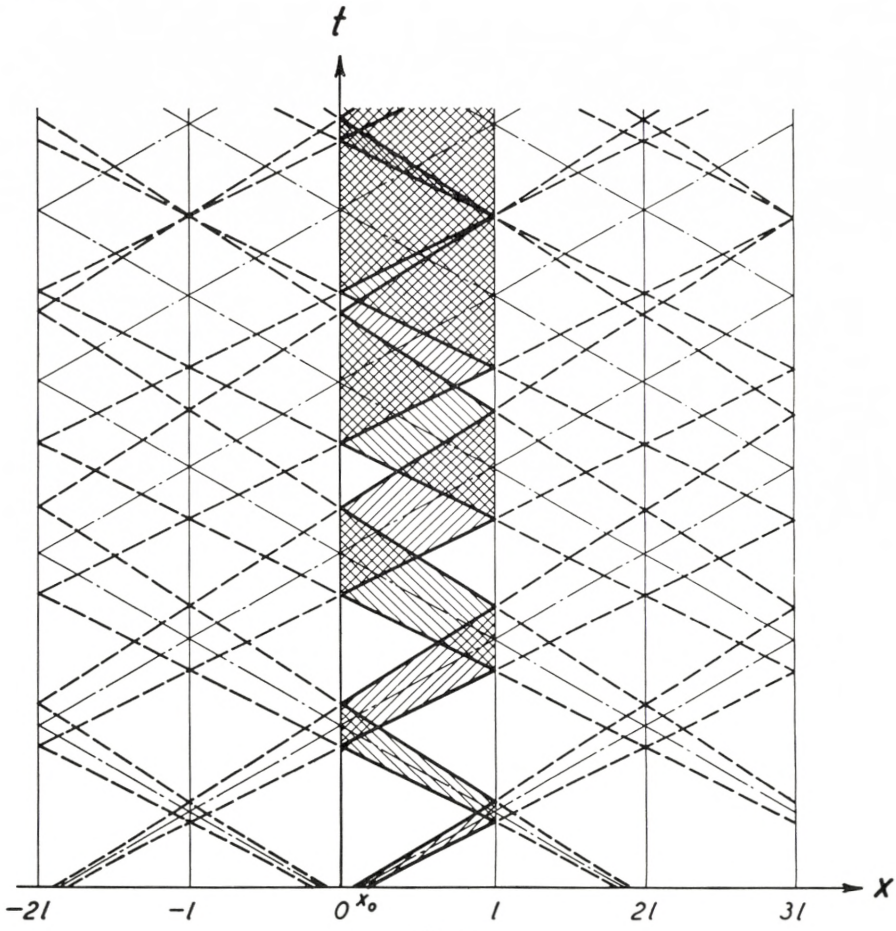

Fig. 2.

perfectly instable and behaves, for $t > t_c$, in an indeterministic manner.

Though this is perfectly trivial, I have never seen it pointed out[1].

3. Reality.

The question what we mean by the expression "physical reality" is closely connected with the previous considerations on

[1] For an unbounded straight line motion, the question of stability has no meaning as there is no range (like l in the Einstein model) with which to compare $\Delta x(t)$. The usual considerations on mechanical determinism miss this essential point of a final range.

continuity and determinism. EINSTEIN, in the paper quoted (4), describes "the programme that, until the introduction of quantum mechanics, was unquestionably accepted for the development of physical thinking" in the following way (translated from the original German): "Everything is to be reduced to conceptual objects situated in space-time and to strict relations which hold for these objects. In this description, nothing appears which refers to empirical knowledge about these objects. A spatial position (relative to the co-ordinate system used) is attributed to, say, the moon at any definite time, quite independently of the question whether observations of this position are made or not. This kind of description is meant if one speaks of the physical description of a "real external world". . . . . EINSTEIN then discusses the question whether quantum mechanics leads to a description of the behaviour of macro-bodies, which corresponds to this notion of reality, and his answer is no. He considers the model of a one-dimensional one-particle gas (discussed above) and compares the classical motion with fairly sharp initial position and velocity with a special solution of the Schrödinger equation

$$\psi = Ae^{iat} \sin bx = \frac{1}{2i} Ae^{i(at+bx)} - \frac{1}{2i} Ae^{i(at-bx)}, \qquad (1)$$

(a and b being properly chosen constants); this represents a state where the momentum has either of two opposite equal values and the probability of position is, for sufficiently high momentum, constant apart from small periodic variations. He continues (translated): "For a macro-system we are sure that it is at any time in a 'real state' which is correctly described with good approximation by classical mechanics. The individual macro-system of the kind considered by us has therefore at any time an almost sharply defined coordinate (of its centre of mass)—at least if averaged over a small interval of time—and an almost sharply defined momentum (defined also in regard to sign). None of these results can be obtained from the ψ-function. It contains only such statements which refer to a *statistical ensemble* of the kind considered". And a few lines later he concludes: "Quantum mechanics describes ensembles of systems, not individual systems. The description with the help of a ψ-function is

thus an *incomplete* description of a single system, not a description of its 'real state'."

This consideration, as it stands, is not conclusive, as the function ψ chosen by EINSTEIN is a very special solution of the wave equation, not adapted to the initial conditions and therefore not suited to illuminate the question whether quantum mechanics is able to describe the individual macro-body in a "realistic" manner—like classical mechanics—or can tackle only statistical ensembles. This question will be treated in some detail in the second part of this paper. Here another point must be discussed, which is implicitly contained in Einstein's publication and obviously foremost in his mind[1].

In the previous sections, it has been shown that no physical meaning can be attributed to a sharp value of a co-ordinate and that therefore the description of a position in Einstein's model should be given in a hazy but realistic manner through a probability density $P(x)$; that, further, the laws of classical mechanics should be formulated not in terms of orbits, but of a time-dependent probability density $P(x, v, t)$. If this is done, classical mechanics is actually not dealing with a single system, but with a statistical ensemble, and Einstein's criticism of quantum mechanics, quoted above, taken literally, fails as it would apply in the same way to the classical theory. However, what EINSTEIN really means, is evident from another sentence of his article which reads (translated): "The fact that, for the macro-system considered, not every function ψ satisfying the Schrödinger equation corresponds approximately to a description of a real phenomenon in the sense of classical mechanics, is particularly obvious by considering a ψ-function which is formed by the superposition of two functions of the type (1) whose frequencies (energies) are essentially different. For, to such a superposition, there is no corresponding 'real case' of classical mechanics (still, however, a statistical ensemble of such 'real cases' according to Born's statistical interpretation)."

Classical mechanics, formulated statistically as it ought to be, is still a "description of reality" according to Einstein's definition,

[1] I have to thank Professor W. PAULI for giving me, in some letters, an explanation of Einstein's ideas, obtained in oral discussions at Princeton, and his own comments.

as one can *think* the single, sharp state as existing (though not observe it with the accuracy demanded by the mathematical concept of sharpness) and then obtain the physical vagueness by applying the ordinary laws of probability. For instance, one can think of a particle in a straight line being at x_1 and then the physical situation "we know that it is near x_1" by a probability density $p(x - x_1)$ (where the function $p(x)$ is different from zero only near $x = 0$). If we only know that the particle is either near x_1 or near x_2, the probability density will be

$$P(x) = a_1 p(x - x_1) + a_2\, p(x - x_2),\ a_1 + a_2 = 1, \tag{2}$$

according to the ordinary rules of probability calculus.

In quantum mechanics the situation, however, is different. If $\varphi(x - x_1)$ is the Schrödinger function describing a particle being near x_1, the probability density is $p(x - x_1) = |\varphi(x - x_1)|^2$. If we know that the particle is either near x_1 or near x_2, the situation is described by the Schrödinger function $\psi(x) = c_1\varphi(x - x_1) + c_2\varphi(x - x_2)$ and the resultant probability is

$$\left.\begin{aligned} P(x) = |\psi(x)|^2 = a_1 p(x - x_1) + a_2\, p(x - x_2) + J(x), \\ a_1 = |c_1|^2,\ a_2 = |c_2|^2, \end{aligned}\right\} \tag{3}$$

where the additional term

$$J(x) = c_1 c_2^* \varphi(x - x_1)\varphi^*(x - x_2) + c_1^* c_2 \varphi^*(x - x_1)\varphi(x - x_2) \tag{4}$$

represents the "interference of probabilities". It has no classical analogue; even if it is practically negligible for $t = 0$, it may become appreciable for certain x-values at later instances.

The existence of this interference phenomenon excludes the possibility to think of the particle as having a definite position (and velocity) at any instant and to connect these positions in imagination to an orbit, and this is the reason why EINSTEIN declares quantum mechanics to be incomplete[1]. He insists that, at least for macro-bodies, a theory cannot be regarded as satisfactory unless it conforms with his idea of reality.

[1] EINSTEIN discusses in this connection the ideas of DE BROGLIE, BOHM, SCHRÖDINGER a. o. who tried, in different ways, to interpret the formalism of quantum mechanics in terms of classical concepts, but he rejects these attempts as unsatisfactory.

This is a philosophical creed which can be neither proved nor disproved by physical arguments. But what can be done is this: one can formulate another concept of physical reality which takes account of the actual existence of the interference phenomenon in the atomistic region and goes over into the traditional one (that accepted by EINSTEIN) for macro-bodies. This I have done in a systematic, but rather abstract way, at another place (5). I shall not repeat these considerations here, but illustrate them only with the help of the model used above, a particle oscillating on a line between two elastically reflecting boundaries.

The main point is that the physicist has not to do with what can be thought of (or imagined), but what can be observed. From this standpoint a state of a system at a time t, when no observation is made, is not an object of consideration. But as soon as an observation is made, the situation found has to be regarded as the final state of the phenomenon defined by a previously observed initial state and, if future observations are envisaged, also as the initial state of the further development. This "reduction of probability" is not characteristic of quantum mechanics, but has also to be applied to classical mechanics if it is formulated in terms of probability: Any observation for checking a predicted probability density "destroys" it and produces a new one which has to serve as initial state for further predictions.

But from this standpoint the interference phenomenon looses much of its paradoxial character. For the one-dimensional model, an actual observation determines not the complex amplitudes $c_1 = \sqrt{a_1}\, e^{i\alpha_1}$, $c_2 = \sqrt{a_2}\, e^{i\alpha_2}$, but only the probabilities (relative frequencies) $a_1 = |\, c_1 \,|^2$, $a_2 = |\, c_2 |^2$; the phases α_1, α_2 remain entirely unknown and undetermined, and the interference term vanishes if averaged over the phase difference $\alpha_1 - \alpha_2$. For more complicated systems (like the optical interferometers), the distribution in the final state may of course show interference fringes, which classical theory cannot explain; but this appears only paradoxial from the traditional (Einstein's) standpoint where a non-observed intermediate state is declared to be just as real as an actually observed final state.

The situation can be illustrated by a detailed discussion of our model. This will be done in the second part of this paper.

Part II. Mathematical Considerations.

The model which will now be investigated in more detail seems to be the simplest mechanical system with a finite range of the variables (co-ordinate, velocity) for which the exact solution can be found. The Hamiltonian has essentially only a kinetic part; the potential energy due to reflection at the boundaries can be replaced by certain periodicity conditions, and the equations of motion then can be solved, in the classical and quantum treatment as well, with the help of Kelvin's method of images. The resulting formulae are simple and well suited for a discussion of several important problems, as the transition from the initial individualistic to the final statistical description, the characteristic distinctions of classical and quantum treatment, the reduction of probability through observation, and the interference of probabilities.

1. Classical treatment of the one-particle one-dimensional gas.

The orbit of a particle in Einstein's model, starting at $t = 0$ from the point $x = x_0$ with the velocity $v = v_0$, is analytically given by

$$\left.\begin{aligned} x &= 2lk - x_0 - v_0 t, && t_{2k-1} \leqslant t \leqslant t_{2k}, \\ x &= -2lk + x_0 + v_0 t, && t_{2k} \leqslant t \leqslant t_{2k+1}, \end{aligned}\right\} \tag{1.1}$$

where

$$t_k = \frac{kl - x_0}{v_0}, \quad k = 0, \pm 1, \pm 2, \ldots . \tag{1.2}$$

It is convenient (as already indicated in Fig. 1) to replace the one-particle system by a periodic system, consisting of an infinite number of synchronized particles, by dropping the conditions $t \geqslant 0$, $0 \leqslant x \leqslant l$ (silently assumed in (1.1)). This procedure will be denoted by the short name "periodic continuation". According to the programme explained in Part I, the "deterministic" description (1.1), (1.2) shall be replaced by a statistical one, with the help of a probability density, $P(x, v, t)$. We have to do with a case of statistical mechanics where the system is not in statistical

equilibrium, but develops in time from a given initial distribution $P(x, v, 0)$. The only condition for $P(x, v, t)$ is that which expresses the conservation of probability; it follows from Liouville's theorem,

$$\frac{\partial P}{\partial t} + [P, H] = 0, \tag{1.3}$$

where $H(x, p)$ is the Hamiltonian as function of coordinate and momentum and

$$[P, H] = \frac{\partial P}{\partial x}\frac{\partial H}{\partial p} - \frac{\partial P}{\partial p}\frac{\partial H}{\partial x} \tag{1.4}$$

the Poisson bracket.

H consists of the kinetic energy $p^2/2m$, and the potential energy representing the reflective power of the walls. As this force is assumed to be infinitely strong, it can be replaced by certain periodicity conditions which will be derived presently. With $H = p^2/2m$ and $p = mv$, (1.4) reduces to

$$\frac{\partial P}{\partial t} + v\frac{\partial P}{\partial x} = 0. \tag{1.5}$$

The periodicity conditions follow from the consideration that the solution must have the same value at a given point x (in $0 \leqslant x \leqslant l$) after each reflection; for instance, after one reflection at $x = 0$, one has

$$P(x, v, t) = P\left(x, -v, t - \frac{2x}{v}\right) \tag{1.6a}$$

and, after two reflections at $x = 0$ and $x = l$,

$$P(x, v, t) = P\left(x, v, t + \frac{2l}{v}\right). \tag{1.6b}$$

The general solution of (1.5) is

$$P(x, v, t) = f(x - vt, v), \tag{1.7}$$

where $f(x, v)$ is an arbitrary function of two arguments, defined for all values $-\infty < x, v < \infty$, which represents the initial state

$$P(x, v, 0) = f(x, v). \tag{1.8}$$

The condition (1.6b) leads to

$$f(x - vt, v) = f(x - vt - 2l, v)$$

and (1.6a) to

$$f(x - vt, v) = f(-x + vt, -v).$$

The first of these conditions says that $f(x, v)$ is periodic in x with the period $2l$,

$$f(x, v) = f(x + 2l, v); \tag{1.9a}$$

the second, that it is symmetric for the inversion

$$f(x, v) = f(-x, -v). \tag{1.9b}$$

These two periodicity conditions define the periodic continuation of $P(x, v, t)$.

The case of a particle having for $t = 0$ almost a fixed position x_0 and fixed velocity v_0 is of particular interest. In order to describe it in a simple way we introduce a function $\varphi(x, v)$ restricted to a narrow domain around $x = 0$, $v = 0$; assuming φ to be normalized, the average of a function $q(x, v)$ is defined by

$$\overline{q} = \int_0^l \int_{-\infty}^{\infty} q(x, v)\, \varphi(x, v)\, dx\, dv, \quad \int_0^l \int_{-\infty}^{\infty} \varphi(x, v)\, dx\, dv = 1, \tag{1.10}$$

and we postulate

$$\overline{x} = 0, \ \overline{v} = 0, \ \overline{x^2} = \sigma_0^2, \ \overline{v^2} = \tau_0^2, \tag{1.11}$$

where $\sigma_0 \ll l$, $\tau_0 \ll v_0$.

Then, the function

$$f(x, v) = \sum_{k=-\infty}^{\infty} \{\varphi(2kl + x - x_0, v - v_0) + \varphi(2kl - x - x_0, -v - v_0)\} \tag{1.12}$$

has all properties requested: it satisfies (1.9a) and (1.9b) and it has, in the interval $0 < x < l$, only one sharp maximum corre-

sponding to the first term for $k = 0$ (as the maximum of the second term, at $-x_0 + 2kl$, is outside the interval for all $k = 0, \pm 1, \pm 2, \ldots$).

Hence, the probability density is, according to (1.7),

$$\left.\begin{aligned} &P(x, v, t) \\ &= \sum_{k=-\infty}^{\infty} \{\varphi(2kl + x - x_0 - vt, v - v_0) + \varphi(2kl - x - x_0 + vt, v - v_0)\}; \end{aligned}\right\} \tag{1.13}$$

it is properly normalized, for

$$\left.\begin{aligned} \int_0^l \int_{-\infty}^{\infty} P(x, v, t)\, dx\, dv &= \sum_{k=-\infty}^{\infty} \int_{-\infty}^{\infty} d\eta \left[\int_{2kl - x_0^+ - (v_0 + \eta)t}^{(2k+1)l - x_0 - (v_0 + \eta)t} \varphi(\xi, \eta)\, d\xi - \int_{2kl - x_0 - (v_0 + \eta)t}^{(2k-1)l - x_0 - (v_0 + \eta)t} \varphi(\xi, \eta) d\xi \right] \\ &= \int_{-\infty}^{\infty} d\eta \int_{-\infty}^{\infty} d\xi \varphi(\xi, \eta) = 1, \end{aligned}\right\} \tag{1.13a}$$

in virtue of (1.10).

If $\varphi(x, v)$ is chosen as a Dirac δ-function, i. e. $\sigma_0 = 0$, $\tau_0 = 0$, this function (1.13) reduces to zero except for the points which satisfy the equations (1.1), (1.2). But this limiting case does not correspond to a real physical situation. We have to consider σ_0 and τ_0 as finite quantities.

By integrating (1.13) over v one obtains the spatial distribution

$$\left.\begin{aligned} P(x, t) &= \int_{-\infty}^{\infty} P(x, v, t)\, dv \\ &= \sum_{k=-\infty}^{\infty} \int_{-\infty}^{\infty} \{\varphi(2kl + x - x_0 - (v_0 + \eta)t, \eta) + \varphi(2kl - x - x_0 - (v_0 + \eta)t, \eta)\} d\eta, \end{aligned}\right\} \tag{1.14}$$

and, by integrating (1.13) over x from 0 to l, the velocity distribution

$$P(v, t) = \int_{-\infty}^{\infty} P(x, v, t)\, dx = \sum_{k=-\infty}^{\infty} \left\{ \int_{2kl - x_0 - vt}^{(2k+1)l - x_0 - vt} \varphi(\xi, v - v_0) d\xi - \int_{2kl - x_0 + vt}^{(2k-1)l x_0 + vt} \varphi(\xi, -v - v_0) d\xi \right\}. \tag{1.15}$$

These two formulae are the analytical expression of the fact that at each reflection the velocity changes its sign. The distribution of the absolute value of the velocity is obviously nothing but the probability that the velocity is either v or $-v$, hence

$$P(|v|, t) = P(v, t) + P(-v, t). \tag{1.16}$$

This quantity is easily found from (1.15) to be independent of time, as should be expected. For the two parts in (1.16) contribute terms in the sum (1.15) which can be combined to integrals from $-\infty$ to ∞ :

$$P(|v|, t) = P(|v|) = \int_{-\infty}^{\infty} \{\varphi(\xi, v - v_0) + \varphi(\xi, -v - v_0)\}\, d\xi. \quad (1.17)$$

As an example for which all calculations can be performed in detail, one can consider $\varphi(x, v)$ as a Gauss function in both arguments. If we put

$$\varphi(x, v) = \frac{1}{2\pi\sigma_0\tau_0} e^{-\frac{x^2}{2\sigma_0^2} - \frac{v^2}{2\tau_0^2}}, \quad (1.18)$$

the equations (1.11) are satisfied. (1.13) becomes

$$P(x, v, t) = \frac{1}{2\pi\sigma_0\tau_0} \left\{ e^{-\frac{(v-v_0)^2}{2\tau_0^2}} \sum_{k=-\infty}^{\infty} e^{-\frac{1}{2\sigma_0^2}(2kl + x - x_0 - vt)^2} + e^{-\frac{(v+v_0)^2}{2\tau_0^2}} \sum_{k=-\infty}^{\infty} e^{-\frac{1}{2\sigma_0^2}(2kl - x - x_0 - vt)^2} \right\}, \quad (1.19)$$

and (1.14)

$$P(x, t) = \frac{1}{\sigma(t)\sqrt{2\pi}} \sum_{k=-\infty}^{\infty} \left\{ e^{-\frac{1}{2\sigma(t)^2}(2kl + x - x_0 - v_0 t)^2} + e^{-\frac{1}{2\sigma(t)^2}(2kl - x - x_0 - v_0 t)^2} \right\}, \quad (1.20)$$

where

$$\sigma(t) = \sqrt{\sigma_0^2 + \tau_0^2 t^2}. \quad (1.21)$$

If now the averages of x, x^2, and $(\Delta x)^2 = (x - \bar{x})^2$ are formed with the distribution (1.20) one finds for $\bar{x}$ exactly the expressions (1.1), (1.2) and further

$$\overline{(\Delta x)^2} = \sigma(t)^2. \quad (1.22)$$

Hence, the width of the distribution increases with time. It becomes equal to the whole range l of x at a critical instant

$$t_c = \frac{1}{\tau_0}\sqrt{l^2 - \sigma_0^2}. \quad (1.23)$$

If $\sigma_0 \ll l$, this is approximately $t_c \sim l/\tau_0$, the value used in Part I. For small τ_0, the epoch t_c is very large but always finite.

It can now be shown that, for $t \to \infty$, $P(x, t)$ becomes constant, independent of x and t. If t is large, one has $\sigma(t) \to \tau_0 t$, and (1.20) reduces to

$$P(x, t) \to \frac{1}{\tau_0 t \sqrt{2\pi}} \sum_{k=-\infty}^{\infty} e^{-\frac{1}{2\tau_0^2}\left(\frac{2lk}{t} - v_0\right)^2};$$

if one puts $\frac{2lk}{t} - v_0 = \eta$, then to an increment $\Delta k = 1$ there corresponds $\Delta\eta = 2l/t$ which, for $t \to \infty$, tends to zero. Hence, the sum goes over into an integral

$$P(x, t) \to \frac{1}{\tau_0 \sqrt{2\pi}} \frac{1}{l} \int_{-\infty}^{\infty} e^{-\frac{\eta^2}{2\tau_0^2}} d\eta = \frac{1}{l}. \tag{1.24}$$

This is the properly normalized "geometrical" probability for finding the particle anywhere in the interval of length l.

However, the distribution for $t \to \infty$ is not that of an ideal gas, as the velocity distribution is different. One obtains from (1.17) and (1.18)

$$P(|v|) \to \frac{1}{\tau_0 \sqrt{2\pi}} \left\{ e^{-\frac{(v-v_0)^2}{2\tau_0^2}} + e^{-\frac{(v+v_0)^2}{2\tau_0^2}} \right\}, \tag{1.25}$$

that means two Gauss distributions with the mean velocities $\pm v_0$, but not a Maxwell distribution.

The result of this consideration is therefore that a motion which starts as that of a practically individualistic particle, in the course of time goes over into a state where the position becomes completely indetermined while the magnitude of the velocity remains unchanged, its direction indetermined.

The question how the model has to be modified so that the final state is an ideal gas will not be investigated here in detail. It is obvious that a mechanism for the exchange of velocities between several mobile objects is needed. I presume that it suffices to replace one of the elastic boundaries by a model of a thermal reservoir (a heavy body with a Maxwell energy distribution) which exchanges energy and momentum with the particle at each collision.

2. Quantum mechanics of the one-dimensional one-particle gas.

To treat the same problem with quantum mechanics one has to solve the time-dependent Schrödinger equation for the wave function $\psi(x, t)$,

$$\frac{\hbar^2}{2m}\frac{\partial^2\psi}{\partial x^2} + \hbar i \frac{\partial\psi}{\partial t} = 0 \tag{2.1}$$

with the boundary conditions

$$\psi(0, t) = 0, \quad \psi(l, t) = 0. \tag{2.2}$$

There are two standard methods, that of d'Alembert and that of Fourier. The d'Alembertian solution is, in the present case, preferable as it leads to results easily comparable with those of the classical treatment. The transformation in a Fourier series can then be easily obtained.

De Broglie has given, in one of his books (6), a solution[1] of (2.1) without boundaries, which corresponds to arbitrary initial values $f(x)$; namely

$$\psi(x, t) = \left(\frac{-im}{2\pi\hbar t}\right)^{1/2} \int_{-\infty}^{\infty} f(\xi) e^{\frac{im}{2\hbar t}(x-\xi)^2} d\xi. \tag{2.3}$$

This can be readily confirmed by direct calculation (substituting into (2.1) and demonstrating that $\psi(x, t) \to f(x)$ for $t \to 0$). Then, following Darwin, he choses for $f(x)$ the function

$$f(x) = \left(\frac{1}{\sigma_0\sqrt{2\pi}}\right)^{1/2} e^{-\frac{(x-x_0)^2}{4\sigma_0^2} + \frac{i}{\hbar} mv_0(x-x_0)}, \tag{2.4}$$

which represents an harmonic wave with momentum mv_0, modulated by a Gauss function with a crest at x_0 and width $\sigma_0\sqrt{2}$. The probability for location $|f(x)|^2$ is normalized,

$$\int_{-\infty}^{\infty} |f(x)|^2 dx = 1, \tag{2.5}$$

[1] De Broglie has actually treated the three-dimensional case.

and the expectation values of coordinate, momentum, and their mean square deviations are

$$\left.\begin{aligned} \overline{x} &= \int_{-\infty}^{\infty} x\, ff^*\, dx = x_0, \\ \overline{p} &= -\hbar i \int_{-\infty}^{\infty} f^* \frac{df}{dx}\, dx = m v_0; \end{aligned}\right\} \tag{2.6a}$$

$$\left.\begin{aligned} \overline{(\Delta x)^2} &= \int_{-\infty}^{\infty} x^2 ff^*\, dx - x_0^2 = \sigma_0^2, \\ \overline{(\Delta p)^2} &= -\hbar^2 \int_{-\infty}^{\infty} f^* \frac{d^2 f}{dx^2}\, dx - m^2 v_0^2 = \frac{\hbar^2}{4\sigma_0^2}. \end{aligned}\right\} \tag{2.6b}$$

If we introduce the uncertainty of the velocity

$$\tau_0 = \sqrt{\overline{(\Delta v)^2}} = \frac{1}{m}\sqrt{\overline{(\Delta p)^2}} = \frac{\hbar}{2\sigma_0 m}, \tag{2.7}$$

we have the Heisenberg uncertainty relation

$$\sqrt{\overline{(\Delta x)^2}\cdot\overline{(\Delta p)^2}} = m\sigma_0\tau_0 = \frac{\hbar}{2}. \tag{2.8}$$

If (2.4) is substituted in (2.3) and the integration performed, one obtains after some reduction

$$\left.\begin{aligned} \psi(x,t) = \left(\frac{s(t)}{\sigma(t)\sqrt{2\pi}}\right)^{1/2} exp\left\{-\left(\frac{x-x_0-v_0 t}{2\sigma(t)}\right)^2\right. \\ \left. -\frac{im}{2\hbar t}\left[\frac{\sigma_0^2}{\sigma(t)^2}(x-x_0-v_0 t)^2 - (x-x_0)^2\right]\right\}_1, \end{aligned}\right\} \tag{2.9}$$

where

$$s(t) = \frac{\sigma_0 - i\tau_0 t}{\sigma(t)}, \qquad |s(t)|^2 = 1. \tag{2.10}$$

$\psi(x, t)$ is the normalized probability amplitude for a group of waves with a crest initially at x_0 moving with the velocity v_0 (from left to right). Then, $\psi(-x, t)$ corresponds to a group of waves with a crest initially at $-x_0$ and moving with the velocity

$-v_0$ (from right to left). For inspection of (2.9) shows that a change of sign of x is equivalent to a change of signs of x_0 and v_0.

Applying the image method, we construct the function

$$\Psi(x,t) = \sum_{k=-\infty}^{\infty} \{\psi(2kl + x, t) - \psi(2kl - x, t)\}; \qquad (2.11)$$

it is obviously periodic in x with period $2l$ and vanishes for $x = 0$ and $x = l$. If $t \to 0$, one has approximately $\sigma(t) \to \sigma_0$, $s(t) \to 1$, and

$$\Psi(x,0) = \left(\frac{1}{\sigma_0\sqrt{2\pi}}\right)^{1/2} \sum_{k=-\infty}^{\infty} \left\{ exp\left[-\left(\frac{2kl + x - x_0}{2\sigma_0}\right)^2 + \frac{imv_0}{\hbar}(2kl + x - x_0)^2\right] \right. \\ \left. - exp\left[-\left(\frac{2kl - x - x_0}{2\sigma_0}\right)^2 + \frac{imv_0}{\hbar}(2kl - x - x_0)^2\right]\right\}. \qquad (2.12)$$

This can be written

$$\Psi(x,0) = \sum_{k=-\infty}^{\infty} \{f(2kl + x) - f(2kl - x)\}, \qquad (2.13)$$

where $f(x)$ is the function defined by (2.4). Hence, the initial state consists in two groups of plane waves travelling to the right and left, both modulated by Gauss functions of width σ_0, and group crests at $x_0 + 2kl$ and $-x_0 + 2kl$ ($k = 0, \pm 1, \pm 2, \cdots$), respectively. Inside the interval $0 \leqslant x \leqslant l$, these waves are equivalent to one wave with a crest initially at x_0, which is repeatedly reflected at the boundaries $x = 0$ and $x = l$. Hence the solution describes, for small σ_0, a repeatedly reflected single particle with slightly uncertain initial position.

The probability of location is

$$P(x,t) = \Psi\Psi^* = \sum_{k=-\infty}^{\infty} \sum_{k'=-\infty}^{\infty} \{\psi(2k'l + x, t) \\ - \psi(2kl - x, t)\}\{\psi^*(2kl + x, t) - \psi^*(2kl - x, t)\}. \qquad (2.14)$$

Now, each term $\psi(2kl + x, t)$ corresponds, in Fig. 1, to a line ascending from left to right (+ line), each term $\psi(2kl - x, t)$ to

a line ascending from right to left (— line). Accordingly, the four products obtained by multiplying out the bracket in (2.14) can be classified into three types and the total probability split into three parts:

$$P(x, t) = P_c(x, t) + P_i(x, t) + P_r(x, t). \tag{2.15}$$

For $k = k'$, the terms $\psi(2kl + x, t)\, \psi^*(2kl + x, t)$ and $\psi(2kl - x, t)\, \psi^*(2kl - x, t)$ represent the superposition of the Gauss function of a (+ line) with itself and a (— line) with itself; they contribute to (2.15)

$$P_c(x, t) = \frac{1}{\sigma(t)\sqrt{2\pi}} \sum_{k=-\infty}^{\infty} \left\{ e^{-\frac{1}{2\sigma(t)^2}(2kl + x - x_0 - v_0 t)^2} + e^{-\frac{1}{2\sigma(t)^2}(2kl - x - x_0 - v_0 t)^2} \right\}, \tag{2.16}$$

which is identical with the probability (1.20) derived from the classical theory.

The remaining terms for $k = k'$, namely $-\psi(2kl + x, t)\, \psi^*(2kl - x, t)$ and $-\psi(2kl - x, t)\, \psi^*(2kl + x, t)$, correspond each to the intersection point of a (+ line) with an equally numbered (— line); all these are (cf. Fig. 1) on the boundary $x = 0$. It is obvious that the other boundary $x = l$, where $k' = k + 1$, contributes terms of the same type and similar magnitude. Collecting all these terms, we obtain

$$\left.\begin{aligned} P_i(x, t) = \frac{-2}{\sigma(t)\sqrt{2\pi}} \sum_{k=-\infty}^{\infty} \Bigg\{ & e^{-\frac{1}{2\sigma(t)^2}[x^2 + (2kl - x_0 - v_0 t)^2]} \\ & \cos \frac{x}{\sigma_0 \tau_0 t} \left[\frac{\sigma_0^2}{\sigma(t)^2} (2kl - x_0 - v_0 t) - 2kl + x_0 \right] \\ + e^{-\frac{1}{2\sigma(t)^2}[(l-x)^2 + (2kl - x_0 - v_0 t)^2]} & \cos \frac{l - x}{\sigma_0 \tau_0 t} \left[\frac{\sigma_0^2}{\sigma(t)^2} (2kl - x_0 - v_0 t) - 2kl + x_0 \right] \Bigg\}. \end{aligned}\right\} \tag{2.17}$$

These terms represent interference effects due to the superposition of an incident with a reflected wave near one of the boundaries. The fringes, described by the cos-terms, are restricted, by the Gauss functions, to a neighbourhood of the boundary of width $\sigma(t)$; if $\sigma_0 \ll l$, these regions of interference remain narrow for a long time ($t \ll t_c$). The remaining terms, all of the type

$k + k'$, correspond either to the superposition of two different (+ lines) or two different (— lines) or to intersection points of a (+ line) and a (—line); outside the region $0 \leqslant x \leqslant l$. If $\sigma(t) \ll l$, their contribution to the probability, $P_r(x, t)$, is small and can be neglected for $t \ll t_c$.

The essential differences between the classical and quantum treatment are now clearly seen to be of two different kinds; there are, firstly, the interference effects near the boundaries, represented by P_i, and, secondly, the Heisenberg uncertainty relation which connects σ_0 and $\tau_0 (= \hbar/2\, m\sigma_0)$ and thus prohibits simultaneously sharp initial position and velocity. Both effects are appreciable only for atomistic particles and negligible for macrobodies (m large).

It is now clear that whenever the interference terms P_i can be neglected, namely when $\sigma_0 \ll l$ and $\tau_0 = \dfrac{\hbar}{2\, m\, \sigma_0} \ll v_0$, or, when

$$\frac{\hbar}{2\, m\, v_0} \ll \sigma_0 \ll l,$$

then $P(x, t)$ approaches, for $t \to \infty$, the constant value $1/l$ as in (1. 24).

We have now to investigate the relation of the solution for an individual particle given above and the solution based on eigenstates (which EINSTEIN uses for his critical considerations). For this purpose we expand the function $\Psi(x, t)$ in a Fourier series; as it is antisymmetric we can write

$$\Psi(x, t) = \sum_{n=1}^{\infty} A_n(t)\, \sin \frac{n\pi}{l} x, \tag{2.18}$$

with

$$A_n(t) = \frac{2}{l} \int_0^l \Psi(x, t)\, \sin \frac{n\pi}{l} x\, dx. \tag{2.19}$$

By substituting (2.18) in the differential equation (2.1), one sees that $A_n\,(t)$ satisfies the equation

$$\hbar i \frac{\partial A_n(t)}{\partial t} - \left(\frac{\hbar\, n\, \pi}{l}\right)^2 \frac{1}{2\, m} A_n(t) = 0, \tag{2.20}$$

and as $E = \hbar i\,\partial/\partial t$ is the energy operator, one has

$$A_n(t) = A_n\, e^{iE_n t/\hbar}, \tag{2.21}$$

where

$$E_n = \left(\frac{\pi\hbar\, n}{l}\right)^2 \frac{1}{2\,m} \tag{2.22}$$

are the eigenvalues of the energy. Therefore it suffices to calculate the constants

$$A_n = A_n(0) = \frac{2}{l}\int_o^l \Psi(x, 0)\, \sin\frac{n\,\pi\, x}{l}\, dx. \tag{2.23}$$

Substituting (2.13) one has

$$\begin{aligned} A_n &= \frac{2}{l}\sum_{k=-\infty}^{\infty}\left\{\int_o^l f(2kl + x)\, \sin\frac{n\,\pi\, x}{l}\, dx - \int_o^l f(2kl - x)\, \sin\frac{n\,\pi\, x}{l}\, dx\right\} \\ &= \frac{2}{l}\sum_{k=-\infty}^{\infty}\int_{2k-1}^{2k+1} f(x)\, \sin\frac{n\,\pi\, x}{l}\, dx, \end{aligned}$$

hence

$$A_n = \frac{2}{l}\int_{-\infty}^{\infty} f(x)\, \sin\frac{n\,\pi\, x}{l}\, dx, \tag{2.24}$$

which shows that the Fourier coefficient of $\Psi(x, 0)$ in the interval $0 \leqslant x \leqslant l$ is the Fourier transform of $f(x)$ in $-\infty < x < \infty$ taken at the points $n\pi/l$ of the reciprocal space.

It follows now readily that $\Psi(x, t)$ is normalized for all t; one has

$$\left.\begin{aligned} \int_o^l \Psi\Psi^*\, dx &= \sum_{n=1}^{\infty}\sum_{n'=1}^{\infty} A_n A_{n'}{}^*\, e^{i(E_n - E_{n'})\, t/\hbar}\int_o^l \sin\frac{\pi\, nx}{l}\, \sin\frac{\pi\, n'x}{l}\, dx \\ &= \frac{l}{2}\sum_{n=1}^{\infty}|\, A_n\,|^2 = \int_{-\infty}^{\infty}|f(x)|^2 dx = 1. \end{aligned}\right\} \tag{2.25}$$

Introducing for $f(x)$ in (2.24) the expression (2.4), one obtains

$$A_n = \frac{\sqrt{2}}{il}\,(\sigma_0\sqrt{2\,\pi})^{1/2}\left\{e^{-\left(\frac{v_0}{2\tau_0} + \frac{\pi\sigma_0 n}{l}\right)^2 + i\frac{\pi nx}{l}} - e^{-\left(\frac{v_0}{2\tau_0} - \frac{\pi\sigma_0 n}{l}\right)^2 - i\frac{\pi nx}{l}}\right\}. \tag{2.26}$$

The absolute value of the momentum in the state n is, according to (2.22),

$$p_n = \sqrt{2mE_n} = \frac{\pi \hbar n}{l}; \tag{2.27}$$

hence, with $\sigma_0 \tau_0 = \hbar/2m$, (2.26) can also be written

$$A_n = \frac{\sqrt{2}}{il}(\sigma_0 \sqrt{2\pi})^{1/2} \left\{ e^{-\frac{1}{4\tau_0^2}(v_0 + p_n/m)^2 + ix_0 p_n/\hbar} - e^{-\frac{1}{4\tau_0^2}(v_0 - p_n/m)^2 - ix_0 p_n/\hbar} \right\}. \tag{2.28}$$

Assume $v_0 > 0$; since in (2.18) $n = 1, 2, \ldots$, p_n is positive. Hence only the exponent of the second term can approach zero, namely for

$$p_n \sim mv_0, \; n_{\max} \sim \frac{mv_0 l}{\hbar \pi}, \; E_{\max} \sim \frac{mv_0^2}{2}. \tag{2.29}$$

For this n one has

$$A_{max} \sim i \frac{\sqrt{2}}{l}(\sigma_0 \sqrt{2\pi})^{1/2} e^{-imv_0 x_0/\hbar}, \tag{2.30}$$

and the expansion (2.18) reduces, for small τ_0, to the leading term:

$$\left.\begin{aligned} \Psi(x, t) &\sim i \frac{\sqrt{2}}{l}(\sigma_0 \sqrt{2\pi})^{1/2} e^{-imv_0 x_0/\hbar} \sin \frac{mv_0 x}{\hbar} \\ &= \frac{1}{\sqrt{2}l}(\sigma_0 \sqrt{2\pi})^{1/2} \left\{ e^{i\frac{mv_0}{\hbar}(x - x_0)} - e^{-i\frac{mv_0}{\hbar}(x + x_0)} \right\}. \end{aligned}\right\} \tag{2.31}$$

This is the solution of the Schrödinger equation used by Einstein (cf. Part I, (1)) to demonstrate the incompleteness of quantum mechanics. However, as the preceding considerations show, it is only an approximation; the correct solution is the wave packet with the coefficients (2.26) or (2.28), and this is completely equivalent to the d'Alembertian solution (2.11) which exhibits the fact that, for a restricted time ($t < t_c$), the motion is properly approximated by the classical, orbital or individualistic description. The quantum formula (2.31) and the classical formula (1.1) are therefore bridged by a continuous transition, and

there is no paradoxial situation for macro-bodies which EINSTEIN believes to exist.

Einstein's objections against quantum mechanics based on the interference of probabilities can also be illuminated by this model. The first point is that one must not add phase factors of the form $e^{i\alpha_k}$ to the terms of the sum (2.11), because then the boundary (periodicity) conditions would be violated. All the different terms in the sum are in phase; only a common phase factor $e^{i\alpha}$ can be added to the whole sum. But this cancels in the probability expression (2.14). Hence, the interference term given in (2.17) is genuine and cannot be destroyed by averaging over phases; these interferences between incident and reflected wave are of the same type as those in certain interferometric optical experiments (standing waves).

But one can now consider the case, discussed at the the end of Part I, where the initial distribution has two sharp maxima, one at x_1, the other at x_2; i. e. one knows only that the particle is either near x_1 or near x_2. The solution $\Psi(x, t)$ is then a linear combination of the two single functions with complex factors; but the relative phase of these is indetermined, one has to average over it and thus no interference phenomenon results from this situation. This must be so; for simple ignorance where a particle is at $t = 0$ cannot produce a physical interference phenomenon. Observable interference can be obtained only by feeding in particles from one source at two places by a physical instrument which divides one de Broglie wave into two "coherent" beams in a similar way as half-silvered plates and similar devices in optics. As soon as an attempt is made to decide on which of the two feeding branches the particle appears, there is a new initial state and no interference is observable.

3. Summary.

It is misleading to compare quantum mechanics with deterministically formulated classical mechanics; instead, one should first reformulate the classical theory, even for a single particle, in an indeterministic, statistical manner. Then some of the distinctions between the two theories disappear, others emerge

with great clarity. Amongst the first is the feature of quantum mechanics, that each measurement interrupts the automatic flow of events and introduces new initial conditions (so-called "reduction of probability"); this is true just as well for a statistically formulated classical theory. The essential quantum effects are of two kinds: the reciprocal relation between the maximum of sharpness for coordinate and velocity in the initial and consequently in any later state (uncertainty relations), and the interference of probabilities whenever two (coherent) branches of the probability function overlap. For macro-bodies both these effects can be made small in the beginning and then remain small for a long time; during this period the individualistic description of traditional classical mechanics is a good approximation. But there is always a critical moment t_c where this ceases to be true and the quasi-individual is transforming itself into a genuine statistical ensemble.

References.

(1) Albert Einstein: Philosopher—Scientist. The Library of Living Philosophers, Vol. VII (Evanston, Illinois, 1949).

(2) Louis de Broglie: C. R., **183**, 447 (1926); **184**, 273 (1927); **185**, 360 (1929); **209**, 1453 (1953).
See also Scientific papers, presented to M. Born (Oliver and Boyd, 1953) p. 21.
Further: La physique quantique restera-t-elle indéterministe? (Paris, Gauthier—Villars, 1953).

(3) E. Schrödinger: Brit. Journ. for the Philos. of Sci. **3**, Part I, 109; Part II, 233 (1952).

(4) A. Einstein: Scient. papers, presented to M. Born (Oliver and Boyd, 1953), p. 33.

(5) M. Born: Physical Reality. Phil. Quarterly, **3**, 139 (1953).

(6) Louis de Broglie: Wellenmechanik (Akad. Verlagsges., Leipzig, 1929).

Indleveret til selskabet den 15. april 1955.
Færdig fra trykkeriet den 22. september 1955.

Det Kongelige Danske Videnskabernes Selskab
Matematisk-fysiske Meddelelser, bind **30**, nr. 3

Dan. Mat. Fys. Medd. **30**, no. 3 (1955)

DEDICATED TO PROFESSOR NIELS BOHR ON THE OCCASION OF HIS 70TH BIRTHDAY

SOME STUDIES ON HEAVY MESON EVENTS IN STRIPPED EMULSIONS

BY

J. K. BØGGILD, J. E. HOOPER, W. C. G. ORTEL,
AND M. SCHARFF

København 1955
i kommission hos Ejnar Munksgaard

CONTENTS

Printed in Denmark
Bianco Lunos Bogtrykkeri A-S

An account is given of 17 K-meson events found in half a stack of stripped emulsions exposed during the Sardinia expedition of 1953. Evidence is presented for the mode of decay $K_\mu \rightarrow \mu + \nu$, where the μ-meson is emitted with $p\beta c = (224 \pm 7)$ MeV., and the best mass of the K_μ-meson is $(990 \pm 16)\ m_e$. An example of χ-decay is also reported and discussed.

I. Introduction.

In the course of a special scan of 106 cm³. of emulsion for stopped K-mesons, 17 examples have been found in which a stopped K-particle emits a fast singly charged secondary, together with one or more neutral particles. In addition, one example of the capture of a negative K-meson, two examples of τ-decay, one probable and one certain excited fragment, 1054 examples of π-μ decay, and 1540 σ-stars were found in the same volume of emulsion. The emulsions searched formed half of a stack of 40 stripped emulsions, each $150 \times 100 \times 0.6$ mm³., exposed by the Sardinia expedition in the summer of 1953. (S 17; exposed on flight 20). The plates reached a maximum altitude of 85,000 feet, and remained above 62,500 feet for seven hours, at which latter altitude the cut-off operated. Full details of the flight data, etc., have been published by Davies and Franzinetti (1954). The plates were later developed in Bristol.

It is difficult to estimate the efficiency of detection of the stopping K-particles which decay with the emission of only a fast charged particle at or near minimum ionization. The grain density in our emulsions is considerably lower than normal (plateau $\approx$ 9 grains per 50 μ) and the grains themselves are small. A guide to the efficiency of observation of the decay tracks from the stopped particles may be had from the ratio of the numbers of ϱ-meson events with and without observed decay electrons.

The observed ratio is 1.15, compared with an expected value ≈ 1. It must be noted, however, that the comparison between the ϱ-mesons and the K-mesons is by no means exact; it is easier to distinguish ϱ-mesons from stopping protons, so that the search for a minimum secondary will be made more carefully.

The method of scanning adopted probably leads to some bias against negative K-events, for, when a negative K-meson is stopped and captured shortly after entering a particular emulsion sheet, the event is not easily distinguished from an ordinary small star. On the other hand, a stopping track with which was associated a lightly ionizing secondary would be traced back into the next emulsion if there were any doubt at all about its nature. Tracing back has been made very simple and quick by the use of frames in which the individual plates are mounted, so that the scanners are always able to follow doubtful examples back quickly.

Table I includes all the data which have been obtained on the examples of K-mesons. Preliminary data (Bøggild et al., 1954) on some of the events have already been included in the table published by Dilworth et al. (1954), but there are changes in the present table due to more detailed measurements which have been made more recently.

II. Mass Measurements on the Primary Particle Tracks.

(a) *Constant Sagitta Method.*

Measurements by the constant sagitta scattering method have been carried out on all the suspected K-particles to rule out the possibility that any of them are examples of hyperons decaying at rest. The cell scheme used was that published by Fay et al., (1954; table 4) which extends from 40 to 10,300 μ and which was designed for a mean sagitta, $\bar{D}$, of 0.500 μ for π-mesons. Taking into account the variation of the scattering constant and $p\beta c$ along the track, a particle of mass $M = 963\, m_e$ would be expected to yield a value of $\bar{D} = 0.288\, \mu$, while one of mass $M = 2330\, m_e$ would give $\bar{D} = 0.193\, \mu$. When the full set of cells is not used, $\bar{D}$ must be corrected by a small factor which is a function of the mass. The scattering was measured using cells,

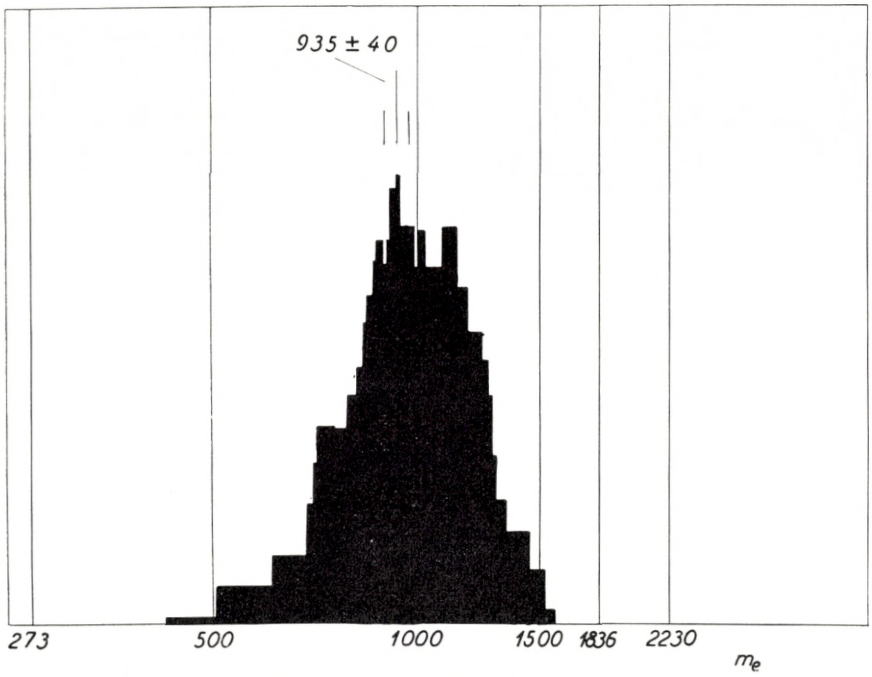

Fig. 1. A weighted distribution of the masses of the 17 K-mesons and one τ-meson measured by the constant sagitta method. Each track is represented by a rectangle whose width is the standard deviation, and whose area corresponds to the statistical weight.

each of which was half the length given in the table. A $4 \times \overline{D}$ cut-off was used and the noise was eliminated between these cells and those of full size, on the assumption that it is independent of cell-size. For steep tracks, the zero point of the cell set was frequently adjusted, so that, on the average, the assumed range was equal to the true range. The value of $\overline{D}$, measured on a track of angle of dip Φ in the unshrunk emulsion, was corrected by a factor $(\cos \Phi)^{3/2}$. This factor was 0.8—0.9 for events $K4$, $K13$, and $K17$, and between 0.6 and 0.8 for events $K8$, $K9$, and $K18$. For all the other events $(\cos \Phi)^{3/2} > 0.9$. The value of $\overline{D}$ from six tracks which were shorter than the full set of cells was corrected on the assumption that the mass was 963 m_e. This correction never exceeded $1\,^0/_0$.

The masses quoted in Table I were calculated, using the relation

$$M = (963\ m_e)\ (0.288\ \mu/\overline{D})^{2.32},$$

while the errors were derived from the number of cells, taking into account the effect of noise. The probability that any of these particles has a mass outside the interval 273 m_e to 2340 m_e is less than 2 %. Taking the measurements of all the particles together, the mean value of $\overline{D} = (0.291 \pm 0.005)\,\mu$, corresponding to a mean mass value of $M = (935 \pm 40)\,m_e$. The weighted distribution of the individual mass values is shown in Fig. 1.

(b) *Mean Gap-Length vs. Range Method.*

In view of the large statistical error inherent in the measurement of mass by the constant sagitta method, we have, in addition, measured, by the mean gap-length vs. range method, the masses of six primary particles whose tracks were flat in the emulsion. As is well known (O'Ceallaigh, 1954; Della Corte et al., 1953, 1954), the mean gap-length is a particularly good measure of ionization, since it is very little dependent on small fluctuations of development in the plates. In our experiment, no corrections for variation of this quantity with depth in the emulsion have been found to be necessary, provided that track within 30 μ of either surface of the shrunk emulsion is not measured. As the greatest fluctuations in the mean gap-length differed by only a few per cent between different parts of the same emulsion, and between different emulsions of this batch, it has only been necessary to make a detailed calibration curve for one of the emulsions of the batch. The curve was then fitted to points corresponding to specific proton ranges obtained from the other emulsion sheets. Of the plates which have been examined in detail, three yield mean gap-lengths as a function of range which are identical to within about 1 % with those obtained from the calibration plate; the mean gap-lengths from three other plates are very close to that of the calibration plate for black tracks, but deviate from it when the mean gap-length becomes larger. The deviations are about 4 % when the ionization is that corresponding to a proton of 5 cm. residual range. As the deviations are small, it is sufficient to assume that the percentage correction of the mean gap-length is proportional to the mean gap-length.

In view of the arguments put forward by Della Corte and his coworkers (1954), such deviations might, at first sight, seem

surprising, but it must be remembered that their arguments only apply to "fully developed" emulsions. Though it is difficult to define in a practical way what exactly is meant by "fully developed", the present stack of emulsions is, by any standards, rather lightly developed. When the mean gap-length in a plate was found to deviate from that in the calibration plate, it was always larger, indicating lighter development. In such plates, the fluctuations of the mean gap-length along a track were found to be very much larger than for those plates in which it did not deviate, and this effect was found to be due to "islands" of low development, in which the mean gap-length was sometimes as much as 10 % above that of the calibration plate. No evidence was found for "islands" in those plates which did not deviate appreciably from the primary calibration. In order to correct for the effects of the "islands", special calibration tracks close to those of the K-mesons were used in those plates which deviated. Some confidence can be felt that all the "islands" which could have led to appreciable errors in the mass determination have been found, for their effects would be expected to show up as large deviations in the apparent mass between different plates. In only one of the six measured examples, $K6$, did the whole of the track lie within the same emulsion sheet. Only two sections of K-track, both on $K7$, were found to pass through the "islands".

A simple cosine correction was applied to the mean gap-length whenever the dip of the track exceeded one in thirty-five in the shrunk emulsion, but as measurements by this method were only made on tracks which were relatively flat, corrections were only used on a few short sections, and they never exceeded 3 %.

In order to test the method for any possible systematic error when applied to particles of K-meson mass, measurements were made, using exactly the same experimental techniques, on the track of a τ-meson. The value obtained for its mass was $(979 \pm 43)\ m_e$, in excellent agreement with the accepted value (e. g., see AMALDI et al., 1954). It should be noted that the error quoted does not take any account of possible errors arising from the calibration.

The errors were found by splitting all the tracks into sections, 1.74 mm long, from each of which a value of the mass was found.

The errors could then be calculated from the internal consistency of each track. From the calibration tracks, the standard deviation of the individual sections from their means were 8.2 %, 8.8 %, and 8.9 % on μ-mesons, π-mesons, and protons, respectively. The standard deviations found from the three longest K-meson tracks were 9.4 %, 5.6 %, and 7.5 % for individual 1.74 mm lengths. Taking all the measured sections of K-meson track together, one finds that the standard deviation is 8.6 %, in good agreement with the above figures. This is consistent with the assumption that all the K-particles have the same mass.

29 individual sections of K-track were measured. If the measurements were completely independent, the final error on the mean would be $(8.6/\sqrt{29})\,\% = 1.6\,\%$. In point of fact, the error calculated from the final masses was only 0.6 %. Though the statistical weight of this figure is small, it appears that the true standard deviation taken from the final mass values cannot be larger than that obtained from the individual sections. This confirms that all the masses are consistent with an unique value, and at the same time shows that any effects due to energy straggling are already included in the error which is deduced from the individual sections. A narrow distribution of the masses determined from long tracks might be a consequence of correlation between energy-loss fluctuations and fluctuations in the grain-density.

The errors quoted for the individual particles in Table I are calculated from the relation s. d. $= (8.6/\sqrt{n})\,\%$, where n is the number of sections in the track. Where mean masses are quoted later in the paper, a further error of 2 % is added, to take into account the possible errors in the calibration. This figure for the calibration error is deduced from the consistency of the apparent masses of all calibration particles. The weighted mass distribution of the K-particles, including the τ-meson, and the calibration tracks whose residual range is > 4 mm, is shown in Fig. 2. The mean mass of the five measured K-particles is $(986 \pm 25)\, m_e$.

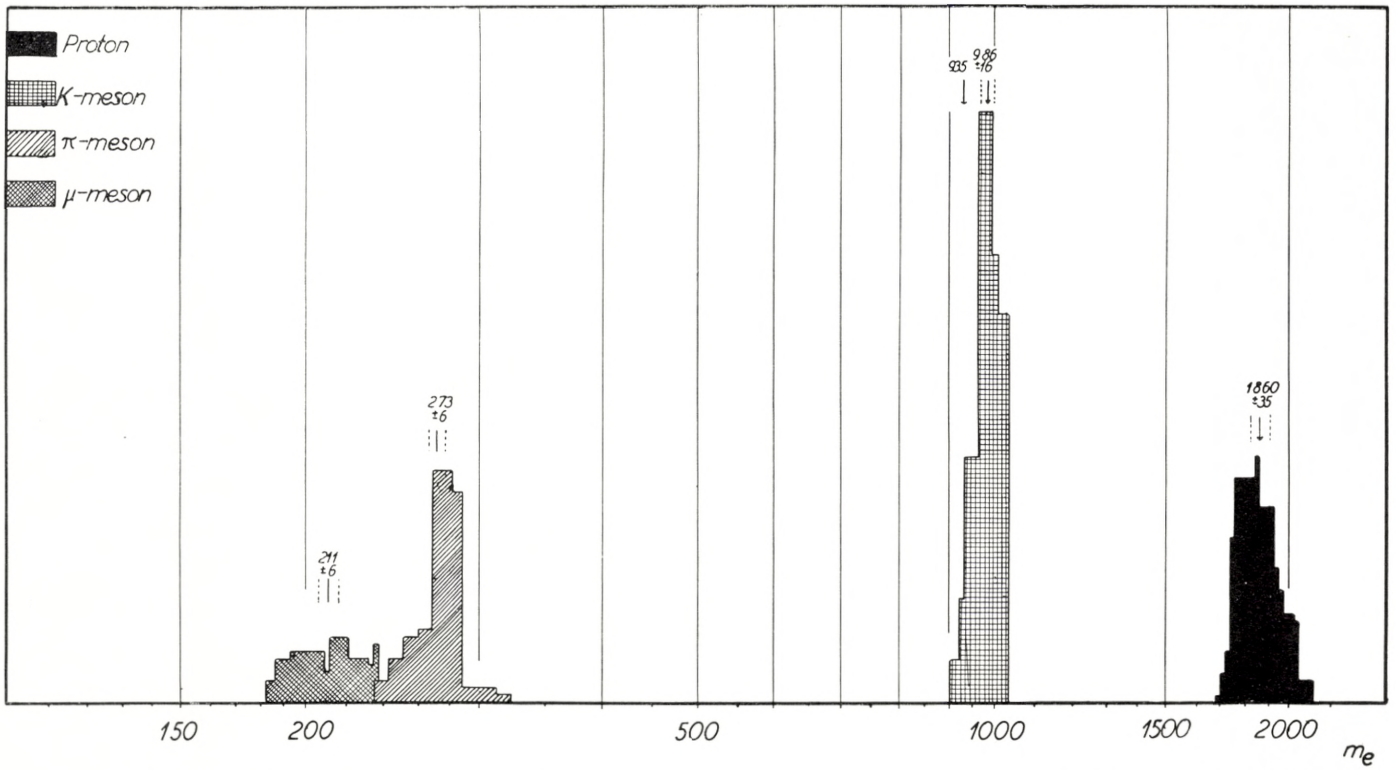

Fig. 2. A weighted distribution (constructed in the same way as Fig. 1) of the masses of the six K-mesons (K 5, K 6, K 7, K 12, K 20, and τ 2) and the calibration particles, obtained from mean gap-length vs. range measurements.

III. Measurements on the Secondary Particle Tracks.

Six of the secondary particles were flat enough to enable reasonably accurate measurements of the grain-density and scattering to be made. Of these six, five lead to values of $p\beta c$ close to 220 MeV., and a grain-density close to plateau. The sixth secondary, that associated with $K5$, was emitted with $p\beta c = (170 \pm 8)$ MeV. and a "blob" density, $b^* = (1.08 \pm 0.02)$ times the plateau value.

The ionization was estimated by comparing the "blob" count with that of nearby electron tracks. It was found to be very important that the electron tracks selected should be near the track under consideration, laterally as well as in depth. It was usually possible to find sufficient electron track which lay within one millimetre of the meson secondary at the same depth in the emulsion. Calibration electrons were chosen by rough scattering measurements which ensured that their energy lay between 30 and 80 MeV. When available, higher energy electrons were used which originated in high energy pairs or other readily identifiable electromagnetic processes. In each plate at least twice as many electron track grains as grains of the secondary track were counted.

The values of the "blob" density, quoted in Table I, are given for the same point on the track as that to which the values of $p\beta c$ given in column 9 refer, while the errors quoted have been calculated from the internal consistency along each track, and not from the number of "blobs" actually counted.

Scattering measurements were made on a Koristka microscope (noise level 0.03 μ independent of cell-length (Bøggild and Scharff, 1954)) by the coordinate method due to Fowler (1950). Each track was measured in 50 μ cells. $\bar{D}$ was calculated, using a $4 \times \bar{D}$ cut-off, and the noise was eliminated between 50 μ and 100 μ cells on the assumption that it was independent of the cell-length. We were able to use such a small cell-size because the total noise on the readings was 0.1 μ, and this was an advantage not only because it increased the statistics, but also because it reduced the effect of distortion. The distortion in these emulsions was low, but corrections were made for some of the

steeper tracks, the distortion being measured directly on neighbouring parallel tracks, and the appropriate correction being added to each second difference.

The values of the scattering from sections of track in different emulsions were plotted as a function of distance from the decay point of the K-mesons, and a straight line, of slope corresponding to the appropriate rate of energy loss, was then fitted to the experimental points by the method of least squares, and was extrapolated back to the decay point. From the value of $\bar{\alpha}$ so found, the value of $p\beta c$ with which the secondary was emitted was calculated.

The value of the scattering constant was checked, on the assumption that the theoretical dependence on velocity and cell size (Williams, 1940; Gottstein et al., 1951) was correct, from measurements on a number of stopping particles in the emulsion. For each section of track, the value of $p\beta c$ was calculated from the range-energy relation published by Baroni et al. (1954), which was first tested at low energy on μ-mesons from the decay of π^+-mesons stopping in the stack. The true μ-meson range was determined independently of the shrinking by the regression method of Fry and White (1954), which, with a slight modification, was adapted to thick emulsions. The mean range of 20 μ-mesons was (0.0 ± 1.4) % from that given by the range-energy relation for 4.11 MeV. μ-mesons. It was found that the scattering constant in these plates should be increased by (3 ± 3) % over the value determined by Voyvodic and Pickup (1952). The errors on the values of $p\beta c$ at emission including those arising from this source are set out separately in column 12 of Table I.

IV. Identification of the Secondary Particles.

The secondaries of $K3$, $K7$, $K12$, $K14$, and $K20$ were all emitted with a value of $p\beta c$ between 215 MeV. and 233 MeV. The deviations of the individual values from the mean, (224 ± 7) MeV., were consistent with the assumption that all five particles were ejected with the same energy. In the following discussion we shall therefore assume that all these particles arose from the same two-body decay process. The ionization of four of them

was the same within experimental limits, but that of $K7$ was considerably higher.

The grain density and scattering results are presented in Fig. 3. The variables chosen for this figure and their theoretical relationship are discussed in the Appendix. The measured "blob" densities, b^*, were converted to grain densities, g^*, on the assumption of an exponential gap-length distribution, using the approximate formula

$$g^* = b^* \left\{ 1 + \frac{\sigma}{G}(g^* - 1) \right\}.$$

Here, G is the mean gap-length and σ is the minimum distance between the centres of resolved grains. We used the value $\frac{\sigma}{G} = 0.1$, which is sufficiently accurate for our purpose, as the quantity $0.1\ (g^* - 1)$ never exceeded 0.02.

The K-meson secondaries are each represented by two points, one calculated on the assumption that the particle is a μ-meson, and the other on the assumption that it is a π-meson. The secondary of $K5$ is well identified as a π-meson, fitting well the points obtained for the calibration tracks. With the exception of $K7$, the other secondaries are best fitted on the assumption that they are μ-mesons. The fast calibration tracks seem to lie below the theoretically calculated limit, but it may be that one of them was a μ-meson.

Independent evidence in favour of the group of secondaries being really μ-mesons is obtained when the mass measurements on the primary particles are taken into account. If we assume that they are π-mesons, and that the events do represent the decay of heavy mesons, then the primary mass, from the observed value of $p\beta c$ at emission of the secondaries, would have to be $(1070 \pm 20)\ m_e$, or greater. This value is well outside the standard error of the combined direct measurements on the tracks of particles $K7$, $K12$, and $K20$, which give a value $(981 \pm 23)\ m_e$. This argument rests on the assumption that we are studying a decay process, but it can be shown that any form of interaction involving a nucleus which could lead to the emission of a π-meson in the required energy region (Rossi, 1954) would require that the spectrum of the secondary emission energies have a width

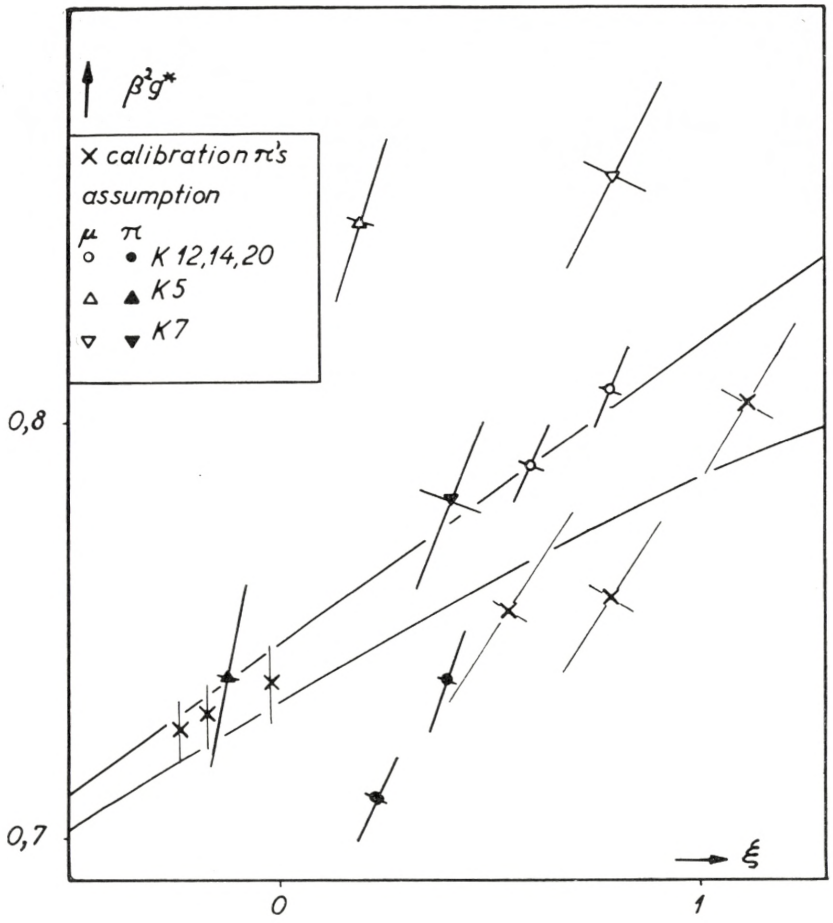

Fig. 3. $\beta^2 g^*$ vs. $\xi = ln \frac{\beta^2}{1-\beta^2} - \beta^2$ for the K-meson secondaries and π-meson calibration tracks. Each secondary particle is represented by two points; one calculated on the assumption that the secondary is a π-meson and the other on the assumption that it is a μ-meson. The curves represent what are believed to be limiting forms of the theoretical relationship (cf. Appendix). They are fitted at the low energy calibration points.

of about 50 MeV., due to the motion of the nucleons in the nucleus. This would be incompatible with the observed homogeneity of the group. It should be remarked, however, that the mean $p\beta c$ of π-mesons, arising from a reaction of the type observed by Rossi, $K^- + n \rightarrow \pi^- + \Lambda^\circ$, would be very close to that of the μ-mesons arising from K_μ decay. In view of the grain-density vs. scattering evidence that $K7$ is a π-meson (Fig. 3), it

might well be possible to interpret this one event as being due to the above reaction. There is good evidence that most of the 18 K-mesons observed are, in fact, positive, since none has been found to be associated with an Auger electron at the end of its range. None of the secondaries was observed to interact in flight, but this evidence is poor, for the total path length in the emulsion was only just over one mean free path, assuming geometrical cross section.

The assumption that the secondary particles are μ-mesons, on the other hand, leads to a mass of the primary particle, calculated from the observed energy of emission of the secondaries, and assuming a decay scheme $K_\mu \rightarrow \mu + \nu$, of $(998 \pm 25)\, m_e$, in good agreement with the measured primary mass. The above decay scheme was proposed by GREGORY et al. (1954) for the so-called K_μ events which they had observed in their double cloud-chamber arrangement at the Pic-du-Midi. It must be remarked, however, that while their evidence suggests that the mass of the K_μ-meson is less than that of the τ-meson, our work suggests that it is the same or greater.

There remains the possibility that some or all of the secondary particles are electrons. This cannot be ruled out on the basis of grain density and scattering measurements for any of the secondaries except that of $K5$. There is, however, no indication of energy loss by bremsstrahlung, although the total track length measured corresponds to more than 8 radiation lengths. This may be seen from Fig. 4, in which the values of $p\beta c$ are plotted as a function of distance from the decay point. The shortest measured length was 2.2 cm., and the total length was 24 cm. The probability that any one secondary is an electron is less than 15 % (EKSPONG, 1955), and if they are indeed a group of particles from events of the same type, the probability that they are all electrons is negligible.

The decay of $K5$, in which a π-meson of initial $p\beta c = (170 \pm 8)$ MeV. is emitted, is clearly an example of the χ-meson, which is believed to decay according to the scheme $\chi^+ \rightarrow \pi^+ + \pi^\circ$. Assuming this decay scheme and using the observed emission energy and the directly measured mass of the primary particle, the mass of the neutral secondary is found to be $(316 \pm 68)\, m_e$. The interpretation of a large number of events similar to $K5$ has recently

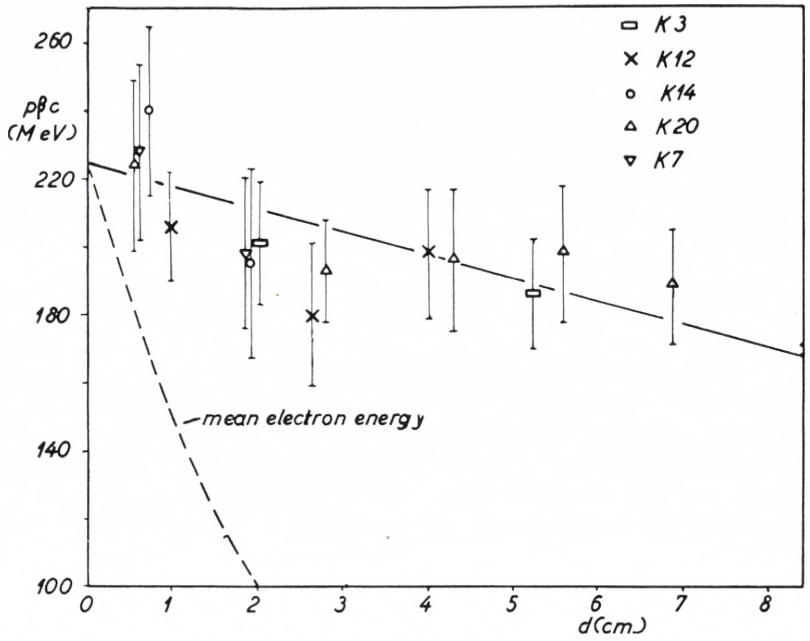

Fig. 4. $p\beta c$ as a function of the distance from the decay point, for the secondary particles. The full line, corresponding to ordinary ionization loss alone, fits the observations well. The dotted curve, based on the assumption that the secondaries are electrons, and taking energy loss by "bremsstrahlung" into account, is much too steep.

been strikingly confirmed by the observation by the Padua group of two examples in a very large stack of stripped emulsions in which the secondaries are brought to rest (ROSTAGNI, private communication). Both in respect of the energy with which the secondary is emitted, and the directly measured mass of the decaying particle, $(996 \pm 34)\, m_e$, $K5$ is in good agreement with the observations hitherto reported (DILWORTH et al., 1954).

V. The Production Stars.

All the K-mesons found in our stack of plates could be traced back to their parent stars, and the classification of each is included in Table I. The mean numbers of heavily and lightly ionizing particles emerging from these stars are very similar to those found by other workers, and no charged hyperons have

been found to emerge from any of the six stars which were examined in detail.

The origin of $K15$ deserves special mention, for it was found to be produced without any other visible associated tracks. Similar origins have been found for K-mesons in Bristol and Bombay, and for a Y^+-particle at Rome. In view of the evidence for associated production obtained at Brookhaven by the Cosmotron group (FOWLER et al., 1954) it seems possible that these events may be of the type

$$n + p \rightarrow Y^\circ + K^+ + n \quad \text{or} \quad n + p \rightarrow Y^+ + K^\circ + n .$$

VI. Discussion and Comparison with other Results.

Evidence for a decay scheme $K_\mu \rightarrow \mu + \nu$ has previously been put forward by GREGORY et al. (1954) on the basis of certain S-events found in the lower chamber of a double cloud-chamber arrangement. Further evidence is provided by some of the events observed in the large multi-plate chamber at M.I.T. (ROSSI, 1954). In both instances two groups of particles were reported; one producing secondaries of range about 100 gm. cm.$^{-2}$ Pb, and another secondaries of range about 60 gm. cm.$^{-2}$ Pb. These particles can be shown to be L-mesons and, on the basis of the directly measured primary masses, the first group cannot be π-mesons, and are therefore assumed to be μ-mesons. The second group of secondary particles is identified with the π-mesons from the decay of the χ-meson, a process previously observed in the nuclear emulsion. The secondary momentum spectrum of slow, charged V-events observed in cloud chambers shows a definite peak, which probably includes both K_μ and χ secondaries. There is no evidence for μ-secondaries with a continuous energy spectrum. The cloud-chamber has provided no strong evidence for a negative counterpart to either the K_μ or the χ-meson.

On the other hand, emulsion work has provided evidence in favour of a particle, named by the Bristol workers the $\varkappa$-meson, which decays with the emission of a μ-meson whose energy varies within wide limits. There has hitherto been no very good

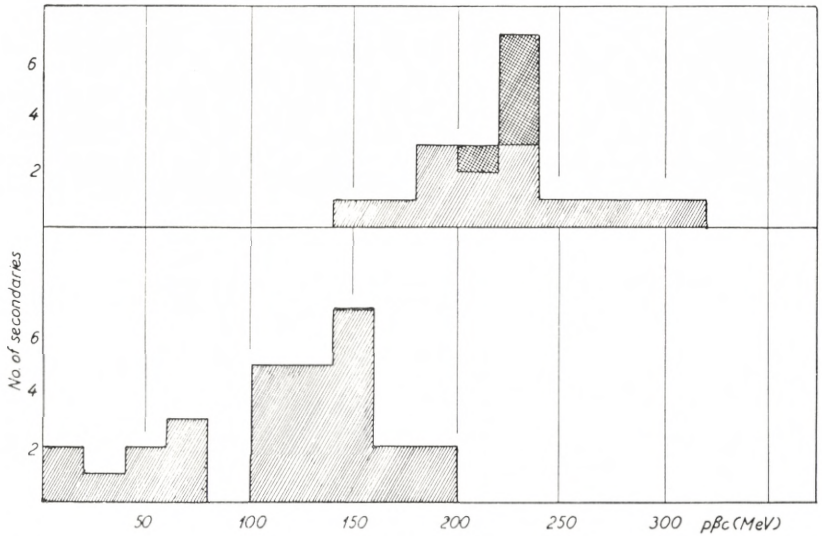

Fig. 5. The momentum spectrum of the secondaries of K-mesons, excluding those which are identified as π-mesons or electrons. The upper diagram includes only events which are likely to be examples of K_μ decay. The lower includes the remainder, and presumably represents the spectrum of secondaries from $\varkappa$ decay. The cross-hatched portion represents our present experimental results.

evidence for a decay of the K_μ type. This is not particularly surprising, for, at least in glass backed plates, it is very difficult to distinguish the peak due to the K_μ decays from the nearby, and possibly overlapping, spectrum of the secondaries of $\varkappa$-decay.

Fig. 5 shows the momentum spectrum of K-meson secondaries which have not been identified as π-mesons or electrons. We have used the collected results listed by DILWORTH et al. (1954) together with our own. Most of these secondaries are probably μ-mesons, for the π-mesons from χ-decay have a grain density appreciably above minimum when they are emitted, and are therefore comparatively easily identified. The upper histogram includes secondaries whose $p\beta c$ at emission was within two standard deviations of 214 MeV., the value expected from K_μ decay if the primary mass is equal to that of the τ-meson. The lower histogram includes the remainder of the examples. To obtain an upper limit to the proportion of K_μ-mesons in the sample, one may assume that the upper diagram includes only K_μ events, and the lower diagram only $\varkappa$ events. Thus, the evidence obtained up to the time of the Padua conference would

TABLE I a. Primary Particles.

1 Event	2 Star	3 Total Length (mm.)	4 Length used for G. R. measurement (mm.)	5 Mass from $\bar{\alpha}$-R (m_e)	6 Mass from G-R (m_e)	Observer*
+ 3	12 + 2p	3.0		1000 ± 300	1110 ± 160 ÷	A. K.
4	11 + 4p	21		1070 ± 180		M. W. H.
5	11 + 12p	30	15.7	850 ± 140	996 ± 29	»
6	6 + 1p	5.3	3.5	620 ± 110	971 ± 59	»
7	16 + 2n	44	14.0	1290 ± 210	998 ± 30	»
8	23 + 9p	15		920 ± 170		»
9	17 + 5p	1.7		610 ± 200		»
10	8 + 4p	8.9		1030 ± 200		»
11	13 + 1p	6.1		1000 ± 190		R. M. P.
12	17 + 2p	36	14.0	740 ± 130	969 ± 29	J. K. B.
13	24 + 3p	19		1100 ± 200		K. N.
14	6 + 2p	22		1200 ± 200		M. W. H.
15	1 + 0n	22		1090 ± 180		»
16	18 + 2n	25		800 ± 120		»
17	19 + 2p	11		1210 ± 300		R. M. P.
18	13 + 2n	11		940 ± 160		M. W. H.
19	5 + 2n	27		1050 ± 180		E. T.
20	3 + 3p	8.1	3.5	890 ± 140	968 ± 59	E. B.

+ Found in an earlier stack.
÷ Measured photoelectrically by VON FRIESEN and his coworkers.
* Observers: Miss E. BACH, Dr. J. K. BØGGILD, Mr. M. WOLF HANSEN, Miss A. KOLDING, Miss K. NIELSEN, Miss R. MØLLER PEDERSEN, Miss E. TROLLE.

seem to suggest that $\varkappa$-mesons were rather more frequently stopped in the emulsion than K_μ-mesons.

While the statistical weight of our result is small, the fact that we have found five probable K_μ-decays and no $\varkappa$-mesons emitting a lower energy μ-meson among six identified events, would seem to require that the K_μ-meson be considerably more common than the $\varkappa$-meson. This is in accord with the results of the cloud-chamber workers, but is very different indeed from that obtained from the earlier emulsion work, discussed above. It is, of course, possible that the discrepancy is a result of different scanning efficiencies. If not, it would seem that a greater proportion of K_μ-mesons is stopped in the larger blocks of emulsion.

TABLE I b. Secondary Particles.

Event	7 Total Length (mm.)	8 Length used for $p\beta c$ measurement (mm.)	9 $p\beta c$ (MeV.)	10 b^*	11 $p\beta c$ at decay (MeV.)	12 ⊕	13 Identity
3+	63	52	199 ± 13	1.00 ± 0.01	220 ± 12	± 13	$(\pi, e)\ \mu$
4△	Nuclear Absorption						
5	58	55	141 ± 8	1.17 ± 0.01	170 ± 6	± 8	π
6	Steep						
7	32	26	218 ± 16	1.02 ± 0.02	221 ± 15	± 16	$(\mu, e)\ \pi$
8	Steep						
9	Steep						
10	Steep						
11	Steep						
12	46	44	199 ± 13	0.97 ± 0.01	215 ± 11	± 13	$(\pi, e)\ \mu$
13	Steep						
14	52	19	228 ± 15	0.98 ± 0.01	233 ± 14	± 15	$(\pi, e)\ \mu$
15	Steep						
16	Steep						
17	Steep						
18	23						
19	Steep						
20	78	69	197 ± 10	0.98 ± 0.01	227 ± 7	± 10	$(\pi, e)\ \mu$

⊕ Error in $p\beta c$ at decay, including the uncertainty in the scattering constant.
△ BØGGILD et al., 1954.

This would imply that the K_μ-mesons are emitted with a higher mean kinetic energy than the $\varkappa$-mesons.

One major difference between our results and those of the cloud-chamber work is the mass of the K_μ-meson. The Pic-du-Midi group quote a best value of $(935 \pm 15)\ m_e$, obtained as a weighted mean between that measured directly, and that obtained indirectly from the assumed decay scheme and the momentum of emission of the secondary. Further, their value of $p\beta c$ at emission, (206 ± 1.5) MeV., is considerably lower than that which we have found. In both experiments there is approximate agreement between the directly and indirectly obtained masses on the basis of the assumed K_μ decay scheme.

In our work, the direct and indirect masses are completely independent. The $p\beta c$ of the secondary particles is obtained by

measurements of the multiple scattering, and depends on the range-energy relation which was used in the determination of the scattering constant. While the range-energy relation in this region could be one or two per cent in error, it does not seem possible on this basis to bring our results down as low as those of the Paris group. Any distortion or noise which was not completely eliminated would increase the apparent scattering and produce too low a value of $p\beta c$, so that correction for such errors would increase the divergence between the two sets of experimental results. Alternatively, if the scattering constant is changed sufficiently to produce agreement, the value of $p\beta c$ with which the secondary of $K5$ is emitted would be reduced from (170 ± 6) MeV. to (153 ± 5) MeV. This would destroy completely the excellent identification of this good event as a χ-meson, and it could not then be identified with any well-established decay scheme.

The directly measured masses in our experiment, obtained from the measurements of mean gap-length, are entirely independent of the range-energy relation and, of course, of the scattering constant. The calibration tracks used for comparison included π- and μ-mesons on the one side, and protons on the other, and there is no evidence for any systematic divergence of the mean gap-length as a function of mass from the expected relation. In view of the complete independence of the direct and indirect measurements, the mean value, $(990 \pm 16)\, m_e$, is statistically significant. As it lies well above the accepted mass of the τ-meson, it is very improbable that the K_μ-meson is the lighter of the two.

In the cloud-chamber work, both the directly and the indirectly measured masses depend to some extent on the range-energy relation chosen. If the relation used has the correct shape, then any change in its absolute value will shift the directly and indirectly measured masses in opposite directions. However, an erroneous range-energy relation can produce an incorrect mass value if both its absolute value and its shape are wrong. Again, it must be emphasized that most cloud-chamber measurements on slow, charged V-particles lend support to the Pic-du-Midi results, rather than to the higher value which we have obtained.

It does not now seem possible to account for the discrepancy between the results of the two experiments, although the similarity

in the mode of decay makes it seem extremely probable that the particles actually being studied are the same. A brief account of this work has already been published by BØGGILD et al. (1955).*

Acknowledgements.

We would like to take this opportunity to thank Professor NIELS BOHR for his hospitality and for the facilities of the Institute which he has put at our disposal to enable us to carry out this work.

One of us, (J.E.H.), is indebted to the Churchill Foundation and the Rask-Ørsted Fund for financial support during the course of this work. Another, (W.C.G.O.), was aided by a U.S. National Science Foundation postdoctoral fellowship during 1953—54.

We have benefited from the work of the participants in the Sardinia expedition of 1953, and we are particularly grateful for the helpful cooperation of the Bristol group under Professor POWELL. Our thanks are also due Professor S. von FRIESEN for the photoelectric measurements of the mass of $K3$.

Mag. scient. N. BRENE has assisted skilfully with the measurements. The contributions of the scanning group, recorded in Table I, are acknowledged with thanks.

* Note added in proof: – Since this paper was written the results presented at the recent International Conference at Pisa have confirmed that the K_μ-meson decays in the emulsion rather more frequently than the χ-meson, and that in large stacks the $\varkappa$-meson is much less frequently found. In addition, the evidence presented suggests that the mass of the K_μ-meson is witin a few electron masses of that of the τ-meson.

Appendix.

By M. Scharff.

It is a well-known fact that the identification of particles on the basis of grain-density and scattering measurements becomes increasingly difficult as the particle velocity, β, approaches unity. Near $\gamma = \frac{1}{\sqrt{1-\beta^2}} = 4$, where g^* as a function of energy has a broad minimum, π- and μ-meson tracks are indistinguishable. Still, at $\gamma = 2.5$, the region of interest in the present experiment, an identification is not quite hopeless, provided that the velocity dependence of g^* is accurately known. The best way to determine this relationship would be to measure the grain density of stopping π- and μ-meson tracks, for which the velocity is known from the range-energy relation. Due to the limited dimensions of our stack, however, the calibration could only be extended to $\gamma = 1.6$ by this method. For higher energy calibration tracks we were forced to use supposed π-mesons ejected from stars, relying upon the rather inaccurate values of β obtained from scattering measurements. There is necessarily some doubt about the identity of such particles, since a μ-meson may sometimes be ejected from a star, or may arise from an unobserved π-μ decay. It therefore seemed desirable to consider whether an extrapolation of the lower energy calibration might not be more reliable. The g^*-β curves obtained by various experimenters differ considerably in the minimum value of g^* and the value of γ for which saturation is reached, and previous experimental results do not provide a safe basis for the extrapolation from $\gamma = 1.6$ to $\gamma = 2.5$. Nevertheless, it turns out that the theoretical relation is, in this region, quite insensitive to rather widely different assumptions as to the mechanism of grain formation, and we feel it may be used with some confidence.

We shall first review the theory which has been developed by several authors. The grain density of a track produced by a particle of relativistic velocity is assumed to be proportional to the mean energy loss of the particle in emulsion (Fowler, 1950) or, more precisely, to the mean energy gained by those

AgBr crystals lying directly along the track (STILLER and SHAPIRO, 1953; MESSEL and RITSON, 1950). To calculate the latter quantity, one may then use the previous results of BETHE (1933) and MØLLER (1932) who calculated the energy loss, neglecting collisions with an energy transfer greater than a certain value, T', and obtained

$$\left(\frac{dE}{dR}\right)_{T'} = BNZ\left[ln\frac{2mc^2 \cdot T'}{I^2} + ln\frac{\beta^2}{1-\beta^2} - \beta^2\right], \qquad (1)$$

where $B = \frac{2\pi e^4}{mc^2} \cdot 1/\beta^2$, Z is the atomic number, N the density of atoms and $I \approx (10\text{ eV.}) \times Z$ is the average excitation potential of the stopping medium. Formula 1 is only valid for γ of the order of unity. At higher energies the relativistic polarization, or "density" effect, of FERMI (1940) enters, causing $(dE/dR)_{T'}$ to saturate at a value which may be obtained from formula (1) by substituting $l = 2\ ln\frac{I}{\hbar\omega_0}$ for the velocity-dependent term $\xi(\beta^2) = ln\frac{\beta^2}{1-\beta^2} - \beta^2$. Here $\omega_0 = \left(\frac{4\pi e^2 NZ}{m}\right)^{1/2}$ is the classical resonance frequency of the electrons in the medium. Taking for *AgBr* $I = 415$ eV. and $\hbar\omega_0 = 34$ eV., one finds $l = 5.0$.

The form of equation (1) suggests that we plot the quantity $\beta^2 g^*$, which may be termed the "reduced grain density", as a function of ξ. If g^* and $(dE/dR)_{T'}$ are in fact proportional, such a plot will, at low energies, be a straight line given by

$$\beta^2 g^* = \text{const} \times (L + \xi), \qquad (2)$$

where $L = ln\frac{2mc^2 \cdot T'}{I^2}$, while at high energies

$$\beta^2 g^* = \text{const} \times (L + l). \qquad (2')$$

L may now be determined empirically from the value $\beta^2 g^* = 0.735$ at $\xi = -0.1$ measured on the stopping meson tracks, taking a saturation value $\beta^2 g^* = 1.0$. The result is $L = 14.3$, from which follows $\beta^2 g^* = 0.79$ at $\xi = 1.0$. This analysis may be refined by introducing a slowly-varying density correction, δ, (A. BOHR, 1948), and assuming $\beta^2 g^* \propto (L + \xi - \delta)$. This correction is

included in curve 1 of Fig. 6, which is normalized to unity, not at $\xi \to \infty$, but in the energy region ($\xi \approx 8$—9) of the electron tracks chosen for standardization of the grain-density measurements. This refinement makes little difference to the curve, the value of L still being ≈ 14. Such a value for L, however, leads to the result $T' \approx 200$ keV., which is at variance with the usual interpretation of T' as the upper limit to the energy of struck electrons which can contribute appreciably to the ionization within the crystal. From this point of view, T' might reasonably be expected to lie between 2 and 10 keV., corresponding to L between 9.5 and 11, which in our stack would lead to a saturation value of $\beta^2 g^* = 1.1$.

Still, this apparent inconsistency can be removed without violating the assumption that grain density is proportional to local energy loss. A major part of the relativistic increase of $\beta^2 g^*$ arises from the effect of the transverse component of the field of the fast particle, and part of the energy lost in this way may be emitted as Čerenkov radiation. The fraction, α, absorbed locally depends on the damping of the atomic oscillators. If we use the theoretical value $L = 10$ and adjust α to fit the calibration point, we obtain curve 2 of Fig. 6, for which $\alpha = 0.70$. Without damping, ($\alpha = 0$), $\beta^2 g^* = 0.78$ at $\xi \to \infty$, while for strong damping, ($\alpha = 1$), $\beta g \to 1.1$, as previously mentioned. Actually, STERNHEIMER (1953) found $1 - \alpha = 0.02$ by a direct approximate calculation, so that it remains doubtful whether our data can be fitted by a consistent theory of this type. For this reason we shall discuss briefly a more general approach.

Let us assume that, for a given development, the probability that a crystal is developed is a function $f(\Delta)$ only of the energy, Δ, transferred to it. The grain density must then behave as $\int_0^\infty f(\Delta)\, \sigma(\Delta)\, d\Delta$, $\sigma(\Delta)$ being the cross section for an energy transfer Δ. The theory discussed above is a consequence of the rather special assumption $f(\Delta) \propto \Delta$. The general case of arbitrary $f(\Delta)$ can be analyzed by means of the distinction, introduced by N. BOHR (1948), between free collisions and resonance collisions, the latter containing the variation with ξ. It may then easily be shown that the reduced energy loss is still represented by expressions of the form (2) and (2′), although the values of L and

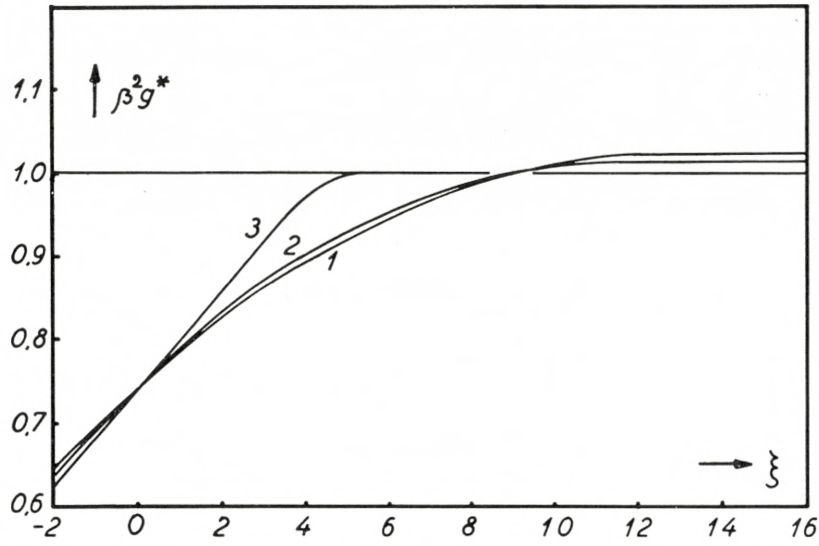

Fig. 6. The theoretical variation of $\beta^2 g^*$ as a function of ξ. The different curves result from the various possible initial assumptions about the mechanism of energy transfer to the silver bromide crystals and about grain formation, which are discussed in the text.

l will depend on $f(\Delta)$ as well as on the distribution of atomic oscillator strengths.

To test the sensitivity of the theoretical $\beta^2 g^*$ vs. ξ curve to the form of $f(\Delta)$, we choose a form which is extremely different from the previous one, viz.

$$f(\Delta) = \begin{cases} 0 \text{ for } \Delta < T_0 \\ 1 \text{ for } \Delta > T_0. \end{cases}$$

Then, g^* will vary as $\int_{T_0}^{\infty} \sigma(\Delta)\, d\Delta$, equivalent to the suggestion of Brown (1953) that a crystal is developed when the energy transferred to it exceeds a certain value T_0, which depends only on development. Curve 3 of Fig. 6 is the result of this assumption, calculated using the simple oscillator distribution of A. Bohr (1948) and assuming strong damping. T_0 was chosen to be 200 eV., to give an absolute plateau grain density of 10 per 50 μ. The curve is a straight line below $\xi = 3$, as in this region the polarization affects only atomic frequencies below $T_0/\hbar$. The slope of the line depends somewhat on the atomic model used, but an upper limit may be calculated from the extreme assumption that the rise is concentrated on oscillators of frequency $T_0/\hbar$.

Previous experimental results fall mainly into two groups. STILLER and SHAPIRO (1953), and FLEMING and LORD (1953), fit their data with curves of the form (2) (or (1)), whereas the results of PICKUP and VOYVODIC (1950), MORRISH (1952), DANIEL et al. (1952), and MICHAELIS and VIOLET (1953) correspond more closely to type (3). From the general treatment of the formation of grains given above, one would not expect such large differences between different batches of plates, but it may well be that, allowing for small differences in experimental techniques, all the data could be fitted by one curve intermediate between (2) and (3). In any case, however, all the empirical curves are consistent with the general scheme, in the sense that each one can be accounted for by some particular choice of $f(\Delta)$, intermediate to the two rather extreme assumptions mentioned above. We are therefore fairly confident that this is also true for the extrapolated curve required in the present experiment.

In Fig. 3, the two limiting curves are fitted so as to deviate about one standard deviation on each side of the calibration points. The upper curve is of type (3) with maximum slope; the lower one is of type (2) with $T' = 1$ keV.

A fuller account of the Appendix will be published shortly.

References.

Amaldi, E., E. Fabri, T. F. Hoang, W. O. Lock, L. Scarsi, B. Touschek, and B. Vitale (1954). Nuovo Cimento **12,** suppl. no. 2, 419.

Baroni, G., C. Castagnoli, G. Cortini, C. Franzinetti, and A. Manfredini (1954). Bureau of Standards, C.E.R.N., Bull. No. 9.

Bethe, H. A. (1933). Handbuch der Physik, 2nd ed., $^{24}/_{1}$, p. 273.

Bohr, A. (1948). Dan. Mat. Fys. Medd. **24,** no. 19.

Bohr, N. (1948). Dan. Mat. Fys. Medd. **18,** no. 8.

Brown, L. M. (1953). Phys. Rev. **90,** 95.

Bøggild, J. K., J. E. Hooper, and M. Scharff (1954), Nuovo Cimento **12,** suppl. no. 2, p. 223.

Bøggild, J. K., J. E. Hooper, W. C. G. Ortel, and M. Scharff (1955). Nuovo Cimento **1,** 1267.

Bøggild, J. K. and M. Scharff (1954). Nuovo Cimento **12,** suppl. no. 2, 374.

Daniel, R. R., J. H. Davies, J. H. Mulvey, and D. H. Perkins (1952). Phil. Mag. **43,** 753.

Davies, J. and C. Franzinetti (1954). Nuovo Cimento **12,** suppl. no. 2, 481.

Della Corte, M. (1953). Nuovo Cimento **10,** 958.

Della Corte, M., M. Ramat, and L. Ronchi (1953). Nuovo Cimento **10,** 509.

Della Corte, M. (1954). Nuovo Cimento **12,** 28.

Dilworth, C. C., A. Manfredini, G. D. Rochester, J. Waddington, and G. T. Zorn (1954). Nuovo Cimento **12,** suppl. no. 2, 433.

Ekspong, A. G. (1955). Arkiv f. Fysik **9,** no. 53.

Fay, H., K. Gottstein, and K. Hain (1954). Nuovo Cimento **11,** suppl. no. 2, 234.

Fermi E., (1940). Phys. Rev. **57,** 485.

Fleming, J. R. and J. J. Lord (1953). Phys. Rev. **92,** 511.

Fowler, P. H. (1950). Phil. Mag. **41,** 169.

Fowler, W. B., R. P. Shutt, A. M. Thorndike, and W. L. Whittemore (1954). Phys. Rev. **93,** 861.

Fry, W. F. and G. R. White (1954). Phys. Rev. **93,** 1427.

Gottstein, K., M. G. K. Menon, J. H. Mulvey, C. O'Ceallaigh, and O. Rochat (1951). Phil. Mag. **42,** 708.

Gregory, B., A. Lagarrigue, L. Leprince-Ringuet, F. Muller, and C. Peyrou (1954). Nuovo Cimento **11,** 292.
Messel, H. and D. M. Ritson (1950). Phil. Mag. **41,** 1129.
Michaelis, P. P. and C. E. Violet (1953). Phys. Rev. **90,** 723.
Morrish, A. H. (1952). Phil. Mag. **43,** 533.
Møller, C. (1932). Ann. d. Phys. (5), **14,** 531.
O'Ceallaigh, C. (1954). Nuovo Cimento **12,** suppl. no. 21, 412.
Pickup, E. and L. Voyvodic (1950). Phys. Rev. **80,** 89.
Rostagni, A. Private Communication.
Rossi, B. (1954). Varenna School lecture notes, unpublished.
Sternheimer, R. M. (1953). Phys. Rev. **91,** 256.
Stiller, B. and M. M. Shapiro (1953). Phys. Rev. **92,** 735.
Voyvodic, L. and E. Pickup (1952). Phys. Rev. **85,** 91.
Williams, E. J. (1940). Phys. Rev. **58,** 292.

Indleveret til selskabet den 29. juni 1955.
Færdig fra trykkeriet den 29. september 1955.

Det Kongelige Danske Videnskabernes Selskab
Matematisk-fysiske Meddelelser, bind **30**, nr. 4

Dan. Mat. Fys. Medd. **30**, no. 4 (1955)

DEDICATED TO PROFESSOR NIELS BOHR ON THE OCCASION OF HIS 70TH BIRTHDAY

HALL COEFFICIENT AND RESISTIVITY OF α- AND β-BRASS FROM 20-600° C

BY

V. FRANK

København 1955
i kommission hos Ejnar Munksgaard

Printed in Denmark
Bianco Lunos Bogtrykkeri A-S

The Hall coefficients and resistivities of *Cu—Zn* alloys in the α- and β-range have been determined by an A.C. method. The observed resistivities are in agreement with earlier results. The sign of the Hall coefficient is normal for all specimens investigated; in the α-range, R_H decreases with increasing *Zn* content more rapidly than predicted by free electron theory and shows a strong temperature dependence for the *Zn* rich alloys. For β-brass, R_H is practically proportional to the resistivity for various temperatures including the temperature range of the order-disorder transition. Some implications of the results for the band structure of these alloys are suggested.

Introduction.

Measurements of the Hall coefficient have for a long time been extensively employed as a means of obtaining some insight into the band structure of pure metals and into the effect of alloying on this band structure. According to current theories, the Hall coefficient should, to a first approximation, be independent of temperature, at least at the higher temperatures where a time of relaxation can be defined. For this reason, and because of experimental difficulties, nearly all measurements have been made at room temperature only. Significant exceptions are the Hall coefficients of ferromagnetic materials, which have recently been studied in greater detail both experimentally and theoretically, and which exhibit strong temperature dependence and other anomalies.

For non-magnetic metals, and especially for alloys, the experimental evidence is scanty concerning the effect of temperature (including the effects of allotropic transformations and melting) on the Hall coefficient. The choice of α- and β-brass for the present investigation was dictated partly by the occurrence of an order-disorder transition in β-brass at moderate temperature, and partly by the availability of results of recent room temperature measurements on these alloys by conventional D.C.methods.

Our results show a pronounced temperature dependence, also for α-brasses, indicating that measurements at one temperature only may be of limited value also in other cases.

Experimental Method.

In order to make reliable determinations of the Hall coefficient at high temperatures we have chosen to use an A.C.apparatus, so that disturbing thermal and Ettinghausen e.m.f.'s are eliminated. Such a method is now in common use; the experimental set up employed in this work presents a modification which permits simultaneous determination both of the Hall coefficient (R_H) and the resistivity (ϱ) with a minimum of probes attached to the sample.

Fig. 1 shows a schematic view of the equipment. The alternating current is taken from a push-pull amplifier (driven by an R-C oscillator) through a shielded transformer (T_1) with very low output impedance. When measuring R_H, the switches S_1 and S_2 are set in position a and the current is passed directly through the sample between A and B; when measuring ϱ, S_1 and S_2 are brought into position b and the current then flows through the series connection of the precision resistance R_1 and the sample. In principle, the Hall voltage, developed across the sample, might be measured directly between probe no. 3 and the sliding contact 4 of the potentiometer P (the ends of which are connected to the probes nos. 1 and 2) if P is first balanced against 3 with zero magnetic field. As the Hall voltage is of the order of micro-volts, this direct method necessitates the use of a stable oscillator and a stable high gain amplifier; a determination of the measuring current is also necessary. These difficulties can be avoided by compensating the Hall voltage, displacing the slide-contact 4 of P; this potentiometer must therefore be calibrated very accurately. The actual construction, which is somewhat more complicated than indicated on Fig. 1, permits readings to one part in a million over a limited range.

The zero indicator connected between 3 and 4 consists of a well shielded input transformer T_3, a battery driven amplifier

A_1, and a selective feedback amplifier A_2. The maximum total gain of this system amounts to 2×10^9. The noise level referred to the input terminals 3 and 4 was about 3×10^{-9} volts when the indicator was tuned to 25 *Hz* (with a bandwidth of 1 *Hz*); this rest signal, usually observed on the oscilloscope, consisted mainly of 50 *Hz* pick-up from the mains.

In order to eliminate from the zero indicator any inductive or capacitive out-of-phase voltages existing between 3 and 4, the secondary of a variable air transformer T_2, the primary of

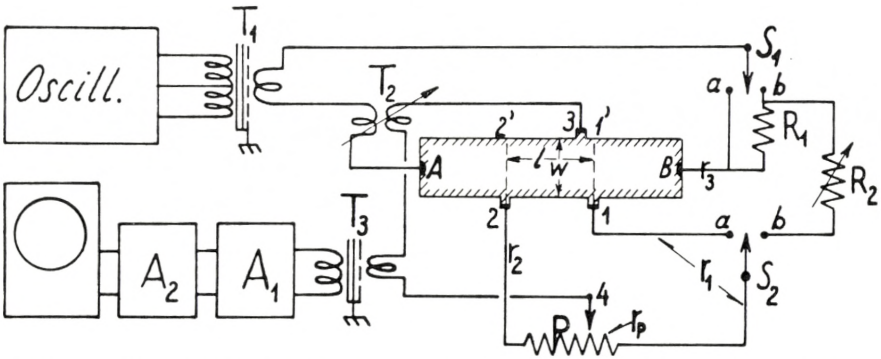

Fig. 1. Block diagram of the sample A—B with the probes 1, 2, and 3 and associated electronic equipment.

which is connected in series with the measuring A.C.current, is inserted in series with the zero indicator.

The samples were rectangular, 45 mm × 10 mm, with the probes 1 and 2 placed at a distance of 15 mm. The connecting conductors consisted of strips of copper foil, silver soldered to the sample by electrical heating with a spot welding apparatus. Insulation was provided by mica sheets, the whole assembly being firmly clamped between two thick copper plates. The outer faces of these plates were furnished with heating elements and thermal insulation; this furnace could be mounted in a box fitting into the air gap of the magnet. To prevent oxidation, carbon dioxide was passed through the box. The temperature was measured by a chromel-alumel couple, the junction being insulated from the sample by a thin mica sheet.

To measure ϱ, P is first balanced with zero magnetic field, while the switches S_1 and S_2 are in position a; S_1 and S_2 are then turned to position b, and the decade resistor R_2 is used

to balance the Wheatstone bridge formed by the resistances R_2, $r_p + r_1 + r_2$, $R_1 + r_3$ and the sample resistance between 1—1' and 2—2'. As $R_2 \rangle\rangle r_p$ we have, irrespective of the placing of probe no. 3,

$$\varrho = \frac{w}{l} t \frac{r_p R_1}{R_2} \left(1 + \frac{r_3}{R_1}\right) \left(1 + \frac{r_1 + r_2}{r_p}\right) \alpha , \qquad (1)$$

where ϱ is the resistivity, t the thickness of the sample, and α is a numerical factor arising from the fact that the measuring current is fed to the sample through the point-like contacts A and B so that the current field in the regions between 1—1' and 2—2' is not quite homogeneous. By separate measurements on samples of different lengths, the value of α for the sample length normally used was determined to 1.010 ± 0.003. The wiring resistances r_1, r_2, and r_3 were suppressed to such values that their effect on the determination of ϱ was less than 1 per cent. The switch S_2 was of the mercury type so that a small and reproducible contact resistance could be obtained.

To measure R_H, P is balanced with the magnetic field on (S_1 and S_2 are in position a); denoting the difference in potentiometer readings for the two field directions by Δx, we have

$$R_H/\varrho = \frac{l}{w} \frac{\Delta x}{2B} \frac{\beta}{\alpha} \Big/ \left(1 + \frac{r_1 + r_2}{r_p}\right), \qquad (2)$$

where B is the induction in the air gap of the magnet and α is the same correction factor as in (1). The correction factor β is different from unity owing to the finite length of the sample; from the published solutions of this problem ([1] . . . . . [6]) we estimate β to 1.010 ± 0.004.

From (1) and (2), R_H may be obtained.

The measurements were carried out with a current of 10—15 amps, a frequency of 25 Hz, and in a field of 0.55 Wb/m^2. Experiments with other values revealed no dependence of ϱ and R_H on these factors.

The accuracy of the results is ± 0.5 % as regards the relative temperature dependence of ϱ and R_H. The absolute values of ϱ and R_H are, however, not better than ± 2 to 3 %, owing to uncertainties in the dimensions of the samples. The temperature is considered correct within $\pm 2°$C.

Results and Conclusions.

Fig. 2 shows the results of resistivity measurements. The copper sample was cut from commercial copper foil, the samples of α-brass were the same as those employed by O. GRAM JEPPESEN [7], and the sample of β-brass was prepared from a cast block with 52.3 atomic $^0/_0$ of copper. The impurity contained in this block, consisting mainly of *Pb*, *Ag*, and *Cd*, was less than 0.03 $^0/_0$. The β-brass sample was milled down from the cast block and given some final rollings combined with a heat treatment at 600° C for a few seconds.

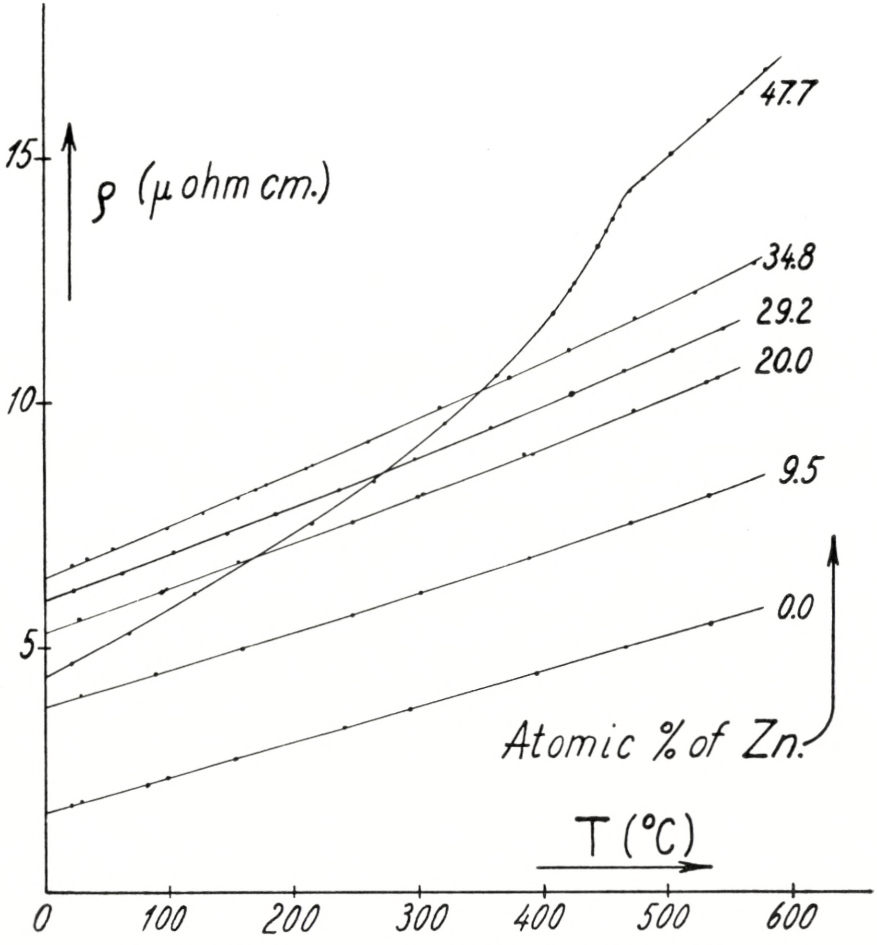

Fig. 2. Resistivity versus temperature for α- and β-brass.

The samples were not systematically annealed, but for each sample at least two measuring series, from 550°C to room temperature, were carried out; in general, the differences between the two measuring series were less than 1 %. This fact and the data from the many annealing experiments on cold worked brasses (cf. the review article by T. BROOM [8]) make us believe that our values of ϱ and R_H represent the true equilibrium values of these quantities. This applies also to β-brass, for which EGGLESTON and BOWMAN [9] have shown that disorder, induced by radiation with α-particles at —100°C, anneals in less than five minutes at 0°C.

The resistivities of the α-brasses are in agreement with earlier results [10]. The ϱ-T curve for the β-brass is in agreement with those obtained by WEBB [11] for single crystals. Especially we observe, in accordance with WEBB, that the slope of the resistivity curve for the disordered state is greater than that for the totally ordered state, to such an extent that, if ϱdisord is extrapolated linearly to 0° K, we obtain a negative residual resistance. Moreover, WEBB states that this effect decreases on approaching the ideal 50 : 50 composition. The data of STEINWEHR and SCHULZE [12] for a single crystal with 50.9 atomic % Cu seem to extrapolate to a slightly positive residual resistance.

It is well known that the anomaly in the specific heat of β-brass extends 100°C above the transition temperature; this is usually attributed to the presence of short range order. Since the effect of this kind of order on the resistivity is not definitely established ([8] § 6.3) it might be of interest to extend the measurements of resistivity to higher temperatures.

R_H versus T is shown in Fig. 3, while Fig. 4 gives the quantity ϱ/R_H (which in the free electron picture of metals is simply the reciprocal of the mobility of the electrons) versus T. The main features of these curves are:

a) The sign of R_H is normal (negative) in the whole temperature range for both α- and β-brass.
b) In the α-range, R_H is nearly a linear function of T, the slope increasing with increasing Zn-content, especially near the phase boundary. For the specimens near this boundary, R_H is almost proportional to ϱ (Fig. 4).

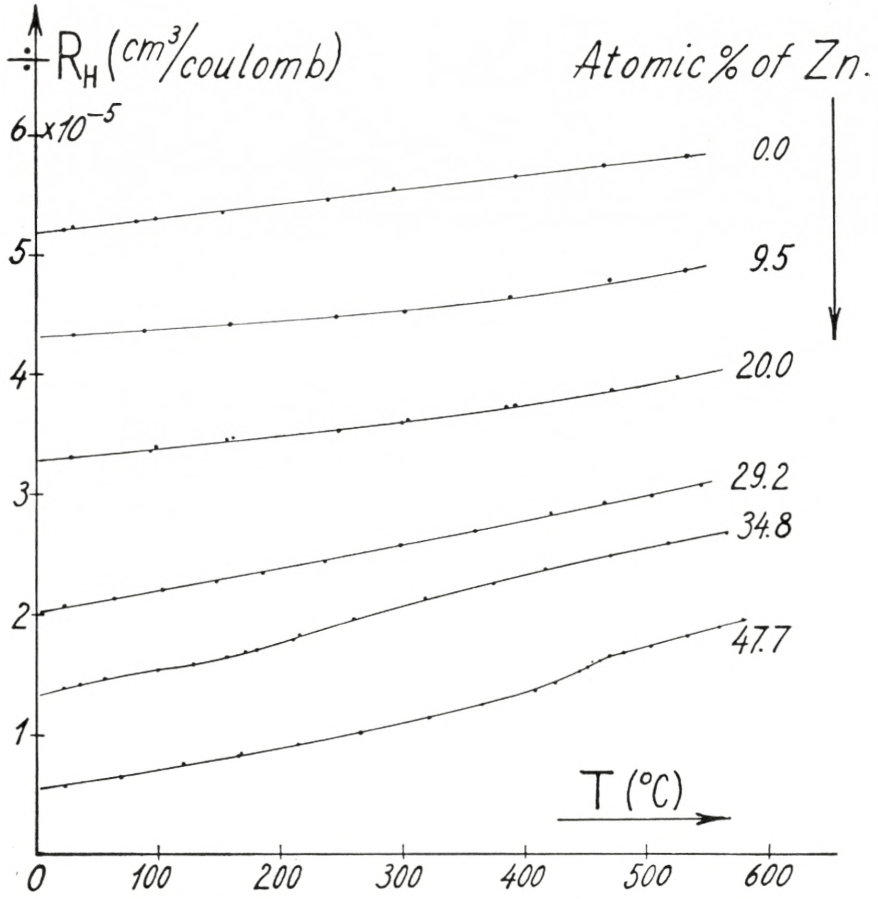

Fig. 3. Hall coefficient versus temperature for α- and β-brass.

c) For β-brass, R_H is also nearly proportional to ϱ, so that the anomaly in R_H is of the same type as that in ϱ. Thus, the sign reversal of R_H observed in Cu_3Au [13] and in Ni_3Mn [14] is not revealed by the order-disorder transition in β-brass. In this connection, we note that the thermoelectric force, as determined by WEBB [11] for β-brass, behaves quite regularly from 0 to 600°C.

d) The room temperature values of R_H for the α-brasses are a few per cent lower than those previously obtained by O. GRAM JEPPESEN [7] from D.C.measurements on the same specimens. The value of R_H for Cu at 20°C is in agreement with newer results ([7], [15]) which center on the value $-(5.25 \pm 0.1)\ 10^{-5}$ cm³ /Coulomb.

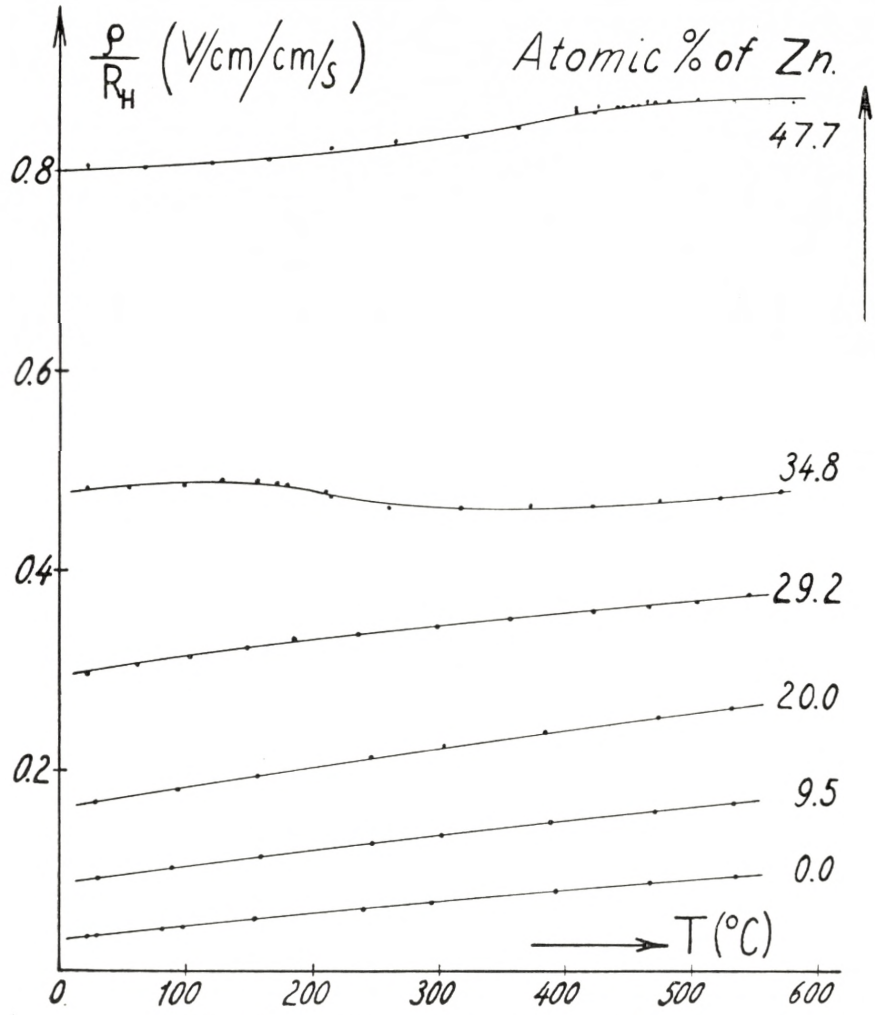

Fig. 4. ϱ/R_H versus temperature for α- and β-brass.

In Fig. 5, R_H is plotted against the content of Zn for $T = 20°\mathrm{C}$ (curve C) and for $T = 600°\mathrm{C}$ (curve B); the values of R_H computed from the Sommerfeld formula (assuming that Cu contributes one and Zn two electrons per atom to the conduction band) have been plotted for comparison (curve A).

Concentrating first upon the low temperature values for the α-brasses, their deviations from the free electron values are easily understood in terms of the deformation of the Fermi surface from spherical symmetry when the Brillouin zone of

the alloys is gradually filled up. It is generally assumed (WILSON pp. 104 ff. [16]) that the instability of the α-phase in alloys like *Cu-Zn* occurs when the Fermi surface due to the filling up of electrons reaches the position corresponding to maximum electron level density. As this Fermi surface will be in contact with the boundaries of the Brillouin zone, it will be strongly deformed. It might therefore be expected that it contributes to the Hall effect an electron-like and a hole-like term which nearly cancel.

The temperature dependence of R_H might be explained by

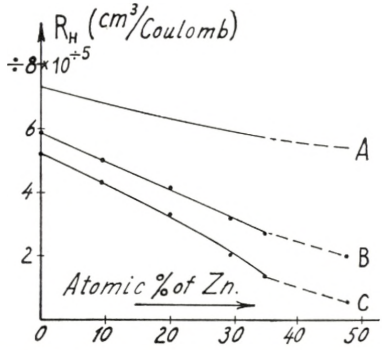

Fig. 5. Hall coefficient versus *Zn* content.
A: calculated according to free electron theory.
B: experimental values for $T = 600°$C.
C: experimental values for $T = 20°$C.

letting the division of the Fermi surface into an electron-like and a hole-like part depend on temperature, but a formal treatment along these lines seems to involve too many arbitrary assumptions to be really significant. Prof. B. L. AVERBACH (private communication) has tentatively suggested that this dependency is due to the thermal smearing of the Fermi surface at elevated temperatures, tending to restore its spherical form and thus reducing the deviation of R_H from the free electron value; this suggestion is supported by the shape of the curves in Fig. 5.

For the disordered state of β-brass, the above remarks on the α-phase may be applied literally, the only difference being that the Brillouin zone of the b.c.c. lattice can hold more electrons per atom than the Brillouin zone of the f.c.c. lattice before the point of maximum level density is reached.

Thus, the rather close agreement between the disordered β-brass and the Zn rich α-brasses does not seem fortuitous; unfortunately the disordered state cannot be quenched, and linear extrapolation to lower temperatures is unsafe, especially because linear extrapolation of the resistivity leads to a negative residual resistivity.

When β-brass is brought into the totally ordered state, i.e. below 200°C, the original Brillouin zone is divided into two equal parts by the formation of interior boundaries (corresponding to the superlattice lines observed in X-ray diffraction). If there is no overlap between the subzones, the energetically lower zone will be full and the higher one will be about half full, as the electron-atom ratio of the β-phase is near $^3/_2$. Thus, we should expect the ordered state to behave like a simple metal, i.e. with R_H close to the free electron value and only slightly temperature dependent, in disagreement with the actual behaviour. If the subzones do overlap to such an extent that both hole and electron conduction occur, a Hall coefficient of small magnitude at low temperatures and with a strong temperature dependence might result, in accordance with experiment.

In the intermediate temperature range from 200°C — 470°C, where the long range order is gradually destroyed, the band structure proposed for the ordered state changes continuously into that of the disordered state; we do not, however, suggest any explanation of the fact that R_H/ϱ is nearly constant during this transition.

The author wants to express his gratitude to Nordisk Kabel- og Traadfabrikker A/S for the preparation of the β-brass, and to Professor T. Bjerge and Professor H. Højgaard Jensen for commenting on the manuscript.

Physics Department,
Technical University of Denmark.

References.

1. F. Kolá̌ček: Ann. Phys. **39**, 1491 (1912).
2. J. Isenberg, B. R. Russell, and R. F. Greene: Rev. Sci. Instr. **79**, 685 (1948).
3. J. Volger: Phys. Rev. **79**, 1023 (1950).
4. V. Frank: Appl. Sci. Res. B, **3**, 129 (1953).
5. W. F. Flanagan, P. A. Flinn, and B. L. Averbach: Rev. Sc. Instr. **35**, 593 (1954).
6. R. F. Wick: Journ. Appl. Phys. **25**, 741 (1954).
7. O. Gram Jeppesen: Nature **173**, 591 (1954).
8. T. Broom: Advances in Physics **3**, no. 9, 26 (1954).
9. R. R. Eggleston and F. E. Bowman: J. Appl. Phys. **24**, 229 (1953).
10. International Critical Tables VI, 172 (1929).
11. W. Webb: Phys. Rev. **55**, 297 (1939).
12. H. v. Steinwehr und A. Schulze: Phys. Zeit. **35**, 385 (1934).
13. A. Komar and S. Sidorov: J. Tech. Phys., U.S.S.R., **11**, 711 (1941).
    — J. Phys., U.S.S.R., **4**, 552 (1941).
14. Simon Foner and Emerson M. Pugh: Phys. Rev., **91**, 220 (A) (1953).
15. Bernard Wiener and Gerhart Groetzinger: Journ. Appl. Phys. **23**, 441 (1952).
16. Wilson: Theory of Metals, Cambridge, 1953.

Indleveret til selskabet den 28. marts 1955.
Færdig fra trykkeriet den 21. september 1955.

Det Kongelige Danske Videnskabernes Selskab

Matematisk-fysiske Meddelelser, bind **30**, nr. 5

Dan. Mat. Fys. Medd. **30**, no. 5 (1955)

DEDICATED TO PROFESSOR NIELS BOHR ON THE OCCASION OF HIS 70TH BIRTHDAY

ON THE POTENTIAL COLLECTIVE FLOW OF A ROTATING NUCLEUS WITH NON-ELLIPSOIDAL BOUNDARY

BY

TORSTEN GUSTAFSON

København 1955

i kommission hos Ejnar Munksgaard

Printed in Denmark
Bianco Lunos Bogtrykkeri A-S

Introduction.

Collective excitation spectra of rotational type are associated with nuclei possessing an equilibrium shape which deviates strongly from spherical symmetry.[1]

The rotational character of the motion is shown by the energy ratios, spins, and intensities, which also give evidence that the nucleus possesses axial symmetry and rotates about axes perpendicular to the symmetry axis.

More detailed information about the collective rotational motion is obtained from the moments of inertia, which can be determined from the observed rotational energy levels. The moments are found to be appreciably smaller than they would be if the nucleus performed a rigid rotation and, in addition, they have a strong dependence on the nuclear deformation. The collective motion of the nucleus has been compared with the hydrodynamical flow, assumed irrotational or potential, of a liquid drop whose boundary is rotating without change of form. The corresponding classical hydrodynamical problem has been studied extensively in connection with the theory of rotating stars (cf. LAMB). An exact solution has been given in the case of a rotating ellipsoid with constant density.[2]

This potential flow for an ellipsoidal boundary has been used by A. BOHR and B. MOTTELSON with a somewhat generalized density distribution such that the surfaces of constant density are similar ellipsoids.

[1] For a survey of the theory of rotational states and of the available experimental evidence, cf. BOHR, 1954; BOHR and MOTTELSON, 1955. Cf. also BOHR, FRÖMAN, and MOTTELSON, 1955; ALAGA, ALDER, BOHR, and MOTTELSON, 1955.

[2] For the rotating ellipsoid, the condition of constant pressure at the surface can be fulfilled, assuming Newtonian attraction, both in the case of irrotational flow and for a flow without internal motion. In the case of a nucleus, the surface condition, of course, has quite another aspect.

For the case of an ellipsoid of revolution of constant density, rotating about an axis perpendicular to its symmetry axis, the moment of inertia is given by

$$\Im = \frac{a^2 e^4}{5\,(2 - e^2)} M, \tag{1}$$

where a is the major semi-axis, e the eccentricity, and M the mass of the nucleus. The nuclear eccentricity may be determined from the quadrupole moment of the nuclear shape

$$Q_0 = \pm \frac{2}{5} a^2 e^2 Z, \tag{2}$$

where Z is the nuclear charge number, and where the positive and negative signs refer to prolate and oblate shape, respectively.

It is found, however, that the moments of inertia, calculated from (1) by means of the observed quadrupole moments, are smaller than the observed moments of inertia by a factor of about three to five. This situation is not appreciably changed by considering the above-mentioned generalized density distribution.

A possible reason for this discrepancy could lie in the assumed density distribution. It has been suggested (Johnson and Teller, 1954) that the protons are more concentrated towards the centre of the nucleus than are the neutrons. Such an effect means a smaller value of "a" in (2) than in (1). This increases the moment of inertia calculated from Q_0. Since, however, the expected differences in "a" are only of the order of 20 %, this effect cannot account for more than a minor part of the discrepancy.

As pointed out by Bohr and Mottelson, another possible way of explaining the discrepancy within the framework of the potential flow model would be to consider nuclear boundaries deviating from the ellipsoidal shape. In order to investigate this point, the potential flow has been calculated for some boundaries of more general form, illustrated in Figs. 1, 2, and 3.

These calculations, reported in the following, show that the moment of inertia as well as the quadrupole moment is quite sensitive to relatively small deviations from ellipsoidal shape, but indicate that the ratio of $\Im/Q^2$, which is the quantity that

can be directly compared with the experimental data, is affected to a much lesser extent.

Our results thus indicate that the model considered cannot be expected to account for the observed magnitude of $\Im/Q_0^2$, and, therefore, suggest significant departures of the collective motion from potential flow.

This conclusion is in accord with the recent findings of BOHR and MOTTELSON (1955) who have investigated the validity of the assumption of potential flow for the nuclear collective motion, and who have shown that important deviations from potential flow are to be expected as a consequence of the nuclear shell structure. The effect is to increase the moment of inertia, and estimates indicate that it is possible in this way to account for the magnitude of the observed moments.

Characteristics of the flow and of the considered nuclei.

Assuming a constant density for the nuclear fluid, the velocity, assumed irrotational, obeys the equations

$$\text{rot } \vec{v} = 0, \quad \text{div } \vec{v} = 0. \tag{3}$$

Introducing $\vec{v} = \text{grad } \Phi$ (for convenience Φ is chosen as the negative of the velocity potential), we get

$$\Delta \Phi = 0. \tag{4}$$

From the rotation, the boundary obtains a velocity whose normal component shall be equal to the normal component of the potential flow. Thus, the boundary condition is time-dependent. A coordinate system fixed in space is denoted by (X, Y, Z), and the rotating system by (xyz). Then the (xyz) depend on (X, Y, Z, t). In the following, Φ and other quantities are expressed in (xyz), and are thus time-dependent.

We first consider the case of an ellipsoid of revolution with axes 2a and 2b, the symmetry axis being 2a. The ellipsoid rotates about an axis perpendicular to its symmetry axis with angular velocity ω. In the body-fixed coordinates, the boundary condition is constant and given by

$$\omega\,(a^2 - b^2)\,xy = \frac{\partial \Phi}{\partial x}\,b^2 x + \frac{\partial \Phi}{\partial y}\,a^2 y, \tag{5}$$

where the axis of rotation is chosen as the z-axis, while the x-axis is the nuclear symmetry axis.

The boundary condition is fulfilled by the potential

$$\Phi = \omega\,\frac{a^2 - b^2}{a^2 + b^2}\,xy. \tag{6}$$

For this flow, one calculates

$$E_{\mathrm{rot}} = \frac{1}{2}\int \varrho\,\vec{v}^2\,d\tau = \frac{1}{2}\,\frac{M\,a^2 e^4}{5\,(2 - e^2)}\,\omega^2, \tag{7}$$

corresponding to the value (1) for the moment of inertia.

In elliptic coordinates, the exact solution for the ellipsoid quoted above has the property of being the first term in an expansion in harmonic functions. There is therefore some advantage in using elliptic coordinates. They are given by (see, e. g., LAMB: Hydrodynamics, p. 139)

$$\left.\begin{aligned} x &= k\,\mu\,\zeta, \\ y &= k\,\sqrt{1 - \mu^2}\cdot\sqrt{\zeta^2 - 1}\,\cos\varphi, \\ z &= k\,\sqrt{1 - \mu^2}\cdot\sqrt{\zeta^2 - 1}\,\sin\varphi. \end{aligned}\right\} \tag{8}$$

For constant $\zeta = \zeta_0$, the curve in μ is an ellipse with $a = k\zeta_0$ and $b = \sqrt{a^2 - k^2}$. Thus, $2\,k$ is the focal distance and $\zeta_0 = e^{-1}$. Constant $\mu = \mu_0$ gives a hyperbola in ζ with $a = k\mu_0$ and $b = \sqrt{k^2 - a^2}$.

We will now seek other boundaries than the ellipsoidal one. This can be done by giving ζ of the boundary as a suitable function of μ. In this note, we will use

$$\zeta = f(\mu) = \zeta_0 + C_0 + C_2\mu^2 + C_4\mu^4. \tag{9}$$

An even function of μ has been chosen in order to describe nuclei with reflection symmetry. For unsymmetric nuclei, the full series in μ would be needed.

For comparison with the ellipsoidal case, two different shapes of the nucleus will be treated, both converging into an ellipsoid for small parameters.

1. The volume and the major axis remain constant.
2. The volume and the quadrupole moment Q_0 remain constant.

First approximation. In the constants C_n, the change of volume is

$$\Delta V = \text{const.} \left[C_0 + \frac{C_2}{3} + \frac{C_4}{5} - e^2 \left(\frac{C_0}{3} + \frac{C_2}{5} + \frac{C_4}{7} \right) \right]. \tag{10}$$

The change of the major axis is

$$\Delta a = k (C_0 + C_2 + C_4). \tag{11}$$

Further,

$$\varepsilon Q_0 = \int d\tau \varrho_e (3 x^2 - r^2), \tag{12}$$

where ε is the total charge.

For ϱ_e constant, we get in first approximation

$$Q_0 = \frac{2}{5} k^2 \left[1 + C_0 \frac{3 e - e^3}{1 - e^2} + C_2 \frac{14 - 5 e^2 - 3 e^4}{7 e (1 - e^2)} + C_4 \frac{36 - 21 e^2 - 5 e^4}{21 e (1 - e^2)} \right]. \tag{13}$$

In the following we will especially illustrate the calculations for the eccentricity $e = {}^4/_5$, which gives a quadrupole moment of the same order as, though somewhat greater than, is common among the rare earth nuclei. This gives the following relations for the C_n in the two cases under consideration.

$$\left.\begin{array}{ll} 1.\ C_0 = -C_2 \cdot 0.1430 & C_4 = -C_2 \cdot 0.8570. \\ 2.\ \overline{C}_0 = -\overline{C}_2 \cdot 0.0863 & \overline{C}_4 = -\overline{C}_2 \cdot 1.267. \end{array}\right\} \tag{14}$$

The coefficients for moderate changes of the surface turn out to be relatively large. In the following we will therefore check the first order approximations of the various physical quantities by numerical calculations for a special surface. We choose case 1 (constant volume and major axis) with $C_2 = 0.4$. To first approximation we get

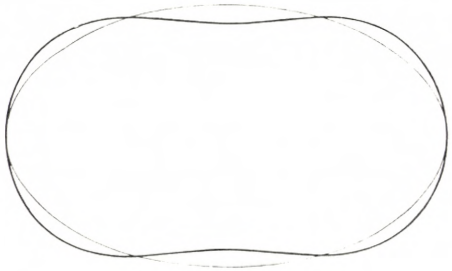

Fig. 1. V and a constant. $C_2 = 0{,}4$

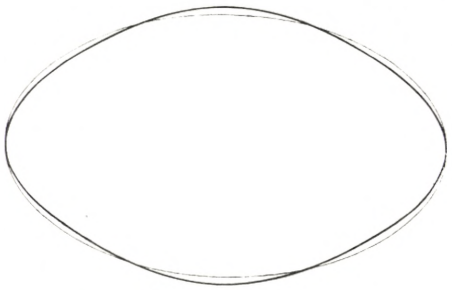

Fig. 2. V and a constant. $C_2 = -0{,}2$

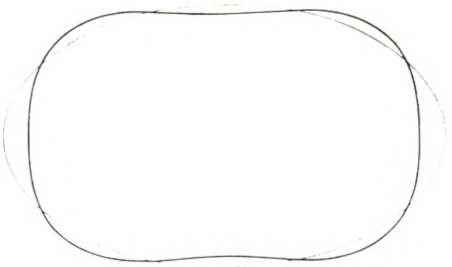

Fig. 3. V and Q_0 constant. $\overline{C}_2 = 0{,}4$

$C_0 = -0.0572$, $C_4 = -0.3428$.

By numerical calculation,

$C_0 = -0.0591$, $C_4 = -0.3409$.

Fig. 1 gives the boundary for these last values. Fig. 2 gives the boundary for $C_2 = -0.2$. Case 2, (constant V and Q_0) with $\overline{C}_2 = 0.4$, is illustrated in Fig. 3.

In case 1 we get the following values of Q_0.

a) First approximation:

$$Q_0 = \frac{2}{5} k^2 [1 + C_2 \cdot 1.091] \quad (15)$$

or for

$$C_2 = 0.4: \; Q_0 = k^2 \cdot 0.5746.$$

b) Numerical calculation

$$Q_0 = k^2 \cdot 0.5780. \quad (16)$$

Calculation of S_0.

It is of some interest to calculate also the 2^4-pole moment of the nuclear shapes considered. This moment may be defined by

$$\varepsilon S_0 = \langle P_4 \rangle = \int d\tau \, \varrho_e (35 \, x^4 - 30 \, x^2 r^2 + 3 \, r^4). \quad (17)$$

For the ellipsoid, this gives

$$S_0^0 = k^4 \cdot 0.6857. \quad (18)$$

In first approximation,

$$S_0 = S_0^0\left[1 + \frac{1}{99\,e^3(1-e^2)}\left\{C_0 \cdot 99\,e^4(3-e^2) + C_2\,11\,(28\,e^2 - 15\,e^4 - 3\,e^6) + C_4\,(88 + 144\,e^2 - 147\,e^4 - 15\,e^6)\right\}\right] \tag{19}$$

Case 1. $$S_0 = S_0^0(1 + C_2 \cdot 0.426) = k^4\ 0.8026. \tag{20}$$

The numerically calculated value is: $S_0 = k^4\ \ 0.8032$.

Case 2. $$S_0 = S_0^0(1 - \overline{C}_2\,1.883) = k^4 \cdot 0.1692. \tag{21}$$

Determination of the flow.

In elliptical coordinates, the potential equation is as follows:

$$\frac{\partial}{\partial\mu}\left[(1-\mu^2)\frac{\partial\Phi}{\partial\mu}\right] + \frac{1}{1-\mu^2}\frac{\partial^2\Phi}{\partial\varphi^2} = \frac{\partial}{\partial\zeta}\left[(1-\zeta^2)\frac{\partial\Phi}{\partial\zeta}\right] + \frac{1}{1-\zeta^2}\frac{\partial^2\Phi}{\partial\varphi^2}. \tag{22}$$

The general solution, free from singularities inside the boundary, is

$$\Phi = \sum_{n,\,s} P_n^s(\mu)\,P_n^s(\zeta)\,[A_{ns}\cos s\,\varphi + B_{ns}\sin s\varphi], \tag{23}$$

where P_n^s is the usual spherical harmonic.

The coefficients A_{ns} and B_{ns} can be obtained from the boundary condition

$$\frac{\partial\Phi}{\partial s_n} = V_n^\omega \tag{24}$$

which expresses the equality on the boundary of the normal velocities of the potential flow and of the rotation ($\zeta = f(\mu)$).

Here,

$$V_n^\omega = \omega k^2 \frac{\sqrt{1-\mu^2}\sqrt{\zeta^2-1}}{B(\mu)}(\mu + \zeta f'(\mu))\cos\varphi \tag{25}$$

with

$$B(\mu) = k\sqrt{\zeta^2-\mu^2}\cdot\sqrt{\zeta^2 - 1 + (1-\mu^2)\,f'(\mu)^2}. \tag{26}$$

Further:

$$\frac{\partial \Phi}{\partial s_n} = \frac{\partial \Phi}{\partial \zeta} \frac{\zeta^2 - 1}{B} - \frac{\partial \Phi}{\partial \mu} \frac{(1-\mu^2) f'(\mu)}{B}. \tag{27}$$

Now, $\frac{\delta \Phi}{\partial s_n} = V_n$ shows that Φ contains the factor $\cos \varphi$.

Thus, $s = 1$; $B_{ns} = 0$.

We get the following expression for Φ:

$$\Phi = \sum_n A_n \sqrt{1 - \mu^2}\, P_n'(\mu) \sqrt{\zeta^2 - 1}\, P_n'(\zeta) \cos \varphi. \tag{28}$$

Before treating the more general case, we give the flow for the ellipsoid treated above, this time in ellipsoidal coordinates.

Then, $f'(\mu) = 0$, and the boundary condition gives

$$\sum_n A_n P_n'(\mu) [\zeta P_n'(\zeta) + (\zeta^2 - 1) P_n''(\zeta)] = \omega k^2 \mu. \tag{29}$$

For constant $\zeta = \zeta_0$ we get: $P_n'(\mu) = \text{const} \cdot \mu$, which means $n = 2$. Thus, for an ellipsoid, the equation is satisfied by the first term in the expansion, with

$$A_2 = \frac{a^2 e^4}{9 (2 - e^2)} \omega. \tag{30}$$

In the more general case, we will try to satisfy the boundary condition by taking into account further terms in the series for Φ. All calculations can be made explicitly. However, the practical difficulties rise rapidly with the number of terms. In the following, only the three first terms of Φ have been used, as they give an accuracy that seems satisfactory in the present case.

The three coefficients A_n in

$$\Phi = \sum_{2,4,6} A_n \Phi_n \tag{31}$$

will be determined by two different methods.

A. The expressions in the boundary condition

$$\frac{\partial \Phi}{\partial s_n} = V_n^{\omega} \tag{32}$$

are developed in power series of μ, and the coefficients for μ, μ^3, and μ^5 are identified. Thus, the condition is best satisfied along the equator of the nuclear drop. The formulae being comparatively long, we only give the results for $e = 4/5$.

$$\left.\begin{aligned} A_2 &= A_2^0(1 - C_0 \cdot 2.354 + C_2 \cdot 1.662 + C_4\, 1.472) \\ A_4 &= -\, C_2 \cdot 0.00369\, \omega k^2 + C_4 \cdot 0.000733\, \omega k^2 \\ A_6 &= -\, C_4 \cdot 1.473 \cdot 10^{-4}\, \omega k^2. \end{aligned}\right\} \quad (33)$$

1. Constant V and a.

$$\left.\begin{aligned} A_2 &= A_2^0 \cdot (1 + C_2 \cdot 0.736) \\ A_4 &= -\, C_2 \cdot 4.314 \cdot 10^{-3}\, \omega k^2 \\ A_6 &= C_2 \cdot 1.26 \cdot 10^{-4}\, \omega k^2. \end{aligned}\right\} \quad (34)$$

2. Constant V and Q.

$$\left.\begin{aligned} A_2 &= A_2^0, \text{ the coefficient for } \overline{C}_2 \text{ being zero.} \\ A_4 &= -\, \overline{C}_2 \cdot 0.00462\, \omega k^2 \\ A_6 &= \overline{C}_2 \cdot 1.87 \cdot 10^{-4}\, \omega k^2. \end{aligned}\right\} \quad (35)$$

B. Since the accuracy of these coefficients is rather important, we compute them, in case 1, with $C_2 = 0.4$ from an integral condition for the flow over the boundary. The quantity $V_n^\omega - \dfrac{\partial \Phi}{\partial s_n}$ represents the flow across the boundary owing to the error in the approximation. Now we try to minimize the square error integral.

Putting

$$\left.\begin{aligned} V_n^\omega \Big/ \sqrt{B(\mu)} &= F(\mu) \cos \varphi \\ \frac{\partial \Phi_m}{\partial s_n} \Big/ \sqrt{B(\mu)} &= \varphi_m(\mu) \cdot \cos \varphi, \end{aligned}\right\} \quad (36)$$

we have the condition

$$W = \pi k \int_0^1 d\mu\, (F(\mu) - \sum A_n \varphi_n(\mu))^2 = \text{minimum}. \quad (37)$$

With usual notations, we get the following system of equations:

$$(F, \varphi_n) = \sum_m A_m (\varphi_m, \varphi_n). \tag{38}$$

The integrals are calculated numerically for $C_2 = 0.4$. We obtain

$$\left.\begin{aligned} A_2 &= 6.908 \cdot 10^{-2} \omega k^2 \\ A_4 &= -1.606 \cdot 10^{-3} \omega k^2 \\ A_6 &= 6.15 \cdot 10^{-5} \omega k^2. \end{aligned}\right\} \tag{39}$$

(For this value of C_2 the numerical coefficients of the first approximation given above are

$6.768 \cdot 10^{-2}$, $-1.726 \cdot 10^{-3}$, $5.04 \cdot 10^{-5}$, respectively).

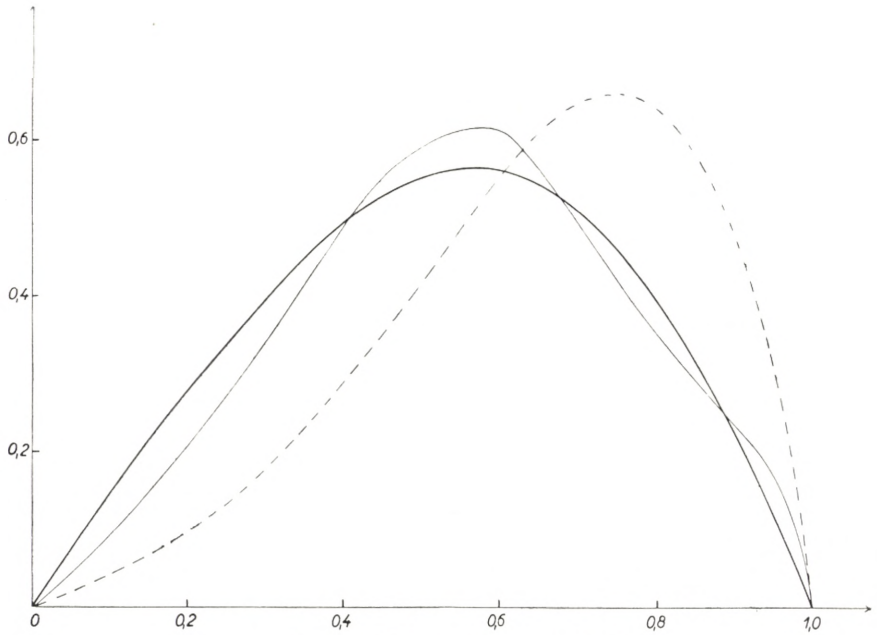

Fig. 4. $F(x)$ solid line thick
$A_2 \psi_2(x)$ dashed line
$\Sigma A_n \psi_n(x)$ solid line thin.

Fig. 4 shows how $F(x) = V_n^{\omega} / B$, where B varies slowly, is approximated by $A_2 \varphi_2 + A_4 \varphi_4 + A_6 \varphi_6$. For comparison, the first term is also inserted, giving the shape of φ_2.

Calculation of E_{rot}.

We use the expressions above for the collective flow to calculate E_{rot}, which is given by the integral over $\frac{1}{2}\,\text{grad}^2\Phi \cdot d\tau$, where $d\tau = k^3 d\mu\, d\zeta\, d\varphi(\zeta^2 - \mu^2)$.

We obtain

$$E_{\text{rot}} = \frac{\pi \varrho k}{2} \int_{-1}^{+1} d\mu \int_{1}^{\zeta} d\zeta\, (G(\zeta, \mu) - G(\mu, \zeta)), \tag{40}$$

where

$$G(\zeta, \mu) = (\zeta^2 - 1)\,[(\sum A_n R_n(\mu)\, P_n'(\zeta))^2 + (\sum A_n P_n'(\mu)\, P_n'(\zeta))^2] \tag{41}$$

with

$$R_n(x) = x P_n'(x) + (x^2 - 1) P_n''(x). \tag{42}$$

First approximation. The terms containing A_4^2, A_6^2, and $A_4 A_6$ can be neglected. In the terms with $A_2 A_4$ and $A_2 A_6$ we can put $\zeta = \zeta_0$. Because of the properties of Legendre functions these integrals are then zero. The only non-zero term is easily calculated.

$$\left.\begin{aligned} E_{\text{rot}} = \frac{81\, M(2 - e^2)}{10\, k^2\, e^2} A_2^2 [1 + \{ C_0(7\, e^5 - 63\, e^3 + 70\, e) + C_2(3\, e^5 \\ - 25\, e^3 + 28\, e) + C_4(5\, e^5 - 49\, e^3 + 54\, e)\, 1/3 \} 1/7 \cdot (2 - e^2)^{-1} \cdot (1 - e^2)^{-1}]. \end{aligned}\right\} \tag{43}$$

We compute E_{rot} for the two cases, V and a constant, V and Q_0 constant.

1. $E_{\text{rot}} = E_{\text{rot}}^0 \cdot (1 + C_2 \cdot 1.827)$.

For $C_2 = 0.4$, the change is $73\,\%$.

This means a rather strong dependence of E_{rot} on the shape of the nucleus.

2. $E_{\text{rot}} = E_{\text{rot}}^0\ (1 - \bar{C}_2 \cdot 0.002)$, which means practically no change of E_{rot} for the change of shape characterized by constant Q_0.

Numerical calculation in case 1 for $C_2 = 0{,}4$.

We will make the calculations for a finite change of the boundary. This, of course, implies long calculations. However, the great change of E_{rot} from the first approximation makes this test desirable.

We write: $E_{\text{rot}} = \sum_{i,j} A_i A_j K_{ij}$, where $(i,j) = (2, 4, 6)$ and the K_{ij} are defined by formulae (40—42).

All calculations can be made explicitly, but the number of terms increases very rapidly for higher indices. Therefore all terms except the first are calculated by an exact integration in ζ and a subsequent numerical integration in μ.

We find the following values:

$$\left.\begin{aligned} E_{\text{rot}} &= \frac{\pi \varrho k}{2}\,(A_2^2 \cdot 37.58 + 2\,A_2 A_4 \cdot 81.4 + A_4^2 \cdot 5985 - 2\,A_2 A_6 \cdot 616 \\ &\quad + 2\,A_4 A_6 \cdot 1.05 \cdot 10^4 + A_6^2 \cdot 3.8 \cdot 10^5) \\ &= \frac{\omega^2 \pi \varrho k^5}{2}\,(0.1793 - 0.0180 + 0.0154 - 0.0052 - 0.0021 + 0.0014) \\ &= \frac{\omega^2 \pi \varrho k^5}{2}\,0.1708. \end{aligned}\right\} \quad (44)$$

Comparing with the first approximation, which gave

$$E_{\text{rot}} = E_{\text{rot}}^0 \cdot 1.73, \quad (45)$$

we find here

$$E_{\text{rot}} = E_{\text{rot}}^0 \cdot 1.93 \quad (46)$$

which shows that the first approximation is qualitatively correct, even if the corrections to the flow are larger than to the static moments.

Comparison of Q_0 and $\Im$.

As mentioned in the Introduction, the quantity which provides the most direct test of the potential flow model is the ratio between Q_0^2 and the moment of inertia $\Im$, obtained from E_{rot}.

Case 1.

First approximation.

$$Q_0^2/\Im = (Q_0^2/\Im)_0 \cdot (1 + C_2 \cdot 0.355). \tag{47}$$

The change would go in the direction indicated by the experiments for negative C_2, illustrated by Fig. 2. However, in any case the change is small.

Finite deviation.

$$\frac{Q_0^2}{\Im} = \left(\frac{Q_0^2}{\Im}\right)_0 \cdot 1.08. \tag{48}$$

This should be compared with the value 1.14 of the first approximation.

Case 2.

For constant V and Q_0 the change in E_{rot} is insignificant.

The calculations show that, for comparatively moderate changes of shape of the nucleus, the quantities $\Im$, Q_0, and S_0 are changed appreciably. The value of $Q_0^2/\Im$, on the contrary, is rather insensitive to such changes in shape which have been considered in these calculations.

On this occasion, I should like to express my deep gratitude to Professor NIELS BOHR for his great interest in my work and enlightening discussions during my many stays in Copenhagen. Further, I want to thank Drs. AAGE BOHR and BEN MOTTELSON for valuable suggestions and for their kind communication of investigations prior to publication. I also thank KERSTIN KJÄLLQUIST, F. M., and ROLF BENGTSSON, F. K., for their helpful aid in carrying through the calculations.

The Institutes of Theoretical Physics
in Lund and Copenhagen.

References.

G. Alaga, K. Alder, A. Bohr, and B. R. Mottelson: Dan. Mat. Fys. Medd. **29,** no. 9 (1955).

A. Bohr: Dan. Mat. Fys. Medd. **26,** no. 14 (1952).

A. Bohr: Dissertation, Copenhagen (1954).

A. Bohr and B. R. Mottelson: Dan. Mat. Fys. Medd. **27,** no. 16 (1953).

A. Bohr and B. R. Mottelson: Dan. Mat. Fys. Medd. **30,** no. 1 (1955).

A. Bohr, P. O. Fröman, and B. R. Mottelson: Dan. Mat. Fys. Medd. **29,** no. 10 (1955).

M. H. Johnson and E. Teller: Phys. Rev. **93,** 357 (1954).

H. Lamb, Hydrodynamics, (1932).

Indleveret til selskabet den 9. juni 1955.
Færdig fra trykkeriet den 3. Oktober 1955.

Det Kongelige Danske Videnskabernes Selskab
Matematisk-fysiske Meddelelser, bind **30,** nr. 6

Dan. Mat. Fys. Medd. **30,** no. 6 (1955)

DEDICATED TO PROFESSOR NIELS BOHR ON THE OCCASION OF HIS 70TH BIRTHDAY

A POLARIMETRIC METHOD FOR THICKNESS CONTROL IN THE PRODUCTION OF INTERFERENCE FILTERS

BY

ALFRED HERMANSEN

København 1955
i kommission hos Ejnar Munksgaard

CONTENTS

Printed in Denmark
Bianco Lunos Bogtrykkeri A-S

Introduction.

In a previous paper [*A*] a general theory for interference filters (with two, three, or four reflective systems of layers) has been developed and numerical calculations of $I(\lambda)$, $R(\lambda)$ (i. e. the intensity distribution in transmitted and reflected light) have been carried out in the special case for the reflective systems consisting of silver layers.

The present paper will deal with the problem of measuring the thickness of the different thin layers during the evaporation process.

In a following paper the apparatus used for producing interference filters of a large area (22 × 22 cm) will be described and experimental results for some filters of different type will be given.

The Different Methods of Thickness Control.

In order to make interference filters of different type with optimum properties and with transmission bands at a specified wavelength it is very important to be able to control the thicknesses of the different thin layers during evaporation, especially the dielectric layers.

The thickness of a silver layer (or another absorbent layer) can be determined with sufficient accuracy by measuring the intensity of light *transmitted* through one or more test plates by means of a photocell. The thickness of the silver layers should only be determined with an accuracy better than about 4 per cent. Measurement of the thickness of a dielectric layer deposited on a glass plate or on a silver layer is much more difficult and should for interference filters be determined with an accuracy better than 0.5 per cent.

In 1949 GREENLAND and BILLINGTON [1] indicated an ingenious method for controlling the thickness of the dielectric layer L_{2m} by production of a Fabry-Perot filter $M L_{2m} M$.

By cementing a prism on to the back of the filter blank total reflection is obtained at the lower boundary of the dielectric layer, and the silver-dielectric layers in this way act as a reflection interference filter at oblique incidence (fig. 1, page 5). As we have $R = 1$ at the bottom of the filter, the condition $\sigma \boldsymbol{R} = 1$ ([*A*] 3,22) is nearly satisfied for the *s*-component and a sharp minimum ("absorption line") will appear in a spectroscope. The position of this minimum is determined by the thickness of the dielectric layer. The relation between $\lambda_m^{(s)}$ and $\lambda_m^{(o)}$ (the position of the transmission band at normal incidence) can either be determined experimentally (as done by GREENLAND [1]) or it can, in principle, be calculated by means of a procedure analogous to [*A*] pages 39—42.

This spectroscopic method of control is independent of optical properties or coatings on the "windows" in the vacuum chamber and can be used in the case of a glass bell jar. The measurement of the optical thickness *nd* by this method will depend upon n, as will be shown below.

DUFOUR [2] has controlled the thickness of dielectric layers by intensity measurements of monochromatic light *reflected* from test plates at normal incidence. This method, which has been improved by JACQUINOT and GIACOMO [3], has especially been used in the making of all-dielectric interference filters ([*A*] § 7). At least two test plates are used, one for the low- and the other for the high-index material (see p. 36). This method depends upon coatings on the "windows", but in theory the measurement of *nd* is independent of n.

To make filters of a large area the filter blank has to be rotated during evaporation, but rotation makes it necessary to place test plates far away from the filter blank, and hence it is of importance to find methods which avoid test plates, so that all the thickness measurements of the dielectric layers are carried out on the filter blank itself.

Such a method of control, which has proved valuable, consists in polarimetric measurements of the phase difference

$\Delta = \delta_p - \delta_s$ $\left(\text{and } tg\ \psi = \frac{\varrho_p}{\varrho_s}\right)$ in *reflected* monochromatic light at an oblique angle of incidence (e. g. 75°) [4]. This method of control is particularly well suited for production of filters with two, three, or four silver layers (treated in [*A*] § 3—5); but it can

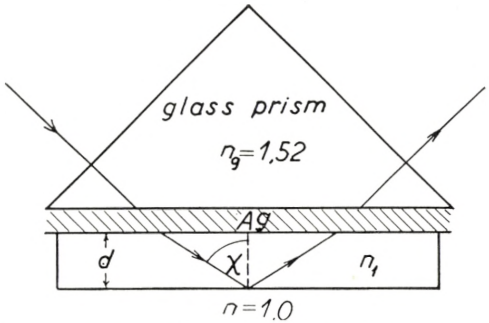

Fig. 1. GREENLAND's method of thickness control.
The silver-dielectric layers act as a reflection interference filter and the narrow absorption band is observed in a spectroscope during evaporation.

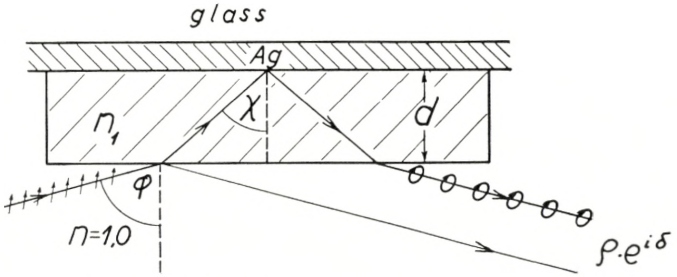

Fig. 2. Polarimetric method of thickness control.
Plane-polarized light (with azimuth about 45°) is reflected from the filter layers and the light (which is elliptically polarized after reflection) is analyzed during evaporation.

also be used for control of all-dielectric filters and for thickness control of reflection interference filters of the HADLEY-DENNISON type.

This method requires two plane windows placed in oblique tubes in the vacuum chamber perpendicularly to the pencil of rays. The method is independent of coatings on the windows, but on the other hand the windows must not be birefringent. Similar to GREENLAND's method the measurement of nd is also here dependent upon n.

Already DRUDE [5] developed formulae which enabled him, from measurements of Δ (and ψ) at oblique incidence, to determine the thickness of very thin dielectric layers (less than 50 Å) on a metal surface. Many years later VAŠIČEK [6] used the same method to determine n and d of thin dielectric layers on a glass base. ROTHEN [7] and ROTHEN and HANSON [8] have used the same method for measurement of dielectric layers as thick as 1—8 λ deposited on a polished steel surface. From their calculations it appeared that the same method could be adapted to control of the thickness of the dielectric layer L_{2m} by production of FABRY-PEROT interference filters $M\,L_{2m}M$. This assumption has been confirmed in recent years in practice in this laboratory [4] and [9].

§ 1. Theory of the Polarimetric Method for Thickness Control.

(Calculation of Δ and ψ)

The problem is:

The FRESNEL factor $r_m = \varrho_m \cdot e^{i\delta_m}$ for a system of m thin layers bounded to vacuum (or air) (fig. 3) is known. To this system is added one more layer consisting of material $m+1$

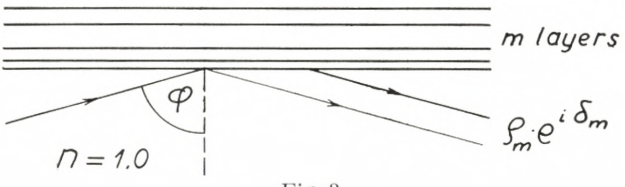

Fig. 3.

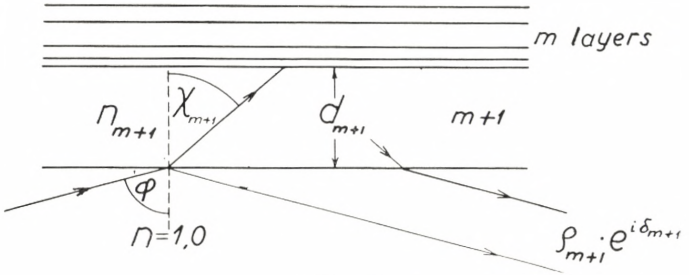

Fig. 4.

(fig. 4), and then $r_{m+1} = \varrho_{m+1} \cdot e^{i\delta_{m+1}}$ for the new system has to be determined.

When r'_{m+1} is the FRESNEL coefficient ([A] 1, 2—3) at the boundary between vacuum and material $m+1$ (fig. 5), the FRESNEL factor $r''_m = \varrho''_m \cdot e^{i\delta''_m}$ in reflection from the system of m

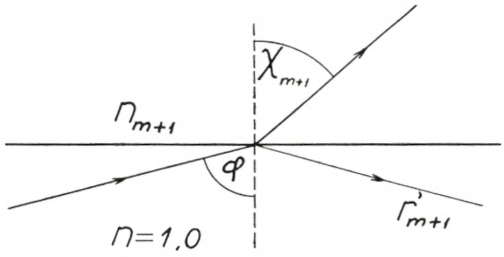

Fig. 5.

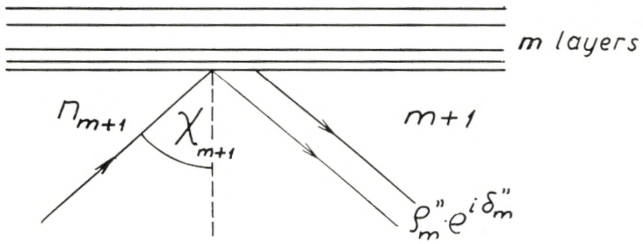

Fig. 6.

layers with material $m+1$ in front (infinite thickness) (fig. 6) is determined from ([A] 2, 7) when $x_m = 0$ is introduced. We obtain

$$r''_m = \varrho''_m \cdot e^{i\delta''_m} = \frac{-r'_{m+1} + \varrho_m \cdot e^{i\delta_m}}{1 - r'_{m+1} \cdot \varrho_m \cdot e^{i\delta_m}}, \qquad (1, 1)$$

and again from ([A] 2, 7) we finally get:

$$r_{m+1} = \varrho_{m+1} \cdot e^{i\delta_{m+1}} = \frac{r'_{m+1} + \varrho''_m \cdot e^{i\delta''_m - ix_{m+1}}}{1 + r'_{m+1} \cdot \varrho''_m \cdot e^{i\delta''_m - ix_{m+1}}} \qquad (1, 2)$$

with

$$x_{m+1} = \frac{360}{\lambda_0} \cdot 2\, d_{m+1} \cdot n_{m+1} \cdot \cos \chi_{m+1} \qquad (1, 3)$$

for the system of $m+1$ layers bounded to vacuum (or air) (fig. 4). λ_0 is the wavelength of the incident plane-polarized light,

which after reflection from the system of thin layers becomes elliptically polarized.

s and p components should be treated separately. The layer $m+1$ added may be absorbent or not; if absorbent also r'_{m+1} and x_{m+1} will be complex numbers. The layer $m+1$ may also be birefringent, in this case $x^{(s)}_{m+1}$ is different from $x^{(p)}_{m+1}$.

The calculation of the observable quantities $\Delta = \delta_p - \delta_s$ and ψ $\left(\operatorname{tg}\psi = \frac{\varrho_p}{\varrho_s}\right)$ can in all cases be carried out *direct from the recurrence formulae* (1, 1—3) *by means of* RYBNER's *tables* [10], when the Fresnel coefficients ([*A*] §1) have first been calculated. If the layer $m+1$ is absorbent (e. g. a silver layer) this procedure will be most convenient. However, if the layer $m+1$ is *not absorbent* (i. e. a dielectric layer) other procedures may be followed.

In this case (1, 1—2) can be written:

$$\varrho''^2_m = 1 - \frac{(1 - r'^2_{m+1})\cdot(1 - \varrho^2_m)}{1 + (r'_{m+1}\cdot\varrho_m)^2 - 2\cdot r'_{m+1}\cdot\varrho_m\cdot\cos\delta_m} \qquad (1,\ 4)$$

$$\varrho^2_{m+1} = 1 - \frac{(1 - r'^2_{m+1})\cdot(1 - \varrho''^2_m)}{1 + (r'_{m+1}\cdot\varrho''_m)^2 + 2\,r'_{m+1}\cdot\varrho''_m\cdot\cos(\delta''_m - x_{m+1})} \qquad (1,\ 5)$$

$$\operatorname{tg}\delta''_m = \frac{\varrho_m\cdot(1 - r'^2_{m+1})\cdot\sin\delta_m}{-r'_{m+1}\cdot(1+\varrho^2_m) + \varrho_m\cdot(1 + r'^2_{m+1})\cdot\cos\delta_m} \qquad (1,\ 6)$$

$$\operatorname{tg}\delta_{m+1} = \frac{\varrho''_m\cdot(1 - r'^2_{m+1})\cdot\sin(\delta''_m - x_{m+1})}{r'_{m+1}\cdot(1+\varrho''^2_m) + \varrho''_m\cdot(1 + r'^2_{m+1})\cdot\cos(\delta''_m - x_{m+1})}, \qquad (1,\ 7)$$

and the derivative $\dfrac{\partial(\delta_{m+1})}{\partial(x_{m+1})}$ can in this case be expressed by

$$-\frac{\partial(\delta_{m+1})}{\partial(x_{m+1})} = \left.\begin{array}{l} \\ \dfrac{\varrho''_m\cdot(1 - r'^2_{m+1})\cdot(\varrho''_m(1 + r'^2_{m+1}) + r'_{m+1}\cdot(1+\varrho''^2_m)\cdot\cos(\delta''_m - x_{m+1}))}{(r'_{m+1}\cdot(1+\varrho''^2_m) + \varrho''_m\cdot(1+r^2_{m+1})\cdot\cos(\delta''_m - x_{m+1}))^2} \cdot \\ \qquad + (\varrho''_m\cdot(1 - r'^2_{m+1})\cdot\sin(\delta''_m - x_{m+1}))^2 \end{array}\right\} \qquad (1,\ 8)$$

Another method to calculate Δ (and ψ) as a function of nd when $m+1$ is a dielectric layer, consists in inversion of complex

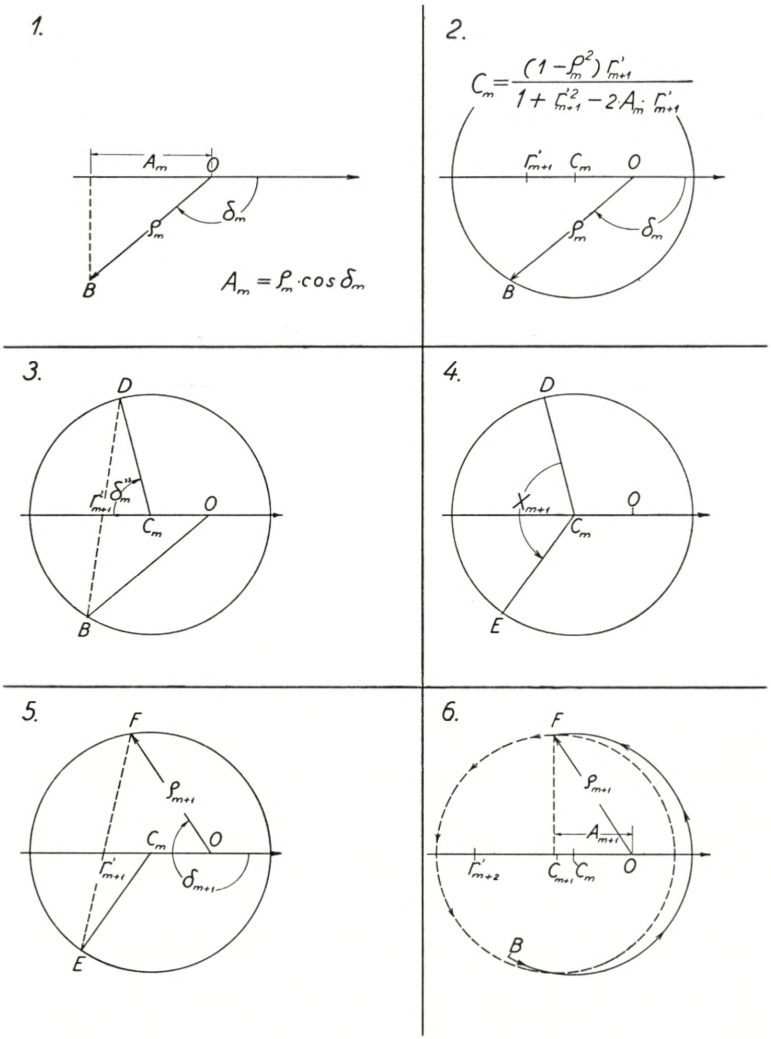

Fig. 7.

1. The complex number (ϱ_m, δ_m) is plotted (point B, clockwise return).
2. The centre $C_m = \dfrac{r'_{m+1}(1-\varrho_m^2)}{1 + r'^2_{m+1} - 2\, r'_{m+1} \cdot \varrho_m \cdot \cos \delta_m}$ is calculated, and a circle is drawn through B with C_m as centre.
3. The point B is inverted to point D (with $(r'_{m+1}, 0)$ as inversion centre).
4. The angle x_{m+1} is plotted (counterclockwise return).
5. The point E is inverted to point F, which is equal to $(\varrho_{m+1}, \delta_{m+1})$.
6. If to the system is added a new dielectric layer $m + 2$ with another index of refraction n_{m+2}, a new centre C_{m+1} is calculated, a new circle is drawn through F (broken line), and the procedure is repeated.

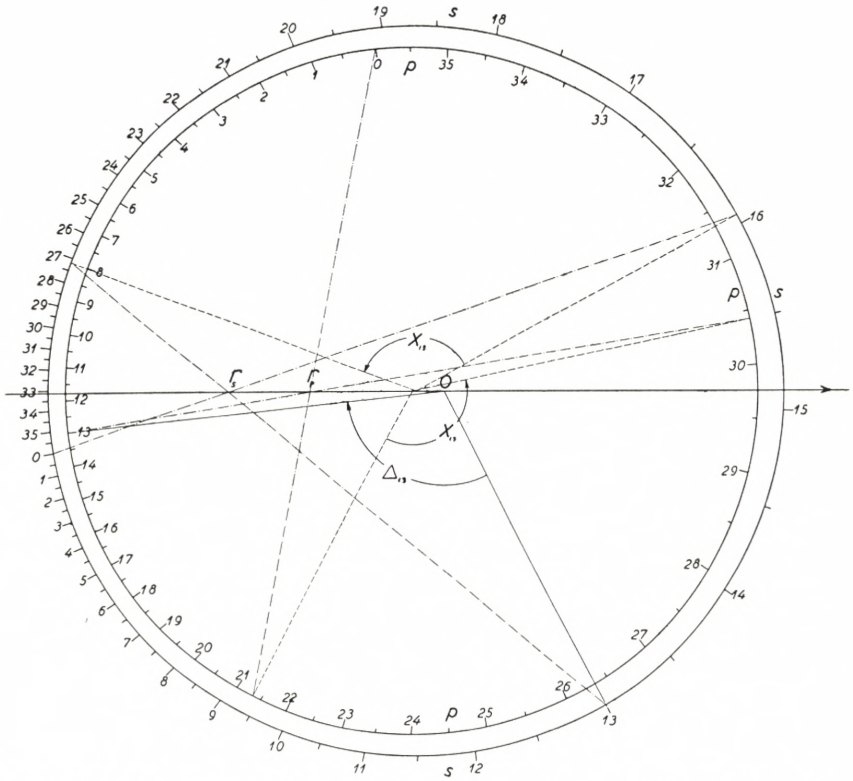

Fig. 8. Graphical calculation of a (Δ, x) curve for a fluoride layer with index of refraction $n = 1.29$ deposited upon a silver layer with $\nu - i\varkappa = 0.1 - i\,3.5$ and thickness $t = 350$ Å. The numbers on the s and the p circles correspond to the same values of x with ten degrees' interval (e. g. 13 corresponds to $x = 130°$). The corresponding (Δ, nd) curve is shown in fig. 28 *p.* 31, unbroken line. In the same way also $\frac{\varrho_p}{\varrho_s} = \operatorname{tg}\psi$ can be derived from fig. 8. Angle of incidence $\varphi = 75°$.

numbers. The different steps in this graphical method (which enable us direct to determine $(\varrho_{m+1}, \delta_{m+1})$ from (ϱ_m, δ_m)) are shown in fig. 7 (1—6). The procedure employed in fig. 7 is a modification of a method indicated by COTTON [11].

In fig. 8 is shown the graphical procedure in the calculation of a (Δ, x) curve for a fluoride layer with a silver layer at the bottom. When a polar coordinathograph for plotting complex numbers (ϱ, δ) is used in the graphical method, the deviations in Δ from the exactly calculated values will be less than $\frac{1°}{3}$, which will be sufficiently accurate in the case of $\varphi = 75°$.

All the (Δ, nd) curves shown in the following figures have been calculated by means of this convenient graphical method. (Δ_0, ψ_0) for the bottom silver layers are calculated direct from (1, 1—2) by means of RYBNER's tables [10].

§ 2. The Accuracy and General Trend of the Polarimetric Method.

In fig. 9 is shown (Δ, nd) curves corresponding to a fluoride layer with $n = 1.28$ (quickly evaporated MgF_2) deposited upon

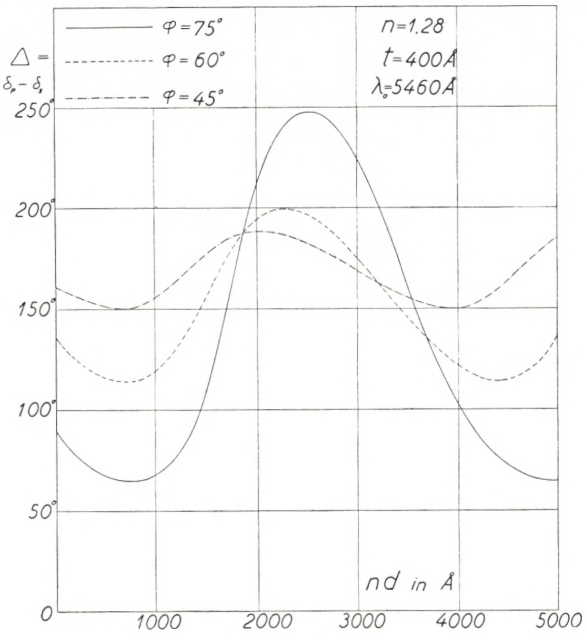

Fig. 9.

a silver layer with $t = 400$ Å. The three curves correspond to different angles of incidence $\varphi = 45°$, $60°$ and $75°$.

Δ is a periodic function of x with 360° as the period or as a function of nd with the period $\frac{\lambda_0}{2 \cos \chi}$, where λ_0 is the wavelength of the polarimeter light and no birefringence is assumed.

The steepness $\frac{\partial \Delta}{\partial (nd)}$ af the curves increases rapidly with increasing angle of incidence.

If n changes its value during evaporation from n to $n + \Delta n$, this gives rise to an uncertainty in the determination of nd and thus also to a change in the position of the transmission band λ_1 for the filter we wish to make. If the evaporation of the dielectric material is stopped at a value of Δ corresponding closely to one whole period ($\Delta \simeq \Delta_0$), the uncertainty in nd can be determined from the derivative of

$$nd = \frac{\lambda_0}{2\sqrt{1 - \frac{\sin^2 \varphi}{n^2}}}.$$

We get

$$\Delta(nd) = \frac{\lambda_0 \cdot \sin^2 \chi}{2\, n \cdot \cos^3 \chi} \cdot \Delta n, \qquad (2,\ 1)$$

and as one whole period on the (Δ, nd) curve corresponds to an interference filter of the second order, the uncertainty $\Delta \lambda_1$, in the position of the transmission band λ_1, will have the same value as $\Delta(nd)$. In Table 1 $\Delta \lambda_1$ is calculated correspondingly to $\lambda_0 =$ 5460 Å when n decreases to $n - 0.01$ during the total period of evaporation. The corresponding uncertainty of GREENLAND's method of control is added in the table. If a change in birefringence $n_p - n_s$ takes place during evaporation, this will give an additional uncertainty for the polarimetric method in contrast to GREENLAND's method, where only the s component is used. In column 4 $\frac{\partial(\Delta)}{\partial(nd)}$ is given for the steep part of the curves in the neighbourhood of $x = 360°$ measured in degrees per Ångström and in column 5,

TABLE 1. ($\Delta\lambda_1$ corresponds to $\Delta n = 0.01$).

	$\cos \chi$ ($n = 1.28$)	$\Delta\lambda_1$ ($n = 1.28$)	$\frac{\partial \Delta}{\partial (nd)}$ ($n = 1.28$)	$\Delta\lambda_1$ ($n = 2.36$)
Greenland's method:	0.54500	92.6 Å		3.4 Å
Polarimetric method:				
$\varphi = 75°$	0.65615	43.3 —	0.090 degree / Å	2.6 —
60°	0.73637	24.6 —	0.045 —	2.0 —
45°	0.83356	11.3 —	0.022 —	1.2 —

$\Delta\,\lambda_1$ is calculated for a high-index layer $n = 2.36$ (ZnS). $\Delta\,n = 0.01$ will in this case give a negligible change in λ_1.

In what follows $\varphi = 75°$ is employed; however, when a photoelectric method is used, $\varphi = 60°$ would give sufficient accuracy.

In fig. 10 (Δ, nd) curves are shown for different values of n, all calculated for $\varphi = 75°$ and with the same silver layer as

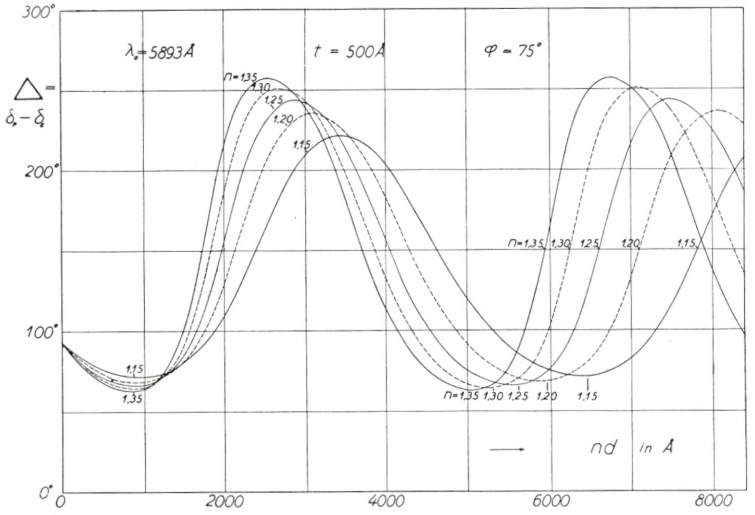

Fig. 10.

"bottom" layer. Fig. 10 shows that even if a dielectric material was available with n as low as 1.15, the polarimetric method of thickness control would give sufficient accuracy. From fig. 10 we are further able to calculate the uncertainty of nd caused by a change in n for all values of nd.

Fig. 10 shows that as n increases $\Delta_{\min}$ will decrease and $\Delta_{\max}$ increase. $\Delta_{\max} - \Delta_{\min}$ (which can be determined during evaporation and which, as calculations show, is independent of small changes in (Δ_0, ψ_0) for the silver layer) determine n of the dielectric layer. If desired, the values of $\Delta_{\max}$ and $\Delta_{\min}$ can be exactly calculated by means of (1, 8) ($n_s d$ is determined in such a way that $\dfrac{\partial(\delta_s)}{\partial(n_s d)} - \dfrac{\partial(\delta_p)}{\partial(n_s d)} = 0$). In Table 2 a few calculations of this type are added. $\varphi = 75°$ $\nu - i\varkappa = 0.1 - i\,3.6$ and $t = 400$ Å for the silver layer.

TABLE 2.

n	Δ_{min}	Δ_{max}	$\Delta_{max} - \Delta_{min}$
1.25	65°.71	243°.28	177°.57
1.30	63.97	250.76	186.79
1.35	62.60	256.61	194.01
1.40	61.46	261.27	199.81

(no birefringence is assumed)

TABLE 3. $\varphi = 75°$.

n	$\cos \chi$	$-r_s$	$-r_p$	
1.15	0.54269	0.41371	0.29161	
...				
1.20	.59336	.46682	.31283	
1.21	.60227	.47584	.31570	
1.22	.61086	.48446	.31846	
1.23	.61910	.49266	.32082	
1.24	.62706	.50052	.32291	
1.25	.63472	.50805	.32476	
1.26	.64211	.51526	.32637	
1.27	.64924	.52218	.32777	
1.28	.65615	.52886	.32899	
1.29	.66282	.53527	.33003	
1.30	.66927	.54145	.33089	
1.31	.67551	.54741	.33164	
1.32	.68155	.55317	.33221	
1.33	.68742	.55874	.33266	
1.34	.69310	.56412	.33299	
1.35	.69861	.56932	.33320	
1.36	.70396	.57438	.33331	
1.37	.70915	.57928	.33332	
1.38	.71420	.58403	.33325	
1.39	.71910	.58864	.33307	
1.40	.72386	.59312	.33281	
1.518	.77132	.63788	.32514	(glass)
2.36	.91240	.78540	.19799	(ZnS)

In Table 3 (r_s, r_p) are calculated for $\varphi = 75°$ and different values of n (from ([A] 1, 1—3)).

For values of nd, where Δ is near a minimum or a maximum, it would be impossible to determine nd with sufficient accuracy.

However, the wavelength λ_0 of the polarimeter light can be changed which alters the position of minimum and maximum on the (Δ, nd) curve, and in this way all values of nd can be controlled with sufficient accuracy on a steep part of a (Δ, nd) curve. (Figs. 27—28, p. 31).

Before the detailed procedure is given which enables us to calculate a (Δ, nd) curve which best fits to the experimental results, it should be emphasized that nd for filters $M\,L_{2m}M$ of the second (or higher orders) ($m \geqslant 2$) can be determined in the simplest manner when the wavelength λ_0 for the polarimeter light is chosen in such a way that x is near 360°, i. e. $\lambda_0 = 2\,dn \cdot \cos\chi$ (or $\lambda_0 = dn \cdot \cos\chi$) (for $\varphi = 75°$ $\lambda_2 = 5050$ Å corresponds to $\lambda_0 = 5461$ Å).

In this case the nd determination will be independent of Δ_0 (the value of Δ when the evaporation of the dielectric layer is started), and without any knowledge of the theory the polarimetric method of control can be used empirically also for compound filters with three or four silver layers (and two or three dielectric layers) and even with a glass bell jar (free from strains) as vacuum chamber.

λ_0 can be altered in practice by means of interference filters in connection with a tungsten band-lamp.

As a (Δ, nd) curve with a silver layer as bottom layer only shows a small dependence upon t (for $t > 350$ Å), an empirical (Δ, nd) curve can be determined and also filters of the first order controlled.

However, theoretical calculations of (Δ, nd) curves or (Δ, λ_m) curves, which best fit the experimental results, will be of great value for determining the physical properties of evaporated thin films and for more complicated filters, such as $M\,L'H_2L'M$, or at all-dielectric filters empirical determination of the (Δ, nd) curve would be much too complicated.

This procedure is more complicated, as previously assumed, because of the following important experimental facts:

1. $\varkappa$ for a silver layer of thickness $t \simeq 400$—500 Å is different from $\varkappa$ for an opaque silver layer.

TABLE 4. $\Delta = \delta_p - \delta_s$.

$\varkappa$ \ v	0.0	0.1	0.2
2.0	63.28	63.29	63.33
2.1	65.34	65.35	65.40
2.2	67.37	67.39	67.43
2.3	69.37	69.38	69.44
2.4	71.33	71.35	71.40
2.5	73.26	73.28	73.33
2.6	75.15	75.17	75.23
2.7	77.00	77.02	77.08
2.8	78.82	78.84	78.89
2.9	80.59	80.61	80.67
3.0	82.33	82.34	82.40
3.1	84.02	84.04	84.10
3.2	85.68	85.70	85.76
3.3	87.29	87.31	87.37
3.4	88.87	88.89	88.95
3.5	90.41	90.43	90.49
3.6	91.91	91.93	91.99
3.7	93.38	93.40	93.45
3.8	94.81	94.83	94.88
3.9	96.20	96.22	96.27
4.0	97.56	97.58	97.63
4.1	98.89	98.90	98.95
4.2	100.18	100.19	100.24
4.3	101.44	101.45	101.50
4.4	102.66	102.68	102.73
4.5	103.86	103.88	103.92
4.6	105.03	105.04	105.09
4.7	106.17	106.18	106.22
4.8	107.28	107.29	107.33
4.9	108.36	108.37	108.41
5.0	109.41	109.42	109.46

TABLE 5. $\operatorname{tg}\psi = \varrho_p/\varrho_s$.

$\varkappa$ \ v	0.1	0.2
2.0	0.9644	0.9301
2.1	.9649	.9310
2.2	.9654	.9320
2.3	.9660	.9331
2.4	.9666	.9343
2.5	.9672	.9355
2.6	.9679	.9367
2.7	.9685	.9380
2.8	.9692	.9393
2.9	.9698	.9406
3.0	.9705	.9419
3.1	.9712	.9432
3.2	.9718	.9445
3.3	.9725	.9458
3.4	.9732	.9471
3.5	.9738	.9483
3.6	.9744	.9495
3.7	.9751	.9507
3.8	.9757	.9519
3.9	.9763	.9531
4.0	.9768	.9543
4.1	.9774	.9554
4.2	.9780	.9565
4.3	.9786	.9576
4.4	.9791	.9586
4.5	.9796	.9596
4.6	.9801	.9606
4.7	.9806	.9616
4.8	.9811	.9625
4.9	.9815	.9634
5.0	.9820	.9643

2. $n^{(v)}$ (n measured in the vacuum container) for a low index layer is different from $n^{(A)}$ (n measured in air) when the material is quickly evaporated. (For MgF_2 we have $n^{(v)} = 1.28$ and $n^{(A)} = 1.365$).

3. A fluoride layer quickly evaporated shows a small birefringence

$$n_p^{(v)} > n_s^{(v)} \quad (\text{for } MgF_2 \quad n_p - n_s \simeq 0.005).$$

For ZnS and other high index layers we have $n^{(v)} = n^{(A)}$.

TABLE 6. ϱ_s.

$\varkappa$ \ ν	0.1	0.2
2.0	0.99073	0.98160
2.1	.99135	.98283
2.2	.99193	.98396
2.3	.99245	.98499
2.4	.99293	.98594
2.5	.99337	.98681
2.6	.99377	.98761
2.7	.99414	.98835
2.8	.99448	.98903
2.9	.99480	.98965
3.0	.99509	.99022
3.1	.99535	.99075
3.2	.99560	.99124
3.3	.99583	.99170
3.4	.99605	.99212
3.5	.99624	.99251
3.6	.99642	.99288
3.7	.99659	.99322
3.8	.99675	.99354
3.9	.99691	.99383
4.0	.99705	.99411
4.1	.99718	.99436
4.2	.99730	.99461
4.3	.99741	.99484
4.4	.99752	.99505
4.5	.99762	.99525
4.6	.99773	.99545
4.7	.99780	.99563
4.8	.99789	.99579
4.9	.99797	.99595
5.0	.99805	.99611

TABLE 7. $180 - \delta_s$ ($\varphi = 75°$).

$\varkappa$ \ ν	0.0	0.1	0.2
2.0	13.29	13.27	13.22
2.1	12.78	12.76	12.71
2.2	12.30	12.28	12.23
2.3	11.85	11.83	11.79
2.4	11.43	11.41	11.37
2.5	11.03	11.02	10.98
2.6	10.66	10.65	10.62
2.7	10.31	10.30	10.27
2.8	9.99	9.98	9.95
2.9	9.68	9.67	9.64
3.0	9.39	9.38	9.36
3.1	9.12	9.11	9.08
3.2	8.86	8.85	8.83
3.3	8.61	8.60	8.58
3.4	8.38	8.37	8.35
3.5	8.16	8.15	8.13
3.6	7.94	7.94	7.92
3.7	7.74	7.74	7.72
3.8	7.55	7.55	7.54
3.9	7.37	7.37	7.36
4.0	7.20	7.19	7.18
4.1	7.03	7.03	7.02
4.2	6.87	6.87	6.86
4.3	7.72	6.72	6.71
4.4	6.58	6.57	6.56
4.5	6.44	6.43	6.43
4.6	6.30	6.30	6.29
4.7	6.17	6.17	6.16
4.8	6.05	6.05	6.04
4.9	5.93	5.93	5.92
5.0	5.82	5.82	5.81

§ 3. Determination of (ϱ_s, δ_s) for a Silver Layer.

To be able to calculate a (Δ, nd) curve it is necessary to know not only (Δ_0, ψ_0) $\left(\Delta_0 = \delta_p - \delta_s;\ \operatorname{tg}\psi_0 = \frac{\varrho_p}{\varrho_s}\right)$, but also (ϱ_s, δ_s) for the silver layer first evaporated.

The first step will be to calculate tables of $\left(\Delta, \frac{\varrho_p}{\varrho_s}\right)$ and (ϱ_s, δ_s)

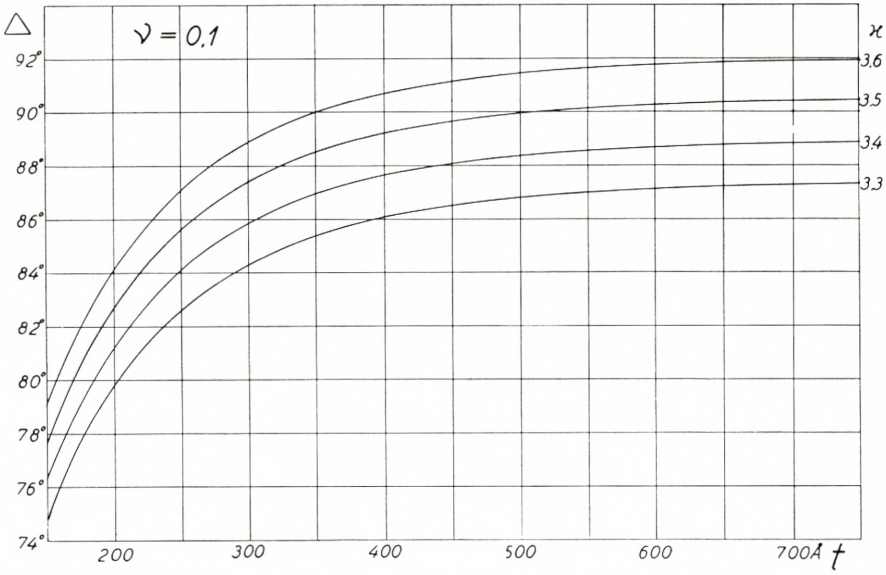
Δ
ν = 0,1
92°
90°
88°
86°
84°
82°
80°
78°
76°
74°
200
300
400
500
600
700Å
t
x
3,6
3,5
3,4
3,3

Fig. 11.

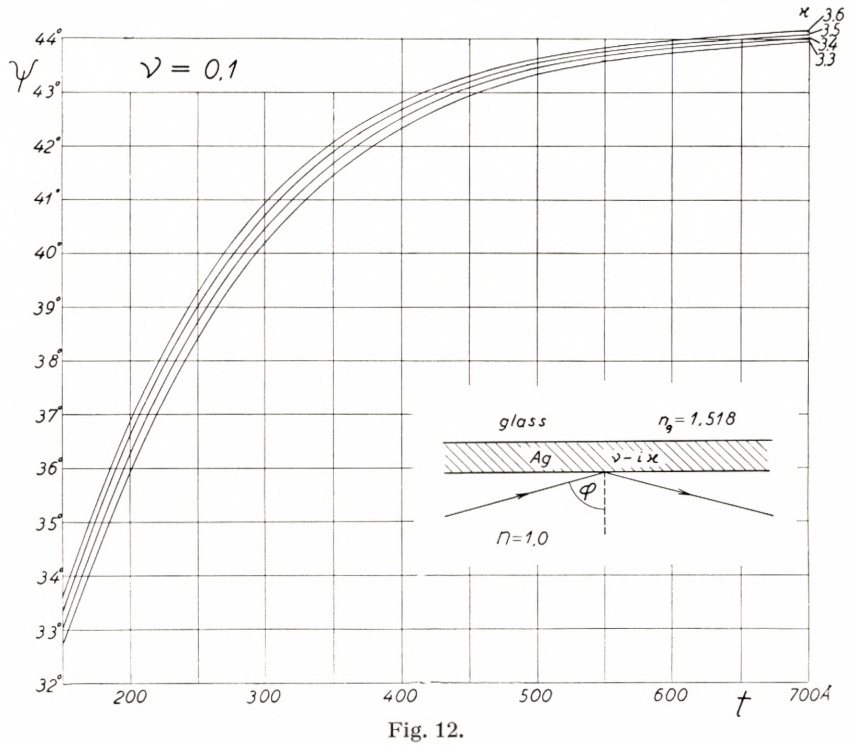
Ψ
ν = 0,1
44°
43°
42°
41°
40°
39°
38°
37°
36°
35°
34°
33°
32°
200
300
400
500
600
700Å
t
x
3,6
3,5
3,4
3,3
glass
$n_g = 1,518$
Ag
ν - i x
φ
n=1,0

Fig. 12.

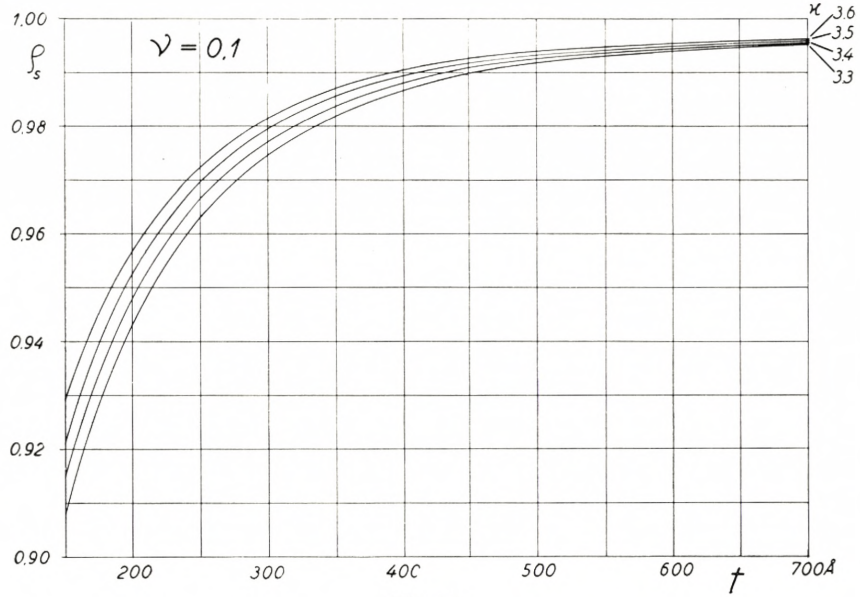
1,00
ρ_s
0,98
0,96
0,94
0,92
0,90
$\nu = 0,1$
$\varkappa$
3,6
3,5
3,4
3,3
200
300
400
500
600
700Å
t

Fig. 13.

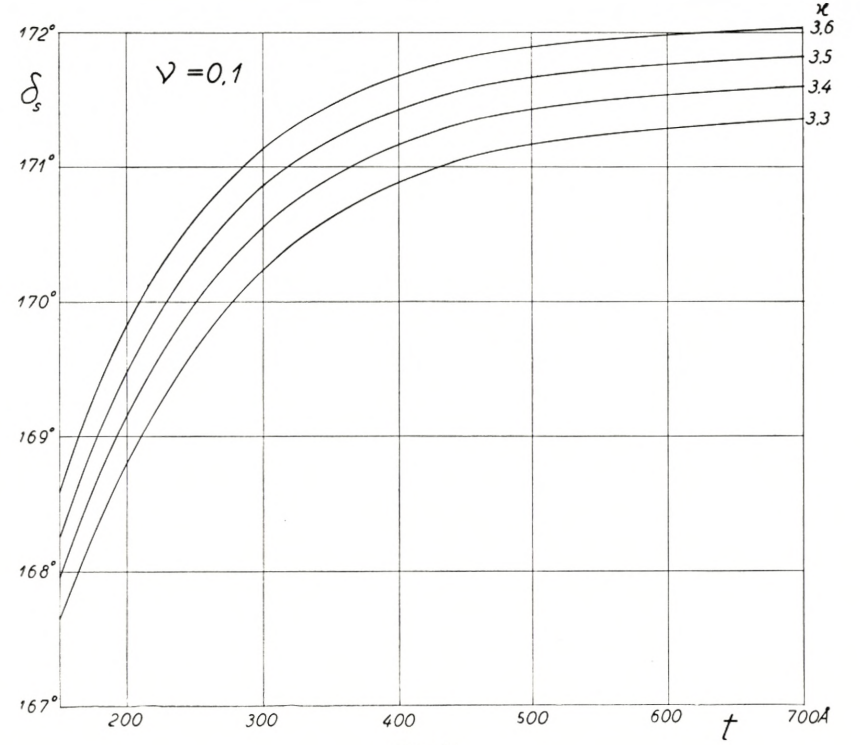
172°
δ_s
171°
170°
169°
168°
167°
$\nu = 0,1$
$\varkappa$
3,6
3,5
3,4
3,3
200
300
400
500
600
700Å
t

Fig. 14.

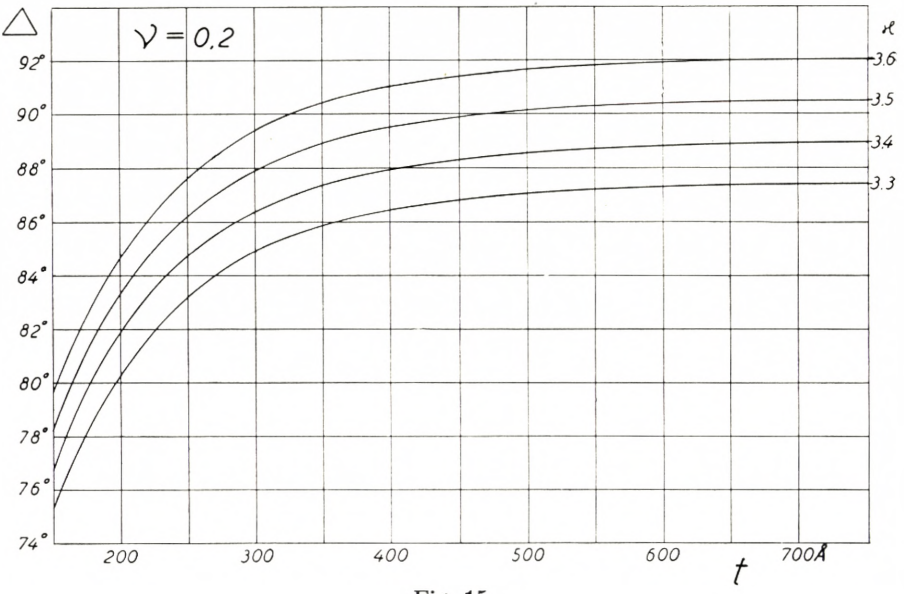
Δ
ν = 0,2
92°
90°
88°
86°
84°
82°
80°
78°
76°
74°
200
300
400
500
600
700Å
t
κ
3.6
3.5
3.4
3.3

Fig. 15.

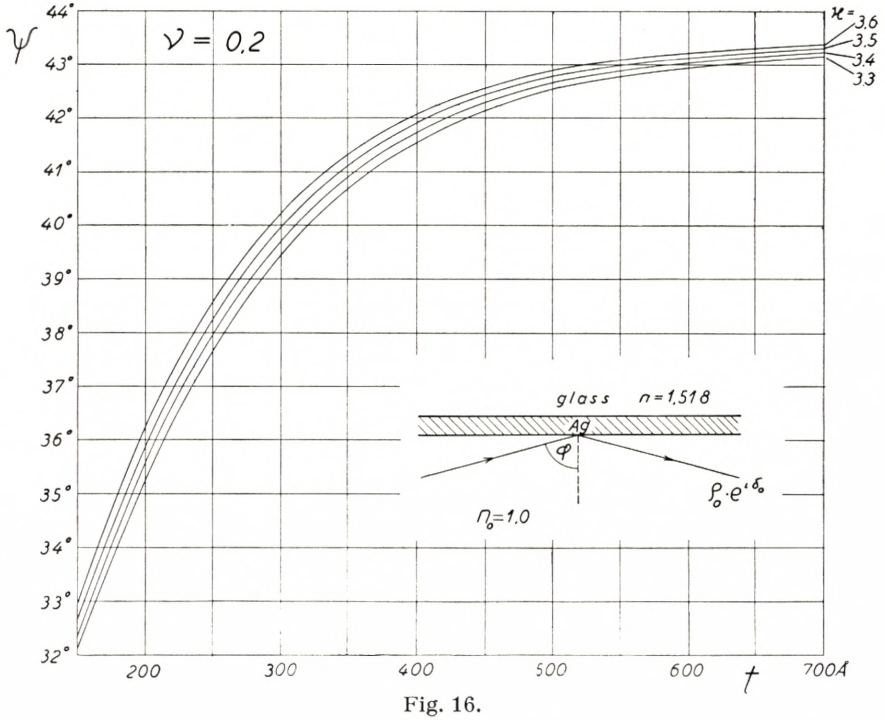
ψ
ν = 0,2
44°
43°
42°
41°
40°
39°
38°
37°
36°
35°
34°
33°
32°
200
300
400
500
600
700Å
t
κ =
3.6
3.5
3.4
3.3
glass n=1,518
Ag
φ
$\rho_0 \cdot e^{i\delta_0}$
n_0=1.0

Fig. 16.

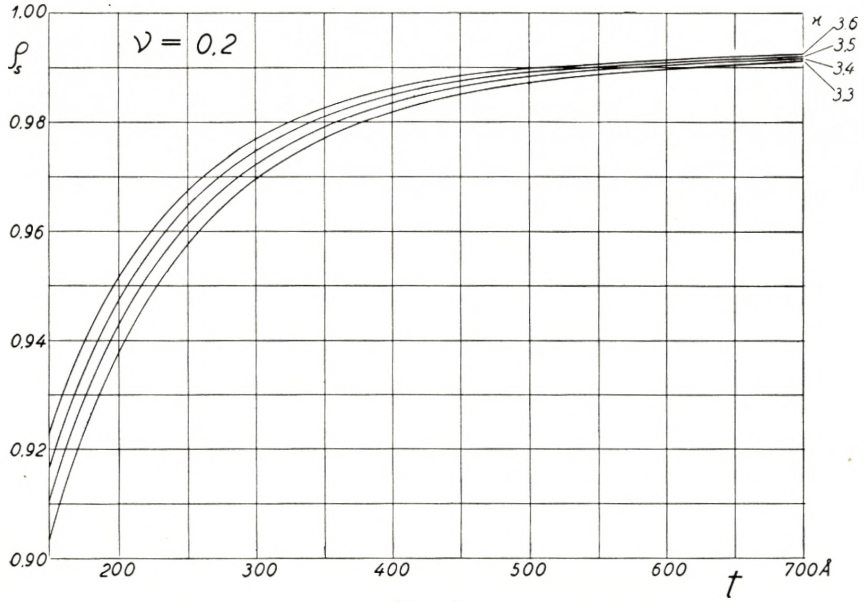
1.00
ρ_s
$\nu = 0.2$
0.98
0.96
0.94
0.92
0.90
200
300
400
500
600
700Å
t
x
3.6
3.5
3.4
3.3

Fig. 17.

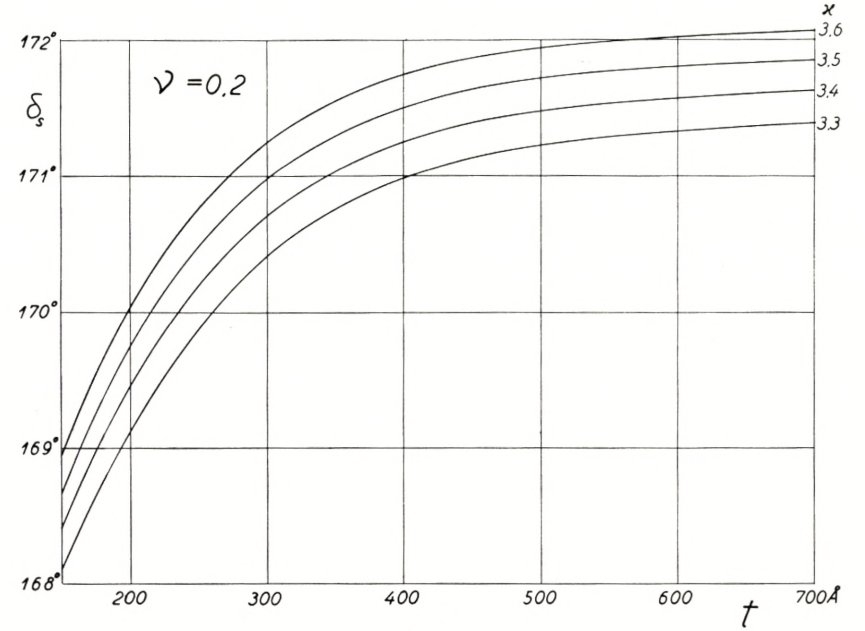
172°
δ_s
$\nu = 0.2$
171°
170°
169°
168°
200
300
400
500
600
700Å
t
x
3.6
3.5
3.4
3.3

Fig. 18.

for an opaque silver layer at $\varphi = 75^\circ$ as a function of $\nu - i\varkappa$. The results of such calculations (carried out by means of ([A] 1, 12—13) are given in Tables 4—7.

The next step will be to calculate the same quantities for different thicknesses t of a silver layer and also for different values of $\nu - i\varkappa$ by means of (1, 1—3). This has been done only for values of $\varkappa$ in the neighbourhood of $\lambda_0 = 5461$ Å, the results being shown in the figs. 11—14 for $\nu = 0.1$ and in the figs. 15—18 for $\nu = 0.2$.

Now the most obvious method would be first to determine $\nu - i\varkappa$ by means of Tables 4—5 from measurements of (Δ_0, ψ_0) for an opaque silver layer. However, experiments show that when the thickness t of a silver layer is increased, Δ reaches a maximum for some definite thickness $t_0 \simeq 450$ Å and then decreases, which according to fig. 11 and fig. 15 means that $\varkappa$ reaches a maximum for $t < t_0$.

As only two observable quantities (Δ_0, ψ_0) are available, we may assume a definite value for ν; when this is done, $\varkappa$ and t can be determined from figs. 11—12 and figs. 15—16. (As a first approximation ν determined for an opaque silver layer can be used). When $\varkappa$ and t are determined for the silver layer, (ϱ_s, δ_s) can be determined from figs. 13—14 and figs. 17—18. It should be emphasized that (ϱ_s, δ_s) in contrast to (ϱ_p, δ_p) only shows a small dependence upon ν and $\varkappa$.

As an example of the above procedure the following experimental results should be given in Table 8.

The measurements are carried out just after evaporation of the layer. The thickness of a silver layer is controlled by transmission measurements at test plates (placed perpendicularly above the evaporation source for silver). A silver layer of thickness $t' = 200$—250 Å is evaporated in one step (only one test plate used) but a silver layer of thickness $t'' = 400$—500 Å is evaporated in two or three steps (two or three test plates are used placed in position in succession). In this way a definite value of $\frac{t''}{t'}$ can be obtained (by means of a photocell). When the current from the photocell is the same for the test plates, we should in theory have $t_2 = 2\,t_1$; $t_3 = 3\,t_1$, etc. in Table 8.

From the measurements it seems as if ν is near 0.1; however,

not until measurements of I_{max} and W_2 for the finished filter have been made, (after the filter has been removed from the vacuum chamber) is it possible to determine ν.

$\varkappa$ depends upon the speed of evaporation, but seems to be independent of the pressure when this is below 10^{-4} mm *Hg*.

TABLE 8. (The transmission through each of the test plates is the same).

Testplate no.	Δ	ψ	$\nu = 0.1$				$\nu = 0.2$			
			t	$\varkappa$	ϱ_s	δ_s	t	$\varkappa$	ϱ_s	δ_s
1	82°80	37°1	210 Å	3.46	0.955	169.54	236 Å	3.32	0.954	169.74
2	90.53	42.5	380	3.60	0.989	171.60	423	3.55	0.987	171.70
3	90.40	43.6	504	3.53	0.993	171.74				
4	90.00	44.0	650	3.48	0.995	171.75				
5	88.74	—		3.40						
6	87.80	—		3.33						
7	87.10	—		3.29						
8	86.40	—		3.24						

For a wavelength λ_0' near 5461 Å figs. 11—18 can still be used if the t-scales are transformed to $t' = t \cdot \frac{\lambda_0'}{5461}$.

§ 4. Determination of n_s and n_p.

When a FABRY-PEROT filter of higher order (e. g. $M\,L_{10}M$) is produced, Δ_{min} and Δ_{max} for several periods of the Δ curve can be measured during evaporation.

Experiments for cryolite and MgF_2 both quickly evaporated now show that small deviations from periodicity are present. We have $\Delta_{min_1} > \Delta_{min_2} > \Delta_{min_3} \ldots$ and $\Delta_{max_1} > \Delta_{max_2} > \Delta_{max_3} \ldots$, which indicates that the evaporated layer is birefringent and that $n_p > n_s$. The film acts as a uniaxial crystal with its optic axis normal to the film. When n_0 is the ordinary and n_e the extraordinary index we have according to BORN [12] or BILLINGS [13]:

$$n_0 = n_s \qquad (4,\ 1)$$

and

$$n_e = \frac{n_p \cdot \sin \chi_p}{\sqrt{1 - \left(\frac{n_p}{n_s}\right)^2 \cos^2 \chi_p}}. \qquad (4,\ 2)$$

(χ_p is determined by $n_p \sin \chi_p = \sin \varphi$).

When birefringence is present, (δ_p, $n_s d$) and (δ_s, $n_s d$) curves must first be constructed separately, and next $\Delta\,(n_s d)$ can be calculated from these curves.

This procedure is illustrated in fig. 19 calculated for $n_s = 1.28$ and $n_p = 1.29$. By means of the p-scale (of $n_s d$) above and the s-scale (of $n_s d$) below in fig. 19 the corresponding (Δ, $n_s d$) curve is constructed in fig. 20 (for $n_s d < 8000$ Å unbroken line and for 8000 Å $< n_s d < 16000$ Å broken line).

As r_p only varies slowly with n (Table 3), fig. 19 can still be used for another value of $n_p = n_p'$ if the p scale (above) is transformed to

$$(n_s d)' = n_s d \cdot \frac{n_p' \cdot \cos \chi_p'}{n_p \cdot \cos \chi_p}. \qquad (4,\ 3)$$

For MgF_2 we have $n_p - n_s \simeq 0.005$. ($n_e - n_0 \simeq 0.009$).

From measurements of $\Delta_{\min_1}$, $\Delta_{\min_2}$ ... and $\Delta_{\max_1}$, $\Delta_{\max_2}$ ... during evaporation it should be possible to determine $n_s^{(v)}$ and $n_p^{(v)}$ (v means measured in vacuum), and from these values and from $\left(\Delta_0, \frac{\varrho_p}{\varrho_s}\right)$ and (ϱ_s,δ_s) for the silver layer the (Δ, $n_s d$) curve can be constructed.

As mentioned above, a great change in n for MgF_2 takes place when air (and H_2O) is admitted to the vacuum chamber and this change in n from $n^{(v)}$ ($= n_s^{(v)}$) to $n^{(A)}$ must be taken into account when we desire to make an interference filter with transmission band at $\lambda_m^{(A)}$ (at normal incidence).

We have ([A] 3, 8)

$$m \cdot \lambda_m^{(A)} = 2\, d n^{(A)} + Z\,(\lambda_m^{(A)},\ n^{(A)}). \qquad (4,\ 4)$$

($Z\,(\lambda_m^{(A)},\ n^{(A)})$ can be determined by means of ([A] fig. 8)), and the evaporation has to be stopped at a value of Δ corresponding to

$$n_s^{(v)} d = \frac{n_s^{(v)}}{2\, n^{(A)}} \cdot (m \cdot \lambda_m^{(A)} - Z\,(\lambda_m^{(A)},\ n^{(A)})). \qquad (4,\ 5)$$

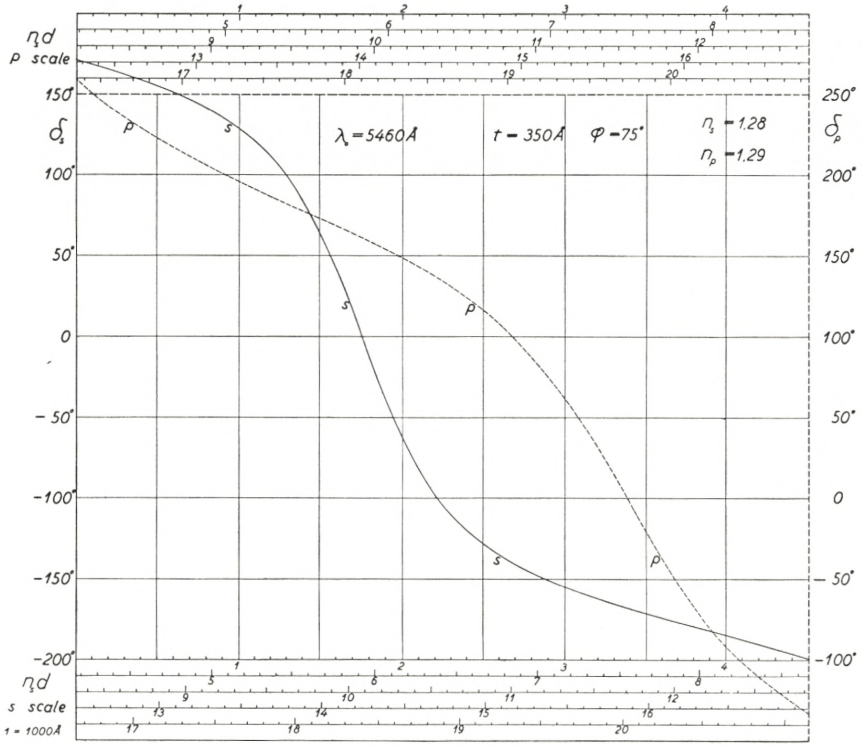
$\eta_1 d$
p scale
δ_s
δ_p
$\lambda_0 = 5460\,Å$
$t = 350\,Å$
$\varphi = 75°$
$n_1 = 1.28$
$n_2 = 1.29$
p
s
150°
100°
50°
0
− 50°
−100°
−150°
−200°
250°
200°
150°
100°
50°
0
− 50°
−100°
$\eta_1 d$
s scale
1 = 1000 Å

Fig. 19.

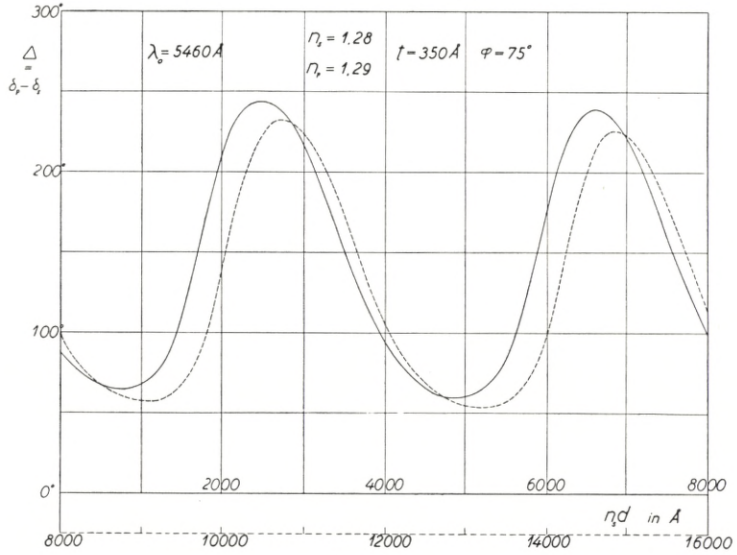
$\Delta = \delta_p - \delta_s$
$\lambda_0 = 5460\,Å$
$n_1 = 1.28$
$n_2 = 1.29$
$t = 350\,Å$
$\varphi = 75°$
300°
200°
100°
0°
2000
4000
6000
8000
8000
10000
12000
14000
16000
$\eta_1 d$ in Å

Fig. 20.

With the apparatus now in use $\lambda_m^{(v)}$ can be measured with a spectroscope (at normal incidence) before air (and H_2O) is admitted to the vacuum chamber.

We have

$$m\lambda_m^{(v)} = 2\, n_s^{(v)} \cdot d + Z(\lambda_m^{(v)},\ n_s^{(v)}). \qquad (4,\ 6)$$

$Z(\lambda_m^{(v)},\ n_s^{(v)})$ can approximately be calculated from ([A] fig. 8) when the λ-scale is transformed. If $\varkappa(\lambda)$ has the value adapted in [A], the observed value of $\lambda_m^{(v)}$ should be equal to the value calculated from (4, 6).

From the observed values of $\lambda_m^{(v)}$ and $\lambda_m^{(A)}$ it is possible to determine $n^{(A)}$ from (4, 4) and (4, 6). As $Z^{(v)} \simeq Z^{(A)}$, we approximately obtain:

$$\lambda_m^{(A)} - \lambda_m^{(v)} = \frac{n^{(A)} - n_s^{(v)}}{n^{(A)}} \left(\lambda_m^{(A)} - \frac{Z(\lambda_m^{(A)},\ n^{(A)})}{m} \right), \qquad (4,\ 7)$$

i. e. the shift in wavelength of the transmission band towards red is proportional to the wavelength especially for filters of higher orders m. For MgF_2 we have very nearly $n^{(v)} = 1.28$ and a shift of $\lambda_2^{(A)} - \lambda_2^{(v)} = 400$ Å is observed when $\lambda_2^{(A)} = 6560$ Å. From (4, 7) we then get $n^{(A)} = 1.365$.

Especially for filters of smaller area (5×5 cm) a cover glass is cemented upon the thin filter layers for protection. The cement most commonly used is a balsam or better a plastic dissolved in xylene or toluene. If porosities are present in the fluoride layer, the cement will fill the pores and a further shift from $\lambda_m^{(A)}$ to $\lambda_m^{(C)}$ towards the red will result. For cryolite quickly evaporated this shift turns out to be as great as $\lambda_2^{(C)} - \lambda_2^{(A)} \simeq 350$ Å ($\lambda_2^{(A)} = 6560$ Å), but here $\lambda_2^{(A)} - \lambda_2^{(v)} = 100$ Å only; however, these shifts are rather unpredictable. For MgF_2 the shift $\lambda_2^{(C)} - \lambda_2^{(A)}$ is only 50—150 Å, but unfortunately this shift seems to be more dependent upon the conditions of evaporation than $n^{(v)}$ and $\lambda_m^{(A)} - \lambda_m^{(v)}$ do. So far experiments seem to show that $n^{(v)}$ is only slightly dependent upon pressure, when this is lower than 10^{-4} mm *Hg*, but is dependent upon the temperature of the crucible ("molybdenum boat"). The higher the temperature the higher $n^{(v)}$ (or the higher $n_p^{(v)} - n_s^{(v)}$) becomes and $\lambda_m^{(C)} - \lambda_m^{(A)}$ becomes smaller, but $\lambda_m^{(A)} - \lambda_m^{(v)}$ will be nearly the same. Recent investigations seem to indicate that this dependence upon the temperature

of the crucible is partly due to impurities in the MgF_2 used and all the above properties, which are so important when making interference filters, require much more experimental investigation with uncontaminated MgF_2 powder.

An alternative determination of $n^{(A)}$ or $(n_s^{(A)}, n_p^{(A)})$ can according to ([A] p. 39—45) be made from observation of $(\lambda_m^{(s)}, \lambda_m^{(p)})$ at an oblique angle of incidence.

In fig. 21 and fig. 22 $(\delta_p, n_s d)$ and $(\delta_s, n_s d)$ curves are shown which are calculated for $n_s = 1.28$, $n_p = 1.285$ and $\lambda_0 = 5460$ Å $(\nu - i\varkappa = 0.1 - i\,3.5)$. The solid curves correspond to $t = 500$ Å and the dotted curves to $t = 200$ Å for the basic silver layer.

Fig. 23 and fig. 24 show the ratios between the s and p circles employed at the construction of figs. 21—22.

Figs. 25—26 are quite analogous to figs. 21—22, but calculated for $\lambda_0 = 7400$ Å $(\nu - i\varkappa = 0.1 - i\,5.0)$. When a red-infrared sensitive photocell is used as reciever in the polarimeter, the application of λ_0 for this spectral region has many advantages because of the optimum conditions for silver layers in this region.

Small changes in the constants from n_s, n_p, λ_0 to n_s', n_p', λ_0' can be compensated for in the figs. 21—22 and 25—26 by transforming the $n_s d$ scales to $(n_s d)' = n_s d \cdot \dfrac{n_p' \cdot \lambda_0 \cdot \cos \chi_p'}{n_p \cdot \lambda_0' \cdot \cos \chi_p}$ (p component) and analogous for the s component.

In fig. 27 the $(\Delta, n_s d)$ curves are constructed from figs. 21—22 (solid curve) and from figs. 25—26 (dotted curve) in the case of $t = 500$ Å $\lambda_m^{(A)}$ and $\lambda_m^{(v)}$ scales calculated from (4, 4—6) and ([A] fig. 8) are added. However, it should be emphasized that fig. 27 may only be regarded as a first approximation. Experiments with uncontaminated MgF_2 powder will be continued for a more accurate determination of n_p and n_s.

From fig. 27 it is apparent that all thicknesses nd up to 6000 Å can be controlled with great accuracy (better than 10 Å), when the conditions of the evaporation process are constant).

In fig. 28 two (Δ, nd) curves have been constructed for $n_p = n_s = 1.29$. $\lambda_0 = 5460$ Å for the solid line curve $(\nu - i\varkappa = 0.1 - i\,3.5)$ and $\lambda_0 = 6560$ Å for the dotted line curve $(\nu - i\varkappa = 0.1 - i\,4.3)$ and $t = 350$ Å for both curves. For a filter of the second order we obtain for a definite $n_s d$, a value of Δ (for $\lambda_0 = 5460$ Å) in fig. 28 which is near the value for Δ we obtain from fig. 27,

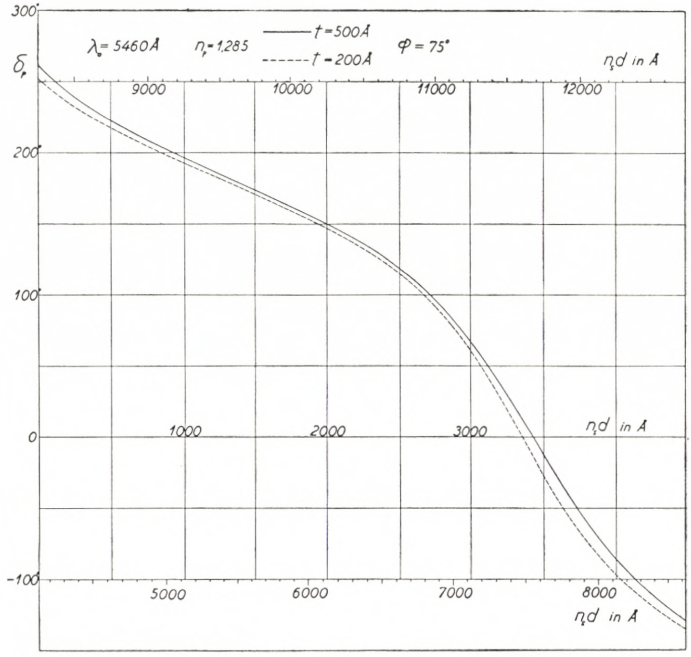
$\lambda_0 = 5460\,Å$
$n_r = 1{,}285$
$t = 500\,Å$
$t = 200\,Å$
$\varphi = 75°$
δ_r
$n_r d$ in Å
300
200
100
0
-100
9000
10000
11000
12000
1000
2000
3000
5000
6000
7000
8000

Fig. 21.

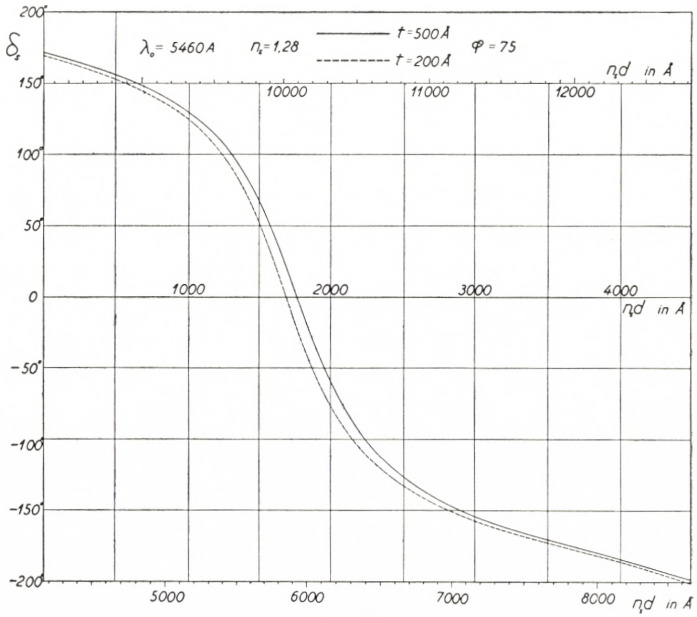
$\lambda_0 = 5460\,Å$
$n_s = 1{,}28$
$t = 500\,Å$
$t = 200\,Å$
$\varphi = 75$
δ_s
$n_s d$ in Å
200
150
100
50
0
-50
-100
-150
-200
10000
11000
12000
1000
2000
3000
4000
5000
6000
7000
8000

Fig. 22.

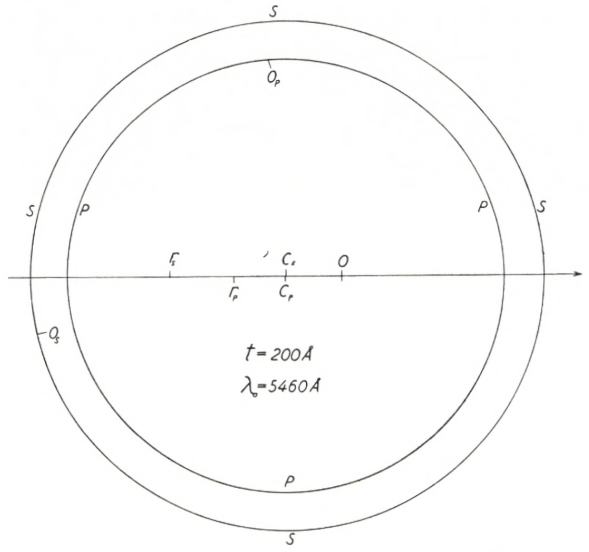

Fig. 23. Proportion between s and p circles for $t = 200$ Å $0_s = (\varrho_s, \delta_s)$ and $0_p = (\varrho_p, \delta_p)$ for the silver layer.

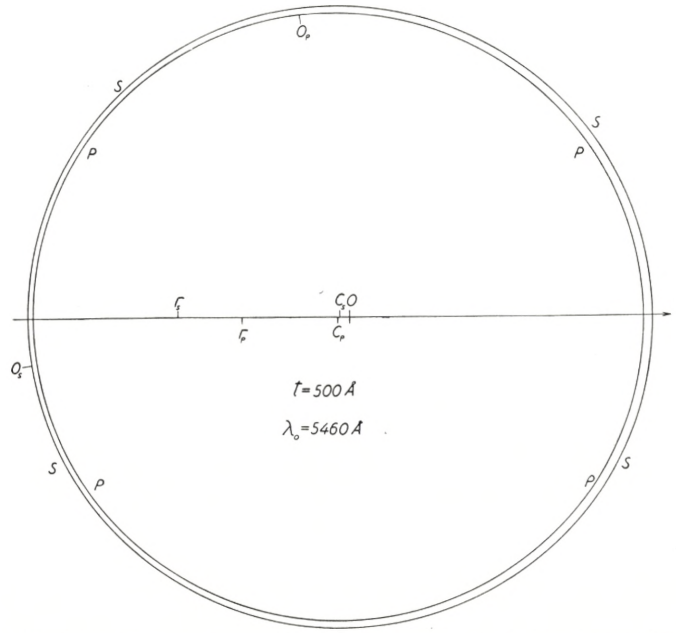

Fig. 24. Proportion between the s- and the p-circle when $t = 500$ Å.

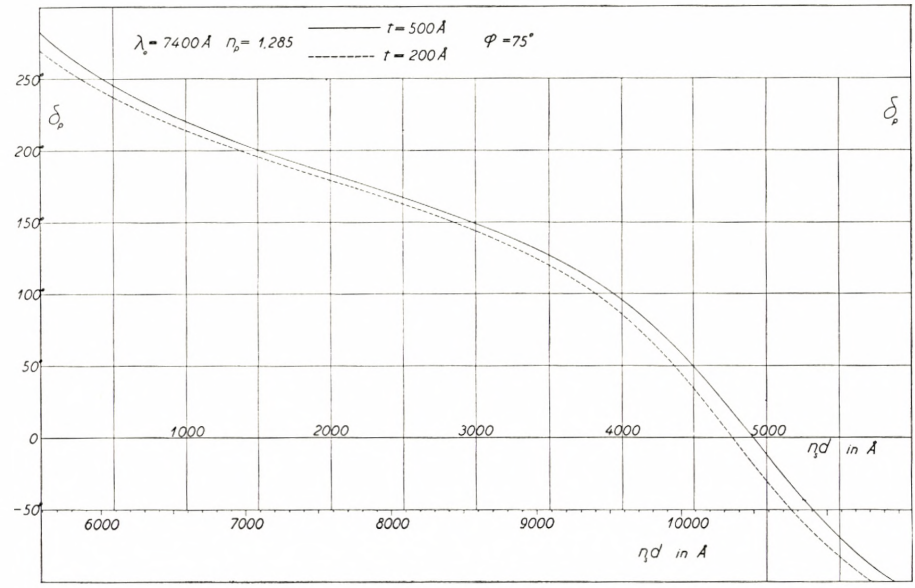
λ₀ = 7400 Å n_p = 1,285
t = 500 Å
t = 200 Å
φ = 75°
δ_p
δ_p
250°
200°
150°
100°
50°
0
-50°
1000
2000
3000
4000
5000
η_p d in Å
6000
7000
8000
9000
10000
η_p d in Å

Fig. 25.

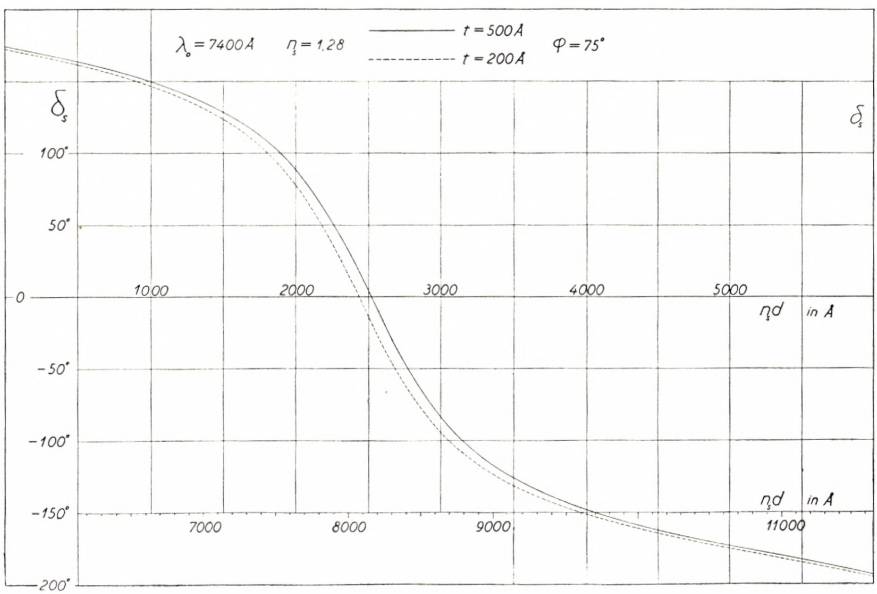
λ₀ = 7400 Å η_s = 1,28
t = 500 Å
t = 200 Å
φ = 75°
δ_s
δ_s
100°
50°
0
-50°
-100°
-150°
-200°
1000
2000
3000
4000
5000
η_s d in Å
7000
8000
9000
11000
η_s d in Å

Fig. 26.

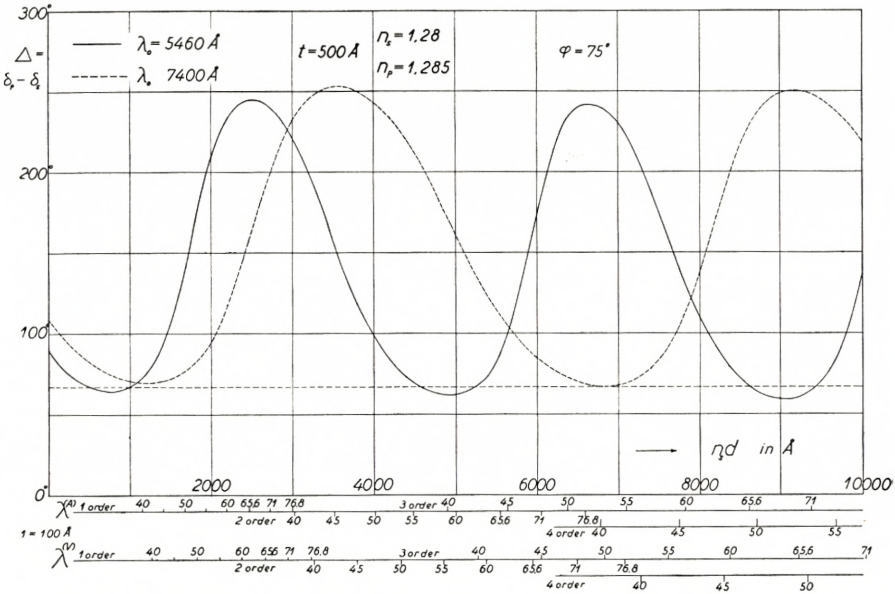
300°
Δ = δ_r − δ_i
λ_o = 5460 Å
λ_e 7400 Å
t = 500 Å
n_e = 1,28
n_p = 1,285
φ = 75°
200°
100°
0°
nd in Å
2000
4000
6000
8000
10000
λ(A) 1 order 40 50 60 65,6 71 76,8
2 order 40 45 50 55 60 65,6 71
3 order 40 45 50 55 60 65,6 71
4 order 40 45 50 55
1 = 100 Å
λ(V) 1 order 40 50 60 65,6 71 76,8
2 order 40 45 50 55 60 65,6 71 76,8
3 order 40 45 50 55 60 65,6 71
4 order 40 45 50

Fig. 27.

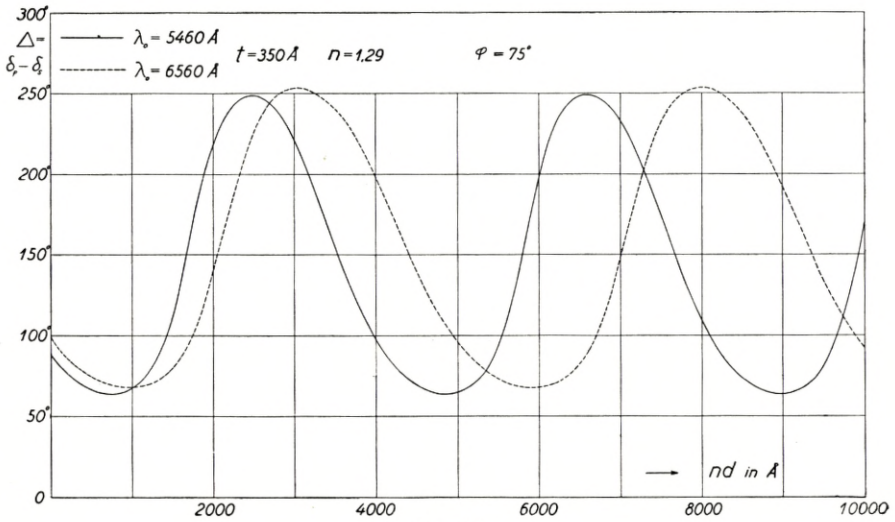
300°
Δ = δ_r − δ_i
λ_o = 5460 Å
λ_o = 6560 Å
t = 350 Å
n = 1,29
φ = 75°
250°
200°
150°
100°
50°
0
nd in Å
2000
4000
6000
8000
10000

Fig. 28.

i. e. if it is assumed that there is no birefringence and n is determined from measurement of $\lambda_m^{(v)}$, we obtain too high a value.

Figs. 27—28 further shows that when three different values of λ_0 are available, also values of $n_s \cdot d$ higher than 6000 Å can be controlled with great accuracy.

At the control of nd only Δ is used. However, also ψ is observed

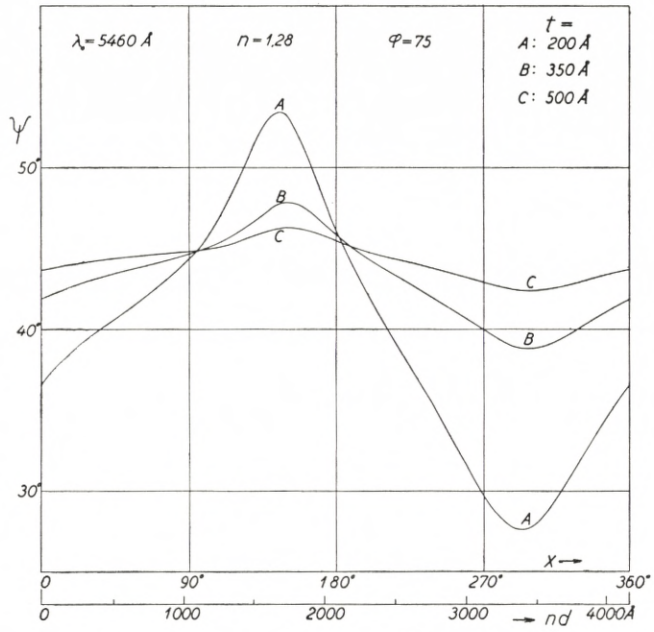

Fig. 29. ψ calculated for different thicknesses t of the basic silver layer. $\operatorname{tg} \psi = \frac{\varrho_p}{\varrho_s}$.

by analyzing the elliptically polarized light reflected from the silver-dielectric layers (fig. 2). Fig. 29 shows (ψ, x) or (ψ, nd) curves all calculated for $n = 1.28$ and for different thicknesses t of the basic silver layer. As opposed to Δ, ψ shows a strong dependence upon t and ν for the basic silver layer. $\psi_{\max} - \psi_{\min}$ can be used for a determination of t if ν is known and at $t = \infty$ be used for a determination of ν, which is independent of small errors in the polarimeter adjustment.

§ 5. Control of the Dielectric Layers for Compound Filters $M'L_{2m}M''L_{2m}M'$ and $M'L_{2m}M''L_{2p}M''L_{2m}M'$.

For these types of filters the polarimetric method for control will be especially well suited because all the measurements take place in *reflected light* and on the filter base itself and because reflection from M', M'' or from the combinations $M'\,L_{2m}M''$ and $M'\,L_{2m}M''\,L_{2p}M''$ (as basic layers for the dielectric layers) result in about the same value for Δ and δ_s (if λ_0 not corresponds to a transmission band for the basic interference filter at $\varphi = 75°$) and the $(\Delta,\ nd)$ curves above (for $t = 500$ Å) can still be used.

As briefly mentioned above the most direct method of control, for a filter of the second or higher order will be to chose the wavelength of the polarimeter light λ_0 in such a way that the evaporation has to be stopped at a value of Δ in the neighbourhood of Δ_0 corresponding to one or more total periods of the $(\Delta,\ nd)$ curve ($\lambda_0 = 2\,dn\cdot\cos\chi$ or $\lambda_0 = dn\cdot\cos\chi$).

Below a table is added which gives λ_0 for filters of the second order (1 period) and of the third order (2 periods) for different values of $\lambda^{(A)}$.

TABLE 9.

$\lambda^{(A)}$	λ_0 $M''L_4M''$	λ_0 $M''L_6M''$
4000 Å	4060 Å	
4500	4730	
5000	5400	4270 Å
5500	6060	4760
6000	6710	5240
6560	7430	5780
7100	8100	6290
7680	8840	6840

In this case the control is independent of the composition of the basic system of layers. In the case where this system consists of a filter $M'\,L_4M''$, as shown in fig. 30 A, $(\Delta,\ \psi)$ of light reflected from A will be the same as $(\Delta,\ \psi)$ for light reflected from a silver layer with thickness $t' + t''$ (fig. 30 B) if $n - i\,\varkappa$ is the same for the three silver layers.

The small birefringence present acts as if $n \cdot \cos \chi$ is greater than in reality. Table 9 is calculated in such a way that $\lambda^{(A)} = 6560$ Å (third order) corresponds to the value of λ_0 actually measured.

When we wish to make a filter $M' L_{2m} M'' L_{2m} M'' L_{2m} M'$ it should further be noted that $n^{(A)} \cdot d$ for the central layer is different from $n^{(A)} \cdot d$ for the outer dielectric layers, as the filters $M' L_{2m} M''$ and $M'' L_{2m} M''$ shall have the same value for $\lambda_m^{(A)}$. The $n_s^{(v)} \cdot d$

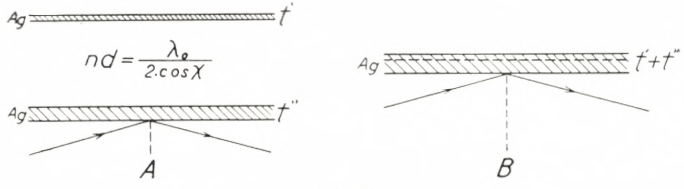

Fig. 30.

values to be used on the $(\Delta, n_s d)$ curve are calculated from (4, 5). The differences betweens the $n_s^{(v)} d$ values for the central and the outer layers vary from about 15 Å at $\lambda_m^{(A)} = 4000$ Å to 115 Å at $\lambda_m^{(A)} = 7700$ Å.

§ 6. Control of the Dielectric Layers for Filters where *L* and *H* Layers are Added to the Silver Layers.

Also at this type of filters (the theory of which is given in ([A] § 6)) all the dielectric layers can be controlled on the filter base itself (fig. 31).

The calculation of the (Δ, nd) curve is carried out graphically by means of a polar coordinathograph (see fig. 7).

As an example fig. 32 shows the (Δ, nd) curve calculated for the simplest filter of this type $M L' H_2 L' M$ in such a way that

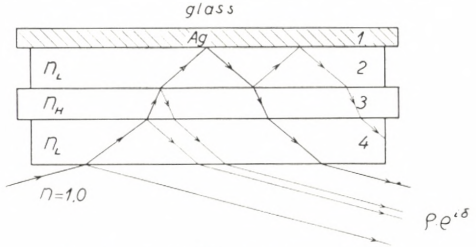

Fig. 31. $ML' HL$ system of layers.

peak transmission occurs at $\lambda = 6560$ Å. Here $\lambda_0 = 5460$ Å will give sufficient accuracy by control of all the dielectric layers, but in most cases (in the case of more complicated filters of this type)

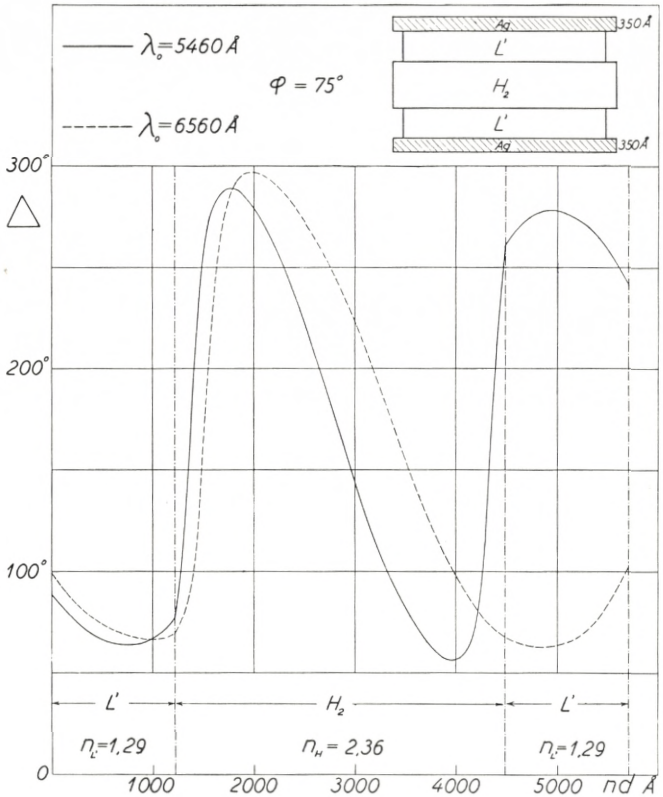

Fig. 32.

the calculation has to be repeated for another value of λ_0 to be able to control all the dielectric layers with sufficient accuracy.

The control of a high-index layer is much easier than for a low-index layer as $n_H^{(v)} = n_H^{(A)} = n_H^{(c)}$ and because of the small value of $\Delta\lambda_1$ (Table 1).

In fig. 32 it is assumed that $n_H = 2.36$ $n_L^{(v)} = 1.29$ and $n^{(A)} = 1.37$.

§ 7. Thickness Control in the Production of All-Dielectric Filters.

As mentioned above, the usual procedure employed for this type of filters is measurement of the intensity $R(d)$ in *reflected* monochromatic light at normal incidence from test plates; at least two test plates are used, one for the low- and the other for the high-index layers. In fig. 33 $R(d)$ is calculated for the test plate with the low-index layer ($n_L^{(v)} = 1.29$, MgF_2) and in fig. 34 $R(nd)$ for the test plate with the high-index layer ($n_H = 2.36$, ZnS). By change of wavelength λ_0 or by measuring the difference $R_1 - R_2$ corresponding to two different wavelengths as indicated in figs. 33—34 it will be possible to control nd for all the layers with an accuracy of about 30 Å (if photocells and an amplifier are used). It should further be mentioned that JACQUINOT and GIACOMO [4] have constructed an apparatus which enables them to measure the derivative $\frac{dR}{d\lambda_0}$ (which can be used for thickness control with great accuracy for thicknesses where $R(d)$ has a maximum or a minimum).

This rather simple test plate procedure offers good results by production of filters of smaller areas. [2] However, as mentioned above, the filter base in the case of production of filters of larger areas must be rotated during evaporation and the test plates placed perpendicularly above the evaporation source and far from the filter base. In this case the test-plate procedure for control would be rather uncertain, and for this reason it would be desirable to control all the filter layers (and especially the 3—5 central layers) on the filter base itself. In the case of this type of filters this is also possible by means of the polarimetric method and with higher accuracy than obtained with the testplate method.

The (Δ, nd) and (ψ, nd) curves are calculated by means of the graphical procedure shown in fig. 7 p. 9.

Such a construction is shown in figs. 35—36. $n_L^{(v)} = 1.29$ and $n_H = 2.36$. λ_0 has been chosen in such a way that $x_H = 180 \cdot \frac{\lambda_1}{\lambda_0} \cdot \cos \chi_H$ is equal to 180° i. e. $\frac{\lambda_1}{\lambda_0} = 1.096$. ($\varphi = 75°$).

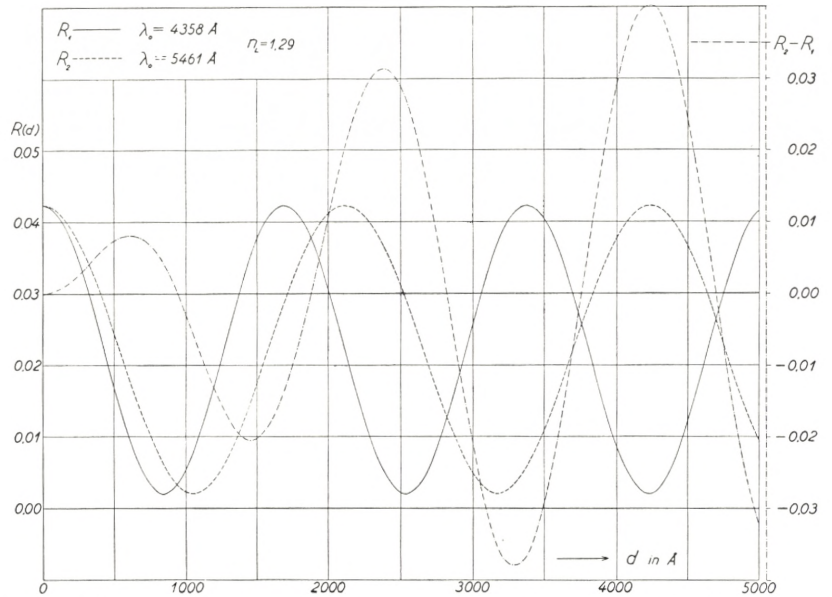

Fig. 33. $R\,(d)$ from a glass surface with $n = 1.518$ coated with a MgF_2 film ($\varphi = 0$).

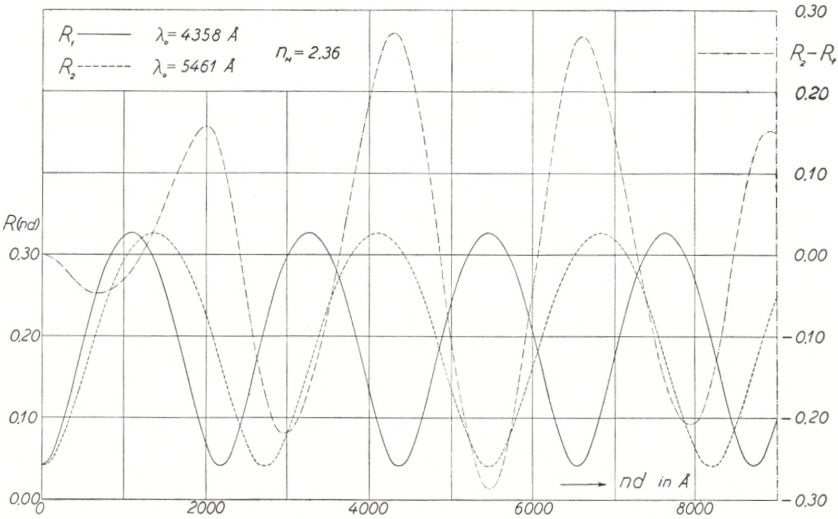

Fig. 34. $R\,(nd)$ from a glass surface with $n = 1.518$ coated with a ZnS film ($\varphi = 0$).

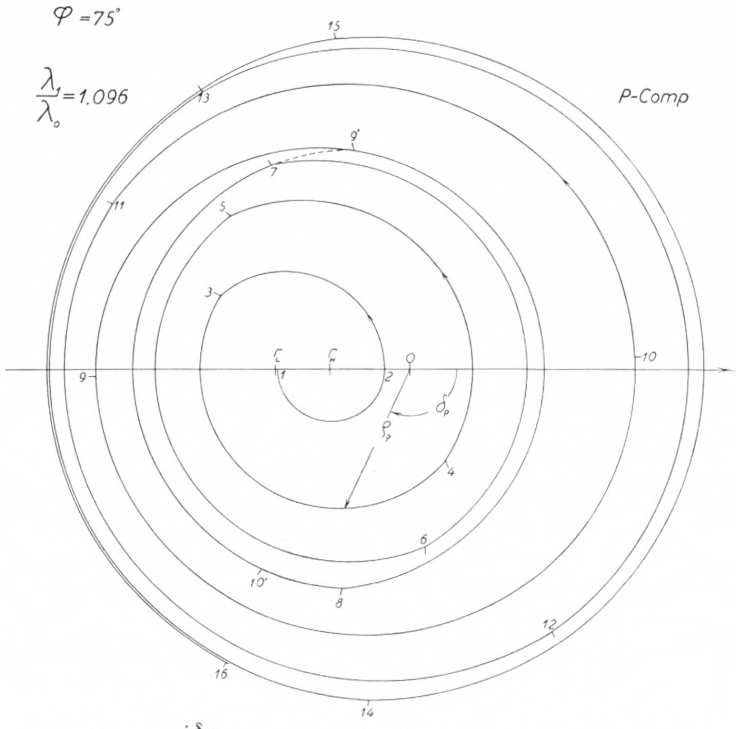

Fig. 35. $\varrho_p \cdot e^{i\delta p}$ during the build-up of the filter $D_7\, L_2\, D_7$.

$x_L = 180 \cdot \dfrac{\lambda_1}{\lambda_0} \cdot \dfrac{n_L^{(v)}}{n_L^{(A)}} \cdot \cos \chi_L$ and when $\dfrac{n_L^{(v)}}{n_L^{(A)}} = 0.9377$ we have $x_L = 122°.62$ ($x_H = x_L = 180°$ for $\lambda = \lambda_1$ and $\varphi = 0$).

Fig. 35 shows (ϱ_p, δ_p) and fig. 36 (ϱ_s, δ_s) (in polar coordinates) for the filter $D_7 L_2 D_7$ as the layers grow simultaneously.

The numbers 1—16 on the spirals denote the values of (ϱ, δ), where the evaporation has to be interrupted and a change to the other dielectric material to take place. E. g. the number 8 means (ϱ, δ) in reflection from the seven layers $D_7 = HLHLHLH$ (1 means (ϱ, δ) for the uncoated glass plate), 9 means reflection from $HLHLHLHL_2$, etc. As $x_H = 180°$, the same construction can be used for the filter $D_8 H_2 D_8$. The number 9′ in figs. 35—36 means (ϱ, δ) corresponding to reflection from the system $D_8 = HLHLHLHL$ (and 10′ in fig. 35 means reflection from D_9; in fig. 36, 10′ is equal to 8).

From figs. 35—36 the corresponding (Δ, nd) and (ψ, nd)

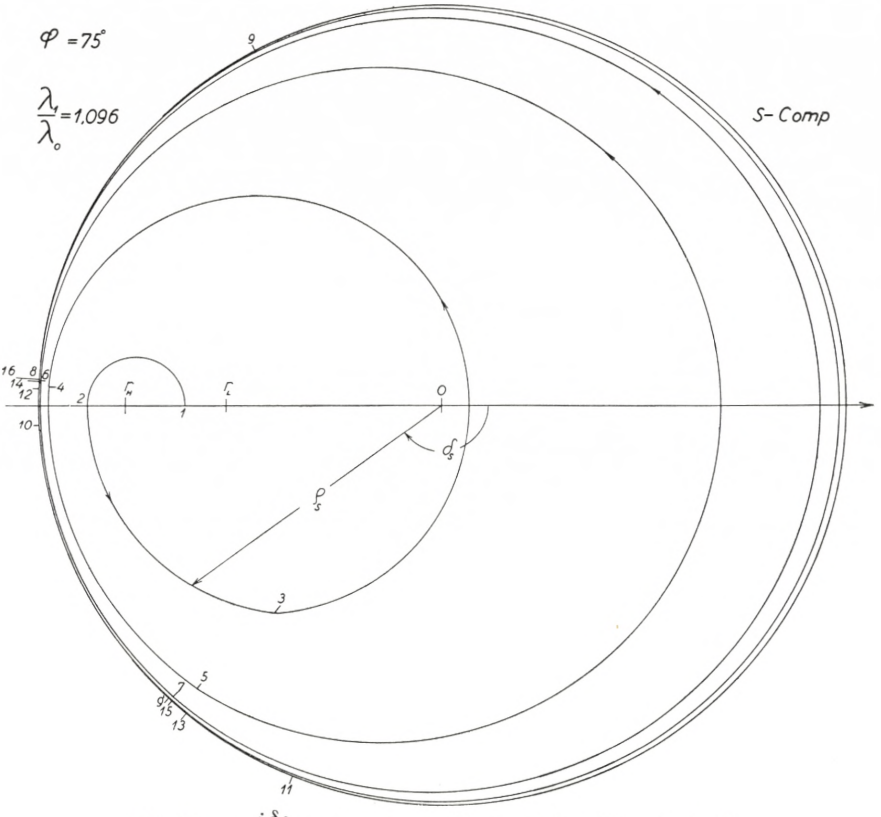

Fig. 36. $\varrho_s \cdot e^{i\delta s}$ during the build-up of the filter $D_1\, L_2\, D_7$.

curves can be constructed (not given here). The positions of the points on the (Δ, nd) curve which correspond to the H and L layers would be still better if λ_0 was chosen still smaller than λ_1 e. g. $\frac{\lambda_1}{\lambda_0} = \frac{6560}{5461} = 1.20$. Unfortunately λ_0 can not be chosen higher than or equal to λ_1, as in this case $\frac{\varrho_p}{\varrho_s}$ would be too low to enable an accurate measurement of Δ.

Another procedure by polarimetric control would be to measure the difference $\Delta(\lambda_0) - \Delta(\lambda_0')$ in Δ corresponding to two neighbouring wavelengths λ_0 and λ_0' (e. g. 5461 Å and 5893 Å). When this difference is measured with an accuracy of 5′ (five minutes of arc) a sufficiently accurate control would be possible for values of nd where Δ has a maximum or a minimum.

Summary.

A polarimetric method for thickness control in the production of interference filters has been treated in detail.

Plane-polarized light with wavelength λ_0 is reflected from the filter layers at an oblique angle of incidence ($\varphi = 75°$) and thus becomes elliptically polarized. λ_0 is chosen in such a way that measurement of $\Delta = \delta_p - \delta_s$ for the elliptically polarized light determines the thickness of a dielectric layer with an accuracy better than 10 Å (when conditions during the evaporation process are constant).

This method of control, which follows the growth of the dielectric layer on the filter base itself, can be applied to all types of interference filters (also reflection interference filters) and is especially well suited for control of the dielectric layers for filters of the types $ML_{2m}M$, $M'L_{2m}M''L_{2m}M'$ and $M'L_{2m}M''L_{2p}M''L_{2m}M'$.

A (Δ, nd) curve for a filter $ML_{2m}M$ can be constructed from measurements of (Δ_0, ψ_0) for the silver layer M first evaporated and from measurements of Δ_{max} and Δ_{min} during evaporation; and the value of Δ at which the evaporation is to be stopped can be calculated corresponding to a definite wavelength for the transmission band λ_m of the filter.

A small birefringence ($n_p - n_s \simeq 0.005$) is present for an evaporated fluoride layer (cryolite or MgF_2) and the index of refraction for rapidly evaporated MgF_2 is much lower in vacuum ($n^{(v)} = 1.28$) than in air ($n^{(A)} = 1.365$). Furthermore measurements of (Δ_0, ψ_0) for silver layers show that $\varkappa$ for a silver layer of the thickness employed for interference filters is different from $\varkappa$ for an opaque silver layer.

The experiments will be continued in order to obtain more refined information about $n_p(\lambda)$ and $n_s(\lambda)$ (in vacuum and air) for thin evaporated MgF_2 films.

Acknowledgement.

These investigations have been carried out at the Physics Department of the Royal Veterinary and Agricultural College, Copenhagen.

I wish to express my gratitude to the Director af the Physics Department, Professor EBBE RASMUSSEN, for the great interest he has taken in this work.

Physics Department
Royal Veterinary- and Agricultural College
Copenhagen.

References.

(*A*) ALFRED HERMANSEN, A Theory of Interference Filters, Dan. Mat. Fys. Medd. **29,** No. 13 (1955).
(1) K. M. GREENLAND and C. BILLINGTON, Proc. Phyc. Soc. B, **63,** 359 (1950) or J. Phys. et le Radium **11,** 419 (1950).
(2) CH. DUFOUR, Le Vide, No. 16—17, 480 (1948) or Theses (Paris 1950).
(3) P. JACQUINOT et P. GIACOMO, J. Phys. et le Radium **13,** 59 A (1952).
(4) A. HERMANSEN, Nature **167,** 104 (1951).
(5) P. DRUDE, Ann. d. Phys. und Chem. **36,** 865 (1889).
— ibid. **39,** 481 (1890).
(6) ANTONIN VAŠÍČEK, J. Opt. Soc. Am. **37,** 145 (1947) and ibid. **37,** 979 (1947).
(7) ALEXANDRE ROTHEN, Rev. Sci. Instr. **16,** 26 (1945).
(8) ALEXANDRE ROTHEN and MARJORIE HANSON, Rev. Sci. Instr. **19,** 839 (1948).
— — ibid. **20,** 66 (1949).
(9) A. HERMANSEN, Nature, **174,** 218 (1954).
(10) JØRGEN RYBNER and K. STEENBERG SØRENSEN, Table for Use in The Addition of Complex Numbers (Jul. Gjellerups forlag, København 1948).
(11) P. COTTON, J. Phys. et le Radium **11,** 321 (1950).
(12) MAX BORN, Optik (1933) (Berlin, Verlag von Julius Springer).
(13) B. H. BILLINGS, J. Opt. Soc. Am. **40,** 471 (1950).

Indleveret til selskabet den 25. april 1955.
Færdig fra trykkeriet den 24. september 1955.

Det Kongelige Danske Videnskabernes Selskab

Matematisk-fysiske Meddelelser, bind **30,** nr. 7

Dan. Mat. Fys. Medd. **30**, no. 7 (1955)

DEDICATED TO PROFESSOR NIELS BOHR ON THE OCCASION OF HIS 70TH BIRTHDAY

ON THE MATHEMATICAL STRUCTURE OF T.D. LEE'S MODEL OF A RENORMALIZABLE FIELD THEORY

BY

G. KÄLLÉN AND W. PAULI

København 1955

i kommission hos Ejnar Munksgaard

Printed in Denmark.
Bianco Lunos Bogtrykkeri A-S

It is shown that the appropriate mathematical formalism of the field theoretical model recently proposed by T. D. LEE must use an indefinite metric to describe the norm of the state vector in the Hilbert space. The appearance of the indefinite metric is intimately connected with a new state of the V-particle having an energy that is below the mass of the "normal" V-particle. It is further shown that the S-matrix for this model is not unitary and that the probability for an incoming V-particle in the normal state and a boson, to make a transition to an outgoing V-particle in the new state and another boson, must be negative if the sum of all transition probabilities for the incoming state mentioned shall add up to one.

Introduction.

In a recent paper[1], T. D. LEE has suggested a very interesting model of a renormalizable field theory. This model is simple enough to allow a more or less explicit solution, but complicated enough to contain many features characteristic of more realistic theories. It uses not only a renormalization of the mass of one kind of particles involved, but also a renormalization of the coupling constant g describing the interaction between the particles. In the explicit solution found by LEE, the ratio between the square of the renormalized coupling constant g and the square of the unrenormalized coupling constant g_0 is given by an expression of the form

$$\frac{g^2}{g_0^2} = 1 - A \cdot g^2, \tag{1}$$

where A is a divergent integral. The ratio (1) is thus equal to $-\infty$. This is a very remarkable result, as according to very general principles[2], this ratio should lie between one and zero. It is the aim of the present note to investigate the mathematical origin of the result (1) and to show that the violation of general principles implied by (1) also has observable consequences insofar as the S-matrix of the theory turns out not to be unitary.

To avoid the manipulation of divergent integrals we introduce a cut-off factor in the interaction. It will then appear that abnormal values of the ratio (1) are also obtained for a finite value of the cut-off and are not immediately connected with the infinities in the original formulation. To make our discussion reasonably self-contained we start with a survey of the foundations of the Lee model and with an outline of the way in which the renormalizations have to be performed in this case.

I. Renormalization of the Lee Model.

Let us consider a system with three different kinds of particles which, following LEE, we call V-particles, N-particles, and θ-particles. To each kind of particles corresponds a field that will be denoted by ψ_V, ψ_N, and a, respectively. The system is governed by the following *unrenormalized* Hamiltonian:

$$H = H_0 + H_{\text{int}}, \tag{2}$$

$$\left.\begin{aligned} H_0 = &\sum_{\bar{p}} E_V(\bar{p})\,\psi_V^*(\bar{p})\,\psi_V(\bar{p}) + \sum_{\bar{p}} E_N(\bar{p})\,\psi_N^*(\bar{p})\,\psi_N(\bar{p}) \\ &+ \sum_{\bar{k}} \omega(\bar{k})\,a^*(\bar{k})\,a(\bar{k}), \end{aligned}\right\} \tag{3}$$

$$H_{\text{int}} = -\frac{g_0}{\sqrt{V}} \sum_{\bar{p}=\bar{p}'+\bar{k}}{}' \frac{f(\omega)}{\sqrt{2\,\omega}} \left(\psi_V^*(\bar{p})\,\psi_N(\bar{p}')\,a(\bar{k}) + a^*(\bar{k})\,\psi_N^*(\bar{p}')\,\psi_V(\bar{p})\right). \tag{4}$$

The operators in (3) and (4) can be thought of as being written in p-space and in a Schrödinger representation. The model does not have invariance with respect to the Lorentz group and it will not be necessary to use the more sophisticated representations of relativistic field theories. The energies $E_V(\bar{p})$, $E_N(\bar{p})$, and $\omega(\bar{k})$ are, in principle, arbitrary functions of the momenta involved and the theory can be treated for any form of these functions. However, for our purpose, it will be sufficient to consider the following special case,

$$E_V(\bar{p}) = E_N(\bar{p}) = m \quad \text{(independent of } \bar{p}), \tag{5}$$

$$\omega(\bar{k}) = \sqrt{\bar{k}^2 + \mu^2}. \tag{6}$$

In particular, *Eq.* (5) will simplify the formal expressions to some extent without interfering with the interesting features of the result. If one wishes, this choice of the energies as functions of the momenta can be thought of as giving a model for the interaction of very heavy V- and N-particles (with equal masses) with light, relativistic θ-particles. The function $f(\omega)$ in (4) is the cut-off function mentioned earlier and is introduced to make the sums, appearing later, convergent. The quantity V is the volume of periodicity.

The field operators obey the following commutation and anti-commutation relations:

$$\{\psi_V^*(\bar{p}),\ \psi_V(\bar{p}')\} = \{\psi_N^*(\bar{p}),\ \psi_N(\bar{p}')\} = \delta_{\bar{p},\bar{p}'}, \tag{7}$$

$$\{\psi_V(\bar{p}),\ \psi_V(\bar{p}')\} = \{\psi_V(\bar{p}),\ \psi_N(\bar{p}')\} = \cdots\cdots = 0, \tag{8}$$

$$[a(\bar{k}),\ a^*(\bar{k}')] = \delta_{\bar{k},\bar{k}'}, \tag{9}$$

$$[a(\bar{k}),\ \psi_V(\bar{p})] = [a(\bar{k}),\ \psi_N(\bar{p}')] = \cdots\cdots = 0. \tag{10}$$

With the aid of these commutators we can set up a representation in the Hilbert space, where each state is characterized by the number of particles present. Further, each state in this representation is an eigenstate of the free-particle Hamiltonian H_0 in (3), but not of the total Hamiltonian (2). Let us denote these states by

$$|n_V,\ n_N,\ n_k\rangle, \tag{11}$$

where n_V, n_N, and n_k are the numbers of "free" V-particles, N-particles, and θ-particles present[3].

With the aid of (7)—(10) it can easily be verified that the following two operators commute with the total Hamiltonian.

$$Q_1 = \sum_{\bar{p}} \psi_V^*(\bar{p})\,\psi_V(\bar{p}) + \sum_{\bar{p}} \psi_N^*(\bar{p})\,\psi_N(\bar{p}), \tag{12}$$

$$Q_2 = \sum_{\bar{p}} \psi_N^*(\bar{p})\,\psi_N(\bar{p}) - \sum_{\bar{k}} a^*(\bar{k})\,a(\bar{k}), \tag{13}$$

$$[H,\ Q_i] = 0, \quad i = 1,2. \tag{14}$$

As each state (11) is also an eigenstate of the operators Q_i, it follows that the eigenstates of the total Hamiltonian H can be built up as linear combinations of states (11) belonging to the same eigenvalue q_i. This will considerably simplify the problem of diagonalizing the total Hamiltonian and, in some cases, even give an explicit solution. As an example, we may mention that there is only one of the states (11) which has $q_1 = q_2 = 0$, *viz.* the state $|0, 0, 0\rangle$ or the "free-particle vacuum". Hence, this state is also an eigenstate of the total Hamiltonian, and a simple calculation gives the eigenvalue zero for this operator. The "physical vacuum" is thus the same as the free-particle vacuum for this model. In the same way, we can show that the physical N-particle states and the physical θ-particle states are identical with the corresponding free-particle states, but that the free V-particle states are *not* eigenstates of the total Hamiltonian. It will be necessary to consider a linear combination of the states $|1_V, 0, 0\rangle$ and $|0, 1_N, 1_k\rangle$ to construct an eigenstate of the total Hamiltonian for this case. We shall later return to this point. For the moment we only remark that, under these circumstances, it will not be necessary to introduce renormalizations of the masses of the N-particles or the θ-particles. The mass renormalization in the model is now performed by adding the following term to the Hamiltonian (this term will *not* change the conservation equations (14)):

$$\delta H = -\delta m \sum_{\bar{p}} \psi_V^*(\bar{p})\,\psi_V(\bar{p}). \tag{15}$$

The constant δm in (15) should, if possible, be determined in such a way that the state corresponding to the physical V-particle has the mass m appearing in H_0. Following the custom in quantum electrodynamics, we also introduce a renormalization of the coupling constant g_0 and of the field operator ψ_V by a factor N in the following way:

$$g = g_0 \cdot N, \tag{16}$$

$$\psi'_V(\bar{p}) = \psi_V(\bar{p})\,\frac{1}{N}. \tag{17}$$

It is important to realize that the constant N in (16) and (17) can by definition be chosen to be real, as there is always an arbitrary phase factor in the field operators. The choice of a

real N only fixes the phase connection between ψ_V and ψ'_V and can have no physical consequences. The value of N is determined by the condition[4)]

$$\langle 0 \left| \psi'_V(\bar{p}) \right| V \rangle = 1. \tag{18}$$

The state $| V \rangle$ in (18) is the physical V-particle state and the state $| 0 \rangle$ the physical vacuum. In what follows, we drop the dash on the renormalized ψ_V-operator as the corresponding unrenormalized operator will not be used again. In terms of our renormalized quantities the Hamiltonian and the canonical commutators will now read

$$H = H_0 + H_{\text{int}} + \delta H, \tag{19}$$

$$H_0 = mN^2 \sum_{\bar{p}} \psi_V^*(\bar{p}) \psi_V(\bar{p}) + m \sum_{\bar{p}} \psi_N^*(\bar{p}) \psi_N(\bar{p}) + \sum_{\bar{k}} \omega(\bar{k}) a^*(\bar{k}) a(\bar{k}), \tag{20}$$

$$H_{\text{int}} = -\frac{g}{\sqrt{V}} \sum_{\bar{p} = \bar{p}' + \bar{k}}' \frac{f(\omega)}{\sqrt{2\omega}} (\psi_V^*(\bar{p}) \psi_N(\bar{p}') a(\bar{k}) + a^*(\bar{k}) \psi_N^*(\bar{p}') \psi_V(\bar{p})), \tag{21}$$

$$\delta H = -\delta m \, N^2 \sum_{\bar{p}} \psi_V^*(\bar{p}) \psi_V(\bar{p}), \tag{22}$$

$$\{ \psi_V^*(\bar{p}), \psi_V(\bar{p}') \} = \frac{1}{N^2} \delta_{\bar{p}, \bar{p}'} \quad \text{(other commutators unchanged).} \tag{23}$$

Eqs. (19)—(23) will be the foundation for the following discussion.

II. The Physical *V*-Particle States and the States Describing the Scattering of one *N*-Particle and one θ-Particle.

We now try to find an eigenstate of the total Hamiltonian of the form

$$| z \rangle = | 1_V, 0, 0 \rangle + \sum_{\bar{k}} \Phi(\bar{k}) | 0, 1_N, 1_k \rangle. \tag{24}$$

In this expression all terms have the same total momentum. In the following formulae, a factor expressing conservation of three-dimensional momentum is very often left out. Calling the eigenvalue of the state (24) $m + \omega_0$, and using (19)—(23), we obtain after some straightforward calculations

$$\omega_0 + \delta m = -\frac{g}{N \cdot \sqrt{V}} \sum_{\bar{k}}' \frac{\Phi(\bar{k}) f(\omega)}{\sqrt{2\omega}}, \tag{25}$$

$$(\omega - \omega_0) \Phi(\bar{k}) = \frac{g}{N\sqrt{V}} \frac{f(\omega)}{\sqrt{2\omega}}. \tag{26}$$

Eliminating $\Phi(\bar{k})$ from (25) and (26) we get the following equation for the determination of the eigenvalue ω_0:

$$\omega_0 + \delta m + \frac{g^2}{2N^2 V} \sum_{\bar{k}}' \frac{f^2(\omega)}{\omega} \frac{1}{\omega - \omega_0} = 0. \tag{27}$$

The constant δm is now determined from the condition that $\omega_0 = 0$ should be one solution of (27). The corresponding eigenstate (24) is, when properly normalized, the physical V-particle state. This gives us

$$\delta m = \frac{-g^2}{2V} \frac{1}{N^2} \sum_{\bar{k}}' \frac{f^2(\omega)}{\omega^2}, \tag{28}$$

$$|V\rangle = C\left[|1_V, 0, 0\rangle + \frac{g}{N\sqrt{2V}} \sum_{\bar{k}}' \frac{f(\omega)}{\omega^{3/2}} |0, 1_N, 1_k\rangle\right], \tag{29}$$

$$C^{-2} = 1 + \frac{g^2}{2VN^2} \sum_{\bar{k}}' \frac{f^2(\omega)}{\omega^3}. \tag{30}$$

Furthermore, using *Eq.* (18), we get

$$C = N \tag{31}$$

or

$$|V\rangle = N|1_V, 0, 0\rangle + \frac{g}{\sqrt{2V}} \sum_{\bar{k}}' \frac{f(\omega)}{\omega^{3/2}} |0, 1_N, 1_k\rangle, \tag{32}$$

$$N^2 = 1 - \frac{g^2}{2V} \sum_{\bar{k}}' \frac{f^2(\omega)}{\omega^3}. \tag{33}$$

The results obtained so far in this paragraph correspond exactly to those obtained by LEE. In particular, *Eqs.* (33) and (16)

together give LEE's result (1) if the form factor is put equal to unity for all values of ω. However, if we have a finite cut-off, *Eq.* (33) can be written

$$N^2 = 1 - \frac{g^2}{g_{\text{crit}}^2}, \tag{34}$$

$$g_{\text{crit}}^{-2} = \frac{1}{2V} \sum_{\bar{k}}' \frac{f^2(\omega)}{\omega^3}. \tag{34a}$$

The value (34) of N^2 lies between zero and one, as was to be expected, only if the renormalized coupling constant g is less than a critical value g_{crit} depending on the cut-off function and defined by (34a). If there is no cut-off, the critical value of the coupling is zero. Further, if the renormalization of the coupling constant is not performed explicitly, but if all quantities are expressed in terms of the original constant g_0, we have to substitute the expression

$$g^2 = \frac{g_0^2 \cdot g_{\text{crit}}^2}{g_0^2 + g_{\text{crit}}^2} \tag{35}$$

for g^2 everywhere in our formulae above. *Eq.* (35) contains the definite prediction that the renormalized coupling is always less than the critical coupling if the Hamiltonian is hermitian, *i.e.* if g_0 is real. As stressed by LEE, it is of some interest to investigate also the case of the renormalized coupling being larger than the critical value and the Hamiltonian being non-hermitian. The crucial question to be answered is whether this violation of the ordinary methods of quantum mechanics will have any observable consequences or if we are able in this way to get an at least partially satisfactory theory.

We now turn to the investigation of the other solutions to the eigenvalue problem (27). Making use of (28) and (33) we can rewrite *Eq.* (27) in the following way:

$$h(\omega_0) \equiv \omega_0 \left[1 + \frac{g^2}{2V} \sum_{\bar{k}}' \frac{f^2(\omega)\,\omega_0}{\omega^3(\omega - \omega_0)} \right] = 0. \tag{36}$$

The second factor in (36) has a pole each time $\omega_0 = \omega_i$, where ω_i is an eigenvalue of the unperturbed Hamiltonian H_0. As the derivative of the last factor in (36) with respect to ω_0 is always positive, this factor must vanish once, and only once, in each interval (ω_i, ω_{i+1}). The corresponding eigenstates (24) describe the scattering of one N-particle and one θ-particle. After some formal manipulations these states can be written,

$$|N, \theta\rangle = |0, 1_N, 1_k\rangle + \sum_{\bar{k}'} \alpha(\bar{k}, \bar{k}') |0, 1_{N'}, 1_{k'}\rangle + \beta(\bar{k}) N |1_V, 0, 0\rangle, \tag{37}$$

$$\alpha(\bar{k}, \bar{k}') = \frac{g}{\sqrt{2V}} \frac{\beta(\bar{k}) f(\omega')}{\sqrt{\omega'}} \left\{ P \frac{1}{\omega' - \omega} + i\pi\delta(\omega' - \omega) \right\}, \tag{38}$$

$$\beta(\bar{k}) = -\frac{gf(\omega)}{\sqrt{2V}\omega^{3/2}} \left[1 + \frac{g^2\omega}{2V} \sum_{\bar{k}} \frac{f^2(\omega')}{\omega'^3} \left(P \frac{1}{\omega' - \omega} + i\pi\delta(\omega' - \omega) \right) \right]^{-1}. \tag{39}$$

In (38) and (39), the limit $V \to \infty$ has been anticipated and these equations contain a prescription how the denominators must be treated when the integration over $\bar{k}'$ is performed. This prescription corresponds to only outgoing waves in the second term of (37). The only incoming particles in these states have momentum $\bar{k}$. From the formulae above it is possible to compute that part of the S-matrix which corresponds to the scattering of N-particles and θ-particles by each other. The result is the unitary matrix

$$\langle N, \theta | S | N', \theta' \rangle = \delta_{\bar{k}, \bar{k}'} + \frac{i\pi g^2}{V} \frac{f^2(\omega)}{\omega} \frac{\delta(\omega' - \omega)}{h(\omega) + i \frac{g^2}{4\pi} |\bar{k}| f^2(\omega)}. \tag{40}$$

From (40) we get the differential cross section

$$\frac{d\sigma}{d\Omega} = \frac{1}{|\bar{k}|^2} \sin^2 \delta \tag{41}$$

with

$$\operatorname{tg} \delta = \frac{g^2}{4\pi} \frac{|\bar{k}| f^2(\omega)}{h(\omega)}. \tag{42}$$

Again, this corresponds exactly to the results obtained by LEE. In the last three formulae, the limit $V \to \infty$ is performed and the

integral appearing in $h(\omega)$ (*Eq.* (36)) is defined to be a principal value.

It remains to discuss the important question whether the states (32) and (37) obtained so far form a complete set or if *there are possibly other states of the form* (24) *which are also eigenstates of the total Hamiltonian*. If other states exist, they must correspond to other solutions of the eigenvalue problem (36). We therefore begin by a more detailed discussion of this equation. The argument given so far has exhausted all roots of this equation in the domain $\omega_0 > \mu^*$. For $\omega_0 < \mu$, we find that the second factor of (36) still has a positive derivative and that it approaches the value $N^2 = 1 - g^2/g_{\text{crit}}^2$ for very large values of $|\omega_0|$. If the coupling constant is less than the critical value, we have no extra root of (36) and the states considered so far form a complete set. On the other hand, *if the coupling is larger than the critical coupling, there will be exactly one extra root of* (36) *for* $\omega_0 < \mu$. The corresponding eigenstate is not a scattering state, but will represent another state of the V-particle.† This state can be constructed explicitly from the formalism given here, and the result is

$$|V_{-\lambda}\rangle = \frac{1}{\sqrt{|h'(-\lambda)|}}\left[N\cdot|1_V, 0, 0\rangle + \frac{g}{\sqrt{2V}}\sum_{\bar{k}}\frac{f(\omega)}{\sqrt{\omega}}\frac{1}{\omega+\lambda}|0, 1_N, 1_k\rangle\right], \quad (43)$$

$$h(-\lambda) = 0; \quad \lambda > 0. \quad (44)$$

The normalization of the state (43) is chosen in a way that will be justified in the next paragraph.

It will be shown in Appendix I that *Eq.* (36) has no non-real roots.

* If the cut-off function vanishes exactly for ω larger than some value Ω, the domain $\omega_0 > \Omega$ needs a special discussion, as the argument after *Eq.* (36) will not be valid there. Actually, it can be shown that there is an extra root in this domain if g is less than the critical value g_{crit}. To avoid inessential complications of the argument, we therefore consider only cut-off functions that have a long tail as, *e. g.*, $f(\omega) = e^{-\omega/\Omega}$, where this question will not appear.

† In footnote 4 of LEE's paper, the possibility of another stable state of the V-particle is briefly mentioned, but no detailed investigation of its properties is given. In our discussion, this state will be of paramount importance.

III. Introduction of an Indefinite Metric in the Hilbert Space.

The negative sign for N^2 in (34), if g is larger than g_{crit}, obviously leads to difficulties with the normalization of the physical V-particle state (32). If we try to correct the normalization of this state by multiplying it with a suitable factor, we are ultimately led to a modification of our renormalization prescriptions insofar as we can no longer use the same factor in (16) and (17) to renormalize the coupling constant and the field operator ψ_V. In this case, extra factors have to be inserted in the interaction Hamiltonian (21), and it can easily be seen that it is not possible in this way to make the theory mathematically consistent. The only possibility of saving the normalization of the state (32) is then to *define* the norm of a state $\alpha \,|\, n_V, n_N, n_k\rangle$ to be $|\alpha|^2(-1)^{n_V}$. As N^2 in our case is real and negative, this indefinite metric will be the appropriate mathematical framework for the Lee model.[5] The introduction of this device will not change many of the formal operations performed earlier, and particularly the scattering states (37) and the S-matrix (40) will be uninfluenced by it. On the other hand, the norm of the state (32) will be now +1 as it stands in the new metric. The norm of the state (43) will be

$$\left.\begin{aligned} &\frac{1}{|h'(-\lambda)|}\left[N^2+\frac{g^2}{2V}\sum_{\bar{k}}\frac{f^2(\omega)}{\omega(\omega+\lambda)^2}\right] \\ &=\frac{1}{|h'(-\lambda)|}\left[1+\frac{g^2}{2V}\sum_{\bar{k}}\frac{f^2(\omega)}{\omega}\left[\frac{1}{(\omega+\lambda)^2}-\frac{1}{\omega^2}\right]\right] \\ =\frac{1}{|h'(-\lambda)|}&\frac{g^2}{2V}\sum_{\bar{k}}\frac{f^2(\omega)}{\omega}\left[\frac{1}{(\omega+\lambda)^2}-\frac{1}{\omega^2}+\frac{\lambda}{\omega^2(\omega+\lambda)}\right]=\frac{h'(-\lambda)}{|h'(-\lambda)|}=-1. \end{aligned}\right\} \quad (45)$$

The norm of the state $|V_{-\lambda}\rangle$ *is negative* and has been normalized to -1 in (43).

To make the formal discussion as simple as possible it will now be convenient to introduce a "metric operator" η[5] which has the following matrix elements for the free-particle states (11):

$$\langle n_V, n_N, n_k|\,\eta\,|n'_V, n'_N, n'_k\rangle = \delta_{n_V n'_V}\cdot\delta_{n_N n'_N}\cdot\delta_{n_k n'_k}\cdot(-1)^{n_V}. \quad (46)$$

For the physical states considered up till now, we have

$$\langle V|\eta|V\rangle = \langle N, \theta|\eta|N, \theta\rangle = 1, \tag{47}$$

$$\langle V_{-\lambda}|\eta|V_{-\lambda}\rangle = -1. \tag{48}$$

The non-diagonal elements of η between these states are all zero. The condition for an operator F to have real expectation values is no longer that it is hermitian, but rather that it is "self-adjoint" in the following sense:

$$F = F^{+} \equiv \eta F^{*} \eta. \tag{49}$$

A detailed examination of the foregoing calculations shows that the introduction of the indefinite metric will make the mathematics formally consistent if the adjoint operators ψ_V^{+}, ψ_N^{+}, and a^{+} are introduced in *Eqs.* (20)—(23) instead of the operators ψ_V^{*}, ψ_N^{*}, and a^{*}. This will make the Hamiltonian self-adjoint. On the other hand, the right-hand side of (23) will no longer have a definite sign, and a negative value of this c-number will not necessarily be inconsistent with the foundations of the theory. A special case of the expectation value of this anticommutator is examined in Appendix I.

If the transformation leading from the free particle states $|n\rangle$ to the physical states $|P\rangle$ is written as a matrix U,

$$|P\rangle = \sum_{|n\rangle} |n\rangle\langle n|U|P\rangle, \tag{50}$$

this matrix will not be unitary, but have the property

$$U^{+}U = \eta U^{*} \eta\, U = 1. \tag{51}$$

It is then important to decide whether the S-matrix of the theory also has the property (51) rather than being unitary. This expectation is not in contradiction with the result (40), as the operator η has only matrix elements $+1$ for the physical states involved there. *Eq.* (51) will have non-trivial consequences only if *physical* states with a non-positive norm are involved. The simplest process of this kind is the scattering of a θ-particle by a V-particle either in its normal state or in the state $|V_{-\lambda}\rangle$. In

the former case, it is to be expected that transitions of the V-particle to its new state take place and that these transitions possibly occur with "negative probabilities". The following paragraph is devoted to a discussion of these problems.

IV. The Scattering of θ-Particles by V-Particles.

We will now study eigenvectors of the total Hamiltonian of the form

$$|z\rangle = \sum_{\bar{k}} \Phi_1(\bar{k}) \cdot N \cdot |1_V, 0, 1_k\rangle + \sum_{\bar{k}, \bar{k}'} \Phi_2(\bar{k}, \bar{k}') |0, 1_N, 1_k, 1_{k'}\rangle. \quad (52)$$

If the eigenvalue is again called $m + \omega_0$, a straightforward calculation will yield the following equations for the coefficients in (52):

$$\Phi_1(\bar{k})(\omega - \omega_0 - \delta m) = \frac{1}{N^2} g \sqrt{\frac{2}{V}} \sum_{\bar{k}'} \Phi_2(\bar{k}, \bar{k}') \frac{f(\omega')}{\sqrt{\omega'}}, \quad (53)$$

$$\Phi_2(\bar{k}, \bar{k}')(\omega + \omega' - \omega_0) = \frac{g}{\sqrt{2V}} \cdot \frac{1}{2} \left[\Phi_1(\bar{k}) \frac{f(\omega')}{\sqrt{\omega'}} + \Phi_1(\bar{k}') \frac{f(\omega)}{\sqrt{\omega}} \right]. \quad (54)$$

In this case, we are not interested in the complete set of states (52), but will only try to find those special states corresponding to the scattering of a θ-particle by a V-particle in its normal state. In other words, we look for solutions to (53) and (54) where $\Phi_1(\bar{k})$ is of the form

$$\Phi_1(\bar{k}, \bar{k}_0) = \delta_{\bar{k}, \bar{k}_0} + \psi(\bar{k}, \bar{k}_0) \quad (55)$$

with outgoing waves only in $\psi(\bar{k}, \bar{k}_0)$ and in $\Phi_2(\bar{k}, \bar{k}')$. The last condition gives us

$$\left.\begin{aligned} \Phi_2(\bar{k}, \bar{k}', \bar{k}_0) = \frac{g}{\sqrt{2V}} \cdot \frac{1}{2} \cdot \Big[\Phi_1(\bar{k}, \bar{k}_0) \frac{f(\omega')}{\sqrt{\omega'}} \\ + \Phi_1(\bar{k}', \bar{k}_0) \frac{f(\omega)}{\sqrt{\omega}} \Big] \left[P \frac{1}{\omega + \omega' - \omega_0} + i\pi\delta(\omega + \omega' - \omega_0) \right] \end{aligned} \right\} \quad (56)$$

or, using (28) and (33),

$$\left.\begin{aligned} &\Phi_1(\bar{k}, \bar{k}_0)\, h(\omega_0 - \omega) \\ &= \frac{g^2}{2V}\frac{f(\omega)}{\sqrt{\omega}} \sum_{\bar{k}'}{}' \frac{f(\omega')\,\Phi_1(\bar{k}', \bar{k}_0)}{\sqrt{\omega'}} \left[P\frac{1}{\omega + \omega' - \omega_0} + i\pi\delta(\omega + \omega' - \omega_0)\right]. \end{aligned}\right\} \quad (57)$$

Contrary to the situation in paragraph II, it will not be possible to find an explicit solution to *Eq.* (57). However, this will not be necessary for our purpose, as it is sufficient here to investigate the properties of the *S*-matrix. This can be done with a method very similar to MØLLER's proof of the unitarity of the *S*-matrix if the Hamiltonian is hermitian.[6] Following MØLLER, we introduce the following quantity

$$\left.\begin{aligned} &U(\bar{k}, \bar{k}_0) \\ &= i\frac{g^2}{2V}\frac{f(\omega)}{\sqrt{\omega}} \sum_{\bar{k}'}{}' \frac{f(\omega')\,\Phi_1(\bar{k}', \bar{k}_0)}{\sqrt{\omega'}} \left[P\frac{1}{\omega + \omega' - \omega_0} + i\pi\delta(\omega + \omega' - \omega_0)\right]. \end{aligned}\right\} \quad (58)$$

From *Eq.* (57) we then conclude

$$\left.\begin{aligned} \sum_{\bar{k}}{}' \Phi_1^*(\bar{k}, \bar{k}_0)\, U(\bar{k}, \bar{k}_0') &= i\frac{g^2}{2V} \sum_{\bar{k}, \bar{k}''}{}' \frac{\Phi_1^*(\bar{k}, \bar{k}_0) f(\omega)}{\sqrt{\omega}} \frac{f(\omega'')\,\Phi_1(\bar{k}'', \bar{k}_0')}{\sqrt{\omega''}} \\ &\times \left[P\frac{1}{\omega + \omega'' - \omega_0'} + i\pi\delta(\omega + \omega'' - \omega_0')\right], \end{aligned}\right\} \quad (59)$$

$$\left.\begin{aligned} \sum_{\bar{k}''}{}' U^*(\bar{k}'', \bar{k}_0)\,\Phi_1(\bar{k}'', \bar{k}_0') &= -i\frac{g^2}{2V} \sum_{\bar{k}, \bar{k}''}{}' \frac{\Phi_1^*(\bar{k}, \bar{k}_0) f(\omega)}{\sqrt{\omega}} \frac{f(\omega'')\,\Phi_1(\bar{k}'', \bar{k}_0')}{\sqrt{\omega''}} \\ &\times \left[P\frac{1}{\omega + \omega'' - \omega_0} - i\pi\delta(\omega + \omega'' - \omega_0)\right]. \end{aligned}\right\} \quad (60)$$

The sum of (59) and (60) vanishes, as does the corresponding sum in MØLLER's paper, only if $\omega_0 < 2\mu$. In this case, $\omega + \omega'' - \omega_0$ never vanishes in the physical interval (μ, ∞) of the frequencies ω, ω'', and the transition $V + \theta \to N + \theta' + \theta''$ cannot occur on the energy shell. In the opposite case, $\omega_0 > 2\mu$, this transition causes a slight complication and we get

$$\left.\begin{aligned}&\delta(\omega_0-\omega_0')\Big[\sum_{\bar{k}}\Phi_1^*(\bar{k},\bar{k}_0)\,U(\bar{k},\bar{k}_0')+\sum_{\bar{k}}U^*(\bar{k},\bar{k}_0)\,\Phi_1(\bar{k},\bar{k}_0')\Big]\\ &=-\frac{\pi g^2}{V}\,\delta(\omega_0-\omega_0')\sum_{\bar{k},\bar{k}''}\Phi_1^*(\bar{k},\bar{k}_0)\,\frac{f(\omega)\,f(\omega'')}{\sqrt{\omega\omega''}}\,\Phi_1(\bar{k}'',\bar{k}_0')\,\delta(\omega+\omega''-\omega_0).\end{aligned}\right\}\tag{61}$$

With the aid of (55), (57), (58), and the vanishing of $h(0)$, we have

$$\psi(\bar{k},\bar{k}_0)\,h(\omega_0-\omega)=i\,U(\bar{k},\bar{k}_0).\tag{62}$$

We write the solution of (62) symbolically as

$$\psi(\bar{k},\bar{k}_0)=i\,\frac{U(\bar{k},\bar{k}_0)}{h(\omega_0-\omega)_+},\tag{63}$$

where the plus sign indicates that outgoing waves are to be chosen at the zeros of $h(\omega_0-\omega)$. Using this result, we can write (61) as

$$\left.\begin{aligned}&\delta(\omega_0-\omega_0')\,[U(\bar{k}_0,\bar{k}_0')+U^*(\bar{k}_0',\bar{k}_0)]\\ &+i\delta(\omega_0-\omega_0')\sum_{\bar{k}}U^*(\bar{k},\bar{k}_0)\,U(\bar{k},\bar{k}_0')\left[\frac{1}{h(\omega_0-\omega)_+}-\frac{1}{h(\omega_0-\omega)_-}\right]\\ &+\frac{\pi g^2}{V}\,\delta(\omega_0-\omega_0')\sum_{\bar{k},\bar{k}''}\Phi_1^*(\bar{k},\bar{k}_0)\,\frac{f(\omega)\,f(\omega'')}{\sqrt{\omega\omega''}}\,\Phi_1(\bar{k}'',\bar{k}_0')\,\delta(\omega+\omega''-\omega_0)=0.\end{aligned}\right\}\tag{64}$$

The second bracket of (64) can be rewritten in the following way:

$$\frac{1}{h(\omega_0-\omega)_+}-\frac{1}{h(\omega_0-\omega)_-}=-2\pi i\sum_{\varrho_i}\frac{1}{h'(\varrho_i)}\,\delta(\omega_0-\omega-\varrho_i),\tag{65}$$

where the summation is over all the roots of the equation $h(x)=0$. To simplify the notations further, we introduce the matrices

$$\langle V,\theta\,|\,R^{(1)}\,|\,V',\theta'\rangle=2\pi\delta(\omega-\omega')\,U(\bar{k},\bar{k}'),\tag{66}$$

$$\langle V_{-\lambda},\theta\,|\,R^{(2)}\,|\,V,\theta'\rangle=2\pi\delta(\omega+\lambda-\omega')\,\frac{U(\bar{k},\bar{k}')}{\sqrt{-h'(-\lambda)}},\tag{67}$$

$$\left.\begin{aligned} &\langle N, \theta', \theta'' \,|\, R^{(3)} \,|\, V, \theta \rangle \\ &= 2\pi\,\delta(\omega' + \omega'' - \omega)\,\frac{g}{\sqrt{2V}}\frac{1}{2}\left[\Phi_1(\bar{k}', \bar{k})\,\frac{f(\omega'')}{\sqrt{\omega''}} + \Phi_1(\bar{k}'', \bar{k})\,\frac{f(\omega')}{\sqrt{\omega'}}\right]. \end{aligned}\right\} \quad (68)$$

It can be shown that the sum over all the roots in (65) corresponding to the scattering states in paragraph II and the last term of (64) can be expressed in terms of the matrix $R^{(3)}$. Using this, we can write (64) as

$$\left.\begin{aligned} &\langle V, \theta \,|\, R^{(1)} + R^{(1)*} + R^{(1)*} R^{(1)} \,|\, V', \theta' \rangle \\ &-\langle V, \theta \,|\, R^{(2)*} R^{(2)} \,|\, V', \theta' \rangle + \langle V, \theta \,|\, R^{(3)*} R^{(3)} \,|\, V', \theta' \rangle = 0. \end{aligned}\right\} \quad (69)$$

It now follows that *the S-matrix of the Lee model* which, for the states considered in this paragraph, is given by

$$S = 1 + R^{(1)} + R^{(2)} + R^{(3)}, \quad (70)$$

is not unitary, because the probability for the transitions $V + \theta \to V_{-\lambda} + \theta'$ is to be counted negative in (69). As was suggested earlier, we see instead that the S-matrix has the property

$$\eta S^* \eta S = 1 \quad (71)$$

if the diagonal elements of η belonging to the states $|\, V_{-\lambda}, \theta \rangle$ are put equal to -1. It can also be shown that, if transitions *from* the states $|\, V_{-\lambda}, \theta \rangle$ are considered, a similar result will be obtained. The non-unitariness of the transformation (50) between the free-particle states and the physical states has its close correspondence in the non-unitariness of the S-matrix and makes the model unacceptable for physical reasons.

At this stage, one might ask if it is not possible to reinterpret the formalism with the aid of an argument similar to hole theory in quantum electrodynamics. One would then, *e. g.*, call the state $|\, V_{-\lambda} \rangle$ the vacuum, and the state which is here called the vacuum a state with one "anti-particle". However, it is easily seen that it is not possible to make the formalism consistent in this way as no reinterpretation along such lines will ever change the non-unitary properties of the S-matrix in (69).

The conclusion of our discussion is then that the model suggested by T. D. LEE is in accordance with the physical probability concept only if a cut-off is introduced and if the renormalized coupling constant is less than the critical value given by *Eq.* (34a). In this case, the constant N^2 lies between zero and one, as is expected from general arguments.[2] If there is no cut-off, the critical value of the coupling constant is zero.

CERN (European Organization for Nuclear Research)
Theoretical Study Division, Copenhagen, Denmark
and
Swiss Federal Institute of Technology,
Zürich, Switzerland.

References.

(1) T. D. LEE, Phys. Rev. **95**, 1329 (1954).
(2) This was first shown by J. SCHWINGER (unpublished) and has since been found by several authors. Cf. H. UMEZAHA and S. KAMEFUCHI, Progr. Theor. Phys. **6**, 543 (1951); G. KÄLLÉN, Helv. Phys. Acta **25**, 417 (1952); H. LEHMANN, Nuovo Cimento **11**, 342 (1954); M. GELL-MAN and F. E. LOW, Phys. Rev. **95**, 1300 (1954). Appendix II of the paper by LEE[1] also contains a proof of this theorem.
(3) The "free-particle states" introduced in this way are of the same kind as the free-particle states used, *e.g.*, in the Tamm-Dancoff method, but entirely different from the so-called "incoming (or outgoing) free-particle states" used in other formulations of relativistic field theories. As will be seen below, the Tamm-Dancoff approach gives the exact solution for this model.
(4) G. KÄLLÉN, Helv. Phys. Acta **25**, 417 (1952).
(5) An indefinite metric has earlier been used in quantum field theory by P. A. M. DIRAC, Proc. Roy. Soc. **A 180**, 1 (1942) in a connection which is not too different from the one used here. Cf. also W. PAULI, Rev. Mod. Phys. **15**, 175 (1943). A result of R. P. FEYNMAN, Phys. Rev. **76**, 749 (1949) particularly p. 756 implies the implicit use of an indefinite metric. Cf. W. PAULI, Prog. Theor. Phys. **5**, 526 (1950). An indefinite metric has also been used in quantum electrodynamics for a treatment of scalar photons. Cf. S. N. GUPTA, Proc. Phys. Soc. **53**, 681 (1950) and K. BLEULER, Helv. Phys. Acta **23**, 567 (1950).
(6) C. MØLLER, Dan. Mat. Fys. Medd. **23**, no. 1 (1945); ibid. **22**, no. 19 (1946).

Appendix I.

In this appendix, we show by an explicit calculation how the indefinite metric is able to account for the negative sign on the right hand of the anticommutator

$$\{\psi_V^+(\bar{p}), \psi_V(\bar{p}')\} = \delta_{\bar{p},\bar{p}'}\frac{1}{N^2}. \tag{A.1}$$

We compute the vacuum expectation value of this quantity for $g > g_{\text{crit}}$ and $p = p'$, and obtain

$$\langle 0 | \{\psi_V^+(\bar{p}), \psi_V(\bar{p})\} | 0 \rangle = \sum_{|z\rangle} |\langle 0 | \psi_V(\bar{p}) | z \rangle|^2 \langle z | \eta | z \rangle. \tag{A.2}$$

In (A.2) the summation is performed over any complete set of states. We can, *e.g.*, sum over all physical states and get contributions from the physical V-particle state, the state $|V_{-\lambda}\rangle$, and the scattering states $|N, \theta\rangle$. According to the result of paragraph II, these contributions will be

$$\left.\begin{aligned} \langle 0 | \{\psi_V^+(\bar{p}), \psi_V(\bar{p})\} | 0 \rangle &= 1 + \sum_{\bar{k}} |\beta(\bar{k})|^2 - \frac{1}{|h'(-\lambda)|} \\ &= 1 + \sum_{\bar{k}} |\beta(\bar{k})|^2 + \frac{1}{h'(-\lambda)}. \end{aligned}\right\} \tag{A.3}$$

If there were no indefinite metric, the right-hand side would be positive and larger than one. This is also the usual proof[2] that N^2 is a positive number less than one. In our case, the last term has a negative sign, and there is no general principle according to which the right-hand side of (A.3) has a definite sign. We shall now show explicitly that this quantity has the correct value given by *Eq.* (33). The proof is essentially based on the fact that the function $h(z)$ defined by (36) and extended to the complex plane by

$$h(z) = z\left[1 + \frac{g^2}{2V}\sum_{\bar{k}}{}' \frac{f^2(\omega)\, z}{\omega^3(\omega - z)}\right] \tag{A.4}$$

has zeros only on the real axis. Indeed, one has with $z = x + iy$,

$$Im\,\frac{h(z)}{z} = \frac{g^2}{2V} Im \sum_{\bar{k}}{}' \frac{f^2(\omega)\, z}{\omega^3(\omega - z)} = \frac{g^2}{2V}\sum_{\bar{k}}{}' \frac{f^2(\omega)\, y}{\omega^2[(\omega - x)^2 + y^2]}, \tag{A.5}$$

which is always different from zero for $y \neq 0$.

Moreover, passing to the limit $V \to \infty$, $h(z)$ transforms into an analytic function given by

$$h(z) = z\left[1 + \gamma z \int_{\mu}^{\infty} f^2(\omega)\frac{\sqrt{\omega^2 - \mu^2}\, d\omega}{\omega^2(\omega - z)}\right] \tag{A.4a}$$

$\left(\text{with the abbreviation } \gamma = \frac{g^2}{4\pi^2}\right)$ which is unique in the complex plane cut along the real axis from μ to positive infinity. The imaginary part of $h(z)$ is discontinuous at this part of the real axis, having opposite signs in the upper and the lower half plane, whilst the real part is continuous. To this ambiguity of $h(z)$ corresponds the circumstance that $z = \mu$ is a branching point of the square root type of $h(z)$ (*cf.* the explicit form given in Appendix II for the particular case $f(\omega) = 1$).

These properties of $h(z)$ enable us to evaluate the integral

$$\frac{1}{2\pi i}\int_C \frac{dz}{h(z)}$$

along the path illustrated in Fig. 1 in two different ways. We first remark that

$$\left.\begin{aligned}\sum_{\bar{k}}{}' |\beta(\bar{k})|^2 &= \gamma \int_{\mu}^{\infty} f^2(\omega)\sqrt{\omega^2 - \mu^2}\, d\omega \left[h^2(\omega) + \left(\frac{\pi\gamma}{\omega} f^2(\omega)\sqrt{\omega^2 - \mu^2}\right)^2\right]^{-1} \\ &= \frac{1}{\pi}\lim_{\varepsilon \to 0} Im \int_{\mu}^{\infty} \frac{d\omega}{h(\omega - i\varepsilon)}.\end{aligned}\right\} \tag{A.6}$$

We now divide the path C into two parts. One of them, C_1, starts from a point $z = R - i\varepsilon$ with arbitrarily large R and arbitrarily

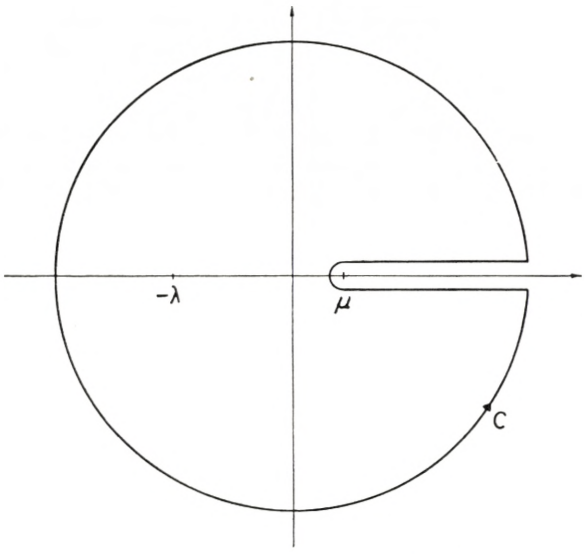

Fig. 1. The path C in *Eq.* (A. 9).

small, positive ε, goes below the real axis at a distance ε from it, encircles the point $z = \mu$ in the negative direction, returns above the real axis at a distance ε, and ends at the point $z = R + i\varepsilon$. The second part, C_R, is a large circle with radius R of which a small part near the positive real axis is omitted.

Performing the limiting process $\varepsilon \to 0$, in which the contribution of the circular arc of C_1 gets arbitrarily small, one first obtains

$$\lim_{\varepsilon \to 0} \int_{C_1} \frac{dz}{h(z)} = -2i \lim_{\varepsilon \to 0} Im \int_{\mu}^{\infty} \frac{dz}{h(z - i\varepsilon)} = -2\pi i \sum_{\bar{k}} |\beta(\bar{k})|^2. \quad \text{(A. 7)}$$

In this limit, the second part C_R of C goes over into the full circle C_R. The corresponding integral is easily evaluated with the aid of the asymptotic form of the function $h(z)$ (cf. the remarks before *Eq.* (43)) and gives

$$\int_{C_R} \frac{dz}{h(z)} = 2\pi i \frac{1}{N^2}. \quad \text{(A. 8)}$$

Hence, in this way we obtain

$$\frac{1}{2\pi i}\int_C \frac{dz}{h(z)} + \sum_{\bar{k}} |\beta(\bar{k})|^2 = \frac{1}{N^2}. \tag{A.9}$$

On the other hand, the absence of non-real zeros of $h(z)$ and a knowledge of the residues of $h(z)^{-1}$ at the poles $z = 0$ and $z = -\lambda$ permits a direct evaluation of the integral

$$\frac{1}{2\pi i}\int_C \frac{dz}{h(z)} = 1 + \frac{1}{h'(-\lambda)}. \tag{A.10}$$

Hence,

$$1 + \sum_{\bar{k}} |\beta(\bar{k})|^2 + \frac{1}{h'(-\lambda)} = \frac{1}{N^2}. \tag{A.11}$$

Eqs. (A.11) and (A.3) together give the expected result (A.1). If the coupling constant is less than the critical value, the integrand in (A.9) will have no pole at $z = -\lambda$, and the last term in (A.10) will be missing. Other matrix elements of the commutators and anticommutators can be treated in similar ways.

Appendix II.

In the *particular case of no cut-off* $f(\omega) = 1$, $1/N = 0$ the function $h(z)$ (cf. (A.4a)) can be expressed in closed form:

$$\left.\begin{aligned} h(\omega \pm i\varepsilon) = \omega + \gamma\left[\omega + \frac{\pi\mu}{2} - \sqrt{\omega^2-\mu^2}\left(\log\frac{\omega+\sqrt{\omega^2-\mu^2}}{\mu} \mp i\pi\right)\right] \\ \text{if} \quad \omega > \mu \quad \text{and} \quad \varepsilon > 0, \end{aligned}\right\} \tag{A.12}$$

$$h(-\lambda) = -\lambda + \gamma\left[-\lambda + \frac{\mu\pi}{2} + \sqrt{\lambda^2-\mu^2}\log\frac{\lambda+\sqrt{\lambda^2-\mu^2}}{\mu}\right] \quad \text{if} \quad \lambda > \mu. \tag{A.13}$$

Apart from the imaginary part in (A. 12) these two cases can also be represented by the same fomula if an absolute value is taken for the argument under the logarithm. For the third interval of the real axis, one has

$$h(\omega) = \omega + \gamma\left[\omega - \sqrt{\mu^2-\omega^2}\arcsin\frac{\omega}{\mu} + \frac{\pi}{2}\frac{\omega^2}{\mu+\sqrt{\mu^2-\omega^2}}\right] \text{ if } -\mu < \omega < \mu. \quad (A.14)$$

These expressions can be used to find the position of the root

$$h(-\lambda) = 0 \quad (A.15)$$

both in the weak and in the strong coupling limit. For weak coupling, we find from (A.13)

$$\lambda \approx \frac{\mu}{2} e^{1/\gamma} \quad \text{if } \gamma << 1, \quad (A.16)$$

which *excludes any kind of power series expansion.** In the strong coupling limit the application of (A.14) gives the following expression for the root:

$$-\omega \equiv \lambda \approx \frac{4}{\pi}\frac{\mu}{\gamma} \quad \text{if } \gamma >> 1 \quad (A.17)$$

with a possibility of an expansion in powers of γ^{-1}.

* This is of some interest in connection with the failure to obtain a power series with a finite radius of convergence by application of perturbation methods to some examples of renormalizable field theories. Cf. C. A. HURST, Proc. Cambr. Phil. Soc. **48**, 625 (1952); W. THIRRING, Helv. Phys. Acta **26**, 33 (1953); A. PETERMANN, Phys. Rev. **89**, 1160 (1953), and R. UTIYAMA and T. IMAMURA, Prog. Theor. Phys. **9**, 431 (1953).

Indleveret til selskabet den 15. april 1955.
Færdig fra trykkeriet den 17. september 1955.

Det Kongelige Danske Videnskabernes Selskab
Matematisk-fysiske Meddelelser, bind **30**, nr. 8

Dan. Mat. Fys. Medd. **30**, no. 8 (1955)

DEDICATED TO PROFESSOR NIELS BOHR ON THE OCCASION OF HIS 70TH BIRTHDAY

TOTAL CHARGES AND ELECTRON CAPTURE CROSS-SECTIONS OF FISSION FRAGMENTS IN GASES

BY

N. O. LASSEN

København 1955
i kommission hos Ejnar Munksgaard

Printed in Denmark.
Bianco Lunos Bogtrykkeri A-S.

1. Introduction.

In the present paper the results of some older measurements are given, the publication of which for various reasons has been delayed a few years. In the meantime a theoretical paper by BOHR and LINDHARD[1]—in the following cited as B. L.—has appeared, and since it affords a new basis for the treatment of the experimental results, a brief report of the latter seems appropriate.

2. Experimental Method.

As mentioned in a previous paper[2] — in the following referred to as I — fission fragments have been deflected in a magnetic field, and from the curvature of the paths the total charges were estimated. Fig. 1, which shows the experimental arrangement, is reproduced from I. Fission fragments from a strip-formed, thin uranium layer (11) passed through a movable slit (12). Through a second slit (16) covered with a mica foil they entered an ionization chamber. The deflection chamber, i. e. the space between the uranium layer and the mica window, could be evacuated or filled with a gas to a low pressure. Records were made for various positions of the intermediate slit, and in this way the deflection distribution was obtained. From the pulse sizes it was possible to distinguish between the two groups of fragments. For further details the reader is referred to I.

Fig. 2 shows some deflection distributions obtained. When the deflection chamber is evacuated no change of charge takes place in it, and the deflections will be determined by the charges with which the fragments leave the surface of the uranium layer or any solid covering foil. The widths of the distributions give

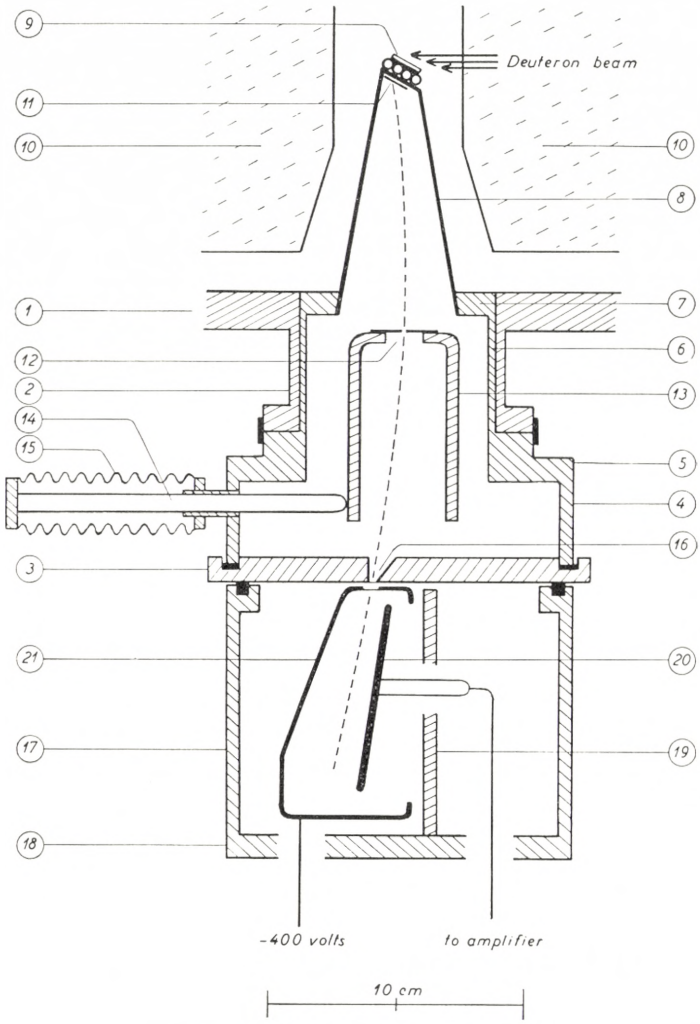

Fig. 1. Experimental apparatus.

information about the charge fluctuations in the solids. When a gas is admitted to the deflection chamber the fragments will, in collisions with the gas atoms, capture and lose electrons along the path, and rather quickly an equilibrium between loss and capture is established. The charge of each fragment will fluctuate around the average value, which will be reached close to the uranium layer if the gas pressure is high. In this case charge

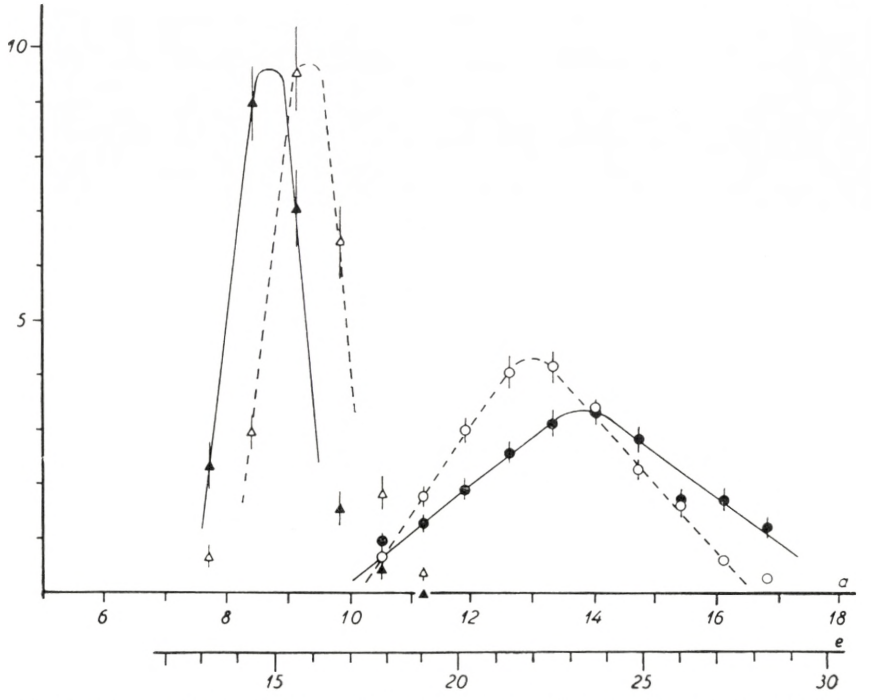

Fig. 2. Charge distributions for fission fragments. The abscissa a is the displacement of the middle slit in the deflection apparatus, given in mm. a is proportional to $\frac{e}{mv}$. Below is given the approximate charge scale (in units of the electronic charge) obtained by using the mean value for mv. Circles refer to fragments having traversed a thin *Be* layer and emerging into vacuum. Triangles refer to fragments emerging into argon at a pressure of 0.9 mm *Hg*. White and black points correspond to the light and heavy fragments, respectively.

exchanges will take place so frequently that the deflection will be determined almost solely by the average charge. The widths of the distributions obtained in this case are due mostly to the geometry of the apparatus. Of course, the gas pressure must not be so high as to cause appreciable stopping of the fragments inside the deflection chamber.

As illustrated by Fig. 2 the charges of fragments leaving solids were observed to be considerably higher than the equilibrium charges in gases. A fragment emerging into the gas will therefore start capturing electrons; if, however, the gas pressure is very low, the equilibrium charge will not be reached until a considerable part of the path in the deflection chamber is

traversed. The distance travelled by the fragments before charge balance is obtained will be a function of the pressure. Accordingly, when the pressure increases from zero the deflection distribution gradually changes (see I, figs. 4—9). Fig. 3 shows the most probable deflections, i. e. the abscissae a for the peaks of the deflection curves, as functions of the argon pressure in the deflection chamber. Neglecting the width of the momentum

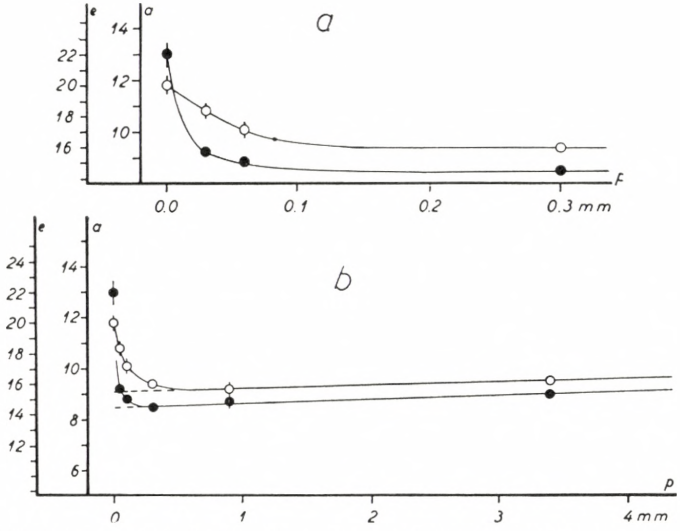

Fig. 3. Most frequent deflection a in mm plotted against the pressure of argon in mm *Hg* in the deflection chamber. Open and full circles refer to the light and heavy fragments, respectively.

distribution of the fragments, the deflections are proportional to the total charges e, the relation being $e = 1.70 \cdot a$, where e is measured in units of the electronic charge, and a in mm. The shape of the decreasing part of the curves for low pressures gives information about the rate of change of charge along the path and enables us to estimate the electron capture cross-sections of the fragments. Regarding the increase in charge for higher pressures, which illustrates the influence of excited states of the fragment ions on electron capture and loss cross-sections, the reader is referred to I (see also [3) 4)]) and to B. L., where a thorough discussion of these phenomena is given.

The estimation of the capture cross-section presents us with the following difficulties. Not only do the fragments capture

electrons in collisions with the gas atoms, but they will of course also in some collisions lose electrons, even when their charges are higher than the equilibrium values. We can measure directly only the difference $\sigma_c - \sigma_l$ between capture and loss cross-sections, and the fact that both cross-sections may be expected to vary with the instantaneous fragment charge further complicates the phenomenon. However, from the fluctuation distributions in Fig. 2 (the right-hand curves) it follows that, for charge values a few units higher than the balance charge, σ_l is negligible as compared with σ_c. Hence, by simply disregarding the loss processes and assuming the capture cross-section to be nearly constant, a first approximation giving the order of magnitude of the average value of the latter could be obtained. Meanwhile, in § 4 of this paper a different method giving a somewhat more exact estimation will be described.

3. Experimental Results.

In I, deflection-pressure curves were given for *A* and H_2. Similar curves were later measured in *He* and N_2. Also, curves were measured in the various gases for slower fragments. In order to slow down the fragments a mica foil of thickness 0.47 mg per cm^2 was placed over the uranium layer. The fragments passed obliquely through the foil. Denoting by v_1 and v_2 the

TABLE 1.
Equilibrium charges of fission fragments.

	Light fragment		Heavy fragment	
	$v_1 \sim 6\, v_0$	$v_1' \sim 5\, v_0$	$v_2 \sim 4\, v_0$	$v_2' \sim 3\, v_0$
H_2	15.8	13.4	12.6	9.2
He	14.1	11.7	11.6	8.6
N_2	15.1	13.8	13.9	10.5
A	15.4	13.7	14.6	10.4
U	20.0		22.0	
Mica		19.4*		18.0*

* In *I* the charges for fragments leaving mica with reduced velocities were erroneously given as 18.8 and 17.2 instead of 19.2 and 17.8. The small differences between the latter figures and those given in the table are due to uncertainty in the zero position for the deflection scale.

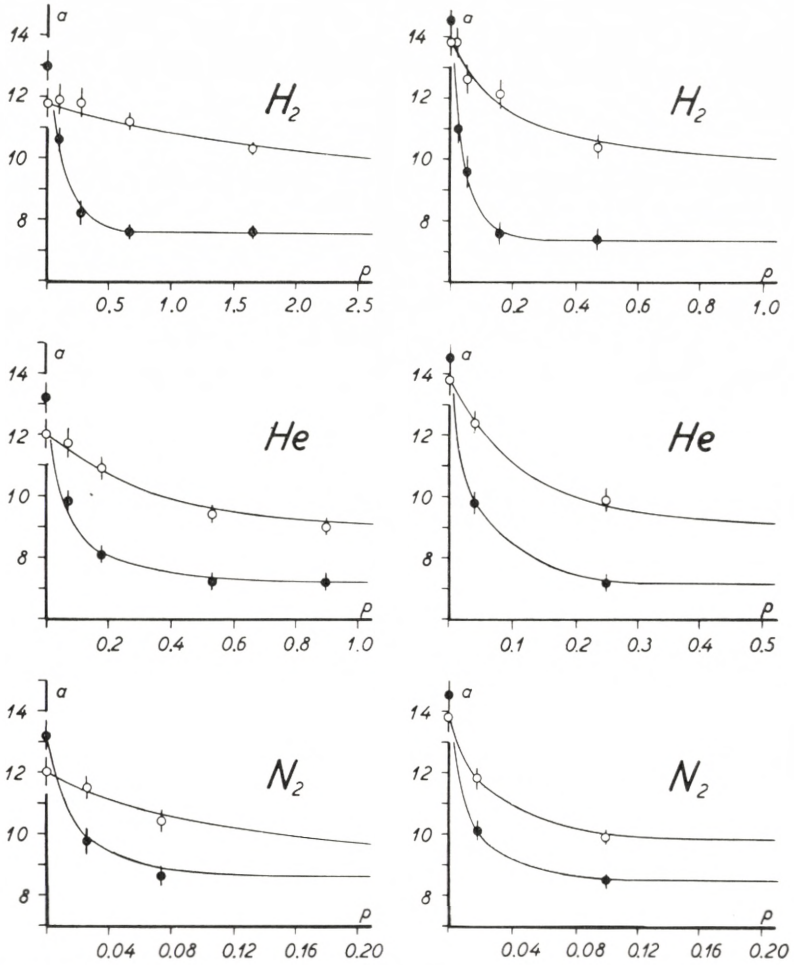

Fig. 4. Deflection vs. pressure curves in various gases. The curves to the left and right side refer to fragments with initial and reduced velocities, respectively. Open and full circles refer to the light and heavy fragments, respectively. The deflection is proportional to $\frac{e}{mv}$. Neglecting the momentum spread we have for fragments with full velocity, $e = 1.70 \cdot a$; for light and heavy fragments with reduced velocities, $e = 1.41 \cdot a$ and $e = 1.24 \cdot a$, respectively, a in mm, and e in units of the electronic charge.

initial velocities of the light and heavy fragments, respectively, and by v_1' and v_2' the velocities after their passage through the foil, one has

$$v_1' = 0.83 \cdot v_1$$
$$v_2' = 0.73 \cdot v_2.$$

The velocities thus happen to be close to 3, 4, 5 and 6 times v_0, the orbital velocity of the hydrogen electron. Fig. 4 gives the beginning of the curves for low pressures in the various gases. In all cases, at least two points corresponding to higher pressures were measured and from the latter points the equilibrium charges were determined. Table 1 summarizes the results. Within experimental errors the charge of the heavy fragment varies in all gases proportional to the velocity, in agreement with the approximative formula given by BOHR[5], $e = Z^{1/3} \cdot \frac{v}{v_0}$, Z being the nuclear charge number of the fragment. The same applies to the light fragment in H_2 and He while, in the heavier gases, the charge of the light fragment varies more slowly with velocity. This result, however, is also in conformity with theoretical expectations, as discussed by BOHR and LINDHARD.

4. Calculation of the Effective Capture Cross-Section.

The derivation of the effective capture cross-section may be illustrated, taking as an example the case of the heavy fragment with reduced velocity in N_2. The theoretical estimates are obtained in the way described by BOHR and LINDHARD. For the capture cross-section we have the formula (B. L. (4.5))

$$\sigma_c = \pi a_0^2 e^2 z^{\frac{1}{3}} \left(\frac{v_0}{v}\right)^3,$$

where z is the atomic number of the stopping gas (here 7), a_0 and v_0 are the radius and orbital velocity of the hydrogen atom in the ground state, and v is the fragment velocity (here $3\,v_0$). In Fig. 5 σ_c is plotted against e. From the experiment the equilibrium charge is known to be 10.5 and, hence, for this abscissa $\sigma_l = \sigma_c$. Assuming σ_l to vary proportionally to e^{-3} (cf. B. L.), the curves for σ_l and $\sigma_c - \sigma_l$, respectively, are drawn. For $e = 18$, the mean charge with which the fragments enter the gas, we find $\sigma_c - \sigma_l = 21\,\pi a_0^2$.

Consider, next, the empirical estimation of $\sigma_c - \sigma_l$. For simplicity, all fragments are assumed to start with $e = 18$.

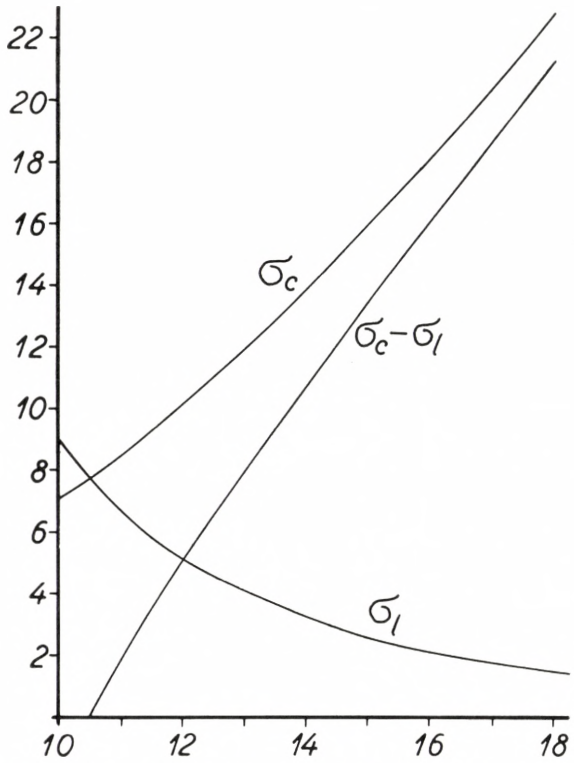

Fig. 5. Capture and loss cross-sections plotted against charge for the heavy fission fragments with $v = 3\,v_0$ in nitrogen at low pressure. Cross-section in units of πa_0^2, where $a_0 = \frac{h}{m\varepsilon^2}$, and the charge in units of the electronic charge ε.

From Fig. 5 it is seen that the effective capture cross-section varies almost linearly with charge. Thus, we assume

$$\sigma_e = \sigma_{18}\frac{e - 10.5}{18 - 10.5}, \qquad e = 18, 17, \ldots,$$

the balance charge being 10.5, and σ_e denoting the effective capture cross-section for a fragment with charge e. Then, for the mean charge $\bar{e}\,(x)$ at a distance x from the uranium layer, we have (cf. B. L. (2.5))

$$\bar{e}\,(x) = 10.5 + 7.5\, e^{-\frac{1}{7.5}\sigma_{18} n x} = 10.5 + 7.5\, e^{-\frac{1}{7.5}\frac{x}{\lambda}},$$

TABLE 2.

Effective capture cross-section $\sigma_c - \sigma_l$ in units of πa_0^2.

	Light fragment				Heavy fragment			
	$v \sim 6\, v_0$		$v \sim 5\, v_0$		$v \sim 4\, v_0$		$v \sim 3\, v_0$	
	exp.	th.	exp.	th.	exp.	th.	exp.	th.
H_2	0.06 ± 0.02	0.04	0.8 ± 0.3	0.13	1.6 ± 0.6	0.9	8 ± 2	3.5
He	0.7 ± 0.3	0.1	$4 \pm 2.$	0.55	9 ± 2	3.7	17 ± 5	15
N_2	1.4 ± 0.5	1.6	8 ± 4	2.7	15 ± 8	13	20 ± 6	21
A	2.5 ± 0.8	2.7		6	24 ± 8	18		30

where n is the number of atoms of the stopping gas per cm^3 and λ is a quantity which may be called the effective mean free path for electron capture by fragments with $e = 18$.

Suppose the gas pressure has such a value p_1 mm Hg that $\lambda = 10$ cm. The function $\bar{e}\,(x)$ may be calculated and, from the known variation of the magnetic field, the deflection of a fictitious fragment travelling with just the mean charge may be found by numerical integration. The deflection value so obtained is assumed to coincide with the peak for the actual deflection distribution, an assumption which is presumably not much in error. By calculating for various pressures, the whole deflection-pressure curve is obtained, the pressure being given in units of p_1. This curve is shown in Fig. 4, p_1 being chosen equal to 0.0008 mm Hg, which fits best with the experimental point. This value corresponds to $\sigma_{18} = 20\, \pi a_0^2$, a result which is in close agreement with the theoretical estimate.

In Table 2 are given the experimental results for $\sigma_c - \sigma_l$ in the various gases and for the different velocities, all estimates being based on the assumption that $\sigma_c - \sigma_l$ varies linearly with charge. The values corresponding to velocities $6\, v_0$, $5\, v_0$, $4\, v_0$, and $3\, v_0$ refer to charge values 20, 19.4, 22, and 18, respectively. For comparison are given theoretical values, kindly estimated by Mr. J. LINDHARD in the way described in B.L. The agreement is satisfactory for the values referring to nitrogen and argon, whereas, in the lighter gases most of the experimental values are rather high as compared with the theoretically computed figures. Since the cross-sections are small in the lighter gases, it is clear that possible impurities in the latter would just tend

to increase the cross-sections. However, great care was taken to avoid impurities; before the experiments the deflection chamber was always filled three times and evacuated carefully between the fillings; during the experiments the chamber was connected to a liquid air trap in order to remove vapors. The tank helium was known to contain three per cent nitrogen, but it was slowly filtered through charcoal in liquid air and should thus be very pure. The tank hydrogen was said to contain less than 0.1 per cent impurities. Also, the small experimental value obtained for $\sigma_c - \sigma_l$ of the light fragment with $v = 6\, v_0$ in H_2 seems to show, quite apart from the good agreement with the theoretical figure, that the possible impurities are much too small to influence essentially the other values for $\sigma_c - \sigma_l$ in hydrogen. As seen, the experiments indicate for the light fragment in H_2 a very strong velocity dependence of the effective capture cross-section. In *He* $\sigma_c - \sigma_l$ is found experimentally to be considerably higher than the theoretical estimate, as well for $v = 6\, v_0$ as for $v = 5\, v_0$, whereas the ratio between the cross-sections corresponding to the two velocities is in agreement with the theory. For the heavy fragment, in H_2 and in *He*, the differences between experimental and theoretical values are less pronounced.

The present work was carried out at the Institute for Theoretical Physics in Copenhagen and the author wishes to express his heartiest thanks to the Director of the Institute, Professor Niels Bohr, for his great interest in the work and his continued encouragement. My thanks are also due Professor J. C. Jacobsen for helpful advice. Furthermore, I wish to thank J. Lindhard, mag. sc., for valuable discussions.

References.

1) N. Bohr and J. Lindhard: Dan. Mat. Fys. Medd. **28**, no. 7, 1954. In the paper referred to as B.L.
2) N. O. Lassen: Dan. Mat. Fys. Medd. **26**, no. 5, 1951. In the paper referred to as I.
3) — Dan. Mat. Fys. Medd. **26**, no. 12, 1951.
4) — Thesis. On The Total Charges and The Ionizing Power of Fission Fragments. Munksgaards Forlag, Copenhagen 1952.
5) N. Bohr: Dan. Mat. Fys. Medd. **18**, no. 8, 1948.

Indleveret til selskabet den 1. juni 1955.
Færdig fra trykkeriet den 3. oktober 1955.

Det Kongelige Danske Videnskabernes Selskab
Matematisk-fysiske Meddelelser, bind **30**, nr. 9

Dan. Mat. Fys. Medd. **30**, no. 9 (1955)

DEDICATED TO PROFESSOR NIELS BOHR ON THE OCCASION OF HIS 70TH BIRTHDAY

QUANTITATIVE BETA TRACK AUTORADIOGRAPHY WITH NUCLEAR TRACK EMULSIONS

BY

HILDE LEVI AND ANNE S. HOGBEN

København 1955
i kommission hos Ejnar Munksgaard

Printed in Denmark.
Bianco Lunos Bogtrykkeri A-S.

The applicability of the nuclear track plate NTB-2 (of Eastman Kodak, Rochester, N.Y.) to quantitative beta track autoradiography has been investigated. A constant source of C-14 beta particles was brought in contact with the emulsion and the number of tracks registered per unit area of the plate was counted. The counting results obtained by four different investigators evaluating a total of 50 images were subjected to statistical analysis. The reproducibility of the track count was studied, both with respect to the counting ability of one and the same investigator repeatedly confronted with a given track pattern, and to the evaluation of the same pattern by different investigators. A statistical analysis of the counting results permits one to estimate the homogeneity of the emulsion in small areas of the plates, to compare the homogeneity of plates from the same batch, and their sensitivity from batch to batch. The efficiency of the plates and the effect of storage conditions have likewise been investigated. The contributions of various sources of error to the uncertainty of the final counting results were estimated.

Introduction.

In 1950, it was shown by Boyd and Levi[1] that beta particles of low energy, e. g., from radio-carbon or radio-sulphur, register as tracks in nuclear emulsions of the type NTB-2, manufactured by the Eastman Kodak Company in Rochester, N.Y. At that time, this was the only photographic emulsion commercially available which would register low energy electrons as tracks. This offered a possibility for improvement of the sensitivity and the resolution of existing autoradiographic techniques. In random grain autoradiography with low energy beta particles, on the average one grain is made developable per particle traveling through a thin emulsion. Therefore, at low level of activity, the blackening of the emulsion has to be established by grain counting. In the case of the NTB-2 emulsion, beta particles entering the emulsion produce tracks which are more easily recognized and counted than are single grains.

The mentioned authors floated sections of tissue containing a C-14 labeled compound on NTB-2 plates and observed—after suitable exposure—beta tracks in the emulsion under the tissue. The number of tracks per unit area under a section of a given

thickness was counted and, besides, the amount of C-14 present in the tissue was determined by means of an ionization chamber. The track count was found to be in satisfactory agreement with the result of ionization chamber measurements on samples of the same tissue. These findings suggested that track autoradiography might be a means of localizing the labeled compounds within the tissue or the individual cells quantitatively and with a resolution higher than that obtained in a random grain autoradiogram on an NTB plate. However, it remained to investigate how high a resolution can be obtained in a beta track autoradiogram; evidence had to be presented that track counting offers a reproducible and quantitative measure of the amount of tracer element present in the tissue under investigation.

In order to verify the applicability and reproducibility of the method, standard conditions for exposure and processing of the plates, and a reproducible technique of track counting under the microscope had to be established. The development of the counting technique brought to our attention so many points of significance that some details of the method are described in the following.

After a number of unsuccessful attempts at preparing a suitably thin and homogeneously active standard which could easily be handled, it was decided to use as a standard a piece of a C-14 polystyrene foil (manufactured by the A.E.C. in Oak Ridge), containing 0.6 microcuries of C-14 per sq. cm. The foil weighs 28 mg/cm^2 and thus represents an "infinitely thick layer" of C-14.

Standard Exposure and Processing.

About 1 sq. cm. of the polystyrene foil was used as a standard in all cases described below. This standard was laid on the NTB-2 plates and covered with a piece of clean glass on which a 50 g load was placed. The exposure time was either 50 min., 100 min. or 150 min. throughout, because exposure for more than 150 min. would give rise to too many tracks per field (cf. below).

The NTB-2 plates were developed for 8 min. in a D-19 developer at 19—20° C, then fixed for 30 min. in 30 % hypo, and washed for approximately one hour in tap water. The plates

were rinsed in distilled water and dried in a horizontal position at room temperature. Finally, the exposed area on each plate was covered with balsam and a cover glass, 150—175 microns thick.

Track Counting Technique.

The tracks were observed in a Leitz Ortholux microscope, transmitted light, with 10 × oculars and a 45 × objective. One ocular contained a square net micrometer (eyepiece reticulum) subdivided into a hundred small squares. The field circumscribed by the square net was in most cases 125 × 125 square microns.[1]

It was found impossible accurately to localize a field to be counted by vernier readings of the movable stage alone. If not characterized by typical landmarks, a given field could not be found again with certainty after the plate had been moved on the stage. Also, there was no definite proof that the position of the plate under the microscope remained exactly the same during counting of a given field. In order to compare, for example, the counts obtained by different investigators, it was found necessary to establish accuracy of placement within a few microns and, therefore, characteristic landmarks were used as points of reference. Every plate registers a few alpha tracks, the end points of which may serve for exact orientation. Since the plastic box used for exposure was contaminated with traces of an alpha emitter, as a rule about 10—20 alpha tracks were registered within 1 sq. cm. of the image (and a similar amount in other areas of the plates).

Before the fields to be counted were chosen, the boundary of the image was measured up on the stage of the microscope and a ten times enlarged picture of the image was drawn. The positions of a number of alpha tracks located in the central part of the image (at least 500 microns from the edge) were chosen for orientation of the fields to be counted. One end of an α-track can be brought to coincide with one corner of the square reti-

[1] In the course of this study, three different microscopes of the same type, and with corresponding optics, were used. It was discovered later that the field sizes were not identical. Uncertainty as to the actual field size during counting of all series–1 plates has caused us to omit this series in the comparison between batches.

culum to an accuracy of 1 micron in either direction. In the same way, background fields situated several millimetres away from the image and to all four sides of the image, were identified by landmarks.

The choice of fields for counting within a given image is random, as the occurrence of the landmarks is random. The question remains, however, whether each landmark should serve to locate one field or whether—at the most—it can be used to describe the position of four adjacent fields. The result of different groupings is discussed below.

The most convenient and reproducible method of counting is to subdivide the field under observation into ten rows of ten small squares and to count one row at a time. If the number of tracks per field is low—as in a background field or after a 50 min. exposure of our standard—it will take an experienced investigator between 5 and 15 min. to count one field. As the number of tracks increases, it becomes increasingly cumbersome to count (15—30 min./field with 50—100 tracks/field). Also, at high track density, it becomes very difficult to disentangle the complex track patterns.

Identification of a "Track".

Electron tracks in photographic emulsions are characterized by their irregular zig-zag path. Moreover, it is typical of these tracks that the grain spacing in the beginning of the tracks is wider than towards their end, when the particles have given off most of their energy by collision. The tracks observed in the NTB-2 emulsion consisted on the average of six grains, tracks up to ten grains long did occur.

A photographic emulsion always shows some developed grains—fog or background—even if the emulsion has not been exposed to irradiation from a radioactive substance. Some of this background which is due to cosmic radiation will appear as electron tracks similar to those produced by carbon-14 betas. Fog due to chemical or mechanical effects, however, appears as randomly distributed grains. With increasing fog, there is thus an increasing probability for three or more grains to fall "in a line", simulating a track. It was decided to consider four grains in a line a minimum requirement for the track pattern. Thereby,

the much more frequent accidental groups of three grains are not included in the track count. On the other hand, the shortest tracks produced by low energy beta particles will thus not be counted. Because of the shape of the energy distribution curve for the beta spectrum of radio carbon, the track count will be only a few per cent too low due to the mentioned minimum requirement.

Outline of Special Problems.

Besides the efficiency of the NTB-2 plates, i. e., the number of tracks registered from a source of given strength, and the relation between track count and exposure time, it is of paramount interest to investigate the reproducibility of the track count on different plates from the same batch and from different batches. Finally, external conditions during storage may affect the properties of the plates and ought to be investigated.

Obviously, however, an interpretation of results obtained by visual counting of tracks under the microscope must be based on a careful investigation into the reproducibility of the data obtained in repeated countings of a given field by one and the same investigator, and by different investigators confronted with the same field. This check was made throughout the present study; the results obtained were considered so important that they are presented in some detail. They demonstrate very clearly that the study of the properties of the plates is intimately connected with a study of the counting ability of the investigator. An attempt has been made to determine the relative sizes of the errors arising from the various sources.

Results.

Eastman Kodak plates of the type NTB-2 from five different factory batches, received in five shipments over a period of two years, were studied. The batches are designated, in order of receipt, series 1 to series 5.

The analysis of the results of track counts (see Tables I and II) is based on the counting data of four different investigators, denoted as A-B-C- and D. Only one of them, investigator B, has counted fields from all images included in the study. Investigators

TABLE 1.

Counting Data from Plates of Series 1 and 2 (cf. the text on pp. 13 and 14).

1 Series	2 Plate	3 Days between arrival and exposure	4 Exposure time in min.	5 Number of exposed fields counted	6 Mean exposed count per $(100)^2\,\mu^2$	7 Net mean count per $(100)^2\,\mu^2$	8 S. E. of net mean count per $(100)^2\,\mu^2$
1	10	2	50	13	32.9	22.0	2.97
1	15	3	50	28	34.5	24.5	1.19
1	3	1	100	32	65.4	51.0	3.29
1	13	3	100	36	67.1	55.5	4.77
1	5	1	100	7	85.3	69.4	5.12
1	17	4	100	6	74.5	62.1	3.72
1	18	4	100	7	88.4	78.8	4.94
1	19	4	100	5	69.4	57.7	4.73
1	11	2	150	24	112.0	99.3	7.49
1	12	2	150	6	101.1	88.4	5.15
2*	19	2	50	12	27.2	22.8	1.26
2*	23	11	50	12	19.8	14.3	0.92
2*	18	2	100	12	38.7	33.8	1.97
2*	34	9	100	12	42.3	34.3	0.83
2*	32	7	150	12	43.9	38.3	1.64
2*	36	11	150	12	45.3	38.0	1.46
2†	37	18	50	12	34.3	24.0	1.02
2†	42	24	50	12	35.0	23.9	1.07
2†	29	14	100	12	60.0	51.2	2.66
2†	42	24	100	12	49.0	38.0	1.32
2†	41	23	150	12	78.5	67.5	2.22
2†	42	24	150	12	66.7	55.7	1.69

* undried. † dried.

Column 1: serial number; the series are designated in order of receipt.
Column 2: plate number; the plates are designated in order of use.
Column 3: time in days which elapsed from arrival of the plates in Copenhagen till their actual use.
Column 4: exposure time in minutes. Multiple exposure plates have been exposed for varying lengths of time in different areas of the same plate (cf. p. 15).
Column 5: number of fields counted within the image.
Column 6: mean number of tracks counted per $(100)^2\mu^2$ of the image; this figure equals the mean of the track counts actually obtained, divided by the ratio: field size in sq. microns/$(100)^2$ sq. microns.

$$\text{Mean of } X_i = \overline{X}_i = \frac{\Sigma^n X_i}{n}.$$

Column 7: net mean track count per $(100)^2\mu^2$; this figure equals the mean track count per $(100)^2$ sq. microns of the image minus mean track count per $(100)^2$ sq. microns from background areas of the same plate.
Column 8: standard error of the net mean track count per $(100)^2\mu^2$. Standard error = s (of net mean count per $(100)^2$ sq. microns)

$$\text{S. E.} = \sqrt{s^2_{\substack{\text{mean exp. count} \\ \text{per } (100)^2\,\mu^2}} + s^2_{\substack{\text{mean background count} \\ \text{per } (100)^2\,\mu^2}}}$$

$$\text{Variance of the mean of } X_i = s^2_{\overline{X}_i} = \frac{s^2_{X_i}}{n}.$$

TABLE 2.

Counting Data from Plates of Series 2–5, as depicted in Fig. 1.

1 Series	2 Plate	3 Days between arrival and exposure	4 Exposure time in min.	5 Number of exposed fields counted	6 Mean exposed count per $(100)^2\ \mu^2$	7 Net mean count per $(100)^2\ \mu^2$	8 S. E. of net mean count per $(100)^2\ \mu^2$
2†	37	18	50	12	34.3	24.0	1.02
2†	42	24	50	12	35.0	23.9	1.07
2†	29	14	100	12	60.0	51.2	2.66
2†	42	24	100	12	49.0	38.0	1.32
2†	41	23	150	12	78.5	67.5	2.22
2†	42	24	150	12	66.7	55.7	1.69
3	A 9	3	50	10	15.6	12.3	1.22
3	A 7	2	100	10	33.6	30.1	1.09
3	A 11	3	100	10	36.1	30.3	1.52
3	A 10	3	150	10	40.6	37.9	1.82
3	B 1	15	50	10	17.3	14.1	1.92
3	B 5	43	50	10	19.8	16.2	1.24
3	B 8	59	50	10	21.4	15.5	0.85
3	B 3	22	100	10	42.6	39.0	1.85
3	B 6	43	100	10	47.0	40.5	1.46
3	B 2	16	150	10	60.0	55.4	2.00
3	C 2	4	50	10	16.1	12.3	0.87
3	C 6	9	50	10	19.5	16.8	0.90
3	C 8	10	50	10	16.4	13.9	1.24
3	C 9	15	50	10	16.5	14.6	0.70
3	C 12	37	50	10	18.2	14.9	1.31
3	C 2	4	100	9	33.9	30.1	1.45
3	C 8	10	100	10	29.0	26.5	1.85
3	C 11	22	100	10	29.0	27.4	1.10
3	C 6	9	150	10	52.4	49.7	2.27
3	C 10	16	150	10	53.8	51.1	1.82
4	5	8	50	10	16.5	13.0	0.96
4	6	9	50	10	14.8	12.4	0.75
4	5	8	100	10	29.6	26.0	2.13
4	6	9	100	10	30.0	27.6	1.69
5	5	4	50	10	15.9	13.3	1.29
5	8	5	50	10	14.0	11.9	1.44
5	6	5	50	10	17.1	15.1	0.85
5	6	5	100	10	26.5	24.5	1.86

† dried.

In computing the standard error of the net mean track count for plates from batches where there is a tendency for contiguous fields to yield similar track counts, the variance of the mean exposed count and of the mean background count was estimated from the variance of the means of groups of contiguous fields (exposed or background). The standard errors are given here for descriptive purposes, only. In view of suggested differences between different plates of a batch and between different batches, they are not considered to be valid estimates of the error of the respective mean track counts.

C and D were students who did not participate in the research work proper, but were trained for the special task of track counting. The purpose of their participation in the counting was for the present authors to gain an impression of the difficulties inherent in this work, especially because it requires personal judgement and a certain consistency of interpretation.

Reproducibility of counting results.

In order to estimate what proportion of the variability observed in the field counts of one investigator is attributable to uncertainty of evaluating a given track pattern, investigator B recounted all ten selected fields on each of four different images (series 3) after a lapse of several months. This investigator also recounted a single field from each of two exposed areas five times on five different days to provide an additional check on her counting variability.

The variance of the two track counts of the same fields was computed for each of the ten fields from each of the four images recounted, and the mean of these ten variances from a given image was calculated. The results provide estimates of investigator B's average variation in evaluating the track pattern at the exposure levels 50 — 100 — 150 minutes, respectively. The average variances found represent, at the 50 min. exposure level, 4 % of the variance of counts of different fields, 6 % at the 100 min. exposure level, and 10 % at the 150 min. exposure level. Thus, the variance of recounting given track patterns increases with increasing number of tracks per field, not only as an absolute value, but also as a percentage of the variance of different fields.

The estimated standard deviation of recounts of fields, the square root of the average variance discussed above, appears to be a fairly constant percentage of mean track count: 4.5 % on the 50 min. exposure level, 4.4 % at the 100 min. exposure level, and 3.5 % at the 150 min. exposure level.

The track counts of the single fields counted on five different days yield variances smaller than any of the average variances of two counts of the same field reported above. Thus, these limited observations provide no evidence of a day to day variance greater than that included in the estimates given above.

No recounts by the other three investigators are available. Since the variance of the field counts is of the same order of magnitude for all four investigators, it is unlikely that the recount variation of the other investigators (especially A) is vastly different from that of B.

The two most experienced investigators, A and B, showed, on the whole, very good agreement. The data give little evidence of any overall tendency of one of these investigators to count, on the average, higher or lower than the other.[1] For seven images on plates of series 3, on each of which the same ten fields were counted by both A and B, the difference between the mean track count of A and of B, in per cent of mean track count, averages less than 4 %. There is no tendency for the percentage difference to increase with increasing track count. This close agreement between mean counts of A and B is confirmed by the data from the other series.

For the eighteen sets of paired counts, the standard deviation of the difference between the counts of the same field by A and B ranges from 2 % to 12 % of the mean track count. On the average, the standard deviation of the differences between A and B is only about 50 % higher than the standard deviation of the differences between two counts of the same field by investigator B.[2]

To *summarize:* for an experienced investigator, the variation in repeated evaluations of the same track pattern at different

[1] Heterogeneity of variance was indicated by the data even within a single exposure level, so the data from different images could not be pooled. For plates of the first two series, the fields counted by both A and B vary in number from image to image. For seven images from series–3 plates, the number of fields from each image counted both by A and B is ten. The mean of the three mean differences was tested by the statistic t. For the three paired means at 50 min., t is + 0.4, at 100 min., t is — 1.3. The single mean difference at 150 min. is positive.

[2] Comparison of the counts obtained by B and D on the first group of plates counted by D (largely series 2) reveals a pronounced and consistent tendency of D to count (on the average 6 %) lower than B. This tendency is not evidenced on plates counted subsequently. As investigator D gained experience, he evaluated the track pattern differently so as to obtain higher counts. Investigator D never attained as good agreement with B as A exhibited during the entire course of the study.

Investigator C counted only plates of series 1. Counts of three investigators, A, B, and C, are available for nine plates. The mean counts of C seldom show good agreement with those of A and B. Investigator C's mean counts differ on the average from those of A and B by two to three times as much as their mean counts differ from each other.

No comparative data are available between investigators C and D.

times appears to be small. The variance of recounting represents an increasing proportion of the investigator's variation in counts of different track patterns from an image as the average number of tracks per field increases; but even at 150 min. exposure (ca. 80 tracks per field), the variance of recounts accounts for only 10 % of the variance of counts of different fields. The standard deviation of recounts—which is the pertinent statistic in terms of error—shows, however, no tendency to increase with increasing track count, and represents only about 4 % of the track count.

Two of the four investigators showed on the whole very good agreement on counts of the same fields. For the great majority of images, there is no consistent tendency for one of these investigators to count on the average higher or lower than the other, and their counts of the same field differ by only about 1.5 times as much as do two counts of the field by the same investigator.

Homogeneity of the plates.

When a number of fields within the image from a standard source are counted, the scattering of the results around a mean value is a function of (A) the statistical fluctuation in the number of disintegrations actually taking place per time unit, (B) the uncertainty of evaluation as discussed above, and (C) the error in the reproduction of the track pattern, which includes the effect of inhomogeneity within a plate. If fields from images on different plates are considered, lack of homogeneity from plate to plate within the same batch, and also variations in sensitivity from batch to batch would introduce further variability. Homogeneity in this sense is synonymous with uniformity of sensitivity. If the photographic emulsions are homogeneous, any unit area at one end of a plate will be as sensitive to incident radiation as a corresponding area at the other end of the same plate, or on a different plate from the same batch, or from another batch.

(i) *Homogeneity within a plate.*

Striking inhomogeneity within one and the same plate was observed on plates of series 1 and on some plates from later

series. On five of the nine plates of series 1, a large number of exposed and background fields was counted in groups of four contiguous fields about a common center (the landmark, cf. p. 5). Scanning of the individual track counts of a given investigator from a given image revealed a striking tendency for contiguous fields to yield similar track counts, which was confirmed by analysis of variance. This phenomenon appears consistently in counts from images of this series and, to some extent, in the background counts as well.

In series 2—5, the exposed fields were counted in groups of two contiguous fields, the background fields usually in groups of four.

The majority of the plates of series 2 show no tendency for contiguous fields to yield similar track counts. However, in this series and also in series 4 and 5, a few sets of counts evidence this grouping effect to a "significant" degree.[1] By contrast, the extensive data from series 3 give no indication of the existence of such a grouping effect. The corresponding background counts suggest that contiguous fields may be more similar than fields in widely separated areas of the plate. The data, however, are inconclusive.

On the basis of the actual counting experience, the investigators maintain that subjective factors cannot explain this tendency for contiguous fields to yield similar track counts. During the counting of plates of series 1, the only batch in which the phenomenon is consistently present, areas as large as a quarter of a field were frequently observed to be completely devoid of tracks. In later series, this phenomenon was observed in rare cases, only. Wherever this grouping effect exists, a lack of homogeneity within very small areas of the plate is suggested.

In the light of these findings, it seems advisable to count separately located fields rather than groups of contiguous fields in order to obtain a maximum amount of information from a given amount of counting labor. Therefore, in series 2—5, the

[1] For four of the five images from series 1, the counts of investigator B yield variance ratios (F) which are significant at the 5 % level of confidence or better. The same is true of two of the five sets of background counts. In addition, three out of twenty-two sets from series 2 (two of which occur on the same plate), one out of six sets from series 4, and one out of seven sets from series 5 yield F ratios which are significant at the 5 % level of confidence. For all of these series, statistical analyses of the counting data of the other investigators give similar results.

exposed fields were counted in groups of two contiguous fields, the backgrounds usually in groups of four.

(ii) *Homogeneity of plates from the same batch.*

In order to study the homogeneity—or uniformity of sensitivity—from plate to plate of the same batch, the net mean track counts from all images of the same exposure level were compared.

The data from series 2 (dried and undried groups considered separately) suggest that within this batch some plates, or areas of them, differ from others in such a way that they record as tracks differing percentages of the radiation received.[1]

Because of variations in the handling of plates of series 3 and other considerations, statistical analysis of this batch of plates is not informative.

Series 4 and 5 comprise only a small number of plates and no evidence of the existence of differences between plates within these batches was found.

(iii) *Sensitivity from batch to batch.*

Figure 1 presents the net mean track counts of investigator B from all images studied, except those from plates of series 1[2] and series 2 undried. The means from plates of series 2 dried are consistently higher at every exposure level than the means from plates of series 3, 4, and 5.

This phenomenon is confirmed by the data from the other investigator (D).

This finding indicates that different batches of plates may differ appreciably in average sensitivity, and it seems not justified to assume that NTB-2 plates from different batches will yield the same number of tracks per field for a given exposure to the same source of radiation.

[1] Counts from images on two different plates are available at the three exposure levels in each group (dried and undried). In each case, the mean difference was tested by the statistic t. For investigator B, three of the six mean differences (at 50 min. in the undried group, at 100 min. and 150 min. in the dried group) are significant at the 2 % level of confidence. Counting data from the other investigator who counted this series yield almost identical results. The possibility of a somewhat reduced reliability of this test when applied to these data must be considered.

[2] Cf. footnote on p. 5.

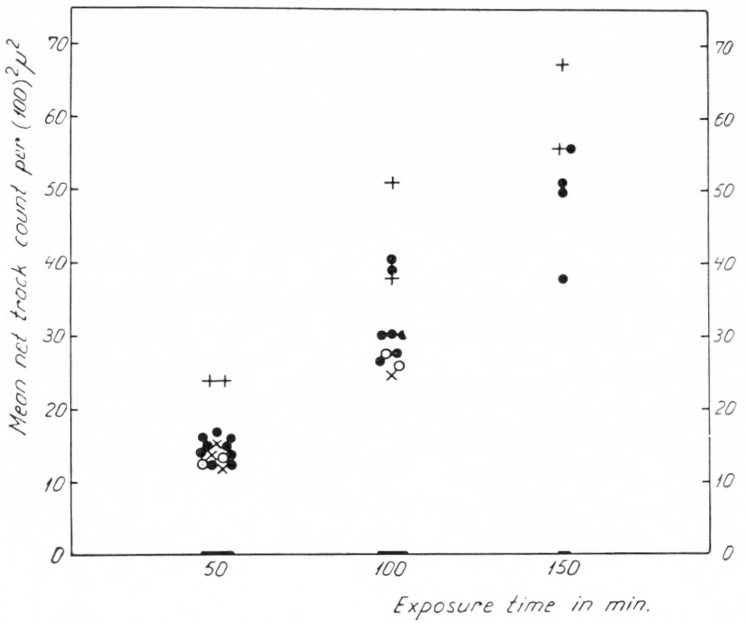

Fig. 1. Mean net track count per field ($(100)^2\mu^2$) versa exposure time in minutes. + series 2; ● series 3; ▦ ○ series 4; × series 5.

Investigation of saturation phenomena (*H* and *D* relation).

The dependence of track count on exposure time was studied applying the exposure times 50 min., 100 min., and 150 min. The experiments were made in two different ways, namely, either by exposing three plates from the same batch, or by exposing different areas of the same plate, for increasing periods of time. The limitation to three different exposure times was necessary because counting is too laborious to allow of a much greater number of images to be evaluated.

The results are illustrated in Fig. 1.

When each batch of plates was considered separately, it was found that the means of the three exposure levels deviate somewhat from the 1:2:3 relationship, and that deviations occur in both directions.

The largest deviation from the 1:2:3 relationship is evidenced by the data from the undried plates of series 2, and is in the direction indicating the presence of a saturation phenomenon,

i. e., the net mean track count increases less than would be expected with increasing exposure time. For the remaining five groups of plates, two exhibit deviation in the direction of saturation, three show deviation of comparable magnitude in the opposite direction.

Three of the seven single plates on which exposures at two or three different levels were made (so-called multiple exposure plates) show deviations from the 1:2:3 relationship almost as large as the largest observed in the means of the batches. However, while two of these plates exhibit substantial deviation in the direction of saturation, the deviation of the third is of comparable magnitude in the opposite direction.

Thus, the data as a whole give little evidence that saturation has been reached. In view of the findings as reported in the previous sections, the sizable deviations from the 1:2:3 relationship observed within some single plates may well be due to inhomogeneity within the plate.

Efficiency of the plates.

When a source of beta particles is brought in contact with a photographic emulsion, only slightly less than 50 $^{0}/_{0}$ of the disintegrations taking place in the source will be "seen" by the emulsion due to geometric conditions. If the source is thick as compared with the range of the beta particles, an additional correction for self-absorption must be applied. In the present case, the source was an "infinitely thick layer" of C-14 labeled polystyrene and therefore, as is well known, only about $^{1}/_{5}$ of the disintegrations in the direction of the detector will reach the emulsion. Taking the correction for geometry and for self-absorption into account, we can expect at the most $^{1}/_{10}$ of the disintegrations taking place in the foil to be registered by the photographic plate.

Some additional loss may occur due to the interspace (of about 1—2 microns) between source and emulsion despite the fact that these surfaces are pressed together, and it is also possible that particles traveling in the emulsion very close to the surface may not be registered as tracks.

We thus arrive at a figure for the number of tracks to be

expected per unit field (100×100 square microns) of the order of 10 % (or somewhat less) of the disintegrations taking place in a piece of the foil of the same surface dimension and a thickness corresponding to the range of the C-14 beta particles.

The standard used contains 0.6 microcuries of C-14 per sq. cm., and, thus, 650 disintegrations take place in the course of 50 min. in 100×100 sq. microns of the foil. The order of magnitude of the track count should therefore be 65 tracks per unit field after 50 min. exposure (or somewhat less).

The actual finding, as illustrated in Fig. 1, is lower than the above estimate by a factor of about 4. The discrepancy may be due to the fact that the C-14 content of the standard foil is not too well-defined. It is also possible—as mentioned above—that the contact between source and emulsion was poorer than anticipated. As pointed out by PELC et. al.[2], this distance is of great importance. Finally, the possibility does exist that the NTB-2 emulsion used did not register all incident particles as tracks, in other words, the efficiency of the emulsion when applied in the manner described here is not one hundred percent. It is worth emphasizing that, in this sense, efficiency is not synonymous with sensitivity, a concept which has been defined and is being used differently.[4]

In experiments carried out with the same standard source placed on an Ilford G-5 emulsion under otherwise identical conditions, the G-5 emulsion registered on the average 45 tracks per unit field after 50 min. exposure, i. e. about 2.5 times more than did the NTB-2 plate.

Effect of storage conditions.

The effect of storage conditions, i. e., temperature, shielding, and humidity, on the efficiency of the plates was studied. It is generally assumed that the lifetime of the plates is prolonged by storage in the cold, that high humidity promotes latent image fading, and that storage in a lead (iron) shield of 5—10 cm thickness will reduce the accumulation of background, especially in the case of emulsions which register electrons from cosmic radiation as tracks. Some of the experiments were extended over

a period of $1^1/_2$ months, and not only the net track count, but also the increase in the background count was considered to be of interest.

The plates of series 3 (a total of three dozen) were stored in different ways in order to study the effect of temperature and

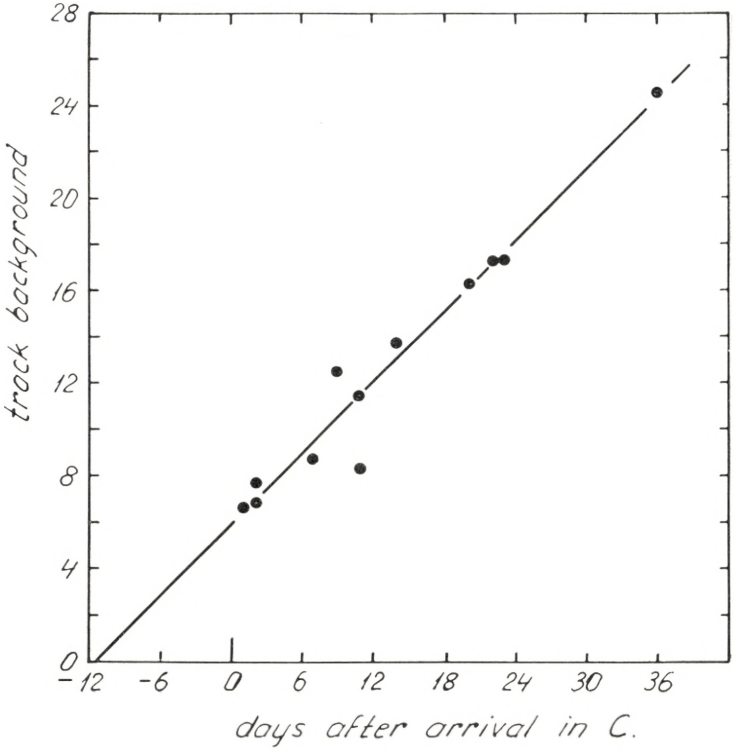

Fig. 2. Increase in track background count per field ($(100)^2\mu^2$) versa time, expressed in days after arrival of the plates in Copenhagen. The day of manufacture is not stated by the producer, shipment took 5 or 6 days.

shielding over an extended period on the properties of the plates. The plates of group A were used within three days after arrival, those of group B were stored at + 5° C in the refrigerator, some for as long as 59 days. The plates of group C were stored at room temperature (20°—22° C) inside a 20 cm iron shield, some for as long as 37 days. Comparison of the data from these three groups reveals no tendency for efficiency to decline with storage under either condition.

At every exposure level, all plates of group B yield higher net mean track counts than any plate of group A. The mean of all group-B plates is higher at every exposure level than the corresponding mean of group-C plates. Comparison of group-A plates with group-C plates yields no consistent difference. The only large difference observed, that between the 150 min. means of the two groups, may be due to differences between plates, as found in other batches.

Fig. 2 shows the increase in background count with time on plates of series 2, which were not shielded during storage. The plates of group C, series 3, stored in a massive iron shield, show no increase in mean background count with time. The background of series-3 B plates stored in the refrigerator, but unshielded remained lower than did that of series 2, although storage was extended over 59 days.

Drying with silica gel prior to exposure was first used with the plates of series 2. At each exposure level, the net mean track counts of dried plates of series 2 are higher than those of undried plates. Application of the theory of combinations reveals that the probability of obtaining such results by chance, i. e., if the drying process actually had no effect on the mean track count, is 1 in 108. Therefore, it seems reasonable to conclude that careful drying of the emulsion prior to exposure does increase the efficiency of the plates of at least some factory batches.

Discussion.

It has been the aim of the present study to investigate the applicability of NTB-2 plates to quantitative β-track autoradiography, for example in connection with tracer studies on biological specimens.

For *practical purposes*, tissue sections, 5—10 microns thick, will be floated on the plates, for example, in the manner described by EVANS[3], and the autoradiogram be observed in the emulsion under the tissue. When using this technique, it must be kept in mind that the sensitivity of the plates is affected by changes in humidity and, therefore, the plates must be dried carefully after having been immersed in water. When most of the moisture has been removed by drying with a fan, the plates must be dried

more thoroughly, e. g., with silica gel. After too rigorous drying, the emulsion begins to peel off, and it will largely be a matter of trial and error to find optimum drying conditions. As long as the humidity of the plates is controled, storage conditions are not critical. The use of a shield is advantageous because accumulation of the track background thereby is suppressed.

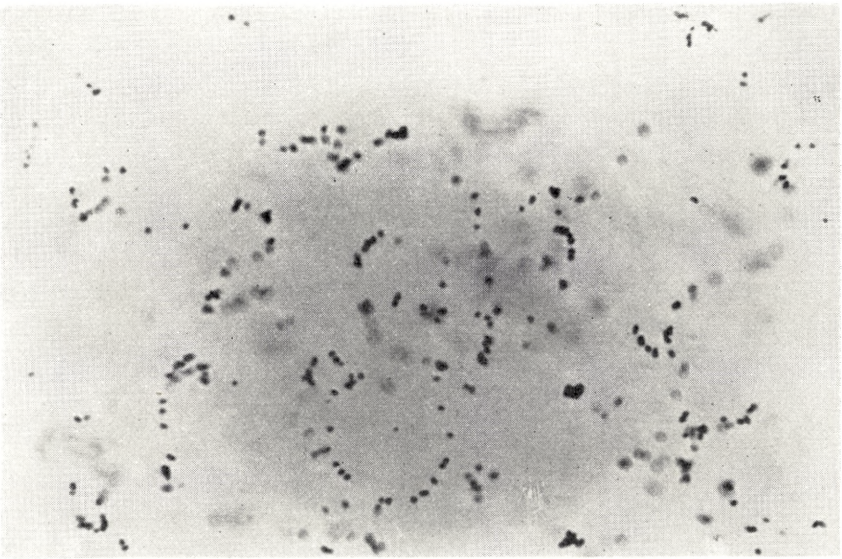

Fig. 3. Photomicrograph of a C-14 beta track pattern in NTB-2 emulsion. Depth of focus about 3 microns.

Exposure time must be such that the number of tracks does not exceed c. 100 per 10^4 sq. microns. At a higher level, counting becomes too difficult. Up to this track density, the number of tracks per field versa exposure time appears to be a linear relation.

Presupposing standardized handling of the emulsion, *the reliability of the counting results* depends on the experience of the investigator and on the properties of the plates.

The investigators must train themselves and establish well-defined criteria on which the interpretation of the track pattern is based. Track counting is not an easy technique, especially because it requires the investigator's full attention and consistency of evaluation. Fatigue is a source of error not to be underestimated. Investigators C and D, participating in this study,

were not particularly interested in perfecting themselves or in improving the method. This is probably part of the reason why their counting results were less reproducible than those of investigators A and B.

In the present study, the standard deviation of recounts of fields was about 4 % of the mean track count. The average difference between the mean track counts obtained by the two main investigators counting the same ten fields of a given image was about 4 %. An estimate of the standard deviation of single net track counts of one investigator (B), i. e., the count from one exposed field less the count from one background field as calculated from the average of the variances within individual plates of a series is given in Table 3.

TABLE 3. Estimated Standard Deviation of Single Net Counts (% of net mean track count).

	50 min.	100 min.	150 min.
series 1	38 %	20 %	18 %
series 2, dried	20 %	12 %	11 %
series 3, 4, and 5	26 %	16 %	13 %

The lack of homogeneity of some of the plates is a serious problem. If the mean track count of fields from a given image is used to estimate the amount of radiation received—as in comparisons between different regions of one image, or between images obtained from unknown sources of radiation—the error calculated from variance of track counts within the exposed areas as mentioned above may seriously overestimate the reliability of the mean count obtained. The differences in sensitivity which were found to exist between different areas of some plates and between plates of some batches are not included in the errors given in the above table. They contribute additionally to the uncertainty of the final results. Differences observed between plates are of such magnitude as to make the error of net track counts from different plates 1.5 to 2 times the error for fields from the same plate. The use of only one plate for all images—even where feasible—cannot be assumed to eliminate this addi-

tional source of error. A further decrease in reliability of the results may arise if images made on plates from different batches are compared.

In practice, this means that a comparison of net track counts per field under different regions of a tissue section can only lead to reasonably accurate results if the regions to be compared are so large that a suitable number of scattered fields can be counted in each region. In view of the inhomogeneity observed within very small areas of some plates, it is advantageous to count separately located fields wherever possible. Comparisons based on single field counts will require the study of serial sections, preferably mounted on one and the same plate.

Very little quantitative information on the *resolution* in a beta track autoradiogram can be obtained from standard exposures with a source of infinitely thick layer. In a medium of density 1 (polystyrene, paraffin, tissue) the range of C-14 betas is about 30 microns, in emulsion (density 4) it is correspondingly less, and in air it is about 3×10^4 microns. When a thick standard source is pressed against the emulsion and the interspace is kept small, the beginning of the tracks will not be too distant from the particles' "points of origin" in the source. With thin tissue sections placed on the emulsion, particles emitted in the direction away from the emulsion can easily reach a medium of low density (air) and can be scattered back into the emulsion, forming a track at considerable distance from their points of origin. It is very tempting, but definitely not justified, to project the starting point of a track as seen in the microscope vertically into the superimposed tissue, assuming that the track originates from this point in the tissue. Systematic investigations into this problem are in progress. The authors' estimate of the resolution obtained when tissue sections containing a C-14 labeled compound are mounted on NTB-2 plates is about 15 microns.

Acknowledgement.

The authors wish to acknowledge the assistance of Miss ELISE FREDERIKSEN (investigator B) whose consciencious co-operation made it possible to collect the data required for the present study.

The mathematical evaluation of the experimental data was begun during A. S. H.'s visit to Copenhagen in 1951, and continued in the United States. The hospitality at the Zoophysiological Laboratory is gratefully acknowledged.

Present address: 3500 Woodridge Ave., Wheaton, Md.

This investigation was supported by the James Picker Foundation on the recommendation of the Committee on Radiology, National Research Council.

Department of Biological Isotope Research,
Zoophysiological Laboratory,
University of Copenhagen.

References.

1. Boyd, G. A. and Hilde Levi: Carbon-14 Beta Track Autoradiography. Science **111**, 58 (1950).
2. Doniach, I. and S. R. Pelc: Autoradiograph Technique Brit. J. Radiology XXIII, 184 (1950).
3. Evans, T. C.: Radioautographs in which tissue is mounted directly on a photographic plate. Proc. Soc. Exptl. Biol. Med. **64**, 313 (1947).
4. Mitchell, J. W.: Fundamental Mechanisms of Photographic Sensitivity. Butterworth Scient. Publ. (1951).

Indleveret til selskabet den 3. maj 1955.
Færdig fra trykkeriet den 1. oktober 1955.

Det Kongelige Danske Videnskabernes Selskab
Matematisk-fysiske Meddelelser, bind **30**, nr. 10

Dan. Mat. Fys. Medd. **30**, no. 10 (1955)

DEDICATED TO PROFESSOR NIELS BOHR ON THE OCCASION OF HIS 70TH BIRTHDAY

OLD PROBLEMS IN THE GENERAL THEORY OF RELATIVITY VIEWED FROM A NEW ANGLE

BY

C. MØLLER

København 1955
i kommission hos Ejnar Munksgaard

CONTENTS

Printed in Denmark
Bianco Lunos Bogtrykkeri A-S

Introduction.

It is a well known consequence of basic assumptions in the general theory of relativity that the rate of an ideal standard clock moving with the velocity v through a gravitational field with the potential χ is determined by the formula

$$d\tau = dt \sqrt{1 + 2\chi/c^2 - v^2/c^2}, \tag{1}$$

where τ is the proper time of the standard clock and t is the coordinate time in a time-orthogonal system of space-time coordinates[1]. Equation (1) is equivalent to the statement that the proper time of a particle is a measure of the length of the time track of the particle in $(3 + 1)$-space. It follows directly from the principle of relativity and the equivalence of gravitational fields and "acceleration fields", together with the assumption that the rate of the standard clock is equal to the rate of the clocks in a local rest system of inertia. The last assumption implies that the acceleration of an ideal standard clock relative to a system of inertia has no influence on the rate of the clock, which thus is entirely determined by its velocity.

The formula (1) is closely connected with the well-known formula for the red-shift of spectral lines emitted by atoms situated at places with a negative gravitational potential, and gives the clue also to a solution, of the so-called clock paradox[2]. On account of the inherent invariance of the length of the time track of a particle, it is clear beforehand that no real contradictions connected with the rate of moving clocks can ever arise in this theory.

However, just for this reason, students of the theory of relativity very often do not find the usual solution of the clock

paradox satisfactory. They maintain—rightly of course—that one has made just such *assumptions* about the behaviour of clocks in gravitational fields that no paradox can occur, and they would like to see a derivation of (1) on the basis of the dynamical laws governing the functioning of a clock or at least of a simple model of a clock. This desire is of a similar kind as that which, in the early days of relativity theory, led to attempts at deriving the Lorentz contraction of moving rigid bodies from the laws governing the constitution of solid bodies. Against such attempts it has been objected that the effects in question are much more elementary and much more directly connected with the principles of the theory than the laws from which they are proposed to be derived, so that the behaviour of moving rigid bodies and standard clocks rather represents a challenge to the theory of the constitution of matter and to the dynamical laws underlying the functioning of clocks. This is certainly a sound objection in the case of the contraction phenomena, since we do not at the moment have a consistent relativistic atomic theory of solid bodies from which the contraction phenomenon could be deduced. However, the situation is somewhat different in the case of the formula (1) for two reasons. Firstly, a clock may be in a certain sense regarded as a much simpler system than a measuring rod, since, for instance, any macroscopic particle performing harmonic oscillations around a centre under the influence of elastic forces may be used as a clock. Thus, in calculating the rate of such a clock, we can neglect all quantal effects and we need only a knowledge of the dynamical laws governing the motion of a macroscopic particle acted upon by an external gravitational field and by a given non-gravitational force. Secondly, as shown by EINSTEIN, INFELD, and HOFFMANN[3], these dynamical laws follow from the gravitational field equations without further assumptions. In particular, it was shown by INFELD and SCHILD[4] that the time track of a freely falling test particle (that is, a particle of vanishing mass) in an arbitrary gravitational background field, is bound to be a geodesic line in the space-time continuum of the background field in order that the field equations can have solutions. This interesting theorem, according to which the equations of motion appear as a kind of integrability conditions for the field equations, is closely connected with

the non-linear character of EINSTEIN's field equations. It is true that the correct equations of motion for a freely falling particle had been derived already long ago on the basis of the principles of relativity and equivalence, but with the extra assumption that the equations of motion do not depend on the second derivatives of the metric tensor with respect to the space-time coordinates. The above mentioned investigations showed, however, that the particle dynamics is intimately connected with the foundations of the theory of gravitational fields and, at least from a didactical point of view, it may now be of some interest to derive Eq. (1) from the dynamics of a simple model of a clock.

Such a derivation also will allow us to formulate certain requirements as to the construction of a clock in order to make it an *ideal* standard clock in the sense of the general theory of relativity. It will turn out, of course, that a real clock can only approximately be considered ideal and that the degree of accuracy with which it may be said to have this property depends on the properties of the gravitational field in which the clock is placed. For a real clock, the formula (1) is therefore also only approximately true.

In recent years, the construction of accurate time measuring instruments has made great progress and the different "atomic clocks" constructed in various laboratories have an accuracy by far exceeding the accuracy of the earth's rotation. The time does not seem far when the accuracy of such clocks is so high that a direct verification of Eq. (1) is possible by comparison of the rates of two clocks situated at places of different gravitational potential on the earth. It is therefore also of interest to verify that the above mentioned conditions for the validity of the formula (1) are satisfied by these clocks.

These problems are dealt with in Section 6. Section 1 contains a review of the three-dimensional formulation of particle dynamics given elsewhere for gravitational fields with zero vector potentials, while the discussion of the most general case is given in the Appendix. The remaining sections are devoted to mainly didactical remarks illustrating the close relationship between the formulae for the mass and energy of a particle in a gravitational field and the Eq. (1). In Section 2, the formula for the gravitational mass of a particle is illustrated by a discussion of a few

"gedanken"-experiments by which this formula, in principle, could be checked. Section 3 presents a similar discussion for the inertial mass. Section 4 brings a derivation of the red-shift formula which is more closely related to the actual mechanism of emission of photons in atomic transitions than usually given in the current text books, the derivation being based directly on a formula describing the influence of gravitational fields on the level scheme of atomic systems. Finally, in Section 5 some of the results obtained in section 3 for the non-relativistic oscillator are derived also for a system with large particle velocities.

1. Particle Dynamics.

The motion of a freely falling particle in an external gravitational field is characterized by the statement that the time track of the particle is a geodesic line. Let us, for simplicity, assume that the system S of space-time coordinates $(x^i) = (x^\iota, ct)$ is time orthogonal*, so that the metric tensor g_{ik}, entering in the interval

$$ds^2 = g_{ik}\, dx^i dx^k, \tag{2}$$

satisfies the three equations

$$g_{\iota 4} = g_{4\iota} = 0. \tag{3}$$

(Latin indices are running from 1 to 4, Greek indices from 1 to 3, only). Then, the spatial line element defining the geometry in the three-dimensional space of our system of reference is simply

$$d\sigma^2 = \gamma_{\iota\varkappa}\, dx^\iota dx^\varkappa, \text{ with } \gamma_{\iota\varkappa} = g_{\iota\varkappa}, \tag{4}$$

and the dynamical action of the gravitational field is determined solely by the scalar gravitational potential $\chi = \chi(x^\iota, t)$ defined by

$$g_{44} = -(1 + 2\chi/c^2). \tag{5}$$

It is now easily seen[5] that the equations of a geodesic in $(3 + 1)$-space are equivalent to a set of equations of motion

* By means of the formulae developped in the Appendix all the considerations of the present paper may easily be carried through also in the most general case.

in 3-space, which can be written in the form of a three-dimensional vector equation. Let $\boldsymbol{u}$ be the three-dimensional velocity vector of the particle with the contravariant and covariant components u^ι and u_ι, respectively, defined by

$$u_\iota = g_{\iota\varkappa}\, u^\varkappa, \quad u^\iota = \frac{dx^\iota}{dt}. \tag{6}$$

Further, let $\mathring{m}_0$ denote the proper mass of the particle as measured in a rest system of inertia; then we define the momentum vector $\boldsymbol{p}$ of the particle by the vector equation

$$\boldsymbol{p} = m\,\boldsymbol{u}, \tag{7}$$

where the factor of proportionality—the inertial mass of the particle in the gravitational field—is given by

$$m = \frac{\mathring{m}_0}{\sqrt{1 + 2\,\chi/c^2 - u^2/c^2}} = \mathring{m}_0 \cdot \Gamma. \tag{8}$$

Here, $u^2 = \left(\frac{d\sigma}{dt}\right)^2 = \gamma_{\iota\varkappa}\, u^\iota u^\varkappa$ is the square of the velocity vector and

$$\Gamma = \frac{1}{\sqrt{1 + 2\,\chi/c^2 - u^2/c^2}} \tag{9}$$

is the generalized Lorentz factor.

The equations of motion then take the form of a three-dimensional vector equation

$$\frac{d_c\, p_\iota}{dt} = K_\iota = -\, m \frac{\partial \chi}{\partial x^\iota}. \tag{10}$$

The left-hand side of this equation is the covariant time derivative of the momentum vector defined by

$$\frac{d_c\, p_\iota}{dt} = \frac{dp_\iota}{dt} - \frac{1}{2} \frac{\partial \gamma_{\varkappa\lambda}}{\partial x^\iota} u^\varkappa p^\lambda, \tag{11}$$

while the right-hand side represents the gravitational force

$$\boldsymbol{K} = -m \operatorname{grad} \chi. \tag{12}$$

The latter is proportional to the negative gradient of the gravitational potential, the factor of proportionality—the gravitational mass—being equal to the inertial mass (8). The last term in (11) is due to the use of curvilinear coordinates in 3-space and is necessary in order to make $\frac{d_e p_\iota}{dt}$ a vector under spatial coordinate transformations.

The equations (10) have the form of usual equations of motion in which the change in the momentum vector $\boldsymbol{p}$ per unit time is equal to the force acting on the particle. They may also be written in Hamiltonian form with the Hamiltonian or the total energy H of the particle in the external gravitational field given by[6]

$$H = \frac{\mathring{m}_0 c^2 (1 + 2\chi/c^2)}{\sqrt{1 + 2\chi/c^2 - u^2/c^2}} = m c'^2. \tag{13}$$

Here,

$$c' = c\sqrt{1 + 2\chi/c^2} \tag{14}$$

is the velocity of light $c' = \frac{d\sigma}{dt}$ at a place where the gravitational potential is χ[7]. Eq. (13) is the generalization of EINSTEIN's energy-mass relation in the presence of gravitational fields. From (7), (8), and (13), we get

$$|\boldsymbol{p}|^2 - \left(\frac{H}{c'}\right)^2 = -\mathring{m}_0^2 c^2, \tag{15}$$

where $|\boldsymbol{p}|^2 = p_\iota p^\iota$ is the square of the momentum vector. Eq. (15) is the generalization of the usual energy-momentum relation for a free particle. In a static field, where $\chi = \chi(x^\iota)$ is time-independent, the energy H is a constant of the motion.

When the particle is acted upon by a force $\mathfrak{F}$, besides the gravitational force $\boldsymbol{K}$, we have to replace the right-hand side of (10) by the sum $\boldsymbol{K} + \mathfrak{F}$ of the two forces. Hence,[8]

$$\frac{d_e \boldsymbol{p}}{dt} = \boldsymbol{K} + \mathfrak{F}. \tag{16}$$

For a force $\mathfrak{F}$ of the usual type, which does not change the proper mass $\mathring{m}_0$, the covariant components $\mathfrak{F}_i$ are connected with the generalized Minkowsky four-force F_i by the relation

$$F_i = \left\{ \Gamma F_\iota, -\frac{\Gamma}{c}(F_\varkappa u^\varkappa) \right\}, \tag{17}$$

Γ being the generalized Lorentz factor (9). In a static gravitational field, the energy conservation law takes the form

$$\frac{dH}{dt} = \mathfrak{F} \cdot \boldsymbol{u} = \mathfrak{F}_\iota u^\iota. \tag{18}$$

Derivations of the equations (6)—(18) are found in loc.cit. [5)—8)]. A short derivation of the corresponding relations for the more general case, where (3) does not hold and where therefore the dynamical action of the gravitational field is described by a vector potential as well as by the scalar potential, is found in the Appendix to the present paper.

2. Gravitational Mass.

By putting $u = 0$ in (8) and (13), we get the following expressions for the rest mass m_0 and the rest energy H_0 of a particle in a gravitational field:

$$m_0 = \frac{\mathring{m}_0}{\sqrt{1 + 2\,\chi/c^2}}, \tag{19}$$

$$H_0 = \mathring{m}_0 c^2 \sqrt{1 + 2\,\chi/c^2} = m_0 \cdot c'^2. \tag{20}$$

Hence, the mass of a body is slightly smaller on the top of a mountain than at sea level, and for the rest energy it is the other way round. Although this variation of the mass is very small (the variation of χ/c^2 is of the order of 10^{-12} between the top of Mount Everest and sea level), it may be of didactical interest to discuss by which experiments the mass (19) in principle could be measured. In this discussion, we shall for simplicity assume that the field is static. Clearly, it will not do to weigh the

particle by means of a balance, since the mass of the weights will vary with χ according to exactly the same formula (19). A balance can therefore only be used for measuring the proper mass $\mathring{m}_0$. On the other hand, if the particle is attached to the end of a string of a given length l, the pendulum thus formed will have a period T which will depend solely on the "gravitational acceleration"

$$G = |-\operatorname{grad} \chi|, \tag{21}$$

at least for small amplitudes and small velocities in the oscillations. Indeed, with these assumptions, the mass m may be treated as a constant, and it will then drop out entirely in the equations of motion (10). Further, if the region in space where the oscillations take place is sufficiently small, we can locally introduce Cartesian coordinates x, y, z (or rather a geodesic system of space coordinates in which the metric tensor $\gamma_{\iota\varkappa}$ may be treated as constant equal to $\delta_{\iota\varkappa}$ inside this region) and, for oscillations along the x-direction, say, the equations of motion (10) reduce to the usual equation of motion for a pendulum

$$\frac{d^2x}{dt^2} = -\frac{G}{l}x. \tag{22}$$

Hence, we get the usual formula for the period

$$T = 2\pi\sqrt{l/G} \tag{23}$$

and measurements by means of a pendulum can therefore only lead to a determination of the gravitational acceleration or the gradient of χ at an arbitrary point.

In order to measure m_0, it is obviously necessary to use an apparatus in which the particle is acted upon by a non-gravitational force which counterbalances the gravitational force. For instance, we may use a spring-balance, where the non-gravitational force is an elastic force $\mathfrak{F}$ proportional to the elongation s of the spring:

$$\mathfrak{F} = ks. \tag{24}$$

When the spring-balance has come to equilibrium, $\boldsymbol{u} = \dot{\boldsymbol{u}} = 0$, and the left-hand side of (16) vanishes. Thus, we get from (12), (16), (21), and (24) the equation

$$m_0 G = ks, \tag{25}$$

from which we can determine m_0 when G, k, and s are known.

However, it must be noted that the elastic constant k itself depends on the gravitational potential χ according to the formula

$$k = \mathring{k} \sqrt{1 + 2\,\chi/c^2}, \tag{26}$$

where $\mathring{k}$ is the value of the elastic constant when the spring is placed at rest in a system of inertia. This fact requires a re-gauging of the spring-balance when it is used at places with different gravitational potentials.

To prove the relation (26) we have simply to make a transformation from the system of coordinates $S: x^i = (x, y, z, ct)$ to a system $\mathring{S}: (\mathring{x}_i)$ which is a local system of inertia at rest relative to S at the space-time point considered. The corresponding transformation equations[9] for the Minkowsky four-force are

$$F_\iota = \mathring{F}_\iota, \quad F_4 = \mathring{F}_4 \sqrt{1 + 2\,\chi/c^2}. \tag{27}$$

Since $\boldsymbol{u} = \mathring{\boldsymbol{u}} = 0$ in our case, we get by (17), (9), and (27), remembering that $\mathring{\chi} = 0$,

$$\mathfrak{F} = \mathring{\mathfrak{F}}/\Gamma = \mathring{\mathfrak{F}} \sqrt{1 + 2\,\chi/c^2}, \tag{28}$$

$$ks = \mathring{k}\mathring{s} \sqrt{1 + 2\,\chi/c^2}. \tag{29}$$

Further, since the relative velocity of the systems S and $\mathring{S}$ is zero, we have

$$s = \mathring{s}, \tag{30}$$

which then leads to the equation (26).

3. Inertial Mass. Harmonic Oscillator.

The mass m_0 determined by the equilibrium condition (25) is of course the gravitational mass, the inertial mass entering only in dynamical problems. As an example, we consider small vibrations of the particle attached to the spring-balance

around the equilibrium position. For sufficiently small amplitudes and velocities in the vibration, the inertial mass m occurring in the vector $\boldsymbol{p}$ on the left-hand side of the equations of motion (16) may be treated as constant and equal to the m_o given by (19) with the value of χ taken at the equilibrium position. Let us further assume that the elastic constant k is so big that the gravitational force $\boldsymbol{K}$ is negligible compared to the elastic force $\mathfrak{F}$. Finally, we may again, for sufficiently small amplitudes, use local Cartesian coordinates with the x-axis in the direction of the vibration. Then, the equations (16) take the form of the usual equations of motion of a harmonic oscillator

$$m_o \frac{d^2 x}{dt^2} = -kx, \tag{31}$$

x being the distance of the particle from the equilibrium position. A solution of (31) is the harmonic oscillation

$$x = A \sin \omega t \tag{32}$$

with the frequency

$$\omega = \sqrt{k/m_o}. \tag{33}$$

Thus we have, according to (19) and (26),

$$\omega = \sqrt{(\mathring{k}/\mathring{m}_0)(1 + 2\chi/c^2)} = \mathring{\omega}\sqrt{1 + 2\chi/c^2}, \tag{34}$$

where $\mathring{\omega}$ is the frequency of the oscillator when it is placed at rest in a system of inertia. By measuring the frequency of the oscillator when placed at different potentials χ, we get a determination of the inertial mass.

When the oscillating particle carries an electric charge, it emits electromagnetic waves of frequency $\nu = \omega/2\pi$, and (34) then expresses the well-known red-shift of light emitted by a macroscopic oscillating system situated at a place of negative gravitational potential. Of course, the system considered is not a good model of a quantum mechanical system like an atom emitting spectral lines. However, in the following section we shall see that the general formula (20) for the rest energy of a particle in a gravitational field provides a simple derivation of the red-shift formula applicable also to atomic systems.

For small velocities we get for the energy (13) of a particle moving with velocity u in a gravitational field, to the first order in u^2/c^2,

$$H = H_0 + \frac{1}{2} m_0 u^2 \tag{35}$$

with m_0 and H_0 given by (19) and (20). Adding to this the elastic potential energy of the oscillator,

$$V = \frac{1}{2} k x^2, \tag{36}$$

we get the total energy of the oscillator in the gravitational field

$$E = H + V = \mathring{m}_0 c^2 \sqrt{1 + 2\chi/c^2} + \varepsilon, \tag{37}$$

where

$$\varepsilon = \frac{1}{2} m_0 u^2 + \frac{1}{2} k x^2 = \frac{1}{2} k A^2 \tag{38}$$

is the usual non-relativistic expression for the energy of an oscillator of mass m_0, elastic constant k and amplitude A.

We shall now compare our oscillator for a given energy state, i. e. a given amplitude A in the gravitational field with the same oscillator placed in a system of inertia. From (37), (38), and (26) we get

$$\varepsilon = \frac{1}{2} \mathring{k} A^2 \sqrt{1 + 2\chi/c^2} = \mathring{\varepsilon} \sqrt{1 + 2\chi/c^2}, \tag{39}$$

$$E = (\mathring{m}_0 + \mathring{\varepsilon}/c^2)\, c^2 \sqrt{1 + 2\chi/c^2} = \mathring{E} \sqrt{1 + 2\chi/c^2}, \tag{40}$$

where

$$\mathring{E} = \mathring{m}_0 c^2 + \mathring{\varepsilon}, \quad \mathring{\varepsilon} = \frac{1}{2} \mathring{k} A^2 \tag{41}$$

is the energy of the oseillator in the system of inertia. A comparison of (40) and (20) shows that the oscillator as a whole has the property of a particle at rest in the gravitational field with a proper mass

$$\mathring{M}_0 = \mathring{m}_0 + \mathring{\varepsilon}/c^2, \tag{42}$$

in accordance with EINSTEIN's energy-mass relation. This may serve as an illustration of the fact that the formula (20) for the rest mass of a particle in a gravitational field holds generally, irrespective of the nature of the mass of the particle.

4. The Red-shift of Spectral Lines.

According to BOHR's theory of atomic spectra, the frequency of the light emitted in a transition between two stationary states of the radiating atom is proportional to the difference in energy of the initial and final states. Therefore, from a didactical point of view, it seems most natural to derive the redshift formula by a consideration of the influence of the gravitational potentials on the energy levels of atomic systems. Let $\mathring{E}_1$, $\mathring{E}_2$, ... $\mathring{E}_n$, ... be the sequence of values of the total energy of the atom in the different stationary states when it is placed at rest in a system of inertia. According to EINSTEIN's mass-energy relation, the proper mass of the atom as a whole in the n'th stationary state is

$$\mathring{M}_{0n} = \mathring{E}_n/c^2. \tag{43}$$

Therefore, by (20), the corresponding energy of the atom when it is placed at rest in a gravitational field must be

$$E_n = \mathring{M}_{0n}c^2\sqrt{1 + 2\,\chi/c^2} = \mathring{E}_n\sqrt{1 + 2\,\chi/c^2}. \tag{44}$$

For the energy release in a transition between two stationary states we then also have

$$\Delta E = \Delta\mathring{E}\sqrt{1 + 2\,\chi/c^2} \tag{45}$$

which, combined with BOHR's energy-frequency relation

$$\Delta E = h\nu, \quad \Delta\mathring{E} = h\mathring{\nu}, \tag{46}$$

immediately leads to the redshift formula

$$\nu = \mathring{\nu}\sqrt{1 + 2\,\chi/c^2}. \tag{47}$$

Thus, the energy and frequency of the photons emitted in a definite transition by atoms at the surface of the sun and by

terrestrial atoms, for instance, differ by the factor $\sqrt{1 + 2\chi/c^2}$. On the other hand, a photon traveling from the sun to the earth may be treated as a "freely falling" particle of proper mass zero and velocity $c' = c\sqrt{1 + 2\chi/c^2}$. Its energy in the static gravitational field is then constantly equal to $h\nu$, which shows that the frequency is unchanged during its travel. After arrival of the photon at the earth, its frequency may be directly compared with the corresponding spectral line emitted by a terrestrial atom.

For $\mathring{m}_0 \to 0$, we get from (15), for the momentum of the photon,

$$p = \frac{H}{c'} = \frac{h\nu}{c'} = \frac{h}{\lambda}, \tag{48}$$

where $\lambda = c'/\nu$ is the wavelength measured with standard measuring sticks. Further, we get from (13), for the "relativistic" mass m of the photon,

$$m = \frac{h\nu}{c'^2}. \tag{49}$$

If we introduce this value for m into the equations of motion (10), we get, after dividing by the common constant factor $h\nu$,

$$\frac{d_c\,(u_\iota/c'^2)}{dt} \equiv \frac{d}{dt}(u_\iota/c'^2) - \frac{1}{2}\frac{\partial \gamma_{\varkappa\lambda}}{\partial x^\iota}\frac{u^\varkappa u^\lambda}{c'^2} = -\frac{1}{c'^2}\frac{\partial \chi}{\partial x^\iota} \tag{50}$$

with

$$u^\iota = \frac{dx^\iota}{dt}, \quad u_\iota u^\iota = c'^2. \tag{51}$$

The equations (50) are the equations of motion of a light ray, as derived, for instance, by Fermat's principle[10], determining the deflection of light in a gravitational field. In this way, the three Einstein effects—the advance of the perihelion, the redshift of spectral lines, and the deflection of light—appear as consequences of the same equations, the equations of motion (10) which, in turn, may be regarded as a kind of integrability conditions for the gravitational field equations.

5. The "Relativistic" Oscillator.

In the derivation of the relation (34) from the equations of motion, we assumed for convenience that

$$u^2/c'^2 \ll 1. \tag{52}$$

This assumption is of course not essential. As an example let us, as in Section 3, consider the case of a macroscopic particle elastically bound to a fixed point 0; but now we shall not assume that the velocities are small. However, we shall stick to the other assumptions made in Section 3, viz. that the gravitational force can be neglected, and that the potential χ can be regarded as a constant over the small domain of the orbit of the particle. For the mass in the equations of motion we then have, according to (8), (14), and (19)

$$m = \frac{m_0}{\sqrt{1 - u^2/c'^2}}, \tag{53}$$

where m_0 and c' are treated as constants. Using again local Cartesian coordinates, we get now, instead of (31),

$$\frac{d}{dt}\left(\frac{m_0 \dot{x}}{\sqrt{1 - \dot{x}^2/c'^2}}\right) = -kx. \tag{54}$$

The total energy E is a constant of the motion. Hence, by (13), (53), and (36),

$$mc'^2 + V \equiv \frac{m_0 c'^2}{\sqrt{1 - \dot{x}^2/c'^2}} + \frac{1}{2} kx^2 = E. \tag{55}$$

If $\pm A$ are the values of x at the turning points of the particle where $\dot{x} = 0$, the constant E in (55) may be written

$$E = m_0 c'^2 + \frac{1}{2} kA^2, \tag{56}$$

and we get for the velocity $\dot{x}$

$$\left(\frac{dx}{dt}\right)^2 \Big/ c'^2 = 1 - [1 + (A^2 - x^2)\,(k/2\,m_0 c'^2)]^{-2}. \tag{57}$$

However, the ratio $k/2\,m_0 c'^2$ is independent of the potential χ. In fact, by (26), (19), and (14),

$$k/2\,m_0 c'^2 = \mathring{k}/2\,\mathring{m}_0 c^2. \tag{58}$$

Therefore, by integration of (57) over one period $T = 1/\nu$, corresponding to a motion of the particle from $x = -A$ to $x = +A$ and back, we get

$$T = \mathring{T}(1 + 2\,\chi/c^2)^{-\frac{1}{2}}, \tag{59}$$

where

$$\mathring{T} = (2/c)\int_{-A}^{A}\left\{1 - [1 + (A^2 - x^2)\,(\mathring{k}/2\,\mathring{m}_0 c^2)]^{-2}\right\}^{-\frac{1}{2}} dx \tag{60}$$

is the period of the same oscillator when placed at rest in a system of inertia. Eq. (59) or

$$\nu = \mathring{\nu}\,\sqrt{1 + 2\,\chi/c^2} \tag{61}$$

is identical with (34), which thus has been derived also for a "relativistic" system.

When

$$\mathring{k}A^2/\mathring{m}_0 c^2 \ll 1, \tag{62}$$

Eq. (60) gives of course the non-relativistic expression $\mathring{\nu} = 1/\mathring{T} = \sqrt{\mathring{k}/\mathring{m}_0}/2\,\pi$; which is independent of the amplitude, but in general the frequency will depend on A and be smaller than this value. This is connected with the fact that the relativistic mass m is larger than the rest mass m_0 which will slow down the motion. The velocity u is therefore always smaller than the value $\sqrt{k/m_0}\,A$ for the maximum velocity in the harmonic oscillation (32):

$$u \leqslant \sqrt{k/m_0}\,A. \tag{63}$$

6. Ideal Standard Clocks.

We shall now turn to the problem, mentioned in the Introduction, of deriving the formula (1) for the rate of a clock in a gravitational field from the dynamics of the clock. Let us first

consider a clock *at rest* in a *static* gravitational field, in which case we should have, according to (1),

$$d\tau = dt\sqrt{1 + 2\,\chi/c^2}. \tag{64}$$

As a simple model of a clock, we may take the oscillator treated in Section 3, consisting of a particle of proper mass $\mathring{m}_0$, which is elastically bound to a fixed point O in the system of reference, the more so as any vibrating system in a certain approximation has the properties of an oscillator. The time shown by the clock is now per definitionem proportional to the number of beats in the oscillation. The ratio $\omega/\mathring{\omega}$, determined by the equation (34), is therefore equal to the ratio of the rates of the clock when placed at potential χ and at zero potential, respectively. Since the coordinate time t may be identified with the time shown by the clock in the latter case, we see that (64) is a consequence of (34).

We shall now establish the general conditions which a clock must satisfy in order that the formula (1) is valid, i. e. the conditions for the oscillating system to be an ideal standard clock. In the derivation of (34) from the equations of motion (16), we have made a number of assumptions. First, we assumed that the velocity of the particle in the oscillation is small compared with the velocity of light, i. e. that (62) is satisfied. However, as shown in Section 5, this is not a necessary but only a convenient assumption. Next, we made the essential assumption that *the gravitational force* $m_0 G$ *in* (16) *could be neglected.* Since the elastic force $\mathfrak{F}$ is of the order kA, the condition for this to be justified is that

$$m_0 G/kA \ll 1. \tag{I}$$

If this condition is not satisfied, the equation of motion for an oscillator in the gravitational field will not have the same form as in a system of inertia. It is true that a constant force $m_0 G$ added to the elastic force of an oscillator will not change the frequency of the oscillator, but only the equilibrium position. However, this holds only for an exact harmonic oscillator; for any potential other than the one given by (36), an additional constant force will change the frequency and invalidate the simple

formula (34). To see this, and to get an estimate of this effect, we let $V(x)$ be the potential of the oscillating particle without the force $m_0 G$. The total potential for the system with the additional force is then

$$\overline{V}(x) = V(x) - m_0 G x. \tag{65}$$

If $\bar{x}_0$ and x_0 are the values of x corresponding to the equilibrium positions of the particle with and without the force $m_0 G$, we have

$$V'(x_0) = 0, \tag{66}$$

$$\overline{V}'(\bar{x}_0) = V'(\bar{x}_0) - m_0 G = 0. \tag{67}$$

From the Taylor expansion of $V(x)$ around the point x_0

$$V(x) = V(x_0) + \frac{1}{2} V''(x_0)(x - x_0)^2 + \frac{1}{3!} V'''(x_0)(x - x_0)^3 + \cdots \tag{68}$$

we see that the system without the force $m_0 G$ may be regarded as a harmonic oscillator with the elastic constant

$$k = V''(x_0), \tag{69}$$

provided that the amplitude A satisfies the condition

$$\frac{V'''(x_0) A}{3 V''(x_0)} = \frac{V'''(x_0) A}{3 k} \ll 1. \tag{70}$$

Hence, by (67), (68), and (69),

$$\bar{x}_0 - x_0 = m_0 G/k, \tag{71}$$

which is small compared with A if (I) is satisfied. The system including the constant force $m_0 G$ may therefore be treated as a harmonic oscillator with the elastic constant

$$\left.\begin{aligned} \bar{k} = \overline{V}''(\bar{x}_0) = V''(\bar{x}_0) &= V''(x_0) + V'''(x_0)(\bar{x}_0 - x_0) \\ &= k + V'''(x_0)\, m_0 G/k. \end{aligned}\right\} \tag{72}$$

Here we have used (65), (68) and (71).

The relative change in k due to the gravitational force is thus

$$\delta k/k = V'''(x_0)\, m_0 G/k^2, \tag{73}$$

and the corresponding change in the frequency $\omega = \sqrt{k/m_0}$ is

$$\delta\omega/\omega = \delta k/2k = V'''(x_0)\, m_0 G/2k^2. \tag{74}$$

This we may also write

$$\delta\omega/\omega = \frac{3}{2}\left(\frac{V'''(x_0)\, A}{3\, k}\right)\cdot\left(\frac{m_0 G}{kA}\right), \tag{75}$$

showing that the degree of accuracy with which the formula (64) is valid depends not only on how strongly (I) is fulfilled, but also on the degree to which the "harmonicity" condition (70) is satisfied.

In the quantum mechanical derivation of the red-shift formula (47) in Section (4), the assumption (I) would mean that the influence of a constant field of the strength $m_0 G$ on the levels of the atomic system, "the gravitational Stark-effect", is negligible.

In the derivation of (34) from (16) it was further assumed that χ in the expression for the mass on the left-hand side of (16) could be treated as a constant, or more precisely, that

$$\frac{dm_0}{dt}\cdot u \ll \mathfrak{F}. \tag{76}$$

For a static field, this gives, on account of (19), (14), (21), and (63),

$$\frac{\mathring{m}_0}{(1+2\chi/c^2)^{3/2}}\left(\frac{\partial\chi}{\partial x^\iota}u^\iota\right)u/c^2 \approx \frac{m_0 G u^2}{c'^2} \leqslant \frac{m_0 G\, kA^2}{c'^2 m_0} \ll kA \tag{77 a}$$

or

$$GA/c'^2 \ll 1. \tag{II}$$

Since u^2 is always smaller than c'^2, (77 a) or (II) will always hold when condition (I) is satisfied.

For a non-static field, we get from (76) the further condition

$$\frac{m_0 u}{c'^2}\frac{\partial\chi}{\partial t} \ll kA, \tag{77 b}$$

which by (63) and (33) may be written

$$\sqrt{\frac{m_0}{k}}\frac{\partial \chi}{\partial t}\Big/c'^2 = \frac{1}{\omega}\frac{\partial \chi}{\partial t}\Big/c'^2 \ll 1\,. \tag{III}$$

Thus, the variation of the dimensionless quantity χ/c^2 during one oscillation must be small.

Finally, the use of Cartesian coordinates in the whole region of oscillation, as was implied in the derivation of the oscillator equation (31), is possible only if the spatial curvature can be neglected inside this region. This leads to the conditions

$$\varkappa A^2 \ll 1 \tag{IV}$$

where $\varkappa$ is the Riemann curvature constant of any "plane" surface of geodesics through the point O. For the "plane" defined by the directions of the x^1- and x^2-coordinate curves in O the curvature constant $\varkappa$ is defined by [11]

$$\varkappa = -P_{1212}/(\gamma_{11}\gamma_{22} - \gamma_{12}^2), \tag{78}$$

where $P_{\iota\varkappa\lambda\mu}$ is the Riemann-Christoffel curvature tensor formed by the spatial metric tensor $\gamma_{\iota\varkappa}$. The corresponding curvatures of the "(23)-" and "(31)-planes" are obtained from (78) by cyclic permutations of the numbers 123.

Up to this point, the centre of the clock, O, has been assumed to be fixed at a definite place in the system of reference. Now, let O be accelerated with the acceleration $\boldsymbol{a}$. As long as the velocity of O is small compared with c', the derivation of (31) from the equations of motion (16) will still be valid if the further condition

$$m_0 a \ll kA \tag{V}$$

is satisfied. Let y^ι and $v^\iota = \dot{y}^\iota$ be the coordinates and velocity of the centre O. For the coordinates and velocity of the particle, we have then

$$x^\iota = y^\iota + \xi^\iota, \quad u^\iota = v^\iota + w^\iota, \tag{79}$$

where ξ^ι is the small vector leading from the centre O to the position of the particle and $w^\iota = \dot{\xi}^\iota$. ($\xi^\iota$ is only approximately a vector!) When (79) is introduced into the left-hand side of (16), it

is seen that the equations of motion under the conditions mentioned above again reduce to an equation of the type (31) with x replaced by ξ.

By (33), the condition (V) implies that

$$\Delta v = a/\omega = a\sqrt{m_0/k} \ll \sqrt{k/m_0} \cdot A = \omega A \approx \dot{\xi}, \tag{80}$$

i. e. the velocity acquired by O during one period of the oscillation is small compared with the mean velocity of the oscillation. The condition (V) is thus the condition for an "adiabatic acceleration" of the clock. Since (80) implies $\Delta v \ll c'$, this condition also gives the justification for using the simple "action at a distance" expression $\mathfrak{F} = k\xi$ for the force in the equations of motion.

If (I) and (V) are not sufficiently well satisfied, we obviously have to add the extra force $m_0 \boldsymbol{G} - \frac{d_c}{dt}(m_0 \boldsymbol{v}) \approx m_0 (\boldsymbol{G} - \boldsymbol{a})$ on the right-hand side of the equations of motion (31). This will cause a change in the frequency which is given by (75), but with G replaced by $|\boldsymbol{G} - \boldsymbol{a}|$. Thus, if the acceleration of the centre of the clock is equal to the gravitational acceleration, as will be the case if the clock is allowed to fall freely, then the two effects dealt with in (I) and (V) will practically cancel and the equations of motion will have the form (31) even if (I) and (V), separately, are not well satisfied.

Finally, when O is moving with the finite velocity $\boldsymbol{v}$, we get again, under the conditions (I) — (V), an equation of the oscillator type (31) for the motion of the particle, but with m_0 replaced by

$$m = \mathring{m}_0 \Gamma(O), \tag{81}$$

where

$$\Gamma(O) = \{ 1 + 2\chi/c^2 - v^2/c^2 \}^{-\frac{1}{2}} \tag{82}$$

is the generalized Lorentz factor corresponding to the velocity of the centre. By a consideration similar to that which in Section 2 lead to the equation (26), we now get for the elastic constant

$$k = \mathring{k}/\Gamma(O), \tag{83}$$

where $\mathring{k}$ is the value of this constant in a local rest system of inertia for the centre O.

Hence, under the above conditions, the frequency ω of an oscillator moving with the velocity $\boldsymbol{v}$ in a gravitational field must be connected with the proper frequency $\mathring{\omega}$ of the same oscillator at rest in a system of inertia by the formula

$$\omega = \mathring{\omega} \sqrt{1 + 2\chi/c^2 - v^2/c^2}, \tag{84}$$

in accordance with the formula (1) for an ideal standard clock.

For given G, $\frac{\partial \chi}{\partial t}$, $\varkappa$ and a, it is obviously always possible to choose the parameters of the clock $\mathring{\omega} = \sqrt{\mathring{k}/\mathring{m}_0}$ and A such that the conditions (I) — (V) are satisfied, i. e. it is always possible to construct clocks which are "ideal" under given circumstances. On the other hand, the degree of accuracy to which a given clock (given $\mathring{k}$, $\mathring{m}_0$ and A) may be regarded as ideal depends of course on the use we want to make of it (i. e. on G, $\frac{\partial \chi}{\partial t}$, $\varkappa$ and a). Let us now see to what degree of accuracy the relations (I) — (V) are satisfied by the "atomic clocks" in order to decide whether the variations in the rate of the clock due to variations in the gravitational field of the earth could in principle be measured by means of such clocks. It is a common feature of these clocks that atomic systems like ammonia molecules act as the "balance" of the clock. The vibrations of the atoms in the molecule, which in this connection may be treated as a classical mechanical system, are to a high degree of accuracy harmonic oscillations. The frequency of the oscillation is of the order

$$\omega \approx 10^{10}\, sec^{-1}. \tag{85}$$

Since the mass of the oscillating particle is of the order

$$m_0 \approx 10^{-24}\, gr \tag{86}$$

the system may be represented by a harmonic oscillator with an elastic constant

$$k = \omega^2 m_0 \approx 10^{-4}\, gr/\mathrm{sec}^2. \tag{87}$$

The amplitude A of the oscillator cannot be larger than atomic dimensions. In the conditions I, and II we can therefore put

$$A \approx 10^{-8} \text{ cm}, \quad c' \approx c = 3 \cdot 10^{10} \text{ cm/sec}, \quad G \approx 10^{3} \text{ cm/sec}^2 \tag{88}$$

for terrestrial gravitational fields.

Hence,

$$m_0 G/k\, A \approx 10^{-9} \tag{89}$$

$$GA/c'^2 \approx 10^{-25}. \tag{90}$$

Further, a straight-forward calculation shows that the quantity on the left hand side of (IV), for a point at the surface of the earth, is of the order $\frac{\partial^2 \chi}{\partial r^2} \frac{A^2}{c^2} \approx (GA/c'^2) \cdot (A/r)$ where r is the radius of the earth.

The conditions (I) — (V) are therefore amply satisfied and the condition (V) is of course also well satisfied even for accelerations considerably larger than the gravitational acceleration. We also see that the oscillator is highly non-relativistic, since

$$\omega^2 A^2/c'^2 \approx 10^{-17} \ll 1. \tag{91}$$

From (75) and (89) we now get

$$\delta\omega/\omega \approx 10^{-9} \, (V'''(x_0) \, A/3 \, k). \tag{91}$$

Thus, if we are aiming at an accuracy of the order of 10^{-12}, the quantity on the left-hand side of (70) which determines the degree of harmonicity of the oscillator must be smaller than 10^{-3}. However, as pointed out on p. 22, the accuracy to which the clock may be considered "ideal" increases considerably if the atomic systems which constitute the balance of the clock are freely falling in the gravitational field, since the effects dealt with in (I) and (V) then almost completely cancel.

In concluding, I wish to thank Dr. D. Frisch for pleasant and illuminating discussions on problems connected with the atomic clocks.

Institute for Theoretical Physics,
University of Copenhagen.

Appendix.

In this Appendix, we shall give a short derivation of the three-dimensional equations of motion in the most general case, where (3) is not satisfied and where the dynamical action of the gravitational field is described by a vector potential

$$\gamma_\iota = g_{\iota 4}/\sqrt{-g_{44}} \tag{A. 1}$$

as well as by the scalar potential defined by (5). In this case, we have, instead of (4), the spatial metric tensor $\gamma_{\iota\varkappa}$ given by

$$d\sigma^2 = \gamma_{\iota\varkappa}\, dx^\iota\, dx^\varkappa, \quad \gamma_{\iota\varkappa} = g_{\iota\varkappa} + \gamma_\iota\, \gamma_\varkappa. \tag{A. 2}$$

Let

$$d\tau = ds/ic = \sqrt{-g_{ik}\, dx^i\, dx^k}/c \tag{A. 3}$$

be the real quantity measuring the length of the time track of a particle in $(3 + 1)$-space, and let F_i be the covariant components of the non-gravitational four-force. Then, using an arbitrary parameter representation, the equations of the time track may be derived from the variational principle

$$\delta \int_{\lambda_1}^{\lambda_2} m_0 c \sqrt{-g_{ik}\, \dot{x}^i\, \dot{x}^k}\, d\lambda - \int_{\lambda_1}^{\lambda_2} F_i\, \delta x^i \frac{d\tau}{d\lambda}\, d\lambda = O, \tag{A. 4}$$

where δx^i are arbitrary variations of the space-time coordinates x^i vanishing for $\lambda = \begin{cases} \lambda^2 \\ \lambda^1 \end{cases}$, and

$$\dot{x}^i = \frac{dx^i}{d\lambda} = \frac{dx^i}{d\tau} \cdot \frac{d\tau}{d\lambda}. \tag{A. 5}$$

Since λ may be chosen arbitrarily, we can, for instance, use the time coordinate $t = x^4/c$ as parameter, in which case $\delta x^4 = O$ in (A. 4) and $\dot{x}^\iota = \dfrac{dx^\iota}{dt} = u^\iota$ is the three-dimensional velocity. Further, in this case one easily gets

$$\frac{d\tau}{d\lambda} = \frac{1}{c}\sqrt{-g_{ik}\, \dot{x}^i\, \dot{x}^k} = \left[\left(\sqrt{1 + 2\chi/c^2} - \gamma_\iota u^\iota/c\right)^2 - u^2/c^2\right]^{\frac{1}{2}} = 1/\Gamma, \tag{A. 6}$$

where Γ is the Lorentz factor in this most general case, and $u^2 = \gamma_{\iota\varkappa} u^\iota u^\varkappa$. With this expression for Γ, the connection between F_i and the components $\tilde{\mathfrak{F}}_\iota$ of the three-dimensional force is then again given by (17).

With this choice of λ, the variational principle (A. 4) takes the form

$$\int_{t_1}^{t_2} \left\{ \delta L(x^\iota, u^\iota) + \tilde{\mathfrak{F}}_\iota \delta x^\iota \right\} dt = O, \tag{A. 7}$$

where

$$L(x^\iota, u^\iota, t) = -\mathring{m}_0 c \sqrt{(c' - \gamma_\varkappa u^\varkappa)^2 - u^2} \tag{A. 8}$$

is the Langrangian of the particle in the gravitational field. Here, $x^\iota = x^\iota(t)$ as a function of the time t is varied in such a way that $\delta x^\iota = O$ for $t = \begin{cases} t_1 \\ t_2 \end{cases}$. In the expression for the Lagrangian, $c' = c\sqrt{1 + 2\chi(x^\iota, t)/c^2}$ is the quantity introduced by (14), but in the present case, ($\gamma_\iota \neq O$), the velocity of light depends on the direction of propagation and c' is now the velocity of light in a direction perpendicular to the space vector γ_ι[7]).

As in (8), the mass of the particle in the gravitational field is defined as $m = \mathring{m}_0 \Gamma$, but with the Lorentz factor given by (A. 6), i. e.

$$m = \mathring{m}_0 \Gamma = \frac{\mathring{m}_0}{\left[\left(\sqrt{1 + 2\chi/c^2} - \gamma_\varkappa u^\varkappa/c\right)^2 - u^2/c^2\right]^{1/2}} \tag{A. 9}$$

is now a function of the four potentials (γ_ι, χ) as well as of the velocity $\boldsymbol{u}$. For the canonically conjugate momentum to the coordinate x^ι, we thus get, by (A. 8) and (A. 9),

$$\pi_\iota = \frac{\partial L}{\partial \dot{x}^\iota} = m u_\iota + m\gamma_\iota (c' - \gamma_\varkappa u^\varkappa) = p_\iota + m\gamma_\iota (c' - \gamma_\varkappa u^\varkappa). \tag{A. 10}$$

Thus, π_ι differs from the momentum $p_\iota = m u_\iota$ of the particle by a term depending on the vector potential in analogy with the case of a particle in an electromagnetic field.

The equations of motion following from the variational principle (A. 7) are

$$\frac{d\pi_\iota}{dt} = \frac{\partial L}{\partial x^\iota} + \tilde{\mathfrak{F}}_\iota. \tag{A. 11}$$

By (A. 9) the Lagrangian (A. 8) can also be written

$$L = -m\,[(c' - \gamma_\varkappa u^\varkappa)^2 - u^2]\,. \tag{A. 12}$$

Thus, by (A. 10) and (A. 12), we get for the Hamiltonian H corresponding to the Lagrangian L

$$\left.\begin{aligned} H \equiv \pi_\iota \dot{x}^\iota - L = m\,(u_\iota u^\iota) + m\,(\gamma_\iota u^\iota)\,[c' - \gamma_\varkappa u^\varkappa] \\ + m\,[(c' - \gamma_\varkappa u^\varkappa)^2 - u^2]\,, \end{aligned}\right\} \tag{A. 13}$$

which leads to the following expression for the energy of the particle in the gravitational field:

$$H = mc'\,(c' - \gamma_\varkappa u^\varkappa)\,. \tag{A. 14}$$

In the special case $\gamma_\iota = 0$, Eqs. (A. 9), (A. 14) are identical with the equations (8), (13) in Section 1.

By using the definitions (A. 10, 13) of π_ι and H, and the equations of motion (A. 11), we get for the time derivative of H

$$\frac{dH}{dt} = \dot{\pi}_\iota u^\iota + \pi_\iota \dot{u}^\iota - \frac{\partial L}{\partial t} - \frac{\partial L}{\partial x^\iota} u^\iota - \frac{\partial L}{\partial u^\iota}\dot{u}^\iota = \mathfrak{F}_\iota u^\iota - \frac{\partial L}{\partial t}, \tag{A. 15}$$

and, by (A. 14), π_ι in (A. 10) may be written

$$\pi_\iota = p_\iota + H\gamma_\iota/c'. \tag{A. 16}$$

Thus, the left-hand side of (A. 11) takes the form

$$\frac{d\pi_\iota}{dt} = \frac{dp_\iota}{dt} + \left(\mathfrak{F}_\varkappa u^\varkappa - \frac{\partial L}{\partial t}\right)\gamma_\iota/c' + H\frac{d}{dt}(\gamma_\iota/c')\,.$$

Further, we get by a simple calculation from (A. 8) and (A. 14)

$$\frac{\partial L}{\partial x^\iota} = \frac{1}{2}\frac{\partial \gamma_{\varkappa\lambda}}{\partial x^\iota} u^\varkappa u^\lambda m - \frac{H}{c'}\left(\frac{\partial c'}{\partial x^\iota} - \frac{\partial \gamma_\varkappa}{\partial x^\iota} u^\varkappa\right) \tag{A. 17}$$

so that the equation of motion may be written

$$\left.\begin{aligned} \frac{d_c p_\iota}{dt} = \mathfrak{F}_\iota - (\mathfrak{F}_\varkappa u^\varkappa)\,\gamma_\iota/c' + \frac{\partial L}{\partial t}\gamma_\iota/c' - H\frac{d}{dt}(\gamma_\iota/c') \\ - \frac{H}{c'}\left(\frac{\partial c'}{\partial x^\iota} - \frac{\partial \gamma_\varkappa}{\partial x^\iota} u^\varkappa\right). \end{aligned}\right\} \tag{A. 18}$$

By this explicit use of the conservation law (A. 15) for the energy, we have achieved that the right-hand side of (A. 18), the force acting on the particle, does not contain the acceleration, but only the coordinates and the velocity of the particle. This expression for the force can be simplified by introducing the antisymmetric spatial tensor $\omega_{\iota\varkappa}$ which is connected to the local rotation of our system of reference with respect to the local systems of inertia. The latter is defined by[12)]

$$\omega_{\iota\varkappa}/c = \left(\frac{\partial}{\partial x^{\iota}} + \frac{\gamma_{\iota}}{c'}\frac{\partial}{\partial t}\right)(\gamma_{\varkappa}/c') - \left(\frac{\partial}{\partial x^{\varkappa}} + \frac{\gamma_{\varkappa}}{c'}\frac{\partial}{\partial t}\right)(\gamma_{\iota}/c'). \qquad \text{(A. 19)}$$

By a somewhat lengthy, but elementary calculation, (A. 18) can be written in the form

$$\frac{d_e p_{\iota}}{dt} = \mathfrak{F}_{\iota} - (\mathfrak{F}_{\varkappa} u^{\varkappa})\,\gamma_{\iota}/c' + mG_{\iota} \qquad \text{(A. 20)}$$

with

$$\left.\begin{aligned} G_{\iota} &= -(1 - \gamma_{\varkappa} u^{\varkappa}/c')^2\left(\frac{\partial \chi}{\partial x^{\iota}} + c'\frac{\partial \gamma_{\iota}}{\partial t}\right) \\ &+ \sqrt{1 + 2\,\chi/c^2}\cdot(c' - \gamma_{\varkappa} u^{\varkappa})\,\omega_{\iota\lambda} u^{\lambda} + \frac{1}{2}\frac{\gamma_{\iota}}{c'}\frac{\partial \gamma_{\varkappa\lambda}}{\partial t} u^{\varkappa} u^{\lambda}. \end{aligned}\right\} \qquad \text{(A. 21)}$$

If we put $\gamma_{\iota} = O$, these equations are reduced to the simple equation (16). Further, in the case of *stationary weak fields*, where time derivations and products of the potentials γ_{ι} and χ can be neglected, we get for the gravitational force

$$K_{\iota} = m\left(-\frac{\partial \chi}{\partial x^{\iota}} + c\,\omega_{\iota\varkappa} u^{\varkappa}\right), \quad \omega_{\iota\varkappa} = \frac{\partial \gamma_{\varkappa}}{\partial x^{\iota}} - \frac{\partial \gamma_{\iota}}{\partial x^{\varkappa}}. \qquad \text{(A. 22)}$$

In a rigid system rotating with constant angular velocity relative to a system of inertia, the equation (A. 22) for K_{ι} gives the usual expressions for the centrifugal and Coriolis forces which therefore are valid for arbitrary velocities of the particle[13)], the only effect of relativity in the equations of motion being the velocity dependence of the mass according to the formula (A. 9).

References.

1) See f. inst. C. MØLLER, The Theory of Relativity, Oxford 1952, (later quoted as C. M.) Chapt. VIII, Eq. (99).
2) A. EINSTEIN, Ann. d. Phys. **17,** 891 (1905); P. LANGEVIN, Scientia **10,** 31 (1911); M. v. LAUE, Phys. Z. **13,** 118 (1912); H. A. LORENTZ, Das Relativitätsprinzip, Haarlemer Vorlesungen, Leipzig 1914; A. EINSTEIN, Naturwiss. **6,** 697 (1918); C. MØLLER, Dan. Mat. Fys. Medd. **20,** No. 19 (1943) and C. M. Chapt. VIII § 98, p. 258.
3) A. EINSTEIN, L. INFELD, and B. HOFFMANN, Ann. Math. **39,** 65 (1938) A. EINSTEIN and L. INFELD, Ann. Math. **41,** 455 (1940) and Can. J. Math. **1,** 209 1949).
4) L. INFELD and A. SCHILD, Reviews of Modern Physics **21,** 408 (1949).
5) C. M. Chapt. X, § 110, p. 290 and C. M. Appendix **7,** p. 378; further the Appendix of the present paper.
6) C. M. Appendix **7,** p. 378.
7) See f. inst. C. M. Chapt. VIII, § 89, Eq. (70).
8) C. M. Chapt. X, § 112.
9) See f. inst. C. M. Chapt. IX, § 104.
10) Eq. (50) is identical with Eq. (98) in C. M. Chapt. X, § 117, if the arbitrary parameter in the latter equation is chosen equal to the time variable.
11) See f. inst. W. PAULI, Relativitätstheorie, Enzyklopädie d. mathem. Wissensch. **V 19** § 17.
12) C. M. Chapt. VIII, § 94, Eq. (110).
13) In C. M. Chapt. X, § 110, p. 292, this was proved only for small velocities.

Indleveret til selskabet den 15. juni 1955.
Færdig fra trykkeriet den 3. oktober 1955.

Det Kongelige Danske Videnskabernes Selskab
Matematisk-fysiske Meddelelser, bind **30**, nr. 11

Dan. Mat. Fys. Medd. **30**, no. 11 (1955)

DEDICATED TO PROFESSOR NIELS BOHR ON THE OCCASION OF HIS 70TH BIRTHDAY

MULTIPOLE ORDER OF THE γ-RAYS FROM $_{81}Tl^{208}$

BY

O. B. NIELSEN

København 1955
i kommission hos Ejnar Munksgaard

Printed in Denmark
Bianco Lunos Bogtrykkeri A-S

The internal conversion lines originating in excited levels of $_{81}Tl^{208}$ have been obtained in coincidence with α-particles from $_{83}Bi^{212}$. Five of the transitions were found to be magnetic dipole from their internal conversion coefficients. In three cases, the multipole order was confirmed by the K/L ratios.

The results are compared with the model of PRYCE[3].

1. Introduction.

In the *Th*-active deposit, $_{81}Tl^{208}$ is formed by the α-decay of $_{83}Bi^{212}$. The α-spectrum consists of six lines, and the corresponding level scheme is of particular interest since $_{81}Tl^{208}$ has one proton hole and one neutron outside a double-closed shell structure.

The levels as indicated by the α-spectrum appear in Fig. 1. From shell model considerations, PRYCE[3] has interpreted the two lowest levels as a doublet resulting from the splitting of an $(s_{1/2}\, g_{9/2})$ configuration. Similarly, the four upper levels can be obtained by the splitting of a $(d_{3/2}\, g_{9/2})$ configuration. Tentatively, the angular momenta shown in Fig. 2 were ascribed to the levels.

The $(\alpha$—$\gamma)$ angular correlation measurements of HORTON and SHERR[4], and of WEALE[5], suggest that the angular momenta of the ground state and the first excited level are (5, 4). This agrees with the subsequent disintegration of Tl^{208}, which decays by β-emission (log $ft \sim 5.5$) to levels with angular momenta 5^- and 4^-, but not to the 3^- level in $_{82}Pb^{208}$[6]. A determination of the multipole order of the γ-rays from the excited levels would provide a further test on the consistency of the assignments of Fig. 2. As the total excitations of the different levels are known with great accuracy from the α-spectrum, the internal conversion coefficients for the γ-transitions can be found merely from the absolute intensity of the β-lines.

The disintegrations taking place in the *Th*-active deposit are shown in Fig. 3. Several of the lines in the composite β-ray spectrum are known to originate in Tl^{208}. The decay of the 40 keV level to the ground state thus results in the very strong L, M, and N conversion lines which, by ELLIS[2], were denoted the A, B, and

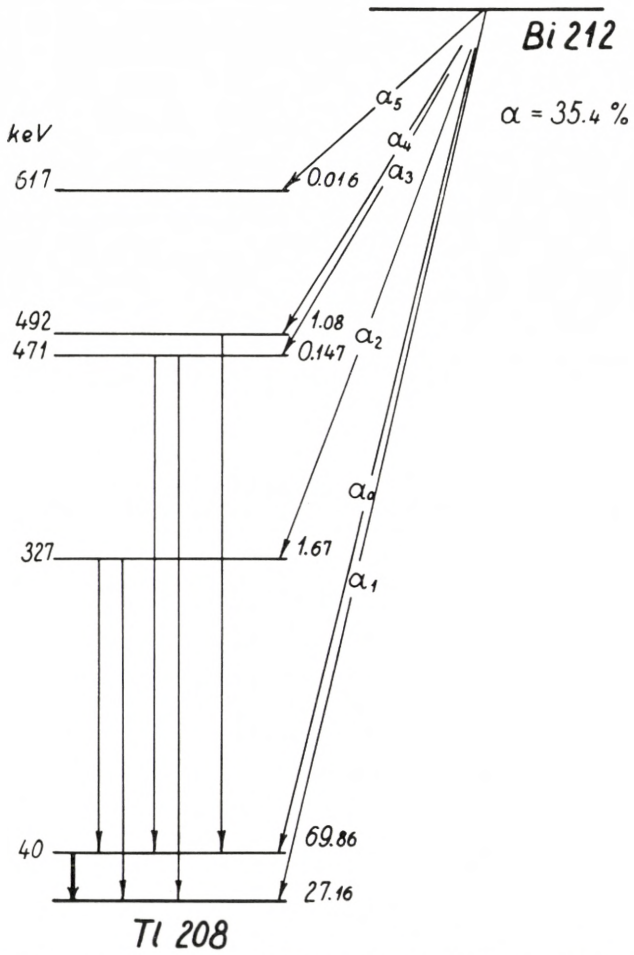

Fig. 1. The decay scheme $Bi^{212} \rightarrow Tl^{208}$. The numbers to the right in the figure indicate the excitation of the levels according to RYTZ[1]. The energies are as found by ELLIS[2]. Transitions observed in this investigation are shown by vertical arrows.

B_b lines. The radiation has been established to be of $M1$ nature from the $L_I:L_{II}:L_{III}$ ratio and from the lifetime[7]. The other lines are much weaker, as can be seen from Fig. 1. The K-conversion line for the transition from the 327 keV level to the 40 keV level (in ELLIS' notation the G_a line) has been measured by FLAMMERSFELD[8]. Some other lines have been recorded on photographic plates[2], but their intensities are not known with sufficient accuracy.

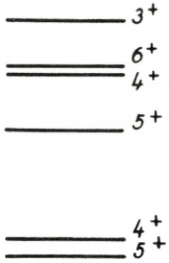

Fig. 2. The angular momenta proposed by PRYCE[3]. The value 6 for the 5th level is not in accordance with experiment.

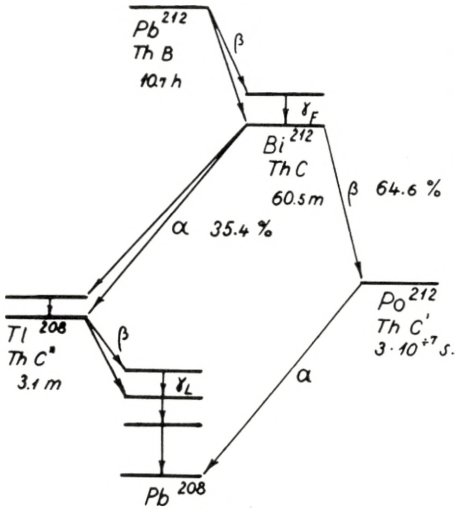

Fig. 3. Decays taking place in the *Th*-active deposit. Only the stronger branches are shown.

The experimental difficulties are due partly to the continuous β-ray background, partly to numerous strong lines from transitions in Bi^{212} and Pb^{208}. The investigation described here represents an attempt to overcome these difficulties by utilizing the coincidence between the β-particles and the internal conversion lines.

2. The Spectrometer.

The β-ray spectrometer[9] which we have recently constructed is especially well suited for coincidence experiments of this type. A 30 mm dia. glass plate covered with a thin layer of *ZnS* powder

was placed immediately behind the source. The glass plate was optically coupled to the photocathode of a multiplier tube RCA 6199 through a vacuum tight lucite window.

This type of counter produces rather strong pulses when hit by α-particles, and gives practically no response to β- and γ-radiation.

The transmission of the spectrometer without the α-counter is about 9 per cent, at a resolution of $\frac{1}{R} \sim 1.5$ per cent. It proved advantageous to place the α-counter so near the source that it covered a fraction of the useful solid angle of the spectrometer, which reduced the transmission to about 8 per cent. More than 35 per cent of the α-particles could then be counted, and the efficiency in the coincident spectrum was between 2.5 and 3 per cent.

β-particles focused in the spectrometer were counted by an anthracene crystal with optical coupling to a multiplier, EMI 6260. The voltage supplied to this photo multiplier tube was varied so as to give pulses of the same height for all energies of the β-particles.

The pulses from the two counters were fed through cathode followers to a coincidence stage with variable resolving time. The counts from the anthracene crystal and the coincidences were recorded on two decade scalers. The magnetic field had only negligible effect on the efficiency of the counters.

For reasons which will be referred to later, it was necessary to use rather strong sources. Usually, the α-counter was hit by about 10^5 α-particles per second. Although *ZnS* is a slow phosphor with a decay time of several μs, a proper shaping of the pulses reduced the blocking of the circuit caused by each pulse to about 1 μs, but the dead time still amounted to about 10 per cent. It was found that the rate of true and random coincidences was reduced to the same extent, and also that the dead time corrections varied with the source strength as predicted by counting theory. The coincidence resolving time was of the order of $^1/_{10}$ μs. It could not be reduced very much below this without loss of true coincidences, presumably because of the slowness of the *ZnS* phosphor.

3. The Sources.

The sources were prepared by activation in *Th*-emanation of small bits of aluminum foil with a thickness of 150 $\mu g/cm^2$. In most cases, these were placed between two larger pieces of the same foil and then fixed to a frame of thin copper wire by means of a small amount of vacuum grease. This mounting of the source prevents the escape of recoiling radioactive atoms, an effect described in more detail by FLAMMERSFELD[8].

Uncovered sources were used for the measurement of lines with energy below 100 keV, and the foils were activated on one side only. The counting of particles having passed through the foil had also to be avoided in these cases, and only three of the gaps of the spectrometer could be utilized.

4. The Coincident Spectrum.

a. Background conditions.

Both the composite spectrum, consisting of all the β-rays from the *Th*-active deposit, and the α-coincident part of it were recorded during the measurements. The correction factor for random coincidences was found simply from the strength of a non-coincident line in the coincident spectrum. For this purpose the *F*-line, the very strong *K*-conversion line for the 238 keV transition in Bi^{212} (see Fig. 3), was generally used. For some different points of the line the number of coincidences was plotted against the total counts. A straight line was then obtained, and the slope giving the correction factor could be found in a few minutes with a statistical uncertainty less than two per cent. Random coincidences were normally less than one per cent of the counts in the composite spectrum.

Fig. 4 shows the final spectrum corrected for random coincidences. The continuous background is due to β-particles in coincidence with α-particles from Po^{212} (see Fig. 3). Since the half life of this isotope is only about $^3/_{10}\,\mu s$, a fraction of the α-particles is emitted so fast that they appear coincident with the β-particles in the continuous spectrum from Bi^{212}. With a resolving time $\sim {}^1/_{10}\,\mu s$, about 8 per cent of these α-particles

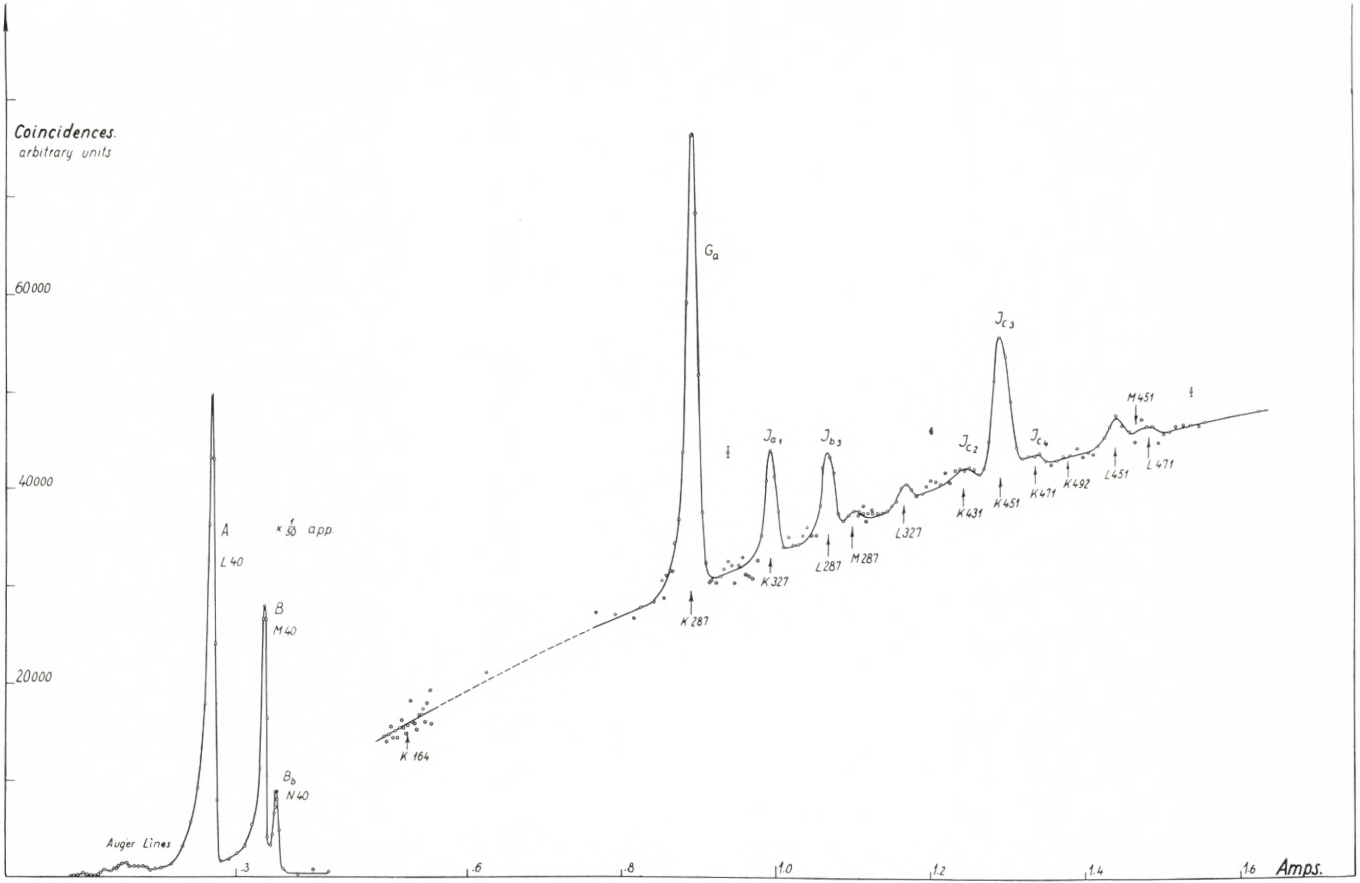

Fig. 4. The coincident spectrum. The lines observed by ELLIS[2] are denoted by the letters introduced by him. The terms below the curve refer to conversion shell and γ-ray energy, the arrows indicating the calculated positions of the lines. Standard statistical fluctuations are indicated by dotted bars above the curve.

were able to produce coincidences, and this background constituted the main experimental difficulty.

If a background consists principally of random coincidences, it varies approximately as the second power of source strength. The outcome of an experiment will then be rather independent of the source strength, since the height of the coincident lines as well as the statistical fluctuations go with first power. This does not hold for the background described above. Sufficient statistical accuracy could be obtained within a reasonable time only when the sources were as strong as possible, the limiting factor being the dead time of the coincidence circuit.

In order to cover a reasonable part of the spectrum within the half life of the source, 10.7 h, counting could not go on more than 10 min. for each point. With this counting period the height of the weaker lines was less than twice the statistical fluctuations. To improve the accuracy, the measurements were repeated, for a certain part of the spectrum 13 times. The magnetic field was adjusted to the same values in each run to make possible a summation of the statistical material.

The spectrum on Fig. 4 contains a summary of the information gained from these experiments. Standard statistical deviations for the different parts are given by the dotted bars above the curve. The section between the arrows M 287 and K 492 was measured with the greatest accuracy, each point corresponding, as mentioned, to more than two hours of counting. Then the three weak lines in the region had a height of more than 6 times the statistical fluctuations. The spectrum represents more than 200 hours of measurements.

b. The strength of the lines.

Of the stronger lines in Fig. 4, B and J_{c3} are completely resolved from non-coincident lines in the composite spectrum. The ratio between their intensities in the two spectra could then be found, thus giving the efficiency of the coincidence arrangement. The results obtained from both lines agreed. Unfortunately, J_{c3} is not strong enough to make the experimental uncertainty less than about 10 per cent, but the relative strength of neighbouring lines is certainly given with rather good accuracy from Fig. 4.

The determination of the absolute intensities involves a comparison in the composite spectrum of the area under at least one of them with the total area of the continuous β-ray spectra, which represents the total number of disintegrations in the source. The line G_a has been measured in this way by FLAMMERSFELD[8], unfortunately, however, with poor statistical accuracy.

The composite spectrum recorded simultaneously with the coincident part could in principle be used in this manner. It appeared, however, that the scattering of particles caused by the α-counter increased the area of the continuous spectrum between 15 and 20 per cent. The general shape was not changed very much, and neither the shape nor the relative strength of the lines was altered. As a number of the stronger lines have been measured absolutely with great care in other cases[8, 10, 11], the intensity of the coincident lines could also have been found merely by using these known lines as standards instead of the continuous spectrum.

It was decided, however, to make an independent determination on the G_a line. As a check of the reliability of the procedure, a few of the strong lines with known intensity were redetermined. These measurements, performed with the α-counter removed, are described in Section 5.

5. Redetermination of the Intensity of G_a and Some Strong Lines.

a. The F and L lines.

The area of the continuous β-ray spectra was obtained by the procedure worked out by FLAMMERSFELD[8] and others[10]. To diminish the uncertainties from the measurement of the low energy β-rays, the method makes use of only the partial spectra of high energy which orginate in Bi^{212} and Tl^{208} (Fig. 3). The separation from the soft component of Pb^{212} was made by extrapolation, according to the spectral shape for ($Bi^{212} + Tl^{208}$) as found by FLAMMERSFELD[8] and by MARTIN and RICHARDSON[10].

Due to the one hour lifetime of Bi^{212} compared to the 10.7 hour lifetime of Pb^{212}, the ($Bi^{212} + Tl^{208}$)-spectrum must be approximately 11 per cent stronger than the spectrum of Pb^{212} when the source is in radioactive equilibrium[10].

The two strong lines, F (148 keV) and L (422 keV), representing different energy regions, were selected. They were obtained with the same resolution as used in the coincident measurements.

The intensity of F was found to be 0.30 ± 0.02 of all disintegrations $Pb^{212} \rightarrow Bi^{212}$. This is in accord with more recent determinations[8, 10, 11]. The measurement was reproducible within 2 per cent, but the experimental uncertainty must be estimated as somewhat higher, due to some arbitrariness in the method of extrapolating.

The ratio between the intensities of the F line and the L line was found to be 45 ± 3, in agreement with MARTIN and RICHARDSON. FLAMMERSFELD has found a ratio of 37, but his results seem to be higher than other determinations for several of the high energy lines.

b. The G_a and I lines.

As mentioned previously, the coincident lines B and J_{c3} are not disturbed by neighbouring lines, and their intensities could thus be deduced from a comparison with the F line. J_{c3} is rather weak, however, and the energy of the B line (36 keV) is so low that a certain loss of true coincidences could not be excluded. Therefore, it was decided to base the determination of the absolute strength of the coincident lines on G_a (202 keV). With the resolution used in the experiments described so far, this line was not resolved from the very much stronger H line from Bi^{212}, which has a momentum only 2 per cent higher. Consequently the resolution was increased to $\frac{1}{R} \sim 0.7$ per cent. Only two of the gaps of the spectrometer were utilized, with the solid angle reduced to ~ 1.5 per cent. The source was about 3×1 mm^2, and the transmission was then 1.2 per cent.

Fig. 5 shows the G, G_a, and H lines which are well resolved at this resolution. The height of G_a relative to F could be found with a statistical uncertainty not exceeding 2 per cent, but the experimental uncertainty was raised somewhat due to the tail of the H line, which contributed to the strength of G_a by a few per cent.

With the intensity of the F line as given above, the strength

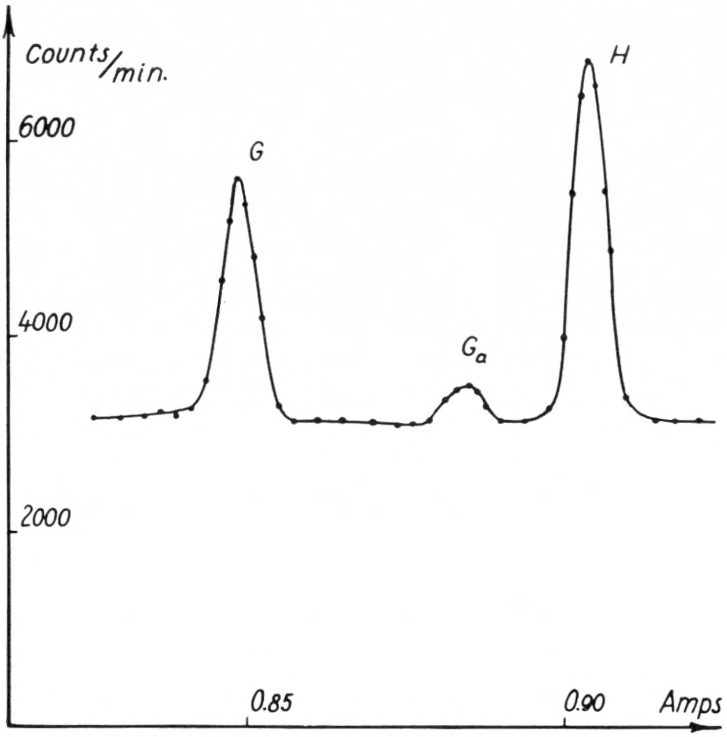

Fig. 5. The G, G_a, and H lines. Resolution 0.7 per cent.

of G_a was found to be $(11.3 \pm 1.2) \times 10^{-4}$ of all disintegrations of $Bi^{212} + Tl^{208}$. This agrees with FLAMMERSFELD's[8] results.

At this resolution, the I line also is separated from the neighbouring lines. The ratio $\frac{F}{I}$, which is the K/L ratio for the 238 keV magnetic dipole[7] γ-ray, was determined to 5.5 ± 0.2, also in accordance with FLAMMERSFELD.

6. The Multipole Order of the Transitions.

The 40 keV transition responsible for the strong low energy lines in Fig. 4 is known to be of M1 nature[7]. An accurate determination of the intensity of these lines was not attempted, but it was found that internal conversion took place in more than

70 per cent of the cases. A better determination of the conversion coefficients has been obtained from measurements of the γ-ray[5, 12].

From Fig. 4, in addition to the low energy lines, 5 K-conversion lines and 3 L-conversion lines can be established. The intensities are roughly in agreement with the results of Ellis[2] for the lines G_a, J_{a1}, and J_{b3}, but J_{c2} turned out to be two times weaker and J_{c3} four times stronger than previously reported. It is remarkable that the lines L 327 and L 451 have not been observed earlier, although they are stronger than J_{c2} and J_{c4}. The strength of the lines on Fig. 4, relative to G_a, is given in Table I.

Table I.

γ-ray energy keV.	Conv. shell	β-line energy keV.	Intensity relative to G_a	γ-ray energy keV.	Conv. shell	β-line energy keV.	Intensity relative to G_a
287	K	202	1	431	K	346	0.035 ± 0.010
287	L	272	0.19 ± 0.01	451	K	366	0.30 ± 0.02
327	K	242	0.24 ± 0.01	451	L	436	0.055 ± 0.010
327	L	312	0.050 ± 0.010	471	K	386	0.022 ± 0.006

Table II shows the corresponding K-shell internal conversion coefficients α_k, and the K/L ratios. The calculation is based on $G_a = 11.3 \times 10^{-4}$, a branching ratio[13]

$$\frac{Bi^{212} \rightarrow Tl^{208}}{Bi^{212} \rightarrow Tl^{208} + Po^{212}} = 0.354,$$

and an excitation of the levels as indicated on Fig. 1. In the two cases where two transitions take place from the same level, only a mean value $\frac{\beta_1 + \beta_2}{\gamma_1 + \gamma_2}$ of the conversion coefficients can be calculated, as the relative intensities of the γ-rays are unknown.

The theoretical conversion coefficients are taken from the tables of Rose et al.[14, 15].

The lifetimes of the excited states must necessarily be of the order of or shorter than the coincidence resolving time, $^1/_{10}\,\mu$s. This excludes multipole orders higher than E1, E2, M1, and M 2, and the conversion coefficients are very different in these cases. The M 1 nature of the transitions in Table II is indicated

TABLE II.

γ-Ray energy keV	α_k observed	α_k theoretical				K/L ratios observed	K/L ratios theoretical	
		$E1$	$E2$	$M1$	$M2$		$E2$	$M1$
287	0.33 ± 0.05	0.027	0.070	0.50	1.55	5.3 ± 0.3	1.2	5.7
327		0.020	0.053	0.35	1.00	5 ± 1	1.6	5.7
431	0.14 ± 0.05	0.011	0.030	0.17	0.44			
471		0.0090	0.024	0.13	0.33			
451	0.10 ± 0.02	0.010	0.027	0.15	0.38	5 ± 1	2.5	5.7

by the conversion coefficients, and for three of them it is confirmed by the K/L ratio. The deviations from the theoretical values are probably due to an admixture of E2 radiation*).

It was not possible to detect the K-lines for transitions from the 492 keV level to 327 keV or to the ground state. An upper limit for their strength is about $^1/_{20}$ of the line K 451. The excitation of the 617 keV level is about 9 times weaker than for 471 keV. It was not attempted to find the corresponding lines.

7. Discussion.

The decay scheme in Fig. 1 is definitely born out by the establishment of coincidences between α-particles and the internal conversion lines. Change in angular momenta of $\Delta I = 0$ or 1 are indicated by the magnetic dipole character of the transitions, which also shows the 5 lower levels to have the same parity.

Thus, the angular momenta of the 327 and 471 keV levels must be either 4 or 5 if the ground state doublet, as supported by earlier experiments, is assumed to be (5, 4). The 492 keV level then most probably has angular momentum 3. A low angular momentum for this level is consistent with the relative intensities of the α-lines. Bi^{212} has angular momentum 1[4], and the α-transition to the 492 keV level is the most favoured of the transitions shown in Fig. 1. An angular momentum of 3 for this

*) Note added in proof: Results recently obtained in Amsterdam suggest that the theoretical $M1$ conversion coefficients are 30–40 per cent too high. G. J. NIJGH and A. H. WAPSTRA: To be published.

level is in disagreement with the assignments of Fig. 2. This is not a serious failure of the model which does not definitely give the order of the levels in a configuration.

Acknowledgements.

The author wishes to express his sincere gratitude to Professor NIELS BOHR for his continuous interest in these problems and for ideal working conditions in his Institute.

I am indebted to Professor M. H. L. PRYCE for helpful suggestions, and to Drs. AAGE BOHR and BEN R. MOTTELSON for valuable discussions.

Institute for Theoretical Physics,
University of Copenhagen,
Denmark.

References.

1. A. Rytz: C. R. **233**, 790 (1951)
2. C. D. Ellis: Proc. Roy. Soc. **A 138**, 318 (1932)
3. M. H. L. Pryce: Proc. Phys. Soc. **65 A** 773, **65 A**; 962, (1952)
4. J. Horton and R. Sherr: Phys. Rev. **90**, 388 (A) (1953)
5. J. W. Weale: Proc. Phys. Soc. **68 A**, 35 (1955)
6. L. G. Elliot, R. L. Graham, J. Walker, and J. L. Wolfson: Phys. Rev. **93**, 356 (1954)
7. R. L. Graham and R. E. Bell: Can. Jour. of Phys. **31**, 377 (1953)
8. A. Flammersfeld: Z. Phys. **114**, 227 (1939)
9. O. B. Nielsen and O. Kofoed-Hansen: Dan. Mat. Fys. Medd. **29**, no. 6 (1955)
10. D. G. E. Martin and H. O. W. Richardson: Proc. Roy. Soc. **A 195**, 287 (1948)
11. N. Feather, J. Kyles, and R. W. Pringle: Proc. Phys. Soc. **61**, 466 (1948)
12. B. B. Kinsey: Phys. Rev. **72**, 526 (1947)
13. P. Marin, G. R. Bishop, and H. Halban: Proc. Phys. Soc. **66 A**, 608 (1953)
14. M. E. Rose, G. H. Goertzel, and C. L. Perry: ORNL-1923 (1953)
15. M. E. Rose, G. H. Goertzel, and C. Swift: L-shell internal conversion coefficients, privately distributed.

Indleveret til selskabet den 24. marts 1955.
Færdig fra trykkeriet den 3. oktober 1955.

Det Kongelige Danske Videnskabernes Selskab
Matematisk-fysiske Meddelelser, bind **30**, nr. 12

Dan. Mat. Fys. Medd. **30**, no. 12 (1955)

DEDICATED TO PROFESSOR NIELS BOHR ON THE OCCASION OF HIS 70TH BIRTHDAY

DEN KLASSISKE MEKANIK I GEOMETRISK BESKRIVELSE

AF

MOGENS PIHL

With an English Summary

København 1955
i kommission hos Ejnar Munksgaard

INDHOLD

Printed in Denmark
Bianco Lunos Bogtrykkeri A-S

Indledning.

Et væsentligt træk i den moderne matematiske fysik er indsigten i den *geometriske udtryksmaades rige muligheder*. En indsigt, som jo ogsaa i stedse mere vidtgaaende grad præger den rene matematik. Og samtidig med denne voksende brug af geometriske udtryksmaader i den matematiske formalisme er vi gennem den almindelige relativitetsteoris beskrivelse af gravitationsfeltet — og de forhaabninger, denne »geometrisering« har givet anledning til — blevet stillet overfor problemet om det *fysiske rums struktur*.

Begge disse tendenser — der ikke skarpt kan adskilles — kan allerede skimtes indenfor den klassiske fysik, og, som det saa ofte er tilfældet indenfor videnskabens historie, har ogsaa her de moderne synspunkter bevirket, at man ser paa visse tidligere antydninger i denne retning med større forstaaelse og varmere sympati, end de oprindeligt mødte. Der er her tale om en sympati, som ikke sjældent i fysikkens historie har givet anledning til en noget misforstaaet proklamering af »forløberskaber« for de traditionelt anerkendte banebrydere, hvorved fortolkningen af de gamles udsagn er gaaet langt udover det historisk mulige*. Men trods denne risiko for at se det tidligere med nutidens briller, vil vi alligevel i det følgende forsøge at minde om, hvorledes den moderne fysiks geometriske synspunkter ogsaa kan findes paa et lidt tidligere tidspunkt af fysikkens udvikling, idet vi samtidig vil antyde den pædagogiske hjælp, den moderne formalisme kan yde i beskrivelsen af de klassiske, os helt fortrolige problemstillinger.

* Et velkendt eksempel herpaa er P. Duhems overvurdering af en vis — tidligere ganske vist helt overset — middelalderlig tankeverdens paastaaede foregriben af den heftige udvikling i mekanikkens historie, vi sædvanligt — og med megen ret — knytter til Galileis navn.

Hvad angaar den *formelle* brug af geometriske udtryksmaader, er det i særdeleshed den *klassiske mekaniks variationsprincipper*, som i denne forbindelse har været af betydning. Klarest træder denne sammenhæng mellem geometri og variationsregning vel frem i en berømt afhandling af P. FINSLER [4], i hvilken der fremsættes en saa almindelig geometri, at et forelagt variationsprincip simpelthen fortolkes som et problem om at finde geodætiske kurver i et rum med en passende metrik, idet man altsaa indretter denne metrik efter variationsprincippet. En tanke, der har mange forløbere, og som f. eks. allerede LIOUVILLE i forbindelse med mekanikkens problemstilling havde været inde paa — som den første spire kan maaske nævnes EULERS paavisning af, at den kraftfri bevægelse af et punkt paa en glat flade foregaar med konstant hastighed langs geodætiske kurver paa fladen. Hos FINSLER og hans mange efterfølgere førte denne indstilling til meget vidtgaaende geometriske generalisationer, hvor det dog var muligt at eftervise mange fra den almindelige geometri fortrolige forhold. I særdeleshed tillader denne »geometrisering« af variationsregningen en smuk fremstilling af de til variationsproblemerne hørende *integrationsteorier* — den Hamilton-Jacobiske teori i mekanikken — og der bestaar her en meget nær overensstemmelse mellem denne geometriske betragtningsmaade og den af HAMILTON indførte *optiske analogi* til behandlingen af saadanne spørgsmaal i mekanikken.

Men det er velkendt (se f. eks. J. L. SYNGE [11]), at den ved relativitetsteorien betingede beskæftigelse med de mere specielle *Riemannske rum* ogsaa viste sig at være af stor betydning for beskrivelsen af den klassiske mekanik, idet man lader den ved den kinetiske energi bestemte kvadratiske form i de generaliserede hastigheder fastlægge metrikken i det til det betragtede mekaniske system hørende konfigurationsrum, hvis koordinater er systemets generaliserede koordinater. Det er dog ikke muligt med denne mere specielle metrik at reducere bevægelseskurverne i dette rum til geodætiske kurver, der gennemløbes med konstant hastighed. Men vi vil i det følgende vise, at det gennem indførelsen af en ekstra koordinat — en saakaldt cyklisk koordinat — er muligt at foretage en saadan reduktion til *inertiens lov* uden at forlade den ved den Riemannske metrik bestemte form for geometri. Det drejer sig her om en ubetydelig drejning af en

tanke, som først klart blev formuleret af J. J. THOMSON, og som i særlig grad ligger til grund for H. HERTZ' bestræbelser paa at eliminere kraftbegrebet i mekanikken.

Med hensyn til spørgsmaalet om det *fysiske rums struktur* er der jo her tale om et problem, som rejste sig, *saasnart* de ikke-euklidiske geometrier var erkendt som tankemuligheder. Vi skal her nøjes med at anføre senere udtalelser af RIEMANN og CLIFFORD, som i særlig grad viser en klar forstaaelse af denne problemstilling.

I det berømte habilitationsskrift »*Ueber die Hypothesen, welche der Geometrie zu Grunde liegen*« skriver RIEMANN [8]: *Die Fragen über das Unmessbargrosse sind für die Naturerklärung müssige Fragen. Anders verhält es sich aber mit den Fragen über das Unmessbarkleine. Auf der Genauigkeit, mit welcher wir die Erscheinungen in's Unendlichkleine verfolgen, beruht wesentlich die Erkenntnis ihres Causalzusammenhangs. Die Fortschritte der letzten Jahrhunderte in der Erkenntniss der mechanischen Natur sind fast allein bedingt durch die Genauigkeit der Construktion, welche durch die Erfindung der Analysis des Unendlichen und die von* ARCHIMED, GALILÄI *und* NEWTON *aufgefundenen einfachen Grundbegriffe, deren sich die heutige Physik bedient, möglich geworden ist. In den Naturwissenschaften aber, wo die einfachen Grundbegriffe zu solchen Construktionen bis jetzt fehlen, verfolgt man, um den Causalzusammenhang zu erkennen, die Erscheinungen in's räumlich Kleine, so weit es das Mikroskop nur gestattet. Die Fragen über die Massverhältnisse des Raumes im Unmessbarkleinen gehören also nicht zu den müssigen. — Setzt man voraus, dass die Körper unabhängig vom Ort existiren, so ist das Krümmungsmass überall constant, und es folgt dann aus den astronomischen Messungen, dass es nicht von Null verschieden sein kann; jedenfalls müsste sein reciprocer Werth eine Fläche sein, gegen welche das unsern Teleskopen zugängliche Gebiet verschwinden müsste. Wenn aber eine solche Unabhängigkeit der Körper vom Ort nicht stattfindet, so kann man aus den Massverhältnissen im Grossen nicht auf die im Unendlichkleinen schliessen; es kann dann in jedem Punkte das Krümmungsmass in drei Richtungen einen beliebigen Werth haben, wenn nur die ganze Krümmung jedes messbaren Raumtheils nicht merklich von Null verschieden ist; noch complicirtere Verhältnisse können eintreten, wenne die vorausgesetzte Darstellbarkeit eines*

Linienelements durch die Quadratwurzel aus einem Differentialausdruck zweiten Grades nicht stattfindet. Nun scheinen aber die empirischen Begriffe, in welchen die räumlichen Massbestimmungen gegründet sind, der Begriff des festen Körpers und des Lichtstrahls, im Unendlichkleinen ihre Gültigkeit zu verlieren; es ist also sehr wohl denkbar, dass die Massverhältnisse des Raumes im Unendlichkleinen den Voraussetzungen der Geometrie nicht gemäss sind, und dies würde man in der That annehmen müssen, sobald sich dadurch die Erscheinungen auf einfachere Weise erklären liessen. — Die Frage über die Gültigkeit der Voraussetzungen der Geometrie im Unendlichkleinen hängt mit der Frage nach dem innern Grunde der Massverhältnisse des Raumes zusammen. Bei dieser Frage, welche wohl noch zur Lehre vom Raume gerechnet werden darf, kommt die obige Bemerkung zur Anwendung, dass bei einer discreten Mannigfaltigkeit das Princip der Massverhältnisse schon in dem Begriffe dieser Mannigfaltigkeit enthalten ist, bei einer stetigen aber anders woher hinzukommen muss. Es muss also entweder das dem Raume zu Grunde liegende Wirkliche eine discrete Mannigfaltigkeit bilden, oder der Grund der Massverhältnisse ausserhalb, in darauf wirkenden bindenden Kräften, gesucht werden. — Die Entscheidung dieser Fragen kann nur gefunden werden, indem man von der bisherigen durch die Erfahrungen bewährten Erscheinungen, wozu Newton den Grund gelegt, ausgeht und diese durch Tatsachen, die sich aus ihr nicht erklären lassen, getrieben allmählich umarbeitet; solche Untersuchungen, welche, wie die hier geführte, von allgemeinen Begriffen ausgehen, können nur dazu dienen, dass diese Arbeit nicht durch die Beschränktheit der Begriffe gehindert und der Fortschritt im Erkennen des Zusammenhangs der Dinge nicht durch überlieferte Vorurtheile gehemmt wird.«

Riemanns habilitationsforelæsning gjorde et stærkt indtryk paa den unge, engelske matematiker W. K. Clifford, som oversatte den til Engelsk og offentliggjorde den i *Nature*. I en lille note fra 1876 skriver han [Clifford 1]:

Riemann has shown that as there are different kinds of lines and surfaces, so there are different kinds of spaces of three dimensions; and that we can only find out by experience to which of these kinds the space in which we live belongs. In particular, the axioms of plane geometry are true within the limits of experience on the surface of a sheet of paper, and yet we know that the sheet

is really covered with a number of small ridges and furrows, upon which (the total curvature not being zero) these axioms are not true. Similarly, he says although the axioms of solid geometry are true within the limits of experiment for finite portions of our space, yet we have no reason to conclude that they are true for very small portions; and if any help can be got thereby for the explanation of physical phenomena, we may have reason to conclude that they are not true for very small portions of space. I wish here to indicate a manner in which these speculations may be applied to the investigation of physical phenomena. I hold in fact

(1) *That small portions of space are in fact of a nature analogous to little hills on a surface which is on the average flat; namely that the ordinary laws of geometry are not valid in them.*

(2) *That this property of being curved or distorted is continually being passed on from one portion of space to another after the manner of a wave.*

(3) *That this variation of the curvature of space is what really happens in that phenomena we call the motion of matter, being ponderable or etherial.*

(4) *That in the physical world nothing else takes place but this variation, subject (possibly) to the laws of continuity.*

I am endeavouring in a general way to explain the laws of double refraction on this hypothesis, but have not yet arrived at any results sufficiently decisive to be communicated.

Og i den velkendte, populære bog *The Common Sense of the Exact Sciences* vender han i et afsnit om *The Bending of Space* tilbage til problemet og skriver her [Clifford 2]:

We may . . . ask . . . whether we may not . . . be treating merely as physical variations effects which are really due to changes in the curvature of our space; whether, in fact, some or all of those causes which we term physical may not be due to the geometrical construction of our space.

Og lidt senere:

We may conceive our space to have everywhere a nearly uniform curvature, but that slight variations of the curvature may occur from point to point, and themselves vary with the time. These variations of the curvature with the time may produce effects which we not unnaturally attribute to physical causes independent of the geometry of our space. We might even go so far as to assign to this

variation of the curvature of space "what really happens in that phenomena which we term the motion of matter".

Desværre findes intetsteds antydninger af, hvorledes CLIFFORD har tænkt sig disse tanker udformet til en matematisk teori, men af det citerede fremgaar tydeligt, at han har været helt klar over de muligheder, vi nu betegner med ordene »fysikkens geometrisering«.

Vi vil nu i det følgende gøre rede for, hvorledes det er muligt at give en geometrisk beskrivelse af den klassiske mekanik, idet vi indleder med en kortfattet og til formaalet tillempet fremstilling af de træk af den helt almindelige geometri — den Finslerske geometri — vi vil faa brug for. Der bliver her tale om rent *formelle* og den moderne fysiker i det væsentlige fortrolige forhold. Den her angivne vej tillader en i pædagogisk henseende lejlighedsvis frugtbar anvendelse af geometriske udtryksmaader, men de anstillede betragtninger er uden betydning for forstaaelsen af problemet om det fysiske (3-dimensionale) rums struktur. *Ethvert felt* kan i denne beskrivelse opfattes som en egenskab ved rummets metriske struktur, saaledes at det ikke er muligt ad denne vej at diskriminere geometrisk mellem de forskellige felter — tyngdefeltet og det elektromagnetiske felt — i den forstand, at disse opfattes som udtryk for forskellige geometriske træk.

I. Geometriske forudsætninger.

Et ved koordinaterne x^i, $i = 1, 2, \ldots, n$, bestemt n-dimensionalt rum siges at være *Finslersk*, saafremt der til hvert punkt x^i og hver kontravariant vektor a^i gives et af valget af koordinatsystem uafhængigt tal $M\,(x^i, a^i)$, som er 0, dersom alle $a^i = 0$, og ellers er positivt, og for hvilket $M\,(x^i, \alpha\, a^i) = \alpha\, M\,(x^i, a^i)$, $\alpha > 0$, d.v.s. at invarianten M skal være *positiv homogen af første grad* i a^i, saaledes at

$$\frac{\partial M}{\partial a^i}\, a^i = M.$$

Invarianten

$$L = \frac{1}{2} M^2 = \frac{1}{2} \frac{\partial L}{\partial a^i}\, a^i = \frac{1}{2}\, a_i\, a^i$$

er da positiv homogen af anden grad i a^i og betegnes som den *metriske fundamentalinvariant.* Størrelserne

$$a_i = \frac{\partial L(x^i, a^i)}{\partial a^i}$$

transformeres som komponenterne af en kovariant vektor: den til a^i hørende kovariante vektor. Til αa^i hører αa_i, men i almindelighed vil den til $a^i + b^i$ hørende kovariante vektor ikke være $a_i + b_i$. Og ligeledes vil i almindelighed det *skalare produkt* $a^i b_i$, der er en invariant, ikke være lig med $a_i b^i$. Man beviser let, at den til $a^i + b^i$ hørende kovariante vektor er $a_i + b_i$, samt at $a^i b_i = a_i b^i$, hvis og kun hvis den metriske fundamentalinvariant er af formen

$$L = \frac{1}{2} g_{ik}\, a^i a^k,$$

hvor g_{ik} er komponenterne af en kovariant tensor af anden orden, kun afhængig af koordinaterne x^i. Rummet siges da, som bekendt, at være *Riemannsk.*

Ved den *numeriske værdi* eller *længden* af den kontravariante vektor a^i forstaas invarianten

$$| a^i | = \sqrt{a^i a_i} = \sqrt{2 L} = M(x^i, a^i).$$

Er $| a^i | = 1$, siges a^i at være en kontravariant *enhedsvektor.* Vi forudsætter, at der til hver kovariant vektor findes en entydig bestemt kontravariant vektor, hvortil den svarer, og ved den numeriske værdi af en kovariant vektor forstaas da den numeriske værdi af den kontravariante vektor, hvortil den svarer. Altsaa $| a_i | = | a^i |$.

Er $a^i b_i = 0$, siges den kontravariante vektor a^i at *staa vinkelret* paa den kovariante vektor b_i. Kun for Riemannske rum vil da den kontravariante vektor b^i staa vinkelret paa den kovariante a_i.

Invarianten M tillader nu umiddelbart indførelsen af *buelængder:* er $x^i = x^i(t)$ en differentiabel kurve, hvor t er en parameter, vil vi ved buelængden fra det ved t_1 til det ved t_2 bestemte punkt forstaa integralet

$$s_{12} = \int_{t_1}^{t_2} M(x^i, \dot{x}^i)\, dt, \quad \text{hvor} \quad \dot{x}^i = \frac{dx^i}{dt},$$

og man ser straks, at et parameterskifte ikke ændrer buelængden, da M er homogen af første grad i $\dot{x}^i$. Iøvrigt er $\dot{x}^i$ en kontravariant vektor: den til parameteren t hørende *hastighed*. Specielt er for den naturlige parameterfremstilling (hvor buelængden til et variabelt punkt er parameteren) hastighedsvektoren

$$r_i = \mathring{x}^i = \frac{dx^i}{ds}$$

en enhedsvektor:

$$M(x^i, \mathring{x}^i) = 1,$$

kaldet *retningsvektoren*. Af

$$\dot{x}^i = \frac{dx^i}{ds} \cdot \frac{ds}{dt} = r_i \frac{ds}{dt}$$

ses da straks, at $|\dot{x}| = \frac{ds}{dt}$.

Størrelserne $\ddot{x}^i$ er ikke vektorkomponenter. Derimod ses let, at de »Lagrangeske afledede«

$$a_i = \frac{d}{dt}\frac{\partial L}{\partial \dot{x}^i} - \frac{\partial L}{\partial x^i}, \quad L = L(x^i, \dot{x}^i)$$

er komponenterne af en kovariant vektor, kaldet den til t hørende *akceleration*. Akcelerationen hørende til det naturlige parametervalg betegnes som *krumningsvektoren:*

$$k_i = \frac{d}{ds}\frac{\partial L}{\partial \mathring{x}^i} - \frac{\partial L}{\partial x^i}, \quad L = L(x^i, \mathring{x}^i).$$

Det ses let, at $r^i k_i = 0$. Den reciproke værdi af $|k_i|$ kaldes for *krumningsradius*. For en vilkaarlig parameter t kan k_i ogsaa bestemmes som

$$k_i = \frac{ds}{dt}\left\{\frac{d}{dt}\frac{\partial M}{\partial \dot{x}^i} - \frac{\partial M}{\partial x^i}\right\}, \quad M = M(x^i, \dot{x}^i).$$

Ved elementære regninger under hensyntagen til, at L er homogen af anden orden i $\dot{x}^i$, paavises umiddelbart den fortrolige kinematiske relation:

$$a_i = \left(\frac{ds}{dt}\right)^2 k_i + \frac{d^2 s}{dt^2} r_i,$$

hvor r_i er den til retningsvektoren hørende kovariante vektor. Af $r^i k_i = 0$ fremgaar, at $a_i = 0$ medfører:

$$\frac{d^2 s}{dt^2} = 0 \quad \text{og} \quad k_i = 0.$$

I det Riemannske rum er da ogsaa

$$a^i = \left(\frac{ds}{dt}\right)^2 k^i + \frac{d^2 s}{dt^2} r^i,$$

hvor a^i og k^i er de til akceleration og krumningsvektor hørende kontravariante vektorer. I eksistensen af denne kendte kinematiske relation kan vi søge berettigelsen af ovennævnte definitioner paa akceleration og krumning.

Rette linjer er nu kurver, der overalt har krumningen *0*. Og af det ovennævnte fremgaar da, at disse kurver er ekstremaler til variationsproblemet:

$$\delta \int_{t_1}^{t_2} L\,(x^i, \dot{x}^i)\, dt = 0$$

og til problemet:

$$\delta \int_{t_1}^{t_2} M\,(x^i, \dot{x}^i)\, dt = 0, \text{ d.v.s. } \delta \int_{s_1}^{s_2} ds = 0.$$

II. Potentialfrie, tidsuafhængige systemer.

Vi begynder med at erindre om det velkendte forhold, at et dynamisk system, der er underkastet holonome, tidsuafhængige baand, og hvori ikke virker andre kræfter end de fra baandene

hidrørende reaktioner, kan beskrives ved hjælp af et variationsprincip

$$\delta \int_{t_1}^{t_2} L_0 \, dt = 0,$$

hvor t er tiden, og hvor den Lagrangske funktion er af formen

$$L_0 = \frac{1}{2} g_{ik} \dot{x}^i \dot{x}^k,$$

saaledes at størrelserne g_{ik} udelukkende er funktioner af de generaliserede koordinater x^i. Af de til variationsprincippet hørende differentialligninger

$$\frac{d}{dt} \frac{\partial L_0}{\partial \dot{x}^i} - \frac{\partial L_0}{\partial x^i} = 0$$

følger straks

$$\text{Energien } H = \frac{\partial L_0}{\partial \dot{x}^i} \dot{x}^i - L_0 = L_0 = \text{konst.},$$

og L_0 betegnes som systemets kinetiske energi = totalenergien H. L_0 er positiv-definit i $\dot{x}$'erne.

Ved g_{ik} er fastlagt en Riemannsk metrik i det ved koordinaterne x^i bestemte *konfigurationsrum:*

$$ds^2 = \frac{1}{2} g_{ik} \, dx^i \, dx^k,$$

hvor ds er bueelementet, og man har da for det dynamiske systems baner i dette rum

$$\left(\frac{ds}{dt}\right)^2 = \frac{1}{2} g_{ik} \dot{x}^i \dot{x}^k = L_0,$$

saaledes at systempunktets hastighed altsaa er *konstant.*

Endvidere har vi for akcelerationen

$$0 = \frac{d}{dt} \frac{\partial L}{\partial \dot{x}^i} - \frac{\partial L}{\partial x^i} = a_i = \left(\frac{ds}{dt}\right)^2 k_i + \frac{d^2 s}{dt^2} r_i = \left(\frac{ds}{dt}\right)^2 k_i,$$

eller

$$k_i = 0,$$

hvoraf ses, at banekurverne er *rette linjer.*

Vi har hermed bevist, at det systemet beskrivende systempunkt i konfigurationsrummet bevæger sig langs rette linjer med konstant hastighed. Hvilken velkendte lov kan karakteriseres som en *generalisation af inertiens lov.*

III. Tidsuafhængige systemer med skalart potential.

Dersom et dynamisk system udover reaktionskræfterne fra de holonome, tidsuafhængige baand er underkastet kræfter, der kan afledes af et tidsuafhængigt, skalart potential, er dets adfærd bestemt ved et variationsprincip som før, men med en Lagrangefunktion af formen

$$L = \frac{1}{2}\, g_{ik}\, \dot{x}^i\, \dot{x}^k + \frac{1}{2}\, g\,(x^i) = L_0 + \frac{1}{2}\, g\,.$$

Energien er her

$$H = \frac{\partial L}{\partial \dot{x}^i}\, \dot{x}^i - L = L_0 - \frac{1}{2}\, g\,,$$

og den er ligeledes konstant. Størrelsen $-\frac{1}{2}\, g$ er systemets potentielle energi og L_0 den kinetiske energi, der er positiv definit i $\dot{x}$'erne.

De til variationsprincippet hørende Lagrangeske ligninger kan skrives paa formen

$$\frac{d}{dt}\frac{\partial L_0}{\partial \dot{x}^i} - \frac{\partial L_0}{\partial x^i} = \frac{\partial \frac{1}{2}\, g}{\partial x^i}\,,$$

og lader vi som før den kinetiske energi $L_0\,(x^i,\ \dot{x}^i)$ fastlægge den metriske fundamentalinvariant, har vi da

$$\textit{akcelerationen} = a_i = \frac{\partial \frac{1}{2}\, g}{\partial x^i} = \textit{kraften.}$$

Vi indfører nu en ved

$$L' = \psi^2 L_0,\ M' = \psi M_0,\ \psi = \psi\,(x^i)$$

bestemt ny metrik og benytter som parameter ikke buelængden u i den nye metrik, men buelængden s i den oprindelige metrik.

Af

$$u = \int_{s_0}^{s} M'(x^i, \mathring{x}^i)\, ds, \quad \mathring{x}^i = \frac{dx^i}{ds}$$

følger da

$$\frac{du}{ds} = M'(x^i, \mathring{x}^i) = \psi M_0(x^i, \mathring{x}^i) = \psi,$$

idet

$M_0(x^i, \mathring{x}^i) = |\mathring{x}^i| = 1$ (nummerisk værdi i den oprindelige metrik).

Ifølge det foregaaende er krumningsvektoren k_i' i den nye metrik givet ved

$$k_i' = \frac{du}{ds}\left\{\frac{d}{ds}\frac{\partial M_i'(x^i, \mathring{x}^i)}{\partial \mathring{x}^i} - \frac{\partial M'}{\partial x^i}\right\} = \psi\left\{\frac{d}{ds}\frac{\partial (M_0\psi)}{\partial \mathring{x}^i} - \frac{\partial (M_0\psi)}{\partial x^i}\right\} =$$

$$\psi^2\left\{\frac{d}{ds}\frac{\partial M_0}{\partial \mathring{x}^i} - \frac{\partial M_0}{\partial x^i}\right\} + \psi\frac{\partial M_0}{\partial \mathring{x}^i}\frac{d\psi}{ds} - \psi M_0\frac{\partial \psi}{\partial x^i} = \psi^2 k_i + \psi\frac{d\psi}{ds}r_i - \psi\frac{\partial \psi}{\partial x^i},$$

idet

$$r_i = \frac{\partial L}{\partial \mathring{x}^i} = M_0\frac{\partial M}{\partial \mathring{x}^i} = \frac{\partial M}{\partial \mathring{x}^i}, \quad \text{da} \quad M(x^i, \mathring{x}^i) = |\mathring{x}^i| = 1.$$

Sammenholdes dette udtryk for k_i' med

$$a_i = \left(\frac{ds}{dt}\right)^2 k_i + \left(\frac{d^2 s}{dt^2}\right) r_i = \frac{\partial \frac{1}{2} g}{\partial x^i}$$

faas

$$k_i' = \left\{\psi^2 - \left(\frac{ds}{dt}\right)^2\right\} k_i + \left\{\psi\frac{d\psi}{ds} - \frac{d^2 s}{dt^2}\right\} r_i - \left\{\psi\frac{\partial \psi}{\partial x^i} - \frac{\partial \frac{1}{2} g}{\partial x^i}\right\}.$$

Tager vi kun saadanne banekurver i betragtning, der hører til samme værdi E af energien, altsaa saadanne for hvilke

$$\left(\frac{ds}{dt}\right)^2 = L_0 = E + \frac{1}{2} g,$$

og sættes

$$\psi^2 = \left(\frac{ds}{dt}\right)^2, \text{ dvs. } \psi = \sqrt{E + \frac{1}{2}g} = \frac{ds}{dt},$$

faas da

$$k_i' = 0.$$

I den nye metrik vil altsaa *de til samme energi hørende banekurver være rette linjer.* Men den hastighed

$$\frac{du}{dt} = \frac{du}{ds} \cdot \frac{ds}{dt} = \psi^2 = E + \frac{1}{2}g,$$

hvormed disse banekurver gennemløbes, vil *ikke* være konstant. Det er altsaa ikke lykkedes at redde hele inertiens lov paa denne maade.

Det her fremførte er selvfølgelig ikke andet end det velkendte *Maupertuiske princip*

$$\delta \int_{s_1}^{s_2} \sqrt{E + \frac{1}{2}g}\, ds = 0,$$

der først blev helt korrekt formuleret af Jacobi.

Fortolker vi i den geometriske optiks aand $\sqrt{E + \frac{1}{2}g}$ som *brydningsforhold n* i det ved den oprindelige metrik bestemte rum, er dette variationsprincip analogt med det Fermatske princip for isotrope legemer:

$$\delta \int_{s_1}^{s_2} n ds = 0.$$

For dynamiske systemer, hvori ogsaa optræder *vektorpotentialer*, altsaa hvis Lagrangefunktion er af formen

$$L = \frac{1}{2} g_{ik}\, \dot{x}^i\, \dot{x}^k + g_i\, \dot{x}^i + \frac{1}{2}g,$$

er det da muligt at udvide den her anførte optiske analogi, idet saadanne systemer svarer til *anisotrope*, optiske medier. Imidlertid kan man — som vi nu skal se — ogsaa gaa en anden vej, idet man indfører en ny generaliseret koordinat, altsaa udvider systemets dimension med 1.

IV. Konservative systemers geometrisering gennem indførelsen af en ny koordinat.

Det drejer sig her om anveldelsen af en oprindeligt af MAXWELL og LORD KELVIN [W.THOMSON 14] antydet tanke, ifølge hvilken former for potentiel energi skulle kunne fortolkes som hidrørende fra kinetisk energi af »skjulte« legemers bevægelse. Senere er denne tanke i almindelig form fremsat af J.J.THOMSON [13] i dennes inspirerende bog *Applications of Dynamics to Physics and Chemistry*. Vi gengiver her J. J. THOMSONS betragtninger med den trivielle tilføjelse, at vi ogsaa tager sigte paa problemer med *vektorpotential*.

Udgangspunktet er den velkendte *Routhske transformation:* hvis de generaliserede koordinater deles i to grupper x^i, $i = 1,2, \ldots l$, og y^α, $\alpha = 1,2, \ldots, m$, og hastighederne $\dot{y}^\alpha$ udtrykkes som funktioner af x^i, y^α, $\dot{x}^i$ og de ved ligningerne

$$p_\alpha = \frac{\partial L}{\partial \dot{y}^\alpha}$$

definerede *impulser* p_α, vil systemets bevægelse være bestemt ved differentialligningerne

$$\frac{d}{dt}\frac{\partial R}{\partial \dot{x}^\alpha} - \frac{\partial R}{\partial x^\alpha} = 0 \quad (\text{»Lagrangeligningerne«})$$

$$\left.\begin{aligned} \dot{y}^\alpha &= -\frac{\partial R}{\partial p_\alpha} \\ \dot{p}_\alpha &= \frac{\partial R}{\partial y^\alpha} \end{aligned}\right\} \quad (\text{»Hamiltonligningerne«}),$$

hvor den Routhske funktion

$$R = L - p_\alpha \dot{y}^\alpha$$

skal opfattes som funktion af x^i, y^α, $\dot{x}^i$ og p_α.

Er nu systemet saaledes beskaffent, at dets potentielle energi er nul, kan dets Lagrangefunktion skrives som

$$L = \frac{1}{2} g_{ik} \dot{x}^i \dot{x}^k + g_{i\alpha} \dot{x}^i \dot{y}^\alpha + \frac{1}{2} g_{\alpha\beta} \dot{y}^\alpha \dot{y}^\beta$$

med de til $\dot{y}^\alpha$ hørende impulser

$$p_\alpha = g_{i\alpha}\,\dot{x}^i + g_{\alpha\beta}\,\dot{y}^\beta$$

og den Routhske funktion

$$R = L - p_\alpha\,\dot{y}^\alpha = \frac{1}{2}\,g_{ik}\,\dot{x}^i\,\dot{x}^k - \frac{1}{2}\,g_{\alpha\beta}\,\dot{y}^\alpha\,\dot{y}^\beta .$$

Og antager vi yderligere, at koordinaterne y^α er *cykliske* (ogsaa kaldet *ignorable*), altsaa at L kun er afhængig af x'erne, $\dot{x}$'erne og $\dot{y}$'erne, men uafhængig af y'erne, vil ifølge de ovennævnte ligninger impulserne p_α være konstante. Da $\dot{y}^\alpha$ kan skrives paa formen

$$\dot{y}^\alpha = g_i^\alpha\,\dot{x}^i + g^\alpha,\ [g_i^\alpha \text{ og } g^\alpha \text{ funktioner af } x^\alpha \text{ og } p_\alpha],$$

bliver R af typen

$$R = \frac{1}{2}\gamma_{ik}\,\dot{x}^i\,\dot{x}^k + \gamma_i\,\dot{x}^i + \frac{1}{2}\gamma ,$$

hvor alle γ'erne er funktioner af x'erne og de konstante p'er. For fastlagte værdier af p'erne kan det ved de generaliserede koordinater x^i bestemte delsystem da udelukkende beskrives ved de Lagrangeske ligninger

$$\frac{d}{dt}\frac{\partial R}{\partial\,\dot{x}^i} - \frac{\partial R}{\partial\,x^i} = 0,\ R = R\,(x^i,\ \dot{x}^i,\ p_\alpha = \text{konst.})$$

og altsaa karakteriseres som et dynamisk system med Lagrangefunktionen R, altsaa et system med skalart og vektoriel potential.

Der gives saaledes former for potentiel energi, som kan fortolkes som hidrørende fra bevægelser i mere omfattende potentialfrie systemer, hvor legemerne kun er bundet af *geometriske baand.*

Det var H. Hertz' [5] grundlæggende tanke, at *alle* i naturen forekommende bevægelser skulle kunne fortolkes paa denne maade. Hans udgangspunkt er et univers af elementarpartikler, der bevæger sig i det sædvanlige, 3-dimensionale, euklidiske rum, og som kun er bundet til hinanden med rent geometriske

baand. Den samlede bevægelse af dette univers beskriver HERTZ ved indførelsen af et flerdimensionalt euklidisk konfigurationsrum og under anvendelsen af det grundlæggende princip, at bevægelsen i dette foregaar med konstant hastighed langs baner, hvis krumning i hvert punkt er den mindst mulige, som er forenelig med de geometriske baand — et princip, der er identisk med GAUSS' sætning om den mindste tvang. Hvad vi iagttager i virkeligheden er kun delsystemer af dette univers, og for disses bevægelser kan dette grundlæggende princip ikke opretholdes, og det kan her være praktisk at indføre en potentiel energi. Hermed er da kraftbegrebet reduceret til en rent matematisk hjælpestørrelse, og det grundlæggende begreb er de geometriske mekanismer, hvis fravær følte som et saa stort savn, da Newton indførte fjernkræfterne i mekanikken. En smuk fremstilling af væsentlige grundtræk af den Hertzske mekanik er givet af H. A. LORENTZ [7].

Det rum, hvormed HERTZ arbejder, er det sædvanlige 3-dimensionale, euklidiske rum, og det konfigurationsrum, han af matematiske hensyn indfører, er ligeledes euklidisk (i det væsentlige er koordinaterne i dette samlingen af elementarpartiklernes cartesiske koordinater i det sædvanlige rum). Der er her altsaa endnu ingenlunde tale om en geometrisering i den forstand, at selve rummets struktur tages op til revision i forbindelse med fysikkens problemstilling — og det samme gælder J. J. THOMSONS betragtninger, der iøvrigt slet ikke er knyttet til geometriske overvejelser. Derimod foreligger der med HERTZ' betydelige værk for første gang en gennemarbejdet anvendelse af den flerdimensionale, euklidiske geometris udtryksmaade til brug i mekanikken.

En væsentlig mangel ved den Hertzske mekanik er det, at han slet ikke paaviser, at det virkeligt er muligt paa rimelig vis at realisere de kendte naturkræfter ved hjælp af geometriske baand i det sædvanlige rum.

En geometrisering i mere moderne forstand af den klassiske fysik kan nu opnaas paa følgende maade:

Lad det betragtede konservative system være beskrevet ved Lagrangefunktionen

$$L = \frac{1}{2} g_{ik} \dot{x}^i \dot{x}^k + g_i \dot{x}^i + \frac{1}{2} g, \quad i, k = 1,2, \ldots, n,$$

hvor g'erne er tidsuafhængige funktioner af x'erne. Ser vi paa det ved Lagrangefunktionen

$$L' = \frac{1}{2} g'_{ik} \dot{x}^i \dot{x}^k + g'_{0i} \dot{x}^0 \dot{x}^i + \frac{1}{2} g'_{00} \dot{x}^{0^2} = \frac{1}{2} g'_{\alpha\beta} \dot{x}^\alpha \dot{x}^\beta,$$

$$\alpha, \beta = 0,1, 2, \ldots, n$$

bestemte dynamiske problem, er hermed givet et $(n + 1)$-dimensionalt rum med den Riemannske metrik

$$ds^2 = \frac{1}{2} g'_{\alpha\beta} \dot{x}^\alpha \dot{x}^\beta.$$

Vi forudsætter nu, at x^0 er cyklisk, altsaa at

$$p_0 = \frac{\partial L'}{\partial \dot{x}^0} = g'_{0i} \dot{x}^i + g'_{00} \dot{x}^0 = \text{konst.}, \quad \dot{x}^0 = \frac{p_0 - g'_{0i} \dot{x}^i}{g'_{00}},$$

og betragter kun saadanne baner i rummet, langs hvilke p_0 til et givet tidspunkt og hermed til alle tidspunkter er *1*. Den Routhske funktion hørende til det ved koordinaterne x^i beskrevne undersystem er da

$$R(x^i, \dot{x}^i, p_0) = L' - \frac{\partial L'}{\partial \dot{x}^0} \dot{x}^0 = \frac{1}{2} g'_{ik} \dot{x}^i \dot{x}^k - \frac{1}{2} g'_{00} \frac{(1 - g'_{0i} \dot{x}^i)^2}{2 g'^2_{00}} =$$

$$\frac{1}{2} \left(g'_{ik} - \frac{g'_{0i} g'_{0k}}{g'_{00}} \right) \dot{x}^i \dot{x}^k + \frac{g'_{0i}}{g'_{00}} \dot{x}^i - \frac{1}{2 g'_{00}},$$

og vælges nu størrelserne g'_{ik}, g'_{0i} og g'_{00} saaledes, at

$$g'_{ik} - \frac{g'_{0i} g'_{0k}}{g'_{00}} = g_{ik}, \quad \frac{g'_{0i}}{g'_{00}} = g_i, \quad -\frac{1}{2 g'_{00}} = \frac{1}{2} g, \text{ d.v.s. } g'_{ik} =$$

$$g_{ik} - \frac{g_i g_k}{g}, \quad g'_{0i} = -\frac{g_i}{g}, \quad g'_{00} = -\frac{1}{g},$$

er

$$R = \frac{1}{2} g_{ik} \dot{x}^i \dot{x}^k + g_i \dot{x} + \frac{1}{2} g = L,$$

saaledes *at det oprindelige system kan opfattes som et delsystem af et potentialfrit system, hvis dimension er 1 større, og hvis konfiguratonsrums metrik* $g'_{\alpha\beta}$ *er bestemt ved det oprindelige systems metrik* g_{ik} *og potentialerne* g_i *og* g.

Fastholdes denne metrik, men vælges værdien p_0 for det til x^0 hørende moment, vil det ved x^i beskrevne delsystem have Lagrangefunktionen (Routhfunktionen):

$$L = \frac{1}{2} g_{ik} \dot{x}^i \dot{x}^k + p_0 g_i \dot{x}^i + \frac{1}{2} p_0^2 g,$$

d.v.s., der foreligger et system af *samme natur* som det oprindelige, men i hvilket der optræder andre konstanter i potentialerne.

V. Tidsafhængige systemers geometrisering.

Selv for iagttagere, der ikke — som vi hidtil stiltiende har forudsat — er i hvile i forhold til et inertialsystem, gælder, at de mest almindelige tidsafhængige systemer, vi er stødt paa i den klassiske fysik, kan beskrives ved et variationsprincip af formen

$$\delta \int_{t_1}^{t_2} L \, dt = 0$$

med en Lagrangefunktion af typen

$$L = \frac{1}{2} g_{ik} \dot{x}^i \dot{x}^k + g_i \dot{x}^i + \frac{1}{2} g, \; i, k = 1, 2, \ldots, n,$$

hvor g'erne er funktioner af de generaliserede koordinater *og af tiden* t.

For at naa frem til en geometrisering af saadanne systemer, bemærker vi først, at hvis hastigheden $\dot{x}^0$ af en cyklisk koordinat *kun* optræder i kombinationen

$$L = \cdots + \dot{x}^0 \dot{x} + \cdots,$$

hvor x er en af de øvrige koordinater, er

$$\frac{\partial L}{\partial \dot{x}^0} = \dot{x} = \text{konst.},$$

d.v.s. x = konst. $t.$ + konst, saaledes at x *kan benyttes som tidsmaal.*

Metoden er da følgende: af ovennævnte formel for Lagrangefunktionen følger

$$L\, dt^2 = \frac{1}{2} g_{ik}\, dx^i\, dx^k + g_i\, dx^i\, dt + \frac{1}{2} g\, (dt)^2,$$

hvor g'erne altsaa er funktioner af x^i og t. Erstatter vi her rent formelt t med x^{n+1} og tilføjes leddet $dx^0 dx^{n+1}$ faas et $(n+2)$-dimensionalt problem med den Riemannske metrik

$$ds^2 = \frac{1}{2} \overline{g}_{ik}\, dx^i dx^k + \overline{g}_i\, dx^i dx^{n+1} + \frac{1}{2} \overline{g}\, (dx^{n+1})^2 + dx^0 dx^{n+1},$$

hvor $\overline{g}_{ik}$, $\overline{g}_i$ og $\overline{g}$ er de funktioner, der fremkommer ved i g'erne at erstatte t med x^{n+1}. I dette rum vil vi nu undersøge det nye dynamiske problem, hvis Lagrangefunktion er

$$L' = \frac{1}{2} \overline{g}_{ik} \dot{x}^i \dot{x}^k + \overline{g}_i \dot{x}^i \dot{x}^{n+1} + \frac{1}{2} g\, (\dot{x}^{n+1})^2 + \dot{x}^0 \dot{x}^{n+1},$$

hvor x^0 altsaa er cyklisk. Her indgaar x^{n+1} — uafhængig af dets forhistorie — som en *rumlig* koordinat paa lige fod med x^i'erne, *og t er stadig parameteren,* saaledes at $\dot{x}$ betyder dx/dt.

Da x^0 kun optræder i kombinationen $\dot{x}^0 \dot{x}^{n+1}$, er $\dot{x}^{n+1}$ konstant = den til x^0 hørende impuls p_0, altsaa

$$x^{n+1} = p_0\, t + q.$$

Vi vælger de baner i det $(n+2)$-dimensionale rum, hvor $p_0 = 1$ og $q = 0$, saaledes at tidsafhængigheden af x^{n+1} er givet ved $x^{n+1} = t$. I almindelighed er x^{n+1} ikke cyklisk — dette gælder kun for oprindeligt *tidsuafhængige* systemer.

Det udvidede systems Lagrangefunktion er konstant, da L' er potentialfri og eksplicit tidsuafhængig. Vi har, idet $\dot{x}^{n+1} = p_0 = 1$:

$$\left.\begin{aligned} L' &= \frac{1}{2}\bar{g}_{ik}\dot{x}^i\dot{x}^k + \bar{g}_i\dot{x}^i + \frac{1}{2}\bar{g} + \dot{x}^0 = \text{konst.} = \alpha = \left(\frac{ds}{dt}\right)^2 \\ &\text{eller} \\ L' &= L + \dot{x}^0, \end{aligned}\right\} \quad (\text{I})$$

hvor L er funktionen

$$\bar{L}(x^i, x^i, x^{n+1}) = \frac{1}{2}\bar{g}_{ik}\dot{x}^i\dot{x}^k + \bar{g}_i\dot{x}^i + \frac{1}{2}\bar{g}.$$

Det ved koordinaterne x^i bestemte undersystem af dimensionen n har den Routhske funktion

$$R = L' - \frac{\partial L'}{\partial \dot{x}^{n+1}}\dot{x}^{n+1} - \frac{\partial L'}{\partial \dot{x}^0}\dot{x}^0 = L' - p_{n+1}\dot{x}^{n+1} - \dot{x}^{n+1}\dot{x}^0 =$$

$$\bar{L} - p_{n+1},$$

og disse koordinaters udvikling er da bestemt ved differentialligningerne

$$\frac{d}{dt}\frac{\partial(\bar{L} - p_{n+1})}{\partial \dot{x}^i} - \frac{\partial(\bar{L} - p_{n+1})}{\partial x^i} = 0,$$

der jo ogsaa gælder, selvom x^{n+1} ikke er cyklisk. Men da den Routhske funktion skal opfattes som funktion af x^i, $\dot{x}^i$, x^{n+1} og p_{n+1} (samt af p_0, men denne størrelse er jo konstant lig med 1), forsvinder leddet p_{n+1} under differentiationerne, og vi faar

$$\frac{d}{dt}\frac{\partial \bar{L}}{\partial \dot{x}^i} - \frac{\partial \bar{L}}{\partial x^i} = 0.$$

Imidlertid er for enhver funktion $\bar{f}(x^i, \dot{x}^i, x^{n+1})$ og $x^{n+1} = t$:

$$\frac{d\bar{f}(x^i, \dot{x}^i, x^{n+1})}{dt} = \frac{\partial \bar{f}}{\partial x^i}\dot{x}^i + \frac{\partial \bar{f}}{\partial \dot{x}^i}\ddot{x}^i + \frac{\partial \bar{f}}{\partial x^{n+1}}\dot{x}^{n+1} =$$

$$\frac{\partial \bar{f}}{\partial x^i}\dot{x}^i + \frac{\partial \bar{f}}{\partial \dot{x}^i}\ddot{x}^i + \frac{\partial \bar{f}}{\partial x^{n+1}} = \frac{\partial f}{\partial x^i}\dot{x}^i + \frac{\partial f}{\partial \dot{x}^i}\ddot{x}^i + \frac{\partial f}{\partial t} = \frac{df(x^i, \dot{x}^i, t)}{dt},$$

saaledes at

$$\frac{d}{dt}\frac{\partial L}{\partial \dot{x}^i} - \frac{\partial L}{\partial x^i} = 0,$$

d.v.s. bevægelsesligningerne for det oprindelige system. Og hermed er da bevist *at det oprindelige system med Lagrangefunktionen L er det ved koordinaterne x^i bestemte delsystem af det $(n+2)$-dimensionale, eksplicit tidsuafhængige og potentialfrie system.* Forudsat, at vi udvælger de baner i totalsystemet, hvor x^{n+1}'s tidsafhængighed er givet ved $x^{n+1} = t$, altsaa forudsat, at konstanten p_0 gives værdien 1. Dersom p_0 ikke vælges lig med 1, føres vi for det ved x^i beskrevne undersystem til den Routh-Lagrangeske funktion

$$L = \frac{1}{2} g_{ik} \dot{x}^i \dot{x}^k + g_i \dot{x}^i p_0 + \frac{1}{2} g p_0^2,$$

altsaa til et system af samme natur som det oprindelige, men med ændrede værdier for konstanterne i potentialerne.

Af (I) følger

$$\dot{x}^0 = \alpha - \bar{L} = \alpha - \bar{L}\,(x^i\,(t),\ \dot{x}^i\,(t),\ x^{n+1}(t))$$

eller, idet $x^{n+1} = t$:

$$x^0 = \alpha t - \int_0^t L\, dt + \beta,$$

hvor α og β er konstanter. I x^0's tidsafhængighed indgaar altsaa *virkningsintegralet*

$$\int_0^t L\, dt.$$

Den her opstillede metrik er i en anden sammenhæng angivet af L. P. Eisenhart [3], som i tilknytning til ovennævnte bestemmelse af x^0 som funktion af tiden har vist, at den tillader en overmaade smuk og forenklet fremstilling af den *Hamilton-Jacobiske integrationsteori.*

Det skal tilslut bemærkes, at ved de ovennævnte udvidelser ophører metrikken i almindelighed med at være positiv-definit i x'erne, hvilket medfører nødvendigheden af i overvejelserne at udelukke de saakaldte *nullinjer*, d.v.s. linjer langs hvilke den metriske fundamentalinvariant forsvinder.

I stedet for at indføre baade $t = x^{n+1}$ og x^0 som nye koordinater kunne man have gaaet følgende vej, idet man giver afkald paa ønsket om, at det betragtede rum skal være Riemannsk:

Indfører vi i Lagrangefunktionen

$$L(\dot{x}^i, \dot{x}^i, t)$$

en ny parameter u i stedet for t, kræver variationsprincippet

$$\delta \int_{t_1}^{t_2} L \, dt = \delta \int_{u_1}^{u_2} L \frac{dt}{du} du = 0,$$

at L transformeres til

$$L' = L \frac{dt}{du},$$

og opfattes nu t som en variabel x^{n+1} paa lige fod med de øvrige koordinater, kan L' skrives paa formen

$$L' = L(x^i, \overset{*}{x}{}^i / \overset{*}{x}{}^{n+1}, x^{n+1}) \overset{*}{x}{}^{n+1},$$

hvor * betyder differentiation med hensyn til u, saaledes at

$$\overset{*}{x}{}^i = \dot{x}^i \overset{*}{x}{}^{n+1}.$$

Som man ser er L' homogen af første grad i samtlige »hastigheder«

$$\overset{*}{x}{}^1, \overset{*}{x}{}^2, \cdots, \overset{*}{x}{}^n, \overset{*}{x}{}^{n+1},$$

og man kan da benytte $\frac{1}{2}(L')^2$ som *metrisk fundamentalinvariant* i en *Finslersk geometri*, saaledes at banekurverne i det herved bestemte $(n+1)$-dimensionale rum bliver *rette linjer*. For nærmere orientering vedrørende geometrisering i denne forstand — hvor man altsaa opgiver ønsket om at arbejde i det mere anskuelige Riemannske rum — henvises til to afhandlinger af H. Rund [9 og 10] samt til nogle mere overfladiske betragtninger af C. Lanczos [6]. J. L. Synge [12] har fornylig vist det nære slægtskab, som består mellem denne metode og den Hamiltonske optiske analogi i dynamikkens integrationsteori.

Summary.

The possibilities of giving a geometrical description of classical mechanics are discussed, starting from a short historical review. A geometrization of this kind requires the general so-called Finsler-geometry, a short account of whose main features, adapted to the purpose, is given. It is then shown that the introduction of an extra coordinate, a so-called cyclic coordinate, allows a reduction to the more specialized Riemann geometry. We are here concerned with a slight change in an idea, originally formulated by J. J. THOMSON, which in particular forms the basis of H. HERTZ' endeavours to eliminate the concept of force in mechanics. It is finally shown that this geometrization also can be applied to time-dependent, holonomic dynamical systems, leading to a geometrical description which already has been studied by L. P. EISENHART.

Litteratur.

1) W. K. Clifford (1882), On the Space-Theory of Matter. Math. Papers, London, p. 71.
2) W. K. Clifford (1891), The Common Sense of the Exact Sciences. New York (1946), Chapter IV, p. 202.
3) L. P. Eisenhart (1928—29), Dynamical Trajectories and Geodesics. Ann. of Math. **30**, p. 591.
4) P. Finsler (1918), Ueber Kurven und Flächen in allgemeinen Räumen. Disp., Göttingen. Genoptrykt (1951) Basel.
5) H. Hertz (1910), Die Prinzipien der Mechanik. Ges. Werke III, 2. Aufl., Leipzig.
6) C. Lanczos (1949), The Variational Principles of Mechanics. Toronto, p. 280.
7) H. A. Lorentz (1907), Some Considerations on the Prinziples of Dynamics, in Connexion with Hertz' "Prinzipien der Mechanik". Abh. üb. theor. Physik, Leipzig. p. 1.
8) B. Riemann (1854), Ueber die Hypothesen, welche der Geometrie zu Grunde liegen. Ges. Math. Werke, 2. Aufl., Leipzig, p. 272.
9) H. Rund (1952), Die Hamiltonsche Funktion bei allgemeinen dynamischen Systemen. Arch. d. Math. **3**, p. 207.
10) H. Rund (1955). Application des méthodes de la géometrie généralisé à la dynamique théorique. Colloques Internationaux du Centre Nationale, nr. 52.
11) J. L. Synge (1926), On the Geometry of Dynamics. Phil. Trans. *A* **226**, p. 31.
12) J. L. Synge (1954), Geometrical Mechanics and de Broglie Waves. Cambridge, p. 142.
13) J. J. Thomson (1888), Applications of Dynamics to Physics and Chemistry. London, Chapter II.
14) W. Thomson (Lord Kelvin) (1884), Steps towards Kinetic Theory of Matter. Math. and Phys. Papers, III, p. 366.

Indleveret til selskabet den 14. juni 1955.
Færdig fra trykkeriet den 24. september 1955.

Det Kongelige Danske Videnskabernes Selskab
Matematisk-fysiske Meddelelser, bind **30**, nr. 13

Dan. Mat. Fys. Medd. **30**, no. 13 (1955)

DEDICATED TO PROFESSOR NIELS BOHR ON THE OCCASION OF HIS 70TH BIRTHDAY

SPECTROSCOPIC INVESTIGATIONS OF SEPARATED KRYPTON ISOTOPES

BY

EBBE RASMUSSEN AND VICTOR MIDDELBOE

København 1955
i kommission hos Ejnar Munksgaard

Printed in Denmark.
Bianco Lunos Bogtrykkeri A-S.

1. Introduction.

The hyperfine structure (hfs) of spectral lines of krypton have previously been examined by various investigators making use of normal krypton containing the isotopes in their natural abundances. The purpose of the earlier investigations was to measure interferometrically with the greatest possible accuracy the wavelengths of certain krypton lines, in an effort to confirm the suggestion that one of them might be more suited to be the primary standard of wavelength than the red line of cadmium. In the course of such investigations C. J. HUMPHREYS[1] in 1931 discovered and measured the hfs of several krypton arc lines, but did not, however, assign the hfs to nuclear properties.

A higher resolving power was obtained in 1933 by H. KOPFERMANN and N. WIETH-KNUDSEN[2], who succeeded in analysing the hfs of some partially resolved lines amongst the group of strong lines in the infra-red. The greater part of the total intensity of each of these lines was concentrated in the central component and this was described as being due to the even isotopes ($Z = 78$, 80, 82, 84, and 86), which compose altogether 88.5 % of natural krypton, whereas the odd isotope ($Z = 83$), composing the remaining 11,5 %, was held responsible for the faint satellites. By assuming the isotope shift to be negligible the authors could determine the most probable value of the nuclear spin of Kr^{83} to be $I = 9/2$.

The determination of such high spin values is always rather uncertain when based upon the Landé interval rule; this is especially the case, when deviations from this rule occur, caused by an electric quadrupole moment, which in the following years was found to exist for a number of nuclei. For these reasons H. KORSCHING[3] preferred to measure the relative intensities of the hfs components; his results, however, were found to con-

firm the spin value given by Kopfermann. Furthermore, Korsching measured deviations from the interval rule for one level and calculated thereby the quadrupole moment of Kr^{83} to be $Q = +0.15 \times 10^{-24}$ cm^2.

The smallness of the splittings in the hfs of the krypton lines and the unfavourable isotopic composition with respect to Kr^{83} in natural krypton makes investigations with separated isotopes most desirable. Such investigations have been made possible by the development of isotope separators during and after World War II. The commencement of spectroscopic work with separated isotopes of the noble gases was brought about in 1949 by means of an electromagnetic isotope separator built by J. Koch[4] at the Institute of Theoretical Physics in Copenhagen, where use was made of a new technique, designed by J. Koch[5], for collecting gaseous ions. This technique is based upon the fact, that when gaseous ions are accelerated by a voltage of about 50 kV and allowed to hit an aluminium target, they will penetrate the surface of the target to a certain depth, from which they can only be released by heating. Some preliminary results have been published on the isotopes of neon, krypton and xenon[6], and a more exhaustive publication has been given on the odd xenon isotopes[7]. The present paper contains results concerning even as well as odd isotopes of krypton.

2. Experimental Procedure.

The arc spectrum of krypton was excited in an ordinary discharge tube, which was made of pyrex glass and given the shape shown in fig. 1. The capillary bore was 1 mm and the total volume of the tube was 25 cm^3. The cylindrical electrodes consisted of aluminium plates $2\frac{1}{2} \times 4$ cm wrapped around themselves; one of these, T, had previously been irradiated in the isotope separator with ions of the isotope in question.

The procedure in preparing the tube was the following: First a helium tube of the shape mentioned, in which two non-irradiated aluminium electrodes were mounted, was manufactured in the usual way, i. e. the glass walls were degassed by heating with a flame and both electrodes were degassed thoroughly by repeated

heating with the aid of a high-frequency coil, which induced currents in the aluminium. The tube was then filled with helium to a pressure of a few mm of *Hg* and sealed off. To make sure that no leaks existed, it was ascertained that the tube still emitted a pure helium spectrum after having stood for a day or two. The tube was then re-opened and the horizontal electrode was replaced by the target plate *T*, containing the isotope in question.

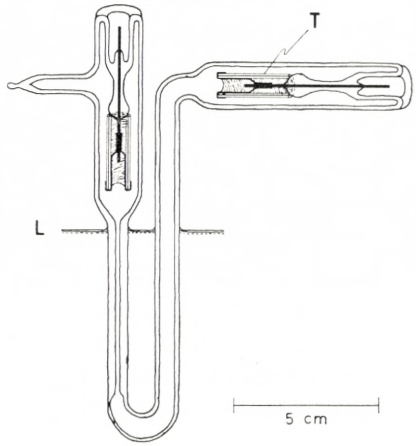

Fig. 1.

Helium was inserted for the second time and after sealing off the spectrum emitted was again seen to be purely helium. Finally, the target electrode was heated by induction currents in order to release the krypton gas collected in it. Helium now acts as a carrier gas enabling the tube to emit a fairly strong krypton spectrum, in spite of the small amounts (50 to 100 micrograms) of krypton available. In order to avoid impurities the target plate was handled exclusively by cleansed tools, and furthermore, the target plate had been degassed thoroughly before it was used as a collector.

The pressure of helium was chosen at 7 mm *Hg*, which was found to give the optimum excitation conditions. The tube was fed with an a.c. from a 7000 volt transformer, connected in series with a balance resistance of 300 000 ohm to enable the tube to be run at a low current (approx. 5 mA) in order to get as sharp lines as possible. The Doppler broadening was

further diminished by inserting the tube in an unsilvered Dewar vessel containing liquid air to the level L indicated in fig. 1.

The spectroscopic equipment consisted of a Steinheil 3-prism glass spectrograph with focal lengths of 650 and 640 mm for the collimator and the camera respectively, and a Fabry-Perot étalon with 60 mm plates, placed in the parallel beam of light between collimator and prism. By means of an achromatic lens with $f = 195$ mm a double-sized image of the capillary tube was projected onto the slit. This illuminating lens, having a diameter of 60 mm, was able to produce full illumination throughout the whole length of the spectral lines.

Special care was taken in adjusting the Fabry-Perot étalons, whose construction allowed the existence of optical contact between the quartz plates and the invar spacer to be verified by the observation of Newton's rings. The final adjustment was carried out with the light from a low pressure mercury lamp and making use of a low power telescope (10×80), whose large exit pupil (8 mm) made it possible to observe the interference rings, even when the eye was moved into different positions. The following spacers were used: 12.5 — 15 — 25 — 35 — 50 mm, and the exact thicknesses were measured to an accuracy of 10^{-5} mm by means of spectral lines of interferometrically known wavelengths.

The strong infra-red krypton lines were photographed on Kodak IRER and Eastman IN emulsions and the visible lines on ordinary Kodak, Ilford or Agfa plates. The plates were measured with a Zeiss comparator, and the line separations were evaluated by the standard method of quadratic interpolation. For clearly separated lines an accuracy of about 0.2×10^{-3} cm^{-1} was obtained.

3. Isotope Shifts between the Even Isotopes*.

In the case of elements containing their natural mixture of isotopes the small isotope shifts of spectral lines can only be observed and measured down to a certain lower limit. This

* A short communication of these results was given at the Rydberg Centennial Conference in Lund in July 1954.

limit is set partly by the resolving power of the spectrographic equipment and partly by the finite line width due to the light source, and is usually of the order of magnitude 0.01 to 0.02 cm^{-1}, depending on the wavelength region. For krypton the isotope shifts are below this limit and can therefore not be observed by using unseparated krypton.

By using separated isotopes, however, it is possible to detect and measure still smaller shifts, far beyond the limit set by the resolving power. This is due to the well known fact, that the uncertainty involved in the measurement of the centre of gravity of a line is some ten times smaller than the half intensity width of the line itself.

Among the even krypton isotopes only 82, 84 and 86 are abundant enough to allow one to collect a sufficient amount within a reasonable time, and the present investigation is therefore confined to these three isotopes. Spectral tubes were made containing Kr^{82}, Kr^{84} and Kr^{86}, respectively, and the tubes were filled with helium to approximately the same pressure ($\pm$ 1 mm *Hg*) in order to avoid relative displacements effectuated by pressure differences.* By means of these tubes interferometer spectrograms were made, with spacers from 25 to 50 mm, using the following method of alternating exposures: First an exposure of, say, Kr^{84} was made; then the plate holder was displaced vertically and an exposure of Kr^{82} was made on a new area of the same plate; finally Kr^{84} was exposed again after a renewed displacement of the photographic plate. This method allows one to control the constancy of the optical device from the beginning to the end of the exposures. Only photographs showing a sufficient constancy were used for measurements. During longer exposures the étalon was placed in an air-tight box (supplied with plane windows) in an effort to counteract the effect of variations in the pressure and temperature of the surrounding air. For the stronger lines, which could be photographed in a few minutes, this precaution could often be avoided.

From such exposures the isotope shift is easily determined by measuring the diameters of the interference rings of both isotopes; the difference between these diameters then simply

* Unpublished work by V. Middelboe on Kr^{84} shows that the displacement caused by a helium pressure difference of 1 mm *Hg* is less than 0.0001 cm^{-1}.

corresponds to the shift between the isotopes. Both the shifts 82—84 and 84—86 were measured and found to be identical within the experimental error. Only the strongest krypton lines have been investigated, namely the $1s - 2p$ combinations (using the Paschen notation) in the infra-red and visible regions, and the $1s - 3p$ combinations in the blue part of the spectrum. The results are collected in table 1, which for each line contains the mean value of the measurements made on a large number of plates; the figures are expected to be accurate to within 10 %.

TABLE 1.

Wave-length Å	Transition	Shift cm^{-1}	Wave-length Å	Transition	Shift cm^{-1}
8928	$1s_5 - 2p_{10}$	2.8×10^{-3}	7685	$1s_2 - 2p_1$	4.4×10^{-3}
8776	$1s_4 - 2p_8$	3.7	7601	$1s_5 - 2p_6$	2.4
8508	$1s_2 - 2p_4$	4.1	7587	$1s_4 - 2p_5$	3.8
8298	$1s_4 - 2p_7$	3.5	5870	$1s_4 - 2p_2$	3.8
8281	$1s_2 - 2p_3$	4.4	5570	$1s_5 - 2p_3$	2.9
8263	$1s_2 - 2p_2$	4.4	4502	$1s_4 - 3p_8$	4.8
8190	$1s_4 - 2p_6$	3.4	4463	$1s_4 - 3p_7$	5.0
8112	$1s_5 - 2p_9$	2.2	4453	$1s_4 - 3p_6$	4.9
8104	$1s_5 - 2p_8$	2.5	4376	$1s_4 - 3p_5$	4.7
8059	$1s_3 - 2p_4$	2.6	4362	$1s_5 - 3p_{10}$	5.0
7854	$1s_3 - 2p_3$	2.8	4319	$1s_5 - 3p_9$	4.0
7694	$1s_5 - 2p_7$	3.5	4273	$1s_5 - 3p_6$	4.0

The sign of the observed shifts was in all cases such that the wavenumbers increased for increasing mass numbers, i. e. in the order 82—84—86, which is the order to be expected when dealing with a normal mass effect. The magnitude of the observed shifts also corresponds rather nearly to that to be expected from a mass effect.

As first recognized by N. BOHR the mass effect for light elements can be ascribed to the motion of the nucleus, the finite mass of which varies slightly from one isotope to another. According to Bohr's theory this gives rise, in the case of one-electron spectra, to a displacement ΔE of a level E given by the formula:

$$\Delta E = E \cdot \frac{M_2 - M_1}{M_1 \cdot M_2} \cdot m$$

where M_1 and M_2 are the masses of the two isotopes in question, and m the mass of the electron, which is $1/1836 = 5.49 \times 10^{-4}$ in chemical mass units. For krypton with $M_1 = 82$ and $M_2 = 84$ one gets

$$\Delta E = E \frac{2}{82 \times 84} 5.49 \times 10^{-4} = 1.6 \times 10^{-7} E.$$

By means of this formula the term displacements in table 2 have been calculated in units of 10^{-3} cm $^{-1}$. In atoms with more than one electron there is, in addition to this simple mass effect, a specific mass effect due to correlations in the motions of the electrons.

The final comparison between the measured line shifts and the calculated term displacements cannot be made until further measurements of higher series members have furnished absolute values for the term shifts. Certain information can be obtained, however, by making the rather crude assumption that the displacements for the higher terms ($2p$ and $3p$) are due mainly to the simple mass effect. Consequently, by adding the observed line shifts to the theoretical displacements for the $2p$ and $3p$ terms one can obtain empirical mean values for the $1s$ term displacements, which can then be compared with the theoretical ones. This has been done in table 2 under the columns ΔE_{calc} and ΔE_{obs}.

From these figures it may be stated that for $1s_5$ and $1s_3$ only small deviations occur, whereas for $1s_4$ and especially for $1s_2$ the simple mass effect alone cannot be responsible for the observed effect. In spite of the smallness of the observed shifts in krypton it is reasonable to conclude, that these shifts for the most part can be accounted for by Bohr's formula, and that only for the deepest term ($1s_2$) a specific mass effect, of the order of magnitude $+ 2 \times 10^{-3}$ cm^{-1}, can be established with certainty.

This result is in accordance with those found by R. Ritschl and H. Schober[8] in neon, where absolute values of term shifts were obtained, and by H. Kopfermann and H. Krüger[9] in

TABLE 2.

	E	ΔE_{cal}	ΔE_{obs}	$\Delta E_{obs} - \Delta E_{cal}$
$1s_5$	32943	5.3	5.8	0.5
$1s_4$	31998	5.1	6.5	1.4
$1s_3$	27723	4.4	5.1	0.7
$1s_2$	27068	4.3	6.7	2.4

		ΔE_{cal}			ΔE_{cal}
$2p_{10}$	21746	3.5	$3p_{10}$	10028	1.6
$2p_9$	20620	3.3	$3p_9$	9799	1.6
$2p_8$	20607	3.3	$3p_8$	9793	1.6
$2p_7$	19950	3.2	$3p_7$	9601	1.5
$2p_6$	19791	3.2	$3p_6$	9552	1.5
$2p_5$	18822	3.0	$3p_5$	9153	1.5
$2p_4$	15319	2.5			
$2p_3$	14996	2.4			
$2p_2$	14970	2.4			
$2p_1$	14060	2.2			

argon, where only relative shifts were measured; the latter results were confirmed later by HORST MEYER[10] using separated isotopes.

4. Hyperfine Structure and Term Intervals of Kr^{83}

The purpose of investigating the odd krypton isotope Kr^{83}, procured by the separation of natural krypton, was to obtain further evidence on the spin value, previously found, and to get an improved value for the electric quadrupole moment of this nucleus. Although the isotopic separation in the present case appeared to be not quite perfect, owing to the large initial abundance of the two neighbouring isotopes 82 and 84, the hfs components of all the observed lines were much better resolved than for natural krypton. The six lines listed in table 3 were selected for measurements, as these lines were by far the best resolved and were most easily analysed. Previous investigators, working with unseparated krypton, also used these lines.

TABLE 3.

Wave-length Å	Transition	Total splitting cm^{-1}	Spacer, max. mm.	Remarks
8508	$1s_2 - 2p_4$	0.245	15	Control of $1s_2$ and $2p_4$
8281	$1s_2 - 2p_3$	0.321	12.5	Control of $1s_2$ and $2p_3$
8059	$1s_3 - 2p_4$	0.192	15	Gives $2p_4$ splitting
7854	$1s_3 - 2p_3$	0.075	35	Gives $2p_3$ splitting
7685	$1s_2 - 2p_1$	0.246	15	Gives $1s_2$ splitting
5570	$1s_5 - 2p_3$	0.238	15	Gives $1s_5$ splitting

Each of these lines was measured on a large number of plates, and the greatest importance was attached to the choice of the largest étalon spacer that could be used in each particular case without the overlapping of neighbouring orders. The following diagrams, figs. 2—7, show the term transitions and below these

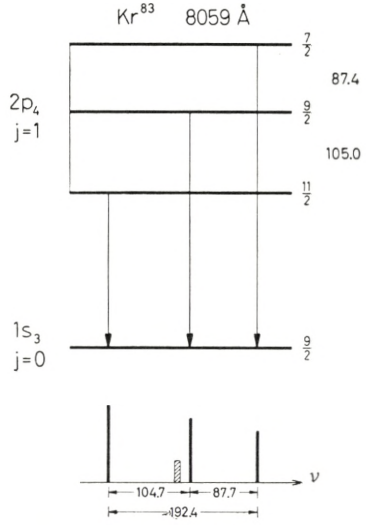

Fig. 2.

the line structures; beneath the latter the mean values of some of the measured intervals are given in units of 10^{-3} cm $^{-1}$, while at the right of each term diagram the finally adopted term intervals are written in the same units. In each line picture the hfs

components are fully drawn and the component due to the even isotopes is shown hatched. The heights of the lines are drawn proportional to the calculated intensities. The reader can find the magnitude (in units of 10^{-3} cm $^{-1}$) of any required line interval, which is not already given, by measuring the particular distance

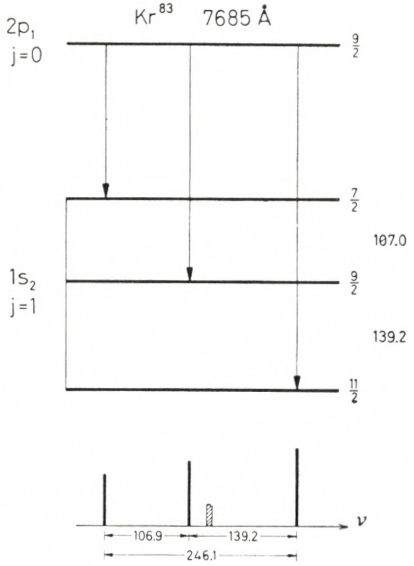

Fig. 3.

in the line picture to the nearest $^1/_{10}$ mm and multiplying by 10. Further, it may be instructive to compare the diagrams fig. 2—7 with the corresponding enlarged photographs of the line structures printed on the special plate at the end of this paper.

In order to explain how the term splittings have been evaluated from the line structures, the individual lines will now be discussed in the proper logical order. For 8059 Å, $1s_3 - 2p_4$, fig. 2, the line structure should be identical with the splitting of $2p_4$, as $1s_3$ with $j = 0$ cannot split. However, only the total splitting can be measured with certainty, because the distance between the component (hatched) coming from the even isotopes and the central hfs component is only about 0.016 cm^{-1}, and this gives rise to an attraction of the central component and thereby a distortion of the intervals.

In order to overcome this difficulty the lines 7685 and 8508 were used as auxiliary lines. For 7685 Å, $1s_2 - 2p_1$, fig. 3, the upper term $2p_1$ cannot split, and the line structure therefore gives the splitting of $1s_2$. Here the disturbance of the intervals

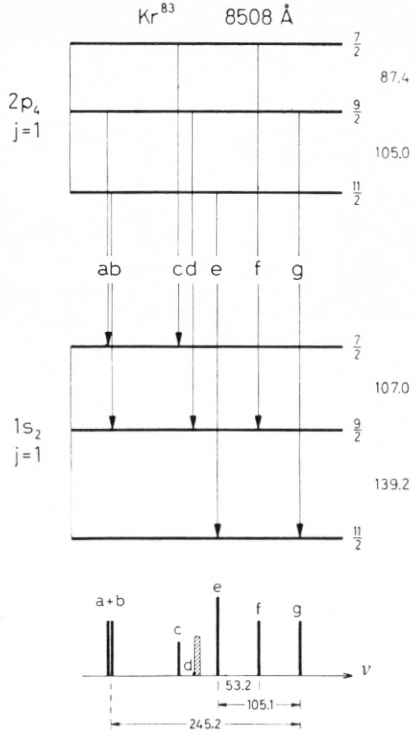

Fig. 4.

is considerably less than for 8059, as the separation of the hatched component and the central hfs component is more favourable, the distance between them being about 0.027 cm^{-1}.

The third line 8508 Å, $1s_2 - 2p_4$, fig. 4, is a combination between the two terms, which have just been discussed, and the measured intervals of this line can therefore give improved values for the splittings of both these terms. For instance the distance e—g gives the larger interval of $2p_4$, and the distance e—f subtracted from the total splitting of $2p_4$ gives the larger interval of $1s_2$. By means of the three lines discussed so far the splittings of the terms $1s_2$ and $2p_4$ can be found without any

one-sided disturbances and with an accuracy of about $\pm 0.2 \times 10^{-3}$ cm^{-1}.

A method similar to the one discussed above was used to determine the splitting of $2p_3$. For the line 7854 Å, $1s_3 - 2p_3$, fig. 5, only the total splitting is reliable, but the line 8281 Å, $1s_2 - 2p_3$, fig. 6, yields the intervals of $2p_3$ undisturbed by the

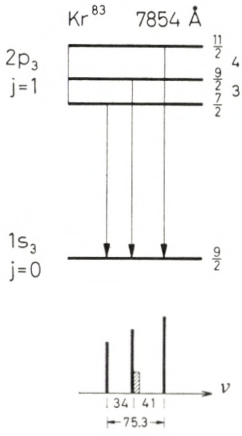

Fig. 5.

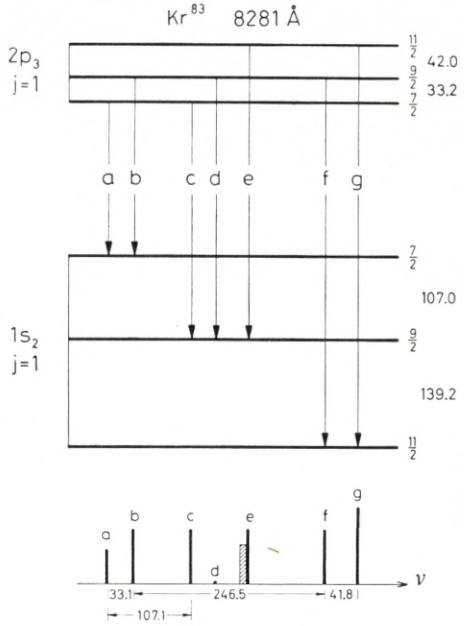

Fig. 6.

hatched component, namely as the distances *a*—*b* and *f*—*g*. Furthermore, the distances *a*—*c* and *b*—*f*, fig. 6, are equal to the smaller interval and the total splitting of $1s_2$, respectively, and this gives a final check on the hitherto measured intervals.

The two intervals of $2p_3$ then being established with some certainty, the next problem was to find the intervals of the term $1s_5$ by means of the line 5570 Å, $1s_5 - 2p_3$, fig. 7. For this particular line the great improvement achieved by the use of separated isotopes is most clearly demonstrated by the fact, that it was possible to distinguish seven separate components. In fig. 7 it will be seen, that the first (largest) interval of $1s_5$ is equal to the distance *h*—*i*, and that the second interval can be found by means

of the distance e—h, when the larger interval of $2p_3$ is known. The third interval of $1s_5$ is equal to the distance d—e and is found, as it happens, to coincide with the smaller interval of $2p_3$. Finally, the fourth and smallest interval of $1s_5$, namely a—b, is so small that a considerable mutual attraction of a and b is believed to take place, with the consequence that the directly measured value

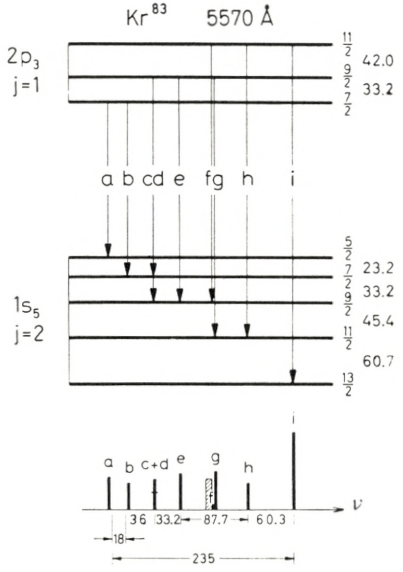

Fig. 7.

(0.018 cm^{-1}) for the distance a—b is too small. The magnitude of the mutual attraction could, however, be evaluated in the following way. The distance from the line $c + d$ to the displaced position of b was found by measurement to be 0.036 cm^{-1}; the true distance between these two lines is seen by consulting the term diagram to be 0.033 cm^{-1}; consequently, the amount by which b has been displaced towards a equals 0.003 cm^{-1}. The corresponding displacement of a towards b can then be calculated to be 0.002 cm^{-1}. This value was obtained by assuming the line shape to be Gaussian, i. e. mainly due to Doppler-broadening, and by taking the intensity ratio of a and b into account. In this way a total mutual attraction of 0.005 cm^{-1} is found, which, when added to the directly measured distance

from a to b, gives the corrected value 0.023 cm^{-1} for the smallest interval of $1s_5$. The finally adopted intervals for $1s_5$, written in fig. 7, will be discussed later.

5. Nuclear Moments of Kr^{83}.

It appears from the fine structure quantum numbers F, written opposite each term component in the figs. 2—7, that one has adopted the spin value $I = {}^9/_2$. If one tries to confirm this value by means of the Landé interval rule, one does not get a complete agreement for any of the observed terms. Table 4 shows the intervals calculated from the measured total splittings by the interval rule for $I = {}^9/_2$, together with the observed intervals. The deviations, which are large for $1s_2$ and $1s_5$ and rather

TABLE 4.

$1s_2$		$1s_5$		$2p_3$		$2p_4$	
obs.	calc.	obs.	calc.	obs.	calc.	obs.	calc.
139.2 ± 0.3	135.4	60.3 ± 0.5	53	42.0 ± 0.4	41.4	105.0 ± 0.2	105.8
107.0 ± 0.3	110.8	45.7 ± 0.5	45	33.2 ± 0.4	33.8	87.4 ± 0.2	86.6
246.2 ± 0.3	246.2	33.2 ± 0.5	36	75.2 ± 0.4	75.2	192.4 ± 0.2	192.4
		23 ± 1	28				
		162 ± 1	162				

small for $2p_3$ and $2p_4$, must in all cases be ascribed to the action of a quadrupole moment of the nucleus. Even the term $2p_4$, which in pure jj-couping should be expected to have a spherically symmetrical electric field in which the quadrupole moment of the nucleus should produce no effect, shows a deviation appreciably larger than the uncertainty of the measurements. The same is found to be the case on calculating the intervals for $I = {}^{11}/_2$; one then gets a deviation for $2p_4$, which is of the same size but of opposite sign.

This dilemma has recently been resolved by an investigation of the hyperfine structure of some krypton lines using the radioactive isotope Kr^{85}, produced by fission processes.[11] Having

two odd isotopes of the same element at ones disposal, i. e. two different nuclei with identical electron configurations, one must find that the ratio between the two deviations from the interval rule is constant from term to term, this constant simply being equal to the ratio between the quadrupole moments of the two nuclei. This was found to be the case only when assuming $I = {}^9/_2$ for both isotopes. The deviation found for $2p_4$ may then be explained as due to a lack of spherical symmetry for this term, owing to the intermediate coupling conditions in krypton.

As the spin value of Kr^{83} thus must be considered to be established with certainty, it is now possible to calculate the nuclear quadrupole moment from the observed intervals. The first step in this calculation will be to separate the magnetic and the electrostatic contributions to the hyperfine structure by evaluating the a- and b-factors by means of the general theory on the interaction between nuclei and electrons.[12)]

According to this theory, the hyperfine structure of a given level can be described by the formula

$$E_F = E_0 + a \cdot \frac{C}{2} + b \left[\frac{3/4\ C(C+1) - I(I+1)\, J(J+1)}{2\, I(2\,I-1)\, J(2\,J-1)} \right]$$

where

$$C = F(F+1) - J(J+1) - I(I+1).$$

E_0 is the energy of the undisplaced level, i. e. without any hyperfine structure, and E_F is the energy of the level component having the fine structure quantum number F. J is the inner quantum number of the level and I the nuclear spin. a and b are the magnetic and electric interval factors, respectively.

The evaluation of the a- and b-factors is simply carried out by the following scheme (table 5), in which the values of E_F are calculated for $I = {}^9/_2$ for the two cases $J = 1$ and $J = 2$. By subtracting adjacent term components E_F the term intervals ΔE, given in the last column, are found. It will be seen from the expressions ΔE, that the Landé interval rule comes out, when $b = 0$, i. e. if no quadrupole moment is present.

By inserting the observed intervals from table 4 in the expressions ΔE one gets the equations, from which the numerical values of a and b can be found. For a term with $J = 1$ ($1s_2$,

TABLE 5.

J	F	C	E_F	ΔE
	11/2	9	$E_{11/2} = E_0 + \frac{9}{2}a + \frac{1}{4}b$	$E_{11/2} - E_{9/2} = \frac{11}{2}a + \frac{11}{12}b$
1	9/2	—2	$E_{9/2} = E_0 - a - \frac{2}{3}b$	$E_{9/2} - E_{7/2} = \frac{9}{2}a - \frac{9}{8}b$
	7/2	—11	$E_{7/2} = E_0 - \frac{11}{2}a + \frac{11}{24}b$	
	13/2	18	$E_{13/2} = E_0 + 9a + \frac{1}{4}b$	$E_{13/2} - E_{11/2} = \frac{13}{2}a + \frac{13}{24}b$
	11/2	5	$E_{11/2} = E_0 + \frac{5}{2}a - \frac{7}{24}b$	$E_{11/2} - E_{9/2} = \frac{11}{2}a$
2	9/2	—6	$E_{9/2} = E_0 - 3a - \frac{7}{24}b$	$E_{9/2} - E_{7/2} = \frac{9}{2}a - \frac{5}{16}b$
	7/2	—15	$E_{7/2} = E_0 - \frac{15}{2}a + \frac{1}{48}b$	$E_{7/2} - E_{5/2} = \frac{7}{2}a - \frac{7}{16}b$
	5/2	—22	$E_{5/2} = E_0 - 11a + \frac{11}{24}b$	

$2p_3$ and $2p_4$) one gets just two equations for the determination of the two quantities a and b. For $1s_5$ with $J = 2$, however, four equations are obtained for the determination of a and b, so in this case a graphical method is preferred in order to obtain the most probable values. The four equations for $1s_5$

$$\text{I} \qquad \frac{13}{2}a + \frac{13}{24}b = 60.3$$

$$\text{II} \qquad \frac{11}{2}a = 45.7$$

$$\text{III} \qquad \frac{9}{2}a - \frac{5}{16}b = 33.2$$

$$\text{IV} \qquad \frac{7}{2}a - \frac{7}{16}b = 23$$

are plotted in the following diagram (fig. 8) as the straight lines I, II, III and IV, which should be expected to intersect in a

single point. This is the case within the accuracy of the measurements, as will be seen by the vertical short lines drawn at the left. These vertical lines indicate the parallel displacements of the four straight lines that correspond to the uncertainties of the

Graphical evaluation of the a- and b-factors

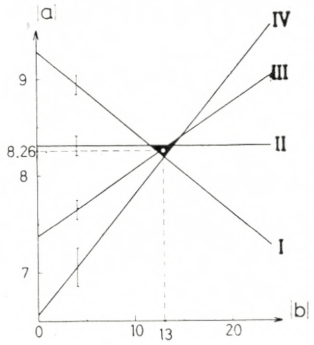

Fig. 8.

four intervals of $1s_5$. From the centre of intersection one gets $a = 8.26$ and $b = 13$.

By using the a- and b-factors, here determined, one can calculate the most reliable intervals for $1s_5$; these are given in fig. 7 and listed in table 6 together with the final results for the other three terms examined. The latter were chosen as making the best overall fit with the experimental results.

For the calculation of the quadrupole moment the term $1s_5$

TABLE 6.

Term	J	F	Intervals	a	b
$1s_2$	1	$\frac{11}{2}\ \frac{9}{2}\ \frac{7}{2}$	— 139.2, — 107.0	— 24.70 ± 0.06	— 3.7 ± 0.4
$1s_5$	2	$\frac{13}{2}\ \frac{11}{2}\ \frac{9}{2}\ \frac{7}{2}\ \frac{5}{2}$	— 60.7, — 45.4, — 33.2, — 23.2	— 8.26 ± 0.08	—13 ± 1
$2p_3$	1	$\frac{11}{2}\ \frac{9}{2}\ \frac{7}{2}$	+ 42.0, + 33.2	+ 7.54 ± 0.08	+ 0.6 ± 0.5
$2p_4$	1	$\frac{11}{2}\ \frac{9}{2}\ \frac{7}{2}$	— 105.0, — 87.4	— 19.23 ± 0.04	+ 0.8 ± 0.3

must be preferred. This term has not only the largest b-factor, but further, quite analogous to xenon,[7] the calculation for this term can be carried out independently of the type of coupling. According to the theory for the quadrupole interaction, the quadrupole moment Q can be found by the expression

$$-Q \cdot \overline{(3\cos^2\theta - 1)} \cdot \overline{\left(\frac{a_0}{r}\right)^3} \cdot 7.89 \cdot 10^{-3} = b \cdot 10^{-24}$$

where $\overline{(3\ cos^2\ \theta - 1)}$ is a measure for the deviation from spherical symmetry of the charge density of the electrons for the electronic state in question and for $1s_5$ will have the value $+ {}^2/_5$. The quantity $\overline{\left(\frac{a_0}{r}\right)^3}$, where a_0 is the radius of the first hydrogen orbit and r the distance of the electron from the centre of the nucleus, can be calculated by the following expression

$$\overline{\left(\frac{a_0}{r}\right)^3} = 0.114 \cdot \Delta \cdot \frac{R'}{Z_i \cdot H}$$

where Δ is the doublet separation of the ground state of the ion, Z_i the effective nuclear charge, and R' and H are relativistic correction factors. With the following numerical values $\Delta = 5220\ \text{cm}^{-1}$, $Z_i = 36 - 4 = 32$, $H = 1.03$ and $R' = 1.045$ one obtains $\overline{\left(\frac{a_0}{r}\right)^3} = 18.9$.

By inserting these quantities in the expression for Q one gets

$$\underline{Q = +(0.22 \pm 0.02) \times 10^{-24}\,\text{cm}^2.}$$

The term $1s_2$, used by KORSCHING[3], is not as well suited as $1s_5$ for the calculation of Q. A comparison between the b-factors of these two terms may, however, be carried out by a consideration quite similar to that used in the case of xenon.[7]

For $1s_2$ the wave function can be written in the form

$$\psi = c_1 \cdot \varphi\left(\frac{3}{2}, \frac{1}{2}\right) + c_2 \cdot \varphi\left(\frac{1}{2}, \frac{1}{2}\right)$$

where the coefficients c_1 and c_2 can be determined from the multiplet structure (i. e. from the relative positions of $1s_2$, $1s_3$, $1s_4$ and $1s_5$) as well as from the Zeeman effect. Both determinations yield $c_1 = 0.156$ and $c_2 = -0.988$. The b-factor of $1s_2$ can then be calculated from the b-factor of the ion ($P_{3/2}$) by the formula

$$b\ (1s_2) = \frac{1}{2} \cdot b\ (P_{3/2}) \left(c_1^2 - \frac{4}{\sqrt{2}} \cdot \frac{S}{R'} \cdot c_1 \cdot c_2 \right)$$

where $R' = 1.045$, $S = 1.07$, and $b\ (P_{3/2}) = b\ (1s_5) = (13 \pm 1) \times 10^{-3}\ \mathrm{cm}^{-1}$. One then gets

$$b\,(1s_2) = \frac{1}{2}\, b\,(1s_5)\,(c_1^2 - 2.89 \cdot c_1\, c_2) = (3.1 \pm 0.3) \times 10^{-3}\ \mathrm{cm}^{-1}$$

to be compared with the observed value $(3.7 \pm 0.4) \times 10^{-3}\ \mathrm{cm}^{-1}$.

The authors wish to thank Professor Niels Bohr for kindly placing spectroscopic equipment at their disposal and Dr. Aage Bohr for valuable theoretical discussions. We are further very grateful to Dr. J. Koch and Mr. K. O. Nielsen, C. E. for the most thorough isotope separations and to Mr. P. W. Streander for the careful construction of apparatus. Finally, we are indebted to the *Carlsbergfond* and to *Statens almindelige Videnskabsfond* for grants given to this work.

Physics Department.
Royal Veterinary and Agricultural College
Copenhagen, Denmark.

References.

1) C. J. Humphreys: Bur. Stand. Jour. Res. **7**, 453, 1931.
2) H. Kopfermann and N. Wieth-Knudsen: Zs. f. Phys. **85**, 353, 1933.
3) H. Korsching: Zs. f. Phys. **109**, 349, 1938.
4) J. Koch and B. Bendt-Nielsen: Dan. Mat. Fys. Medd. **21**, No. 8, 1944.
5) J. Koch: Nature **161**, 566, 1948.
6) J. Koch and E. Rasmussen: Phys. Rev. **76**, 1417, 1949, **77**, 722, 1950.
7) Aa. Bohr, J. Koch and E. Rasmussen: Ark. f. Fys. **4**, 455, 1952.
8) R. Ritschl and H. Schober: Phys. Zeitschr. **38**, 6, 1937.
9) H. Kopfermann and H. Kruger: Zs. f. Phys. **105**, 389, 1937.
10) Horst Meyer: Helv. Phys. Acta. **26**, 811, 1953.
11) E. Rasmussen and V. Middelboe: Zs. f. Phys. **141**, 160, 1955.
12) H. B. G. Casimir: Teylers Tweede Genootschap. Haarlem 1936.

Indleveret til selskabet den 7. juni 1955.
Færdig fra trykkeriet den 1. oktober 1955.

Fig 2 a. 8059 Å

Fig. 3 a. 7685 Å

Fig. 4 a. 8508 Å

Fig. 5 a. 7854 Å

Fig. 6 a. 8281 Å

Fig. 7 a. 5570 Å

Photographs of single orders of Kr-83 lines, enlarged 10–20 times. The direction of increasing wave numbers is from left to right, as in the corresponding diagrams figs. 2–7, but in the photographs the scale is of course not linear.

Det Kongelige Danske Videnskabernes Selskab
Matematisk-fysiske Meddelelser, bind **30**, nr. 14

Dan. Mat. Fys. Medd. **30**, no. 14 (1955)

ON BRÖNSTED'S PRINCIPLE OF SPECIFIC INTERACTION

BY

E. A. GUGGENHEIM

København 1955
i kommission hos Ejnar Munksgaard

Printed in Denmark
Bianco Lunos Bogtrykkeri A-S

The principle of specific interaction of ions was formulated by BRÖNSTED[1] in 1921 two years before the publication of the theory of DEBYE and HÜCKEL[2] in 1923. These two theories were later combined into a single formulation by GUGGENHEIM[3]. The mathematical aspect of this formulation has recently been analysed and criticized by SCATCHARD[4]. The present article is inspired by SCATCHARD's analysis. Starting from different premises I reach conclusions the most important of which confirm SCATCHARD's. It is more difficult to say whether we are in complete agreement because SCATCHARD's article is unfortunately so condensed that clarity has been sacrificed to brevity. In particular some of the symbols used by SCATCHARD are inadequately defined and I have been unable to interpret them. I shall return later to a discussion of SCATCHARD's analysis.

Consider a solution containing n_w moles of the solvent water and n_i moles of the ionic species i. The Gibbs function G can be expressed in the form

$$G = n_w \mu_w^0 + \Sigma_i n_i \mu_i^{\ominus} - RT \Sigma_i \left(n_i - n_i \ln \frac{n_i}{n_w} \right) + G^{corr} + G^{el} + G^s \qquad (1)$$

where μ_w^0 denotes the chemical potential of pure water and $\mu_i^{\ominus}$ is at the given temperature a constant characteristic of the ionic species i at infinite dilution in water. The terms $RT \Sigma_i$ are an approximate form for an ideal dilute solution and G^{corr} denotes terms, unimportant at high dilution, to correct for the previous terms being only approximate. G^{el} denotes the contribution due to electrostatic interactions between the ions regarded as rigid charged spheres with a common diameter. The form of G^{el} is given by the theory of DEBYE and HÜCKEL[2], modified if neces-

sary according to the treatment of GRONWALL[5]. The term G^s represents the remaining contribution due to short range interactions. This article is concerned with G^s, but not with G^{corr} nor with G^{el}.

The osmotic coefficient φ is defined by

$$\mu_w^0 - \mu_w = \varphi RT \frac{\Sigma_i n_i}{n_w} \tag{2}$$

where μ_w denotes the chemical potential of water in the solution and μ_w^0 the chemical potential of pure water. The activity coefficient γ_i of the ionic species i is defined by

$$\mu_i - \mu_i^{\ominus} = RT \ln \frac{n_i \gamma_i}{n_w} \tag{3}$$

where μ_i denotes the chemical potential of the ionic species i. It is scarcely necessary to mention that quantities such as μ_i and γ_i are physically significant only when combined to relate to salts or other combinations with zero net charge[6]. For the sake of tidiness we have used mole ratios n_i/n_w instead of the more usual molalities m_i. If we were to replace n_i/n_w by m_i in formula (3) the value of $\mu_i^{\ominus}$ would be changed by a constant term, but the value of the activity coefficient γ_i would be unaffected.

From comparison of (1) with (2) and (3) it is evident that when G^{corr}, G^{el} and G^s vanish, φ and all γ_i's become unity. It is further clear that $1 - \varphi$ and $\ln \gamma_i$ can be decomposed linearly in the same manner as G, namely

$$1 - \varphi = 1 - \varphi^{el} - \varphi^{corr} - \varphi^s \tag{4}$$

$$\ln \gamma_i = \ln \gamma_i^{corr} + \ln \gamma_i^{el} + \ln \gamma_i^s. \tag{5}$$

In formula (4) it is implied that φ^{el} is given by the theory of Debye and Hückel and that φ^{el} is comparable with unity, while φ^{corr} and φ^s are much smaller quantities. This article is concerned only with the terms φ^s and $\ln \gamma_i^s$. Incidentally the superscript ^{s} corresponds to the superscript $'''$ used by SCATCHARD.

The essential approximation underlying GUGGENHEIM's treatment is that G^s should have a form analogous to that for a regular

mixture of non-electrolytes. For such a mixture of molecular species α, β, ... we have the useful and simple approximation

$$G^s = \frac{1}{2} \frac{\Sigma_\alpha \Sigma_\beta n_\alpha n_\beta l_{\alpha\beta}}{\Sigma_\alpha n_\alpha} \quad (l_{\alpha\beta} = l_{\beta\alpha}) \tag{6}$$

where n_α denotes the number of moles of the species α and $l_{\alpha\beta}$ is a constant characteristic of the pair $\alpha\beta$. For the solution of ionic species i, k, ... in water w we write correspondingly

$$G^s = \frac{1}{2} \frac{n_w^2 l_{ww}}{n_w + \Sigma_i n_i} + \frac{n_w \Sigma_i n_i l_{wi}}{n_w + \Sigma_i n_i} + \frac{1}{2} \frac{\Sigma_i \Sigma_k n_i n_k l_{ik}}{n_w + \Sigma_i n_i}. \tag{7}$$

We now expand in powers of n_i/n_w and neglect terms of second and higher order, obtaining

$$\left.\begin{aligned} G^s = \frac{1}{2} n_w l_{ww} - \frac{1}{2} \Sigma_i n_i l_{ww} + \frac{1}{2} \frac{(\Sigma_i n_i)^2}{n_w} l_{ww} - \ldots \\ + \Sigma_i n_i l_{wi} - \frac{\Sigma_i n_i \Sigma_k n_k l_{wk}}{n_w} + \ldots \\ + \frac{1}{2} \frac{\Sigma_i \Sigma_k n_i n_k l_{ik}}{n_w} - \ldots \end{aligned}\right\} \tag{8}$$

Differentiating with respect to n_w and denoting the mole ratio n_i/n_w by r_i, we obtain for the corresponding term μ_w^s of μ_w

$$\mu_w^s = -\frac{1}{2} (\Sigma_i r_i)^2 l_{ww} + \Sigma_i r_i \Sigma_k r_k l_{wk} - \frac{1}{2} \Sigma_i \Sigma_k r_i r_k l_{ik} \tag{9}$$

and consequently

$$\frac{\varphi^s RT}{\Sigma_i r_i} = \frac{1}{2} l_{ww} - \Sigma_i y_i l_{wi} + \frac{1}{2} \Sigma_i \Sigma_k y_i y_k l_{ik} \tag{10}$$

where

$$y_i = \frac{r_i}{\Sigma_k r_k} = \frac{n_i}{\Sigma_k n_k} \text{ so that } \Sigma_i y_i = 1. \tag{11}$$

We can now rewrite (10) in the form

$$\frac{\varphi^s RT}{\Sigma_i r_i} = \frac{1}{2} \Sigma_i \Sigma_k y_i y_k L_{ik} \tag{12}$$

where L_{ik} is defined by

$$L_{ik} \equiv l_{ik} - l_{wi} - l_{wk} + l_{ww}. \tag{13}$$

Alternatively we can write

$$\frac{\varphi^s RT}{\Sigma_i r_i} = \frac{1}{2} \Sigma_i \Sigma_k y_i y_k M_{ik} + \frac{1}{2} \Sigma_i y_i L_{ii} \tag{14}$$

where M_{ik} is defined by

$$M_{ik} \equiv L_{ik} - \frac{1}{2} L_{ii} - \frac{1}{2} L_{kk} = l_{ik} - \frac{1}{2} l_{ii} - \frac{1}{2} l_{kk} \tag{15}$$

so that

$$M_{ii} = 0. \tag{16}$$

It is important to distinguish sharply M_{ik} occurring in (14) and satisfying the identity (16) from L_{ik} occurring in the formally simpler (12) but not satisfying any identity analogous to (16). This distinction between M_{ik} and L_{ik} was overlooked by GUGGENHEIM, nor is the distinction clearly defined by SCATCHARD.

Up to this point no distinction has been made between cations and anions. We now denote cations by R and anions by X. Formula (14) becomes

$$\left.\begin{aligned} \frac{\varphi^s RT}{\Sigma_i r_i} &= \Sigma^{+-} y_R y_X \left(M_{RX} + \frac{L_{RR}}{2 y_-} + \frac{L_{XX}}{2 y_+} \right) \\ &+ \frac{1}{2} \Sigma_R \Sigma_{R'} y_R y_{R'} M_{RR'} + \frac{1}{2} \Sigma_X \Sigma_{X'} y_X y_{X'} M_{XX'} \end{aligned}\right\} \tag{17}$$

where Σ^{+-} denotes summation over pairs of ions of opposite sign, and y_+, y_- are defined by

$$y_+ \equiv \Sigma^+ y_R \qquad y_- = \Sigma^- y_X \quad \text{so that} \quad y_+ + y_- = 1. \tag{18}$$

We now introduce BRÖNSTED's principle of specific interaction: "In a dilute salt solution of constant total concentration ions will be uniformly influenced by ions of their own sign." This implies

$$M_{RR'} = M_{RR} \equiv 0 \quad \text{and} \quad M_{XX'} = M_{XX} \equiv 0 \tag{19}$$

so that (17) reduces to

$$\frac{\varphi^s RT}{\Sigma_i r_i} = \Sigma^{+-} y_R y_X \left(M_{RX} + \frac{L_{RR}}{2 y_-} + \frac{L_{XX}}{2 y_+} \right). \tag{20}$$

We can rewrite (20) formally as

$$\frac{\varphi^s RT}{\Sigma_i r_i} = \Sigma^{+-} y_R y_X N_{RX} \tag{21}$$

where N_{RX} is defined by

$$N_{RX} = M_{RX} + \frac{L_{RR}}{2 y_-} + \frac{L_{XX}}{2 y_+} \tag{22}$$

but N_{RX} is not independent of the composition of the solution.

If all the cations have the same charge and all the anions have the same charge, so that every electrolyte present consists of the same number ν_+ of cations and the same number ν_- of anions, then

$$y_+ = \frac{\nu_+}{\nu_+ + \nu_-} \qquad y_- = \frac{\nu_-}{\nu_+ + \nu_-} \tag{23}$$

and N_{RX} becomes a constant characteristic of the electrolyte composed of the ions R and X. When electrolytes of more than one electrical type are present, N_{RX} varies with the relative proportions of electrolytes of the several types. N_{RX} is then not a constant. This is the important conclusion reached by SCATCHARD, but expressed rather differently.

So much for the osmotic coefficient. We shall now derive analogous relations for the activity coefficients. By differentiation of (8) with respect to n_i we obtain, using the definitions (11), (13) and (15),

$$\left.\begin{aligned} \ln \gamma_i^s &= \frac{\Sigma_k n_k (l_{ww} - l_{wk} - l_{wi} + l_{ik})}{n_w} = \Sigma_k y_k L_{ik} \\ &= \Sigma_k y_k \left(M_{ik} + \frac{1}{2} L_{kk} + \frac{1}{2} L_{ii} \right). \end{aligned}\right\} \tag{24}$$

When we introduce the notation R, R' for cations and X, X' for anions formula (24) becomes

$$\left.\begin{aligned} ln\,\gamma_h^s &= \Sigma_{X'}\, y_{X'}\left(M_{RX'} + \frac{1}{2}L_{X'X'} + \frac{1}{2}L_{RR}\right) \\ &\quad + \Sigma_{R'}\, y_{R'}\left(\frac{1}{2}L_{R'R'} + \frac{1}{2}L_{RR}\right) \\ &= \Sigma_{X'} y_{X'}\left(M_{RX'} + \frac{1}{2}L_{X'X'}\right) + \Sigma_{R'} y_{R'}\frac{1}{2}L_{R'R'} + \frac{1}{2}L_{RR} \end{aligned}\right| \qquad (25)$$

where we have used the principle of specific interaction in the form

$$M_{RR'} = M_{R'R'} = 0. \qquad (26)$$

We now consider an electrolyte composed of ν_R ions R and ν_X ions X and we define

$$q_R = \frac{\nu_R}{\nu_R + \nu_X} \qquad q_X = \frac{\nu_X}{\nu_R + \nu_X}. \qquad (27)$$

From (26) and the analogous formula for γ_X^s we deduce for the mean activity coefficient of the electrolyte

$$\left.\begin{aligned} ln\,\gamma_{R,X}^s &= \Sigma_{X'} y_{X'}\left(q_R\, M_{RX'} + \frac{1}{2}L_{X'X'} + \frac{1}{2}\frac{q_R\, L_{RR}}{y_-}\right) \\ &\quad + \Sigma_{R'}\, y_{R'}\left(q_X\, M_{R'X} + \frac{1}{2}L_{R'R'} + \frac{1}{2}\frac{q_X\, L_{XX}}{y_+}\right). \end{aligned}\right| \qquad (28)$$

If, but only if, all the electrolytes present are of the same electrical type so that

$$y_+ = q_R \qquad y_- = q_X \qquad (29)$$

formula (28) reduces to

$$ln\,\gamma_{R,X}^s = q_R\,\Sigma_{X'} y_{X'} N_{RX'} + q_X\,\Sigma_{R'} y_{R'} N_{R'X} \qquad (30)$$

where each N_{RX} is independent of the composition and is given by

$$N_{RX} = M_{RX} + \frac{L_{XX}}{2\,q_R} + \frac{L_{RR}}{2\,q_X}. \qquad (31)$$

This conclusion is also in agreement with SCATCHARD's.

If we want to obtain formulae of comparable simplicity in mixtures of electrolytes of several types, we have to supplement the principle of specific interaction

$$M_{RR'} = M_{RR} = 0 \qquad M_{XX'} = M_{XX} = 0 \tag{32}$$

by the additional assumptions

$$L_{RR} = L_{R'R'} = L_{XX} = L_{X'X'} = L. \tag{33}$$

Formula (20) then reduces to

$$ln\, \gamma^s_{R,X} = q_R \Sigma_{X'} y_{X'} M_{RX'} + q_X \Sigma_{R'} y_{R'} M_{R'X} + L. \tag{34}$$

This may be rewritten in the form

$$ln\, \gamma^s_{R,X} = q_R \Sigma_{X'} y_{X'} N_{RX'} + q_X \Sigma_{R'} y_{R'} N_{R'X} \tag{35}$$

where $N_{RX'}$, $N_{R'X}$ defined by

$$N_{RX'} = M_{RX'} + \frac{L}{q_R} \tag{36}$$

$$N_{R'X} = M_{R'X} + \frac{L}{q_X} \tag{37}$$

respectively depend on the electrical type of the electrolyte whose activity coefficient is being considered, but not on the electrical type of the other electrolytes present. It seems that GUGGENHEIM's previous treatment of mixtures of electrolytes of different electrical types involved the tacit assumption expressed by (33). I can see no convincing physical basis for this assumption except as an approximation on the grounds that L_{RR} and L_{XX} are likely to be much less specific than M_{RX}.

I now return to an examination of SCATCHARD's analysis. SCATCHARD begins his discussion with his formula (10)

$$B = \frac{\Sigma_i c_i b_i}{c} + \frac{1}{2} \frac{\Sigma_{ij} c_i c_j b_{ij}}{c^2} \tag{S 10}$$

where c_i denotes the equivalent concentration of species i and c the total equivalent concentration. I am not at all clear why this formula contains equivalent concentrations rather than ionic

concentrations; nor am I sure whether SCATCHARD attaches importance to the distinction. The situation is complicated by his quoting as the relation between equivalent concentrations c_i and molalities m_i

$$\nu c = \Sigma_i c_i \nu_i = \Sigma_i m_i$$

Since neither ν nor ν_i is defined, I cannot say with certainty that this formula is wrong, but it does look strange. However, I shall assume that these matters are trivial and return to the discussion of formula (S 10). SCATCHARD attaches special importance to the presence of the terms in b_i and states that "GUGGENHEIM avoids the thermodynamic error by the usually improbable assumption that every b_i is zero". Now we can always define quantities b'_{ij} by

$$b'_{ij} = b_{ij} + \frac{1}{2} b_i + \frac{1}{2} b_j$$

and then, since $\Sigma_i c_i = 2c$ rewrite (S 10) as

$$B = \frac{1}{2} \frac{\Sigma_{ij} c_i c_j b'_{ij}}{c^2}$$

The question whether the b_i are zero or not is consequently meaningless until the b_{ij} have been unambiguously defined and SCATCHARD has omitted to do this. Presumably SCATCHARD's b_{ij} correspond closely to my M_{ij} and not to my L_{ij}. To sum up, SCATCHARD's premises are ambiguous but my premises lead to conclusions in considerable, if not complete, agreement with his.

References.

1) Brönsted: Dan. Mat. Fys. Medd. (1921), **4**, 4; J. Am. Chem. Soc., (1922), **44**, 877.
2) Debye and Hückel: Physikal. Zeit. (1923), **24**, 185.
3) Guggenheim: Rep. of Scandinavian Science Congress, Copenhagen (1929), p. 298; Phil. Mag., (1935), **19**, 588.
4) Scatchard: J. Phys. Chem., (1954), **58**, 600.
5) La Mer, Gronwall and Greiff: J. Phys. Chem., (1931), **35**, 2245.
6) Guggenheim: J. Phys. Chem., (1929), **33**, 842.

Indleveret til selskabet den 16. marts 1955.
Færdig fra trykkeriet den 19. september 1955.

Det Kongelige Danske Videnskabernes Selskab
Matematisk-fysiske Meddelelser, bind **30,** nr. 15

Dan. Mat. Fys. Medd. **30,** no. 15 (1956)

ROTATIONAL PERTURBATIONS IN NUCLEI — APPLICATION TO WOLFRAM 183

BY

A. K. KERMAN

København 1956
i kommission hos Ejnar Munksgaard

CONTENTS

Printed in Denmark
Bianco Lunos Bogtrykkeri A-S

I. Introduction.

Rotational spectra have been well established as an important feature of the excited states in heavy nuclei. The theory of rotational states and the supporting evidence have been given by Bohr, Mottelson, and co-workers (cf. Bohr, 1952; Bohr and Mottelson, 1953; Bohr, 1954; Bohr and Mottelson, 1954; Bohr, Fröman, and Mottelson, 1955; Alaga, Alder, Bohr, and Mottelson, 1954).

Deviations from the simple rotational spectrum have been found for the most part to be small and to often exhibit the character of rotation-vibration corrections, especially in even-even nuclei (Bohr, 1954). As is well known, such corrections arise as an effect of the centrifugal force on the intrinsic structure of the rotating system. The fact that the observed deviations are usually small implies that the centrifugal force excites only high energy modes of the intrinsic structure. By high energy we mean large compared to the characteristic rotational energy.

An examination of the rotational spectra in Wolfram 183 reveals a deviation from the simple structure, which cannot be accounted for by the rotation-vibration correction. It is proposed that this deviation is caused by the action of the rotation in exciting low energy states of the particle structure. When suitable low energy states exist, the rotational motion is no longer separable and we must treat it as strongly coupled to the degrees of freedom in question. This effect is well known in molecules, where it has been called the Rotational Perturbation (cf., e.g., Herzberg, 1950, pp. 285–6).

The analogy to molecules, although of great use, must not be carried too far when it comes to detailed discussions. For example, in molecules the heavy particles provide a rather stable field in which the electrons can move; while in the nucleus it is

the nucleons which must provide, in a self-consistent way, the field in which they themselves move. Also, the mass of a nucleon compared to the nucleus is much larger than is the case for electrons in molecules. One may therefore expect that most perturbations will play a more important role in nuclei than they do in molecules.

We can also expect that the rotational perturbations in particular will be less important in even-even nuclei than in odd nuclei, at least near the ground state. The reason for this is the fact that, in even-even nuclei, the first excitation of the particle structure appears to be rather high ($\sim$ 1 MeV), probably because of the interaction between pairs of nucleons. Thus, there are no very low energy states which can be coupled to the rotation.

In the following sections, the consequences of the rotational perturbations are developed, using a simplified model at the start in order to keep the essential points foremost. Then, a rather detailed application is made to the accurately measured energy spectrum of Wolfram 183 (cf. MURRAY et. al., 1955). From this we obtain good evidence that the interpretation is well founded. A similar analysis of other odd nuclei will be of interest, but this must await the accumulation of more data.

II. Rotational Perturbations.

In order to make clear the origin and generality of the particular rotational perturbation in which we are most interested here, it is useful to consider a simple model. Subsequently, we shall generalize this model in order to make it applicable to the actual case of nuclei. In doing so, the role of other rotational perturbations will become clear.

Therefore, we first restrict ourselves to the system of a single particle coupled to a rigid top by a potential. The Hamiltonian for this system is simply

$$H = \frac{p^2}{2m} + V(\bar{r}) + \sum_{k=1}^{3} \frac{\hbar^2}{2\Im_k} (I_k - j_k)^2, \qquad \text{(II.1)}$$

where $\bar{p}$, $\bar{j}$, and $\bar{r}$ are respectively the linear momentum, angular momentum, and position vectors of the particle in the system of

coordinates corresponding to the instantaneous position of the principal axes of the top. The vector $\bar{I}$ is the total angular momentum of the system; $\Im_k$ are the principal moments of inertia of the top; V is the potential energy between the particle and the top; and m is the reduced mass of the system.

For the analogy with nuclei it is useful to consider first the case where both the top and the potential V have axial symmetry. In particular this means

$$\Im_1 = \Im_2 \equiv \Im. \tag{II.2}$$

The Hamiltonian (1) can then be written in the more convenient form

$$H = H_0 + \frac{\hbar^2}{2\Im_3}(I_3 - j_3)^2 + \frac{\hbar^2}{2\Im}(I^2 - I_3^2 - j_3^2) + RPC, \tag{II.3}$$

with

$$H_0 = \frac{p^2}{2m} + V(\bar{r}) + \frac{\hbar^2}{2\Im} j^2, \tag{II.4}$$

and

$$RPC = -\frac{\hbar^2}{2\Im}(I_+ j_- + I_- j_+), \tag{II.5}$$

where

$$I_\pm = I_1 \pm iI_2, \; j_\pm = j_1 \pm ij_2. \tag{II.6}$$

The term defined in equation (5) is an effect of the Coriolis force on the particle and will be given the name "rotation-particle coupling" (*RPC*). When *RPC* is neglected, it is clear because of the axial symmetry, that I_3 and j_3 will be good quantum numbers. These have usually been designated by K and Ω, respectively. The Hamiltonian H_0 can, in principle, be solved for the particle motion with Ω as one of the quantum numbers (for example, see NILSSON, 1955; GOTTFRIED, 1955). Then, the energy spectrum will be given by

$$E = E_\Omega^{(0)} + \frac{\hbar^2}{2\Im_3}(K - \Omega)^2 + \frac{\hbar^2}{2\Im}(I(I+1) - K^2 - \Omega^2). \tag{II.7}$$

All available data on rotational spectra in nuclei indicates that only states with $K = \Omega$ occur in the regions of low excitation, i.e. the spectrum has the form

$$E = E_K^{(0)} + \frac{\hbar^2}{2\Im}(I(I+1) - 2K^2). \tag{II.8}$$

This is equivalent to the statement that rotations about the symmetry axis require high energies, or simply that

$$\Im_3 \ll \Im. \tag{II.9}$$

The effects of the rotation-particle coupling can be simply investigated. For this, we first need the non-vanishing matrix elements

$$(IK \mid I_\pm \mid IK \pm 1) = \sqrt{(I \mp K)\,(I \pm K + 1)}, \tag{II.10}$$

$$(j\Omega \mid j_\mp \mid j\,\Omega \pm 1) = \sqrt{(j \mp \Omega)\,(j \pm \Omega + 1)}. \tag{II.11}$$

Using these matrix elements we note the general property that the *RPC* preserves the quantum number $(K - \Omega)$ even though it destroys both K and Ω separately. This is an important property, because it means that matrix elements to the lowest lying states, which have $K - \Omega = 0$ in common with the ground state, do not vanish.

Whether or not the *RPC* will be important depends essentially on the spectrum of energies for the Hamiltonian H_0. If the spacings in this spectrum are large compared to the rotational energies, or, in other words, if the rotation is adiabatic with respect to the particle motion, then the *RPC* is a small perturbation and the simple rotational spectrum (8) is to be expected. This corresponds to a strong coupling of the particle to the rotator. In the opposite limit, when the particle is almost decoupled from the rotator, the quantum numbers Ω and K are not appropriate and the non-spherical part of the coupling energy $V(\bar{r})$ should be treated as the perturbation. We shall be interested in the case of partial decoupling. By this is meant the situation where the great mass of the particle spectrum is high in energy, but where there may be one or a few levels which are low enough so that they cannot be simply treated in perturbation theory. The *RPC*, acting through these levels, partly decouples the particle from the rotator. In the following section, we shall discuss this case in detail.

An important example of partial decoupling is the case where $\Omega = {}^1/_2$ and the rotator has axial symmetry. Because of this symmetry, the states Ω and $-\Omega$ are degenerate and the wave function is a "symmetrical" combination of the two (cf. Bohr, 1952).

Then, for the special case $\Omega = {}^1/_2$, the *RPC* has a diagonal matrix element, and this contributes the so-called "decoupling term" to the rotational spectrum (DAVIDSON and FEENBERG, 1953; BOHR and MOTTELSON, 1953; see also equation (III.1) below). There are many cases of odd nuclei with $\Omega = {}^1/_2$ where this decoupling effect has been met with.

Up to this point, we have been considering the simple model of a particle coupled to an axially symmetric rigid top. We shall now proceed to generalize on this model. Our first step is to relax the restriction as to axial symmetry. This leads to the following four perturbations.

$$H' = H_1' + H_2' + H_3' + V'(\bar{r}) \tag{II.12}$$

$$\begin{aligned} = \left(\frac{\hbar^2}{8\,\Im_1} - \frac{\hbar^2}{8\,\Im_2}\right) \Big\{ & -2\,(I_+ j_+ + I_- j_-) + (j_+ j_+ + j_- j_-) \\ & + (I_+ I_+ + I_- I_-) \Big\} + V'(\bar{r}), \end{aligned} \tag{II.13}$$

where $V'(\bar{r})$ is the axial asymmetry in the particle potential energy, and the moment of inertia $\Im$ in (7) is now the harmonic mean of $\Im_1$ and $\Im_2$. All of these perturbations are such that they do not preserve the quantum number $(K - \Omega)$. In view of the condition (9), this means that they couple only to high energy states. Therefore, in this case, H' can be treated as a small perturbation. The analogous perturbations have been previously examined by BOHR (1952) for the model of a particle interacting with an incompressible liquid drop, in which case an explicit expression for $V'(\bar{r})$ is also obtained.

It can easily be seen, using equations (10) and (11) and second order perturbation theory, that H_1' and H_3' lead to a renormalization of $\Im$, while $V'(\bar{r})$ and H_2' lead to a renormalization of $E_K^{(0)}$. The energy H_3' gives in addition a new type of term which is negative and proportional to $I^2\,(I+1)^2$.

It is quite clear, both from general ideas of nuclear dynamics and from the data on rotational spectra, that the nuclear rotational motion is not that of a rigid body. In fact, the measured moments of inertia lie between those for irrotational flow and for a rigid body (cf. BOHR and MOTTELSON, 1955). These moments depend

on the shape of the nucleus which, in turn, depends upon the internal nucleon configuration. However, as long as the moments of inertia are essentially constants of the motion, the considerations above will still apply.

Small deviations from the constant values arise from the fact that the rotational motion will distort the nuclear shape somewhat. This distortion is essentially a stretching, which increases the moment of inertia. Therefore, the moment of inertia can be expanded as a function of $I(I+1)$, and to first order this introduces a term in the energy which is negative and proportional to $I^2(I+1)^2$. This is the so-called rotation-vibration energy and its magnitude depends on the deformability of the nucleus and on the dependence of the moment of inertia on the deformation. Other effects of the deformability will arise if the rotation causes a deviation from axial symmetry. (The extreme case where the nucleus is not stable with respect to vibrations about axial symmetry, so-called γ-vibrations, has been considered by BOHR and MOTTELSON, 1953, and by WILETS and JEAN, 1955.) Then, as we have already seen, the energies (13) lead to a renormalization of $E_K^{(0)}$ and $\Im$ as well as providing another rotation-vibration-like correction. For regions far removed from closed shells, where the rotational energies are small (< 100 keV), all the evidence is that the rotation-vibration effects are also small. In addition, the evidence suggests that, as one approaches closed shells, these effects will increase to a point where one would have to treat the rotation-vibration coupling in a more exact manner than second order perturbation theory. This would be an analogous situation to the one considered here for the *RPC*. For the nuclei near magic numbers, where one expects a spherical equilibrium shape, the rotation-vibration coupling is so strong that it makes no real sense to speak of rotations. The collective motion then takes the form of oscillations analogous to the surface vibrations of a liquid drop. One has some evidence that this is the case (GOLDHABER and WENESER, 1955).

We must keep in mind the fact that in nuclei the moments of inertia arise as a collective effect of all the particles. Actually, the inertia of the rotational motion is intimately associated with the *RPC*; and in fact the moment of inertia can be traced back to a second order effect of the *RPC* on all the particles (cf. below).

The decoupling effects which we consider here arise in cases where higher order terms are important so that it is necessary to describe more explicitly the corresponding degrees of freedom. Essentially, this is the case when there exist low lying states of excitation of the particle structure, or special degeneracies, as in the case of $\Omega = {}^1/_2$ with axial symmetry. Such low lying excitations, with energies comparable to rotational energies, are usually found in odd-A nuclei and we therefore expect decoupling effects to be especially important in these cases.

Finally, it is emphasized that the *RPC*, which we consider acting between low lying configurations of the rotating nucleus, is of a very general nature (Coriolis force) and its existence is independent of any specific assumptions about the intrinsic nuclear structure.

III. Mixing of Two Rotational Bands.

Let us consider the simplest possible case where the *RPC* will have an important effect. This is the situation when there is a single low-lying configuration which is coupled to the ground state by the *RPC*. In this case, the energy can be simply diagonalized (cf., e.g., HERZBERG, 1950, p. 283) and the various limits considered afterwards. Without the *RPC* there is associated with each of the configurations a rotational band having energies*

$$E_K(I) = E_K^{(0)} + E_K^{(1)} \left\{ I(I+1) + \delta_{K,\,1/2}\, a\, (-1)^{I+1/2} \left(I + \frac{1}{2} \right) \right\}, \quad \text{(III.1)}$$

where the parameter $E_K^{(1)}$ and the decoupling parameter a depend in some way upon the nucleon configuration, and where $E_K^{(0)}$ is conventionally chosen so that $E_K(K)$ will have the experimental energy.

The rotational spectra corresponding to the close configurations K and $K+1$ will be mixed by the *RPC* (only states with

* For reasons of simplicity, we have disregarded the rotation-vibration term

$$- E_K^{(2)} \left\{ I(I+1) + \delta_{K,\,1/2}\, a\, (-1)^{I+1/2} \left(I + \frac{1}{2} \right) \right\}^2, \quad \text{1(a)}$$

although there is no difficulty in including it if the accuracy of the data requires this.

the same I can mix) and the resulting energy spectrum will be given by*

$$\left.\begin{aligned} E(I) &= {}^1/_2 \left\{ E_{K+1}(I) + E_K(I) \right\} \\ \pm {}^1/_2 \sqrt{\left\{ E_{K+1}(I) - E_K(I) \right\}^2 + 4 A_K^2 (I-K)(I+K+1)} \end{aligned}\right\} \quad \text{(III.2)}$$

where

$$A_K = \left| \left(K \left| \frac{\hbar^2}{2\Im} J_- \right| K+1 \right) \right| \qquad \text{(III.3)}$$

$$J_- = \sum_{\text{particles}} j_- . \qquad (3)\text{a}$$

We note that the state $I = K$ is not affected because it has no perturbing partner in the $(K + 1)$ spectrum. It is clear that the parameter A_K has roughly the order of magnitude of a rotational energy, although it may be considerably smaller if the two configurations have a small overlap.

The amplitudes of mixing will be expressed in the following notation. We write the wave functions as

$$\Psi_I^{H,L} = a_I^{H,L} \Psi_{IK} + b_I^{H,L} \Psi_{IK+1}, \qquad \text{(III.4)}$$

$$a_I^2 + b_I^2 = 1, \qquad \text{(III.5)}$$

where the superscripts H and L denote the higher and lower energy solutions, respectively, and the dependence on other quantum numbers is left implicit. In terms of the ratio

$$R_K(I) = \frac{\left| \left\{ E_{K+1}(I) - E_K(I) \right\} \right|}{2 A_K \sqrt{(I-K)(I+K+1)}} \qquad \text{(III.6)}$$

the mixing amplitudes are

$$a_I^{H,L} = \left\{ 1 + \left[\pm R + \sqrt{1 + R^2} \right]^2 \right\}^{-1/2}, \qquad \text{(III.7a)}$$

$$b_I^H = a_I^L ; \quad b_I^L = - a_I^H . \qquad \text{(III.7b)}$$

* In general there is also the possibility for the *RCP* to connect different states of the same parity both of which have $K = {}^1/_2$. This arises on account of the symmetrization of the wave function discussed before. The considerations are the same as those presented here and the only difference is that we put $K = -{}^1/_2$ in the matrix element A_K.

We have conventionally considered the particle state $K+1$ to be higher than the state K. For the opposite case we have only to interchange the roles of a_I and b_I in (7).

One is interested in the electromagnetic transition probabilities between the mixed states. These will be given in terms of the above mixing amplitudes and the usual γ-ray transition matrix elements. The latter are expressed in general by the formulae (cf. NILSSON, 1955)

$$\left.\begin{aligned} B(E2) &= \frac{5}{16\pi} e^2 \{(I\,2\,I'K' \mid IK\,2,\ K'-K) \\ &+ b_{E2}^{KK'}(-1)^{I'+K'}(I\,2\,I', -K' \mid IK\,2, -K'-K)\}^2 (Q^{KK'})^2 \end{aligned}\right\} \quad \text{(III.8)}$$

$$\left.\begin{aligned} B(M1) &= \frac{3}{4\pi}\left(\frac{e\hbar}{2MC}\right)^2 \{(I\,1\,I'K' \mid IK\,1,\ K'-K) \\ &+ b_{M1}^{KK'}(-1)^{I'+K'}(I\,1\,I', -K' \mid IK\,1, -K'-K)\}^2 (G^{KK'})^2, \end{aligned}\right\} \quad \text{(III.9)}$$

where Q, G, b_{M1}, b_{E2} depend upon the intrinsic wave functions. For the diagonal transitions (diagonal in K), these have the usual interpretation in terms of electric quadrupole moments and magnetic g-factors.
Thus

$$Q^{KK} = Q_0^K, \quad \text{(III.10)}$$

the electric quadrupole moment in the state K; and

$$G^{KK} = K(g_K - g_R), \quad \text{(III.11)}$$

related to the magnetic g-factors in the state K (cf. BOHR and MOTTELSON, 1953, p. 109).

In quadrupole transitions, the off-diagonal matrix elements and the quantities b_{E2} can usually be neglected because they are single-particle effects, while the diagonal matrix elements are essentially the large collective electric quadrupole moments. For magnetic transitions the term containing b_{M1} enters only in the diagonal case $K = K' = {}^1/_2$. The factor which determines the effect of b_{M1} is the ratio (see (14))

$$f^{II'} = (-1)^{I'+1/2} \frac{(I1\,I', -1/2 \,|\, I\,1/2\,1, -1)}{(I1\,I'\,1/2 \,|\, I\,1/2\,1\,0)} = \frac{(-1)^{I+1/2}}{\sqrt{2}} \begin{cases} 1 & , \quad I' = I-1 \\ (2I+1), & I' = I \\ -1 & , \quad I' = I+1. \end{cases} \tag{III.12}$$

The reduced transition probabilities between the mixed states (neglecting the single-particle $E2$ effects) are then

$$B(E2) = \frac{5}{16\pi} e^2 \{ a_I a_{I'} Q_0^K (I\,2\,I'K \mid IK\,2\,0) + b_I b_{I'} Q_0^{K'} (I\,2\,I'K' \mid IK'\,2\,0) \}^2 \tag{III.13}$$

$$B(M1) = \frac{3}{4\pi} \left(\frac{e\hbar}{2Mc} \right)^2 \{ a_I a_{I'} G^{KK} (I\,1\,I'K \mid IK\,1\,0) [1 + \delta_{K,1/2} f^{II'} b_{M1}] + b_I b_{I'} G^{K'K'} (I\,1\,I'K' \mid IK'\,1\,0) + a_I b_{I'} G^{KK'} (I\,1\,I'K' \mid IK\,1\,1) + a_{I'} b_I G^{K'K} (I\,1\,I'K \mid IK'\,1, -1) \}^2 \tag{III.14}$$

with

$$K' = K + 1\,; \quad G^{KK'} = -G^{K'K}. \tag{III.14a}$$

The transition probabilities are given in the usual way by

$$T(E2) = \frac{4\pi}{75} \frac{1}{\hbar} \left(\frac{\Delta E}{\hbar c} \right)^5 B(E2) \tag{III.15}$$

$$T(M1) = \frac{16\pi}{9} \frac{1}{\hbar} \left(\frac{\Delta E}{\hbar c} \right)^3 B(M1). \tag{III.16}$$

We can easily examine the extreme case where the interacting particle states are almost degenerate. If, for example, we take $K \neq 1/2$, $E_K^{(1)} = E_{K+1}^{(1)}$, and assume that the rotational family is degenerate in zero order, the energy spectrum is

$$E(I) = E_K^{(0)} + E_K^{(1)} \left\{ I(I+1) \pm \left(\frac{A_K}{E_K^{(1)}} \right) \sqrt{(I-K)(I+K+1)} \right\}, \tag{III.17}$$

while the mixing is fifty fifty, i. e.

$$a_I^H = b_I^H = a_I^L = \frac{1}{\sqrt{2}}; \quad b_I^L = -\frac{1}{\sqrt{2}}. \tag{III.18}$$

One sees, therefore, that the decoupling can have a rather large effect on the rotational spectrum, enough in some cases to make it almost unrecognizable as such (cf. also the decoupling effect when $K = {}^1/_2$. It is not expected that this extreme case will occur, except by some accident, but nevertheless it is instructive as an example of the kind of effect which can occur. It is more instructive to examine the opposite extreme where perturbation theory is useful, and this is done in the next section.

IV. Perturbation Limit for *RPC.*

When the energies of the two configurations (K and $K+1$) are very different, i.e. the difference is large compared to the rotational energies, we expect that the mixing can be treated as a perturbation. The different orders of the perturbation series are simply obtained by an expansion of the equations in Section III. The relevant expansion parameter is the ratio $R_K(I)^{-1}$. It is clear that whether or not perturbation theory is applicable depends to some extent on the total angular momentum I in view of the I dependence of R_K. In general, the perturbation series becomes less useful, the larger I is.

For the energies in the perturbed ground state band, one obtains the formula*

$$E(I) = E_K^{(1)} \left\{ 1 - \frac{A_{K<}}{E_K^{(1)}} \frac{A_{K<}}{\Delta E} \right\} [I(I+1) - K(K+1)] + \frac{A_{K<}^2}{\Delta E} \left\{ \frac{(E_{K'}^{(1)} - E_K^{(1)})}{\Delta E} + \left(\frac{A_{K<}}{\Delta E} \right)^2 \right\} [I(I+1) - K(K+1)]^2 + \cdots \tag{IV.1}$$

* The result (1) is for the case where there is only one state ($K \pm 1$) which interacts with the ground state K. Of course, the perturbation result can just as easily be obtained for the more general case where there are an arbitrary number of interacting states. In higher orders, we would then have to include states with $K \pm 2$, etc., and this might change the results in specific cases. Equation (1) is displayed in order to show the kind of effects which may be expected.

where K labels the ground state band, and K' the interacting band ($K' = K \pm 1$). The quantity ΔE is the energy difference, taken as positive, between the interacting configurations. The necessary condition for this expansion is

$$\frac{A_{K<}}{\Delta E} \ll 1 . \tag{IV.2}$$

There are two general remarks which can be made on consideration of this result. First, the *RPC* can significantly increase the moment of inertia for the ground state rotational band; and second, it can provide a vibration-rotation-like term which has a positive sign. We shall look first at the former effect.

In second order perturbation theory, one sees that the moment of inertia is increased by the factor (cf. equation (1))

$$\left\{ 1 + \frac{A_{K<}}{E_K^{(1)}} \frac{A_{K<}}{\Delta E} \right\} \tag{IV.3}$$

and, hence, when there are appropriate low-lying configurations, the last few nucleons can have a rather large effect on the moment of inertia, even when perturbation theory is still valid. For example, in a nucleus with $A \approx 200$, each particle can be said to contribute on the average one half of one percent of the moment of inertia, while the last few nucleons might easily give rise to a contribution of ten per cent. Of course, if the contribution is too large, perturbation theory will not be adequate, especially for the higher states in the band. The empirical evidence shows a general tendency for larger moments in the odd nuclei than in neighbouring even nuclei (cf. Bohr and Mottelson, 1955; Bohr, Fröman, and Mottelson, 1955). This would indicate that the last few nucleons do indeed have low-lying states, and that the *RPC* is operating as described above. In many cases, the difference is so large as to indicate that a perturbation treatment of the *RPC* is not suitable. In the next section we will discuss the case of ${}_{74}W^{183}$ where this situation exists.

One can recall the remark made earlier that we expect the *RPC* to be rather intimately connected with the moment of inertia. In fact, Inglis (1954) and Bohr and Mottelson (1955) have shown that the total moment of inertia can be derived in time-dependent perturbation theory as an effect of the rotation on the

particle structure; an effect quite equivalent to the *RPC* when one takes into account all of the particles and uses second order perturbation theory.

It is not surprising to see that the second term in (1) is proportional to $I^2(I+1)^2$. The interesting fact is that the coefficient can in principle have a positive sign. For the particular case we have studied here, the positive sign is obtained as long as the moment of inertia of the interacting band (K') is not too large compared to that of the band (K) under consideration. As has been discussed above, this type of term in the energy can arise as a direct effect of the centrifugal force on the moment of inertia (rotation-vibration interaction) or as an effect of the energy H_3 (eq. (II.12)) in second order perturbation theory. In both cases the coefficient is negative. The reason one can have a positive sign from the *RPC* is that the $I^2(I+1)^2$ term first arises in fourth order perturbation theory. (The same is true for the less important perturbation H_1). Since the *RPC* can usually couple to states of lower energy it may be rather more important than the other couplings, even in fourth order. Thus we may expect in some cases to find an anomalously small or even a positive "rotation-vibration"-like correction.

We seem to have an example of both of these effects (renormalization of moment of inertia and positive rotation-vibration correction) in the excited rotational band of ${}_{74}W^{182}$ which has been assigned as odd parity and $K = 2$ (cf., e.g., ALAGA et al., 1955). At this excitation energy (1.29 MeV for the first state of the band) one expects that the level density is higher than in the ground state region, and then the *RPC* may play a role, as it does in the neighbouring odd isotope. This seems to be the case because the excited band has a higher moment of inertia than the ground state band (15 % higher); and also it has a positive rotation-vibration-like correction, while that of the ground state band is, as usual, negative.

In the perturbation limit, the effect of the rotational admixtures on the electromagnetic transition amplitudes can be easily obtained. To first order in $(A_{K<}/\Delta E)$, the mixing amplitudes are*

* This is for the case where the configuration $K+1$ is higher in energy than the configuration K. For the reverse case the roles of a_I and b_I are interchanged (cf. III equation (7)).

$$a_I^L = b_I^H \sim 1\,; \quad a_I^H = -b_I^L \sim \left(\frac{A_{K<}}{\Delta E}\right)\sqrt{(I-K)\,(I+K+1)}. \quad \text{(IV.4)}$$

Let us first consider transitions between rotational states in the same band. The following results are obtained, using equations (4), (III.13), and (III.14) along with certain properties of the vector addition coefficients. For $E2$ transitions ($I' = I - 2$) and $M1$ transitions ($I' = I - 1$) within a band (K), we have respectively

$$\left.\begin{aligned} B(E2) &= \frac{5}{16\,\pi}\,e^2\,(I\,2\,I'\,K \mid I\,K\,2\,0)^2 \\ &\left\{ Q_0^K + \left(\frac{A_{K<}}{\Delta E}\right)\sqrt{\frac{2}{3}}\,Q^{KK'}\,f_{E2}^{KK'} \right\}^2; \quad K_< \neq {}^1/_2 \end{aligned}\right\} \quad \text{(IV.5)}$$

$$\left.\begin{aligned} B(M1) &= \frac{3}{4\,\pi}\left(\frac{e\hbar}{2Mc}\right)^2 (I\,1\,I'\,K) \mid IK\,1\,0)^2 \\ &\left\{ G^{KK}\left[1 + \delta_{K,{}^1/_2}\,\frac{(-1)^{I+{}^1/_2}}{\sqrt{2}}\,b_{M1}\right] + \left(\frac{A_{K<}}{\Delta E}\right)\sqrt{2}\;G^{KK'}\,f_{M1}^{KK'} \right\}^2 \end{aligned}\right\}, \quad \text{(IV.6)}$$

where $K' = K \pm 1$ labels the perturbing band. The values of $f^{KK'}$ are given in Table I.

TABLE I.

$f_{M1}^{KK'}$	$f_{E2}^{KK'}$	K'	
$-(K+1)$	$-(2K+3)$	$K+1$	K is ground state band
$(K-1)$	$(2K-3)$	$K-1$	
$(K+1)$	$(2K+3)$	$K+1$	K is excited band
$-(K-1)$	$-(2K-3)$	$K-1$	

One sees from (5) and (6) that, when the rotational admixtures are small, they do nothing more than "renormalize" what are understood as the electric quadrupole moments and the magnetic g-factors. The I dependence of the transition amplitudes remains the same as they are without the admixtures. The renormalization of Q_0 will be quite unimportant because the correction term, in addition to being small because of $(A_{K<}/\Delta E)$, is made smaller still because the off-diagonal matrix elements Q^{KK} are

expected to be unimportant compared to the intrinsic quadrupole moments Q_0^K.

For transitions between mixed rotational bands, in the usual case where the quadrupole moments of the two bands are nearly equal, we get simply

$$\left.\begin{aligned} B(E2) = \frac{5}{16\pi} e^2 (I\,2\,I'K' \mid IK\,2,\, K'-K)^2 \\ \left\{\left(\frac{A_{K<}}{\Delta E}\right)\sqrt{6}\, Q_0^K + Q^{K'K}\right\}^2, \end{aligned}\right\} \quad \text{(IV.7)}$$

when

$$Q_0^K = Q_0^{K'};\ K' = K \pm 1;\ K_< \neq {}^1/_2.$$

This is a result previously derived and used by ALAGA et al. (1955). One can obtain a similar result in the $M1$ amplitudes, but the necessary condition $G^{KK} = G^{K'K'}$ is not likely to be fulfilled. In equation (7) one sees that the off-diagonal particle term can be important because the strong collective term is cut down by the small factor $(A_{K<}/\Delta E)$.

V. Application to $_{74}W^{183}$.

The energy levels in the odd nucleus $_{74}W^{183}$ have been very accurately determined up to an energy of 450 keV from a study of the γ-transitions and internal conversion following the β-decay of $_{73}Ta^{183}$ (MURRAY et al, 1955). The level scheme suggested by MURRAY et al. can be interpreted in terms of two intermixed rotational bands accompanying configurations with $K = {}^1/_2$ and $K = {}^3/_2$* (cf. Fig. 1).

A semi-empirical fit of the ground state rotational band, $(K = {}^1/_2)$, using the usual formula (III.1) with the correction III. (1a), is successful in a qualitative way, and leads to the parameters $E^{(1)}_{1/2} = 13.027$ keV, $a = 0.1904$, and $E^{(2)}_{1/2} = 0.003182$ keV. The energy of the $K = {}^1/_2$, $I = {}^9/_2$ level (G) using these parameters is only some 8 keV lower than the experimental value.

* This interpretation has also been considered by CHRISTY (1954).

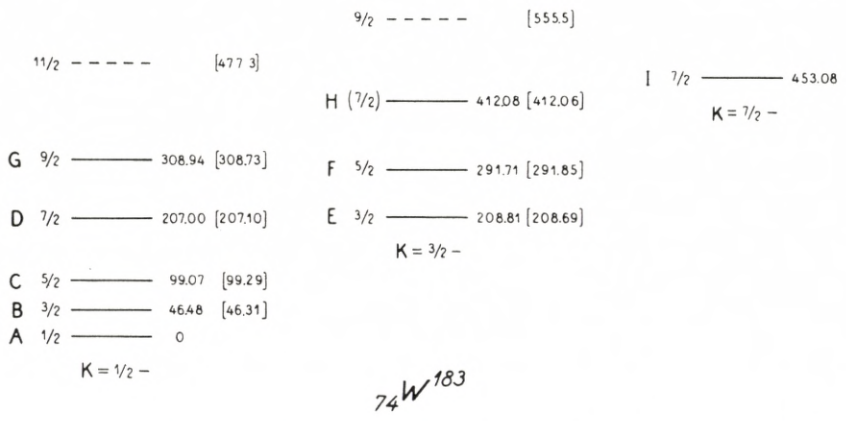

Fig. 1. The level scheme in W^{183} suggested by MURRAY et al. has been drawn so as to display clearly the interpretation in terms of rotational bands. The different bands are horizontally displaced, and the numbers in square brackets are the energies calculated using the parameters (V. 1).

Since it does not fit in with the other rotational sequences we postulate that the level I (spin 7/2) begins a new rotational band with $K = 7/2$. Because the *RPC* cannot directly mix bands with $\Delta K > 1$, the $K = 7/2$ band cannot mix with $K = 1/2$ or 3/2 bands. Therefore the level I can be disregarded in dealing with the mixing of the other two bands.

The spin for the state *H* has been postulated to be 7/2 rather than 5/2 as suggested by MURRAY et al. This seems to be a reasonable assignment because of the lack of an $E2$ transition to the ground state. The spin 7/2, however, is contrary to the multipolarity assignment $M1$ for the transition *HE*. This assignment is based on internal conversion evidence (measurement of the *K* conversion coefficient), but appears not to be entirely conclusive. In addition, the theory predicts a 7/2 state with just the properties of the observed level *H*. A conclusive measurement of this spin would of course be very interesting.

This discrepancy, however, is something one would like to understand. In view of (1) the fact that there is a close lying $K = {}^3/_2$ configuration, and (2) that the parameter $E^{(1)}_{1/2}$ (13.027 kev) is 22 % less than the value of $E^{(1)}_0$ (16.767 keV) in the neighbouring even-even nucleus $_{74}W^{182}$, it would seem likely that the 8 keV discrepancy is a result of the *RPC*. Then, using the first part of equation (IV.1), we can simply estimate that $A_{1/2} = 28$ keV. This only serves as a first estimate, because the 8 keV discrepancey implies that a fourth order perturbation treatment is not valid. The large effect on the moment of inertia implies the same thing.

The formula (III.2) has been applied to the first five levels above the ground state, and the resulting parameters are

$$\left.\begin{aligned} E^{(1)}_{1/2} &= 15.853 \text{ keV.} \qquad a = 0.1684 \text{ keV.} \\ E^{(1)}_{3/2} &= 14.050 \text{ keV.} \qquad A_{1/2} = 21.735 \text{ keV.} \\ E^{(0)}_{3/2} &= 146.74 \text{ keV.} \end{aligned}\right\} \quad (V.1)$$

The numbers in square brackets in Fig. 1 give the energies as calculated, using these parameters. We note that the discrepancy has been reduced to the order of one fifth of a kilovolt. This remainder might easily be caused by the neglect of other rotation-vibration-like terms in the energy. Just as important, the value of $E^{(1)}_{1/2}$ is now much closer to the analogous quantity in the neighbouring even-even nucleus. Again, the remaining discrepancy might easily be a result of other higher order effects. Finally, it is interesting to note that the matrix element $A_{1/2}$ has the expected order of magnitude of a rotational energy, which we had already seen in the perturbation estimate above.

Making use of the parameters (1) along with equations (III. 1), (III. 6), and (III. 7), a table of mixing amplitudes can be simply constructed.

TABLE II.

I	$^3/_2$	$^5/_2$	$^7/_2$	$^9/_2$
$a^H_I = -b^L_I$	.24	.35	.47	.51
$a^L_I = b^H_I$	.97	.94	.88	.86

Now a_I is the amplitude of $K = {}^1/_2$, b_I is the amplitude of $K = {}^3/_2$, and H, L refer to the high and low energy states of the same total angular momentum I. Especially for the higher angular momenta, the mixing is considerable, and one does not expect that perburbation theory would be adequate.

Having determined the mixing amplitudes we can now go on to an examination of the electromagnetic transition probabilities. One has a great wealth of data on relative decay probabilities (cf. MURRAY et al., 1955) and also some data on Coulomb excitation (HUUS et al., 1955; MCCLELLAND et al., 1954; MARK et al., 1955; STELSON and MCGOWAN, 1955). Although this data is

quite extensive and accurate it would be very useful to have even more detailed measurements; for example the $E2/M1$ mixtures would be quite interesting and also decisive for the interpretations which follow.

The easiest transitions to discuss are those which are pure $E2$. This is so because here the parameters are roughly known. First, it is not expected that the collective quadrupole moment will vary drastically from one state to another, i.e., we expect $Q_0^{3/2}$ and $Q_0^{1/2}$ to be roughly equal. The fact that the moments of inertia for these two states are closely equal can be considered as evidence for this. Hence, we can take

$$Q_0^{3/2} \approx Q_0^{1/2}. \qquad \text{(V.2a)}$$

To the same approximation we can also use

$$Q^{3/2\,1/2} \approx 0$$

because this is a single particle effect.

MURRAY et al. have measured only one intensity ratio for a pair of $E2$ transitions. This is the ratio for the transitions HE and HB in W^{183} (see Fig. 1) which they find to have the value 0.27. A direct calculation, using (2), gives 0.34, which agrees within the accuracy of the measurements. Without the rotational admixture this ratio is too small by a factor ten even for a more favourable choice of $Q^{1/2\,3/2}$.

Making use of the same assumptions (2) we can construct a table of relative Coulomb excitation probabilities. Thus, fixing $Q_0 \approx 6.5 \cdot 10^{-24}$ cm^2 to fit the value given by of HUUS et al., (1955), we can calculate the other excitation probabilities. The value of $B_{\text{exc}}\,(E2)$ for the highest state is roughly one-sixth of the values for the two low states. Without the rotational admixture this would be reduced by more than a factor ten. Recently the excitation AF has indeed been observed (cf. STELSON and MCGOWAN, 1955) and the value of $B_{\text{exc}}(E2)$ determined agrees with the value given in the table, indicating that the estimate (2) is roughly correct. Since the value for Q_0 is consistent with values in the neighbouring nuclei (cf. HUUS et al., 1955) the interpretation seems well confirmed.

TABLE III.

Transition	AB	AC	AE	AF
Energy (keV.)	46.5	99.1	208.8	291.7
$I \to I^1$	$1/2 \to 3/2^L$	$1/2 \to 5/2^L$	$1/2 \to 3/2^H$	$1/2 \to 5/2^H$
$B_{\text{exc}} \cdot (E2) e^{-2} \cdot 10^{48}\,\text{cm}^{-4}$	1.6	2.2	0.099	0.30

The above estimates show that the rotational admixtures play an essential role for certain transitions. In a more quantitative discussion one should consider the quantities $Q_0^{3/2}$, $Q^{1/2\,3/2}$, and $b_{E2}^{KK'}$ as parameters to be fitted by the data. The accuracy of the present experiments is not sufficient to determine these parameters although it indicates that the choice (2) is a good one.

There is much more data available with respect to the $M1$ transition intensities. MURRAY et al. have measured twelve intensity ratios in W^{183} which can serve as a good test of the theory. Because W^{183} has a ground state spin $I = {}^1/_2$ we see from (III.14) that there are four parameters, leaving eight pieces of data which the theory must fit. The $M1$ amplitudes are linear expressions in the four derived parameters α, β, g_3, g_{13}.

$$\alpha = \left(\frac{\hbar}{MC}\right)\left(1 - \frac{1}{\sqrt{2}}\, b_{M1}\right)(G^{1/2\,1/2}/Q_0^{1/2}), \tag{V.3}$$

$$\beta = \left(\frac{\hbar}{MC}\right)\left(1 + \frac{1}{\sqrt{2}}\, b_{M1}\right)(G^{1/2\,1/2}/Q_0^{1/2}), \tag{V.4}$$

$$g_3 = \left(\frac{\hbar}{MC}\right)(G^{3/2\,3/2}/Q_0^{1/2}), \tag{V.5}$$

$$g_{13} = \left(\frac{\hbar}{MC}\right)(G^{1/2\,3/2}/Q_0^{1/2}) = -g_{31}. \tag{V.6}$$

Note that the new parameters are defined in units of the ground state quadrupole moment $Q_0^{1/2}$. Since we are dealing with intensity ratios, we are led to a set of twelve quadratic equations in four unknows. We have proceeded by a trial and error method, and have succeeded in finding values for the parameters which

TABLE IV.

Transition	t_{exp}	t_{theo}	% $E2$ (theo)	Relative $E2/M2$ phases
BA	—	110	.6	(±)
CA	(28)	28	100	
CB	30	20	3	(±)
DB	(400)	400	100	
DC	900	1100	1	(±)
EA	220	370	20	(±)
EB	1400	830	10	(∓)
EC	(144)	144	5	(∓)
FA	1330	840	100	
FB	—	460	9	(±)
FC	60	87	70	(∓)
FD	(300)	300	.8	(∓)
FE	47	82	20	(∓)
GC	(1790)	1790	100	
GD	65	67	10	(±)
HB	1860	2500	100	
HC	15900	12000	2	(∓)
HD	(1900)	1900	2	(∓)
HE	490	840	100	
HF	160	130	50	(∓)
HG	110	280	1	(∓)

fit the data extremely well considering the uncertainties involved*. The fit is presented in Table IV.

Since transition probabilities are a good test of wave functions, this fit is considered as evidence that the general ideas employed are correct. It would be very interesting to have more measurements, particularly on the $E2/M1$ mixtures. The theory predicts the percentage of $E2$ in the $M1$ radiation, and also the relative phases. Such measurements would be a further very exacting test of the theory, particularly in the cases where there are relatively large admixtures.

* One of the uncertainties in our wave functions has to do with the possibility that the upper ($K = {}^3/_2$) band is perturbed by a still higher band with the same parity and $K = {}^1/_2$ or ${}^5/_2$. In fact the high moment of inertia for this band (cf. (1)) indicates that this may be the case.

Caption to Table IV.

We compare here the relative transition probabilities measured by MURRAY et al. to those calculated with the expressions (III. 13) and (III. 14). For convenience, we use natural units ($\hbar = c = 1$; one atomic mass unit = 931 MeV; $10^{13}\,\mathrm{cm}^{-1} = 197$ MeV; $10^{24}\,\mathrm{sec}^{-1} = 658$ MeV; $e^2 = 137^{-1}$) and then the parameters which give the fit are (in MeV).

$$\alpha = \mp 0.037 \quad \beta = \mp 0.100 \quad g_3 = \pm 0.042 \quad g_{13} = \pm 0.006.$$

The theoretical quantity tabulated is

$$t = 10^9\, T / \left\{ e^2 \left(Q_0^{1/2}\right)^2 \right\}$$

and this has the dimensions $(\mathrm{MeV})^5$ in natural units.

The experimental quantities are relative intensities of γ-ray lines from a given level. Thus we have normalized the intensities in a given group so that one of the experimental values agrees with the corresponding theoretical value for t. This intensity is put in brackets in the table. In the last two columns we have also included the percentage of $E2$ radiation and its phase relative to the $M1$ radiation as predicted by the theory with the above parameters. The $E2/M1$ phases are not unique because a fit of the intensity ratios determines the $M1$ parameters only up to an overall sign relative to the $E2$ parameters. However, once this sign is fixed by a measurement of one of the $E2/M1$ phases, the rest will be determined by the fit. In the table we have given the $E2/M1$ phases to correspond with the signs of the parameters as written above.

The transition FB was not seen by MURRAY et al. because it is masked by very intense radiation of nearly the same energy, originating in level I (compare transitions ID and IE in Fig. 1). Our calculation shows that this transition (FB) is quite comparable in intensity to the others from level F and therefore it should be possible to see it, for example, in Coulomb excitation, where the level I is not excited. Actually the relative intensity FB must be included in an accurate estimate of $B(E2)$ for the level F when this is measured by Coulomb excitation (the value for $B_{\mathrm{exc}}(E2)$ by STELSON and MCGOWAN, is calculated by neglecting FB).

It is probably possible to improve the fit by a more exhaustive analysis using four parameters as above, or by including as parameters the $E2$ matrix elements which have only been roughly estimated here. However, the fit as presented, is probably sufficiently good so that we can say there is some sense in the ideas underlying it.

The percentage $E2$ mixtures in the table are presented only as an indication of the order of magnitude predicted by the theory. The rough estimates as to the $E2$ matrix elements make the values somewhat uncertain.

Conclusion.

We have seen that the *RPC* can have a rather important effect in an odd nucleus as exemplified by ${}_{74}W^{183}$. It is not expected that this is an atypical case. For example, the systematic effect on the moment of inertia has been noted already (cf. above). In some cases (e.g., ${}_{73}Ta^{181}$, ${}_{71}Lu^{175}$, and ${}_{63}Eu^{153}$), the excited state which might cause a rotational admixture has been seen. More data in such nuclei would be very revealing. From the discussion above it would seem that Coulomb excitation is an excellent tool with which to look for the admixed band, because the mixing greatly enhances the excitation probability for these higher states.

The author offers his thanks to Drs. A. Bohr and B. R. Mottelson for their critical reading of this manuscript and for many stimulating discussions and suggestions. He is also grateful to the Canadian National Research Council for a Postdoctorate Overseas Fellowship, and to Professor Niels Bohr who has generously extended to him the hospitality of this institute.

Institute for Theoretical Physics
University of Copenhagen, Denmark.

References.

G. Alaga, K. Alder, A. Bohr, and B. R. Mottelson (1955), Dan. Mat. Fys. Medd. **29**, no. 9.

A. Bohr (1952), Dan. Mat. Fys. Medd. **26**, no. 14.

A. Bohr and B. R. Mottelson (1953), Dan. Mat. Fys. Medd. **27**, no. 16.

A. Bohr (1954), Rotational States in Atomic Nuclei. Ejnar Munksgaard, Copenhagen.

A. Bohr and B. R. Mottelson (1954), chapter 17 of "Beta and Gamma Ray Spectroscopy", ed. by K. Siegbahn, North Holland Publishing Co., Amsterdam.

A. Bohr, P. O. Fröman, and B. R. Mottelson (1955), Dan. Mat. Fys. Medd. **29**, no. 10.

A. Bohr and B. R. Mottelson (1955), Dan. Mat. Fys. Medd. **30**, no. 1.

R. F. Christy (1954), Phys. Rev. **96**, 858 (A).

J. P. Davidson and E. Feenberg (1953), Phys. Rev. **89**, 856.

K. Gottfried (1955), thesis, M. I. T.

G. Herzberg (1950), "Spectra of Diatomic Molecules", second edition, D. Van Nostrand Co. Inc., Toronto.

T. Huus, J. Bjerregaard, and B. Elbek (1956), Dan. Mat. Fys. Medd. **30**, no. 17.

D. Inglis (1955), Phys. Rev. **97**, 701.

H. Mark, C. McClelland, and C. Goodman (1955), submitted for publication.

C. L. McClelland, H. Mark, and C. Goodman (1954—55), Phys. Rev. **93**, 904; Phys. Rev. **97**, 1191.

J. J. Murray, F. Boehm, P. Marmier, and J. W. M. Dumond (1955), Phys. Rev. **97**, 1007.

J. J. Murray, P. Snelgrove, P. E. Marmier, and J. W. M. Dumond (1954), Phys. Rev. **96**, 858 (A).

S. G. Nilsson (1955), Dan. Mat. Fys. Medd. **29**, no. 16.

G. Scharff-Goldhaber and J. Weneser (1955), Phys. Rev. **98**, 212.

P. H. Stelson and F. K. McGowan (1955), Phys. Rev. **99**, 112.

L. Wilets and M. Jean, to be published.

Indleveret til selskabet den 5. september 1955.
Færdig fra trykkeriet den 16. marts 1956.

Det Kongelige Danske Videnskabernes Selskab
Matematisk-fysiske Meddelelser, bind **30**, nr. 16

Dan. Mat. Fys. Medd. **30**, no. 16 (1956)

STELLAR MODELS

BASED ON THE PROTON-PROTON REACTION

BY

PETER NAUR

København 1956
i kommission hos Ejnar Munksgaard

CONTENTS

Printed in Denmark
Bianco Lunos Bogtrykkeri A-S

1. Introduction.

With the recognition that the proton-proton chain reaction may provide the greater part of the energy production of dwarf stars[1] a type of stellar model, which has not so far been studied in any great detail, becomes of interest. Indeed, since the temperature enters into the rate of the proton-proton reaction only with a power of about four, the energy production will take place in an extended region around the center of the star. Consequently, the existence of the convective core, which is a pronounced feature of point-source models and carbon-cycle models, is by no means certain. And even in cases where the convective core exists an appreciable fraction of the energy is likely to be produced outside the core, and it is necessary to take the variation of the flux of energy through the star into account.

Previous investigations, which are important in this connexion, include papers by I. Epstein[2], and by I. Epstein and L. Motz[3]. These papers give models for the Sun, in which the proton-proton reaction is taken into account. A paper by Osterbrock[4] gives models for red dwarf stars, calculated on the assumption that convective layers, extending downwards from the surface, exist. A. Reiz[5] has calculated a model which is applicable to stars composed entirely of hydrogen and helium. It is a special case of the type of model considered in the present paper.

The aim of the present investigation is to answer the question: Given an energy production law of the form

$$\varepsilon = \varepsilon_0 \varrho T^4 \tag{1}$$

how do the properties of the star vary with the opacity law?

In answering this question the methods for integrating the equations of the equilibrium of the star will first be discussed (section 2). Section 3 gives the main results of using the punched

card equipment of the IBM Watson Scientific Computing Laboratory, New York City, for solving the differential equations. Altogether twenty different opacity laws have been considered. Detailed tables are given for eleven models. Finally, in section 4, the models are used to construct the Hertzsprung-Russell diagram for stars composed entirely of hydrogen and helium. It will be found that the results confirm those obtained independently by REIZ[5].

In appendix 1 the power expansions for the behaviour of the solutions near the center of the star are developed, while appendix 2 gives tables for the eleven models discussed in section 3.

2. A method for the integration of the equations of stellar equilibrium.

2.1. *The fundamental equations.* The stellar models to be considered in the present paper are specified in the following way: 1) The chemical composition is uniform throughout the star. 2) The star is in radiative equilibrium except for a possible convective core around the center. Convective zones near the surface are not considered. 3) The radiation pressure can be neglected. 4) The energy production is given by a law of the form

$$\varepsilon = \varepsilon_0 \varrho^{\delta} T^{\nu} \tag{2}$$

where ε is the production of subatomic energy per gram per second, ϱ the density, T the temperature, and ε_0, δ, and ν, constants. 5) The opacity is given by a law of the form

$$\varkappa = \varkappa_0 \varrho^{1-\alpha} T^{-3-s} \tag{3}$$

where $\varkappa$ is the mass opacity of the stellar material and $\varkappa_0$, α, and s, are constants. 6) The stellar material behaves like an ideal gas.

The fundamental equations governing the structure of a star of these properties are well known. In the present section they shall be discussed with special attention to the fact that the energy production takes place in an extended region around the center of the star. Also, a set of variables, which is particularly suited for solution by means of automatic computing machines, shall be introduced.

The starting point is the four standard equations of a star in equilibrium:[6)]

$$dP/dr = -GM_r \varrho r^{-2} \tag{4}$$

$$dM_r/dr = 4\pi \varrho r^2 \tag{5}$$

$$dL_r/dr = 4\pi \varrho r^2 \varepsilon \tag{6}$$

$$dT/dr = \begin{cases} -3(16\pi ac)^{-1} \varkappa \varrho L_r r^{-2} T^{-3} & \text{rad. eq. (7a)} \\ 0.4\ TP^{-1}\, dP/dr & \text{conv. eq. (7b)} \end{cases}$$

Here r denotes the distance from the center of the star, P the pressure, M_r the mass contained within the sphere of radius r, concentric with the star, L_r the flux of energy across this sphere, G the constant of gravitation, a the Stefan-Boltzmann constant, and c the velocity of light.

The physical contents of these equations can be stated as follows. The first equation is the condition that the star is in mechanical equilibrium in its own gravitational field, *i. e.* that the gravitational attraction on any element of matter will be compensated by the pressure gradient. Equation (7) is the equation governing the transport of energy from the center towards the surface. It assumes one of two forms, depending on whether the main agent of transport of energy is electro-magnetic radiation or convective currents, or, in other words, whether the point in question is in radiative or convective equilibrium. In radiative equilibrium the gradient of the radiation pressure, $aT^4/3$, becomes proportional to the flux of energy, $L_r r^{-2}$, and the opacity per unit volume, $\varkappa\varrho$. Where convective currents are present the matter will be in adiabatic equilibrium, with the ratio of the specific heats equal to 5/3, valid for monatomic gases, and the temperature gradient is independent of the flux of energy. Equations (5) and (6) express the relation between the microscopic quantities, ϱ and $\varrho\varepsilon$, and the macroscopic quantities, M_r and L_r. To these equations we must add the equation of state of the stellar material, in our case of a perfect gas,

$$P = \Re \mu^{-1} \varrho T \tag{8}$$

where μ is the mean molecular weight, and $\Re$ is the gas constant.

The quantities $\varkappa$ and ε describe the physical behaviour of the stellar material, $\varkappa$ measuring the interaction of the radiation and the matter, ε giving the output of subatomic energy. Thus it is clear that they will depend on the physical parameters of the matter and the chemical composition, *i. e.* we can write

$$\varkappa = \varkappa(\varrho,\ T,\ \text{chemical composition})$$
$$\varepsilon = \varepsilon(\varrho,\ T,\ \text{chemical composition}).$$

The problem of computing the structure of a star with a given radius R, mass M, and total energy output L, is now equivalent to finding a solution of the eq. (4) to (8) which satisfies the boundary conditions

$$\left.\begin{aligned} M_r &= M \\ L_r &= L \\ P &= 0 \\ T &= \text{surface temperature} \end{aligned}\right\} \text{for } r = R \tag{9}$$

$$\left.\begin{aligned} L_r &= 0 \\ M_r &= 0 \end{aligned}\right\} \text{for } r = 0. \tag{10}$$

The surface temperature can be put equal to zero without any appreciable error being introduced. The problem is thus one of four simultaneous differential equations with two point boundary conditions—the fundamental problem of all such work as the present.

In order to illustrate the character of the problem we will now briefly discuss two different, though mathematically equivalent, methods for solving the problem by means of stepwise numerical integrations, namely a) by integrating from the surface and b) by integrating from the center of the star.

a) Suppose R, M, and L, to be given. If we then *assume* a chemical composition we can, by stepwise integration, calculate the run of the quantities P, T, L_r, and M_r, as functions of r, going from the surface towards the center. In general we will find, however, that the two conditions $L_r = M_r = 0$ for $r = 0$ are not satisfied. In order to get the proper solution we must, therefore, carry out a number of integration runs, varying systematically *two* chemical parameters.

b) In order to start a numerical calculation from the center

we must assume given the chemical composition and the central values of the density and the temperature, ϱ_c, and T_c. As the condition that our model is physically possible we have the one condition that ϱ and T must vanish for the same value of r. Such a model can be found by carrying out integrations for systematically varied ϱ_c, say. Thus, for given composition and T_c we will, in general, determine one definite star with certain values of R, L, and M. By also varying T_c we can find solutions with prefixed values of, for instance, M. In this way we have arrived at the celebrated theorem of VOGT and RUSSELL: Given the chemical composition and the mass of the star, the radius and luminosity follow. Finally we arrive at the same conclusion as when discussing a), that in order to fit the solutions to given values of R and L, as well as M, we must vary *two* chemical parameters.

Although the conclusions of the two discussions a) and b) are equivalent, the two procedures are still quite different, in that a) requires two parameters to be varied in order to find the solution with given R, L, and M, while in b) four parameters must be varied in order to obtain the same result. This is the reason why calculations of the structure and composition of given definite stars, as for instance EPSTEIN's work on solar models, is carried out in the manner described as a). Even then a considerable amount of work is required before the eigensolution is found, and it is highly desirable to reduce the number of parameters to be varied to one, when a more extensive program of calculations of stellar models is undertaken, even at the cost of some accuracy. This is accomplished by the application of homology transformations.

2.2. *Homology transformations.* We speak of two stellar models being homologous when values of the physical variables describing one of them can be obtained by multiplying the corresponding values for the other model by definite scale factors. Denoting by T_0, L_{r0}, ϱ_0, M_{r0}, the variables at the point r_0 in one model, we get for the point $r = r_1$ in the homologous model

$$\left.\begin{aligned} r_1 &= C_r r_0 \\ T_1 &= C_T T_0 \\ L_{r1} &= C_L L_{r0} \\ \varrho_1 &= C_\varrho \varrho_0 \\ M_{r1} &= C_M M_{r0} \end{aligned}\right\} \qquad (11)$$

The existence of models described by quantities with suffix 1 is established only if these variables satisfy the equations (4) to (8). In the case of the equations (4), (5), and (8), this is apparently so, provided the scale factors satisfy suitable conditions. Equations (6) and (7), which contain the, as yet, unspecified functions $\varkappa$ and ε, must, however, be considered in some detail. First we have, by assumption,

$$dT_0/dr_0 = -3\,(16\,\pi\,ac)^{-1}\,\varkappa_0\,(\varrho_0\,T_0)\,\varrho_0 L_{r0}\,r_0^{-2}\,T_0^{-3} \tag{12}$$

The condition that the configuration (11) does, in fact, satisfy eq. (7a) is

$$dT_1/dr_1 = -3\,(16\,\pi\,ac)^{-1}\,\varkappa_1\,(\varrho_1\,T_1)\,\varrho_1 L_{r1} r_1^{-2}\,T_1^{-3} \tag{13}$$

or, using (11),

$$\left.\begin{aligned} &C_T C_r^{-1}\,dT_0/dr_0 = \\ &-3\,(16\,\pi\,ac)^{-1}\,C_\varrho C_L C_r^{-2} C_T^{-3}\,\varkappa_1\,(\varrho_1\,T_1)\,\varrho_0 L_{r0} r_0^{-2}\,T_0^{-3}. \end{aligned}\right\} \tag{14}$$

Comparing (12) and (14) we find that two models are homologous if their laws of opacity satisfy the functional equation

$$\varkappa_0\,(\varrho_0\,T_0) = C_\varrho C_L C_r^{-1} C_T^{-4}\,\varkappa_1\,(\varrho_0 C_\varrho,\ T_0 C_T) \tag{15}$$

This will always be the case if the opacity can be written on the form

$$\varkappa = \varkappa_0\,\varrho^{1-\alpha}\,T^{-3-s} \tag{16}$$

where α and s denote constants, while $\varkappa_0$ is a quantity which varies from one model of the homologous family to the next. In quite a similar manner we deduce from eq. (6) that in order to make the homologous transformation valid we must have

$$\varepsilon = \varepsilon_0\,\varrho^{\delta}\,T^{\nu}. \tag{17}$$

An application of this result will introduce an important simplification in the problem if the opacity and energy production can be written as (16) and (17), where the chemical composition enters only through the factors $\varkappa_0$ and ε_0. In that case the change of the chemical composition will only cause the model to vary within the same homologous family of solutions. Consequently, once a single member of the family has been found, it will be a

simple matter to discuss the relation between the chemical composition and the parameters of the stellar model, R, M, and L.

We shall now proceed on the assumption of the validity of the expressions (16) and (17), postponing the discussion of their physical applicability. Then the problem is solved as soon as one solution with the proper boundary conditions is known. Adopting the method b) we can now chose arbitrary values for $\varkappa_0$, ε_0, and T_c. By varying ϱ_c we find the solution which satisfies the condition $\varrho = 0$ and $T = 0$ simultaneously for some value of r, R. This will give us a stellar model with definite values of R, L, M, T_c, ϱ_c, $\varkappa_0$, ε_0, and μ. Of these quantities $\varkappa_0$, ε_0, and μ, are assumed to be functions of the chemical composition. If the structure for some other values of R, L, and M, is wanted we only have to use scale factors. Of the three conditions to be satisfied, one determines the central temperature. The others impose two conditions on the chemical parameters. One of these is Eddington's mass-luminosity relation, the other one is the condition that the total energy released by nuclear processes equals the luminosity.

It should be mentioned that a simplification of the integration procedure does not appear in the approach described in a), and it is quite obvious that the method b) should be used.

2.3. *Homology invariant variables.* The method for finding the eigensolutions of the fundamental equations outlined above could probably be used for the actual numerical procedure. Additional simplifications may, however, be introduced by using different variables, with the further important advantage that the equations become far better suited for solution with the aid of automatic computing machinery. Indeed, as will be demonstrated presently, it will be a great advantage to use as variables the homology invariant quantities

$$V = -d\log P/d\log r = GM_r\varrho\, r^{-1}P^{-1} \tag{18}$$

$$U = d\log M_r/d\log r = 4\pi\varrho\, r^3 M_r^{-1} \tag{19}$$

$$W = d\log L_r/d\log r = 4\pi\varepsilon_0\, r^3\varrho^{1+\delta}\, T^{\nu}L_r^{-1} \tag{20}$$

$$\left.\begin{aligned} H = V/(n+1) &= -d\log T/d\log r \\ &= 3\varkappa_0(16\pi ac)^{-1}\varrho^{2-\alpha}L_r r^{-1}T^{-7-s} \end{aligned}\right\} \tag{21}$$

Of these variables V and U are well known, H is closely related to the equally well known polytropic index, n, while W has been introduced by Osterbrock and the present author[7]). As can readily be shown, the boundary conditions for these variables are

$$U = W = 3, \qquad V = H = 0 \qquad \text{for } r = 0 \tag{22}$$

$$U = W = 0, \qquad V \to \infty, \; H \to \infty \qquad \text{for } R = r. \tag{23}$$

The differential equations satisfied by these variables are deduced by logarithmic differentiation of the eq. (18) to (21), making use of eq. (4) to (8) and also of the equations themselves. We get

$$dV/V = (U + H - 1)\, dr/r \tag{24}$$

$$dU/U = (3 - V + H - U)\, dr/r \tag{25}$$

$$dW/W = (3 - (1 + \delta)\, V - (\nu - 1 - \delta)\, H - W)\, dr/r \tag{26}$$

$$dH/H = ((9 + s - \alpha)\, H - (2 - \alpha)\, V + W - 1)\, dr/r. \tag{27}$$

It is now apparent that we can eliminate the last physical variable, r, simply by choosing the independent variable among the four homology invariants. The most convenient variable for this purpose appears to be V* and we are then left with the equations

$$dU/dV = U\,(3 - V + H - U)\, V^{-1}\,(U + H - 1)^{-1} \tag{28}$$

$$\left.\begin{aligned} dW/dV = {} & W\,(3 - (1 + \delta)\, V \\ & - (\nu - 1 - \delta)\, H - W)\, V^{-1}\,(U + H - 1)^{-1} \end{aligned}\right\} \tag{29}$$

$$\left.\begin{aligned} dH/dV = {} & H\,((9 + s - \alpha)\, H \\ & - (2 - \alpha)\, V + W - 1)\, V^{-1}\,(U + H - 1)^{-1}. \end{aligned}\right\} \tag{30}$$

The great advantages of using the variables V, U, H, and W, now become apparent. In fact, expressed in these variables, the four fundamental differential equations are reduced to three differential equations and a quadrature. For, in order to return to the physical variables from a solution expressed in the homology invariant variables, we only have to perform a quadrature, *e. g.*

* A similar method has been used by Levee[8]), who choses W as his independent variable.

$$\log r/r_0 = \int_{V_0}^{V} V^{-1} (U + H - 1)^{-1} \, dV \tag{31}$$

and then use the equations (18) to (21). Also, the differential equations are very convenient for treatment by means of automatic computing machinery, because they do not involve exponentials.

Having now demonstrated the advantage of using the variables (18) to (21) we only have to understand their behaviour at the boundaries before we can use them for actual computations. We have already given the boundary conditions for all our variables at the center and the surface of the star, eq. (22) and (23). Integrating, as we intend to do, from the center towards the surface, the new independent variable, V, varies from zero to infinity. In practise one must, of course, break off at some suitably large value of V. As to the conditions at the center we find, by inserting the values of the variables at the center in the eq. (28) to (30), that $V = 0$ is a singularity, so that a parameter is necessary to label a solution starting at the center. This is not surprising, when compared with the procedure for solving the problem in physical variables discussed above. It is quite clear that, also when using the new variables, it will be necessary to carry out trial computations, varying one parameter, before the solution satisfying the boundary conditions both at the center and at the surface is found. As the parameter labeling the trial solutions it has been found convenient to use

$$H_0' \equiv (dH/dV)_{V=0} = (n_c + 1)^{-1} \tag{32}$$

where n_c denotes the polytropic index at the center of the star. The numerical solution cannot be started from the center where all derivates become indeterminate. We have, therefore, expanded H, U, and W, in powers of V, the coefficients of the series being functions of H_0'. The evaluation of the power series is elementary, but rather lengthy, and has been given in appendix 1.

Suppose now that a value of H_0' is chosen. Using the expansions of appendix 1 we can then compute H, W, and U, for a value of V close to zero, *e. g.* $V = 0.2$. From here we can continue the solution of the equations (28) to (30) to some large value

of V ($V = 15$ is convenient) by step-by-step numerical integration. The question is now, what is the criterion that H_0' is chosen in such a way that the solution corresponds to a configuration in which P and T simultaneously tend to zero? In order to find this condition we observe that near the surface of the star we must have an approximate relation of the kind

$$P \propto T^q \tag{33}$$

where q is some positive number which is left undetermined for the moment. But from this relation it follows that near the surface we have

$$n + 1 = V/H = d(\log P)/d(\log T) = q \tag{34}$$

i. e. near the surface the polytropic index must tend to a finite positive limit. The actual value of this can now easily be found from the eq. (30). Near the surface we can neglect the constants and the functions U and W in comparison with H and V, which increase beyond any limits. Writing n_0 for the value of n at the surface, we have then

$$H = V/(n_0 + 1) \tag{35}$$

and we find

$$n_0 + 1 = (8 + s - \alpha)/(2 - \alpha). \tag{36}$$

The required criterion is that the quantity V/H tends to this limit for large V.

It is of considerable interest to know what happens if the parameter H_0' is not chosen to be equal to the eigenvalue. The numerical work shows that the solutions are extremely sensitive to variations of this parameter. In fact, if H_0' is chosen only slightly below the eigenvalue, H will reach a maximum and the denominator $U + H - 1$ will become zero for some finite value of V. If, on the other hand, H_0' is chosen larger than the eigenvalue, H will increase so as to make $n + 1 = V/H < 2.5$ at some value of V. At this point the equation of radiative equilibrium will cease to be valid. Only if H_0' is chosen quite close to the eigenvalue will the solution ever reach $V = 15$. Generally, the sensitivity of the solutions can be understood from the presence of the rather large coefficient $9 + s - \alpha$ in eq. (30). In the eigen-

solution the quantity $(9 + s - \alpha) H - 1 + W - (2 - \alpha) V$ will remain small only because the first and the last term nearly cancel. Any deviation from this solution will quickly be amplified, when the solution is followed towards larger V.

Once the eigensolution, expressed in homology invariant variables, have been found, there remains the problem of calculating the solutions expressed in physical variables. This calculation necessitates one further integration, *e. g.* the quadrature (31). The variables M_r, L_r, P, and T, could then be found by means of the eq. (18) to (21). The automatic computing machinery being available it was, however, more convenient to evaluate all of the physical variables by means of quadratures. From the eq. (18) to (21) and (24) to (27) we find

$$\left.\begin{aligned} \log P &= -\int_{V_0}^{V} dV/(U + H - 1) + \text{constant} \\ \log T &= -\int_{V_0}^{V} H dV/V\,(U + H - 1) + \text{constant} \\ \log M_r &= \int_{V_0}^{V} U dV/V\,(U + H - 1) + \text{constant} \\ \log L_r &= \int_{V_0}^{V} W dV/V\,(U + H - 1) + \text{constant} \end{aligned}\right\} \tag{37}$$

The constants of integration were chosen so that the functions $\log r/R$, $\log P/P_c$, $\log T/T_c$, $\log M_r/M$, and $\log L_r/L$, resulted. For $\log r$ and $\log M_r$ this made an analytic approximation of the solutions beyond $V = 15$ necessary. This was derived in the following manner.

2.4. *Expansions valid near the surface of the star.* Let us, following C. M. and H. Bondi[9], introduce the three homology invariant variables

$$Q = -\, d \log r / d \log P = V^{-1} \tag{38}$$

$$S = -\, d \log M_r / d \log P = U/V \tag{39}$$

$$N = \quad d \log T / d \log P = (n + 1)^{-1} = H/V. \tag{40}$$

These variables are convenient near the surface where V and H tend to infinity. Using eq. (18) to (21) and remembering that $L_r = L$ near the surface we now get

$$dQ/Q = dr/r - dM_r/M_r + dT/T = (-Q + S + N)\, dP/P \tag{41}$$

$$dS/S = 4\, dr/r - 2\, dM_r/M_r + dP/P = (1 - 4\, Q + 2\, S)\, dP/P \tag{42}$$

$$\left.\begin{aligned} dN/N &= (2-\alpha)\, dP/P - (8 + s - \alpha)\, dT/T - dM_r/M_r \\ &= \left[(2-\alpha) - (8 + s - \alpha)\, N + S\right] dP/P. \end{aligned}\right\} \tag{43}$$

Owing to its close relation to V we shall find it convenient to use Q as the independent variable, rather than S as used by Bondi and Bondi. We then get the differential equations

$$dS/dQ = S(1 - 4\, Q + 2\, S)\, Q^{-1}\, (S + N - Q)^{-1} \tag{44}$$

$$dN/dQ = N((2-\alpha) - (8 + s - \alpha)\, N + S)\, Q^{-1}\, (S + N - Q)^{-1}. \tag{45}$$

We intend to use these only for $V \geqslant 15$, i. e. for $0 < Q \leqslant 1/15$. Also, S is small near the surface, and thus we have approximately

$$dS/dQ = SQ^{-1}\, N_0^{-1} \tag{46}$$

whence

$$S = A^{-1} Q^{1/N_0} \tag{47}$$

where A is a constant. This approximation is better than might at first be expected. This is due to the fact that N, in the applications, usually is close to $^1/_4$, so that $N\,(1 - 4\, Q + 2\, S)\,(S + N - Q)^{-1}$ remains close to unity even for rather large values of Q.

The variable N will be nearly constant equal to

$$N_0 = (1 + n_0)^{-1} = (2 - \alpha)/(8 + s - \alpha) \tag{48}$$

near the surface. A better approximation can be found if eq. (45) is analysed with respect to the importance of the various terms. It becomes apparent that for small variations of N it makes sense to regard $N/(N + S - Q)$ as a constant at the same time as the variation of $(2 - \alpha) - (8 + s - \alpha)\, N + S$ is taken into account. In fact, this latter quantity can be written

$$-(8 + s - \alpha)\ (N - N_0) + S.$$

At the surface we have $S = 0$, and near the surface the two terms are comparable. This suggests that it would be a good approximation to write

$$N - N_0 = BS \tag{49}$$

where B is a suitable constant. For its determination we get from (45)

$$BdS/dQ = N_0 (N_0 + S - Q)^{-1} SQ^{-1} (1 - (8 + s - \alpha) B)$$

or, using (46),

$$B = N_0 (3 - \alpha - \eta (n_0 + 1) Q)^{-1}. \tag{50}$$

Strictly, S and Q are zero where the approximations are valid. The form given, eq. (50), suggests that slightly better results would be obtained for finite values of Q if a coefficient B, which is slowly increasing with Q, is used, η being a factor less than, but of the order of, unity.

We now get from eq. (38) and (41), corresponding to (31),

$$\log r/R = -\int_0^Q (N + S - Q)^{-1} dQ. \tag{51}$$

Beginning with the most important, the order of magnitude of the quantities is, N_0, Q, S, and $N - N_0$. We can therefore expand the integrand

$$(N + S - Q)^{-1} = (N_0 - Q)^{-1} - (1 + B) (N_0 - Q)^{-2} S \ldots \tag{52}$$

where we have used (49). The first term can be integrated exactly. In the second term we use the first two terms of the expansion for $(N_0 - Q)^{-2}$. In this way we get

$$\left.\begin{aligned} \log_{10} r/R = {} & \log_{10} (1 - QN_0^{-1}) \\ & + \frac{(n_0 + 1)^2}{n_0 + 2} \left(1 + \frac{2 (n_0 + 1) (n_0 + 2)}{n_0 + 3} Q\right) SQ \log e \, (1 + B) \end{aligned}\right\} \tag{53}$$

where we have used eq. (48).

The approximation for $\log M_r/M$ is derived in the following way. Using eq. (39) and (41) we find

$$\log M_r/M = -\int_0^Q SQ^{-1}\,(N - Q + S)^{-1}\,dQ \tag{54}$$

Inserting the expansion (52) we find that none of the terms can be integrated exactly, and we have to expand $(N_0 - Q)^{-1}$ and $(N_0 - Q)^{-2}$ in power series in QN_0^{-1}. Using (47) we can integrate term by term, and get, after some reduction,

$$\left.\begin{aligned}\log_{10} M_r/M = &-U \log e\left[\frac{1}{n_0+1}\frac{Q}{N_0}+\frac{1}{n_0+2}\left(\frac{Q}{N_0}\right)^2+\frac{1}{n_0+3}\left(\frac{Q}{N_0}\right)^3\ldots\right]\\ &+\left(\frac{Q}{N_0}\right)^2 U^2(1+B)\log e\left[\frac{1}{2\,n_0+2}+\frac{2}{2\,n_0+3}\frac{Q}{N_0}\ldots.\right].\end{aligned}\right\} \tag{55}$$

As an illustration of the use of these relations we take the following values which have been obtained from one of the integrations described in section 3. The constants of the model are

$$\begin{aligned}\alpha &= 0.5\\ s &= -2.1.\end{aligned}$$

We then find from (36)

$$n_0 + 1 = N_0^{-1} = 3.6.$$

The integration from the center gives for $V = 15$:

$$U = 0.2162.$$

Then, from (38) and (39),

$$\begin{aligned}S &= 0.0144\\ Q &= 0.0667.\end{aligned}$$

From (50) we find

$$B = 0.12,$$

and from (53) and (55)

$$\begin{aligned}\log_{10} r/R &= 9.8826 - 10\\ \log_{10} M_r/M &= 9.9926 - 10.\end{aligned}$$

The expansions are equally useful for starting integrations from the surface. In this case each solution will be specified by the value of the parameter A (eq. (47)). Choosing a starting value for V the expansions will provide values of N, r/R, and M_r/M.

2.5. *Invariant parameters of the models.* In addition to the functions (37), the invariant parameters, which specify the models, must be found. Corresponding to the homology transformations each model can be characterized by four parameters. In an obvious extension of the convention adopted by CHANDRASEKHAR[10] we choose the parameters to be the following:

The ratio of central density to mean density,

$$F = \varrho_c/\bar{\varrho}, \tag{56}$$

the central temperature constant,

$$E = T_c R/\mu M, \tag{57}$$

the constant in the mass-luminosity relation,

$$C = \frac{L R^{3\alpha+s} \varkappa_0}{M^{5+s+\alpha} \mu^{7+s}} \left(\frac{k}{G m_H}\right)^{7+s} \frac{3}{4\,(4\pi)^{3-\alpha} ac}, \tag{58}$$

which, expressing L, R, and M, in solar units, becomes

$$\log C = -27.0448 + 0.3274\,\alpha - 7.3638\,s + \log \frac{L R^{3\alpha+s} \varkappa_0}{M^{5+s+\alpha} \mu^{7+s}},$$

and the ratio of central energy production rate to mean energy production rate,

$$D = \varepsilon_c M/L. \tag{59}$$

Using the eq. (18) to (21) it can be shown that these parameters satisfy the relations

$$F = (T/T_c)\,(M_r/M)\,(P/P_c)^{-1}\,(r/R)^{-3}\,(U/3) \tag{60}$$

$$E = (M_r/M)\,(r/R)^{-1}\,(T/T_c)^{-1}\,V^{-1}\,G\,(k/m_H)^{-1} \tag{61}$$

$$C = (M_r/M)^{5+s+\alpha}\,(r/R)^{-3\alpha-s}\,(L_r/L)^{-1}\,H U^{-2+\alpha}\,V^{-7-s} \tag{62}$$

$$D = (L_r/L)\,(P/P_c)^{-\delta}\,(M_r/M)^{-1}\,(T/T_c)^{\delta-\nu} W U^{-1}. \tag{63}$$

It should be noted that the quantities on the right hand side are independent of the point in the star which is used in their determination. This constancy can serve as a check on the last stage of the calculation of the solutions.

2.6. *Convective cores.* Up to this point the question of convective cores has been ignored. It is, however, very easy to extend the already developed procedure for integrating the equations of equilibrium of a star to the case of a star with a convective core. As is well known, the structure of a convective core is described by

$$T = T_c\, \theta\, (\xi) \tag{64}$$

$$\varrho = \varrho_c\, \theta\, (\xi)^{3/2} \tag{65}$$

where θ is the Emden function for the polytropic index $n = 3/2$, and ξ is proportional to r. The function θ, together with V and U expressed as functions of ξ, have been tabulated[11]. Furthermore we have

$$H = V/(n+1) = 2\, V/5. \tag{66}$$

Suppose now that the core extends to a value of $V = V_{core}$. Outside this point eq. (30) replaces (66). At V_{core} all our variables, including V, U, H, and W, must be continuous, and we can find the proper starting point for the numerical integrations from their values on the boundary of the core. Of these V and U are known from the tables quoted above, and H is found from eq. (66). The variable W, finally, can be found for any point in the core, using (20), (6), (17), (64), and (65), which give

$$W = \xi^3\, \theta^{\nu+3\,\delta/2} \Big/ \int_0^{\xi} \theta^{\nu+3\delta/2}\, \xi^2\, d\xi\,. \tag{67}$$

This quantity is a function of ξ and $\nu + 3\,\delta/2$ only and has been tabulated by the present author[12].

Having thus determined V, U, W, and H, on the boundary of the core we can carry out the stepwise integration of eq. (28) to (30) to see whether the condition (36) is satisfied for large V. If not, it is a sign that the core has not been assigned the right extent.

2.7. *Summary of the method.* As a summary of the present section, here is a short directory in the use of the method:

Given the four exponents, α, s, δ, and ν, find the series expansions valid near the center, using the formulae of appendix 1. It is most convenient to choose a suitable small value of V, *e.g.*

0.2, and then, by using the Taylor series, to find U, W, and H, as polynomials in H_0'. (If it is known already from other evidence that the model possesses a convective core, this calculation and the following one can, of course, be omitted.)

In order to determine whether a convective core is present or not, compute a trial solution, starting with $n_c = 3/2$, *i.e.* $H_0' = 0.4$, and using (28) to (30) for a step-by-step integration. If H or $U + H - 1$ become zero, a convective core is actually present. If, on the other hand, H increases so rapidly as to make $n + 1 = V/H$ smaller than 2.5 at some point no convective core is present.

Trial solutions corresponding to varying initial conditions must now be calculated until a solution is found for which the polytropic index $n + 1 = V/H$ approaches the proper surface value (36) for large values of V. The parameter to be varied is H_0' in the cases of no convective core, and V_{core} when a core is present. In the latter case the initial values are taken from the tables of the Emden functions, as described in section 2.6.

The run of the physical variables can now be found, r following from (31), and the other variables from eliminations among the eq. (18) to (21), or from the quadratures (37). If the five physical variables are expressed in units of R, P_c, T_c, M, and L, the series expansions (53) and (55) will be useful.

With the complete solution thus computed the constants of the model follow from (60) to (63).

3. Numerical results.

3.1. *The use of the punched card equipment.* In the preceding section it has been shown that the calculation of the structure of a star with the opacity given by $\varkappa = \varkappa_0 \varrho^{1-\alpha} T^{-3-s}$ and the energy production given by $\varepsilon = \varepsilon_0 \varrho^{\delta} T^{\nu}$ can be reduced to the stepwise integration of the eq. (28) to (30). In this section we shall describe how the calculations for the case $\varepsilon = \varepsilon_0 \varrho T^4$ have been carried out by means of the IBM punched card equipment at the Watson Laboratory, New York City, and the results obtained will be given.

Before any numerical calculations can be made, the differential equations must be approximated so as to permit a solution

in a finite number of algebraic operations, which is, essentially, a problem of replacing the integrals by suitable summations. For this purpose a process of successive approximations was used. In the first approximation the solution was computed by repeated expansions, using only the first term of the Taylor series, according to the formulae

$$\left.\begin{aligned} U_{m+1} &= U_m + \Delta V\,(dU/dV)_m \\ W_{m+1} &= W_m + \Delta V\,(dW/dV)_m \\ H_{m+1} &= H_m + \Delta V\,(dH/dV)_m \end{aligned}\right\} \qquad (68)$$

where ΔV stands for the constant steplength of the independent variable, and we have used the subscript m to denote the value of the variables at the point $V_m = V_0 + m \Delta V$. Thus, in the first approximation, we get tables of the three variables U, W, and H, which, however, do not exactly satisfy the differential equations. These tables can then be used to calculate good approximations for second order terms in the expansions, *e.g.*

$$^1/_2\,(\Delta V)^2\,(d^2 U/dV^2)_m \approx U_{m+1} - 2\,U_m + U_{m-1} \qquad (69)$$

and a second order run can then be computed using

$$U_{m+1} = U_m + \Delta V\,(dU/dV)_m + {}^1/_2\,(\Delta V)^2\,(d^2 U/dV^2)_m \qquad (70)$$

and similarly for W and H.

The efficiency of this method depends strongly on the steplength, ΔV, which must be chosen small in order to make the process converge rapidly. A value of ΔV of 0.1 was found suitable when four decimal places were carried. In fact, no higher approximations than the second were needed.

In the course of the calculations extensive use was made of the excellent collection of computing machines at the IBM Watson Laboratory. However, the only particular technique worth mentioning in the present connexion is the one used for solving the eq. (28) to (30) by means of the model 604 electronic calculating punch. This machine has a rather small capacity for numbers, a total of only 50 digits. It was found possible to solve the differential equations only by using two punched cards to advance the variables by one step. In this way numbers may be stored provisionally on a card while it passes from the punch station to the

second reading station. Use of this technique, and of the selective circuits of the machine, made it possible to fit the variables into the capacity of the machine. The speed of the process was 50 integration steps per minute. During the search for the eigensolutions several hundred integration runs were performed.

The other problem of the numerical solution of the equations is the sensitivity of the solutions against variations in the initial values. Owing to this sensitivity any deviation of the trial value of H_0' from the eigenvalue will cause the solution to end at a physically impossible point, either $n = \infty$ or $n = 0$. The sensitivity is so strong that a solution which is started from the point $V = 0.2$ and calculated with four decimal places will rarely go beyond $V = 6$ before an impossible point is reached. Thus one can have two starting values of H_0' at $V = 0.2$, differing by one unit in the fourth decimal, one of which will cause n to vanish at $V = 6$, while the other will send n off to infinity before $V = 6$. One way of overcoming this difficulty would be to carry more decimals. This was, however, not possible with the 604. Another method is suggested by the following table, which shows some results of two runs:

	$H_0' = 0.3605$			$H_0' = 0.3610$		
V	U	W	H	U	W	H
0.2	2.9232	2.6846	0.0708	2.9233	2.6844	0.0709
3.0	1.8551	0.3200	0.8340	1.8662	0.3213	0.8682
5.4						∞
5.8			0.0000			

It is apparent that the two solutions, which differ widely at $V = 5.5$ are still close together at $V = 3$. It therefore suggests itself to start further runs from $V = 3$, interpolating the initial values between the two solutions:

$$\left.\begin{aligned} V &= 3 \\ U &= 1.8551 + 0.0111\,\gamma \\ W &= 0.3200 + 0.0013\,\gamma \\ H &= 0.8340 + 0.0342\,\gamma \end{aligned}\right\} \quad (71)$$

where γ is a parameter to be determined by further integrations. This method proved to be quite satisfactory, but had to be used

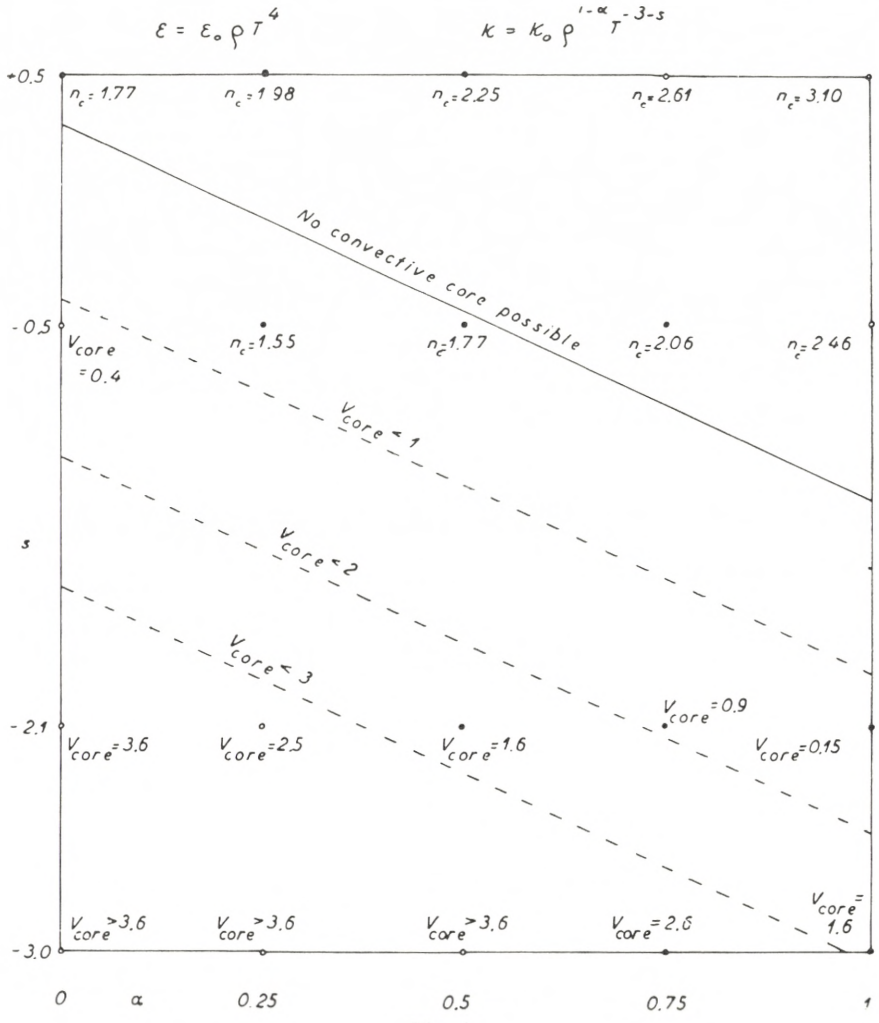

Fig. 1.

several times for increasing values of V, usually at V equal to 3, 6, and 10. Only the solutions started at $V = 10$ could be followed as far as $V = 15$. The result of this procedure was a pair of solutions lying closely on either side of the eigensolution for each of the intervals in V between 0, 3, 6, and 10. The finally adopted solution was found by linear interpolation between these pairs, use being made of the interpolation factors γ as defined above. As a check, the final solution was compared with the differential equations. Usually the error in the increase of the

solution for one step was found to be within one unit in the fourth decimal, and only in a single case a deviation of as much as four units was encountered. This fully justifies the procedure. It is interesting to note that if all runs had been calculated all the way from $V = 0.2$, at least ten decimals would have been necessary in the calculations.

3.2. *The behaviour of the convective core.* During the initial stages of the work twenty different opacity laws were considered, *viz.* all combinations of $\alpha = 0.0$, 0.25, 0.5, 0.75, and 1.00, and $s = +0.5, -0.5, -2.1$, and -3.0. In this way the two important cases of constant opacity ($\alpha = 1$, $s = -3.0$) and Kramers opacity ($\alpha = 0$, $s = +0.5$) and a number of intermediate cases were covered. At the later stages only eleven of the cases were investigated. However, the material gives information concerning the extent of the convective core for all of the twenty models. This information is represented in figure 1. This diagram also shows the results of applying the criterion for the existence of a convective core to the model in question[7], [12]. It is apparent that this criterion alone is sufficient for a reasonably good first indication as to whether a core may be expected or not.

3.3. *Invariant parameters of eleven models.* Table 1 gives the invariant parameters of the eleven models which have been considered in detail, calculated according to eq. (60) to (63). For R, M, and L, solar units have been used.

The principal results of an inspection of this table are the following:

a) For given R, M, and μ, T_c increases for increasing α and s. Speaking in terms of figure 1, T_c increases towards the upper right of the diagram. For models along the line connecting Kramers and constant opacity the central temperature is nearly constant, decreasing slightly towards the latter.

b) Qualitatively, the ratio $\varrho_c/\bar{\varrho}$ varies in the same way as the central temperature. However, the drop of the density concentration towards the constant opacity end of the diagram is more pronounced than is the drop of central temperature.

c) The ratio $\varepsilon_c M/L$ is nearly constant, independent of the opacity law.

TABLE 1.

$\varepsilon = \varepsilon_0 \varrho T^4 \qquad \varkappa = \varkappa_0 \varrho^{1-\alpha} T^{-3-s}$

Model no.	α	s	$\log RT_c/\mu M = \log E$	$\log \varrho_c/\bar{\varrho} = \log F$	$\log C + 10$	$\log \varepsilon_c M/L = \log D$
1	0.00	+ 0.5	7.317	1.642	4.076	0.942
2	0.25	+ 0.5	7.416	2.005	4.567	0.951
3	0.50	+ 0.5	7.604	2.658	5.385	0.964
4	0.25	— 0.5	7.295	1.529	4.761	0.942
5	0.50	— 0.5	7.397	1.913	5.206	0.951
6	0.75	— 0.5	7.615	2.664	6.002	0.965
7	0.50	— 2.1	7.204	1.153	5.761	0.925
8	0.75	— 2.1	7.280	1.431	6.022	0.942
9	1.00	— 2.1	7.434	1.982	6.465	0.963
10	0.75	— 3.0	7.174	1.040	6.508	0.915
11	1.00	— 3.0	7.253	1.316	6.716	0.933

3.4. *The structure of the models.* In appendix 2 the variation of the physical parameters through the eleven models is given. In the calculations four decimals were carried throughout. The figures given have been rounded to three decimals.

The figures termed *variations* give variations of the fundamental variables U, W, and H, for variations of the initial values. They correspond to the coefficients of γ as used in eq. (71). The corresponding variations of the initial values could not be determined with any accuracy.

4. Applications of the models.

4.1. *The Sun.* The integrations described in section 3 have been used for the construction of two different models for the Sun. During this work the integrations were only used to describe the central parts of the Sun, use being made of the variations explained in section 3.4, while the exterior regions were convered to a large extent by the series expansions of section 2.4. It was found possible to fit the model to a physically given opacity, which contained contributions from the heavy elements, free-free transitions in hydrogen and helium, and scattering on free electrons. Details of these models have been published elsewhere[13].

4.2. *The hydrogen-helium star.* The most natural application of the models is the construction of the Hertzsprung-Russell diagram for stars composed entirely of hydrogen and helium, since the models are based on an energy production law of the type (1). Indeed, the energy production by the proton-proton reaction is given by[14]

$$\varepsilon = 10^{-29.0054} X^2 \varrho T^4.$$

Here X is the abundance of hydrogen, by mass. However, in such a star the opacity will be due to scattering on free electron and free-free transitions in hydrogen and helium, and cannot directly be expressed in the form (16). The principal question is thus how to apply our models to stars in which these two agents both contribute to the opacity. In this question we choose the following approach.

According to the theorem of VOGT and RUSSELL the structure of a star is uniquely determined by the mass and the chemical composition. In a mixture of hydrogen and helium there is only one chemical parameter. Consequently our stars form a two-parametrical sequence, the parameters being the mass, M, and the hydrogen abundance, X. Consider now the two contributions to the opacity. In general it will, of course, be necessary to take both of them into account. It seems likely, however, that in a certain region of the (M, X)-diagram the electron scattering will be negligible. The behaviour of our stars in this region will then be given by the model based on an opacity law of the form

$$\varkappa = 2.74 \cdot 10^{22} (1 + X) \varrho T^{-3.5} \tag{72}$$

where the constant is the one used in the construction of the solar models[13].

Correspondingly, we expect to find, in another region of the (M, X)-diagram, that the free-free transitions can be neglected in the opacity. In this region we can then use the model based on

$$\varkappa = 0.2 (1 + X). \tag{73}$$

In the remaining part of the (M, X)-diagram we must take both the free-free transitions and the scattering into account. Here we may hope that one or more of the models, based on

opacity laws intermediate between the two already quoted will be of use. As explained below this is indeed the case.

Model 1.

Free-free transitions predominate.

Our first task, when using this model, is to determine the region in the (M, X)-diagram in which the scattering is negligible. We therefore first investigate how the opacity varies through this model, using the table of appendix 2,

V	r/R	$\log (\varrho/\varrho_c)\,(T/T_c)^{-3.5}$
0	0.00	0.00
6	0.41	0.45
15	0.72	0.63

We see that the Kramers opacity factor increases outwards in the star. We therefore only have to know that the scattering is relatively unimportant at the center to conclude that it is so through the whole star. On the basis of the four invariant constants of the model and the homology transformations we can convert the condition that the ratio of scattering opacity to free-free opacity has a definite value at the center into a relation between M and X. Indeed, using eq. (56) to (59) and demanding that the scattering opacity of eq. (73) is less than 10 % of the free-free opacity of eq. (72) we get

$$\log M \leqslant -1.0597 + \frac{1}{32}\log (1+X)\, X^2\, \mu^{-46}. \qquad (74)$$

Table 2 gives this function together with some more data for the corresponding stars.

Table 2.

Model 1. The sequence for which $\varkappa_{\text{scattering}}/\varkappa_{\text{free-free}} = 0.1$ at the center of the star.

X	Max $\log M$	$\log R$	$\log T_c$	$\log \varrho_c$	$\log L$	$^1/_4 \log LR^{-2}$
1.00	9.38	9.85	6.55	0.85	6.49	9.20
0.75	9.27	9.75	6.60	1.03	6.51	9.25
0.50	9.13	9.63	6.67	1.26	6.53	9.32
0.25	8.94	9.45	6.78	1.61	6.53	9.41
0.10	8.80	9.26	6.91	2.03	6.50	9.49

The model does not possess a convective core.

It is apparent that the present model is valid only for very red dwarfs.

MODEL 8.

Free-free opacity and scattering opacity compete.

We shall now try to find a model which can be made to represent the case that the opacities from the two sources, eq. (72) and (73), are of the same order of magnitude. It is therefore necessary to adopt a method for combining the two contributions. In the present survey it was judged sufficiently accurate simply to add them together. We thus represent our physical opacity by the expression.

$$\varkappa_{\text{physical}} = 2.74 \cdot 10^{22} (1 + X) \varrho T^{-3.5} + 0.3 (1 + X) \qquad (75)$$

where the customary factor of 3/2 has been applied to the scattering. We now want to find a model in which the opacity, given by (75), runs closely to a function of the form (16). For this purpose we proceed as follows: Using the tables of appendix 2 we can compute the run of the actual opacity through each of our models. We have, in fact,

$$\varkappa/\varkappa_{\text{center}} = (\varrho/\varrho_c)^{1-\alpha} (T/T_c)^{-3-s}. \qquad (76)$$

Also, we can compute the run of the free-free opacity from

$$\varkappa_{\text{free-free}}/\varkappa_{\text{free-free, center}} = (\varrho/\varrho_c) (T/T_c)^{-3.5} \qquad (77)$$

The condition that the particular model is useful in the present context then becomes that there exists a relation of the kind

$$(\varrho/\varrho_c)^{1-\alpha} (T/T_c)^{-3-s} = x (\varrho/\varrho_c) (T/T_c)^{-3.5} + y \qquad (78)$$

where x and y are positive.

This test was carried out for the nine models available with the result that it was found that in model 8 we have

$$(\varrho/\varrho_c)^{0.25} (T/T_c)^{-0.9} = 0.110 (\varrho/\varrho_c) (T/T_c)^{-3.5} + 0.954 \qquad (79)$$

within an accuracy of 6 % throughout the star.

The two terms on the right hand side of (79) represent the contributions from the free-free transitions and the scattering.

At the center we thus have a contribution from the free-free transitions of $10\,^0/_0$. At $r/R = 0.73$ they contribute by $44\,^0/_0$.

The present model places a strict condition on the value of the opacity at the center of the star. In fact, for the terms of eq. (75) and (79) to be proportional at the center we must have

$$\varrho_c T_c^{-3.5} = \frac{0.3 \cdot 0.110}{0.954 \cdot 2.74 \cdot 10^{22}} = 10^{-23.90}. \tag{80}$$

Further, the constant of the opacity law becomes

$$\varkappa_0 = 0.3145\,(1 + X). \tag{81}$$

The invariant constants of the model now give

$$32 \log M = 16.666 + \log (1 + X)\,\varepsilon_0\,\mu^{-49}. \tag{82}$$

This gives a one-dimensional sequence of stars. It has been tabulated in Table 3.

TABLE 3.

Model 8. The sequence of stars in which the free-free transitions contribute $10\,^0/_0$ of the opacity at the center and $44\,^0/_0$ at $r/R = 0.73$.

X	$\log M$	$\log R$	$\log T_c$	$\log \varrho_c$	$\log L$	$^1/_4 \log LR^{-2}$
1.00	0.08	9.86	7.20	1.31	0.26	0.13
0.75	9.96	9.76	7.25	1.48	0.24	0.18
0.50	9.81	9.64	7.31	1.70	0.22	0.23
0.25	9.62	9.46	7.41	2.05	0.17	0.31
0.10	9.46	9.27	7.53	2.46	0.09	0.39

The convective core extends in this model to $r/R = 0.16$, includes $10\,^0/_0$ of the mass and $51\,^0/_0$ of the energy production.

MODEL 9.

Electron scattering predominates.

This model was computed on the assumption that $\varkappa$ is constant. The condition that it is useful in the present investigation is that the opacity due to the free-free transitions is small. We therefore

first consider the variation of the corresponding factor through the star:

V	$\log\ (\varrho/\varrho_c)\ (T/T_c)^{-3.5}$
0	0.00
5	0.65
10	1.03

It is apparent that the importance of the free-free transitions increases as one moves outwards in the star, like in model 1 and 8. This increase continues even to the surface. Here we have, in fact, $P \propto T^4$ so

$$\varrho\ T^{-3.5} \propto T^{-0.5} \qquad \text{(near the surface)}. \quad (83)$$

Since there exists no region where this model is strictly applicable we must contend ourselves with some reasonable condition for the unimportance of the free-free transitions. As such we adopt that they must contribute by $10\,^0/_0$ or more only at points exterior to $V = 15$, $r/R = 0.74$. Table 4 has been calculated on this assumption.

TABLE 4.

Model 11. In the sequence of stars given the free-free transitions contribute by $10\,^0/_0$ to the opacity at $r/R = 0.74$.

X	$\log M$	$\log R$	$\log T_c$	$\log \varrho_c$	$\log L$	$^1/_4 \log LR^{-2}$	P_r/P_c
1.00	0.60	9.98	7.58	1.37	2.35	0.60	0.035
0.75	0.48	9.88	7.63	1.53	2.33	0.64	
0.50	0.33	9.76	7.69	1.76	2.31	0.70	
0.25	0.14	9.58	7.79	2.10	2.26	0.78	
0.10	9.98	9.39	7.91	2.51	2.18	0.85	0.056

The convective core in this model includes $24\,^0/_0$ of the radius, $22\,^0/_0$ of the mass, and $78\,^0/_0$ of the energy production. P_r is the radiation pressure at the center.

The Hertzsprung-Russell diagram.

The results quoted have been collected in the accompanying HR-diagram. Additional results, for stars with $\log M = 0.5$, have been plotted. With this value of the mass the radiation pressure

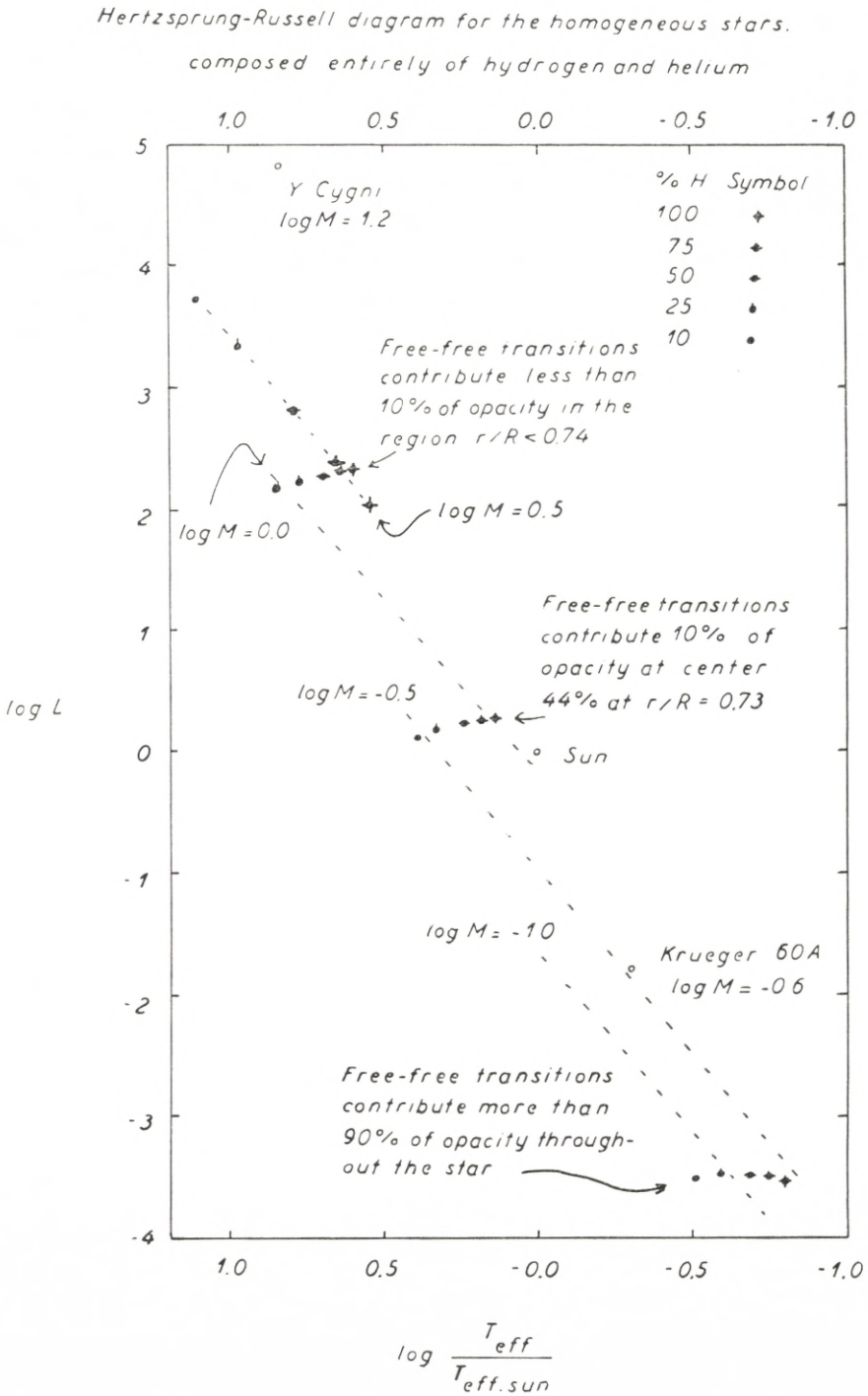
Hertzsprung-Russell diagram for the homogeneous stars.
composed entirely of hydrogen and helium
1.0
0.5
0.0
- 0.5
- 1.0
5
4
3
2
1
0
- 1
- 2
- 3
- 4
log L
γ Cygni
log M = 1.2
% H Symbol
100
75
50
25
10
Free-free transitions contribute less than 10% of opacity in the region r/R < 0.74
log M = 0.0
log M = 0.5
Free-free transitions contribute 10% of opacity at center 44% at r/R = 0.73
log M = -0.5
Sun
log M = -1.0
Krueger 60A
log M = -0.6
Free-free transitions contribute more than 90% of opacity throughout the star
1.0
0.5
- 0.0
- 0.5
- 1.0
log T_eff / T_eff. sun

Fig. 2.

becomes appreciable, and the basis of the model breaks down. For comparison the points corresponding to the data for the Sun, Y Cygni and Krueger 60 A, have also been plotted (fig. 2).

The results of the present section may be compared with those obtained by A. REIZ[5]. REIZ has calculated a model of the type considered in the present paper, based on the opacity law

$$\varkappa = \varkappa_0 \varrho^{0.5} T^{-1.75}. \tag{84}$$

It is found that the present results agree well with those found by REIZ.

The writer is grateful to Dr. W. J. ECKERT for placing the facilities of the Watson Scientific Computing Laboratory at his disposal. He also wishes to thank the staff of this laboratory for their generous help during the work with the punched card machines.

Finally, he wishes to thank Ole Rømer Fondet, Copenhagen, and The International Astronomical Union for the grants, which made the stay at New York City possible, and the U. S. Educational Foundation in Denmark for a Fulbright Travel Grant.

Appendix 1.

Expansions for the central region of the star.

In this appendix the series expansions valid at the center of the star will be derived. V will be taken as the independent variable throughout. Thus, dashes denote derivatives with respect to V, and subscript zero values of the functions at $V = 0$, *i.e.* at the center of the of the star. The formulae will be derived such as to be equally useful for a star in convective and radiative equilibrium at the center. Expressions whose validity is confined to one of these cases will be distinguished by *rad. eq.* or *conv. eq.* written in the bracket together with its number.

It will, in this section, be convenient to introduce symbols for some particular functions. Thus we define

$$T = H/V \tag{85}$$

$$g = 9 + s - \alpha \tag{86}$$

$$S = (g H - (2 - \alpha) V + W - 1)/(U + H - 1) \tag{87}$$

$$P = U/(U + H - 1) \tag{88}$$

$$Q = (3 - V + H - U)/V \tag{89}$$

$$A = W/(U + H - 1) \tag{90}$$

$$b = \nu - \delta - 1 \tag{91}$$

$$B = (3 - (1 + \delta)\, V - bH - W)/V \tag{92}$$

Then the differential equations (28) to (30) can be written

$$H' = ST \qquad \text{(93 rad. eq.)}$$

$$U' = PQ \tag{94}$$

$$W' = AB \tag{95}$$

In convective equilibrium eq. (93 rad. eq.) is replaced by

$$H_0'' = H_0''' = H_0^{\text{iv}} \text{ etc.} = 0 \qquad \text{(96 conv. eq.)}$$

On the basis of these expressions we want to find the first and higher derivatives of U and W, and the second and higher derivatives of H, at $V = 0$, subject to the conditions

$$U_0 = W_0 = 3 \tag{97}$$

$$H_0 = 0 \tag{98}$$

In all these derivatives H_0' will enter as a parameter (cfr. section 2.3).

First differentiation.

Using (98) we have the Taylor expansion

$$H = H_0' V + {}^1/_2\, H_0'' V^2 + \frac{1}{6} H_0''' V^3 \ldots \tag{99}$$

Then from (85)

$$T = H_0' + {}^1/_2\, H_0'' V + \frac{1}{6} H_0''' V^2 \ldots \tag{100}$$

$$T_0 = H_0'. \tag{101}$$

From (87) and (88) we get

$$S_0 = 1 \tag{102}$$

$$P_0 = 3/2. \tag{103}$$

At $V=0$, Q becomes indeterminate. We can find the limiting value by using the standard rule of differentiating the numerator and denominator seperately (this rule will be used frequently in what follows) and obtain

$$Q_0 = -1 + H_0' - U_0'. \tag{104}$$

Further, using (94), we get

$$U_0' = P_0 Q_0 = -\frac{3}{2}(1 - H_0' + U_0') \tag{105}$$

and solving for U_0'

$$U_0' = -\frac{3}{5}(1 - H_0'). \tag{106}$$

Then (104) becomes

$$Q_0 = -\frac{2}{5}(1 - H_0'). \tag{107}$$

The following quantity will also be useful

$$U_0' + H_0' = (8 H_0' - 3)/5. \tag{108}$$

From (90) and (92) we now get

$$A_0 = 3/2 \tag{109}$$

$$B_0 = -(1 + \delta) - bH_0' - W_0' \tag{110}$$

and from (95)

$$W_0' = A_0 B_0 = -3(1 + \delta)/2 - 3 bH_0'/2 - 3 W_0'/2. \tag{111}$$

Solving for W_0':

$$W_0' = -3((1 + \delta) + bH_0')/5 \tag{112}$$

and inserting in (110)

$$B_0 = 2 W_0'/3 = -2((1 + \delta) + bH_0')/5. \tag{113}$$

Second differentiation.

Differentiating (100) we get

$$T' = {}^1/_2\, H_0'' + H_0''' \, V/3 \tag{114}$$

and

$$T_0' = {}^1/_2\, H_0''. \tag{115}$$

Further, from (87),

$$\left.\begin{aligned} S' &= (gH' - (2-\alpha) + W')/(U + H - 1) \\ &\quad - (gH - (2-\alpha)\, V + W - 1)\,(U' + H')\,(U + H - 1)^{-2}. \end{aligned}\right\} \tag{116}$$

Using (97), (108), and (112), we obtain

$$S_0' = ((5\,g - 3\,b - 8)\, H_0' - 10 + 5\,\alpha - 3\,\delta)/10. \tag{117}$$

Now, from (93), (115), and (101)

$$H_0'' = S_0\, T_0' + S_0'\, T_0 = {}^1/_2\, H_0'' + H_0' S_0' \qquad \text{(118 rad. eq.)}$$

and solving for H_0'', using (117),

$$H_0'' = H_0'\,((5\,g - 3\,b - 8)\, H_0' - 10 + 5\,\alpha - 3\,\delta)/5. \qquad \text{(119 rad. eq.)}$$

Differentiation of (88) yields

$$P' = U'/(U + H - 1) - U\,(U' + H')\,(U + H - 1)^{-2} \tag{120}$$

and inserting (106)

$$P_0' = 3\,(1 - 6\, H_0')/20. \tag{121}$$

Differentiation of (89) gives

$$\left.\begin{aligned} Q' &= (-1 + H' - U')/V - (3 - V + H - U)/V^2 = \\ &\quad (-1 + H' - U' - Q)/V. \end{aligned}\right\} \tag{122}$$

By the standard limiting rule we get

$$Q_0' = H_0'' - U_0'' - Q_0' \tag{123}$$

or

$$Q_0' = {}^1/_2\, H_0'' - {}^1/_2\, U_0''. \tag{124}$$

We can now calculate

$$\left.\begin{aligned} U_0'' &= P_0 Q_0' + P_0' Q_0 \\ &= 3\,H_0''/4 - 3\,U_0''/4 - 3\,(6\,H_0'^2 - 7\,H_0' + 1)/\,50 \end{aligned}\right\} \quad (125)$$

and, solving for U_0'', obtain the results

$$U_0'' = 3\,H_0''/7 - 6\,(6\,H_0'^2 - 7\,H_0' + 1)/175 \quad (126)$$

$$Q_0' = 2\,H_0''/7 + 3\,(6\,H_0'^2 - 7\,H_0' + 1)/175. \quad (127)$$

Inserting (119) in (126) we get

$$\left.\begin{aligned} U_0'' &= 3\,((25\,g - 15\,b - 52)\,H_0'^2 \\ &\quad + (25\,\alpha - 15\,\delta - 36)\,H_0' - 2)/175. \end{aligned}\right\} \quad (128 \text{ rad. eq.})$$

By differentiation of (90) we get

$$\left.\begin{aligned} A' &= W'\,(U + H - 1)^{-1} - W\,(U' + H')\,(H + U - 1)^{-2} \\ &= W'\,(U + H - 1)^{-1} - A\,(U' + H')\,(U + H - 1)^{-1} \end{aligned}\right\} \quad (129)$$

and, using (108) and (112), the limit

$$A_0' = -3\,((8 + 2\,b)\,H_0' + 2\,\delta - 1)/20. \quad (130)$$

For B' we get, from (92),

$$\left.\begin{aligned} B' &= (-(1 + \delta) - bH' - W')/V - (3 - (1 + \delta)\,V \\ &\quad - bH - W)/V^2 = (-(1 + \delta) - bH' - W' - B)/V \end{aligned}\right\} \quad (131)$$

which gives the limit

$$B_0' = -{}^1/_2\,bH_0'' - {}^1/_2\,W_0''. \quad (132)$$

Now the equation for W'' can be derived from (95), (130), and (132). Solving this equation we get

$$\left.\begin{aligned} W_0'' &= 6\,((8\,b + 2\,b^2)\,H_0'^2 + (8 + b + 8\,\delta + 4\,\delta\,b)\,H_0' \\ &\quad - 1 + \delta + 2\,\delta^2)/175 - 3\,bH_0''/7. \end{aligned}\right\} \quad (133)$$

Then B_0' can be found:

$$\left.\begin{aligned} B_0' &= -3\,((8\,b + 2\,b^2)\,H_0'^2 + (8 + b + 8\,\delta + 4\,\delta\,b)\,H_0' \\ &\quad - 1 + \delta + 2\,\delta^2)/175 - 2\,bH_0''/7. \end{aligned}\right\} \quad (134)$$

Inserting (119) into (133) we get

$$\left.\begin{aligned} W_0'' = 3\,((56\,b + 19\,b^2 - 25\,bg)\,H_0'^2 \\ + (16 + 52\,b + 16\,\delta - 25\,\alpha\,b + \\ 23\,\delta\,b)\,H_0' - 2 + 2\,\delta + 4\,\delta^2)/175. \end{aligned}\right\} \quad (135 \text{ rad. eq.})$$

Third differentiation.

The general procedure for deriving the derivatives having been made clear during the two first differentiations, we need only give the principal results of the third differentiation.

$$\left.\begin{aligned} S_0'' = H_0''(-10 + 7\,g - 3\,b)/14 + [H_0'^2(484 + 216\,b - 280\,g + \\ 12\,b^2) + H_0'(398 - 57\,b + 216\,\delta + 105\,g - 280\,\alpha + 24\,\delta\,b) \\ - 210 - 57\,\delta + 105\,\alpha + 12\,\delta^2]/350. \end{aligned}\right\} \quad (136)$$

$$\left.\begin{aligned} H_0''' = 3\,\lfloor H_0'^3(350\,g^2 + 120\,b^2 - 390\,g\,b - 1370\,g + 822\,b + 1332) \\ + H_0^2(525\,\alpha\,g - 285\,b\,\alpha - 315\,g\,\delta + 195\,\delta\,b - 1090\,\alpha - 945\,g + \\ 513\,b + 702\,\delta + 2018) \\ + H_0'(175\,\alpha^2 + 75\,\delta^2 - 210\,\alpha\,\delta - 595\,\alpha + 363\,\delta + 490)]/700. \end{aligned}\right\} \quad (137)$$

$$P_0'' = -6\,H_0''/7 + 3\,(348\,H_0'^2 - 196\,H_0' + 23)/700. \quad (138)$$

$$\left.\begin{aligned} U_0''' = H_0'''/3 + 2\,(1 - 2\,H_0')\,H_0''/7 \\ + 4\,(12\,H_0'^3 - 20\,H_0'^2 + 9\,H_0' - 1)/175. \end{aligned}\right\} \quad (139)$$

$$\left.\begin{aligned} U_0''' = [H_0'^3(350\,g^2 + 120\,b^2 - 390\,g\,b - 1770\,g + 1062\,b + \\ 2164) + H_0'^2(525\,\alpha\,g - 285\,b\,\alpha - 315\,g\,\delta + 195\,\delta\,b - 745\,g - \\ 1490\,\alpha + 393\,b + 942\,\delta + 2178) + H_0'(175\,\alpha^2 + 75\,\delta^2 - \\ 210\,\alpha\,\delta - 395\,\alpha + 243\,\delta + 234) - 16]/700. \end{aligned}\right\} \quad (140 \text{ rad. eq.})$$

$$\left.\begin{aligned} A_0'' = 3\,H_0''(-5 - b)/14 + 3\,[H_0'^2(8\,b^2 + 144\,b + 484) + \\ H_0'(16\,\delta\,b + 144\,\delta - 38\,b - 234) + 8\,\delta^2 - 38\,\delta + 23]/700. \end{aligned}\right\} \quad (141)$$

$$\left.\begin{aligned} W_0''' = &-bH_0'''/3 + 2H_0''\left[H_0'(13b + 3b^2) + 3\delta b + 5\delta + 5\right]/35 \\ &+ 2\left[H_0'^3(2b^3 - 24b^2 - 146b) + H_0'^2(6\delta b^2 + 15b^2 - 48\delta b\right. \\ &+ 69b - 146\delta - 146) + H_0'(6\delta^2 b + 30\delta b + 3b - 24\delta^2 \\ &\left. + 69\delta + 93) + 2\delta^3 + 15\delta^2 + 3\delta - 10\right]/875. \end{aligned}\right\} \quad (142)$$

$$\left.\begin{aligned} W_0'''' = &\left[H_0'^3(-1750\,bg^2 - 944\,b^3 + 2550\,b^2 g + 9450\,bg\right. \\ &- 6822\,b^2 - 11988\,b) + H_0'^2(-2625\,b\alpha g + 2175\,bg\delta \\ &+ 2025\,b^2\alpha - 1647\,\delta b^2 + 8050\,\alpha b + 4725\,bg - 3645\,b^2 - \\ &7014\,b\delta + 1000\,g + 1000\,g\delta - 15338\,b - 2768\,\delta - 2768) + \\ &H_0'(-875\,b\alpha^2 - 687\,b\delta^2 + 1650\,\alpha\delta b + 2975\,b\alpha - 2775\,\delta b \\ &+ 1000\,\alpha\delta - 792\,\delta^2 - 2426\,b - 2048\,\delta + 1000\,\alpha - 1256) \\ &\left. + 16\,\delta^3 + 120\,\delta^2 + 24\,\delta - 80\right]/3500. \end{aligned}\right\} \quad (143 \text{ rad. eq.})$$

Summary of the equations.

The definitions which will be needed when using the equations of the present appendix are given in eq. (2), (3), (86), and (91). The general form of the results is described in section 2.3.

The developments are arranged so as to be equally useful for convective and radiative equilibrium. The particular formulae to be used in the two cases are the following:

Function	Convective equilibrium	Radiative equilibrium
H_0'	$H_0' = 0.4$	H_0' is the fundamental parameter
U_0'	eq. (106)	eq. (106)
W_0'	(112)	(112)
H_0''	$H_0'' = 0$	(119)
U_0''	(126)	(126) or (128)
W_0''	(133)	(133) or (135)
H_0'''	$H_0''' = 0$	(137)
U_0'''	(139)	(139) or (140)
W_0'''	(142)	(142) or (143)

Appendix 2.

The run of the physical variables through 11 stellar models.

MODEL 1.

$$\varkappa = \varkappa_0 \varrho\, T^{-3.5}.$$

V	U	W	H	$\log r/R$	$\log P/P_c$	$\log T/T_c$	$\log M_r/M$	$\log L_r/L$
0.0	3.000	3.000	0.000	$-\infty$	0.000	0.000	$-\infty$	$-\infty$
0.5	2.808	2.253	0.172	9.007	9.891	9.962	8.621	9.431
1.0	2.616	1.640	0.330	9.160	9.780	9.924	9.037	9.733
1.5	2.424	1.155	0.474	9.251	9.668	9.888	9.268	9.861
2.0	2.234	0.784	0.607	9.318	9.552	9.852	9.424	9.926
2.5	2.045	0.512	0.731	9.372	9.432	9.816	9.539	9.960
3.0	1.860	0.320	0.848	9.407	9.307	9.780	9.628	9.979
3.5	1.678	0.193	0.960	9.457	9.177	9.744	9.698	9.989
4.0	1.502	0.111	1.068	9.493	9.042	9.707	9.756	9.995
4.5	1.334	0.061	1.175	9.526	8.901	9.670	9.803	9.998
5.0	1.175	0.031	1.281	9.557	8.754	9.632	9.842	9.999
5.5	1.027	0.015	1.386	9.586	8.603	9.594	9.874	0.000
6.0	0.891	0.007	1.492	9.613	8.447	9.554	9.900	0.000
6.5	0.767	0.003	1.599	9.638	8.289	9.515	9.920	0.000
7.0	0.658	0.001	1.706	9.662	8.130	9.476	9.937	0.000
7.5	0.562	0.001	1.815	9.684	7.972	9.438	9.951	0.000
8.0	0.478	0.000	1.925	9.704	7.815	9.400	9.961	0.000
8.5	0.408	0.000	2.037	9.722	7.663	9.364	9.969	0.000
9.0	0.347	0.000	2.149	9.739	7.515	9.328	9.976	0.000
9.5	0.297	0.000	2.262	9.755	7.373	9.294	9.981	0.000
10.0	0.254	0.000	2.376	9.769	7.237	9.262	9.984	0.000
10.5	0.219	0.000	2.490	9.781	7.107	9.231	9.987	0.000
11.0	0.189	0.000	2.604	9.793	6.983	9.201	9.990	0.000
11.5	0.164	0.000	2.719	9.804	6.864	9.173	9.992	0.000
12.0	0.143	0.000	2.834	9.813	6.752	9.147	9.993	0.000
12.5	0.125	0.000	2.949	9.822	6.645	9.122	9.994	0.000
13.0	0.110	0.000	3.063	9.830	6.543	9.097	9.995	0.000
13.5	0.098	0.000	3.176	9.837	6.445	9.074	9.996	0.000
14.0	0.086	0.000	3.288	9.844	6.352	9.052	9.997	0.000
14.5	0.077	0.000	3.398	9.850	6.262	9.032	9.997	0.000
15.0	0.068	0.000	3.504	9.856	6.176	9.011	9.998	0.000

Variations

V	ΔU	ΔW	ΔH
3	+111	+13	+342
6	39	1	229
10	27	0	519

Model 2.

$$\varkappa = \varkappa_0 \varrho^{0.75} T^{-3.5}.$$

V	U	W	H	log r/R	log P/P_c	log T/T_c	logM_r/M	log L_r/L
0.0	3.000	3.000	0.000	$-\infty$	0.000	0.000	$-\infty$	$-\infty$
0.5	2.800	2.263	0.160	8.876	9.891	9.964	8.591	9.414
1.0	2.600	1.652	0.306	9.032	9.778	9.929	9.012	9.722
1.5	2.399	1.164	0.438	9.126	9.662	9.894	9.247	9.855
2.0	2.199	0.787	0.559	9.195	9.542	9.860	9.407	9.922
2.5	2.000	0.509	0.671	9.251	9.415	9.825	9.526	9.959
3.0	1.803	0.313	0.776	9.300	9.282	9.790	9.619	9.979
3.5	1.609	0.183	0.875	9.344	9.140	9.754	9.693	9.989
4.0	1.420	0.101	0.971	9.384	8.989	9.716	9.754	9.995
4.5	1.238	0.052	1.064	9.422	8.827	9.678	9.805	9.998
5.0	1.066	0.024	1.157	9.458	8.655	9.637	9.847	9.999
5.5	0.904	0.010	1.249	9.493	8.472	9.595	9.881	0.000
6.0	0.757	0.004	1.342	9.527	8.279	9.552	9.909	0.000
6.5	0.625	0.002	1.436	9.559	8.078	9.507	9.931	0.000
7.0	0.510	0.000	1.532	9.590	7.871	9.462	9.948	0.000
7.5	0.413	0.000	1.629	9.618	7.662	9.416	9.962	0.000
8.0	0.333	0.000	1.727	9.645	7.456	9.371	9.972	0.000
8.5	0.268	0.000	1.827	9.670	7.254	9.328	9.979	0.000
9.0	0.216	0.000	1.929	9.692	7.060	9.286	9.984	0.000
9.5	0.175	0.000	2.031	9.712	6.875	9.246	9.988	0.000
10.0	0.143	0.000	2.134	9.730	6.700	9.209	9.991	0.000
10.5	0.117	0.000	2.238	9.746	6.535	9.174	9.993	0.000
11.0	0.097	0.000	2.342	9.760	6.380	9.141	9.995	0.000
11.5	0.081	0.000	2.446	9.773	6.233	9.110	9.996	0.000
12.0	0.068	0.000	2.551	9.785	6.095	9.080	9.997	0.000
12.5	0.057	0.000	2.655	9.796	5.965	9.052	9.997	0.000
13.0	0.049	0.000	2.760	9.805	5.841	9.026	9.998	0.000
13.5	0.042	0.000	2.864	9.814	5.724	9.001	9.998	0.000
14.0	0.036	0.000	2.968	9.822	5.614	8.978	9.999	0.000
14.5	0.031	0.000	3.070	9.830	5.508	8.955	9.999	0.000
15.0	0.027	0.000	3.172	9.836	5.407	8.934	9.999	0.000

Variations

V	ΔU	ΔW	ΔH
3	+32	+4	+93
6	61	1	298
10	32	0	737

Model 3.

$$\varkappa = \varkappa_0 \varrho^{0.5} T^{-3.5}.$$

V	U	W	H	$\log r/R$	$\log P/P_c$	$\log T/T_c$	$\log M_r/M$	$\log L_r/L$
0.0	3.000	3.000	0.000	$-\infty$	0.000	0.000	$-\infty$	$-\infty$
0.5	2.792	2.275	0.146	8.647	9.890	9.967	8.553	9.394
1.0	2.582	1.668	0.279	8.805	9.776	9.934	8.979	9.709
1.5	2.372	1.176	0.399	8.901	9.656	9.902	9.219	9.847
2.0	2.161	0.792	0.508	8.974	9.530	9.869	9.384	9.918
2.5	1.950	0.506	0.607	9.034	9.396	9.835	9.508	9.957
3.0	1.739	0.304	0.698	9.087	9.250	9.801	9.605	9.978
3.5	1.530	0.170	0.784	9.135	9.092	9.765	9.685	9.990
4.0	1.325	0.087	0.866	9.182	8.919	9.726	9.751	9.995
4.5	1.124	0.040	0.945	9.227	8.727	9.686	9.806	9.998
5.0	0.932	0.016	1.023	9.272	8.512	9.641	9.853	9.999
5.5	0.751	0.005	1.101	9.318	8.271	9.592	9.891	0.000
6.0	0.586	0.001	1.180	9.365	8.002	9.539	9.922	0.000
6.5	0.442	0.000	1.260	9.412	7.705	9.481	9.947	0.000
7.0	0.322	0.000	1.342	9.460	7.386	9.419	9.965	0.000
7.5	0.230	0.000	1.427	9.505	7.056	9.356	9.977	0.000
8.0	0.162	0.000	1.515	9.547	6.730	9.294	9.985	0.000
8.5	0.115	0.000	1.604	9.585	6.418	9.235	9.990	0.000
9.0	0.082	0.000	1.695	9.618	6.128	9.180	9.994	0.000
9.5	0.060	0.000	1.787	9.647	5.860	9.130	9.996	0.000
10.0	0.044	0.000	1.879	9.672	5.614	9.084	9.997	0.000
10.5	0.034	0.000	1.972	9.694	5.389	9.041	9.998	0.000
11.0	0.026	0.000	2.065	9.714	5.182	9.002	9.998	0.000
11.5	0.020	0.000	2.159	9.731	4.990	8.966	9.999	0.000
12.0	0.016	0.000	2.253	9.746	4.813	8.933	9.999	0.000
12.5	0.013	0.000	2.348	9.759	4.648	8.902	9.999	0.000
13.0	0.010	0.000	2.444	9.771	4.493	8.873	0.000	0.000
13.5	0.008	0.000	2.542	9.782	4.349	8.846	0.000	0.000
14.0	0.007	0.000	2.642	9.792	4.213	8.820	0.000	0.000
14.5	0.006	0.000	2.745	9.801	4.085	8.796	0.000	0.000
15.0	0.005	0.000	2.853	9.809	3.965	8.773	0.000	0.000

Variations

V	ΔU	ΔW	ΔH
3	+132	+19	+340
6	37	0	150
10	1	0	55

Model 4.

$$\varkappa = \varkappa_0 \varrho^{0.75} T^{-2.5}.$$

V	U	W	H	log r/R	log P/P_c	log T/T_c	log M_r/M	log L_r/L
0.0	3.000	3.000	0.000	$-\infty$	0.000	0.000	$-\infty$	$-\infty$
0.5	2.817	2.242	0.185	9.049	9.892	9.959	8.638	9.446
1.0	2.632	1.628	0.352	9.200	9.783	9.919	9.051	9.741
1.5	2.447	1.146	0.503	9.290	9.673	9.881	9.278	9.866
2.0	2.262	0.780	0.641	9.354	9.560	9.844	9.431	9.928
2.5	2.078	0.513	0.769	9.406	9.445	9.808	9.543	9.961
3.0	1.898	0.325	0.888	9.450	9.325	9.772	9.630	9.979
3.5	1.721	0.198	1.003	9.488	9.202	9.736	9.699	9.989
4.0	1.550	0.116	1.114	9.522	9.073	9.700	9.755	9.994
4.5	1.386	0.066	1.223	9.553	8.941	9.663	9.801	9.997
5.0	1.231	0.036	1.330	9.582	8.804	9.626	9.839	9.999
5.5	1.085	0.019	1.437	9.609	8.663	9.589	9.870	9.999
6.0	0.951	0.010	1.545	9.634	8.519	9.552	9.895	0.000
6.5	0.828	0.005	1.654	9.657	8.373	9.514	9.916	0.000
7.0	0.718	0.002	1.763	9.679	8.226	9.477	9.933	0.000
7.5	0.621	0.001	1.874	9.699	8.080	9.441	9.946	0.000
8.0	0.536	0.001	1.986	9.718	7.936	9.405	9.957	0.000
8.5	0.462	0.000	2.099	9.735	7.795	9.370	9.966	0.000
9.0	0.399	0.000	2.213	9.750	7.658	9.336	9.972	0.000
9.5	0.345	0.000	2.328	9.765	7.526	9.304	9.978	0.000
10.0	0.299	0.000	2.444	9.778	7.399	9.272	9.982	0.000
10.5	0.260	0.000	2.560	9.790	7.277	9.243	9.985	0.000
11.0	0.227	0.000	2.677	9.800	7.160	9.214	9.988	0.000
11.5	0.199	0.000	2.795	9.810	7.049	9.187	9.990	0.000
12.0	0.175	0.000	2.912	9.819	6.942	9.161	9.992	0.000
12.5	0.154	0.000	3.030	9.828	6.841	9.136	9.993	0.000
13.0	0.137	0.000	3.148	9.835	6.744	9.113	9.994	0.000
13.5	0.122	0.000	3.265	9.842	6.651	9.090	9.995	0.000
14.0	0.108	0.000	3.381	9.849	6.562	9.069	9.996	0.000
14.5	0.097	0.000	3.497	9.855	6.476	9.048	9.996	0.000
15.0	0.087	0.000	3.610	9.860	6.394	9.019	9.997	0.000

Variations

V	ΔU	ΔW	ΔH
3	+91	+9	+260
6	18	0	83
10	23	0	301

Model 5.

$$\varkappa = \varkappa_0 \varrho^{0.5} T^{-2.5}.$$

V	U	W	H	$\log r/R$	$\log P/P_c$	$\log T/T_c$	$\log M_r/M$	$\log L_r/L$
0.0	3.000	3.000	0.000	$-\infty$	0.000	0.000	$-\infty$	$-\infty$
0.5	2.808	2.254	0.171	8.911	9.891	9.962	8.605	9.426
1.0	2.613	1.643	0.323	9.065	9.780	9.925	9.023	9.729
1.5	2.418	1.158	0.460	9.157	9.667	9.889	9.255	9.858
2.0	2.222	0.785	0.584	9.225	9.549	9.854	9.413	9.924
2.5	2.026	0.511	0.698	9.280	9.426	9.818	9.530	9.960
3.0	1.833	0.317	0.803	9.327	9.297	9.783	9.620	9.979
3.5	1.642	0.188	0.903	9.369	9.160	9.747	9.694	9.989
4.0	1.456	0.105	0.999	9.407	9.016	9.710	9.753	9.995
4.5	1.277	0.055	1.092	9.444	8.862	9.672	9.803	9.998
5.0	1.106	0.026	1.184	9.478	8.698	9.633	9.844	9.999
5.5	0.946	0.012	1.276	9.511	8.525	9.593	9.878	0.000
6.0	0.799	0.005	1.368	9.542	8.344	9.551	9.905	0.000
6.5	0.667	0.002	1.462	9.573	8.154	9.508	9.928	0.000
7.0	0.550	0.001	1.557	9.602	7.960	9.464	9.945	0.000
7.5	0.451	0.000	1.654	9.629	7.763	9.421	9.959	0.000
8.0	0.368	0.000	1.752	9.654	7.568	9.378	9.969	0.000
8.5	0.299	0.000	1.852	9.677	7.376	9.336	9.977	0.000
9.0	0.244	0.000	1.953	9.698	7.191	9.296	9.982	0.000
9.5	0.199	0.000	2.056	9.717	7.014	9.257	9.987	0.000
10.0	0.164	0.000	2.160	9.735	6.845	9.221	9.990	0.000
10.5	0.136	0.000	2.264	9.750	6.686	9.186	9.992	0.000
11.0	0.113	0.000	2.369	9.764	6.535	9.154	9.994	0.000
11.5	0.095	0.000	2.474	9.777	6.393	9.123	9.995	0.000
12.0	0.080	0.000	2.580	9.788	6.258	9.094	9.996	0.000
12.5	0.068	0.000	2.687	9.799	6.131	9.067	9.997	0.000
13.0	0.058	0.000	2.793	9.808	6.010	9.041	9.997	0.000
13.5	0.050	0.000	2.900	9.817	5.896	9.016	9.998	0.000
14.0	0.043	0.000	3.008	9.825	5.788	8.993	9.998	0.000
14.5	0.038	0.000	3.116	9.832	5.684	8.971	9.999	0.000
15.0	0.033	0.000	3.225	9.839	5.586	8.950	9.999	0.000

Variations

V	ΔU	ΔW	ΔH
3	+50	+6	+126
6	30	0	115
10	22	0	383

Model 6.

$$\varkappa = \varkappa_0 \varrho^{0.25} T^{-2.5}.$$

V	U	W	H	$\log r/R$	$\log P/P_c$	$\log T/T_c$	$\log M_r/M$	$\log L_r/L$
0.0	3.000	3.000	0.000	$-\infty$	0.000	0.000	$-\infty$	$-\infty$
0.5	2.797	2.268	0.154	8.647	9.891	9.965	8.562	9.403
1.0	2.592	1.660	0.292	8.804	9.778	9.931	8.986	9.714
1.5	2.385	1.170	0.414	8.899	9.660	9.898	9.224	9.850
2.0	2.176	0.790	0.523	8.970	9.536	9.864	9.387	9.920
2.5	1.967	0.507	0.621	9.029	9.404	9.830	9.509	9.958
3.0	1.758	0.307	0.711	9.081	9.262	9.796	9.605	9.978
3.5	1.550	0.173	0.795	9.129	9.107	9.760	9.684	9.990
4.0	1.345	0.090	0.874	9.174	8.938	9.722	9.749	9.995
4.5	1.144	0.042	0.950	9.218	8.750	9.682	9.804	9.998
5.0	0.951	0.017	1.025	9.262	8.539	9.638	9.851	9.999
5.5	0.768	0.006	1.099	9.307	8.303	9.590	9.889	0.000
6.0	0.600	0.002	1.174	9.354	8.038	9.538	9.921	0.000
6.5	0.452	0.000	1.251	9.401	7.743	9.481	9.946	0.000
7.0	0.329	0.000	1.331	9.448	7.423	9.419	9.964	0.000
7.5	0.233	0.000	1.413	9.494	7.090	9.356	9.977	0.000
8.0	0.163	0.000	1.498	9.537	6.757	9.294	9.985	0.000
8.5	0.114	0.000	1.586	9.576	6.437	9.234	9.991	0.000
9.0	0.081	0.000	1.675	9.610	6.138	9.178	9.994	0.000
9.5	0.058	0.000	1.765	9.640	5.863	9.127	9.996	0.000
10.0	0.043	0.000	1.856	9.666	5.610	9.080	9.997	0.000
10.5	0.032	0.000	1.948	9.688	5.379	9.037	9.998	0.000
11.0	0.024	0.000	2.040	9.708	5.166	8.998	9.999	0.000
11.5	0.019	0.000	2.132	9.726	4.970	8.961	9.999	0.000
12.0	0.015	0.000	2.224	9.741	4.788	8.927	9.999	0.000
12.5	0.012	0.000	2.316	9.755	4.619	8.896	0.000	0.000
13.0	0.010	0.000	2.409	9.767	4.461	8.866	0.000	0.000
13.5	0.008	0.000	2.502	9.778	4.312	8.839	0.000	0.000
14.0	0.006	0.000	2.594	9.789	4.173	8.813	0.000	0.000
14.5	0.005	0.000	2.687	9.798	4.041	8.789	0.000	0.000
15.0	0.004	0.000	2.780	9.806	3.916	8.766	0.000	0.000

Variations

V	ΔU	ΔW	ΔH
3	+78	+12	+178
6	19	0	66
10	11	0	282

Model 7.

$$\varkappa = \varkappa_0 \varrho^{0.5} T^{-0.9}.$$

V	U	W	H	$\log r/R$	$\log P/P_c$	$\log T/T_c$	$\log M_r/M$	$\log L_r/L$
0.0	3.000	3.000	0.000	$-\infty$	0.000	0.000	$-\infty$	$-\infty$
0.5	2.824	2.231	0.200	9.191	9.892	9.957	8.686	9.475
1.0	2.655	1.608	0.400	9.338	9.786	9.914	9.093	9.762
1.5	2.494	1.126	0.600	9.423	9.681	9.872	9.312	9.879
2.0	2.338	0.769	0.769	9.483	9.578	9.832	9.455	9.935
2.5	2.180	0.514	0.918	9.529	9.475	9.793	9.560	9.964
3.0	2.022	0.336	1.057	9.567	9.371	9.755	9.639	9.980
3.5	1.867	0.215	1.190	9.599	9.266	9.719	9.702	9.989
4.0	1.717	0.135	1.318	9.627	9.160	9.684	9.753	9.994
4.5	1.573	0.083	1.444	9.652	9.052	9.649	9.795	9.997
5.0	1.435	0.050	1.569	9.675	8.944	9.614	9.829	9.998
5.5	1.306	0.030	1.693	9.696	8.836	9.580	9.857	9.999
6.0	1.185	0.018	1.818	9.715	8.727	9.547	9.881	0.000
6.5	1.073	0.010	1.943	9.732	8.619	9.515	9.900	0.000
7.0	0.970	0.006	2.068	9.748	8.512	9.483	9.916	0.000
7.5	0.876	0.004	2.195	9.763	8.406	9.452	9.930	0.000
8.0	0.790	0.002	2.323	9.776	8.303	9.422	9.941	0.000
8.5	0.714	0.001	2.452	9.788	8.201	9.392	9.950	0.000
9.0	0.645	0.001	2.582	9.800	8.102	9.364	9.958	0.000
9.5	0.583	0.000	2.712	9.810	8.006	9.336	9.964	0.000
10.0	0.528	0.000	2.843	9.820	7.913	9.310	9.970	0.000
10.5	0.479	0.000	2.975	9.828	7.823	9.284	9.974	0.000
11.0	0.435	0.000	3.107	9.836	7.736	9.260	9.978	0.000
11.5	0.396	0.000	3.239	9.844	7.652	9.236	9.981	0.000
12.0	0.361	0.000	3.372	9.851	7.572	9.213	9.983	0.000
12.5	0.330	0.000	3.504	9.857	7.494	9.191	9.986	0.000
13.0	0.302	0.000	3.636	9.863	7.418	9.170	9.988	0.000
13.5	0.277	0.000	3.767	9.868	7.346	9.150	9.989	0.000
14.0	0.255	0.000	3.897	9.873	7.276	9.130	9.990	0.000
14.5	0.234	0.000	4.026	9.878	7.208	9.112	9.992	0.000
15.0	0.216	0.000	4.153	9.883	7.142	9.093	9.993	0.000

Variations

V	ΔU	ΔW	ΔH
6	+18	0	+108

Model 8.

$$\varkappa = \varkappa_0 \varrho^{0.25} T^{-0.9}.$$

V	U	W	H	log r/R	log P/P_c	log T/T_c	log M_r/M	log L_r/L
0.0	3.000	3.000	0.000	$-\infty$	0.000	0.000	$-\infty$	$-\infty$
0.5	2.824	2.231	0.200	9.089	9.892	9.957	8.661	9.467
1.0	2.655	1.609	0.394	9.237	9.786	9.914	9.068	9.754
1.5	2.483	1.131	0.554	9.323	9.679	9.874	9.289	9.872
2.0	2.308	0.774	0.697	9.385	9.572	9.835	9.438	9.931
2.5	2.132	0.514	0.827	9.434	9.463	9.798	9.546	9.962
3.0	1.958	0.331	0.947	9.475	9.350	9.762	9.630	9.980
3.5	1.787	0.206	1.060	9.511	9.234	9.726	9.697	9.989
4.0	1.620	0.124	1.168	9.542	9.115	9.690	9.751	9.994
4.5	1.459	0.073	1.275	9.572	8.992	9.655	9.796	9.997
5.0	1.305	0.041	1.380	9.598	8.865	9.619	9.833	9.998
5.5	1.161	0.023	1.484	9.623	8.734	9.584	9.864	9.999
6.0	1.027	0.012	1.589	9.646	8.601	9.548	9.889	0.000
6.5	0.903	0.006	1.695	9.668	8.466	9.512	9.910	0.000
7.0	0.791	0.003	1.802	9.688	8.330	9.477	9.927	0.000
7.5	0.691	0.002	1.910	9.707	8.194	9.442	9.941	0.000
8.0	0.602	0.001	2.019	9.724	8.059	9.408	9.952	0.000
8.5	0.525	0.000	2.131	9.740	7.926	9.374	9.961	0.000
9.0	0.457	0.000	2.243	9.755	7.797	9.342	9.968	0.000
9.5	0.399	0.000	2.357	9.769	7.671	9.311	9.974	0.000
10.0	0.348	0.000	2.471	9.781	7.550	9.281	9.979	0.000
10.5	0.305	0.000	2.587	9.793	7.433	9.252	9.982	0.000
11.0	0.268	0.000	2.703	9.803	7.320	9.224	9.986	0.000
11.5	0.236	0.000	2.820	9.813	7.212	9.198	9.988	0.000
12.0	0.209	0.000	2.936	9.822	7.109	9.172	9.990	0.000
12.5	0.185	0.000	3.054	9.830	7.010	9.148	9.992	0.000
13.0	0.165	0.000	3.171	9.837	6.915	9.125	9.993	0.000
13.5	0.147	0.000	3.288	9.844	6.824	9.103	9.994	0.000
14.0	0.132	0.000	3.405	9.850	6.737	9.081	9.995	0.000
14.5	0.118	0.000	3.522	9.856	6.653	9.061	9.996	0.000
15.0	0.107	0.000	3.638	9.862	6.572	9.041	9.996	0.000

Variations

V	ΔU	ΔW	ΔH
5	+25	+2	+81
10	7	0	106

Model 9.

$\varkappa = \varkappa_0 T^{-0.9}$.

V	U	W	H	log r/R	log P/P_c	log T/T_c	log M_r/M	log L_r/L
0.0	3.000	3.000	0.000	$-\infty$	0.000	0.000	$-\infty$	$-\infty$
0.5	2.820	2.237	0.189	8.892	9.892	9.957	8.618	9.444
1.0	2.635	1.625	0.351	9.042	9.784	9.918	9.030	9.738
1.5	2.445	1.146	0.491	9.132	9.673	9.880	9.258	9.863
2.0	2.254	0.780	0.614	9.197	9.559	9.844	9.412	9.926
2.5	2.060	0.512	0.723	9.250	9.440	9.809	9.527	9.960
3.0	1.867	0.321	0.822	9.296	9.315	9.773	9.616	9.979
3.5	1.676	0.192	0.913	9.336	9.183	9.738	9.689	9.989
4.0	1.488	0.109	1.000	9.374	9.042	9.702	9.748	9.994
4.5	1.305	0.058	1.084	9.410	8.890	9.665	9.798	9.997
5.0	1.129	0.029	1.166	9.444	8.729	9.626	9.840	9.999
5.5	0.963	0.014	1.248	9.477	8.555	9.586	9.874	0.000
6.0	0.810	0.006	1.330	9.509	8.370	9.545	9.903	0.000
6.5	0.671	0.002	1.414	9.540	8.175	9.502	9.926	0.000
7.0	0.548	0.001	1.500	9.570	7.971	9.458	9.944	0.000
7.5	0.443	0.000	1.588	9.599	7.761	9.413	9.958	0.000
8.0	0.356	0.000	1.678	9.626	7.551	9.369	9.969	0.000
8.5	0.285	0.000	1.771	9.652	7.343	9.325	9.977	0.000
9.0	0.228	0.000	1.866	9.675	7.140	9.283	9.983	0.000
9.5	0.183	0.000	1.962	9.696	6.946	9.243	9.988	0.000
10.0	0.148	0.000	2.058	9.715	6.761	9.205	9.991	0.000
10.5	0.120	0.000	2.156	9.732	6.586	9.169	9.993	0.000
11.0	0.098	0.000	2.255	9.747	6.421	9.135	9.995	0.000
11.5	0.081	0.000	2.354	9.761	6.266	9.103	9.996	0.000
12.0	0.067	0.000	2.453	9.774	6.118	9.073	9.997	0.000
12.5	0.057	0.000	2.552	9.785	5.980	9.044	9.997	0.000
13.0	0.048	0.000	2.650	9.795	5.848	9.018	9.998	0.000
13.5	0.040	0.000	2.748	9.805	5.724	8.992	9.998	0.000
14.0	0.034	0.000	2.845	9.813	5.605	8.968	9.999	0.000
14.5	0.030	0.000	2.942	9.821	5.493	8.945	9.999	0.000
15.0	0.025	0.000	3.036	9.828	5.385	8.923	9.999	0.000

Variations

V	ΔU	ΔW	ΔH
3	+53	+5	+112
6	19	1	59

Model 10.

$$\varkappa = \varkappa_0 \varrho^{0.25}.$$

V	U	W	H	$\log r/R$	$\log P/P_c$	$\log T/T_c$	$\log M_r/M$	$\log L_r/L$
0.0	3.000	3.000	0.000	$-\infty$	0.000	0.000	$-\infty$	$-\infty$
0.5	2.824	2.231	0.200	9.232	9.892	9.957	8.699	9.478
1.0	2.655	1.608	0.400	9.380	9.786	9.914	9.105	9.765
1.5	2.494	1.126	0.600	9.465	9.681	9.872	9.324	9.881
2.0	2.342	0.768	0.800	9.524	9.578	9.831	9.467	9.937
2.5	2.198	0.514	1.000	9.569	9.478	9.791	9.569	9.966
3.0	2.059	0.338	1.156	9.605	9.380	9.753	9.645	9.981
3.5	1.919	0.220	1.296	9.635	9.282	9.716	9.705	9.989
4.0	1.782	0.141	1.432	9.661	9.184	9.680	9.754	9.994
4.5	1.648	0.089	1.565	9.684	9.086	9.645	9.793	9.997
5.0	1.520	0.056	1.697	9.705	8.988	9.612	9.826	9.998
5.5	1.398	0.035	1.827	9.724	8.890	9.579	9.853	9.999
6.0	1.284	0.022	1.958	9.740	8.793	9.547	9.876	0.000
6.5	1.176	0.013	2.090	9.756	8.697	9.515	9.895	0.000
7.0	1.077	0.008	2.222	9.770	8.602	9.485	9.910	0.000
7.5	0.985	0.005	2.354	9.783	8.508	9.455	9.924	0.000
8.0	0.901	0.003	2.487	9.795	8.416	9.427	9.935	0.000
8.5	0.824	0.002	2.621	9.806	8.326	9.399	9.944	0.000
9.0	0.754	0.001	2.756	9.816	8.239	9.372	9.952	0.000
9.5	0.691	0.001	2.890	9.825	8.154	9.346	9.959	0.000
10.0	0.633	0.000	3.026	9.833	8.071	9.321	9.964	0.000
10.5	0.581	0.000	3.162	9.841	7.990	9.296	9.969	0.000
11.0	0.534	0.000	3.297	9.848	7.912	9.273	9.973	0.000
11.5	0.491	0.000	3.432	9.855	7.837	9.250	9.977	0.000
12.0	0.452	0.000	3.567	9.861	7.764	9.228	9.980	0.000
12.5	0.418	0.000	3.700	9.867	7.693	9.207	9.892	0.000
13.0	0.386	0.000	3.832	9.872	7.625	9.187	9.984	0.000
13.5	0.357	0.000	3.962	9.877	7.558	9.168	9.986	0.000
14.0	0.330	0.000	4.091	9.882	7.494	9.149	9.988	0.000
14.5	0.307	0.000	4.216	9.886	7.431	9.131	9.989	0.000
15.0	0.285	0.000	4.339	9.891	7.371	9.113	9.990	0.000

Model 11.

$\varkappa = \varkappa_0$.

V	U	W	H	$\log r/R$	$\log P/P_c$	$\log T/T_c$	$\log M_r/M$	$\log L_r/L$
0.0	3.000	3.000	0.000	$-\infty$	0.000	0.000	$-\infty$	$-\infty$
0.5	2.824	2.231	0.200	9.134	9.892	9.957	8.678	9.474
1.0	2.655	1.608	0.400	9.281	9.786	9.914	9.084	9.761
1.5	2.494	1.126	0.600	9.366	9.681	9.872	9.303	9.878
2.0	2.336	0.770	0.759	9.426	9.577	9.832	9.447	9.934
2.5	2.174	0.514	0.894	9.472	9.473	9.793	9.552	9.964
3.0	2.010	0.336	1.018	9.511	9.367	9.756	9.633	9.980
3.5	1.847	0.213	1.133	9.544	9.259	9.720	9.698	9.989
4.0	1.687	0.132	1.244	9.574	9.148	9.685	9.750	9.994
4.5	1.532	0.080	1.351	9.601	9.034	9.650	9.793	9.997
5.0	1.384	0.047	1.457	9.625	8.918	9.616	9.829	9.998
5.5	1.243	0.027	1.563	9.648	8.798	9.581	9.859	9.999
6.0	1.111	0.015	1.669	9.669	8.677	9.547	9.884	0.000
6.5	0.989	0.008	1.775	9.689	8.555	9.514	9.904	0.000
7.0	0.877	0.005	1.883	9.707	8.432	9.480	9.921	0.000
7.5	0.776	0.003	1.992	9.724	8.308	9.447	9.935	0.000
8.0	0.685	0.002	2.103	9.740	8.186	9.415	9.947	0.000
8.5	0.604	0.001	2.216	9.754	8.066	9.383	9.956	0.000
9.0	0.533	0.000	2.330	9.768	7.948	9.353	9.964	0.000
9.5	0.470	0.000	2.445	9.780	7.833	9.323	9.970	0.000
10.0	0.416	0.000	2.561	9.792	7.722	9.294	9.975	0.000
10.5	0.368	0.000	2.678	9.802	7.614	9.267	9.979	0.000
11.0	0.327	0.000	2.797	9.812	7.509	9.240	9.983	0.000
11.5	0.291	0.000	2.916	9.821	7.409	9.215	9.985	0.000
12.0	0.259	0.000	3.035	9.829	7.313	9.190	9.988	0.000
12.5	0.232	0.000	3.155	9.836	7.220	9.167	9.990	0.000
13.0	0.208	0.000	3.275	9.844	7.131	9.144	9.991	0.000
13.5	0.187	0.000	3.396	9.850	7.045	9.123	9.992	0.000
14.0	0.169	0.000	3.516	9.856	6.963	9.102	9.993	0.000
14.5	0.153	0.000	3.636	9.862	6.883	9.082	9.994	0.000
15.0	0.139	0.000	3.757	9.867	6.807	9.063	9.995	0.000

Variations

V	ΔU	ΔW	ΔH
5	+14	+1	+44

References.

1) B. Strömgren, A. J., **57**, 65 (1952).
2) I. Epstein, Ap. J., **114**, 438 (1951).
3) I. Epstein and L. Motz, Ap. J., **117**, 311 (1953).
4) D. E. Osterbrock, Ap. J., **118**, 529 (1953).
5) A. Reiz, Ap. J. **120**, 342 (1954).
6) S. Chandrasekhar, An Introduction to the Study of Stellar Structure (Chicago: University of Chicago Press, 1938).
7) P. Naur and D. E. Osterbrock, Ap. J., **117**, 306 (1953).
8) R. D. Levee, Ap. J., **117**, 200 (1953).
9) C. M. Bondi and H. Bondi, M. N., **109**, 62 (1949).
10) S. Chandrasekhar, Astrophysics, A Topical Symposium, ed. J. A. Hynek (New York: McGraw-Hill Book Co., 1951), chapter 14.
11) Brit. Ass. Math. Tables, Vol II. (1932).
12) P. Naur, Dan. Mat. Fys. Medd. **29**, no. 5 (1954) = Publ. Cop. Obs. no. 164.
13) P. Naur, Ap. J., **119**, 365 (1954).
14) E. E. Salpeter, Ap. J., **116**, 649 (1952).

Indleveret til selskabet den 25. september 1954.
Færdig fra trykkeriet den 18. Januar 1956.

Det Kongelige Danske Videnskabernes Selskab
Matematisk-fysiske Meddelelser, bind **30**, nr. 17

Dan. Mat. Fys. Medd. **30**, no. 17 (1956)

MEASUREMENTS OF CONVERSION ELECTRONS FROM COULOMB EXCITATION OF THE ELEMENTS IN THE RARE EARTH REGION

BY

TORBEN HUUS, JØRGEN H. BJERREGAARD,
AND BENT ELBEK

København 1956
i kommission hos Ejnar Munksgaard

CONTENTS

Printed in Denmark.
Bianco Lunos Bogtrykkeri A-S.

The paper deals with the experimental problems connected with measurements of the conversion electrons produced by Coulomb excitation of the heavier elements. It contains the results of a series of measurements on elements with the atomic numbers 25, 26, 47, 60, 62 to 75, and 77 to 79. Reduced transition probabilities are computed from the data and are compared with the results derived from lifetime measurements. By means of the unified model, nuclear moments are calculated from the measured excitation energies and transition probabilities. The values obtained are compared with the theory as well as with other experimental evidence and in general the agreement is found to be satisfactory.

I. Introduction.

The excitation of nuclei by the electric field of impinging heavy particles provides a powerful method for studying the collective nuclear energy spectra. In the two years that have passed since such Coulomb excitation processes were first investigated, one has obtained extensive information* which has yielded many tests of the theoretical predictions based on the unified nuclear model (Bo 1).

According to this model, the collective excitations have a particularly simple character for nuclei possessing large deformations, as encountered in regions far removed from closed shell configurations. Such strongly deformed nuclei are expected to exhibit excitation spectra of simple rotational type, characterized by numerous regularities in energies and transition probabilities. The rotational spectra also have especially small excitation energies and large electric quadrupole matrix elements, making them highly suitable for Coulomb excitation studies.

The region of the periodic table, which offers the best possibility for a systematic study of rotational states by means of Coulomb excitation, is the comparatively large interval between the nuclei having 82 neutrons and mass numbers around $A = 140$, and the doubly closed shell configuration of $_{82}Pb^{208}$. In the present paper, the results of some Coulomb excitation measurements of nuclei in this region are reported.

In the investigation of the radiation from the Coulomb excited

* For a complete list of experimental investigations employing the Coulomb excitation process, the reader is referred to a forthcoming review article (Al 1). We may here especially point to the extensive investigations by N. P. Heydenburg and G. M. Temmer (He 1); C. L. McClelland, H. Mark, and C. Goodman (Mc 1); and P. H. Stelson and F. K. McGowan (St 1).

nuclei we have studied the internal conversion electrons rather than the emitted γ-rays. This method offers the following advantages:

a) The relatively high resolution obtainable with β-spectrometers is useful, in particular when targets of separated isotopes are difficult to obtain, as is the case with the rare earth elements.

b) The presence of lighter elements in the target is comparatively harmless, as a consequence of their small conversion coefficients. This was important in our work since the rare earths were only available in very small quantities and in the form of oxides, which give rise to a γ-ray background under proton bombardment. This background is considerably smaller when α-particles are employed as projectiles which, however, in most instances requires an acceleration voltage of more than the 2 MV at our disposal.

c) The relative intensity of the electrons from the various atomic shells yields information about the multipolarity of the transitions.

On the other hand, the use of the thin targets, which are preferable for the lower electron energies, gives rise to additional uncertainties in the measured cross sections. This is particularly true because of the difficulty of producing stable and homogeneous targets when only very small quantities of the materials are available.

In the present investigation, it was aimed at obtaining a preliminary survey of rotational excitations in the region of the elements considered and, in addition, at estimating nuclear moments on the basis of the observed cross sections. In particular, the trends of the nuclear quadrupole deformations and their relation to the moments of inertia appear to be of interest for current theoretical developments.

In Chapter II, the theory of rotational states and of the Coulomb excitation process is summarized, while the experimental problems are dealt with in Chapter III. The data obtained are tabulated and commented on in Chapter IV, whereas the results are discussed in Chapter V. The theory of a background radiation, important for the measurements, is outlined in the Appendices I and II.

II. Summary of Theory.

A. Rotational States.

In this section, we give a brief summary of the theory of nuclear rotational states, as developed by BOHR and MOTTELSON (Bo 1), and present the formulae which are employed in the present work.

Rotational spectra are associated with nuclei possessing large deformations. For such nuclei one may distinguish between intrinsic and rotational excitations. The former involve a change of configuration of individual particles or vibrations of the nuclear shape, the latter correspond to a collective rotational motion of the nucleus with preservation of the intrinsic structure.

Energy Spectra and Effective Moments of Inertia.

If the nuclear shape possesses axial symmetry, as appears to be the case for all strongly deformed nuclei, the component of the total angular momentum along the symmetry axis is a constant of the motion. The corresponding quantum number 'K' is the same for all the members of a rotational band. For $K \neq 1/2$, the rotational excitation energy ΔE_r is given by

$$\Delta E_r = \frac{\hbar^2}{2\,\Im}\left[I\,(I+1) - K\,(K+1)\right], \tag{1}$$

where I is the total nuclear angular momentum and $\Im$ the effective moment of inertia.

Even-even nuclei have $K = 0$ in their ground state and the corresponding rotational band contains the states

$$I = 0,\ 2,\ 4,\ \ldots \text{ even parity.} \tag{2 a}$$

For odd-A nuclei, or odd-odd nuclei, the spin sequence is

$$I = K,\ K+1,\ K+2,\ \ldots \text{ all same parity,} \tag{2 b}$$

and K thus equals the ground state spin I_0.

In the special case of odd-A nuclei with $K = 1/2$, the spin of the last odd particle is partially decoupled from the rotational

motion. The rotational excitation energy then contains an additional term and is given by

$$\Delta E_a = \Delta E_r + a \cdot \frac{\hbar^2}{2\Im} \cdot \left[1 + (-1)^{I+1/2}(I+1/2)\right], \qquad (3)$$

where the decoupling parameter 'a' is related to the wave function for the last odd nucleon by

$$a = -\sum_j (-1)^{j+1/2}(j+1/2) \cdot |c_j|^2. \qquad (4)$$

In this expression, $|c_j|^2$ represents the probability that the particle possesses a total angular momentum j. The decoupling parameter may be positive or negative, and for $|a| > 1$ formula (3) implies level inversions. Thus, a nucleus with $I_0 = 3/2$ could, in principle, have $K = 1/2$ and an anomalous rotational spectrum.

For rotational spectra of the simple type (1), the ratio of the energies of the second and first excited states depends only on I_0 and is, for odd-A nuclei, given by

$$\frac{\Delta E_2}{\Delta E_1} = \frac{2I_0+3}{I_0+1} = \begin{cases} 2.40 & I_0 = 3/2 \\ 2.29 & I_0 = 5/2 \\ 2.22 & I_0 = 7/2. \end{cases} \qquad (5)$$

The separation between rotational and intrinsic motion depends on the smallness of the rotational frequencies as compared with the frequencies of the intrinsic motion. The finiteness of the rotational frequencies thus gives rise to small deviations from the pure rotational spectra. For the strongly deformed nuclei, these deviations from (1) are expected not to exceed one per cent for the lowest rotational states, except in special cases where the rotational motion may be perturbed by a low-lying intrinsic excitation (cf. Ke 1).

The rotational motion of the nucleus is essentially different from that of a rigid body, and may be pictured as a wave travelling around the nuclear surface. The corresponding moment of inertia is appreciably smaller than for rigid rotation and is related to the magnitude of the nuclear deformation. A simple model,

which has been considered, describes the rotational motion in terms of an irrotational flow. For an ellipsoidal nucleus of constant density, one then obtains

$$\Im_{\text{irrot}} = \frac{2}{5} A_2 M_0 (\Delta R)^2, \tag{6}$$

where ΔR is the difference between the major and the minor semi-axis, while A_2 is the nuclear mass number, and M_0 the nucleonic mass.

In a recent more detailed analysis (Bo 2), it has been found, however, that the nuclear shell structure implies deviations from the model of irrotational flow with moments of inertia larger than (6) in magnitude. Empirical data on the relationship between $\Im$ and ΔR may yield information on the 'purity' of the individual particle motion in the nucleus.

Electric Quadrupole Moments and Transition Probabilities.

The reduced transition probabilities B_{E2} for electric quadrupole excitation* are given by the intrinsic quadrupole moment Q_0 through the expressions

$$B_{E2} = \frac{15}{16\pi} e^2 Q_0^2 \frac{I_0}{(I_0+1)(I_0+2)} \qquad I_0 \to I_0 + 1, \tag{7}$$

$$B_{E2} = \frac{15}{8\pi} e^2 Q_0^2 \frac{1}{(2I_0+3)(I_0+2)} \qquad I_0 \to I_0 + 2. \tag{8}$$

The spectroscopically measured quadrupole moment Q is related to Q_0 by

$$Q = \frac{I_0}{I_0+1} \frac{2I_0-1}{2I_0+3} Q_0. \tag{9}$$

These formulae also hold in the case $I_0 = 1/2$.

By comparison with (2), it is seen that such transitions only reach the first excited rotational state in the even-even nuclei, and the first and second in the odd-A nuclei.

* In the present paper, the letter B always denotes the reduced transition probability corresponding to the excitation, and not to the decay.

For a uniformly charged nucleus of spheroidal shape, one has

$$Q_0 = \frac{4}{5} Z_2 R_0 \cdot \Delta R, \tag{10}$$

where $Z_2 e$ is the charge and R_0 the average radius of the nucleus. By eliminating ΔR by means of (6) and putting $R_0 = A_2^{1/3} r_0$, one obtains*

$$\frac{\hbar^2}{2\,\Im_{\text{irrot}}} \cdot Q_0^2 = \frac{4}{5} \frac{Z_2^2}{A_2^{1/3}} \cdot \frac{\hbar^2 \cdot r_0^2}{M_0} \simeq 5 \frac{Z_2^2}{A_2^{1/3}} \text{ keV} \cdot 10^{-48} \text{ cm}^4, \tag{11}$$

which provides a convenient relation for testing the irrotational estimate for $\Im$.

Magnetic Dipole Moments and Transition Probabilities.

The nuclear magnetic moment and the $M1$ transition probabilities between successive rotational states can be expressed in terms of the two gyromagnetic ratios g_K and g_R, of which the first is associated with the intrinsic angular momentum K and the second with the rotational motion.

The ground state magnetic moment is given by

$$\mu = \frac{I_0^2}{I_0 + 1} \cdot g_K + \frac{I_0}{I_0 + 1} \cdot g_R \qquad \text{n. m.}, \tag{12}$$

holding for $K \neq 1/2$. For $K = 1/2$, the moment contains an additional term, similar to that in (3). (Cf., e. g., Ni 1).

For an $M1$ transition from a state I to a state $I + 1$ in a rotational band with $K = I_0 \neq 1/2$, the reduced transition probability is given by

$$B_{M1} = \frac{3}{4\pi} \cdot \left(\frac{e\hbar}{2 M_0 c} \right)^2 \cdot (g_K - g_R)^2 \cdot \frac{I_0^2 \,(I + 1 - I_0)\,(I + 1 + I_0)}{(I + 1)\,(2\,I + 1)}. \tag{13}$$

Thus, from measurements of μ and B_{M1}, one may determine the quantities g_K and g_R. It is of interest to compare g_R with the value

* Here and in the following, we have employed the value $r_0 = 1.20 \cdot 10^{-13}$ cm.

$$(g_R)_{\text{uniform}} = \frac{Z_2}{A_2}, \tag{14}$$

corresponding to a rotational motion of uniformly charged nuclear matter.

For odd-A nuclei, the radiative decay of rotational excitations can be of the mixed $M1 + E2$ type. The mixing ratio is denoted by δ; its square, which gives the ratio of the number of $E2$ gamma quanta to the number of $M1$ quanta emitted in the decay $I + 1 \to I$, is, for $K \neq 1/2$, given by

$$\delta^2 = \frac{3}{20} \frac{1}{I(I+2)} \cdot \left[\frac{(Q_0 \cdot \Delta E) : (\hbar^2/M_0)}{g_K - g_R} \right]^2. \tag{15}$$

With the usual convention (cf., e. g., Bi 1), $(g_K - g_R)$ should be given the same sign as the ratio $Q_0 : \delta$, but if this sign is not known, one can only determine $|g_K - g_R|$.

If one denotes the transitions from the second to the first rotational state by the subscript 21, and those from the first to the ground state by 1, it follows from (15) that

$$\delta_1^2 : \delta_{21}^2 = \left(\frac{\Delta E_1}{\Delta E_{21}} \right)^2 \frac{(I_0 + 1)(I_0 + 3)}{I_0 (I_0 + 2)} = \left\{ \begin{array}{ll} 1.10 & I_0 = 3/2 \\ 1.04 & I_0 = 5/2 \\ 1.02 & I_0 = 7/2 \end{array} \right\} \tag{16}$$

if one inserts the theoretical energy ratios given by (5).

The mixing ratios can either be determined directly from the $K:L$ ratios or from angular correlation measurements. In addition, they can be obtained from the branching ratio of the cascade to cross-over decay of the second rotational state, if that ratio is known for the $E2$ part of the transition. For rotational states, one has for the quadrupole γ-transition probabilities $T_{E2}\{\gamma\}$ the ratio

$$T_{E2}\{\gamma_2\} : T_{E2}\{\gamma_{21}\} = \frac{1}{2} \left(\frac{\Delta E_2}{\Delta E_{21}} \right)^5 \cdot \frac{(2I_0 + 1)(I_0 + 3)}{I_0^2 (2I_0 + 3)}, \tag{17}$$

where subscript 2 denotes the transition from the second rotational state to the ground state. This formula is valid also for $I_0 = 1/2$.

For a rotational spectrum (1), one finds, by means of (5),

$$T_{E2}\{\gamma_2\}:T_{E2}\{\gamma_{21}\} = \left\{\begin{array}{ll} 9.87 & I_0 = 3/2 \\ 5.86 & I_0 = 5/2 \\ 4.21 & I_0 = 7/2\,. \end{array}\right\} \quad (18)$$

B. Internal Conversion.

In order to determine the transition energies from the energies of the electrons ejected from the K, L or M shells of the target atoms by the process of internal conversion, one will of course have to know the corresponding binding energies. We have used the values compiled in the table published by HILL *et al.* (Hi 1). For the L electrons, most weight has been given to the value for the L_I sub-shell in the case of $M1$ transitions, and to the other two sub-shells for $E2$ transitions. The comparison of the values for the transition energy found from the different conversion lines provides a check on the reliability of the energy determinations and shows also whether the transition has been assigned to the right element.

In order to find the total number of nuclei excited in a given state from yield measurements on a conversion line, one will have to know the corresponding decay fraction $\varepsilon\{n\}$, i. e. the fraction of the excitations which de-excite through that particular mode of decay, represented by the principal quantum number 'n' for the atomic shell. If the conversion coefficients $\alpha\{K\}$, $\alpha\{L\}$, $\alpha\{M\}$, etc. are known, one can calculate ε from

$$\varepsilon\{n\} = \frac{\alpha_{M1}\{n\} + \delta^2\alpha_{E2}\{n\}}{\left(1 + \sum_{\nu}\alpha_{M1}\{\nu\}\right) + \delta^2\left(1 + \sum_{\nu}\alpha_{E2}\{\nu\}\right)} \cdot \beta, \quad (19)$$

where β is the branching fraction, i. e. the fraction of the excitations which decays to the final state in question. For the conversion coefficients, we have used the values represented by the curves in Figs. 1 and 2. They are based mainly on the tables of ROSE *et al.* (Ro 1).* In most instances, the conversion coefficients are so large that the K and L conversion lines together

* We are very grateful to Professor ROSE for sending us his results prior to publication.

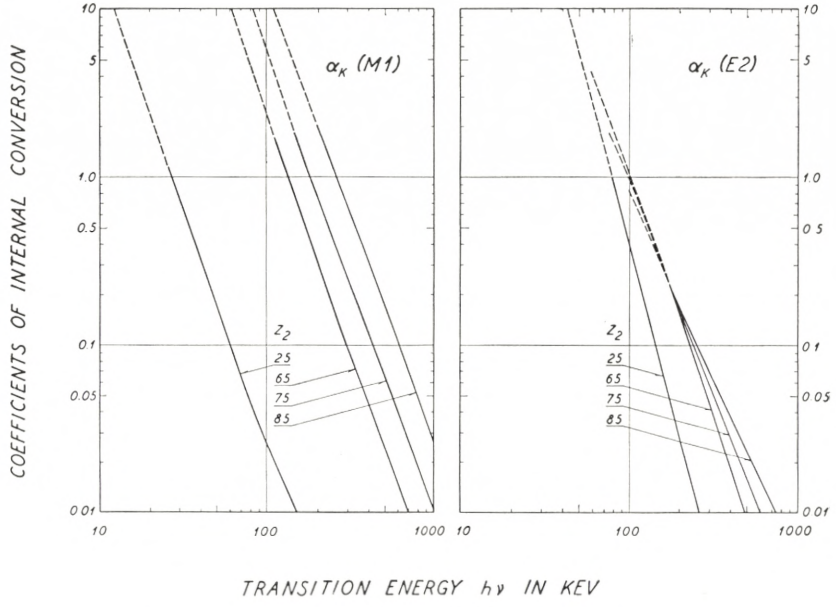

Fig. 1. Internal conversion coefficients for the K shell.* The curves are mainly based on the theoretical results obtained by Rose (Ro 1).

contain the majority of all the decays, which means that $\varepsilon\{K\} + \varepsilon\{L\}$ approaches the value β, almost independent of the conversion coefficients and of δ^2. It is, therefore, important to determine the yield of both these lines or, e. g., the yield of the L line and the $K:L$ ratio.

For the transitions in which a spin change $\Delta I = 2$ is involved, one knows of course that $\delta^2 = \infty$ and, since the $E2$ transitions ordinarily have conversion coefficients corresponding to $K:L < 1$, one can in general obtain a good transition yield determination from the theoretical $K:L$ ratio and measurements on the L line. For the case $\Delta I = 1$, the value of δ^2 is not known a priori, and one will have to measure the $K:L$ ratio also. Thereby one obtains, however, an explicit value of δ^2, since one has

$$\delta^2 = \frac{\alpha_{M1}\{K\}}{\alpha_{E2}\{K\}} \cdot \frac{(L:K)_{\text{obs}} - (L:K)_{M1}}{(L:K)_{E2} - (L:K)_{\text{obs}}}, \tag{20}$$

* Note added in proof. It seems that the finite size of the nucleus gives rise to a significant correction to the $M1$ coefficients which, for $Z_2 \simeq 70$, should be about 25 per cent smaller than given by Fig. 1 (cf. Al 1). The effects on the $K:L$ ratios and the $E2$ coefficients are considerably smaller.

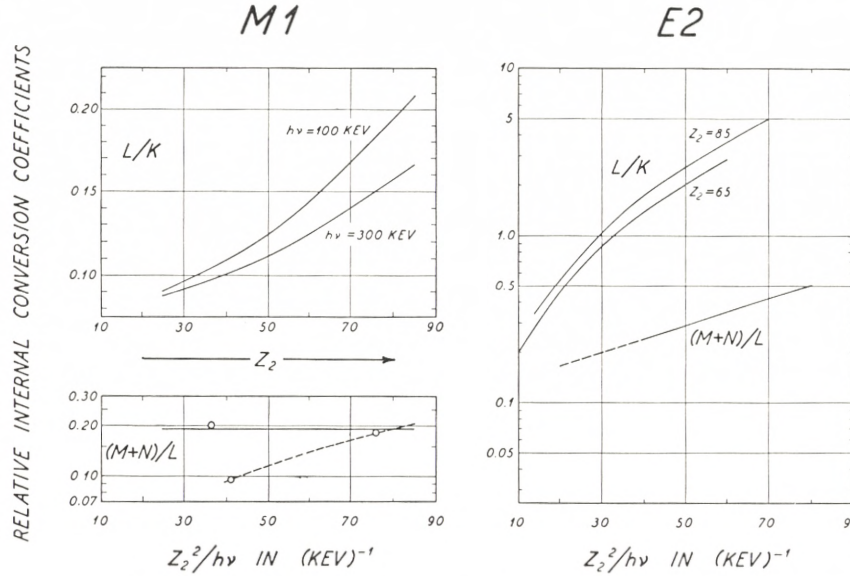

Fig. 2. Semi-empirical ratios for the internal conversion coefficients for the various shells. In the case of the $L:K$ ratios the values are based mainly on the work of Rose (Ro 1)*. For the $M1$ radiation, it should be mentioned that the 500 keV curve is falling in between the 100 keV and 300 keV curves. For the $E2$ radiation, the $Z_2 = 65$ curve is based mainly on empirical data. In the case of the $(M + N):L$ ratios we have taken the values from the paper of H. de Waard (Wa 1), with the exception that, for the $M1$ radiation, we have employed the full drawn curve, which seems as reasonable as the dashed curve given by de Waard.

where $L:K$ stands for the corresponding ratio of the conversion coefficients. In this way, one is able to determine the magnetic matrix element in terms of the quadrupole matrix element. In order to obtain absolute values for these matrix elements from the measured cross sections, the branching fraction β must also be known (cf. (19)). For the first excited state, we have $\beta = 1$, and for the second excited state, the branching can be determined in terms of δ^2 for the mixed transitions, as one has

$$\frac{\beta_{21}}{1-\beta_{21}} = \frac{\beta_{21}}{\beta_2} = \frac{\left(1+\sum_{\nu}\alpha_{M1}\{\nu_{21}\}\right):\delta_{21}^2 + \left(1+\sum_{\nu}\alpha_{E2}\{\nu_{21}\}\right)}{1+\sum_{\nu}\alpha_{E2}\{\nu_2\}} \cdot \frac{T_{E2}\{\gamma_{21}\}}{T_{E2}\{\gamma_2\}}, \quad (21)$$

where $T_{E2}\{\gamma_{21}\}:T_{E2}\{\gamma_2\}$ is given by formula (17) from the theory for the rotational states. If β_{21} is close to unity, the simul-

* Note added in proof. All L shell coefficients have now been computed also for $Z_2 = 55$. For the $E2$ transitions, the $L:K$ ratios come out about 1.5 times smaller than corresponding to the Z_2 dependence indicated in Fig. 2.

taneous measurements on the cascade and the cross-over lines lead to the best determination of $(g_K - g_R)$ through the equation (21), which essentially provides a means of comparing this quantity with the value of Q_0 determined from the excitation of the second excited state. Which way the above formulae are used in the present work depends on the particular example; usually, however, it is most convenient to test the nuclear theory by determining δ^2 from $K:L$ and β from δ^2, and then to check the consistency of the results by comparing the Q_0-values obtained from the excitation of the first and second excited states.

C. Electromagnetic Excitations.

If one bombards nuclei having the charge $Z_2 e$ by projectiles with the charge $Z_1 e$ and an energy E_1 small compared to the Coulomb barrier, i. e.,

$$E_1 < \frac{Z_1 Z_2}{A_2^{1/3}} \cdot \frac{e^2}{r_0}, \tag{22}$$

then the predominant process will be the excitation of the nuclei through the effect of the long range electromagnetic forces. The theory for this process has recently been worked out in great detail by ALDER and WINTHER (Al 2). The total excitation cross sections are given by

$$\sigma_{E\lambda} = \left(\frac{b}{2}\right)^{2-2\lambda} \cdot \frac{B_{E\lambda}}{e^2} \cdot \left(\frac{Z_1 e^2}{\hbar v_i}\right)^2 \cdot \left(\frac{v_f}{v_i}\right)^{2\lambda-2} \cdot f_{E\lambda}\{\xi\} \tag{23}$$

$$\sigma_{M\lambda} = \left(\frac{b}{2}\right)^{2-2\lambda} \cdot \frac{B_{M\lambda}}{e^2} \cdot \left(\frac{Z_1 e^2}{\hbar c}\right)^2 \cdot \left(\frac{v_f}{v_i}\right)^{2\lambda-2} \cdot f_{M\lambda}\{\xi\} \tag{24}$$

$$b = \frac{Z_1 Z_2 e^2}{\frac{1}{2} M v_i^2}; \qquad \xi = \frac{Z_1 Z_2 e^2}{\hbar}\left(\frac{1}{v_f} - \frac{1}{v_i}\right). \tag{25}$$

Here, M means the reduced mass, whereas v_i and v_f are the initial and final relative velocities of the projectiles. The dimensionless functions $f\{\xi\}$ are tabulated in the work of ALDER and WINTHER (Al 2), and the values reproduced here in Fig. 3 for

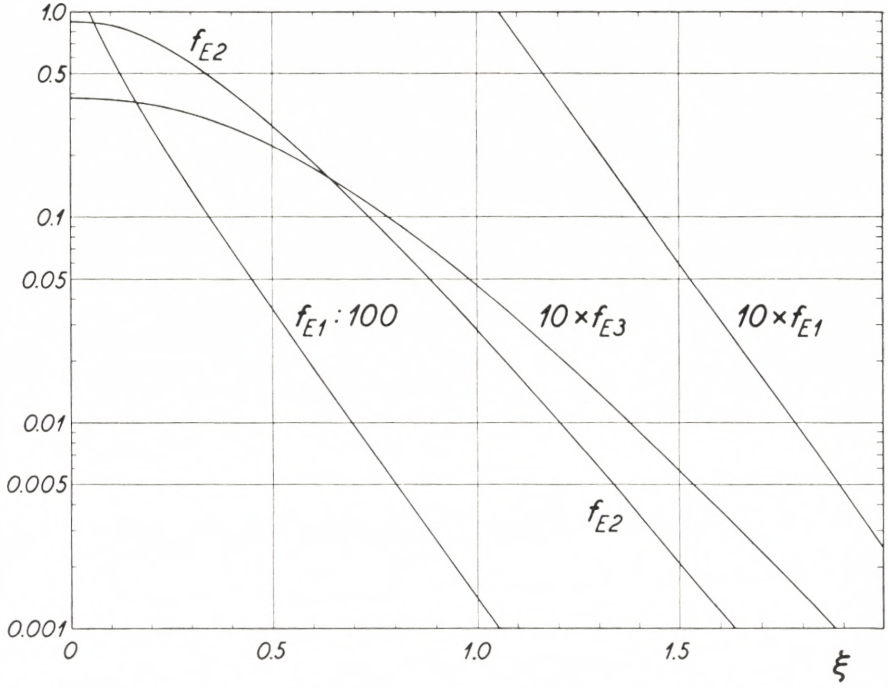

Fig. 3. Curves giving the f-functions defined in the text. The values are taken from the work of ALDER and WINTHER (Al 2).

the electric excitations. The quantities B are the reduced transition probabilities for the excitation.

The collective rotational excitations are of electric quadrupole type. For these, the total cross section can be written in the form

$$\sigma_{E2} = \left(\frac{69.4}{Z_2}\right)^2 \cdot \frac{A_1 (E_1 - \Delta E')}{(1 + A_1 : A_2)^2} \cdot \frac{B_{E2}}{e^2} \cdot f_{E2}\{\xi\} \text{ millibarn}, \quad (26)$$

if one inserts the effective excitation energy $\Delta E'$ and the LAB bombarding energy E_1 in MeV as well as the $B_{E2} : e^2$ in units of 10^{-48} cm^4. The number A_1 here denotes the exact mass of the projectiles in units of the nucleon mass, and $\Delta E'$ is related to the actual excitation energy ΔE by the equation

$$\Delta E' = (1 + A_1 : A_2) \cdot \Delta E. \quad (27)$$

For all types of transitions one has, for the energies in MeV,

$$\xi = \frac{Z_1 A_1^{1/2}}{E_{av}^{3/2}} \cdot \frac{Z_2 \, \Delta E'}{12.65}, \tag{28}$$

where E_{av} is the 'average' bombarding energy defined by

$$E_{av}^{3/2} \equiv \frac{1}{2}\left[\left(1 - \frac{\Delta E'}{E_1}\right)^{1/2} + \left(1 - \frac{\Delta E'}{E_1}\right)\right] \cdot E_1^{3/2} \simeq \left(E_1 - \frac{1}{2}\Delta E'\right)^{3/2}. \tag{29}$$

This means that different projectiles will have very nearly the same ξ-value if only they have bombarding energies in proportion to $Z_1^{2/3} A_1^{1/3}$. Without knowing the value of ΔE, one can therefore determine the multipole order λ of the excitation by comparing the reaction cross sections for bombardments with different particles (Bj 1). With the type of the transition known, one can determine ΔE through the f-function by measuring the excitation function for one kind of particles. Such a procedure may be useful for the interpretation of the results. Combined with measurements where the angular distributions of the emitted radiations have been observed, it allows a rather unambiguous level assignment.

The reduced transition probabilities for the excitations are the same as those for the corresponding de-excitation process, except for a trivial spin weight factor. Their determination from the excitation cross sections is therefore equivalent to measurements of the lifetimes for the decay of the states excited. One has for the transition probability (cf., e. g., Bo 1)

$$T_{E2}\{\gamma\} = 1.23 \cdot 10^{13} \frac{2\,I_0 + 1}{2\,I + 1} \Delta E^5 \frac{B_{E2}}{e^2} \sec^{-1}, \; I \to I_0 \tag{30}$$

if ΔE is inserted in MeV and the $B_{E2}{:}e^2$ for the $E2$ excitation in units of 10^{-48} cm^4. The half-life of the state I is given by

$$\tau_{1/2} = \frac{0.693 \; \varepsilon\{\gamma_{I \to I_0}\}}{(1 + \delta^{-2})\, T_{E2}\{\gamma\}}, \tag{31}$$

where the decay fraction $\varepsilon\{\gamma\}$ for the γ-transition to the ground state of course depends on the mixing ratio δ^2 and the branching fraction β. (Formula (19) can also be used for $\varepsilon\{\gamma\}$ if the α's in the numerator are replaced by unity). It is seen that the con-

version coefficients come in twice when one compares half-lives with excitation cross sections and, for this reason, rather large uncertainties are introduced when these coefficients are only known approximately.

III. Experimental Problems.

A. Calibration of Apparatus.

Two pieces of direct information can immediately be obtained by the detection of a conversion peak in the spectrum of momenta for the electrons emitted from a bombarded target: the energy of the electrons and their rate of production. In the previous chapter, it has been outlined how one can compute the relevant nuclear properties from these data. In the present chapter, we discuss the factors which enter in the determination of the experimental quantities.

The spectrometer which has been used in the present work is shown in Fig. 4. The magnetically analyzed beam of particles accelerated in the 2 MV electrostatic generator (Br 1) enter the spectrometer through the collimator tube C. Each end of this tube is supplied with stops of tungsten foil, both having circular apertures, 2 mm in diameter. They serve to define the position of the beam so that targets placed on the target holder T can be bombarded only on the spot which constitutes the source point for the spectrometer. The collimator tube and the target holder are supported by lucite and given electric potentials of about $+$ 100 volts with respect to the rest of the spectrometer, which is grounded. This is in order to prevent the secondary electrons from seriously distorting the current measurements of the beam integrator. For the same reason, it is necessary to keep the spectrometer chamber under high vacuum by means of a diffusion pump. The target holder can be turned around its axis, allowing up to 12 different targets to be put into the bombarding position.

The fast electrons emitted from the target are analyzed in the magnetic field between the two plane and approximately semicircular pole faces P_1 and P_2, which define a wedge-shaped gap with the axis passing through the source- and focal-points

of the spectrometer. This field has double-focusing properties (Ko 1), viz. in the direction of the field because of the rotational symmetry around the axis, and in the direction of the axis because of the shape of the curves defining the extension of the field where the electrons enter and leave the deflecting region. This type of spectrometer is convenient for the present purpose, because it utilizes a relatively large solid angle and, in addition, permits the source to be 'viewed' easily from the same side as that bombarded.

The number of projectiles scattered from the target and entering through the entrance stop which defines the bunch of electrons accepted by the spectrometer greatly exceeds the number of electrons. A background arises therefore from these heavy particles, if they can reach the counter by one more scattering on the wall of the vacuum chamber. However, in order to trap the majority of them, one only has to place a kind of Venetian blind at the wall opposite to the target and the counter, in the way indicated in the figure. In the few measurements where a crystal and a photomultiplier tube were employed for detection, this system of stops also served to attenuate the effects of stray light. Actually, the bombarded targets often emitted fluorescent light which, e. g., in the case of the various rare earth oxides, was of a very high luminousity and brightly coloured.

In the present investigation, practically all the measurements were made with a Geiger counter as the detector. It had a round window, 7 mm in diameter and covered by a 1 mg/cm^2 mica foil; the limiting stops employed in front of the window were always smaller and had rectangular apertures. The counter cylinder inside the Geiger counter was insulated from the window frame and given a potential of + 100 volts with respect to it. Thereby, the sensitive region of the counter was narrowed, so that a decrease by a factor of three in the efficiency for γ-rays was obtained without changing the efficiency for the electrons which enter through the window.

The current in the magnetizing coils of the spectrometer was used as a measure of the momentum of the electrons focussed on the counter stop. Provided that the current was changed so that it was never decreased and always brought up to the same maximum value before being switched off, the reproducibility

was in general better than $\pm$ 0.5 per cent. The linearity of the scale was checked by measuring the 24.5, 148, and 222 keV conversion lines of the $Th\,(B + C + C'')$ spectrum. The remanence was found to be about 2 per cent of the field corresponding to the 148 keV line. The absolute calibration of the scale was made by frequent measurements on the Coulomb excitation of the 100 keV level in W^{182}. This calibration disagreed about 1 per cent with the ThB measurement. The energy scale used is, however, believed to be correct within about $\pm$ 1 per cent.

The area $P\{n\}$ of a conversion peak 'n' in a spectrum is a measure of the corresponding yield. If the peaks are sharp, one can disregard the back-scattered electrons which will have lost sufficient energy to disappear in the continuous background. The production yield $Y\{n\}$ will thus be given by

$$Y\{n\} = C\{p\} \cdot \frac{P\{n\}}{p} \cdot \frac{z_f \cdot \bar{f}}{\Delta z} \cdot \frac{4\pi}{d\Omega} \cdot \frac{e}{q}, \qquad (32)$$

where the momentum of the conversion electrons is denoted by 'p'. The factor $C\{p\}$ is applied in order to correct for the loss due to the finite probability that the electrons of momentum p cannot penetrate the counter foil. The correction factor used for the 1 mg/cm^2 mica foil is shown in Fig. 5. For the higher momenta, the values are those given by Saxon (Sa 1), whereas the low momentum values have been estimated from measurements on the background electrons (cf. following paragraph). The average dispersion factor $\bar{f}$ was determined from measurements performed with various dimensions of the counter stop; it was found that $\bar{f} \simeq 2.9$ for the electron orbits accepted by the entrance stop shown in Fig. 4. The distance between source and focus was $2\,z_f = 120$ mm and the counter stop generally used had a length of $\Delta z = 3.0$ mm. The effective solid angle $d\Omega$ corresponding to the entrance stop employed was determined by a comparison between the intensity obtained with this stop and that obtained with another stop, which subtended a known solid angle and was so small that no electrons passing through it could get lost in the pole faces or elsewhere. The value found in this way was $d\Omega/4\,\pi = 0.90$ per cent, if one includes also the effect of the

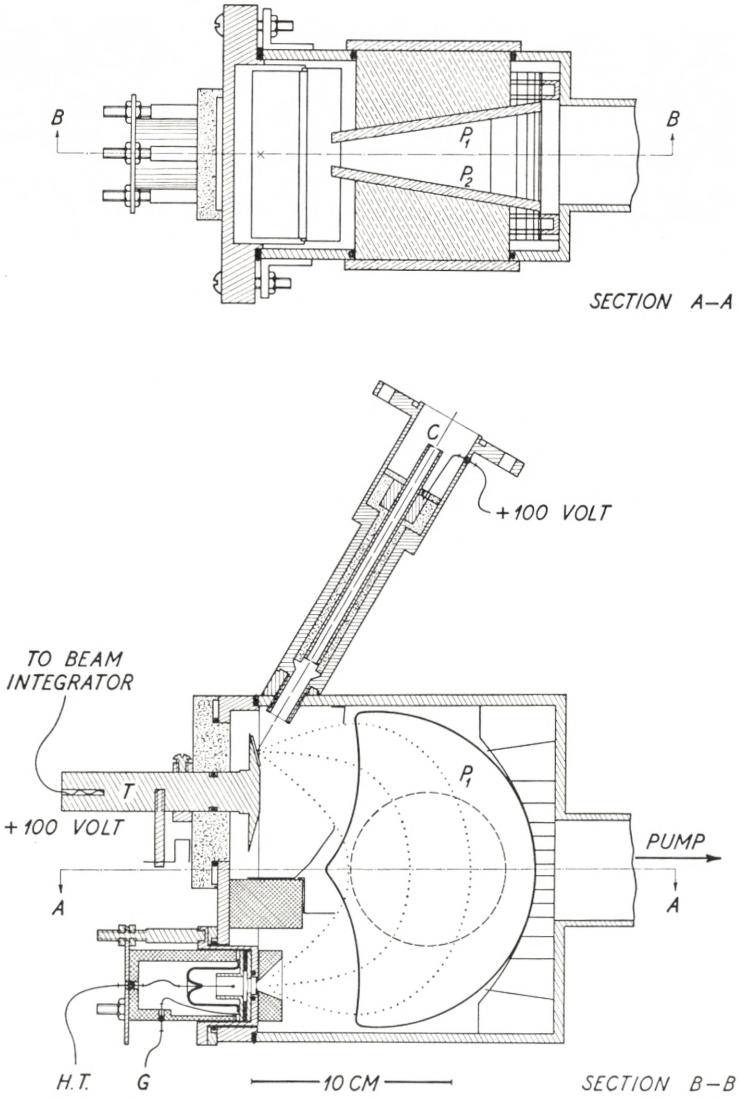

Fig. 4. Beta spectrometer of the wedge-gap type. For a description, confer the text.

finite width of the counter stop, which was $\Delta x = 3.5$ mm. The theoretical angular distributions of the emitted electrons have so far only been evaluated for the K shell (cf. Ro 2, Al 2), and the relatively small effects expected because of anisotropies have therefore been neglected everywhere in the present paper. The last factor in equation (32) contains the total charge 'q' carried

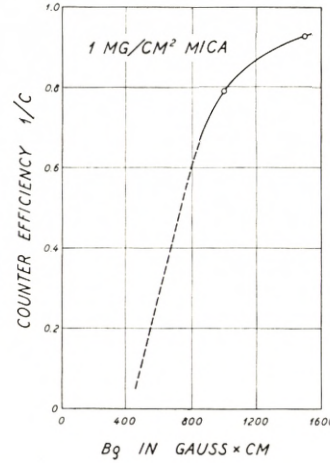

Fig. 5. Counter efficiency of Geiger counter with a 1 mg/cm² mica window. The part of the curve which has been drawn in full is based on the curves given by Saxon (Sa 1). For the extrapolation, confer the text.

by the collected projectiles, and this quantity was measured with a glim-discharge beam integrator, which had proved reliable to within a few per cent.

The Coulomb excitation cross section σ is related to the thin target yield by the equation

$$\sigma \cdot \varepsilon\{n\} = \frac{1}{N} \cdot \frac{d\left(Y\{n\}\right)}{ds}, \tag{33}$$

where $\varepsilon\{n\}$ is the decay fraction (cf. eq. (19)) and N the number of atoms of the kind investigated, which is contained in one cubic centimeter of the target material. The target thickness 's' means the thickness in centimeters measured along the direction of the beam.

In the case of thin targets, it is often more convenient to measure the thickness in mass per unit area. If we denote the thickness, measured in these units and perpendicular to the surface, by 't', then

$$t = s \cdot \varrho \cdot \cos\,\theta, \tag{34}$$

where θ is the angle between the beam and the direction perpendicular to the surface. The specific density ϱ of the target material need not be known when it is the thickness 't' which has been

measured, because in that case only ϱ/N enters in the cross section determination (33). This ratio corresponds to the molecular weight, and is therefore only influenced by the admixture of other atoms in the target, present either in the form of chemical compounds or otherwise.

Direct measurements of 't' by weighing of the targets give only the thicknesses averaged over relative large areas and are, consequently, insensitive to the effects of target inhomogeneities which may have arisen either during the preparation or during the bombardment. As discussed in the last paragraph of this chapter, we have therefore also tried to measure the thicknesses by other means. One method which immediately suggests itself is to employ the background radiation produced in the target atoms (cf. following paragraph).

B. Background Radiation.

In principle, one can reduce as much as wanted background radiations such as that of the scattered projectiles or, e. g., that generated by neutrons in the case of deuteron bombardments. This is not true for the background of electrons produced by the bombardment through direct atomic processes in the target atoms, although the promptness of the ejection of these electrons still provides a means of distinguishing them from the electrons emitted during the more delayed nuclear de-excitation processes (Hu 2). It is therefore important to know in which way the production of these fast stopping electrons is dependent on the experimental conditions.

In the Appendix I, it is shown how one can estimate the probability for the direct ejection of an electron into the continuum with the kinetic energy E_δ by means of a non-relativistic theory neglecting screening effects. To a first approximation, one obtains the following expression for the differential cross section $d\sigma$:

$$\frac{d\sigma}{dE_\delta} \simeq 10^{-18} \cdot Z_1^2 \cdot \left(\frac{E_1}{A_1}\right)^4 \cdot Z_2^4 \cdot \frac{(e^2 \cdot mc^2)^2}{E_\delta^9}, \qquad (35)$$

where the rest energy mc^2 of the electron is introduced for convenience. If one applies the counter foil correction factor (cf.

ref. Sa 1 in the preceding paragraph) to the semi-empirical expression given earlier (Zu 1), one obtains practically the same cross section as that given by the above formula (35). The extrapolated values of the correction factor $C\{p\}$ (cf. Fig. 5) have been obtained from measurements on the stopping electrons, assuming the energy dependence (35) to be valid also at lower electron energies. However, a preliminary measurement, which we have made recently with the Geiger counter replaced by an anthracene scintillation counter, seems to indicate that this procedure leads to reasonable results.

According to formula (35), deuterons should give yields which, under the same conditions, are 16 times smaller than for bombardments with protons. Actually, the yield is found to decrease only by a factor of about 10, but this may not be surprising in view of the experimental uncertainties and the approximations involved in the derivation of the formula (cf. Appendix I). It is nevertheless illustrative for the present purpose to discuss the optimum experimental conditions on the basis of formulae (23), (28), and (35). They imply that the background of stopping electrons depends on the parameters of the bombardment through

$$Z_1^2 \cdot \left(\frac{E_1}{A_1}\right)^4 \simeq \text{const.} \frac{Z_1^{14/3}}{(A_1 \cdot \xi)^{8/3}}. \tag{36}$$

In the case of low-energy conversion lines, where this background will usually be dominant, it obviously is not favourable to go to much higher bombarding energies than those for which the cross sections for Coulomb excitation increase approximately as E_1^4, because then the signal to noise ratio will begin to decrease. For $E2$ excitations, this optimum condition corresponds to $\xi \simeq 0.5$, as is evident from Fig. 6. The equation (36) is a consequence of formula (28) for ξ, which, as mentioned earlier, implies that, in order to obtain a certain ξ-value for a given transition, one will have to employ bombarding energies in proportion to $Z_1^{2/3} A_1^{1/3}$. The maximum signal to noise ratio will thus, for the $E2$ excitations given by (26), be proportional to $(A_1 : Z_1)^4$, which means that deuterons and α-particles should be 16 times better than protons, as far as the influence of the background of stopping electrons is concerned. As mentioned

above, the deuterons are not quite as good as that, and in addition they give the strong 'outer' background due to the neutrons produced (cf. Fig. 10). α-particles will therefore in general be preferable to protons and deuterons in measurements at low electron energies; in addition, at the optimum conditions they have the largest absolute values for the cross sections (cf. Eq. (26)). However, in the search for K-conversion lines, where the corresponding excitation energy is considerably higher than the

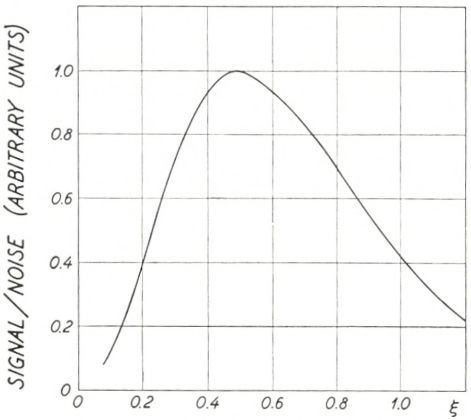

Fig. 6. Relative cross sections for $E2$ Coulomb excitation and the production of stopping electrons, as a function of the bombarding conditions.

electron energy, it often takes a comparatively high bombarding energy to obtain $\xi = 0.5$. The necessary energies are, as shown above, 2.5 times larger for α-particles than for protons, whereas they are only 1.25 times larger for deuterons than for protons. When only a limited acceleration voltage is available it may therefore often occur that the relative smallness of the cross sections then obtainable with α-particles (cf. Eq. (26) or ref. Bj 1) excludes the employment of these projectiles and makes the deuterons best fitted for the purpose.

For the higher electron energies, it will be preferable to bombard with protons and to employ all the acceleration voltage available, since for these electrons the general machine background will usually be more important than the contributions from the stopping electrons. According to equation (26), α-particles can never give $E2$ cross sections more than four times the cross sections corresponding to protons of the same energy,

and as thick targets are preferable here, this advantage will be more than counteracted by the smaller effective target thickness (cf. following paragraph) and the approximately 8 times larger stopping power, which is to be expected for the α-particles.

In order to calculate the thick target yields corresponding to the cross section (35) one must know to what extent the electrons can penetrate the target material. For very thin targets, the yields will of course be proportional to the target thickness, but, as the thickness is increased, the yield of electrons emerging from the surface with a certain energy will increase relatively less. This is due to the fact that the electrons will be scattered and lose energy on their way out of the target, so that those coming from the deeper lying layers will have to be generated with a higher energy, and therefore, according to formula (35), are produced at a much lower rate.

Since the production rate is approximately proportional to E_δ^{-9}, one would expect the effective layer of a thick target to correspond to an energy loss for the electrons of about 10 per cent. However, the scattering of the electrons is so strong in targets of the heavy elements, that their direction of movement is completely changed before they have travelled even this small distance. The way in which the electrons emerge from such targets is thus to some extent similar to a diffusion process. Consequently, the effective target thickness depends most critically on the scattering cross section.

In Appendix II, it is shown that in the diffusion approximation one obtains a yield Y which, for a target thickness t, is related to the corresponding thick target yield Y_∞ by

$$Y \simeq Y_\infty \left[1 - \exp\left\{-t/t_\infty\right\}\right], \tag{37}$$

where the effective thickness t_∞ of the thick target is given by

$$t_\infty \simeq \left(\frac{E_\delta}{50}\right)^2 \text{mg/cm}^2 \tag{38}$$

if one inserts E_δ in keV.* It follows from these equations and from

* The estimate for t_∞ published earlier (Zu 1) does not include the effects of the scattering and is five times larger than (38). However, the neglect of the grain size effect (cf. next paragraph), and an error in the value employed for the dispersion factor practically completely compensated the effect of this overestimate.

(33) — (35) that the thick target yields should be proportional to Z_2^3 in approximate agreement with the experimental findings. We have also checked the above estimates with respect to absolute magnitude, by bombarding silver and gold targets with protons of so high an energy that the thickness (38) can be considered nearly infinitesimal for the projectiles. These elements were

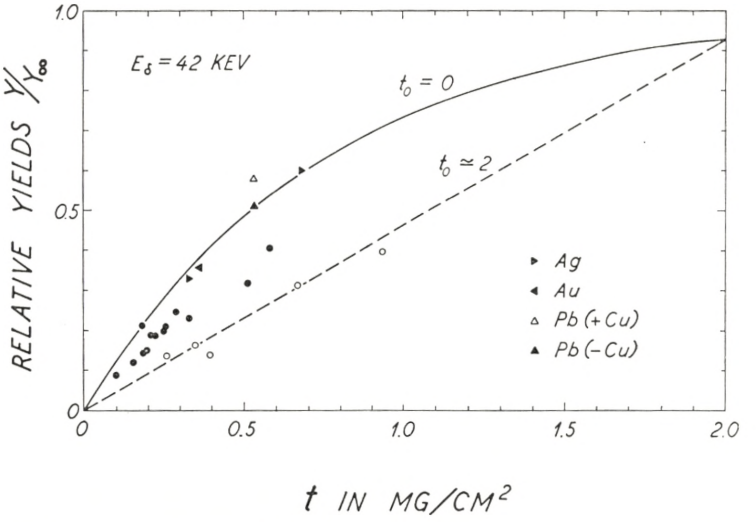

Fig. 7. Thin to thick target yields of stopping electrons emerging from the target surface with an energy of approximately 42 keV. The theoretical variation (37) with the thickness 't' (perpendicular to the surface) of a homogeneous target, is represented by the solid curve. The dashed line indicates the effect of target inhomogeneities corresponding to grain sizes of the order of 2 mg/cm², if 't' is interpreted as the mean thickness. The triangle points correspond to measurements on targets prepared by evaporation; the Ag and Au targets were made on glass, the Pb target on copper. The black circles correspond to measurements on sprayed targets prepared on a support of aluminum; the point on the solid curve corresponds to a target made by means of a particularly thin solution. The open circles correspond to measurements on targets prepared by the suspension method; the yields have been corrected for the contributions from the brass support (cf. the text). For the plotted points, 't' refers to the heavy atoms only.

chosen because they are easy to evaporate onto glass plates in vacuum and give thin targets which are optically homogeneous. The thicknesses were determined by weighing. The result of the comparison is shown in Fig. 7. In view of the approximations involved one would be inclined to consider the good agreement somewhat accidental.

In cases where oxide targets of the type X_2O_3 are used, one

would expect t_∞ to be about 10 per cent smaller than given by (38), so that the thick target yields should be about 80 per cent of the values for the pure targets.

C. Target Preparation and Thickness Determination.

The amounts of the rare earth oxides which were available to us for the target preparation, at the beginning of the present investigation, were in most of the cases only of the order of 10 mg. Attempts to prepare the targets by letting solutions of the materials dry out were not successful; the compounds became deposited as crystals when the evaporation of the liquid was slow, and in very uneven layers when the evaporation was speeded up by heating. Instead, we therefore employed the following more simple technique. We made a suspension of the fine oxide powder in alcohol and allowed proper amounts of it to dry out slowly on small brass disks, which had been pressed down in holes made in a thick rubber plate. Such targets appeared to give relatively reproducible results, but they were certainly not ideally suited for the measurements, especially in view of the effect of the grain size of the oxide powders.

It did not seem likely that reliable thickness determinations could be obtained by means of weighing, since the bombarded area often looked rather damaged when the targets were taken out of the spectrometer after the bombardment. The continuous background of the stopping electrons measured nearly simultaneously with the conversion lines appeared to offer a better measure for the thickness of the targets in the region actually bombarded in the experiment. However, in the beginning we did not realize how important the scattering of the electrons was for the determination of the effective target thickness (38), which we overestimated by a factor of about 5 (cf. Zu 1). Consequently, we ignored the significance of the grain size, and it was only from a closer examination of the continuous background in the measured spectra that it became clear that this was not justified.

The relatively slow variation of $Y : Y_\infty$ as a function of the electron energy, which was found even for small values of this ratio, indicated that the grain sizes were in general comparable

to t_∞ for electron energies as high as 50 keV. A similar behaviour was found for some of the pure metallic targets of, e. g., Ta and W, which had been prepared by evaporation in vacuum and visually showed a clear crystalline structure. For a calibration, it would therefore not be correct to employ the curve in Fig. 7, which corresponds to the homogeneous targets. If one were to idealize the grains as chips of a constant thickness t_0 mg/cm^2 which are not overlapping, then the relative yields would be related linearily to the average thickness $t \leqslant t_0$ in the way indicated by the dashed line in Fig. 7 for the case $t_0 = 2$ mg/cm^2. Investigations of the targets in a microscope showed that the grain sizes were of the general order of 3 microns for the oxides used, corresponding to a diameter of about 2 mg/cm^2, and thus somewhat larger than the estimates derived from (38) and the relative yield dependence.

As long as better targets were not available, we therefore considered it the best compromise to estimate their thicknesses by employing a calibration curve somewhere in between the two curves shown in Fig. 7. In the calculations we first subtracted the full yield of stopping electrons measured for the bare brass support, since this should be correct for the very thin targets, and give errors of only minor importance for the thicker ones. The transition probabilities arrived at in this way could, however, not be expected to be reliable to more than about a factor of 1.5.

Recently, larger samples of most of the rare earth oxides have been put at our disposal by courtesy of Professor Spedding and the Iowa State College.* It has thereby been possible to produce more stable and homogeneous targets, in particular by employing the technique of spraying the dissolved material onto a hot surface.

When preparing the targets by this method we proceeded in the following way. First, a small amount of the oxide powder was dissolved in a few drops of pure concentrated nitric acid which was then heated until only the rare earth nitrate was left. This compound was dissolved in distilled water and put into the bottle of a commercial perfume atomizer, which was adjusted to give the finest possible spray when operated by means of clean compressed

* We are very grateful to Professor Spedding for the great improvement of the measurements, which has been possible in this way.

air. The solution was then sprayed onto the hot surface of a small polished disk of either brass or aluminum, in small bursts of duration of less than a second.

The temperature of the disk is rather critical and should usually be about 300° C. Also the concentration of the solution seemed to be of great importance. With a concentration of about 1 mg per 10 cm^3 of water it was possible to produce rather homogeneous targets on brass supports, but with an efficiency of only about 10 per cent. When such thin solutions were employed with aluminum as the support, we usually did not succeed in making the material condense on the polished surfaces. In these cases, we had to use concentrations of the order of 1 mg per cm^3, which gave rather good efficiencies but, on the other hand, also a somewhat poorer homogeneity. After having finished the spraying we heated the targets to approximately 500° C in order to decompose all the nitrate to the oxide. The targets produced in this way were very stable and usually sufficiently homogeneous within areas of the order of 10 mm^2.

In this manner, we first made a thin target of Yb_2O_3 on a support of brass, which had been covered with a very thin layer of aluminum, so that the target thickness could be determined through a measurement of the energy shift of one of the well-known Al^{27} (p, γ) resonances (the so-called sandwich method). The cross sections for Coulomb excitation, which were found by means of such a thickness calibration, were about three times smaller than the values found previously, and even smaller than those corresponding to the thickness found directly by means of weighing. The latter thickness was, moreover, considerably larger than that determined from the yield of the background electrons by means of the curve in Fig. 7 corresponding to homogeneous targets. These facts indicated that the target did not consist of the pure oxide, but that, in addition, it contained large amounts of light atoms.

It was therefore clear that a method was needed, by which one could determine the number of heavy atoms per unit area independently of the inhomogeneity and composition of the targets. Fortunately, this demand can easily be met through measurements on the spectrum of the elastically scattered projectiles. These particles can penetrate the target layers with energy

losses which are smaller than the energies transferred to the recoils in the collisions with the light atoms. The peak, which in the spectrum of the scattered particles corresponds to the collisions with the heavy atoms, will therefore fall in a region above that in which the contributions from the light atoms are found. Moreover, it will be by far the strongest peak in the spectrum, since the cross section for Rutherford scattering increases as the square of the charge.

We therefore decided to set up a heavy particle spectrometer, which could view the bombarded targets through the pumping tube shown in Fig. 4. The direction of observation formed an angle of 104° with respect to the beam. The spectrometer consists of a 90° deflection magnet with a radius of 42.5 cm. The entrance stop was 2.5 mm in diameter and the distance between this stop and the target 104 cm. The exit slit was placed just outside the end of the plane pole shoes, and was adjusted to a width of 0.85 mm. The particles were detected by means of an anthracene crystal counter. The homogeneous magnetic field was generated by means of permanent magnets, which were magnetized corresponding to an energy of about 1.7 MeV for the protons accepted by the spectrometer. The so-called profile curves were then measured by varying the bombarding energy instead of the spectrometer setting.

An example of a profile curve measured for a thin target of Gd_2O_3 on a support of aluminum is shown in Fig. 8 together with the profile measured for a thick metallic W target. A thick Gd_2O_3 target would have given a yield approximately 50 per cent smaller than that of the thick W target, and the figure therefore shows that the sprayed target gives a maximum yield which is only about half of what it should have been. This clearly demonstrates that the sprayed target is either inhomogeneous, or it contains a large amount of light atoms. A similar result was obtained with the above mentioned Yb_2O_3 target, except for the fact that the profile curve in this case did not go down to zero at the higher bombarding energies. The reason is that in this region the scattering from the brass support gives a contribution which overlaps the peak corresponding to the collisions with the heavy atoms, as a consequence of straggling effects in the target. By means of the profile curve, it was possible to explain

the discrepancies between the previously mentioned thickness determinations for the target as being due to an admixture of larger amounts of light atoms.

It thus appears that thickness calibrations by means of the background electrons are unreliable when the targets are strongly inhomogeneous, whereas the admixture of lighter atoms is of minor importance because they do not contribute very much to

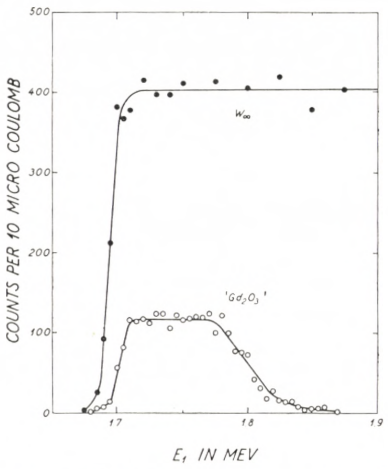

Fig. 8. Profile curves for a thick W target and a sprayed target of Gd_2O_3 (on Al), obtained by measuring the yield of elastically scattered protons as a function of the bombarding energy E_1. The thin target contained 0.26 mg Gd per cm².

either the production or the scattering of the δ-rays. When the thicknesses are determined by the sandwich method or directly by weighing, the situation is the opposite. Here the inhomogeneities are not so dangereous, whereas lack of knowledge about the composition of the target may give rise to larger errors.

The method employing the profile curves should be very reliable, particularly if one uses a light element like aluminum as support. From the measured profiles one can compute the thicknesses in the following way. The peak measured for a pure and homogeneous thin target (such as, e. g., the evaporated Au target mentioned earlier) reaches the thick target yield, and one can determine the thickness directly from the measured half-width when the stopping power of the material is known. As a consequence of inhomogeneities and light element im-

purities the peak will, as we have seen above, be smeared out to a lower and broader one, but in such a way that its area does not change. One can therefore easily determine the half-width which would have been found if the target had been pure and homogeneous; all one has to know is the thick target yield for the pure element. These yields were obtained by extrapolating as $Z_2^{3/2}$ from that found, e. g., for the thick W target, since this dependence is in accordance with both theory and experiment. The accuracy in the thickness determinations by means of this method is therefore only dependent on the energy scale for the accelerated particles, on the relative yields of thin to thick targets, and on the stopping power for the projectiles.

The largest errors are probably introduced through the stopping powers employed. We have used values 10 per cent higher than those obtained from the semi-empirical expression given by C. B. Madsen (Ma 2), since this seems to be in better accordance with the latest experiments. For 1.7 MeV protons on W, the value employed is approximately 50 keV per mg/cm^2. By means of this stopping power we compute for the scattering a theoretical thick target yield which is only about 10 per cent larger than found experimentally. However, the measured yields showed a dependence on the way in which the beam came through the stops of the collimator tube (*C* in Fig. 4), and the absolute yields are therefore not so reliable. For the thickness determination this is of minor importance, since the measured yields were always immediately compared with the thick W yield measured under the same conditions. For the present purpose, the errors in the calibration of the scale of the voltmeter of the electrostatic generator are of no importance.

We repeated the measurements of most of the main conversion lines found in the old thin target experiments with new targets made by spraying the more concentrated of the above mentioned solutions onto 0.5 mm thick disks of aluminum. The yields of background electrons from these targets relative to the corresponding pure thick target yields obtained from interpolations have been compared with the thicknesses determined from the respective profile curves. The result is shown in Fig. 7 and indicates that the new targets were also somewhat inhomogeneous. Comparison between the yield of conversion electrons found in the old and new measurements, respectively, made it possible

to calculate the true average thickness for the old targets, which it was not possible to measure directly because of the fact that they were very inhomogeneous and made on a support of brass. The results obtained for the even elements are shown in Fig. 7. They seem to indicate that the grain diameters in the old targets were of the order of 2 mg/cm^2, in agreement with the microscopic evidence.

For some of the elements, the energies of the conversion electrons are large enough to permit the use of targets which are thick compared to the range of the bombarding particles. In order to determine a nuclear cross section σ from the corresponding thick target yield, it is in general necessary to measure the dependence of this yield on the bombarding energy E_0. However, the absolute value of $\sigma\{E_0\}$ can also be found from a single thick target yield measurement if the relative variation of the cross section is known, so that the theoretical ratio between the thick and thin target yields can be computed. This is the case for the Coulomb excitations, where σ is expected to have the dependences given by equations (23).

For the present purpose, it is therefore convenient to express the thick target yield in terms of an effective target thickness dE_λ, which is measured in energy units and defined in such a way that equation (33) gives the correct value for the cross section corresponding to the energy E_0, if one makes the substitution

$$\frac{d\{Y\{n\}\}}{ds} \rightarrow \frac{Y\{n\}}{dE_\lambda} \cdot \frac{dE}{ds} \tag{39}$$

with all the quantities on the right-hand side taken at the energy E_0.

For bombarding energies in the region of interest for Coulomb excitation experiments, it seems that the stopping power dE/ds of almost all substances follows an energy dependence approximately proportional to the inverse square root of the energy of the projectiles (cf. Ma 2, Li 1). Employing such a relation one obtains, from (23), the effective target thickness

$$dE_\lambda = \frac{2}{3} E_0 \frac{\xi_0^{\frac{4\lambda}{3}-1}}{f_{E\lambda}\{\xi_0\}} \cdot \int_{\xi_0}^{\infty} \frac{f_{E\lambda}\{\xi\}}{\xi^{\frac{4\lambda}{3}}} d\xi, \tag{40}$$

where ξ_0 is the ξ-value (28) appropriate for the bombarding energy E_0. The values of dE_λ calculated from (40) are plotted in Fig. 9; they are rather insensitive to changes in the assumed energy dependence of the stopping power.

In the evaluation of the Coulomb excitation cross sections, we have employed the thicknesses given in the third column of Table I. The values have been determined in one of the ways

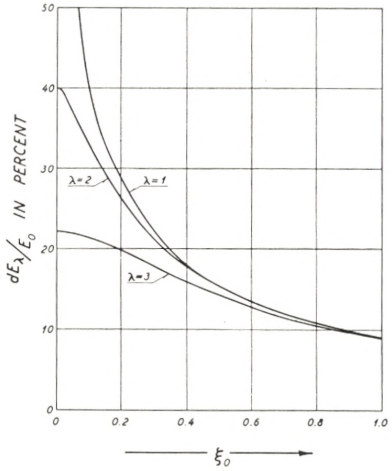

Fig. 9. Effective target thicknesses for $E\lambda$ Coulomb excitations, as defined by equation (40). The stopping power has been assumed to depend on the energy of the projectiles as $E^{-1/2}$, but the curves are rather independent of this assumption. The changes would be the largest for the small ξ_0-values, but even the assumption of an energy-independent stopping power would only increase the value for $\lambda = 2$ and $\xi_0 = 0$ from the 40 per cent given in the figure to a value of 50 per cent.

described above. The two methods with the profile curves and with the thick targets have been used in the majority of the cases and are the only ones which are expected to give reliable results.

IV. Results.

About three fifths of the elements with an odd number of protons have just one stable isotope, and the rest have no more than two. The results obtained with natural samples of these elements are therefore relatively simple to interpret. With five exceptions, of which only $_{71}Lu^{176}$ has a significant abundance

(2.6 per cent), all naturally occurring nuclides with an odd $Z \geqslant 9$ have an even number of neutrons and thus $I_0 \neq 0$. According to the considerations in Chapter II, one can therefore in general expect to excite the first two rotational states by the bombardment of these nuclides, and, in favourable instances, one should be able to detect three sets of conversion lines. It is of particular interest here to know the $K:L$ ratios of the $\Delta I = 1$

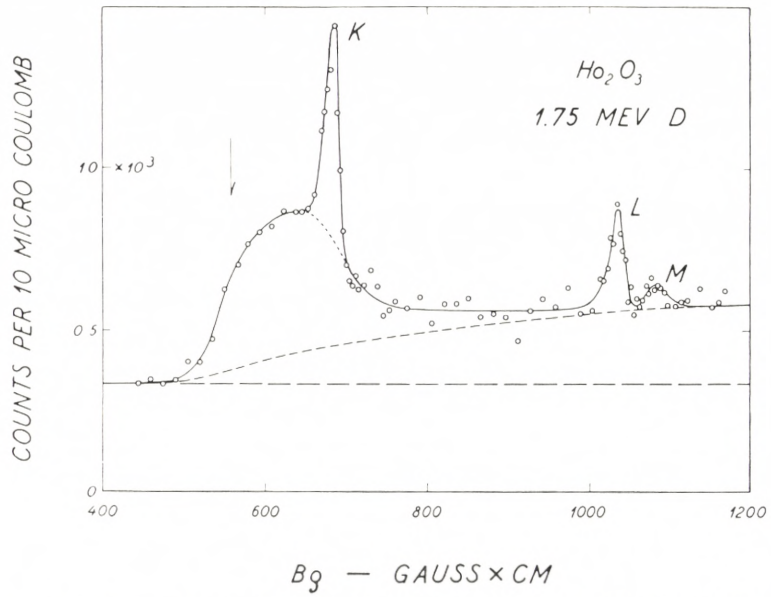

Fig. 10. Spectrum of internal conversion electrons from the K, L, and M shells of $_{67}Ho^{165}$ corresponding to the decay of the first rotational state. The excitations were produced by means of bombardment with 1.75 MeV deuterons, and the target contained 0.22 mg Ho per cm². The background consists of three parts. The first is field-independent and probably mainly produced by neutrons; the second is due to β-activities induced in light elements present in the target, and the third comes from the stopping electrons ejected from the holmium atoms (dotted peak). The latter two are cut-off at approximately 600 Gauss-cm, as an effect of the 1 mg/cm² mica foil covering the counter window.

decays, where the radiations will be of the mixed $M1$ and $E2$ type. As discussed earlier, under the present conditions, it is often easier to measure the K lines corresponding to the decays of the first rotational states, if one produces the excitations by means of bombardments with deuterons.

An example of a spectrum obtained with 1.75 MeV deuterons is shown in Fig. 10. Only one set of conversion lines is visible on

the spectrum; they correspond to the first excited state of the nuclide $_{67}Ho^{165}$, which has an isotope abundance of 100 per cent. The measured points scatter relatively much, because the deuterons induce a strong background of penetrating radiation (cf. Fig. 10), which fluctuates with the performance of the accelerator. The deuteron bombardments also produce β-activities in light atoms present in the targets and their supports. For this reason, the use of graphite or aluminum as support materials was excluded, and all the deuteron measurements have been carried out with targets prepared on a brass backing. On the other hand, it is also evident from Fig. 10 that the background of stopping electrons, to which the deuterons give rise, is sufficiently reduced to allow a relatively good measurement of the K peak; with proton bombardments, this peak only appeared as a hump on a much stronger background of stopping electrons.

Just as for Ho, most of the other odd-Z elements investigated proved to have first excited states which decayed predominantly through K conversion as a consequence of large $M1$ transition probabilities. For these elements, the measured excitation cross sections are not so reliable, since the determinations of the K line yields are rather dependent on the applied counter foil correction and the background conditions. For some of them, it was necessary to determine the K conversion yields from the measured L lines by employing K:L ratios known from other sources. For the even-even nuclides the situation is more favourable, since here the K lines are of relatively less importance.

The elements with an even Z often have three or more isotopes which are stable and comparatively abundant. Most frequently the mass numbers A are then also even and the ground state spin, consequently, $I_0 = 0$. For these nuclei, one cannot reach more than the first rotational state by an $E2$ excitation (cf. Chapt. II), and the decay will also have to be a pure $E2$ transition. Consequently the amount of K conversion is known theoretically (cf. Fig. 1), and since the coefficients in general are smaller than for the L shell, one can obtain rather reliable excitation cross sections from the measured L peaks, even if the K peaks are not measurable because of the background conditions.

Fig. 11 shows the spectrum of the L and M $(+N)$ peaks

measured for Er, where the first excited states of most of the even-even isotopes practically coincide. Another example, where this is not the case, is shown in Fig. 12. These two examples are typical of the even-Z elements also in that rather abundant odd-A isotopes are present in the natural samples. The L lines from the first rotational states of these isotopes will probably fall in the neighbourhood of those of the even ones. They will, however, be

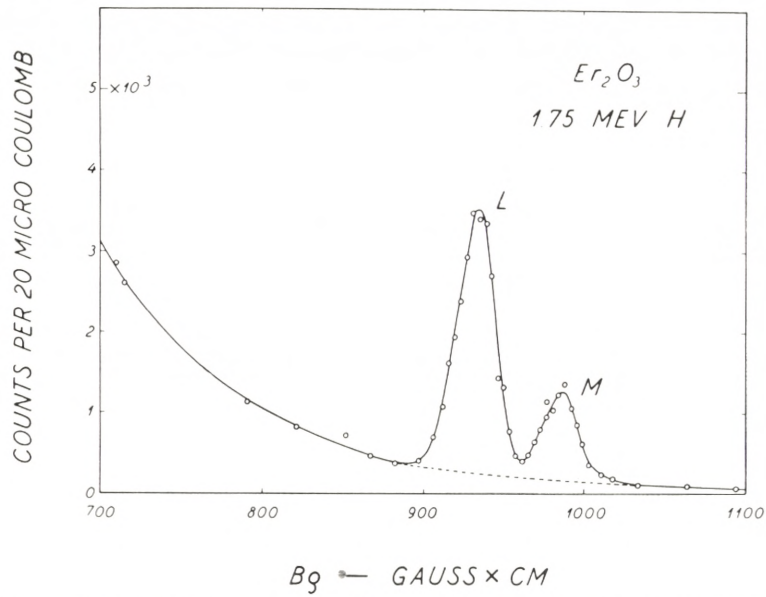

Fig. 11. The L and M (+ N) conversion peaks obtained by a 1.75 MeV proton bombardment of a target which contained 0.33 mg Er per cm². The transitions are assigned to the first excited states of the even erbium isotopes, which are supposed to have practically coincident excitation energies. The background is due to stopping electrons.

difficult to observe because of their relatively small intensities, which are a consequence partly of the smaller L conversion of the mixed transitions, and partly of the difference in the spin-weight factors appearing in the equations (7) and (8). Because of the comparatively small abundances it is also difficult to observe the very low lying K lines, and we have therefore in general disregarded the contributions from such isotopes. The situation may be different for elements such as W, where the odd isotope has a ground state spin $I_0 = 1/2$ and thus a rotational spectrum of the anomalous type (3).

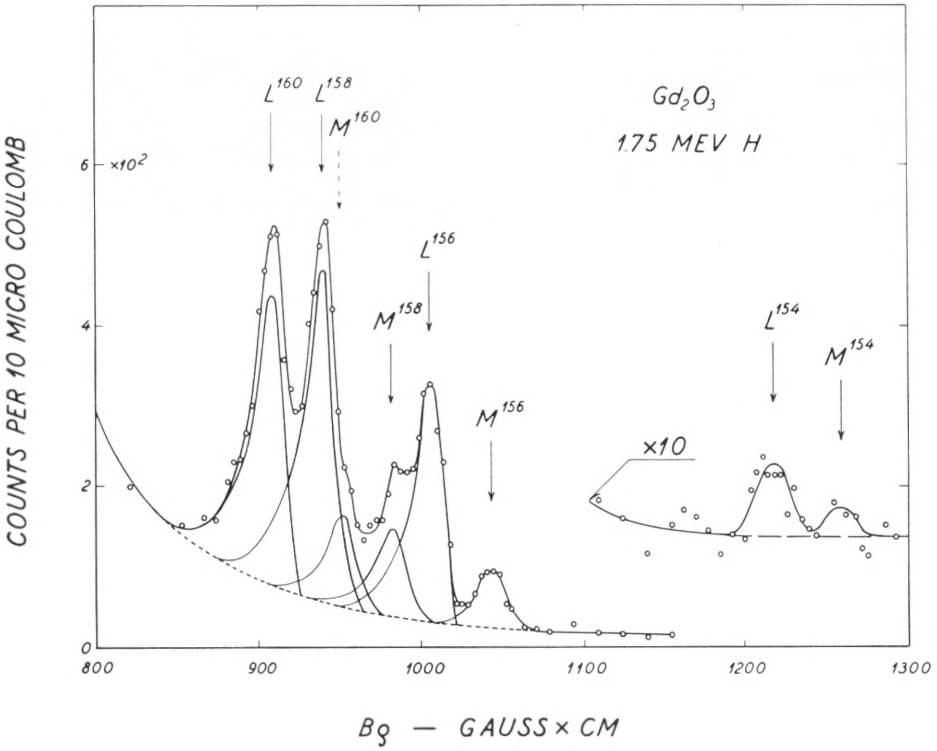

Fig. 12. Spectrum of conversion lines obtained by proton bombardment of a target which contained 0.26 mg Gd per cm². The peaks drawn indicate the contributions from the various isotopes, as assigned on the basis of the energy systematics (cf. the text).

Additional examples of the spectra discussed below are reproduced in previous publications (Hu 3, Bj 1).

In the Tables I and II, we have summarized the results which we have obtained so far from our investigations of a number of elements. In general, the spectra were only scanned for electron energies below 170 keV. The conversion lines found in the experiments have been assigned to the atomic shells of the various isotopes on the basis of the general systematics (cf., e. g., Bo 1), as well as by comparison with the information available from other experiments (cf., e. g., He 1, Mc 1, St 1, and Ho 1). From the measured peak areas we have computed the corresponding B-values by employing the natural isotope abundances given in the paper by HOLLANDER *et al.* (Ho 1). It has been assumed that all the excitations are of the $E2$ type, and that

the decays correspond to pure $E2$ transitions for the even-even nuclei, and mixed $M1 + E2$ transitions for the odd ones. In the following, we shall briefly comment on the transition energies and probabilities given in the tables. Our data can be compared with the results of the γ-measurements made by other investigators, but, in the present paper, we will only make a few remarks on those occasions in which major discrepancies are found. For a more detailed comparison between the various experimental results, the reader is referred to a forthcoming review article (Al 1).

---

25. MANGANESE. The thick target employed had been prepared by electro-plating. The surface was coloured and looked as if the manganese were covered with some sort of deposit; this may possibly imply that the value given in Table II for the excitation energy is somewhat too low. The main purpose of our Mn measurement was to demonstrate the extent to which the method of detecting the conversion electrons could be employed for lighter elements, and this element was known to have a large excitation cross section. Other investigators (Ma 1, Te 1) have measured a value of $0.07 \cdot 10^{-48}$ cm^4 for $\varepsilon \{\gamma_1\} B{:}e^2$, which, compared with the present result, indicates that the decay is a rather pure $M1$ transition. Thus, a $Q_0 \simeq 1$ barn would be found if the excitations were interpreted as rotational.

26. IRON. A thick target consisting of iron enriched about 20 times in Fe^{57} was employed for the measurements. We found two lines which we assigned to this isotope because of the good agreement with the conversion lines seen in the decay of $_{27}Co^{57}$ (cf. Al 3). Due to the 50 per cent content of other Fe-isotopes in the target, the signal to noise ratio was comparatively small, and the $L + M$ lines were not measurable. However, the $K{:}L$ ratio is not either a good measure of the mixing, since it is about equal for the $M1$ and $E2$ transitions in this region. The multipolarity can be determined much better from the α_K coefficients (cf. Al 3), which show that the 122 keV decay corresponds to a nearly pure $M1$ transition, whereas the 137 keV decay is of the $E2$ type. From the measured partial B-values one

can therefore determine the branching fractions, β, for the transitions to the ground state and to the first excited state at about 14 keV, respectively, as well as the total B-value for the second excited state. The multipolarities found for the transitions evidently conform with those corresponding to a normal rotational spin sequence 1/2, 3/2, 5/2, for which the data would yield the Q_0-value given in Table II.

47. SILVER. The K lines corresponding to the lowest collective excitation in each isotope could barely be measured, and those corresponding to the cross-over and stop-over transitions from the next collective state around 410 keV were not detectable. Large uncertainties must be ascribed to the total B-values obtained. More reliable results can be derived from the γ-ray measurements (cf. He 2, St 1, Mc 2). The level schemes for the silver isotopes have been discussed briefly elsewhere (Hu 2) on the assumption that the excitations may be described in terms of rotational states.

58. CERIUM. No lines were found in the investigation.

59. PRASEODYMIUM. No lines were found in the investigation.

60. NEODYMIUM. The two weak lines found were assigned to a low-lying first excited state in the heavy isotope Nd^{150}, which has an abundance of less than 6 per cent. The assignment was made because it was known that the higher mass numbers in this region correspond to the lower excitation energies (Bo 1). Recent γ-measurements on separated targets (He 1, Si 1) show that the assignment is correct and that the estimated B-values are approximately right. In the case of Nd, the measurements have not been repeated with sprayed targets, while this has been done for all the following elements of the rare earths.

62. SAMARIUM. With this element the region of strongly deformed nuclei is approached and the excitation cross sections become correspondingly large. Unfortunately, the K_1 line of Sm^{152} appears to coincide with an L_1 line of Sm^{154}. The yield of the composite peak depends on the bombarding energy in a way which indicates that most of it is due to L conversions. The fraction which corresponds to K conversion has been estimated

from the yield of the L_1 line of Sm^{152} by means of the $K:L$ ratios given in Fig. 2. In the same way we can then calculate the yield which should be expected for the K_1 line of Sm^{154}. However, the energy for these electrons is only about 36 keV and they are therefore difficult to observe. Deuteron measurements made at an early stage did not give any clear evidence for the expected peak. From our data we estimate partial B-values for γ-emission, which are 0.7 and 2.0 times those obtained for Sm^{152} and Sm^{154}, respectively, through direct measurements of the emitted γ-rays (He 1).

63. EUROPIUM. The two most important peaks in the spectrum were interpreted as the L_1 and K_2 lines of the 52 per cent abundant isotope Eu^{153}, because the other stable isotope Eu^{151} has less than 90 neutrons and is therefore expected to have appreciably higher excitation energies (cf. Bo 1); that this is the correct interpretation follows moreover from recent γ-coincidence measurements and β-decay evidence (cf. He 1, Ma 3). Thus, we obtain a value of 2.30 for the ratio between the excitation energies of the second and first excited states, in good agreement with the value corresponding to rotational excitations of a nucleus with $I_0 = 5/2$ (cf. Eq. (5)). Our absolute values for the excitation energies seem, however, to be somewhat higher than found in the γ-ray measurements. Our earlier deuteron measurements indicate that $K:L \sim 1$ for the decay of the first excited state, and with this value for the ratio B-values consistent with the nuclear theory are obtained by means of the formulae (16) to (21). Although the indications of a peak corresponding to the expected stop-over L_{21} line also fits into the picture, it is still only a very crude determination of the $M1$ contributions, as the yield of the weak K_2 line is rather uncertain. However, the fact that this line is observed shows clearly that the $M1$ transition probabilities must be relatively small. Comparison with the partial B-value found for the corresponding γ-ray (He 1) indicates that the cross-over transitions should actually be even stronger than we have found.

64. GADOLINIUM. Evidently there is some ambiguity in the way in which the yield corresponding to the large group of peaks in Fig. 12 has been divided among the various L and M

lines, which are only partly resolved from each other. On the whole, the curves shown correspond to $(M+N):L$ ratios which are somewhat lower than those given in Fig. 2. However, the computed B-values agree well with the recent results obtained from γ-measurements (He 1), except for the isolated, but very weak $L_1{}^{154}$ line. From our data we estimate a partial B-value for the γ-emission corresponding to this line, which is about 1.8 times smaller than that found directly. Higher energy radiations from the odd Gd-isotopes have been observed in the same γ-experiments, but with the yields reported, we would not be able to detect the corresponding conversion lines. (Cf. also the discussion in the beginning of the present chapter).

65. TERBIUM. The only terbium line which could be detected with certainty was the L_1 line at 49 keV. From the yield of this line alone it is not possible to determine the total B-value, as it does not give the magnitude of the mixing ratio. However, on the basis of the rotational description, one would expect the nucleus to have a second excited state at approximately 139 keV (cf. Eq. (5)), and the fact that the corresponding transitions to the ground state did not give any detectable conversion lines, implies that the cascade transitions must be the strongest, and thus predominantly of the $M1$ type. We find that more than 80 per cent, and probably as much as 90 per cent, of the L_1 peak must be due to $M1$ transitions. Consequently, it ought to be possible to detect the cascade lines, even though the background is higher at the lower energies; unfortunately, however, all the terbium samples available were more or less contaminated with dysprosium, and the comparatively strong lines from this element concealed the presence of the stop-over lines. However, the data seem consistent with the mentioned degree of mixing. Recently, HEYDENBURG and TEMMER (He 1) have succeeded in measuring the γ-rays from the cross-over transitions. They find an energy of 136 keV and a yield which is about 1.6 times larger than that which we estimate on the basis of the above assumption.

66. DYSPROSIUM. The two strong transitions observed are assigned to the two most abundant even isotopes on the basis of the energy systematics found in this region of the elements.

From the data we estimate partial B-values for γ-emission which are about 1.5 times larger than the values measured directly (He 1). From the arguments given in the introduction to this chapter it is not expected that the odd Dy isotopes would give rise to any measurable intensities, and no lines corresponding to these nuclei were observed.

67. HOLMIUM. This element provides a typical example, showing the ways in which one can test some of the regularities predicted by the theory. The only stable isotope of holmium is Ho^{165}. The L electrons corresponding to the first excited state of this nucleus were easily measured in the proton experiments, but for the K line it turned out that the best results were obtained from deuteron bombardments. From the measured $K:L$ ratio for these transitions we determine the branching and mixing ratios for the transitions from the second excited state, as computed by means of the formulae (16) to (21). In the proton measurements we also found a weak line corresponding to the L_{21} transitions and we can therefore calculate the total B-values for both states. The experimental results are seen to be consistent with the rotational description, which predicts an energy ratio of 20:9 and a ratio for the B-values of 35:9, whereas the measured ratios are 2.21 and $\simeq$ 3.2, respectively. In addition, the indications of K conversion peaks from the decays of the second excited state have estimated intensities in agreement with the theoretical expectations. It must, however, be admitted that the transition probabilities given for the second excited state are computed on the basis of very uncertain yield measurements. It is therefore not surprising that our estimate of the partial B-value for the cross-over γ-ray is about two times larger than the value obtained directly from the γ-measurements (He 1). This indicates that the $M1$ transitions are even stronger than those corresponding to the mixing ratios given in Table II, but this would only be of minor importance for the total B-value computed for the first excited state.

68. ERBIUM. The masses of the erbium isotopes fall in the middle of the region where the energies for the first excited states of the even-even nuclides change only slowly with the mass num-

ber. The excitation energies can consequently be expected to be practically the same for all the even Er isotopes, and to these nuclei we therefore assign the pair of conversion lines shown in Fig. 11. The coincidence between the excitation energies is evidently complete within the limits of the experimental resolution. As for most other even-Z nuclides we do not find the lines from the odd-A isotopes.

69. THULIUM. The spin of the only stable thulium isotope Tm^{169} is known to be 1/2 (cf., e. g., Li 2), and one can therefore expect to find the anomalous rotational spectrum given by formula (3). The strongest Coulomb excited line in both the conversion electron and the γ-ray measurements (He 1) corresponds to a transition energy of approximately 110 keV. The peak found at the position of the M line from this transition appeared too strong relative to the L line to be a pure M peak, and the clear indication of a peak, which was found at a slightly higher energy, also supports the impression that additional transitions are present, corresponding to an energy about 119 keV. Relative to the L peak, the composite peak does not appear to be weaker at the lower proton energies, and we are therefore led to an assignment in which the two transitions belong to a 119 keV excited state, decaying mainly via the stop-over to a first excited state at about 8 keV, but also to some extent by the cross-over to the ground state. As a check, we have measured the excitation function for the 110 keV transitions; it was found to conform with an excitation energy of about 120 keV, even though the evidence was not quite conclusive. In addition, the above interpretation seems to be consistent with recent β-decay experiments (Jo 1).

For a normal spin sequence the assumed level scheme leads to the value $a = 0.79$ for the decoupling parameter in equation (3), and a moment of inertia which would correspond to an energy of $6\,\hbar^2/2\Im \simeq 75$ keV for a first excited state in a similar even-even nucleus. These values are in good accord with recent theoretical estimates (Mo 1). The measured yields show that the presumed stop-over lines correspond to rather pure $M1$ transitions, put the $K{:}L$ ratio is so large that only an upper limit to the cross-over branching fraction can be obtained in this way. Instead, we have determined this quantity directly by comparison with the

measured cross-over yield, and Table II therefore contains only one value for the total transition probability.

70. YTTERBIUM. The situation here is completely similar to that of erbium, and the remarks made there apply also to the ytterbium measurements. In addition, we found in the α-bombardement of Yb a weak indication of a peak in the spectrum at an energy around 57 keV. If the peak is real it is most probably an L peak associated with a 66 keV transition, but we have no basis for further assignment.

71. LUTECIUM. The only conversion lines we detected with certainty were those from the decay of the first excited state of the 97 per cent abundant isotope Lu^{175}. The measured $K:L$ ratio shows that the majority of the decays correspond to $M1$ transitions, indicating that cross-over transitions from the expected second rotational state should be comparatively weak. The corresponding γ-ray has been observed in the experiments of HEYDENBURG and TEMMER (He 1), who find the ratio between the excitation energies to agree well with the theoretical value. On the basis of our data, we estimate a partial B-value for the cross-over γ-ray, which is about 4 times larger than the value found directly in the above mentioned γ-measurements. However, our value for the mixing ratio is derived from equation (20) and depends critically on the $K:L$ ratio, which only has to be decreased by 20 per cent in order to remove the apparent discrepancy. This change would only be of minor importance for the computed total B-value for the first excited state, which is also found to be in good agreement with the results obtained by the above experimentors. On the other hand, for $|g_K - g_R|$, it would imply that the correct value should be approximately 1.8 times smaller than given in Table II. The yields which should be expected for the conversion lines associated with the decay of the second excited state are so small relative to the respective backgrounds that they would only be measurable under improved experimental conditions.

72. HAFNIUM. Our measurements on this element have so far only been made by bombardment of a comparatively thick HfO_2 target, which had been prepared by the suspension method. When viewed in a microscope after the bombardment, the target

layer appeared to consist of rather small grains which were evenly distributed and which covered approximately 90 per cent of the surface. The thickness determination by means of weighing should therefore not be so bad in the present case.

In hafnium, the odd-A isotopes have excitation energies for the first rotational state, which are higher than those for the even ones. In spite of their comparatively small intensities, it was therefore also possible to detect the L conversion lines for the odd isotopes. The corresponding K lines were too weak to be measurable, but indications gave estimated $K{:}L$ ratios of the order of 2. This ratio would correspond to partial B-values for γ-emission, which agree reasonably well with the γ-ray measurements (He 1, St 1, Mc 1). However, for Hf^{177} the transition from the first excited state has been reported (Ma 4) to have $\delta^2 \lesssim 0.02$, and it is by employing this value that the very low B-value given in Table II has been computed. We have assumed that $I_0 = 7/2$ in agreement with the observed rotational energy intervals (cf. He 1), but this is of minor importance for the computed transition probabilities. For the even isotopes, a similar comparison with the γ-ray measurements is less uncertain and the measured intensities are found to agree approximately with each other. The target was relatively thick and therefore the resolution obtained was not very good. Only in the α-particle bombardments could the weak Hf^{176} lines be detected simultaneously with those from the more abundant isotopes, and this was because of the better resolution which was obtained as a consequence of the smaller effective target thickness. Comparison with the γ-ray measurements made with separated targets (Mc 1, He 1) shows that all our energy determinations for the hafnium lines are 1 or 2 keV too high, but that the assignments made are correct.*

73. TANTALUM. The Ta^{181} nucleus is one of those for which more detailed studies have been made by means of Coulomb excitation experiments, and in several papers the results have been discussed in terms of the rotational interpretation (cf., e. g., Bo 5). All three γ-rays from the excitation of the two lowest

* Note added in proof. Repeated measurements on sprayed targets have yielded partial B-values which are somewhat smaller than those given in Table I. For the $L_1^{178,\,180}$ peak, the average is $2.3 \cdot 10^{-48}$ cm^4, corresponding to a quadrupole moment $Q_0 = 7.0$ barn.

excited states have been detected, and coincidence experiments as well as angular distribution measurements have confirmed that the energy ratio and the spin sequence for the levels are as predicted for a rotational spectrum.

The energies given in Table II are, as mentioned earlier, calibrated against the 100 keV transitions found for excited W; the values are slightly lower than those published earlier (Hu 3, Hu 1), but the ratio is still found to be 2.21 in excellent agreement with the theory. If we add all the partial B-values which we have measured for the first rotational state and, by means of equations (7) and (8), compare this total with the partial B-value measured for the practically unconverted cross-over γ-transitions from the second state, then we find that one should expect that 80 per cent of the transitions from the second level have decayed via the cascade to the first level. This means that $\delta^2 \simeq 0.14$ or that the cascade transitions are practically pure $M1$ decays in agreement with the measured conversion coefficients, as well as with the angular distribution measurements of McGowan (Mc 3). With these values for the branching and the mixing ratio we can determine the total B-value for the second excited state from the measured stop-over conversion lines and thus obtain a practically independent check on the branching fraction. The total B-value is found to be 3.6 times smaller than for the first excited state, in excellent agreement with the theory. This is of course somewhat coincidental, since the yield of the stop-over conversion lines are not very accurately measured, but, nevertheless, it gives a relatively good confirmation of the values for the branching fractions, and therefore also of the determination of the mixing ratio and $|g_K - g_R|$.

74. TUNGSTEN. With targets of natural tungsten there are several coincidences in the position of the conversion lines from the various isotopes. In bombardments with α-particles of sufficiently low energy the only lines which remained were those corresponding to the low-lying first excited state of W^{183}. The $M + N$ peak from the decay of this level was easier to measure than the L peak, as the background was much higher for the latter peak which, moreover, was very close to the foil cut-off. The conversion coefficients are known from the β-decay work

of MURRAY *et al.* (Mu 1). Using their results we can compute the total B-value from the M peak alone, if we look apart from the fact that our $L:(M+N)$ ratio seems too low. The computed B-value is however rather uncertain, and we have therefore repeated the experiment with a sprayed target made of WO_3 enriched in W^{183}. These measurements confirm that the transitions take place in the odd isotope; unfortunately, however, we cannot evaluate a reliable transition probability from the data until information on the isotopic composition of the target material becomes available. The spin of W^{183} is 1/2 and the second excited collective state is found to have an energy of 99.1 keV (Mu 1, Mc 4). This is 2.13 times the excitation energy for the first collective state and corresponds to $a = 0.19$ and $3\,\hbar^2/\Im = 78$ keV, which is in good accord with theoretical expectations (Mo 2, Ke 1). The excitation energy for the first excited state in the even isotope W^{182} is 100.1 keV (cf. Bo 3), which is very close to the value for the second excited state of the odd isotope. We cannot expect to be able to discriminate between these two $E2$ transitions in our measurements and, for this reason, we cannot determine the yield corresponding to the second excited state in W^{183}, or the amount of W^{182} in the enriched target. For the natural targets, the yield of the composite L peak will be due mainly to the even isotope, for which one can therefore obtain a rather reliable B-value determination. For the measured peak we estimate the W^{183} contributions to be about 20 per cent, if we assume that $Q_0 = 6.5$ barns (as interpolated from Fig. 13) rather than the uncertain 8.4 barns given in Table II.

Also for the other two even isotopes, coincidences of the positions of the M and L conversion peaks make an accurate comparison of the total B-values difficult, as we have to employ the relative conversion coefficients given in Fig. 2. The average value computed for all the even isotopes corresponds to a partial B-value for γ-emission, which is in good agreement with our previously published measurements (Hu 1), and with those of STELSON and MCGOWAN (St. 1).

The value found in the experiments of MCCLELLAND *et al.* (Mc 1) is about three times smaller; their measurements on separated targets have confirmed the assignments given in Table I (cf. Mc 4).

75. RHENIUM. The pure metal of this element was only available in the form of a powder consisting of comparatively large grains. Consequently, our earlier experiments made with targets prepared by the suspension method were not very reliable, and we have therefore repeated the measurements with sprayed targets. In addition to the group of L and M lines from the decay of the first excited state of each of the two stable isotopes Re^{185} and Re^{187}, the spectrum also showed the corresponding K line associated with the latter nuclide. The $K:L$ ratio thus obtained is in good agreement with the value found from measurements on the β-decay of $_{76}Os^{187}$ (cf. Ho 1). For Re^{187} we can therefore compute the total B-value in the usual way; the corresponding value for γ-emission turns out to be about two times larger than that obtained directly in the experiments of McClelland *et al.* The K line associated with Re^{185} could not be detected with certainty, but the indications are that the $K:L$ ratio is lower than for Re^{187}. For the lighter isotope the ratio is not known from other sources, and we have therefore only given the two limits for the total B-value, which correspond to either a pure $M1$ or a pure $E2$ decay.

76. OSMIUM. Many small peaks were seen in the measured spectrum, but they were all of the same magnitude as the experimental fluctuations in the background and no lines were established with certainty.

77. IRIDIUM. The spectrum measured for this element is very similar to that obtained in the bombardment of rhenium. The measurements were made with a thick target of the pure metal, but the L peaks from the de-excitation of the two stable isotopes were clearly resolved due to the fact that the layer corresponding to the effective target thickness is comparatively thin for electrons with energies above 100 keV. The determination of the yield of the measured M peak was rather uncertain and we only found weaker indications for the K peaks. The $K:L$ ratios for the two levels are however known from β-decay experiments (Ho 1, Wa 1), and we can thus compute the B-values and the corresponding moments in the usual way.

78. PLATINUM. Bombardment of a thick target of pure platinum metal yielded only two weak lines; they correspond

to the energies for the K and L electrons from a 210 keV decay. This transition has previously been found by McCLELLAND *et al.* (Mc 1), and by TEMMER *et al.* (Te 1). By means of separated targets the former authors have shown that the process takes place in Pt^{195}. This nucleus is of the even-Z odd-A type, and has a spin $I_0 = 1/2$. The L peak was barely visible, but the $K:L$ ratio is definitely so large that the decay must be mainly $M1$, and the level therefore has $I = 3/2$.

79. GOLD. For this element the deviation from the spherically symmetric form of the closed-shell nuclei has become so small, that, in the present experiment, it was difficult to detect the Coulomb excitation of the collective states. These states, however, have been investigated in detail by the γ-ray technique, and angular distribution measurements have shown that $\delta^2 \lesssim 0.6$ for the first excited state at 279 keV (cf. Mc 3). With this value for the mixing ratio we have computed the total B-value from the estimated size of the K peak.

92. URANIUM. After having replaced the Geiger counter with an anthracene detector we looked for the L conversion line from the decay of the 44 keV first excited state in U^{238}. However, the background of stopping electrons was so strong at these low energies that the line could not be detected with certainty.

The partial B-values for γ-emission, which we estimate from our data by means of the conversion coefficients given in Figs. 1 and 2, are on the whole in satisfactory agreement with the results obtained from the γ-ray experiments. On the average, the deviations seem to be about 25 per cent, and this is of the same order of magnitude as the experimental uncertainties.

An additional check on the experiments, which at the same time constitutes a test of the theory of Coulomb excitation, can be obtained by computing the reduced transition probabilities for the excitations from the directly measured lifetimes of the excited states. As mentioned in Chapter II, such a comparison is independent of any particular nuclear model, but it demands a rather good knowledge of the magnitude of the various conversion coefficients (cf. Eq. (31)), because the $E2$ γ-transitions

often constitute only a small fraction of the decays. However, the above mentioned agreement between the conversion electron and γ-ray measurements indicates that the applied conversion coefficients are approximately correct, and the comparison should therefore be a significant test of the theory of the excitation process.

The half-lives for the decays of the first excited state of several of the even-even nuclei in which we are interested here have been measured in recent years (cf. Su 1), and these transitions are particularly well suited for comparison, because they have no magnetic contributions. In Table III, we have given the values for the half-lives as well as the corresponding reduced transition probabilities, corrected for the spin weight factors so that they can be compared directly with the B-values of Table II (cf. Eq. (30)). The approximate agreement between the B-values obtained by the two different kinds of experiments seems very satisfactory when one considers all the uncertainties involved. A similar result has been obtained by HEYDENBURG and TEMMER (He 1), who have compared their data with the lifetimes by means of total conversion coefficients taken from the paper of SUNYAR. The values of $\varepsilon\{\gamma\}$, which we have employed in Table III, deviate by less than 10 per cent from those given by SUNYAR.

V. Discussion.

From the experimental results summarized in Table II, one can compute the nuclear moments and gyromagnetic ratios by means of the formulae given in Chapter II, on the assumption that the observed excitations are of rotational character. This interpretation is suggested by the large electric quadrupole transition probabilities characterizing the excitations, as well as by the systematic trends in the properties of the observed levels (cf. below). For a few of the odd-A nuclei where two excitations could be observed (Eu, Ho, and Ta), the predictions of the theory have also been tested, in a more quantitative way, by the measured ratios of the energies and excitation cross sections for the two levels. As far as the relative cross sections are concerned,

the consistency of experiment and theory is evident from the approximate equality of the Q_0-values derived from the excitations of the two levels (cf. Table II).

A. Quadrupole Moments.

The Q_0-values obtained from the present measurements and listed in Table II are plotted in Fig. 13 as a function of the nuclear mass number A_2. They exhibit a rather smooth variation, with fluctuations not exceeding the experimental uncertainties.

These intrinsic quadrupole moments may be compared with those derived from spectroscopic measurements for odd-A nuclei, by means of the relation (9). Previous comparisons of this type (cf., e. g., Bo 4) indicated that the latter Q_0-values somewhat exceed those derived from transition probabilities. However, for $_{71}Lu^{175}$ and $_{73}Ta^{181}$, where the discrepancies were largest, a

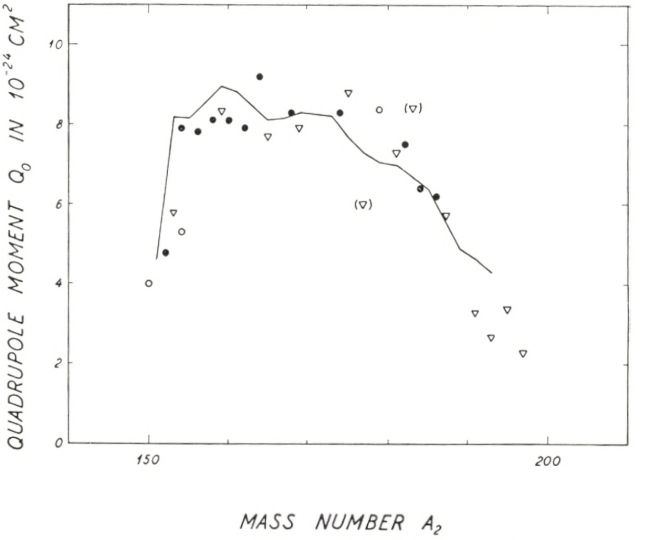

Fig. 13. The Q_0-values given in Table II plotted as a function of the mass number A_2.* The circles represent the even-A nuclides and the triangles the odd-A nuclides. The uncertainties are supposed to be of the order of 10 % for the black points, and 20 % or more for the rest of the points. The points in parentheses correspond to $_{72}Hf^{177}$ and $_{74}W^{183}$, (cf. the comments in Chapt. IV). The broken line represents the theoretical moments for the odd-A nuclides, corresponding to $r_0 = 1.20 \cdot 10^{-13}$ cm (cf. Mo 1).

* Cf. footnote p. 45.

recent more detailed analysis of the electronic configurations has led to a considerable decrease in the spectroscopic Q-values (Ka 1). For $_{71}Lu^{175}$ and $_{73}Ta^{181}$ the revised spectroscopic analysis yields Q_0-values of about 12 barns and 9 barns, respectively, to be compared with the values 9 barns and 7 barns, listed in Table II. The remaining deviation is hardly significant, in view of the existing experimental uncertainties.

Recently, a theoretical estimate of nuclear quadrupole moments has been made on the basis of the calculation of the binding energies for individual nucleons in deformed potentials (Mo 1). The equilibrium deformation has been determined by minimizing the total energy of the system of nucleons. The quadrupole moments, calculated in this way for the odd-A nuclei between $A_2 = 151$ and $A_2 = 193$, are shown in Fig. 13, where the theoretical points are connected by a broken line. The absolute magnitudes correspond to the value $r_0 = 1.20 \cdot 10^{-13}$ cm. The agreement is very satisfactory, except for $_{73}Eu^{153}$, where our experimental quadrupole moment is about 30 per cent lower than the theoretical Q_0-value.

B. Moments of Inertia.

The nuclear moments of inertia $\Im$ derived from the observed excitation energies by means of equations (1) or (3) show a similar variation with A_2 as the quadrupole moments, with a broad maximum in the region around $A_2 = 170$.

Of special interest, from a theoretical point of view, is the relation between the moments of inertia and the nuclear deformations. This is illustrated by Fig. 14, where the $\Im$-values determined from the energies given in Table II are plotted against Q_0. The correlation of the two quantities is evident from the grouping of the points around the dashed line shown in the figure, with the largest deviation from the general trend again occurring for $_{63}Eu^{153}$. For comparison, the $\Im$-values calculated from the relation (11), corresponding to the assumption of irrotational flow for the rotational motion, are also shown in the figure. It is seen that such a model gives moments of inertia which are smaller than the observed moments by factors of more than four, as has also been recognized previously (Bo 1, Fo 1, Su 1).

The relation (11) assumes a simple ellipsoidal nuclear shape, and an increase of the moments of inertia for the irrotational model could arise from the occurrence of higher multipoles in the shape. It appears, however, (Gu 1) that while such an effect is not unexpected and may have an appreciable influence on the moment of inertia, the ratio of $\Im$ and Q_0^2 is much less affected.

A recent analysis of the nuclear rotational motion (Bo 2) has also shown that important deviations from irrotational flow

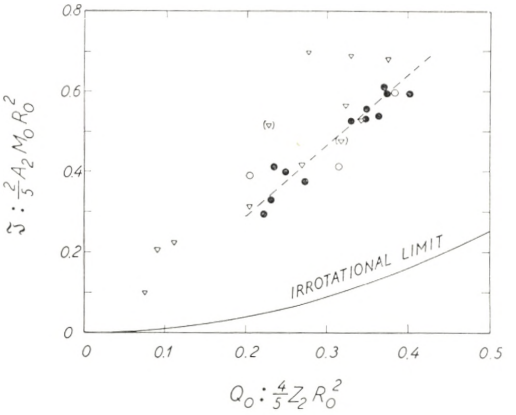

Fig. 14. Moments of inertia determined from the excitation energies by means of equations (1) or (3), and plotted against the corresponding nuclear deformations, as represented by the Q_0-values (cf. Table II).* For the average nuclear radius we have employed the value $R_0 = r_0 \cdot A_2^{1/3}$, with $r_0 = 1.20 \cdot 10^{-13}$ cm. A correlation between the two quantities is indicated by the grouping of the points around the broken line. The points are marked in the same way as in Fig. 13.

are to be expected as a consequence of the nuclear shell structure. Thus, it is found that for pure independent particle motion in a deformed potential, the moment would be approximately equal to that for rigid rotation. The effect of residual interactions between the particles, not included in the average nuclear field, results in smaller moments of inertia, which increase with increasing deformation. The values for irrotational flow are approached when the interactions become so strong that they destroy the shell structure. The observed magnitude and trend of the moments of inertia are interpreted as indicating a strength of interaction about three times smaller than corresponding to this limit (Bo 2).

* Cf. footnote p. 45.

C. Magnetic Moments.

The $M1$ transition probabilities are measures of the quantities $|g_K - g_R|$ (cf. Table II), and if, in addition, the magnetic moments of the ground states are known, the values of the two gyromagnetic ratios can be determined separately by means of equation (12). However, the ambiguity in the sign of $(g_K - g_R)$ implies that two sets of g-values come into consideration. When the experimental data are uncertain, one is therefore left with a very large range of possible g-values, and only little can be learned from the measurements. This applies to most of the elements considered here, with the exception of the nuclei $_{63}Eu^{153}$ and $_{73}Ta^{181}$. For the former, the occurrence of the comparatively strong cross-over transitions shows that the magnetic transitions must be weak, and consequently the gyromagnetic ratios g_K and g_R must be approximately equal. From spectroscopic evidence the magnetic moment is known to be about 1.6 n. m., which corresponds to the values $g_K \simeq g_R \simeq 0.64 \pm 0.1$, whereas the estimate (14) yields a value of $g_R \simeq 0.41$. As mentioned in the comments on $_{73}Ta^{181}$, one has for this nucleus a comparatively good determination of the magnetic transition probabilites, which, by means of the value $g_R = 0.40$ estimated from (14), yields the magnetic moments 0.1 n.m. or 2.9 n.m. for the ground state. The former of these values is excluded by the angular distribution measurements (Mc 3) which show that $(g_K - g_R)$ is positive if Q_0 is positive (cf. Chapter II A), as is indicated by the spectroscopic Q-values. The spectroscopically determined magnetic moment is 2.1 n.m. (Br. 2), and combined with our data this value would correspond to $g_R = 0.17$.

In order to obtain more information about the gyromagnetic ratios, better measurements of both the magnetic moments and the transition probabilities are needed. The present measurements have shown that, in general, the magnetic transition probabilities are large, and this implies, as mentioned in Chapter II, that they are best determined by direct measurements of the branching fractions for the second excited states. One should, thus, compare the yield of the cross-over γ-rays with the yield of the cascade conversion lines. Reliable measurements of the latter demand a better experimental technique than the one

employed in the present work. It would probably be advantageous to monitor the electron yields by means of the elastically scattered projectiles, and to stabilize the position of the beam so that a higher resolution could be employed in the β-spectrometer. This would also improve the accuracy in the measurements of the yields in the decays of the first excited states, since the movements of the beam are responsible for the uncertainty in the determination of the half-widths and peak areas of the measured lines. Further improvements would imply the use of thin-walled counters and evaporated or painted (Gl 1) targets, as well as considerations of the angular distributions of the conversion electrons. We hope to be able to investigate some of the more interesting nuclei in this manner, when the new 4-MeV electrostatic generator of this Institute comes into regular operation.

In conclusion, we want to express our gratitude to Professor NIELS BOHR for his continued interest in our work and for the excellent working conditions offered at his institute. In addition, we would like to thank Drs. A. BOHR and B. R. MOTTELSON for much advice and for great help in the attempts to interpret the obtained data. We are also grateful to cand. mag. B. S. MADSEN for his aid with the electronic equipment and for his assistance in some of the experiments. Finally, we gratefully acknowledge the kindness by which many samples of the rare earth oxides have been put at our disposal by various institutions, in particular by the 'Iowa State College', Iowa City, U.S.A., and by 'Chalmers Tekniska Högskola', Göteborg, Sweden.

Appendix I.

The non-relativistic theory for the ionization of the K shell by bombardment with heavy particles has been treated by HENNEBERG (He 3) on the basis of the Born approximation. For the present purpose, it is of interest to extend these calculations to include also the higher shells, and we shall therefore briefly outline a simple derivation of Henneberg's formula.

In the evaluation of the matrix elements one is, according to HENNEBERG (l. c.), justified in employing the Born approximation, i. e., to replace the product of the initial and final wave functions for the bombarding particle by the product of two plane waves, and this is true because the radii of the electron orbits are large compared to the classical distance of closest approach for the projectiles. With such a substitution, the integration over the coordinates of the bombarding particle is straightforward, and one obtains (cf. Be 1) the following expression for the differential cross section for the emission of an electron of energy E_δ:

$$\frac{d\sigma}{dE_\delta} \simeq 4\,\pi Z_1{}^2 \frac{M_1}{E_1}\frac{e^4}{\hbar^2}\int_{q_{\min}}^{\infty} |V\{q\}|^2 \frac{dq}{q^3} \qquad (43)^*$$

$$V\{q\} \equiv \int e^{i\vec{q}\cdot\vec{r}} \cdot \psi_f{}^*\{\vec{r}\} \cdot \psi_i\{\vec{r}\}\, d\vec{r}\,, \qquad (44)$$

where $Z_1 \cdot e$, M_1, and E_1 are the charge, mass, and energy of the bombarding particle which has suffered a momentum change $\hbar\vec{q}$ in the C. M. system. From the conservation of energy and momentum, it follows that

$$\hbar q_{\min} \simeq (E_B + E_\delta) \cdot \sqrt{\frac{M_1}{2E_1}}, \qquad (45)$$

where E_B is the actual binding energy of the ejected electron. Consequently, $\exp\{i\vec{q}\cdot\vec{r}\}$ will be a rapidly varying function as compared to the electron wave functions ψ, provided that one or both of the following two conditions are fulfilled:

$$E_B > E_0 \text{ or } E_\delta > E_0, \qquad (46)$$

where E_0 is the maximum energy which an electron can obtain in a free collision with the bombarding particle, i. e.

$$E_0 \simeq 4\,m\frac{E_1}{M_1}, \qquad (47)$$

if 'm' denotes the electron mass.

Provided that the condition (46) holds, one can easily show, by expanding $\exp\{i\vec{q}\cdot\vec{r}\}$ in spherical harmonics and performing repeated partial integrations, that, to leading order in $1/q$, only

* N. B.: Formulae numbers 41 and 42 are omitted.

s-states contribute to the integral V. For these states one obtains in the same way

$$V_s = \int_0^\infty \frac{\sin\{qr\}}{qr} \cdot R_{sf}\{r\} \cdot R_{si}\{r\} \cdot r^2 \cdot dr \simeq -\frac{2}{q^4}\left[\frac{d}{dr}(R_{sf} \cdot R_{si})\right]_{r=0} \quad (48)$$

or, from the differential equation for the radial wave functions R_s,

$$|V_s|^2 \simeq \frac{2^4}{q^8}\left(\frac{Z_2}{a_0}\right)^2 \cdot |R_{sf}\{0\}|^2 \cdot |R_{si}\{0\}|^2, \quad (49)$$

where $Z_2 e$ is the charge of the target nuclei and a_0 the Bohr radius of the hydrogen atom.

If one neglects screening effects, one has (cf., e. g., SOMMERFELD (So 1)) for the n^{th} shell

$$|R_{si}\{0\}|^2 = 2^2 \cdot \left(\frac{Z_2}{n\, a_0}\right)^3 \quad (50)$$

and

$$|R_{sf}\{0\}|^2 = 2^2 \frac{m}{\hbar^2}\frac{Z_2}{a_0}\left[1 - \exp.\left\{-2\pi \frac{Z_2}{a_0}\sqrt{\frac{\hbar^2}{2m\,E_\delta}}\right\}\right]^{-1}, \quad (51)$$

where the final wave function is normalized per unit energy range.

From these equations one obtains the differential cross section for the n^{th} shell, which per atom is

$$\frac{d\sigma_n}{dE_\delta} = \frac{2^{18}\,\pi}{5} \cdot Z_1^2 \cdot e^4 \left(\frac{m\,E_1}{M_1}\right)^4 \cdot \frac{(n\,E_B')^3}{(E_B + E_\delta)^{10}}, \quad (52)$$

where E_B' is the unscreened binding energy defined by

$$E_B' = \frac{e^2}{2\,a_0}\left(\frac{Z_2}{n}\right)^2. \quad (53)$$

In equation (52) we have omitted the last factor in (51) as it is of no practical importance. The equation is the same in the laboratory coordinates,* since $(2\,E_1 : M_1)^{1/2}$ is the velocity of the bombarding particle relative to the nucleus which is initially at rest, and since, furthermore, the center-of-mass velocity can be

* Note, however, that small center-of-mass corrections are neglected in equation (45).

neglected as compared to the velocities of the ejected electrons. Their angular distribution should, therefore, also be approximately isotropic in the laboratory system.

From the above equations, we find, as a total for all the shells, the differential cross section

$$\frac{d\sigma}{dE_\delta} = 1.0 \cdot 10^{-17} \cdot Z_1{}^2 \cdot \left(\frac{E_1}{A_1}\right)^4 \cdot Z_2{}^4 \cdot \frac{(e^2 \cdot mc^2)^2}{E_\delta{}^9} \cdot S, \tag{54}$$

where, for convenience, the rest energy mc^2 of the electron has been introduced. The sum S is given by

$$S = \sum_n \frac{1}{n^3} \cdot \frac{u^9}{(c_n + u)^{10}}, \tag{55}$$

where

$$u = \frac{E_\delta}{E_{K'}} \text{ and } c_n = \frac{E_B}{E_{K'}}. \tag{56}$$

Taking as appropriate values the figures $c_1 = 0.8$; $c_2 = 0.16$; $c_3 = 0.04$, and $c_4 = 0 = c_5 = \ldots$, we obtain the contributions shown in Fig. 15 for the various shells. They add up to a total

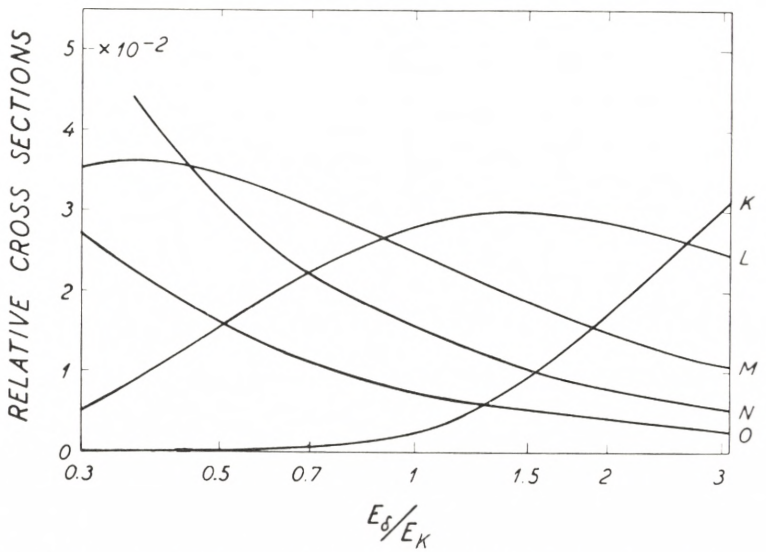

Fig. 15. Relative contributions to the stopping electrons of energy $E\delta$ from the various shells, as calculated on the basis of a non-relativistic theory neglecting screening effects.

which is nearly independent of u and has a value around 0.1 which, inserted in (54), gives the equation (35) used in Chapter III.

The comparatively good agreement between the cross sections computed from this formula and the measured ones must be somewhat coincidental. The relativistic effects appear to increase the contributions, in particular from the K shell, by large factors,§ which however will be counteracted to some extent by the effects of the screening, especially in the case of the higher shells. A correct theory would also have to take into account the higher terms in the $1/q$ expansion which, on the other hand, means that also the contributions from the p sub-shells etc. should be considered. The present derivation seems, however, to be sufficient to show the general dependence of the cross section on the various parameters and brings out the main problems necessarily involved in a more complete treatment.

Appendix II.

When free electrons are generated with an energy E_δ^* in an infinitisimal layer dx at the depth x below the surface of a target, then the fraction $W dE_\delta$ which reaches the surface by diffusion-like processes and emerges with energies between E_δ and $E_\delta + dE_\delta$, will be given by (cf. Be 2)

$$W\{E_\delta, E_\delta^*, x\}\, dE_\delta = \frac{x}{(4\pi\tau)^{1/2}} \cdot e^{-x^2/4\tau} \cdot \frac{1}{\tau} \left| \frac{d\tau}{dE_\delta} \right| dE_\delta, \qquad (57)$$

where

$$\tau\{E_\delta, E_\delta^*\} = \frac{1}{6} \int_{E_\delta}^{E_\delta^*} \lambda\{E_\delta'\} \frac{dE_\delta'}{|dE_\delta'/dx|}. \qquad (58)$$

The function τ has been tabulated by BETHE (cf. Table II of ref. Be 2), but the values given must be changed somewhat for the low electron energies which we consider here.

Firstly, the transport mean free path λ should not be calculated on the basis of the Born approximation, but rather by employ-

§ Private communication from Č. ZUPANČIČ.

ment of the classical approximation (cf., e. g., Bo 6), since for $E_\delta \approx 50$ keV and $Z_2 \approx 70$ one has the collision index

$$\varkappa^2 = 2\frac{(Z_2 \cdot e)^2}{E_\delta \cdot a_0} \approx 5 > 1. \tag{59}$$

This means that the screening cut-off takes place at a scattering angle which is $\varkappa$ times larger than in the case of the Born approximation, so that one obtains a larger λ given by

$$\left.\begin{aligned} \varrho\lambda &= 4\frac{M_0}{\pi e^4}\frac{A_2}{Z_2^2}\cdot E_\delta{}^2 \cdot \left[\log_e\left\{\frac{8\,E_\delta\,a_0}{Z_2{}^{2/3}\cdot e^2}\right\} - \log_e\left\{\varkappa^2\right\}\right]^{-1} \\ &\simeq \frac{E_\delta{}^2}{170\sqrt{Z_2}}\ \mathrm{mg/cm^2}\ \text{for}\ E_\delta\ \text{in keV}. \end{aligned}\right\} \tag{60}$$

Secondly, the specific stopping power dE_δ/dx for the electrons will, in the region which we are considering here, not be independent of the electron energy. The most probable energy loss for electrons which have travelled the distance dx will be better represented by the expression (cf., e. g., Segrè (Se 1))

$$\left.\begin{aligned} -\frac{1}{\varrho}\frac{dE_\delta}{dx} &= \frac{\pi e^4}{M_0}\cdot\frac{Z_2}{A_2}\cdot\frac{1}{E_\delta}\cdot\log_e\left\{5.5\,\frac{Z_2}{A_2}\frac{\pi a_0{}^2}{M_0}\varrho\,dx\right\} \\ &\simeq \frac{650}{E_\delta\cdot\sqrt{Z_2}}\ \frac{\mathrm{kev}}{\mathrm{mg/cm^2}}\ \text{for}\ E_\delta\ \text{in keV}, \end{aligned}\right\} \tag{61}$$

and for $\varrho\,dx \approx 0.3$ mg/cm^2.

Consequently, one obtains from equation (58) the following approximate expression for τ:

$$\varrho^2\,\tau\left\{E_\delta, E_\delta{}^*\right\} \simeq \left(\frac{E_\delta}{40}\right)^4 \cdot \left[\left(\frac{E_\delta{}^*}{E_\delta}\right)^4 - 1\right] (\mathrm{mg/cm^2})^2 \text{ for } E_\delta \text{ in keV}. \tag{62}$$

This energy dependence together with that of equation (35) for the production cross section leads, in combination with the distribution (57), to the following estimate for the yield of electrons from a target which has a thickness t/ϱ in the direction perpendicular to the surface:

$$\left.\begin{aligned} Y\{E_\delta\}\,dE_\delta &= \frac{\varrho\,dE_\delta}{A_2 M_0 \cos\theta}\int_0^{t/\varrho}\int_{E_\delta}^{\infty} W\{E_\delta, E_\delta^*, x\}\,\frac{d\sigma}{dE_\delta^*}\,dE_\delta^*\,dx \\ &= Y_\infty\,dE_\delta\,\frac{t}{t_\infty}\,\frac{1}{\sqrt{4\pi}}\int_0^{\infty}\frac{\left[1-e^{-z}\right]\cdot z^{3/2}}{\left[\left(\frac{3\sqrt{\pi}}{16}\,\frac{t}{t_\infty}\right)^2+z\right]^3}\,dz, \end{aligned}\right\} \quad (63)$$

where the effective thickness for a thick target is denoted by t_∞ and is given approximately by

$$t_\infty \simeq \frac{4}{3\sqrt{\pi}}\left(\frac{E_\delta}{40}\right)^2 \simeq \left(\frac{E_\delta}{50}\right)^2 \text{ mg/cm}^2 \quad (64)$$

if one inserts the electron energy E_δ in keV.

The dependence of the function (63) on the ratio t/t_∞ deviates less than 5 per cent from the simple exponential expression (37). In the above derivation, it has been assumed that the target support gives a back-scattering equal to that of the target material, but without contributing to the production of free electrons. Hence, the way in which the yield will actually depend on the target thickness may be somewhat different from that given by (63), even though the fact that the yield is decreasing so strongly with the energy implies a rather small back-scattering effect. Also the application of the diffusion approximation is not quite justified, and we have therefore only employed the more simple expression for comparison with the experiments.

Table I.

The figures given in the seven columns of this table have the following meaning.

1. Electron energies for the measured conversion lines. The probable errors are estimated to be about $\pm 1\ ^0/_0$.
2. Bombarding conditions; H = protons, D = deuterons, and α = He^+ ions. The bombarding energies are given in the laboratory system.
3. Target thicknesses and the materials employed by the preparation. The figures given refer only to the weight of the heavy atoms per unit area, since in many cases the amounts of light elements in the targets are not known. The values are obtained in the following ways (cf. Chapter III C).

   a) Effective layer of thick target as determined by means of Fig. 9 (angle between beam and surface equal to 45°).
   b) Thickness of target evaporated on a brass support, as determined by means of the curve $t_0 = 0$ in Fig. 7.
   c) Thickness of target prepared on a support of brass by means of the suspension method, as determined by means of the curve $t_0 = 2$ in Fig. 7.
   d) Thickness of target prepared on a support of brass by means of the suspension method, as determined by comparison with measurements on sprayed targets.
   e) Thickness of target prepared on a support of brass by means of the suspension method, as determined by weighing.

   In all other cases, the targets have been prepared either by evaporation or by means of spraying, and their thicknesses determined through measurements on the elastically scattered protons. The evaporated targets were made on a support of graphite in the case of Ta, and on copper in the case of W. The sprayed targets were made on a support of aluminum, with the exception of those used for the deuteron measurements, where brass supports were employed.
4. Total yields of conversion electrons from the 'n' shells of the atoms (n = K, L, or M). The values are computed by disregarding anisotropies, and correspond to 10^{10} projectiles. For computional reasons,

the values are given with two significant figures. The errors are estimated to be smaller than 25 per cent, except in the cases denoted with the signs $\simeq$ or $\sim$, where it may be expected that they can be as large as corresponding to factors of 1.5 and 2, respectively.

5. Assignments with respect to atomic shell and nuclear transition. Subscript 1 refers to transitions from the first collective state to the ground state; subscripts 21 and 2 refer to transitions from the second collective state to the first, and to the ground state, respectively. For composite lines, the fraction assigned to the various isotopes is given in the left-hand side of the column.
6. Transition energies for the decays corresponding to the assignments given in column 5. The binding energies have been taken from the table published by HILL *et al.* (Hi 1).
7. Partial B_{E2}-values for the various conversion lines as computed from the partial cross sections by means of equation (26). The uncertainties are indicated in the same manner as in column 4.

TABLE Ia.

$E\{n\}$	projec.	target	$Y\{n\}$	frac.	assign.		$\Delta E\downarrow$	$\varepsilon\{n\}\cdot B:e^2$
keV	A_1 MeV	mg/cm² Z_2	per 10^{10}		n	A_2	keV	10^{-48} cm⁴
118.3	H 1.75	4.3[a] Mn	$\simeq$ 5.9	1	K_1	55	124.8§	$\simeq$ 0.0009
115.2	H 1.75	4.2[a] 50 % Fe^{57}	$\sim$ 1.8	1	K_{21}	57	122.3	$\sim$ 0.0007
129.8	«	«	$\sim$ 1.2	1	K_2	57	136.9	$\sim$ 0.0004
283	H 1.75	2.7[a] Ag	$\sim$ 0.21	1	K_1	109	308	$\sim$ 0.0026
297	«	2.6[a] «	$\sim$ 0.16	1	K_1	107	322	$\sim$ 0.0023
299	«	2.6[a] Ag^{107}	$\sim$ 0.28	1	K_1	107	324	$\sim$ 0.0021
—	H 1.75	$\simeq$ 0.70[c] CeO_2	—					
—	H 1.75	$\simeq$ 0.81[c] Pr_6O_{11}	—					
88.0	H 1.75	$\simeq$ 0.51[c] Nd_2O_3	($\sim$ 0.5)	1	K_1	150	131.6	—
125.7	«	«	$\sim$ 0.36	1	L_1	150	132.4	$\sim$ 0.31
75.7	H 1.75	0.24 Sm_2O_3	16	0.8	L_1	154	83.1	2.9
«	«	«	«	0.2§	K_1	152	122.5	—
81.7	«	«	$\simeq$ 3.1	1	M_1	154	83.1	—
115.3	«	«	2.4	1	L_1	152	122.7	0.56
122.1	«	«	$\simeq$ 0.5	1	M_1	152	123.5	—
($\sim$35)	D 1.75	0.66[d] Eu_2O_3	($\lesssim$ 20)	1	K_1	153	—	—
77.0	«	«	$\simeq$ 18	1	L_1	153	84.7	—
«	H 1.75	«	9.5	1	L_1	153	«	0.65
82.9	«	«	$\simeq$ 2.4	1	M_1	153	84.3	—
$\sim$103	«	«	($\lesssim$ 0.3)	1	L_{21}	153	$\sim$ 111	($\lesssim$0.05)
146.3	«	«	$\simeq$ 0.34	1	K_2	153	194.8	$\simeq$ 0.051
$\sim$189	«	«	i	1	L_2	153	$\sim$ 196	—

§ See comments. i = indication.

TABLE Ib.

$E\{n\}$	projec.	target	$Y\{n\}$	frac.	assign.	$\Delta E\downarrow$	$\varepsilon\{n\}\cdot B:e^2$
keV	A_1 MeV	mg/cm² Z_2	per 10^{10}	n	A_2	keV	10^{-48} cm⁴
67.9	H 1.75	0.26 Gd_2O_3	15	1 L_1	160	75.7	3.4
72.7	«	«	21	0.2 M_1	160	(74)	—
«	«	«	«	0.8 L_1	158	80.5	3.4
78.9	«	«	$\simeq$ 3.9	1 M_1	158	80.4	—
83.0	«	«	11	1 L_1	156	90.8	2.8
88.4	«	«	$\simeq$ 1.9	1 M_1	156	89.9	—
116.3	«	«	$\simeq$ 0.24	1 L_1	154	124.1	$\simeq$ 0.73
49.4	D 1.75	0.58 Tb_4O_7	$\simeq$ 40	1 L_1	159	57.9	$\simeq$ 0.45
57.0	«	«	—	1 M_1	159	58.6	—
65.4	«	«	($\sim$ 10)	1 Dy	ctm	—	—
72.4	«	«	($\sim$ 13)	$\sim$ 0.5§ L_{21}	159	80.9	($\sim$ 0.2)
«	«	«	«	$\sim$ 0.5 Dy	ctm	—	—
80.3	«	«	—	$\sim$ 0.5§ M_{21}	159	81.9	—
«	«	«	—	$\sim$ 0.5 Dy	ctm	—	—
66.0	H 1.75	0.10 Dy_2O_3	10	1 L_1	164	74.6	4.8
73.1	«	«	8.3	0.3 M_1	164	(74.8)	—
«	«	«	«	0.7 L_1	162	81.7	3.2
80.2	«	«	$\simeq$ 1.2	1 M_1	162	81.9	—
39.5	D 1.75	0.31 Ho_2O_3	$\simeq$ 45	1 K_1	165	95.1	$\simeq$ 1.6
59.5	H 1.90	0.69[d] «	i	1 K_{21}	165	(115.1)	—
87.1	D 1.75	0.31 «	$\simeq$ 8.0	1 L_1	165	96.0	—
«	H 1.75	0.22 «	4.3	1 L_1	165	«	0.32
94.9	«	«	$\simeq$ 1.4	1 M_1	165	96.7	—
107.5	«	«	$\sim$ 0.32	1 L_{21}	165	116.4	$\sim$ 0.074
(156)	H 1.90	0.69[d] «	i	1 K_2	165	(212)	—

§ See comments. i = indication. ctm = contamination.

TABLE Ic.

$E\{n\}$	projec.	target		$Y\{n\}$	frac.	assign.		$\Delta E\downarrow$	$\varepsilon\{n\}\cdot B:e^2$
keV	A_1 MeV	mg/cm²	Z_2	per 10^{10}		n	A_2	keV	10^{-48} cm⁴
71.9	H 1.75	0.33	Er_2O_3	58	1	L_1	164, 166	80.8	3.6
79.3	«	«		≃ 17	1	M_1	168, 170	81.1	—
51.0	H 1.75	0.29	Tm_2O_3	≃ 28	1	K_{21}	169	110.4	≃ 2.1
101.6	«	«		4.2	1	L_{21}	169	111.2	0.32
109.7	«	«		2.4	*0.4	M_{21}	169	111.6	—
«	«	«		«	0.6	L_2	169	119.3	0.11
117.8	«	«		(~ 0.3)	1	M_2	169	119.7	—
68.3	H 1.75	0.18	Yb_2O_3	28	1	L_1	170, 172	77.9	3.9
75.0	«	«		≃ 10	1	M_1	174, 176	77.0	—
51.0	H 1.75	0.21	Lu_2O_3	≃ 17	1	K_1	175	114.3	—
104.3	«	«		≃ 3.1	1	L_1	175	114.9	0.36
112.2	«	«		~ 0.77	1	M_1	175	114.2	—
~ 80	α 1.75	≃ 1.2[e]	HfO_2†	i	1	L_1	176	90	—
84.4	H 1.75	«		≃ 110	1	L_1	178, 180	94.7	≃ 3.4†
~ 89	α 1.75	«		i	1	M_1	176	91	—
92.9	H 1.75	«		≃ 35	1	M_1	178, 180	95.0	—
104.0	«	«		≃ 4.7	1	L_1	177	114.3	≃ 0.57†
112.1	«	«		≃ 2.6	*0.4	M_1	177	114.2	—
«	«	«		«	0.6	L_1	179	122.7	0.28†
~122	«	«		i	1	M_1	179	124	—

* Cf. Fig. 2. i = indication. † Cf. footnote p. 45.

TABLE Id.

$E\{n\}$	projec.	target		$Y\{n\}$	frac.	assign.		$\Delta E\downarrow$	$\varepsilon\{n\}\cdot B:e^2$
keV	A_1 MeV	mg/cm²	Z_2	per 10^{10}	n		A_2	keV	10^{-48} cm⁴
68.7	H 2.00	0.28	Ta	17	1	K_1	181	136.2	1.4
97.4	«	«		$\simeq 0.58$	1	K_{21}	181	164.9	$\simeq 0.22$
124.4	«	«		2.6	1	L_1	181	135.9	0.21
133.5	«	«		$\simeq 0.83$	1	M_1	181	135.7	$\simeq 0.066$
153.5	«	«		~ 0.074	1	L_{21}	181	165.0	~ 0.029
34.9	α 1.45	0.35[a]	W	($\lesssim 2$)	1	L_1	183	(46.4)	—
44.3	«	«		~ 0.91	1	M_1	183	46.6	~ 0.53
89.6	H 1.75	0.23	«	7.0	0.8	L_1	182	100.4	2.7
«	«	«		«	~ 0.2	L_2	183	(~ 100)	—
100.3	«	«		6.1	0.3	M_1	182	(102.6)	—
«	«	«		«	0.6	L_1	184	111.1	1.7
111.5	«	«		3.8	0.3	M_1	184	(113.8)	—
«	«	«		«	0.7	L_1	186	122.3	1.4
121.8	«	«		$\simeq 0.55$	1	M_1	186	124.1	—
63.1	H 1.75	0.30	Re	~ 5.1	1	K_1	187	134.8	—
113.6	«	«		$\simeq 1.1$	1	L_1	185	125.7	$\simeq 0.30$
122.8	«	«		$\simeq 1.2$	0.2	M_1	185	125.2	—
«	«	«		«	0.8	L_1	187	134.9	$\simeq 0.18$
132.8	«	«		~ 0.24	1	M_1	187	135.2	—
—	H 1.75	~ 1[c]	Os	—					
116.4	H 1.75	5.0[a]	Ir	$\simeq 6.3$	1	L_1	191	129.6	$\simeq 0.12$
126.2	«	«		$\simeq 5.6$	0.2	M_1	191	128.6	—
«	«	4.8[a]	«	«	0.8	L_1	193	139.4	$\simeq 0.061$
135.4	«	«		~ 1.8	1	M_1	193	138.0	—
131.7	H 1.75	3.5[a]	Pt	~ 1.7	1	K_1	195	210.1	~ 0.15
196.4	«	«		~ 0.44	1	L_1	195	209.8	—
200.0	H 2.00	3.8[a]	Au	~ 1.9	1	K_1	197	280.7	~ 0.072
—	α 1.75	~ 0.5[b]	U	—§					

§ See comments.

Table II.

The eleven columns of this table contain:

1. Nuclei investigated.
2. Excitation energy of collective states found by the measurements.
3. Conversion lines used for the computations (cf. column 5 of Table I).
4. $K:L$ ratios obtained either from the data in Table I, or from Fig. 2, or from the results of measurements on radioactive elements (cf. Ho 1).
5. Reciprocal of the square of the mixing ratios as computed from the equation (20) and the values in column 4, or as known from other sources. (See comments).
6. Branching fractions as computed from the equation (21) and the values in column 5, or as determined directly (cf., e. g., the case $_{26}Fe^{57}$).
7. Reciprocal of the decay fractions corresponding to the modes of decay given in column 3. (Cf. Eq. (19)).
8. Total B_{E2}-values as computed from the values of column 7 and the partial B_{E2}-values of Table I. The uncertainties are indicated in the same manner as in column 4 of Table I.
9. Spin of the ground state. (Cf. Ho 1).
10. Intrinsic quadrupole moments as computed from equations (7) and (8).
11. Gyromagnetic ratios computed by means of equation (15). (Note the discussion in Chapt. V).

Where the mixing ratios are only known to lie within certain limits, the values given in columns 7, 8, and 10 are those corresponding to the two limits, with the $M1$ limit given first.

TABLE IIa.

nucleus	level keV	line n	$K:L$	$1:\delta^2$	β	$1:\varepsilon\langle n\rangle$	$B:e^2$ 10^{-48} cm^4	I_0	Q_0 10^{-24} cm^2	$\lvert g_K-g_R\rvert$
$_{25}Mn^{55}$	125§	K_1	$\gtrsim 7$	—	1	64 6.6	$\simeq 0.057$ $\simeq 0.006$	3/2	1.1 (0.4)†	—
$_{26}Fe^{57}$	137	K_{21}	—	$\gtrsim 10$§	0.92§	65	~ 0.044	1/2	0.9	—
«	137	K_2	—	0	0.08§	100				
$_{47}Ag^{107}$	323	K_1	—	—	1	78 53	~ 0.17 ~ 0.12	1/2	2.1 1.7	—
$_{47}Ag^{109}$	308	K_1	—	—	1	67 50	~ 0.18 ~ 0.13	1/2	2.1 1.8	—
$_{60}Nd^{150}$	132	L_1	*1.4	0	1	5.1	~ 1.6	0	4.0	
$_{62}Sm^{152}$	123	L_1	*1.1	0	1	4.0	2.3	0	4.8	
$_{62}Sm^{154}$	83	L_1	*0.57	0	1	2.2	6.2	0	7.9	
$_{63}Eu^{153}$	84	L_1	~ 1	~ 0.4	1	2.5	1.6	5/2	5.8	$\lesssim 0.1$
«	195	L_{21}	—	«	(~ 0.35)	(~ 11)	($\lesssim 0.6$)	5/2	—	
«	195	K_2	*2.2	0	$\simeq 0.65$	11	$\simeq 0.56$	5/2	5.8§	
$_{64}Gd^{154}$	124	L_1	*1.0	0	1	3.8	$\simeq 2.8$	0	5.3	
$_{64}Gd^{156}$	90	L_1	*0.59	0	1	2.3	6.0	0	7.8	
$_{64}Gd^{158}$	80	L_1	*0.48	0	1	2.0	6.5	0	8.1	
$_{64}Gd^{160}$	76	L_1	*0.43	0	1	1.9	6.4	0	8.1	
$_{65}Tb^{159}$	58	L_1	—	($\gtrsim 50$)§	1	7.7§	$\simeq 3.5$	3/2	8.3	
«	139	L_{21}	—	«	$\gtrsim 0.95$§	—	—	3/2	—	$\gtrsim 2$
$_{66}Dy^{162}$	82	L_1	*0.43	0	1	1.9	6.1	0	7.9	
$_{66}Dy^{164}$	75	L_1	*0.37	0	1	1.8	8.5	0	9.2	
$_{67}Ho^{165}$	96	L_1	$\simeq 4.9$	~ 11	1	$\simeq 7.7$	$\simeq 2.5$	7/2	7.7	0.51
«	212	L_{21}	—	«	0.9	$\simeq 10$	~ 0.76	7/2	8.4	

§ See comments. * Cf. Fig. 2.

TABLE IIb.

nucleus	level keV	line n	$K:L$	$1:\delta^2$	β	$1:\varepsilon\{n\}$	$B:e^2$ 10^{-48} cm^4	I_0	Q_0 10^{-24} cm^2	$\lvert g_K - g_R\rvert$
$_{68}$Er even	81	L_1	*0.37	0	1	1.9	6.8	0	8.3	
$_{69}$Tm^{169}	119	K_{21}	$\simeq 6.5$	$\gtrsim 20$	0.9	1.8	3.7	1/2	7.9	—
«	119	L_2	*0.69	0	~ 0.09§	~ 34				
$_{70}$Yb even	77	L_1	*0.25	0	1	1.8	6.8	0	8.3	
$_{71}$Lu^{175}	114	L_1	$\simeq 5.5$	(~ 20)§	1	8.9	3.2	7/2	8.8	(~ 1.0)§
$_{72}$Hf^{177}	114	L_1	$\lesssim 2$	$\lesssim 0.02$§	1	(2.6)	~ 1.5§	7/2§	6.0	$\lesssim 0.03$§
$_{72}$Hf^{178}										
$_{72}$Hf^{180}	95	L_1	*0.38	0	1	2.0	$\simeq 6.9$†	0	8.3†	
$_{73}$Ta^{181}	136	K_1	6.5	7.0§	1	1.7	2.3	7/2	7.3	0.56
«	301	K_{21}	~ 7	7.1§	0.80§	2.8	$\simeq 0.62$	7/2	7.6	
$_{74}$W^{182}	100	L_1	*0.36	0	1	2.0	5.5	0	7.5	
$_{74}$W^{183}	46	M_1+N_1		—	1	5.3§	~ 2.8	1/2	8.4	—
$_{74}$W^{184}	112	L_1	*0.45	0	1	2.3	4.0	0	6.4	
$_{74}$W^{186}	123	L_1	*0.54	0	1	2.7	3.8	0	6.2	
$_{75}$Re^{185}	125	L_1	—	—	1	9.2 2.7	$\simeq 2.7$ $\simeq 0.81$	5/2	7.6 4.2	—
$_{75}$Re^{187}	135	L_1	$\simeq 5.1$	~ 8.7	1	8.7	$\simeq 1.6$	5/2	5.8	0.63
$_{77}$Ir^{191}	129	L_1	2.1§	0.86	1	4.8	$\simeq 0.56$	3/2	3.3	0.29
$_{77}$Ir^{193}	139	L_1	3.7§	3.6	1	6.2	$\simeq 0.38$	3/2	2.7	0.53
$_{78}$Pt^{195}	210	K_1	~ 3.8	~ 1	1	3.2	~ 0.47	1/2	3.4	—
$_{79}$Au^{197}	281	K_1	$\gtrsim 3$	∞ $\simeq 1.7$§	1	3.2 4.2§	~ 0.23 ~ 0.30	3/2	2.1 2.4	$\gtrsim 0.36$

§ See comments. §) Cf. Fig. 2. † Cf. footnote p. 45.

TABLE III.

Comparison of the B-values from the present Coulomb excitation measurements (summarized in Table II and repeated here in column 5) with those (column 4) computed from the half-lives (column 3) by means of equations (30) and (31). The half-lives have been taken from the tables published by SUNYAR (Su 1).

Nucleus	$h\nu$	$\tau_{1/2}$	$B_{E2}: e^2$ (from $\tau_{1/2}$)	$B_{E2}: e^2$ (from C. E.)
Z_2	keV	10^{-9} sec.	10^{-48} cm^4	10^{-48} cm^4
$_{62}Sm^{152}$	122	1.4	3.3	2.3†
$_{64}Gd^{154}$	123	1.2	3.4	$\simeq$ 2.8†
$_{66}Dy^{160}$	85	1.8	5.0	—
$_{66}Dy^{162}$	82	—	—	6.1
$_{68}Er^{164}$	90	1.4	5.5	—
$_{68}Er^{166}$	81	1.7	6.0	6.8
$_{70}Yb^{170}$	84	1.57	5.2	6.8
$_{72}Hf^{176}$	89	1.35	5.1	—
$_{72}Hf^{180}$	93	1.4	4.8	$\simeq$ 6.9
$_{74}W^{182}$	100	1.27	4.1	5.5

† The values will be relatively higher if the $K:L$ ratios are increased (cf. footnote p. 12).

References*.

Al 1 K. ALDER, A. BOHR, T. HUUS, B. R. MOTTELSON, A. WINTHER; a review article on Coulomb excitation, to be submitted to Rev. Mod. Phys.

Al 2 K. ALDER and A. WINTHER, Phys. Rev. **96**, 237 (1954); Dan. Mat. Fys. Medd. **29**, no. 19 (1955); CERN/T/KA-AW-4 (1955).

Al 3 D. E. ALBURGER and M. A. GRACE, Proc. Phys. Soc. A **67**, 280 (1954).

Be 1 H. A. BETHE, Ann. d. Phys. **5**, 325 (1930).

Be 2 H. A. BETHE, M. E. ROSE, and L. P. SMITH, Proc. Amer. Phil. Soc. **78**, 573 (1938).

Bi 1 L. C. BIEDENHARN and M. E. ROSE, Rev. Mod. Phys. **25**, 729 (1953).

Bj 1 J. H. BJERREGAARD and T. HUUS, Phys. Rev. **94**, 204 (1954).

Bo 1 A. BOHR and B. R. MOTTELSON, Dan. Mat. Fys. Medd. **27**, no. 16 (1953).

Bo 2 A. BOHR and B. R. MOTTELSON, Dan. Mat. Fys. Medd. **30**, no. 1 (1955).

* For a complete list, the reader is referred to the review article (Al 1).

Bo 3 F. Boehm, P. Marmier, and J. W. M. DuMond, Phys. Rev. **95**, 864 (1954).
Bo 4 A. Bohr and B. R. Mottelson, Chapter 17 'Beta- and Gamma-Ray Spectroscopy', ed. by K. Siegbahn, North-Holland Publ. Co. (1955).
Bo 5 A. Bohr, Dissertation (Einar Munksgaards Forlag, Copenhagen 1954).
Bo 6 N. Bohr, Dan. Mat. Fys. Medd. **18**, No. 8 (1948).
Br 1 K. J. Broström, T. Huus, and R. Tangen, Phys. Rev. **71**, 661 (1947).
Br 2 B. M. Brown and D. H. Tomboulian, Phys. Rev. **88**, 1158 (1952).

Fo 1 K. W. Ford, Phys. Rev. **95**, 1250 (1954).

Gl 1 K. M. Glover and P. Borrel, J. Nucl. Energy, 1, 215 (1955).

Gu 1 T. Gustafson, Dan. Mat. Fys. Medd. **30**, no. 5 (1955).

He 1 N. P. Heydenburg and G. M. Temmer, Phys. Rev. **100**, 150 (1955); (cf. also Phys. Rev. **93**, 906 (1954).
He 2 N. P. Heydenburg and G. M. Temmer, Phys. Rev. **95**, 861 (1954).
He 3 W. Henneberg, Z. f. Phys. **86**, 592 (1933).
Hi 1 R. D. Hill, E. L. Church, and J. W. Mihelich, Rev. Sci. Instr. **23**, 523 (1952).
Ho 1 J. M. Hollander, I. Perlman, and G. T. Seaborg, Rev. Mod. Phys. **25**, 469 (1953).
Hu 1 T. Huus and Č. Zupančič, Dan. Mat. Fys. Medd. **28**, no. 1 (1953).
Hu 2 T. Huus and A. Lundén, Phil. Mag. **45**, 966 (1954).
Hu 3 T. Huus and J. H. Bjerregaard, Phys. Rev. **92**, 1579 (1953).

Jo 1 S. A. E. Johannson, private communication.

Ka 1 T. Kamei, private communication to A. Bohr.
Ke 1 A. Kerman, Dan. Mat. Fys. Medd. 29, no. 15 (1955).
Ko 1 O. Kofoed-Hansen, J. Lindhard and O. B. Nielsen, Dan. Mat. Fys. Medd. **25**, no. 16 (1950).

Li 1 J. Lindhard and M. Scharff, Dan. Mat. Fys. Medd. **27**, no. 15 (1953).
Li 2 K. H. Lindenberger and A. Steudel, Naturwiss. **42**, 41 (1955).

Ma 1 H. Mark, private communication.
Ma 2 C. B. Madsen, Dan. Mat. Fys. Medd. **27**, no. 13 (1953).
Ma 3 N. Marty, C. R. **238**, 2516 (1954).
Ma 4 P. Marmier and F. Boehm, Phys. Rev. **97**, 103 (1955).
Mc 1 C. L. McClelland, H. Mark, and C. Goodman, Phys. Rev. **97**, 1191 (1955).

Mc 2 C. L. McClelland, private communication.
Mc 3 F. K. McGowan and P. H. Stelson, Phys. Rev. **99**, 127 (1955).
Mc 4 C. L. McClelland, H. Mark and C. Goodman, Phys. Rev. **93**, 904 (1954).
Mo 1 B. R. Mottelson and S. G. Nilsson, Phys. Rev. **99**, 1615 (1955).
Mo 2 B. R. Mottelson and S. G. Nilsson, to appear in Dan. Mat. Fys. Medd.
Mu 1 J. J. Murray, P. Snelgrove, P. E. Marmier, and J. W. M. DuMond, Phys. Rev. **96**, 858 (1954).

Ni 1 S. G. Nilsson, Dan. Mat. Fys. Medd. **29**, no. 16 (1955).

Ro 1 M. E. Rose, G. H. Goertzel, B. I. Spinrad, J. Harr, and P. Strong, Phys. Rev. **83**, 79 (1951).
Ro 2 M. E. Rose, L. C. Biedenharn, and G. B. Arfken, Phys. Rev. **85**, 5 (1952).

Sa 1 D. Saxon, Phys. Rev. **81**, 639 (1951).
Se 1 E. Segrè, Experimental Nuclear Physics I (J. Wiley and Sons, New York 1953).
Si 1 B. E. Simmons, P. M. van Patter, K. F. Famularo, and R. V. Stuart, Phys. Rev. **97**, 89 (1955).
So 1 A. Sommerfeld, Atombau und Spektrallinien II (F. Vieweg und Sohn, Braunschweig 1939).
St 1 P. H. Stelson and F. K. McGowan, Phys. Rev. **99**, 112 (1955).
Su 1 A. W. Sunyar, Phys. Rev. **98**, 653 (1955).

Te 1 G. M. Temmer and N. P. Heydenburg, private communication.

Wa 1 H. de Waard, Dissertation (Uitgeverij Excelsior, The Hague, 1954).

Zu 1 Č. Zupančič and T. Huus, Phys. Rev. **94**, 205 (1954).

Indleveret til selskabet den 15. august 1955.
Færdig fra trykkeriet den 27. februar 1956.

Matematisk-fysiske Meddelelser
udgivet af
Det Kongelige Danske Videnskabernes Selskab
Bind **30,** no. 18

Mat. Fys. Medd. Dan. Vid. Selsk. **30,** no. 18 (1956)

ON THE RESTRICTED PROBLEM OF THREE BODIES

BY

J. F. STEFFENSEN

København 1956
i kommission hos Ejnar Munksgaard

Synopsis.

Three bodies are assumed to move in a plane, subject to Newton's law of gravitation, one of the bodies being infinitely small, and the two others moving in circles around their common centre of gravitation. To expand the coordinates of the small body in powers of the time is generally assumed to be impractical, but it is shown here that by introducing certain auxiliary dependent variables, the equations of motion are transformed into a differential system of the *second degree*, permitting to calculate the coefficients of the series by a set of recurrence formulas particularly adapted to the modern calculating machines. Sufficient conditions for the convergence of the resulting series are obtained, and a simple numerical example is given.

Printed in Denmark
Bianco Lunos Bogtrykkeri A-S

1. We have in view the well-known particular case of the Problem of Three Bodies where the movement takes place in a plane, and two of the masses describe circles about their common centre of gravity, while the mass of the third body is infinitely small. Expansion of the coordinates in powers of the time t can be obtained by successive differentiations of the equations of motion, but this way of calculating the coefficients of the powers of t has been given up as too tedious[1]. We intend to show here that the calculation of the coefficients can be carried out with comparative ease when the equations of motion are transformed into a differential system of the *second degree*, permitting to calculate the coefficients of t^ν by a set of recurrence formulas, particularly adapted to the modern calculating machines. The process is closely related to that employed in one of my papers on the differential equations of G. W. HILL[2].

The equations of motion are given in Darwin's paper, p. 103. We write them, with a change of notation[3],

$$\left.\begin{aligned} \frac{d^2p}{dt^2} - 2N\frac{dq}{dt} + Mp\,(r^{-3} - 1) + (p-1)\,(s^{-3} - 1) &= 0, \\ \frac{d^2q}{dt^2} + 2N\frac{dp}{dt} + Mq(r^{-3} - 1) + q(s^{-3} - 1) &= 0, \end{aligned}\right\} \tag{1}$$

where

$$r^2 = p^2 + q^2, \qquad s^2 = r^2 + 1 - 2p, \tag{2}$$

$$N^2 = M + 1. \tag{3}$$

[1] G. H. DARWIN: "Periodic Orbits". Acta mathematica, 21 (1897), 129—132.

[2] J. F. STEFFENSEN: "On the Differential Equations of Hill in the Theory of the Motion of the Moon (II)". Acta mathematica, 95 (1956), 25—37.

[3] Darwin's x, y, n, ν, ϱ, C have in succession been replaced by p, q, N, M, s, K.

Jacobi's integral is

$$M(r^2 + 2r^{-1}) + (s^2 + 2s^{-1}) - \left(\frac{dp}{dt}\right)^2 - \left(\frac{dq}{dt}\right)^2 = K. \tag{4}$$

In these equations p and q are the coordinates of the infinitesimal body, the masses of the finite bodies are M and 1, their distance from each other 1, and the angular velocity of the system N.

Referring for further particulars to Darwin's paper we put

$$X = r^{-3} - 1, \qquad Y = s^{-3} - 1, \tag{5}$$

so that

$$\left.\begin{aligned} r\frac{dX}{dt} + 3(X+1)\frac{dr}{dt} &= 0, \\ s\frac{dY}{dt} + 3(Y+1)\frac{ds}{dt} &= 0. \end{aligned}\right\} \tag{6}$$

while (1) can be written

$$\left.\begin{aligned} \frac{d^2p}{dt^2} - 2N\frac{dq}{dt} + MpX + pY - Y &= 0, \\ \frac{d^2q}{dt^2} + 2N\frac{dp}{dt} + MqX + qY &= 0. \end{aligned}\right\} \tag{7}$$

For the determination of p, q, r, s, X, Y we have the 6 equations (7), (6) and (2) which we propose to satisfy by power series in t without making use of Jacobi's integral. We put

$$p = \sum_{\nu=0}^{\infty} a_\nu t^\nu, \qquad q = \sum_{\nu=0}^{\infty} b_\nu t^\nu, \tag{8}$$

$$r = \sum_{\nu=0}^{\infty} c_\nu t^\nu, \qquad s = \sum_{\nu=0}^{\infty} d_\nu t^\nu, \tag{9}$$

$$X = \sum_{\nu=0}^{\infty} e_\nu t^\nu, \qquad Y = \sum_{\nu=0}^{\infty} f_\nu t^\nu. \tag{10}$$

Inserting these series in the 6 equations and demanding that the coefficient of t^n shall vanish, we find by (7)

$$\left.\begin{aligned}
&(n+1)(n+2)\,a_{n+2} - 2N(n+1)\,b_{n+1} + M\sum_{\nu=0}^{n} a_\nu e_{n-\nu} \\
&\qquad + \sum_{\nu=0}^{n} a_\nu f_{n-\nu} - f_n = 0, \\
&(n+1)(n+2)\,b_{n+2} + 2N(n+1)\,a_{n+1} + M\sum_{\nu=0}^{n} b_\nu e_{n-\nu} \\
&\qquad + \sum_{\nu=0}^{n} b_\nu f_{n-\nu} = 0,
\end{aligned}\right\} \quad (11)$$

by (6)

$$\left.\begin{aligned}
&\sum_{\nu=0}^{n}(\nu+1)\,e_{\nu+1}c_{n-\nu} + 3\sum_{\nu=0}^{n}(\nu+1)\,c_{\nu+1}e_{n-\nu} \\
&\qquad + 3(n+1)\,c_{n+1} = 0, \\
&\sum_{\nu=0}^{n}(\nu+1)\,f_{\nu+1}d_{n-\nu} + 3\sum_{\nu=0}^{n}(\nu+1)\,d_{\nu+1}f_{n-\nu} \\
&\qquad + 3(n+1)\,d_{n+1} = 0,
\end{aligned}\right\} \quad (12)$$

and by (2)

$$\left.\begin{aligned}
&\sum_{\nu=0}^{n} c_\nu c_{n-\nu} = \sum_{\nu=0}^{n} a_\nu a_{n-\nu} + \sum_{\nu=0}^{n} b_\nu b_{n-\nu}, \\
&\sum_{\nu=0}^{n} d_\nu d_{n-\nu} = \sum_{\nu=0}^{n} c_\nu c_{n-\nu} - 2\,a_n \qquad (n>0), \\
&d_0^2 = c_0^2 + 1 - 2\,a_0.
\end{aligned}\right\} \quad (13)$$

As initial values (constants of integration) we choose the coordinates and components of velocity of the infinitely small body at the time $t = 0$, that is a_0, a_1, b_0, b_1. Hence we find by (13), c_0 and d_0 being positive (since r and s represent distances from the finite masses)

$$c_0 = \sqrt{a_0^2 + b_0^2}, \qquad d_0 = \sqrt{c_0^2 + 1 - 2a_0}, \qquad (14)$$

whereafter by (10) and (5)

$$e_0 = c_0^{-3} - 1, \qquad f_0 = d_0^{-3} - 1. \qquad (15)$$

The remaining constants are calculated by the recurrence formulas (11) — (13). We state these in the form and order in which they are to be employed.

$$2\,c_0 c_n = \sum_{\nu=0}^{n} a_\nu a_{n-\nu} + \sum_{\nu=0}^{n} b_\nu b_{n-\nu} - \sum_{\nu=1}^{n-1} c_\nu c_{n-\nu}. \tag{16}$$

$$2\,d_0 d_n = \sum_{\nu=0}^{n} c_\nu c_{n-\nu} - \sum_{\nu=1}^{n-1} d_\nu d_{n-\nu} - 2\,a_n. \tag{17}$$

$$-nc_0 e_n = 3\sum_{\nu=1}^{n} \nu c_\nu e_{n-\nu} + \sum_{\nu=1}^{n-1} \nu e_\nu c_{n-\nu} + 3\,nc_n. \tag{18}$$

$$-nd_0 f_n = 3\sum_{\nu=1}^{n} \nu d_\nu f_{n-\nu} + \sum_{\nu=1}^{n-1} \nu f_\nu d_{n-\nu} + 3\,nd_n. \tag{19}$$

$$\left.\begin{aligned} -n(n+1)\,a_{n+1} = M\sum_{\nu=0}^{n-1} a_\nu e_{n-\nu-1} + \sum_{\nu=0}^{n-1} a_\nu f_{n-\nu-1} \\ -2\,Nnb_n - f_{n-1}. \end{aligned}\right\} \tag{20}$$

$$-n(n+1)\,b_{n+1} = M\sum_{\nu=0}^{n-1} b_\nu e_{n-\nu-1} + \sum_{\nu=0}^{n-1} b_\nu f_{n-\nu-1} + 2\,Nna_n. \tag{21}$$

We give below the first few of these recurrence formulas.

$$\left.\begin{aligned} c_0 c_1 &= a_0 a_1 + b_0 b_1. \\ d_0 d_1 &= c_0 c_1 - a_1. \\ -c_0 e_1 &= 3\,c_1(e_0+1). \\ -d_0 f_1 &= 3\,d_1(f_0+1). \end{aligned}\right\} \tag{22}$$

$$\left.\begin{aligned} -2\,a_2 &= Ma_0 e_0 + f_0(a_0-1) - 2\,Nb_1, \\ -2\,b_2 &= Mb_0 e_0 + f_0 b_0 + 2\,Na_1. \\ 2\,c_0 c_2 &= 2\,a_0 a_2 + a_1^2 + 2\,b_0 b_2 + b_1^2 - c_1^2. \\ 2\,d_0 d_2 &= 2\,c_0 c_2 + c_1^2 - d_1^2 - 2\,a_2. \\ -c_0 e_2 &= 2\,c_1 e_1 + 3\,c_2(e_0+1). \\ -d_0 f_2 &= 2\,d_1 f_1 + 3\,d_2(f_0+1). \end{aligned}\right\} \tag{23}$$

$$\left.\begin{aligned} -6\,a_3 &= M(a_0 e_1 + a_1 e_0) + f_0 a_1 + f_1(a_0-1) - 4\,Nb_2. \\ -6\,b_3 &= M(b_0 e_1 + b_1 e_0) + b_0 f_1 + b_1 f_0 + 4\,Na_2. \end{aligned}\right\} \tag{24}$$

$$\left.\begin{aligned} c_0 c_3 &= a_0 a_3 + a_1 a_2 + b_0 b_3 + b_1 b_2 - c_1 c_2 . \\ d_0 d_3 &= c_0 c_3 + c_1 c_2 - d_1 d_2 - a_3 . \\ -3\, c_0 e_3 &= 5\, c_1 e_2 + 7\, c_2 e_1 + 9\, c_3 (e_0 + 1) . \\ -3\, d_0 f_3 &= 5\, d_1 f_2 + 7\, d_2 f_1 + 9\, d_3 (f_0 + 1) . \end{aligned}\right\} \quad (24)$$

It is seen that these forms lend themselves easily to the calculating machine.

2. In order to examine the convergence we write (16)—(21) in the following form where the constants of integration and those of zero order have been isolated. In (25), (29) and (30) we assume $n \geqslant 3$, in (26)—(28) $n \geqslant 2$.

$$\left.\begin{aligned} c_0 c_n &= a_0 a_n + a_1 a_{n-1} + b_0 b_n + b_1 b_{n-1} - c_1 c_{n-1} \\ &\quad + \frac{1}{2} \sum_{\nu=2}^{n-2} (a_\nu a_{n-\nu} + b_\nu b_{n-\nu} - c_\nu c_{n-\nu}) . \end{aligned}\right\} \quad (25)$$

$$d_0 d_n = c_0 c_n - a_n + \frac{1}{2} \sum_{\nu=1}^{n-1} (c_\nu c_{n-\nu} - d_\nu d_{n-\nu}) . \quad (26)$$

$$-n c_0 e_n = 3\, n c_n (e_0 + 1) + 2 \sum_{\nu=1}^{n-1} \nu c_\nu e_{n-\nu} + n \sum_{\nu=1}^{n-1} c_\nu e_{n-\nu} . \quad (27)$$

$$-n d_0 f_n = 3\, n d_n (f_0 + 1) + 2 \sum_{\nu=1}^{n-1} \nu d_\nu f_{n-\nu} + n \sum_{\nu=1}^{n-1} d_\nu f_{n-\nu} . \quad (28)$$

$$\left.\begin{aligned} -n(n+1)\, a_{n+1} &= a_0 (f_{n-1} + Me_{n-1}) + a_1 (f_{n-2} + Me_{n-2}) + \\ &\sum_{\nu=2}^{n-2} a_\nu (f_{n-\nu-1} + Me_{n-\nu-1}) + a_{n-1} (f_0 + Me_0) - f_{n-1} - 2\, Nn\, b_n . \end{aligned}\right\} \quad (29)$$

$$\left.\begin{aligned} -n(n+1)\, b_{n+1} &= b_0 (f_{n-1} + Me_{n-1}) + b_1 (f_{n-2} + Me_{n-2}) \\ &+ \sum_{\nu=2}^{n-2} b_\nu (f_{n-\nu-1} + Me_{n-\nu-1}) + b_{n-1} (f_0 + Me_0) + 2\, Nn a_n . \end{aligned}\right\} \quad (30)$$

We now put, as in an earlier paper[1],

$$K_\nu = \frac{\lambda^\nu}{\nu(\nu+1)} \qquad (\lambda > 0) \quad (31)$$

[1] Acta mathematica, 93 (1955), 173.

and assume that it has been proved for $2 \leqslant \nu \leqslant n$ that

$$| a_\nu | \leqslant AK_\nu, \qquad | b_\nu | \leqslant BK_\nu \tag{32}$$

and for $1 \leqslant \nu \leqslant n-1$ that

$$| c_\nu | \leqslant CK_\nu, \quad | d_\nu | \leqslant DK_\nu, \quad | e_\nu | \leqslant EK_\nu, \quad | f_\nu | \leqslant FK_\nu. \tag{33}$$

We then find sufficient conditions, by (25) — (28) for the validity of (33) in the case $\nu = n$, and by (29) — (30) for (32) in the case $\nu = n+1$, so that the inequalities (32) and (33) are valid for all ν under consideration. We proceed as in the paper quoted, making use of the identity

$$\left.\begin{aligned} K_\nu K_{m-\nu} = \lambda^m \Bigg[\left(\frac{1}{\nu} + \frac{1}{m-\nu}\right) \frac{1}{m(m+1)} - \\ \left(\frac{1}{\nu+1} + \frac{1}{m-\nu+1}\right) \frac{1}{(m+1)(m+2)} \Bigg]. \end{aligned}\right\} \tag{34}$$

From this, writing for abbreviation

$$s_n = \sum_{\nu=1}^{n} \frac{1}{\nu} \tag{35}$$

we obtain the sums[1]

$$\sum_{\nu=1}^{n-1} K_\nu K_{n-\nu} = 2 \frac{n-1+2s_{n-1}}{n(n+1)(n+2)} \lambda^n, \tag{36}$$

$$\sum_{\nu=2}^{n-2} K_\nu K_{n-\nu} = \left(2 \frac{n-1+2s_{n-1}}{(n+1)(n+2)} - \frac{1}{n-1}\right) \frac{\lambda^n}{n}, \tag{37}$$

$$\sum_{\nu=2}^{n-2} K_\nu K_{n-\nu-1} = \left(2 \frac{n-2+2s_{n-2}}{n(n+1)} - \frac{1}{2(n-2)}\right) \frac{\lambda^{n-1}}{n-1}, \tag{38}$$

$$\sum_{\nu=1}^{n-1} \nu K_\nu K_{n-\nu} = \frac{n-1+2s_{n-1}}{(n+1)(n+2)} \lambda^n. \tag{39}$$

[1] Interpreted as zero, if the upper limit of summation is less than the lower.

3. Dealing first with (25), we obtain, c_0 being positive, by (32) and (33)

$$\left.\begin{aligned} c_0 \mid c_n \mid &\leqslant (A \mid a_0 \mid + B \mid b_0 \mid) K_n \\ &+ (A \mid a_1 \mid + B \mid b_1 \mid + C \mid c_1 \mid) K_{n-1} \\ &+ \frac{1}{2}(A^2 + B^2 + C^2) \sum_{\nu=2}^{n-2} K_\nu K_{n-\nu} \end{aligned}\right\}$$

or

$$\left.\begin{aligned} c_0 \mid c_n \mid &\leqslant (A \mid a_0 \mid + B \mid b_0 \mid) \frac{\lambda^n}{n(n+1)} \\ &+ (A \mid a_1 \mid + B \mid b_1 \mid + C \mid c_1 \mid) \frac{\lambda^{n-1}}{(n-1)n} \\ &+ \frac{1}{2}(A^2 + B^2 + C^2)\left(2\frac{n-1+2s_{n-1}}{(n+1)(n+2)} - \frac{1}{n-1}\right)\frac{\lambda^n}{n}. \end{aligned}\right\} \quad (40)$$

If, now, we demand that the right-hand side of this inequality shall be $\leqslant c_0 C K_n = c_0 C \dfrac{\lambda^n}{n(n+1)}$, we obtain after multiplication by $n(n+1)\lambda^{-n}$ as a sufficient condition for the validity of $|c_\nu| \leqslant CK_\nu$ in all cases under consideration

$$\left.\begin{aligned} &A \mid a_0 \mid + B \mid b_0 \mid + (A \mid a_1 \mid + B \mid b_1 \mid + C \mid c_1 \mid)\frac{n+1}{n-1}\cdot\frac{1}{\lambda} \\ &+ \frac{1}{2}(A^2 + B^2 + C^2)\left(2\frac{n-1+2s_{n-1}}{n+2} - \frac{n+1}{n-1}\right) \leqslant Cc_0. \end{aligned}\right\} \quad (41)$$

We replace this condition by a simpler but more rigid condition obtained by replacing the factors depending on n by absolute numbers which are at least as large.

Since $\dfrac{n+1}{n-1} = 1 + \dfrac{2}{n-1}$, this factor is constantly decreasing and may for $n \geqslant 2$ be replaced by 3.

Putting next

$$S_n = 2\frac{n-1+2s_{n-1}}{n+2} - \frac{n+1}{n-1}, \quad (42)$$

and observing that

$$s_n \leqslant 1 + \frac{1}{2} + \frac{1}{3} + \frac{n-3}{4} = \frac{13}{12} + \frac{n}{4} \tag{43}$$

so that

$$s_{n-1} \leqslant \frac{5}{6} + \frac{n}{4}$$

or $4\, s_{n-1} \leqslant n + \frac{10}{3}$, we find by inserting this in (42)

$$S_n \leqslant 2 - \frac{14}{3\,n+6} - \frac{2}{n-1}.$$

Hence

$$S_n < 2. \tag{44}$$

Observing finally that $\frac{n+1}{n-1} \leqslant 3$ for $n \geqslant 2$, we may replace (41) by the more rigid condition

$$\left.\begin{aligned} A \mid a_0 \mid + B \mid b_0 \mid + (A \mid a_1 \mid + B \mid b_1 \mid + C \mid c_1 \mid)\frac{3}{\lambda} \\ + A^2 + B^2 + C^2 \leqslant c_0 C \end{aligned}\right\} \tag{45}$$

which is independent of n.

4. Next, as regards (26), we find by (36), corresponding to (41), the sufficient condition

$$Cc_0 + A + (C^2 + D^2)\frac{n - 1 + 2\,s_{n-1}}{n+2} \leqslant Dd_0. \tag{46}$$

The condition that the factor depending on n shall be steadily decreasing may be written in the form

$$s_{n-1} > \frac{5}{2} + \frac{2}{n} \tag{47}$$

which is satisfied for $n \geqslant 10$. We therefore have in this region[1]

$$\frac{n - 1 + 2\,s_{n-1}}{n+2} < \frac{3}{4} + \frac{1}{6}s_9 < \frac{5}{4} \tag{48}$$

[1] A table of s_n is found in S. SPITZER: Tabellen für die Zinses-Zinsen und Renten-Rechnung, Wien 1897, 369—370.

which is also valid for $n < 10$. We may therefore replace (46) by the simpler but more rigid condition

$$Cc_0 + A + \frac{5}{4}(C^2 + D^2) \leqslant Dd_0. \tag{49}$$

5. From (27) we obtain by (39) and (36) as a sufficient condition

$$3 \mid e_0 + 1 \mid C + 4\,CE\frac{n - 1 + 2\,s_{n-1}}{n+2} \leqslant Ec_0, \tag{50}$$

and from this, by (48), the more rigid sufficient condition

$$3 \mid e_0 + 1 \mid C + 5\,CE \leqslant Ec_0. \tag{51}$$

Since (28) is obtained from (27) by a simple exchange of letters we may at once by (51) write down the following sufficient condition, resulting from (28)

$$3 \mid f_0 + 1 \mid D + 5\,DF \leqslant Fd_0. \tag{52}$$

6. As regards (29), we have, by (31)—(33) and (38),

$$\left.\begin{aligned} n\,(n+1) \mid a_{n+1} \mid \leqslant \mid a_0 \mid (F + ME)\frac{\lambda^{n-1}}{(n-1)\,n} \\ + \mid a_1 \mid (F + ME)\frac{\lambda^{n-2}}{(n-2)\,(n-1)} \\ + A\,(F + ME)\left(2\frac{n - 2 + 2\,s_{n-2}}{n\,(n+1)} - \frac{1}{2\,(n-2)}\right)\frac{\lambda^{n-1}}{n-1} \\ + A \mid f_0 + Me_0 \mid \frac{\lambda^{n-1}}{(n-1)\,n} + F\frac{\lambda^{n-1}}{(n-1)\,n} + 2\,NB\frac{\lambda^n}{n+1}. \end{aligned}\right\} \tag{53}$$

If we demand that the right-hand side of this shall be $\leqslant n\,(n+1)\,AK_{n+1} = A\frac{n}{n+2}\lambda^{n+1}$, we obtain after multiplication by $\frac{n+2}{n}\lambda^{1-n}$ the condition

$$\left.\begin{aligned} &[\,|\,a_0\,|\,(F+ME)+A\,|\,f_0+Me_0\,|\,+F]\,\frac{n+2}{(n-1)\,n^2} \\ +\,2\,NB\,&\frac{n+2}{n\,(n+1)}\,\lambda+|\,a_1\,|\,(F+ME)\,\frac{n+2}{n\,(n-1)\,(n-2)}\,\frac{1}{\lambda} \\ &+A\,(F+ME)\,R_n \leqslant A\,\lambda^2 \end{aligned}\right\} \tag{54}$$

where

$$R_n=\frac{2\,(n+2)}{n\,(n-1)}\left(\frac{n-2+2\,s_{n-2}}{n\,(n+1)}-\frac{1}{4\,(n-2)}\right). \tag{55}$$

We proceed to show that

$$R_n \leqslant \frac{1}{8} \qquad (n \geqslant 3). \tag{56}$$

We write (55) in the form

$$R_n=\left(\frac{2}{n-1}+\frac{4}{n\,(n-1)}\right)\left(2\,\frac{s_{n-2}-1}{n\,(n+1)}+\frac{3}{4}\,\frac{n-3}{(n+1)\,(n-2)}\right.$$

where we may assume $n \geqslant 5$, since $R_3 = 0$, $R_4 = \frac{1}{8}$. Now the first factor in R_n is evidently decreasing, and the second factor is the sum of two decreasing expressions, since

$$\frac{s_{n-2}-1}{n\,(n+1)} > \frac{s_{n-1}-1}{(n+1)\,(n+2)} \qquad (n \geqslant 5)$$

which can be written

$$2\,(s_{n-2}-1) > 1+\frac{1}{n-1},$$

and

$$\frac{n-3}{(n+1)\,(n-2)} > \frac{n-2}{(n+2)\,(n-1)} \qquad (n \geqslant 5)$$

which can be written

$$n\,(n-5)+2 > 0.$$

The remaining factors depending on n in (54) are steadily decreasing, and we find for $n \geqslant 3$

$$\frac{n+2}{(n-1)\,n^2} = \frac{1}{(n-1)\,n} + \frac{2}{(n-1)\,n^2} \leqslant \frac{5}{18}, \tag{57}$$

$$\frac{n+2}{n\,(n+1)} = \frac{1}{n+1} + \frac{2}{n\,(n+1)} \leqslant \frac{5}{12}, \tag{58}$$

$$\left.\begin{aligned} \frac{n+2}{n\,(n-1)\,(n-2)} &= \frac{1}{(n-1)\,(n-2)} \\ &+ \frac{2}{n\,(n-1)\,(n-2)} \leqslant \frac{5}{6}. \end{aligned}\right\} \tag{59}$$

Inserting finally the limits (56) — (59) in (54), we obtain the more rigid, but of n independent, sufficient condition

$$\left.\begin{aligned} &\frac{5}{18}\left[\,|\,a_0\,|\,(F+ME) + A\,|\,f_0 + Me_0\,|\, + F\right] + \frac{5}{6}\,NB\lambda \\ &+ \frac{5}{6}\,|\,a_1\,|\,(F+ME)\,\frac{1}{\lambda} + \frac{1}{8}\,A\,(F+ME) \leqslant A\lambda^2. \end{aligned}\right\} \tag{60}$$

7. As regards finally (30), a comparison with (29) shows that we obtain the same form as (53), the only difference being that a and b, A and B have been exchanged and the term $F\,\dfrac{\lambda^{n-1}}{(n-1)\,n}$ left out. We may therefore immediately write down the sufficient condition corresponding to (60)

$$\left.\begin{aligned} &\frac{5}{18}\left[\,|\,b_0\,|\,(F+ME) + B\,|\,f_0 + Me_0\,|\,\right] + \frac{5}{6}\,NA\lambda \\ &+ \frac{5}{6}\,|\,b_1\,|\,(F+ME)\,\frac{1}{\lambda} + \frac{1}{8}\,B\,(F+ME) \leqslant B\lambda^2. \end{aligned}\right\} \tag{61}$$

8. The result of the preceding investigation is that, if for a certain $n \geqslant 3$ it has been proved that (32) is satisfied for $2 \leqslant \nu \leqslant n$ and (33) for $1 \leqslant \nu \leqslant n-1$, and if, besides, the inequalities

(45), (49), (51), (52), (60) and (61) are all satisfied, then the expansions (8) — (10) are convergent, provided that $\Sigma K_\nu \mid t \mid^\nu$ converges, that is, for $\mid t \mid \leqslant \frac{1}{\lambda}$.

The question arises whether, when the constants of integration are arbitrarily given, it is always possible to find such values of λ, A, B, C, D, E, F that the six inequalities are all satisfied. We proceed to prove that this is really so.

To begin with, λ can always be chosen so large that (60) and (61) are satisfied, no matter what values the other constants possess, and (45) can for sufficiently large λ be replaced by

$$A \mid a_0 \mid + B \mid b_0 \mid + \frac{5}{4}(A^2 + B^2) < C\left(c_0 - \frac{5}{4} C\right) \tag{62}$$

while the three remaining inequalities which we write in the form

$$A + C\left(c_0 + \frac{5}{4} C\right) \leqslant D\left(d_0 - \frac{5}{4} D\right), \tag{63}$$

$$3 \mid e_0 + 1 \mid C \leqslant E\,(c_0 - 5\,C), \tag{64}$$

$$3 \mid f_0 + 1 \mid D \leqslant F\,(d_0 - 5\,D), \tag{65}$$

are unchanged. Now it follows from (64) and (65) that we must choose

$$C < \frac{1}{5} c_0, \qquad D < \frac{1}{5} d_0, \tag{66}$$

after which (64) and (65) are satisfied, provided that we choose E and F sufficiently large. After this, (62) will be satisfied, if we choose A and B sufficiently small in comparison with C, and (63) if A and C are sufficiently small in comparison with D. In thus choosing small values for A, B, C and D we do not run into difficulties, because (31) — (33) show that small values of these constants can be compensated by choosing λ sufficiently large.

There is, thus, always a solution for sufficiently small values of $\mid t \mid$, if $c_0 > 0$, $d_0 > 0$ as assumed in (14).

9. If at the time $t = 0$ we have $q = 0$, $\frac{dp}{dt} = 0$, that is $b_0 = 0$, $a_1 = 0$, certain simplifications occur. In that case there are only the two arbitrary constants a_0 and b_1 left, and we find first by (14) and (15), if $a_0 \neq 0$ and $a_0 \neq 1$,

$$\left.\begin{aligned} c_0 = |\, a_0 \,|, \quad d_0 = |\, a_0 - 1 \,|, \quad e_0 = |\, a_0 \,|^{-3} - 1, \\ f_0 = |\, a_0 - 1 \,|^{-3} - 1. \end{aligned}\right\} \tag{67}$$

The recurrence formulas now show that b_ν vanishes when ν is an even number, and the other coefficients when ν is odd. Under these circumstances the working formulas (16) — (21) are best written thus

$$\left.\begin{aligned} -(2n-1)\,2n a_{2n} = M \sum_{\nu=0}^{n-1} a_{2\nu} e_{2n-2\nu-2} + \sum_{\nu=0}^{n-1} a_{2\nu} f_{2n-2\nu-2} \\ - 2N(2n-1)\, b_{2n-1} - f_{2n-2}. \end{aligned}\right\} \tag{68}$$

$$\left.\begin{aligned} 2 c_0 c_{2n} = \sum_{\nu=0}^{n} a_{2\nu}\, a_{2n-2\nu} + \sum_{\nu=1}^{n} b_{2\nu-1} b_{2n-2\nu+1} \\ - \sum_{\nu=1}^{n-1} c_{2\nu} c_{2n-2\nu}. \end{aligned}\right\} \tag{69}$$

$$2 d_0 d_{2n} = \sum_{\nu=0}^{n} c_{2\nu} c_{2n-2\nu} - \sum_{\nu=1}^{n-1} d_{2\nu} d_{2n-2\nu} - 2 a_{2n}. \tag{70}$$

$$-n c_0 e_{2n} = 3 \sum_{\nu=1}^{n} \nu c_{2\nu} e_{2n-2\nu} + \sum_{\nu=1}^{n-1} \nu e_{2\nu} c_{2n-2\nu} + 3 n c_{2n}. \tag{71}$$

$$-n d_0 f_{2n} = 3 \sum_{\nu=1}^{n} \nu d_{2\nu} f_{2n-2\nu} + \sum_{\nu=1}^{n-1} \nu f_{2\nu} d_{2n-2\nu} + 3 n d_{2n}. \tag{72}$$

$$\left.\begin{aligned} -2n(2n+1)\, b_{2n+1} = M \sum_{\nu=1}^{n} b_{2\nu-1} e_{2n-2\nu} \\ + \sum_{\nu=1}^{n} b_{2\nu-1} f_{2n-2\nu} + 4 N n a_{2n}. \end{aligned}\right\} \tag{73}$$

The first few of these formulas are

$$\left.\begin{aligned} -2\,a_2 &= Ma_0e_0 + f_0(a_0-1) - 2\,Nb_1. \\ c_0c_2 &= a_0a_2 + \frac{1}{2}b_1^2. \\ d_0d_2 &= c_0c_2 - a_2. \\ -c_0e_2 &= 3\,c_2(e_0+1). \\ -d_0f_2 &= 3\,d_2(f_0+1). \end{aligned}\right\} \quad (74)$$

$$-6\,b_3 = Mb_1e_0 + b_1f_0 + 4\,Na_2. \quad (75)$$

$$\left.\begin{aligned} -12\,a_4 &= M(a_0e_2 + a_2e_0) + f_2(a_0-1) + a_2f_0 - 6\,Nb_3. \\ 2\,c_0c_4 &= 2\,a_0a_4 + a_2^2 + 2\,b_1b_3 - c_2^2. \\ 2\,d_0d_4 &= 2\,c_0c_4 + c_2^2 - d_2^2 - 2\,a_4. \\ -c_0e_4 &= 2\,c_2e_2 + 3\,c_4(e_0+1). \\ -d_0f_4 &= 2\,d_2f_2 + 3\,d_4(f_0+1). \end{aligned}\right\} \quad (76)$$

$$-20\,b_5 = M(b_1e_2 + b_3e_0) + b_1f_2 + b_3f_0 + 8\,Na_4. \quad (77)$$

$$\left.\begin{aligned} -30\,a_6 &= M(a_0e_4 + a_2e_2 + a_4e_0) + f_4(a_0-1) + a_2f_2 \\ &\quad + a_4f_0 - 10\,Nb_5. \\ c_0c_6 &= a_0a_6 + a_2a_4 + b_1b_5 + \frac{1}{2}b_3^2 - c_2c_4. \\ d_0d_6 &= c_0c_6 + c_2c_4 - d_2d_4 - a_6. \\ -3\,c_0e_6 &= 3(c_2e_4 + 2\,c_4e_2 + 3\,c_6e_0) + e_2c_4 + 2\,e_4c_2 + 9\,c_6. \\ -3\,d_0f_6 &= 3(d_2f_4 + 2\,d_4f_2 + 3\,d_6f_0) + f_2d_4 + 2\,f_4d_2 + 9\,d_6. \end{aligned}\right\} \quad (78)$$

10. As a simple numerical example of the application of (74) — (78) we choose $a_0 = \frac{1}{2}$, $b_1 = -1$ besides the already assumed $b_0 = 0$, $a_1 = 0$ leading to (67). For N and M we choose the values $N = 1{\cdot}1$, $M = {\cdot}21$ which satisfy (3). The results are given in the table below.

ν	a_ν	c_ν	d_ν
0	·5	·5	·5
2	·2825	1·2825	·7175
4	—·4332729	—4·407273	—2·4107271
6	1·3130591	19·199425	8·728045

ν	e_ν	f_ν	ν	b_ν
0	7·	7·	1	—1·
2	—61·56	—34·44	3	1·2045
4	527·3519	214·5577	5	—2·687845
6	—4442·1231	—1319·5487		

A partial check on these calculations is obtained by calculating the value of Jacobi's constant K by (4) for various values of t. I have found

$$t = 0, \qquad K = 4{\cdot}1425$$
$$t = {\cdot}03, \qquad K = 4{\cdot}1424999$$

which seems satisfactory.

As regards the convergence, (32) and (33) are satisfied by the coefficients given in the table if, for instance, we choose $\lambda = 20$, $A = {\cdot}005$, $B = {\cdot}002$, $C = {\cdot}02$, $D = {\cdot}04$, $E = 1{\cdot}2$, $F = 3.2$, and since these values also satisfy all the six inequalities (45), (49), (51), (52), (60) and (61), the expansions (8) — (10) are at least convergent for $|t| \leqslant \frac{1}{20}$.

This space of time may at first appear to be small, but the expansion for q shows that it corresponds to a movement in the vertical direction of nearly one tenth of the original distance of the infinitesimal body from either of the two finite bodies.

Indleveret til selskabet den 30. januar 1956.
Færdig fra trykkeriet den 29. maj 1956.

Matematisk-fysiske Meddelelser
udgivet af
Det Kongelige Danske Videnskabernes Selskab
Bind **30,** no. 19

Mat. Fys. Medd. Dan. Vid. Selsk. **30,** no. 19 (1956)

QUASI-CLASSICAL PATH INTEGRALS

BY

H. J. GROENEWOLD

København 1956
i kommission hos Ejnar Munksgaard

Synopsis.

Various time-independent and time-dependent expansions for non-relativistic motion are considered with a "semi-classical" zero order term. The expansions are expressed with the help of quasi-classical paths. They are all easily combined with a Born expansion. The connection with the BWK method and with the Feynman path integrals is pointed out.

Printed in Denmark
Bianco Lunos Bogtrykkeri A-S

1. Introduction.

Quasi-classical path integrals occur in various ways in quantum mechanics. Their purpose may range from an expression of a hidden pining for the good old classical theory to a practical tool in an approximation process. Two characteristic forms are the time-independent integrals of, e. g., the BWK approximation[1] and the time-dependent Feynman path integrals[2]. The BWK method is usually restricted to essentially 1-dimensional problems. We shall first deal with the question in how far this restriction is essential to the approximation. Meanwhile we may combine BWK approximation and Born approximation. We further discuss the connection between the time-independent and the time-dependent forms (all non-relativistic). Finally, we consider the singular case of quasi-classical propagation, which occurs in weak fields.

2. 1-dimensional stationary Schrödinger waves.

Consider a particle with mass m in a potential

$$V(x) = V_0(x) + V_1(x). \tag{2.01}$$

The part $V_0(x)$ will be involved in a BWK expansion, the part $V_1(x)$ in a Born expansion. One of them may be zero. The eigenfunctions $\psi(x)$ of the time-independent Schrödinger equation

$$\left\{ E + \frac{\hbar^2}{2m}\frac{d^2}{dx^2} - V_0(x) \right\} \psi(x) = V_1(x)\ \psi(x) \tag{2.02}$$

with energy eigenvalue E can arbitrarily be split up into

$$\psi(x) = \psi_+(x) + \psi_-(x) \tag{2.03}$$

with

$$\psi_{\pm}(x) = A_{\pm}(x)\; e^{\frac{i}{\hbar} S_{\pm}(x)}\;;\; A_{\pm}(x) = B_{\pm}(x)\, A(x), \quad (2.04)$$

where $A(x)$ is an arbitrary normalization function and

$$S_{\pm}(x) = \int^{x} dx'\; p_{\pm}(x')\,; \quad (2.05)$$

$$p_{\pm}(x) = \pm\, p(x) = \pm \left\{ 2m\,(E - V_0(x)) \right\}^{1/2}. \quad (2.06)$$

The splitting (2.03) can be made unique by an auxiliary condition on the B's. If we choose for this

$$\frac{d\left\{ B_{+}(x)\; A(x)/C(x) \right\}}{dx} e^{\frac{i}{\hbar} S_{\pm}(x)} + \frac{d\left\{ B_{-}(x)\; A(x)/C(x) \right\}}{dx} e^{\frac{i}{\hbar} S_{-}(x)} = 0, \quad (2.0$$

with an arbitrary splitting function $C(x)$, insertion into (2.02) gives for the B's the equations

$$\left.\begin{aligned} \pm \frac{dB_{\pm}(x)}{dx} e^{\frac{i}{\hbar} S_{\pm}(x)} &= \frac{1}{2}\left\{ \pm\left(2\frac{A'}{A} + \frac{p'}{p} \right) \right. \\ &\quad \left. + \frac{\hbar}{ip}\left(\left(\frac{C'}{C} \right)^2 + \left(\frac{C'}{C} \right)' \right) + \frac{2mi}{\hbar^2} V_1 \right\} B_{\pm}\, e^{\frac{i}{\hbar} S_{\pm}} \\ &\quad + \frac{1}{2}\left\{ \pm\left(2\frac{C'}{C} + \frac{p'}{p} \right) \right. \\ &\quad \left. + \frac{\hbar}{ip}\left(\left(\frac{C'}{C} \right)^2 + \left(\frac{C'}{C} \right)' \right) + \frac{2mi}{\hbar^2} V_1 \right\} B_{\mp}\, e^{\frac{i}{\hbar} S_{\mp}}. \end{aligned}\right\} \quad (2.08)$$

The dashes denote the derivatives with respect to x.

We consider such cases for which the coefficients in the right-hand member can be regarded as small, viz., the V_1 terms according to the Born expansion, the derivative terms according to the BWK expansion. So we expand

$$B_{\pm}(x) = \sum_{r=0}^{\infty} B_{\pm}^{(r)}(x), \quad (2.09)$$

with

$$B_{\pm}^{(0)}(x) = B_{\pm}^{(0)} \quad \text{(constant)}; \tag{2.10}$$

$$\left.\begin{aligned} \pm \frac{dB_{\pm}^{(r+1)}(x)}{dx} e^{\frac{i}{\hbar} S_{\pm}(x)} &= \frac{1}{2}\left\{ \pm\left(2\frac{A'}{A} + \frac{p'}{p}\right)\right. \\ &\left. + \frac{\hbar}{ip}\left(\left(\frac{C'}{C}\right)^2 + \left(\frac{C'}{C}\right)'\right) + \frac{2mi}{\hbar^2} V_1 \right\} B_{\pm}^{(r)} e^{\frac{i}{\hbar} S_{\pm}} \\ &+ \frac{1}{2}\left\{ \pm\left(2\frac{C'}{C} + \frac{p'}{p}\right)\right. \\ &\left. + \frac{\hbar}{ip}\left(\left(\frac{C'}{C}\right)^2 + \left(\frac{C'}{C}\right)'\right) + \frac{2mi}{\hbar^2} V_1 \right\} B_{\mp}^{(r)} e^{\frac{i}{\hbar} S_{\mp}} \\ &(r = 0,1, \ldots). \end{aligned}\right\} \tag{2.11}$$

In as far as $\psi_+(x)$ and $\psi_-(x)$ are interpreted as the wave components propagating in the + and — directions, respectively, the first part of the right-hand member of (2.11) describes the transmission, and the second part the reflection. The r'th order approximation then accounts for the r-fold transmissions and reflections. But the arbitrariness of the splitting (2.03) according to the choice of the condition (2.07) and the splitting function $C(x)$ (and also the arbitrariness of the normalization function $A(x)$) should be kept in mind.

Integrating (2.11) we have to care for (*i*) the singular points ("reflection points"), where $E - V_0(x) = 0$ and (*ii*) the range of (x). For the moment we restrict ourselves to the simplest case of a 2-sided infinite range $-\infty \leq x \leq \infty$ without singularities ($V_0(x) < E$). Then we have the boundary conditions

$$B_{\pm}^{(r+1)}(x) \xrightarrow[x \to \mp\infty]{} 0 \qquad (r = 0, 1, \ldots), \tag{2.12}$$

and integration of (2.11) gives

$$\left.\begin{aligned} B_{\pm}^{(r+1)}(x) = \int_{\mp\infty}^{x} dx' \frac{1}{2}\Bigg[&\left\{\left(2\frac{A'}{A} + \frac{p'}{p}\right)\right. \\ &\left. \pm \frac{\hbar}{ip}\left(\left(\frac{C'}{C}\right)^2 + \left(\frac{C'}{C}\right)'\right) \pm \frac{2mi}{\hbar} V_1 \right\} B_{\pm}^{(r)} e^{\frac{i}{\hbar} S_{\pm}} \end{aligned}\right\} \tag{2.13}$$

$$+\left\{\left(2\frac{C'}{C}+\frac{p'}{p}\right)\pm\frac{\hbar}{ip}\left(\left(\frac{C'}{C}\right)^2\right.\right. \tag{2.13}$$

$$\left.\left.+\left(\frac{C'}{C}\right)'\right)\pm\frac{2mi}{\hbar}V_1\right\}B_{\mp}^{(r)}e^{\frac{i}{\hbar}S_{\mp}}\Bigg]e^{-\frac{i}{\hbar}S_{\pm}}\quad(r=0,1,\ldots).\Bigg\}$$

This corresponds to the iterative solution of the integral equation for $\psi(x)$

$$\psi(x)=\psi^0(x)+\int_{-\infty}^{\infty}dx'\frac{1}{2}\Bigg[\left(\frac{A'}{A}+\frac{C'}{C}+\frac{p'}{p}\right)(\psi_+(x')-\psi_-(x'))\Bigg.$$

$$\left.+\left(-\frac{A'}{A}+\frac{C'}{C}\right)\frac{x-x'}{|x-x'|}\psi(x')\right\} \tag{2.14}$$

$$\left.+\left\{\frac{\hbar}{ip}\left(\left(\frac{C'}{C}\right)^2+\left(\frac{C'}{C}\right)'\right)+\frac{2mi}{\hbar^2}V_1\right\}\psi(x')\Bigg]\frac{A(x)}{A(x')}e^{\frac{i}{\hbar}|S_{\pm}(x)-S_{\pm}(x')|}\right\}$$

with

$$\psi^0(x)=\psi_+^0(x)+\psi_-^0(x)=B_+^0A(x)e^{\frac{i}{\hbar}S_+(x)}+B_-^0A(x)e^{\frac{i}{\hbar}S_-(x)}. \tag{2.15}$$

As long as the continuous potential $V_0(x)$ is approximated by a step potential, the splitting (2.03) can be regarded as unique in each step interval. The continuous limit then corresponds to the choice $C(x)=1$ for the splitting function. This representation has been used by various authors[3) 4)]. The BWK part of the "reflection coupling coefficient" in (2.11) is then of 1st order, that of the "transmission coupling coefficient" can be made equal to zero by the choice of $A(x)=p(x)^{-1/2}$ for the normalization function.

The choice of $A(x)=C(x)=p(x)^{-1/2}$ reduces the BWK part of all 1st order coefficients to zero and in general will lead to a more rapid convergence (if at all) of the iteration process.

Up to the order $r=1$ this last choice corresponds to the genuine B[5)]W[6)]K[7)] approximation[1)]. In higher orders the expansions are different, because the genuine method uses an expansion of S rather than of B.

There are many other modifications of the method (e. g. references 8), 9), 10)).

3. 1-dimensional stationary classical waves.

It is well known that the BWK method is actually very much older than quantum mechanics and that much more initials would be needed to do justice to all inventors. We shortly point out the connection with 1-dimensional stationary classical waves (e. g. electromagnetic waves, sound waves) with wave equations of the type

$$\chi(x) - \frac{Z(x)}{i\,k(x)} \frac{d\psi(x)}{dx} = 0; \tag{3.01}$$

$$i\,k(x)\,Z(x)\,\psi(x) - \frac{d\chi(x)}{dx} = 0, \tag{3.02}$$

where $k(x)$ is the wave number and $Z(x)$ the impedance. The method of section 2 now leads to the integral equation

$$\left.\begin{aligned}\psi(x) = \psi^{(0)}(x) + \int_{-\infty}^{\infty} dx' \frac{1}{2}\Bigg[&\left(\frac{A'}{A} + \frac{C'}{C} + \frac{Z'}{Z}\right)(\psi_+(x') - \psi_-(x')) \\ &+ \left(-\frac{A'}{A} + \frac{C'}{C}\right)\frac{x - x'}{|x - x'|}\psi(x') \\ + \frac{1}{Z}\left\{\frac{Z}{ik}\left(\frac{C'}{C}\right)^2 - \frac{Z}{ik}\left(\frac{C'}{C}\right)' - \left(\frac{Z}{ik}\right)'\frac{C'}{C}\right\}&\psi(x')\Bigg]\frac{A(x)}{A(x')}\, e^{i|R_\pm(x) - R_\pm(x')|}\end{aligned}\right\} \tag{3.03}$$

with

$$R_\pm(x) = \pm\int^x dx'\, k(x'). \tag{3.04}$$

The BWK part of section 2 is a special case of the present one with

$$Z(x) = k(x) = \frac{p(x)}{\hbar}; \qquad R_\pm(x) = \frac{S_\pm(x)}{\hbar}. \tag{3.05}$$

4. Difficulties with more-dimensional stationary waves.

Now consider an N-dimensional system of particles in a total potential

$$V(x) = V_0(x) + V_1(x), \tag{4.01}$$

where (x) stands for all the coordinates $x_1, x_2, \ldots x_N$, and the splitting is done in the same way as in (2.01). The mass of the particle of which x_i is one of the coordinates is written as m_i. We may also add vector potentials

$$A_i(x) = A_{0i}(x) + A_{1i}(x), \tag{4.02}$$

depending on the set of three coordinates of which x_i is one. From the gauge condition of zero divergence we only need the total condition

$$\sum_{i=1}^{N} \frac{1}{m_i} \frac{\partial A_{0i}(x)}{\partial x_i} = \sum_{i=1}^{N} \frac{1}{m_i} \frac{\partial A_{1i}(x)}{\partial x_i} = 0. \tag{4.03}$$

The time-independent Schrödinger equation is then

$$\left.\begin{aligned} &\left\{ E - \sum_i \frac{1}{2 m_i} \left(\frac{\hbar}{i} \frac{\partial}{\partial x_i} - A_{0i}(x) \right)^2 - V_0(x) \right\} \psi(x) \\ &\quad = \left\{ - \sum_i \frac{1}{m_i} A_{1i}(x) \left(\frac{\hbar}{i} \frac{\partial}{\partial x_i} - A_{0i}(x) \right) \right. \\ &\qquad \left. + \sum_i \frac{1}{2 m_i} A_{1i}^2(x) + V_1(x) \right\} \psi(x). \end{aligned}\right\} \tag{4.04}$$

In order to proceed in a similar way as in section **2**, one needs a set of solutions $S_{0\Lambda}(x)$, depending on an $(N-1)$-dimensional parameter Λ, of the time-independent classical Hamilton-Jacobi equation

$$E - \sum_i \frac{1}{2 m_i} \left(\frac{\partial S_{0\Lambda}(x)}{\partial x_i} - A_{0i}(x) \right)^2 - V_0(x) = 0 \tag{4.05}$$

for the action function $S_{0\Lambda}(x)$. For a given Λ, the $(N-1)$-dimensional surfaces of constant action can be labelled by a 1-dimensional parameter ξ_Λ

$$S_{0\Lambda}(x) = S_{0\Lambda}(\xi_\Lambda). \tag{4.06}$$

Their orthogonal trajectories are the classical paths. ξ_A can serve as a parameter along these paths. In analogy to (2.03), $\psi(x)$ can be written as

$$\psi(x) = \int dA\, \psi_A(x) \tag{4.07}$$

with

$$\psi_A(x) = A_A(x)\, e^{\frac{i}{\hbar} S_{0A}(\xi_A)}. \tag{4.08}$$

As a first attempt one might try to choose the A's constant on the surfaces of constant action

$$A_A(x) = A_A(\xi_A). \tag{4.09}$$

In this case, one should first investigate whether with (4.09) the expansion (4.07) is always possible. Then one would have to account for the coupling throughout the (x)-space between the waves $\psi_A(x)$ with different A's. But, as surfaces of constant action for different A's in general do not coincide, this coupling could not be described directly in terms of the $A_A(\xi_A)$'s. (In case the classical motion is reversible, the surfaces of reverse solutions A and $-A$ conicide. Besides, an auxiliary condition can be imposed upon all pairs $A_A(\xi_A)$ and $A_{-A}(\xi_{-A})$. But, still, the difficulty concerning the coupling with other A's remains).

Instead of an overall coupling between the $\psi_A(x)$'s with different A's, one could try a local coupling in the point (x) between the $\psi_A(x)$'s along the orthogonal trajectory of the corresponding $S_{0A}(\xi_A)$ (classical path) through (x) with different A's. Then, instead of making the restriction (4.09), one would have to impose other auxiliary conditions upon the A's in such a way that (analogous to section **2**) the coupling equations do not contain their second order derivatives and can be separated with regard to the first order derivatives in the direction of the corresponding path. It seems difficult to choose the auxiliary conditions so that we get rid of the second order derivatives, which may be said to describe "scattering" (cf. section **5**). Instead, we shall consider another choice of auxiliary conditions, by which we get rid of "coupling".

5. More-dimensional stationary treatment.

With this other choice it is possible instead of (4.04) to take a more general N-dimensional Schrödinger equation

$$\{E - \boldsymbol{H}_0(x)\}\,\psi(x) = \boldsymbol{H}_1(x)\,\psi(x), \tag{5.01}$$

where in the Hamiltonian operator

$$\boldsymbol{H}(x) = \boldsymbol{H}_0(x) + \boldsymbol{H}_1(x) \tag{5.02}$$

the part $\boldsymbol{H}_1$ will again be involved in the Born expansion.

In order to introduce quasi-classical paths we have to define a quasi-classical N-dimensional Hamiltonian $H_0(p,x)$ corresponding to the hermitian operator $\boldsymbol{H}_0(x)$. We can do this, e. g., by means of WEYL's rule of correspondence[11] between (real) functions $a(p,x)$ and (hermitian) operators $\boldsymbol{a}$, which we put in the form[12]

$$\left.\begin{aligned} \boldsymbol{a} &= \int\!\!\int d\xi^N\, d\eta^N\, e^{\frac{i}{\hbar}\sum_i(\xi_i \boldsymbol{p}_i + \eta_i \boldsymbol{x}_i)}\, \alpha(\xi,\eta) \longleftrightarrow a(p,x) \\ &= \int\!\!\int d\xi^N\, d\eta^N\, e^{\frac{i}{\hbar}\sum_i(\xi_i p_i + \eta_i x_i)}\, \alpha(\xi,\eta); \end{aligned}\right\} \tag{5.03}$$

$$\left.\begin{aligned} \alpha(\xi,\eta) &= \frac{1}{\hbar^N}\ \mathrm{Trace}\left(e^{\frac{i}{\hbar}\sum_i(\xi_i \boldsymbol{p}_i + \eta_i \boldsymbol{x}_i)}\, \boldsymbol{a}\right) \\ &= \frac{1}{\hbar^{2N}} \int\!\!\int dp'^N\, dx'^N\, e^{\frac{-i}{\hbar}\sum_i(\xi_i p'_i + \eta_i x'_i)}\, a(p',x'). \end{aligned}\right\} \tag{5.04}$$

The operators $(\boldsymbol{p})$ and $(\boldsymbol{x})$ read in x-representation

$$\boldsymbol{p}_i = \frac{\hbar}{i}\frac{\partial}{\partial x_i}; \qquad \boldsymbol{x}_i = x_i. \tag{5.05}$$

In practice, $H(p,x)$ defined in this way does not contain $\hbar$. Otherwise, one might (at least in sections **5** and **6**) instead of $H(p,x)$ also use

$$H_c(p,x) = \lim_{\hbar \to 0} H(p,x), \tag{5.06}$$

which can directly be obtained from

$$H_c(p, x) = \lim_{\hbar \to 0} e^{-\frac{i}{\hbar}\sum_i p_i x_i} \boldsymbol{H}(x)\, e^{\frac{i}{\hbar}\sum_i p_i x_i}. \tag{5.07}$$

If there were a difference at all between H and H_c, it would be at least of 2nd order in $\hbar$. This also holds for other possible choices of the rules of correspondence.

Owing to the relation

$$\frac{\hbar}{i}\frac{\partial}{\partial x_i} e^{\frac{i}{\hbar}S(x)} A(x) = e^{\frac{i}{\hbar}S(x)} \left(\frac{\partial S}{\partial x_i} + \frac{\hbar}{i}\frac{\partial}{\partial x_i}\right) A(x) \tag{5.08}$$

we have[13]

$$\left\{E - \boldsymbol{H}_0(x)\right\} e^{\frac{i}{\hbar}(x)} A(x) = e^{\frac{i}{\hbar}S(x)} \left\{ \left[E - H_0\left(\frac{\partial S}{\partial x}, x\right)\right] - \left[\sum_i \frac{\partial H_0\left(\frac{\partial S}{\partial x}, x\right)}{\partial \frac{\partial S}{\partial x_i}} \frac{\hbar}{i}\frac{\partial}{\partial x_i} + \sum_i \frac{\hbar}{2i} \frac{\partial^2 H_0\left(\frac{\partial S}{\partial x}, x\right)}{\partial x_i \partial \frac{\partial S}{\partial x_i}} \right] - \boldsymbol{Q}_0(x) \right\} \boldsymbol{A}(x). \tag{5.09}$$

The hermitian operator $\boldsymbol{Q}_0(x)$ (or $\boldsymbol{Q}_{c0}(x)$ if H_{c0} is used instead of H_0) is at least of 2nd order in $\hbar$. In case of the ordinary Schrödinger equation (4.04), it is

$$\boldsymbol{Q}_0(x) = \sum_i \frac{\hbar^2}{2 m_i}\frac{\partial^2}{\partial x_i^2}. \tag{5.10}$$

The form (5.09) can be used in various ways. If, e. g., one takes $\boldsymbol{H}_1(x) = 0$ and puts

$$\psi(x) = A(x)\, e^{\frac{i}{\hbar}S(x)} \tag{5.11}$$

with real amplitude andp hase functions $A(x)$ and $S(x)$, then the real and imaginary parts can each be equated to zero. This is done (with a longing for the good old classical theory) in the "pilot wave" theories[14) 15)] for the case (4.04), where $\boldsymbol{Q}_0(x)$, according to (5.10), is real and therefore is taken together with the first square brackets of (5.09).

At present we consider, just as in section **4**, a set of solutions $S_{0A}(x)$ of the time-independent Hamilton-Jacobi equation for the action function $S_{0A}(x)$

$$E - H_0\left(\frac{\partial S_{0A}}{\partial x}, x\right) = 0 \tag{5.12}$$

and the corresponding solution $A_{0A}(x)$ of

$$\left[\sum_i \frac{\partial H_0\left(\frac{\partial S_{0A}}{\partial x}, x\right)}{\partial \frac{\partial S_{0A}}{\partial x_i}} \frac{\partial}{\partial x_i} + \sum_i \frac{1}{2} \frac{\partial^2 H_0\left(\frac{\partial S_{0A}}{\partial x}, x\right)}{\partial x_i \partial \frac{\partial S_{0A}}{\partial x_i}}\right] A_{0A}(x) = 0 \tag{5.13}$$

or

$$\sum_i \frac{\partial}{\partial x_i}\left\{\frac{\partial H_0\left(\frac{\partial S_{0A}}{\partial x}, x\right)}{\partial \frac{\partial S_{0A}}{\partial x_i}} A_{0A}(x)^2\right\} = 0. \tag{5.14}$$

The classical paths are again the orthogonal trajectories of the surfaces of constant action (4.06). (5.14) is the stationary continuity equation for the classical density $A_{0A}(x)^2$ along the paths of the system A in a statistical ensemble. Along each path of the solution A we introduce a parameter s_A, for which

$$ds_A = \sum_i dx_{iA} \frac{\partial H_0\left(\frac{\partial S_{0A}}{\partial x}, x\right)}{\partial \frac{\partial S_{0A}}{\partial x_i}} \Big/ \sum_i \left(\frac{\partial H_0\left(\frac{\partial S_{0A}}{\partial x}, x\right)}{\partial \frac{\partial S_{0A}}{\partial x_i}}\right)^2, \tag{5.15}$$

where (dx_A) is an infinitesimal element of the path. Instead of the sums in (5.15) we can also take, say, the i^{th} terms only. Integration of (5.13) along that path of the solution A, which goes to (x) from a point (x'), gives

$$A_{0A}(x) = A_{0A}(x') \exp\left\{-\frac{1}{2}\int_{(x')}^{(x)} ds''_A \sum_i \frac{\partial^2 H_0\left(\frac{\partial S_{0A}}{\partial x''}, x''\right)}{\partial x''_i \frac{\partial S_{0A}}{\partial x''_i}}\right\}. \tag{5.16}$$

(x') and $A_{0\Lambda}(x')$ still have to be suitably determined. In the 1-dimensional case, where there is no divergence of paths, the density simply becomes inversely proportional to the velocity

$$A_0(x) = \text{const.} \left(\frac{\partial H_0\left(\frac{\partial S_0}{\partial x}, x\right)}{\partial \frac{\partial S_0}{\partial x}} \right)^{-\frac{1}{2}}. \tag{5.17}$$

In the representation (4.07), (4.08) we now use the auxiliary conditions on the $A_\Lambda(x)$'s, at least in such a way that the $\psi_\Lambda(x)$'s for various values of Λ separately satisfy (5.01). Writing

$$A_\Lambda(x) = B_\Lambda(x)\, A_{0\Lambda}(x), \tag{5.18}$$

that together with (5.09), (5.12), and (5.13) gives the equation

$$\left.\begin{aligned} &\sum_i \frac{\partial H_0\left(\frac{\partial S_{0\Lambda}}{\partial x}, x\right)}{\partial \frac{\partial S_{0\Lambda}}{\partial x_i}} \frac{\partial}{\partial x_i} B_\Lambda(x) \\ &= \frac{-\frac{i}{\hbar}}{A_{0\Lambda}(x)} \left\{ \boldsymbol{Q}_0(x) + \boldsymbol{H}_1(x) \right\} \left\{ B_\Lambda(x)\, A_{0\Lambda}(x) \right\}. \end{aligned}\right\} \tag{5.19}$$

We consider again such cases where the operators in the right-hand member can be regarded as effectively small, so that we can make the expansion

$$B_\Lambda(x) = \sum_{r=0}^{\infty} B_\Lambda^{(r)}(x) \tag{5.20}$$

with

$$B_\Lambda^{(0)}(x) = B_\Lambda^0 \quad \text{(constant)} \tag{5.21}$$

and

$$\left.\begin{aligned} &\sum_i \frac{H_0\left(\frac{\partial S_{0\Lambda}}{\partial x}, x\right)}{\partial \frac{\partial S_{0\Lambda}}{\partial x_i}} \frac{\partial}{\partial x_i} B_\Lambda^{(r+1)}(x) \\ &= \frac{-\frac{i}{\hbar}}{A_{0\Lambda}(x)} \{\boldsymbol{Q}_0(x) + \boldsymbol{H}_1(x)\} \{B_\Lambda^{(r)}(x) A_{0\Lambda}(x)\} \quad (r = 0, 1, \ldots). \end{aligned}\right\} \quad (5.22)$$

These equations might be said to describe the "scattering" of the separate semi-classical waves

$$\psi_\Lambda^0(x) = A_{0\Lambda}(x)\, e^{\frac{i}{\hbar} S_{0\Lambda}(x)} \quad (5.23)$$

due to the "quantum potential" operator $\boldsymbol{Q}_0(x)$ and the "Born potential" operator $\boldsymbol{H}_1(x)$ in a similar loose hazy way as (2.11) was said to describe the coupling between the various (two) semi-classical waves.

Integrating (5.22) we have to take care of (*i*) the occurrence of "reflection and scattering singularities" and (*ii*) the range of the coordinates (x) and the boundary conditions. As to (*i*), singularities may occur not only due to the vanishing of the velocity vector in the left-hand member of (5.22), but also due to the operators $\boldsymbol{Q}_0$ and $\boldsymbol{H}_1$ in the right-hand member, e. g., along the envelopes (caustics) of the classical path for a given Λ. For the moment we restrict ourselves to the simple cases where they do not occur. As to (*ii*), we assume that the region of (x)-space, in which $\boldsymbol{Q}_0$ and $\boldsymbol{H}_1$ are effectively different from zero, can be enclosed in an $(N-1)$-dimensional surface Σ (which may tend to infinity). Let us denote the points where the classical paths cut this surface with the velocity vector pointing towards the inside direction by (x'). Further we assume that the "incoming wave" $\psi^0(x')$ given on Σ can be represented by

$$\psi^0(x') = \int d\Lambda\, \psi_\Lambda^0(x') \quad (5.24)$$

with

$$\psi_\Lambda^0(x') = B_\Lambda^0\, A_{0\Lambda}(x')\, e^{\frac{i}{\hbar} S_{0\Lambda}(x')} \quad (5.25)$$

and a suitable choice for B_A^0 (e. g. 1) and $A_{0A}(x')$. These choices for (x') and $A_{0A}(x')$ will be used in (5.16).

Now we have for (5.22) the boundary conditions

$$B_A^{(r+1)}(x') = 0 \quad (r = 0, 1, \ldots) \tag{5.26}$$

and (5.22) can be integrated along the classical path of the solution $S_{0A}(x)$ which goes to (x) from the corresponding point (x') on Σ

$$\left.\begin{aligned} B_A^{(r+1)}(x)\, A_{0A}(x) = \int_{(x')}^{(x)} ds_A'' \frac{A_{0A}(x)}{A_{0A}(x'')} \frac{-i}{\hbar} \\ \{\boldsymbol{Q}_0(x'') + \boldsymbol{H}_1(x'')\}\{B_A^{(r)}(x'')\, A_{0A}(x'')\} \quad (r = 0, 1, \ldots). \end{aligned}\right\} \tag{5.27}$$

This corresponds to the iterative solution of the integral equation for $\psi_A(x)$

$$\left.\begin{aligned} \psi_A(x) = \psi_A^0(x) + \int_{(x')}^{(x)} ds_A'' \frac{A_{0A}(x)}{A_{0A}(x'')} \frac{-i}{\hbar} \\ \{\boldsymbol{Q}_0(x'') + \boldsymbol{H}_1(x'')\}\left\{e^{\frac{i}{\hbar}\{S_{0A}(x) - S_{0A}(x'')\}} \psi_A(x'')\right\} \end{aligned}\right\} \tag{5.28}$$

with

$$\psi_A^0(x) = B_A^0\, A_{0A}(x)\, e^{\frac{i}{\hbar} S_{0A}(x)} \tag{5.29}$$

as the semi-classical incoming wave.

The genuine BWK approximation, if extended to more than one dimension in higher orders, would again use an expansion of S rather than of B. The present expansion coincides with it up to the order $r = 1$. It seems that in non-separable more-(3-) dimensional problems it has not been used in higher approximation than $r = 0$ (semi-classical waves)[16].

If, for the left-hand member of (5.01), we take the ordinary form (4.04) with $N \leqslant 3$ for a free particle ($A_{0i}(x) = V_0(x) = 0$), the integrations can be carried out for various sets of free particle solutions $S_{0A}(x)$, which all result in the usual Born expansion.

It goes without saying that besides the treatments discussed so far there are many other possibilities (e. g. ref. 17)).

6. Time-dependent treatment.

The notions of coupling in section 2 and of scattering in section 5 should become somewhat clearer in a time-dependent description. The method of section 2 appears not suited to introduce time dependence in a straightforward way, but the method of section 5 can be made more readily fit for it.

Instead of (5.01) we take the time dependent N-dimensional Schrödinger equation

$$\left\{-\frac{\hbar}{i}\frac{\partial}{\partial t} - \boldsymbol{H}_0(x,t)\right\}\psi(x,t) = \boldsymbol{H}_1(x,t)\ \psi(x,t). \qquad (6.01)$$

The Hamiltonian operators may now also depend on time.

Whereas the stationary problem in general is to find the eigenfunctions (and eigenvalues) of (5.01) with certain boundary conditions, the general time dependent problem is to derive from $\psi(x,t')$ at a given time t' (initial condition) $\psi(x,t)$ at other times t. This connection can be expressed by

$$\psi(x,t) = \int dx'^N K(x,t;x',t')\,\psi(x',t'), \qquad (6.02)$$

where $K(x,t;x',t')$ is determined by

$$\left\{-\frac{\hbar}{i}\frac{\partial}{\partial t} - \boldsymbol{H}_0(x,t)\right\}K(x,t;x',t') = \boldsymbol{H}_1(x,t)\,K(x,t;x',t') \qquad (6.03)$$

with the initial condition

$$\lim_{t-t'\to 0} K(x,t;x',t') = \delta^N(x-x') \qquad (6.04)$$

and (if (6.03) is understood to be valid for all $t-t'$) a somewhat different representation[18] is obtained if $K(x,t,x',t')$ is multiplied by a factor $\varepsilon(t-t')$, which is 1 for $t>t'$ and 0 for $t<t'$) the inversion condition

$$K(x,t;x',t') = K^*(x',t';x,t). \qquad (6.05)$$

The asterisk denotes the complex conjugate.

In order to introduce quasi-classical paths, we define $H(p,x;t)$ in the same way as $H(p,x)$ in section **5**. Instead of (5.09) we now have

$$\left.\begin{aligned}&\left\{-\frac{\hbar}{i}\frac{\partial}{\partial t}-\boldsymbol{H}_0(x,t)\right\}e^{\frac{i}{\hbar}I(x,t;x',t')}D(x,t;x',t')\\&=e^{\frac{i}{\hbar}I(x,t;x',t')}\left\{\left[\frac{\partial I}{\partial t}-H_0\left(\frac{\partial I}{\partial x},x;t\right)\right]\right.\\&-\left[\frac{\hbar}{i}\frac{\partial}{\partial t}+\sum_i\frac{\partial H_0\left(\frac{\partial I}{\partial x},x;t\right)}{\partial\frac{\partial I}{\partial x_i}}\frac{\hbar}{i}\frac{\partial}{\partial x_i}\right.\\&\left.\left.+\sum_i\frac{\hbar}{2i}\frac{\partial^2 H_0\left(\frac{\partial I}{\partial x},x;t\right)}{\partial x_i\,\partial\frac{\partial I}{\partial x_i}}\right]-\boldsymbol{Q}_0(x,t)\right\}D(x,t;x',t').\end{aligned}\right\}\quad(6.06)$$

The remarks in section **5**, regarding $\boldsymbol{Q}_0(x)$, also hold for the present $\boldsymbol{Q}_0(x,t)$.

Proceeding in an analogous way as in section **5**, we consider the solutions $I_{0\lambda}(x,t;x',t')$ of the time-dependent Hamilton-Jacobi equation for the principle function ("eikonal") $I_0(x,t;x',t')$ with $t>t'$

$$\frac{\partial I_{0\lambda}(x,t;x',t')}{\partial t}-H_0\left(\frac{\partial I_{0\lambda}(x,t;x',t')}{\partial x},x;t\right)=0\quad(6.07)$$

and the corresponding solutions $D_{0\lambda}(x,t;x',t')$ also with $t>t'$) of

$$\left.\begin{aligned}&\left[\frac{\partial}{\partial t}+\sum_i\frac{\partial H_0\left(\frac{\partial I_{0\lambda}}{\partial x},x;t\right)}{\partial\frac{\partial I_{0\lambda}}{\partial x_i}}\frac{\partial}{\partial x_i}\right.\\&\left.+\sum_i\frac{1}{2}\frac{\partial^2 H_0\left(\frac{\partial I_0}{dx},x;t\right)}{\partial x_i\,\partial\frac{\partial I_0}{\partial x_i}}\right]D_{0\lambda}(x,t;x',t')=0\end{aligned}\right\}\quad(6.08)$$

or

$$\left.\begin{aligned} &\frac{\partial}{\partial t} D_{0\lambda}(x, t; x', t')^2 \\ &+ \sum_i \frac{\partial}{\partial x_i} \left\{ \frac{\partial H_0\left(\frac{\partial I_{0\lambda}}{\partial x}, x; t\right)}{\partial \frac{\partial I_{0\lambda}}{\partial x_i}} D_{0\lambda}(x, t; x', t')^2 \right\} = 0. \end{aligned}\right\} \quad (6.09)$$

If there are different solutions $I_{0\lambda}(x, t; x', t')$ (distinguished by hte suffix λ), they correspond to different classical paths from (x') at a time t' to (x) at a time t[19]. Analogous to (5.14), (6.09) is the dynamical continuity equation for the classical density function $D_{0\lambda}(x, t; x', t')^2$. But, whereas (5.14) refers to the paths of the system Λ (all with the same energy E), (6.09) refers to the paths λ starting from (x') at a time t'. This common starting point of diverging paths (which occasionally may also occur in (5.14)*) gives rise to a singularity for $t - t' \to 0$. For the direct (almost straight) classical path from (x') to (x) during the infinitesimal time interval from t' to t we have in (6.08), (6.09)

* Professor A. Bohr informs me about a time-independent 3-dimensional treatment initiated by Christy[32]) and generalized by Fröman[33]), in which one chooses a special system Λ of paths which start from points (x') on a surface Σ (which now may also be inside the region where $\boldsymbol{Q}_0$ and $\boldsymbol{H}_1$ are effective) and converge towards a point (x). For this system Λ, the treatment of section **5** becomes more analogous to that of section **6**. Instead of $S_\Lambda(x)$ and $A_\Lambda(x)$ we may then write $S_\Lambda(x, x')$ and $A_\Lambda(x, x')$. Analogous to (6.10) one has for $(x') \to (x)$ the singularity

$$\lim_{(x')\to(x)} \sum_i \frac{\partial}{\partial x_i'} \frac{\partial H_0\left(\frac{\partial S_0}{\partial x}, x'\right)}{\partial \frac{\partial S_0}{\partial x_i'}} = \left\{ \sum_i \left(\frac{\partial H_0\left(\frac{\partial S_0}{\partial x}, x\right)}{\partial \frac{\partial S_0}{\partial x_i}} \right)^2 \right\}^{1/2} \lim_{(x')\to(x)} \frac{N-1}{\left|\vec{x'} - \vec{x}\right|}. \quad (i)$$

Then

$$J(x, x') = A_\Lambda(x, x')\, e^{\frac{i}{\hbar} S_{0\Lambda}(x, x')} \quad (ii)$$

is a special solution of (5.01) (in the special form (4.04) with $N = 3$; $A_{0i}(x) = 0$, with the singularity

$$\lim_{(x')\to(x)} J(x, x') = \lim_{(x')\to(x)} A_{0\Lambda}(x, x') = \lim_{(x')\to(x)} \frac{1}{\left|\vec{x'} - \vec{x}\right|}. \quad (iii)$$

A general solution $\psi(x)$ is then in Fröman's method with the help of Green's formula expressed as

$$\left.\begin{aligned} &\lim_{t-t'\to 0} \sum_i \left\{ \frac{\partial}{\partial x_i} \frac{\partial H_0\left(\frac{\partial I_{0\lambda_0}}{x}, x; t\right)}{\partial \frac{\partial I_{0\lambda_0}}{\partial x_i}} \right\} \\ &= \lim_{t-t'\to 0} \sum_i \left\{ \frac{\partial}{\partial x_i} \frac{x_i - x_i'}{t-t'} \right\} = \lim_{t-t'\to 0} \frac{N}{t-t'}. \end{aligned}\right\} \tag{6.10}$$

For the parameter s_λ along the path introduced in analogy to (5.15) we can now take the time t. (6.08) could formally be integrated along the path λ from (x', t') to (x, t)

$$\left.\begin{aligned} &D_{0\lambda}(x, t; x', t') = D_{0\lambda}(x', t'; x', t') \\ &\exp\left\{ -\frac{1}{2} \int_{(x', t')}^{(x, t)} dt''_\lambda \sum_i \frac{\partial^2 H_0\left(\frac{\partial I_{0\lambda}}{\partial x}, x''; t''\right)}{\partial x_i'' \partial \frac{\partial I_{0\lambda}}{\partial x_i''}} \right\} \end{aligned}\right\} \tag{6.11}$$

similar to (5.16). The singular function $D_{0\lambda}(x', t'; x', t')$ is left undetermined. For a classical path λ_0, which for an infinitesimal time interval $t - t'$ is a direct (almost straight) path, the limit

$$\lim_{t-t'\to 0} D_{0\lambda_0}(x, t; x', t') \; (t-t')^{\frac{N}{2}} \tag{6.12}$$

remains finite. If $L\left(x, \frac{dx}{dt}; t\right)$ is a 2nd order polynomial in $\left(\frac{dx}{dt}\right)$, then $D_{0\lambda}^2$ is explicitly given by VAN HOVE's solution[20] (cf. also ref, 16)) of (6.09)

$$D_{0\lambda}(x, t; x', t')^2 = c_\lambda \left\| \frac{\partial^2 I_{0\lambda}(x, t; x', t')}{\partial x_i \partial x_j'} \right\|. \tag{6.13}$$

$$\psi(x) = -\frac{1}{4\pi} \int_\Sigma d\Sigma' \left\{ \frac{\partial J(x, x')}{\partial x_n} \psi(x') - J(x, x') \frac{\partial \psi(x')}{\partial x_n} \right\}, \tag{iv}$$

where n denotes the direction of the normal on Σ towards (x). This expression (which is analogous to that of KIRCHHOFF in optics; cf. also ref. 16)), has been used with the semi-classical approximation $J^{(0)}$ for J.

The double bar denotes the determinant of the square matrix ($i, j = 1, 2, \ldots N$). For more general functions $L\left(x, \frac{dx}{dt}; t\right)$, (6.13) still satisfies (6.09), as can directly be checked with the help of (6.07). Contrary to (6.11), (6.13) fixes the limit for $t - t' \to 0$. As long as the determinant becomes nowhere zero, the constant c_λ can be chosen so that (6.13) is positive. Otherwise, the singularities of $D_{0\lambda}$ have to be carefully investigated. It may be observed that a representation of the solution of (5.14) in terms of $S_{0\lambda}$ analogous to the solution (6.13) of (6.09) in terms of $I_{0\lambda}$ cannot be given.

As the principal function $I_{0\lambda}(x, t; x', t')$ is equal to the path integral of the Langrangian $L_0\left(x, \frac{dx}{dt}; t\right)$

$$I_{0\lambda}(x, t; x', t') = \int_{(x', t')}^{(x, t)} dt''_\lambda L_0\left(x'', \frac{dx''}{dt''}; t''\right), \tag{6.14}$$

the (singular) initial condition for $t - t' \to 0$ for the direct (almost straight) path λ_0 from (x') to (x) during the infinitesimal time interval from t' to t is

$$\lim_{t-t' \to 0} I_{0\lambda_0}(x, t; x', t') = \lim_{t-t' \to 0} (t - t')\ L_0\left(x^v, \frac{x - x'}{t - t}; t\right), \tag{6.15}$$

where (x^v) lies between (x') and (x). The corresponding singularity of (6.13) is then given by

$$\lim_{t-t' \to 0} D_{0\lambda_0}(x, t; x', t')^2 = c_{\lambda_0} \lim_{t-t' \to 0} \left\| \left\{ (t-t') \frac{\partial^2}{\partial x_i \partial x_j} + \frac{\partial^2}{\partial x_i \partial \left(\frac{x_j - x'_j}{t - t'}\right)} - \frac{\partial^2}{\partial \left(\frac{x_i - x'_i}{t - t'}\right) \partial x_j} - \frac{1}{t - t'} \right. \right.$$
$$\left. \left. \frac{\partial^2}{\partial \left(\frac{x_i - x'_i}{t - t'}\right) \partial \left(\frac{x_j - x'_j}{t - t'}\right)} \right\} L_0\left(x^v, \frac{x - x'}{t - t'}; t\right) \right\| \tag{6.16}$$

in agreement with (6.12).

If, for $t < t'$, we define

$$I_{0\lambda}(x, t; x', t') = -I^{*}_{0\lambda}(x', t'; x, t) \tag{6.17}$$

(with the asterisk for the case it might become complex) and

$$D_{0\lambda}(x, t; x', t') = D^{*}_{0\lambda}(x', t'; x, t), \tag{6.18}$$

then, for $t < t'$, $I_{0\lambda}(x,t;x',t')$ and $D_{0\lambda}(x,t;x',t')$ in the equations (6.07) — (6.13) have to be replaced by $-I^{*}_{0\lambda}(x, t; x', t')$ and $D^{*}_{0\lambda}(x,t;x',t')$, $\partial/\partial t$ and $\partial/\partial x_i$ by $\partial/\partial t'$ and $\partial/\partial x'_i$, c_λ by $-c_\lambda$. (If the classical motion is reversible, the restrictions of the equations to either $t > t'$ or $t < t'$ can be dropped).

In order to proceed along similar lines as in section **5**, we might (summing over all classical paths from (x') at t' to (x) at t) try to put

$$K(x, t; x', t') = \sum_{\lambda} K_\lambda(x, t; x', t') \tag{6.19}$$

with

$$K_\lambda(x, t; x', t') = D_\lambda(x, t; x', t')\, e^{\frac{i}{\hbar} I_{0\lambda}(x, t; x', t')} \tag{6.20}$$

and make an expansion

$$D_\lambda(x, t; x', t') = \sum_{r=0}^{n} B^{(r)}_\lambda(x, t; x', t')\, D_{0\lambda}(x, t; x', t') \tag{6.21}$$

with

$$B^{(0)}_\lambda(x, t; x', t') = B^{0}_\lambda(x', t'), \tag{6.22}$$

and for $t > t'$

$$\left.\begin{aligned} &\left\{\frac{\partial}{\partial t} + \sum_i \frac{\partial H_0\left(\frac{\partial I_{0\lambda}}{\partial x}, x; t\right)}{\partial \frac{\partial I_{0\lambda}}{\partial x_i}} \frac{\partial}{\partial x_i}\right\} B^{(r+1)}_\lambda(x, t; x', t') \\ &\quad = \frac{-\frac{i}{\hbar}}{D_{0\lambda}(x, t; x', t')} \left\{\boldsymbol{Q}_0(x, t) + \boldsymbol{H}_1(x, t)\right\} \\ &\qquad \left\{B^{(r)}_\lambda(x, t; x', t')\, D_{0\lambda}(x, t; x', t')\right\}. \end{aligned}\right\} \tag{6.23}$$

With regard to (6.05) and (6.17), (6.18) we should have for $t < t'$

$$B_\lambda^{(r)}(x, t; x', t') = B_\lambda^{(r)*}(x', t'; x, t). \tag{6.24}$$

Now, if only $I_{0\lambda}$ and $D_{0\lambda}$ would satisfy an initial condition

$$\lim_{t-t' \to 0} \sum_\lambda B_\lambda^0(x', t') D_{0\lambda}(x, t; x', t') e^{\frac{i}{\hbar} I_{0\lambda}(x, t; x', t')} = \delta^N(x - x') \tag{6.25}$$

for a suitable (perhaps not unique) set of B^0's, we would have for (6.23) the initial conditions

$$\lim_{t-t' \to 0} B_\lambda^{(r+1)}(x, t; x', t') = 0 \quad (r = 0, 1, \ldots). \tag{6.26}$$

If further no „reflection and scattering singulatities" would occur along the classical paths λ from (x') at t' to (x) at t, then (6.23) could be integrated along these paths

$$\left.\begin{aligned} &B_\lambda^{(r+1)}(x, t; x', t') D_{0\lambda}(x, t; x', t') \\ &= \int_{(x', t')}^{(x, t)} dt_\lambda'' \frac{D_{0\lambda}(x, t; x', t')}{D_{0\lambda}(x'', t''; x', t')} \frac{-i}{\hbar} \{ \boldsymbol{Q}_0(x'', t'') + \boldsymbol{H}_1(x'', t'') \} \\ &\{ B_\lambda^{(r)}(x'', t''; x', t') D_{0\lambda}(x'', t'', x', t') \} \quad (r = 0, 1, \ldots). \end{aligned}\right\} \tag{6.27}$$

This would correspond to the iterative solution of the integral equation for $K_\lambda(x, t; x', t')$

$$\left.\begin{aligned} &K_\lambda(x, t; x', t') = K_\lambda^0(x, t; x', t') \\ &+ \int_{(x', t')}^{(x, t)} dt_\lambda'' \frac{D_{0\lambda}(x, t; x', t')}{D_{0\lambda}(x'', t''; x', t')} \frac{-i}{\hbar} \{ \boldsymbol{Q}_0(x'', t'') + \boldsymbol{H}_1(x'', t'') \} \\ &\{ K_\lambda(x'', t''; x' t') e^{\frac{i}{\hbar} I_{0\lambda}(x, t; x'', t'')} \} \end{aligned}\right\} \tag{6.28}$$

with

$$K_\lambda^0(x, t; x', t') = B_\lambda^0(x', t') D_{0\lambda}(x, t; x', t') e^{\frac{i}{\hbar} I_{0\lambda}(x, t; x', t')} \tag{6.29}$$

as the semi-classical approximation.

If it were only the non-uniqueness of the choice of the $B_\lambda^0(x', t')$ in (6.25), which determines the amplitudes with which the dif-

ferent paths from (x', t') to (x, t) take part in the representation of the propagation process, the problem might be to choose them so as to obtain as good convergence as possible, if convergence is possible at all. The crucial points of the solution are the absence of singularities and the limiting condition (6.25).

For the moment, we restrict ourselves to cases without singularities. It is likely that the occurrence of more than one path λ from (x', t') to (x, t) entails the occurrence of singularities[19]. This would mean that, with our restriction, we have cut off the discussion of such cases.

For the ordinary time-dependent form of the Schrödinger equation (4.04), the limit of the term (6.25) for the direct (almost straight) path from (x') to (x) during the infinitesimal time interval $t - t'$ has been investigated by many authors. It has been done particularly carefully by CHOQUARD[19], who also derived the limits of the other terms for the indirect paths. In fact he finds the latter to be zero, so that our corresponding $B^0_\lambda(x', t')$ in (6.25) would be left indetermined in this case, if it were justified to deal with them at all. The limit for the direct paths actually does give a δ-function in this case. It need not do so for Hamiltonians $H_0(p, x; t)$ which are not 2nd order polynomials in (p). If it does, $B^0_{\lambda_0}(x', t')$ can be determined from

$$\left.\begin{aligned} &\lim_{t-t'\to 0} D_{0\lambda_0}(x, t; x', t')\, e^{\frac{i}{\hbar} I_{0\lambda_0}(x, t; x', t')} \\ &= \delta^N(x - x') \lim_{\tau\to 0} \int du^N \left\{ c_{\lambda_0} \left\| \tau \frac{\partial^2 L^{(as)}(x', u; t)}{\partial u_i \partial u_j} \right\| \right\}^{\frac{1}{2}} e^{\frac{i}{\hbar} \tau L_0^{(as)}(x', u; t)} , \end{aligned}\right\} \quad (6.30)$$

where for $L^{(as)}$ we may take the leading term of L in the asymptotic expression for $\sum_i u_i^2 \to \infty$.

It seems that, just as in section 5, the present expansion has not been used in higher approximations than $r = 0$.

In the present expansion, the "quantum potential" $\boldsymbol{Q}_0$ and the "Born potential" $\boldsymbol{H}_1$ are treated on the same footing. They can also be separated by first taking $K_0(x, t; x', t')$ as the solution of (6.03), (with (6.04), (6.05)) or (6.28) without the terms with $\boldsymbol{H}_1$. Then (cf. [18]), owing to (6.04), $K(x, t; x', t')$ is the solution of the integral equation

$$\left.\begin{aligned} K(x,t;x',t') &= K_0(x,t;x',t') \\ -\frac{i}{\hbar}\int_{t'}^{t} dt'' \int dx''^N K_0(x,t;x'',t')\boldsymbol{H}_1(x'',t'')K(x'',t'';x',t'). \end{aligned}\right\} \quad (6.31)$$

If $\boldsymbol{H}_1$ is effectively small, (6.31) can again be solved in a Born expansion by iteration.

7. Feynman path integrals.

Another expansion than that of section **6** is used in the Feynman path integrals [2) 20) 21) 22)]. This representation for a time interval from t' to t is obtained by iteration of the (zero order) solution of section **6** for infinitesimal time intervals and then taking the limit (if we were able to do so) of zero time intervals. In this section, we consider the solutions for infinitesimal time intervals from a different point of view than in section **6**, avoiding at the same time the difficulties with possible indirect classical paths.

We use again Weyl's rule of correspondence (5.03), (5.04), from which it follows[12)] that the kernel $a(x,x')$ in x-representation of the operator $\boldsymbol{a}$

$$\boldsymbol{a}\psi(x) = \int dx'^N a(x,x')\psi(x') \quad (7.01)$$

is connected with the function $a(p,x)$ by

$$a(x,x') = \frac{1}{h^N}\int dp'^N e^{\frac{-i}{\hbar}\sum_i (x_i - x_i')p_i'} a\left(p', \frac{x+x'}{2}\right). \quad (7.02)$$

The solution of (6.03) with (6.04) and (6.05) for an infinitesimal time interval dt is in first order

$$\left.\begin{aligned} K(x,t+dt;x',t) &= \left\{1 - \frac{i}{\hbar}dt\boldsymbol{H}_0(x,t) - \frac{i}{\hbar}dt\boldsymbol{H}_1(x,t)\right\}\delta^N(x-x') \\ &= 1 - \frac{i}{\hbar}dt\,H_0(x,x';t) - \frac{i}{\hbar}dt\,H_1(x,x';t). \end{aligned}\right\} \quad (7.03)$$

The term with H_1 will again be treated as a small perturbation. For the other terms we write, using (7.02),

$$
\left.\begin{aligned}
&K_0(x, t+dt; x', t) \\
&\quad = \delta^N(x-x') - \frac{i}{\hbar}\,dt\,H_0(x, x'; t) \\
&\quad = \frac{1}{h^N}\int dp'^N\, e^{\frac{i}{\hbar}\sum_i (x_i - x_i')\,p_i'}\left\{1 - \frac{i}{\hbar}\,dt\,H_0\left(p', \frac{x+x'}{2}; t\right)\right\} \\
&\quad \approx \frac{1}{h^N}\int dp'^N\, e^{\frac{i}{\hbar}\left\{\sum_i (x_i - x_i')\,p_i' - dt\,H_0\left(p', \frac{x+x'}{2}; t\right)\right\}}.
\end{aligned}\right\} \quad (7.04)
$$

In order to obtain the Lagrangian rather than the Hamiltonian, we make, for a suitably chosen (p), the expansion

$$
\left.\begin{aligned}
&\sum_i \frac{x_i - x_i'}{dt}\,p_i' - H_0\left(p', \frac{x+x'}{2}; t\right) \\
&\quad = \left\{\sum_i \frac{x_i - x_i'}{dt}\,p_i - H_0\left(p, \frac{x+x'}{2}; t\right)\right\} \\
&\quad + \sum_i \left\{\frac{x_i - x_i'}{dt} - \frac{\partial H_0\left(p, \frac{x+x'}{2}; t\right)}{\partial p_i}\right\}(p_i' - p_i) \\
&\quad - \frac{1}{2!}\sum_{i,j} \frac{\partial^2 H_0\left(p, \frac{x+x'}{2}; t\right)}{\partial p_i\,\partial p_j}(p_i' - p_i)(p_j' - p_j) - \cdots\cdots
\end{aligned}\right\} \quad (7.05)
$$

Then we could try in (7.04) a stationary phase approximation by choosing (p) so that the first order terms in (7.05) vanish

$$
\frac{\partial H_0\left(p, \frac{x+x'}{2}; t\right)}{\partial p_i} = \frac{x_i - x_i'}{dt}. \quad (7.06)
$$

For this choice of (p) the zero order terms just give

$$
\sum_i \frac{x_i - x_i'}{dt}\,p_i - H_0\left(p, \frac{x+x'}{2}; t\right) = L_0\left(\frac{x+x'}{2}, \frac{x-x'}{dt}; t\right), \quad (7.07)
$$

where $L\left(x, \frac{dx}{dt}; t\right)$ is the Lagrangian corresponding to the Hamiltonian $H(p, x; t)$.

The integral (7.04) can now readily be evaluated if the higher than second order terms in (7.05) are zero, i. e. if $H_0(p, x; t)$ is a polynomial in (p) of 2nd order. In this case, we obtain

$$\left.\begin{aligned} K_0(x, t + dt; x', t) = \left(\frac{1}{i h\, dt}\right)^{\frac{N}{2}} \\ \left\| \frac{\partial^2 H_0\left(p, \frac{x + x'}{2}; dt\right)}{\partial p_i\, \partial p_j} \right\|^{-\frac{1}{2}} e^{\frac{i}{\hbar} dt\, L_0\left(\frac{x + x'}{2}, \frac{x - x'}{dt}; t\right)}, \end{aligned}\right\} \quad (7.08)$$

provided the determinant of the second order derivatives of H_0 does not vanish. (Thus, the singular case that $H_0(p, x; t)$ is linear in (p) must be excluded). With the help of (7.06) and the inverse relation

$$\frac{\partial L_0\left(\frac{x + x'}{2}, \frac{x - x'}{dt}; t\right)}{\partial\left(\frac{x_i - x_i'}{dt}\right)} = p_i \quad (7.09)$$

this determinant can (even if H_0 is not a second order polynomial in (p)) be expressed in terms of L_0 by

$$\left.\begin{aligned} \left\| \frac{\partial^2 H_0\left(p, \frac{x + x'}{2}; t\right)}{\partial p_i\, \partial p_j} \right\|^{-\frac{1}{2}} = \left\{ \frac{\partial(p)}{\partial\left(\frac{x - x'}{dt}\right)} \right\}^{\frac{1}{2}} \\ = \left\| \frac{\partial^2 L_0\left(\frac{x + x'}{2}, \frac{x - x'}{dt}; t\right)}{\partial\left(\frac{x_i - x_i'}{dt}\right) \partial\left(\frac{x_j - x_j'}{dt}\right)} \right\|^{\frac{1}{2}}. \end{aligned}\right\} \quad (7.10)$$

The expression in curled brackets denotes the Jacobian. The resulting

$$K_0(x, t + dt; x', t)$$

$$= \left\| \frac{-i}{h\,dt} \frac{\partial^2 L_0\left(\frac{x+x'}{2}, \frac{x-x'}{dt}; t\right)}{\partial\left(\frac{x_i - x_i'}{dt}\right)\partial\left(\frac{x_j - x_j'}{dt}\right)} \right\|^{\frac{1}{2}} e^{\frac{i}{\hbar} dt\, L_0\left(\frac{x+x'}{2}, \frac{x-x'}{dt}; t\right)} \tag{7.11}$$

is precisely the zero order contribution (with correct normalization factor) of the direct classical path in section **5** (if also there the correspondence is chosen according to Weyl's rule), in agreement with Choquard's theorem[19] that for infinitesimal time intervals there is no contribution from indirect classical paths.

The case that $H_0(p, x; t)$ is a second order polynomial in (p) is equivalent to the case that $L_0\left(x, \frac{dx}{dt}; t\right)$ is a second order polynomial in $\left(\frac{dx}{dt}\right)$. In other cases, the integral (7.04) will in general not be exactly equal to (7.08) or (7.11) although, according to the principle of stationary phase, the latter expressions might be regarded as more or less appropriate approximations to the first ones—or vice versa.

(7.11) has likewise to satisfy the initial condition (6.04) before it can be regarded as a competitor of (7.04) for giving the most correct description.

If $K_0(x, t; x', t')$ has been found for infinitesimal $t - t'$, it can for finite time intervals formally be obtained by iteration in the well-known way. If $t - t'$ is divided into n infinitesimal intervals $t^{(k+1)} - t^{(k)} = dt^{(k)}$ $(k = 0, 1, \ldots n; (x^{(0)}, t^{(0)}) = (x', t'), (x^{(n+1)}, t^{(n+1)}) = (x, t))$, then

$$K(x, t; x', t') = \lim_{\substack{dt^{(k)} \to 0 \\ (k = 0, 1, \ldots n)}} \prod_{k=0}^{n} \int dx^{(k)^N} \left\{ K_0(x^{(k+1)}, t^{(k+1)}; x^{(k)}, t^{(k)}) - \frac{i}{\hbar} dt^{(k)} \boldsymbol{H}_1(x^{(k)}, t^{(k)})\, \delta(x^{(k+1)} - x^{(k)}) \right\}. \tag{7.12}$$

By lack of an appropriate practical calculus (another formal representation has been given by Davison[22]), this limit can only be treated by approximation methods. Feynman considered it to result from the contributions of all kinematical paths from (x', t')

over $(x^{(1)}, t^{(1)})$, $(x^{(2)}, t^{(2)})$, ... $(x^{(n)}, t^{(n)})$ to (x, t) for all values of $(x^{(1)})$, $(x^{(2)})$, ... $(x^{(n)})$. Because, for infinitesimal $t^{(k+1)} - t^{(k)} = dt^{(k)}$, $K_0(x^{(k+1)}, t^{(k+1)}; x^{(k)}, t^{(k)})$ can in this picture of paths be regarded as due to the direct classical path from $(x^{(k)}, t^{(k)})$ to $(x^{(k+1)}, t^{(k+1)})$, those kinematical paths which, in the limit of all $dt^{(k)} \to 0$, would not tend to what we vaguely shall call „smooth" paths, will not effectively contribute to (7.12). The criterion when a path is considered to be „smooth" remains to be established.

For the case that (7.11) may be used for K_0 in (7.12), an approximation by stationary phase has been considered by CÉCILE MORETTE[20]. The $L_0\left(\frac{x^{(k+1)} + x^{(k)}}{2}, \frac{x^{(k+1)} - x^{(k)}}{dt^{(k)}}; t^{(k)}\right)$'s in the exponents are expanded in powers of the $(x^{(k)} - x_\lambda^{(k)})$'s for suitably chosen $(x_\lambda^{(k)})$'s. In order to make the phase stationary, the first order terms must be made to vanish. They do cancel if the $(x_\lambda^{(k)})$'s are chosen on a classical path λ from (x', t') to (x, t) at the times $t^{(k)}$. Owing to the conditions for infinitesimal time intervals, λ has to be a "smooth" path. The zero order terms, which can be taken before the integral signs in (7.12), then contribute the factor

$$e^{\frac{i}{\hbar}\int_{(x', t')}^{(x, t)} dt''_\lambda L_0\left(x'', \frac{dx''}{dt''}; t''\right)} = e^{\frac{i}{\hbar} I_{0\lambda}(x, t; x', t')} . \qquad (7.13)$$

If higher than second order terms in the Taylor expansion may be neglected according to the principle of stationary phase, it is seen from comparison with section **6** that, in this approximation, (7.12) is again given by the semi-classical approximation (6.29). Thus, from all the kinematical paths, only the classical path λ yields in the lowest order an effective contribution. It does not seem as if the higher order terms in the present expansion will be less intractable than those in the expansion of section **6**. Besides, also here, we come into difficulties if more than one "smooth" classical path is possible from (x', t') to (x, t). The convergence of the Taylor expansion giving a stationary phase near one of them becomes particularly doubtful near the others. One might try to make such an expansion near each of them and hope that contributions from space-time regions far from all of them could be neglected because of phase cancellation, so that (7.12) would

split up according to (6.19). In order to determine the amplitudes of the contributions $K_\lambda(x, t; x', t')$ of the various paths, one would even then have to deal with the junctions, with possible singularities along the paths and with possible discontinuities of the paths (or even of their existence) in their dependence on (x, t) and (x', t'). One might hope that (e. g. for fixed (x) and (x') and decreasing $t - t'$) the contributions of paths would turn out to decrease with decreasing "smoothness". Anyhow, these speculations are cut off by the restrictions on the scope of the present paper.

It does not seem that the treatment of the present section could be improved by choosing other rules of correspondence than those of WEYL.

8. Quasi-classical distributions.

In this section, we discuss the particular role of the quasi-classical paths from a somewhat different point of view. To this purpose we use a rather queer and even treacherous representation of quantum mechanics, which (apparently independently and with quite different intentions and interpretations) has been given by a number of authors (cf., e. g., refs. 23), 24), 25), 12)).

To the operators $\boldsymbol{a}$ representing observables and to the statistical operators $\boldsymbol{k}$ representing quantum mixtures[26] we relate functions $a(p, x)$ and $k(p, x)$ in such a way that the expectation value of the observable for the mixture can be written as

$$\text{Trace } (\boldsymbol{k}\,\boldsymbol{a}) = \frac{1}{h^N}\iint dp^N\, dx^N\, h(p, x)\; a(p, x). \tag{8.01}$$

If we relate $a(p, x)$ to $\boldsymbol{a}$ according to Weyl's rule of correspondence (5.03), (5.04), then we have to relate $k(p, x)$ to $\boldsymbol{k}$ in the same way[12]. $k(p, x)$ is then the Wigner distribution[27]. For the special case of a pure quantum state with wave function $\psi(x)$ in the (x)-representation, this becomes

$$k(p, x) = \int d\xi^N\, \psi^\dagger\left(x + \frac{\xi}{2}\right) e^{\frac{i}{\hbar}\sum_i p_i \xi_i}\, \psi\left(x - \frac{\xi}{2}\right). \tag{8.02}$$

In order to transform the equations of motion, e. g. those in Schrödinger representation

$$\frac{\partial}{\partial t}\boldsymbol{k}(t) = -\frac{i}{\hbar}[\boldsymbol{H}(t), \boldsymbol{k}(t)], \tag{8.03}$$

into the (p, x)-representation, we need the expression which corresponds to the commutator brackets

$$\frac{i}{\hbar}[\boldsymbol{a}, \boldsymbol{b}] = \frac{i}{\hbar}(\boldsymbol{a}\,\boldsymbol{b} - \boldsymbol{b}\,\boldsymbol{a}). \tag{8.04}$$

This turns out to be[12)]

$$a(p, x)\frac{2}{\hbar}\left\{\sin\frac{\hbar}{2}\sum_i\left(\frac{\overleftarrow{6}}{6p_i}\frac{\partial}{\partial x_i} - \frac{\overleftarrow{6}}{6x_i}\frac{\partial}{\partial p_i}\right)\right\}b(p, x), \tag{8.05}$$

where the $\overleftarrow{6}$ symbol denotes differentiation to the left. The equation of motion for the Wigner quasi-distribution function $k(p, x)$ thus becomes (in Schrödinger representation)

$$\left.\begin{aligned}\frac{\partial}{\partial t}k(p, x; t) &= -H(p, x; t)\\ \frac{2}{\hbar}\sin&\left\{\frac{\hbar}{2}\sum_i\left(\frac{\overleftarrow{6}}{6p_i}\frac{\partial}{\partial x_i} - \frac{\overleftarrow{6}}{6x_i}\frac{\partial}{\partial p_i}\right)\right\}k(p, x; t).\end{aligned}\right\} \tag{8.06}$$

This stochastic equation is only then a point-to-point transformation of the type of classical statistical mechanics

$$\frac{\partial}{\partial t}k_c(p, x; t) = \sum_i\left(\frac{\partial k_c(p, x; t)}{\partial p_i}\frac{dp_i}{dt} + \frac{\partial k_c(p, x; t)}{\partial x_i}\frac{dx_i}{dt}\right), \tag{8.07}$$

if the right–hand member of (8.06) reduces to[12)]

$$-(H(p, x; t),\ k(p, x; t)) \tag{8.08}$$

with the Poisson brackets

$$(a(p, x), b(p, x)) = a(p, x)\left\{\sum_i\left(\frac{\overleftarrow{6}}{6p_i}\frac{\partial}{\partial x_i} - \frac{\overleftarrow{6}}{6x_i}\frac{\partial}{\partial p_i}\right)\right\}b(p, x). \tag{8.09}$$

If we use Heisenberg instead of Schrödinger representation, we obtain a similar condition for the bracket expression of a and H

instead of k and H. The conditions are only satisfied for all operators k and a if $H(p, x; t)$ is a polynomial of 2nd order in (p) and (x).

For the two-sided operators in (8.05) and (8.09) we use the abbreviations

$$\sum_i \left(\frac{\overleftarrow{\partial}}{\partial p_i} \frac{\partial}{\partial x_i} - \frac{\overleftarrow{\partial}}{\partial x_i} \frac{\partial}{\partial p_i} \right) = \mathfrak{P} \tag{8.10}$$

and

$$\frac{2}{\hbar} \sin\left(\frac{\hbar}{2} \mathfrak{P} \right) = \mathfrak{P} + \mathfrak{R}. \tag{8.11}$$

With other rules of correspondence than those used here, $\mathfrak{R}$ may be different. But it is a fundamental feature of correspondence[12] that, for no linear rule of correspondence, the commutator brackets and the Poisson brackets can correspond to each other identically. Therefore $\mathfrak{R}$ cannot vanish identically. It is of 2nd order in $\hbar$. If $\mathfrak{R}$ and $\boldsymbol{H}_1(p, x; t)$ in

$$H(p, x; t) = H_0(p, x; t) + H_1(p, x; t) \tag{8.12}$$

can be treated as effectively small, we can try the expansion

$$k(p, x; t) = \sum_{r=0}^{\infty} k^{(r)}(p, x; t) \tag{8.13}$$

with

$$\frac{\partial k^{(0)}(p, x; t)}{\partial t} + (H_0(p, x; t), k^{(0)}(p, x; t)) = 0, \tag{8.14}$$

$$\left.\begin{aligned} &\frac{\partial k^{(r+1)}(p, x; t)}{\partial t} + (H_0(p, x; t), k^{(r+1)}(p, x; t)) \\ &= -\left\{ H_0(p, x; t)\, \mathfrak{R} + H_1(p, x; t)\, \mathfrak{P} \right\} k^{(r)}(p, x; t) \\ &\qquad (r = 0, 1, \ldots). \end{aligned}\right\} \tag{8.15}$$

According to (8.14), $k^{(0)}(p, x; t)$ varies with time in exactly the same way as a classical distribution function (cf. (8.07)) moves along the classical paths corresponding to the Hamiltonian $H(p, x; t)$. If the classical path, which reaches (p, x) at the time t, starts at the time t' from (p', x'), then

$$k^{(0)}(p, x; t) = k^{(0)}(p', x'; t'). \tag{8.16}$$

Integration of (8.15) along this path gives

$$\left.\begin{aligned} k^{(r+1)}(p, x; t) &= k^{(r+1)}(p', x'; t') \\ -\int_{(p', x'; t')}^{\bullet(p, x; t)} dt''_\lambda \{ H_0(p'', x''; t'') \mathfrak{R} + H_1(p'', x''; t'') \mathfrak{P} \} k^{(r)}(p'', x''; t'') & \\ (r = 0, 1, \ldots). & \end{aligned}\right\} \tag{8.17}$$

In the present representation there is just one single classical path.

(8.16) and (8.17) correspond to the iterative solution of the integral equation

$$\left.\begin{aligned} k(p, x; t) &= k(p', x'; t') \\ -\int_{(p', x'; t')}^{\bullet(p, x; t)} dt''_\lambda \{ H_0(p'', x''; t'') \mathfrak{R} + H_1(p'', x''; t'') \mathfrak{P} \} k(p'', x''; t''). & \end{aligned}\right\} \tag{8.18}$$

The operators $H_0\mathfrak{R}$ and $H_1\mathfrak{P}$ (operating on k) again represent the "quantum scattering" and the "Born scattering". The present equation (8.18) (for the statistical operator $\boldsymbol{k}$) in the variables (p), (x), t, t' more or less corresponds to the equation (6.29) (for the dynamical transformation operator $\boldsymbol{K}(t, t')$) in the variables (x), (x'), t, t', as far as the latter is valid. We shall not try for the moment to transform (8.18) directly from one representation to the other.

The quasi-classical features of the present representation can be seen as an expression of the correspondence principle. The treacherous touch is that it seems to meet to a certain extent that pining for the good old classical theory. It cannot actually do so for various reasons. One of them is the fact that, in any correspondence between quantum operators and quasi-classical functions, the infinitesimal unitary transformations represented by commutator brackets in the quantum representation cannot in general correspond in the same sense to the infinitesimal canonical transformations represented by Poisson brackets in the quasi-classical representation. This leads to „quantum scattering" described by the operator $\mathfrak{R}$. But even in those singular cases (considered in the next section) where this "quantum scattering" is effectively absent, there are still other prohibitive reasons[28) 12)] which fall outside the scope of the present paper.

9. Weak potentials.

If, as in the case of the ordinary Schrödinger equation (4.04), $H_0(p, x; t)$ is a 2nd order polynomial in (p) $\left(\text{and } L_0\left(x, \frac{dx}{dt}; t\right)\right.$ a 2nd order polynomial in $\left.\left(\frac{dx}{dt}\right)\right)$, the limiting condition (6.25) in section **6** and the equivalence of (7.04) and (7.11) in section **7** can be considered as assured. One speaks of a Schrödinger equation with "weak potentials" (or shortly of "weak potentials") if $H_0(p, x; t)$ is a 2nd order polynomial in (p) and (x) $\left(\text{and } L_0\left(x, \frac{dx}{dt}; t\right)\right.$ a 2nd order polynomial in (x) and $\left.\left(\frac{dx}{dt}\right)\right)$. We have seen in section 8 that, in the latter case (and only then), the "quantum scattering" is absent. Then the methods of the preceding sections must also work out rather simply.

In weak potentials there is only one single classical path from (x', t') to (x, t). Difficulties with more than one path do not appear. We may drop the index λ. There is also no ambiguity in $H(p, x; t)$ by the choice of the rules of correspondence.

We shall separate the "Born potential" $\boldsymbol{H}_1$ according to (6.31) and only consider $K_0(x, t; x', t')$.

In weak potentials the expressions

$$\lim_{t-t' \to 0} \frac{\partial^2 I_0(x, t; x', t')}{\partial x_i \, \partial x_j'}, \quad \frac{\partial}{\partial t} \frac{\partial^2 I_0(x, t; x', t')}{\partial x_i \, \partial x_j'} \tag{9.01}$$

are independent of (x), (x') and therefore also

$$\frac{\partial^2 I_0(x, t; x', t')}{\partial x_i \, \partial x_j'}; \; D_0(x, t; x', t')^2. \tag{9.02}$$

If we exclude singularities, the same can be said about $D_0(x, t; x', t')$. Then all successive higher order terms ($r = 0, 1, \ldots$) of (6.27) (without $\boldsymbol{H}_1$) become zero and (still apart from singularities) the semi-classical expression (6.29) is the exact solution of (6.03), (6.04), (6.05).

The Taylor expansion of L_0 used in section **7** breaks off after

the 2nd order terms in the case of weak potentials, and we obtain the same exact solution as according to section 6. So, as is well known, in weak potentials no other Feynman paths yield effective contributions than the one single classical path.

In the representation of section 8 the time dependence of the quasi-distribution $(k(p, x; t)$ in a weak potential is actually described by a point-to-point transformation of the type of classical statistical mechanics (although $k(p, x; t)$ has not the proper type of a classical distribution function).

This case once more illustrates the rather singular behaviour of quantum systems in weak potentials, e. g., the harmonic oscillator[29) 30) 12)]. In particular it shows how dangerous it may be without further investigation to generalize conclusions which have been derived only for the case of weak potentials also to other cases.

10. Conclusion.

The foregoing expansions are just some examples out of a great variety, all with a quasi-classical lowest order term. Even in "weak potentials", where this is the only term, it does not open the gate to the lost classical paradise. For some problems the expansions may be useful as practical approximation methods. In particular the lowest order BWK approximation works in some respects surprisingly well[31)].

As soon as singularities occur, e. g. connected with "classical reflections", the situation near and beyond these points has to be carefully investigated, as it has been done in the stationary 1-dimensional BWK approximation. These singularities are also of importance for the unsolved problem how to deal with various competing classical paths.

A generalization to a relativistic treatment could more readily be performed for the boson than for the fermion case.

CERN Theoretical Study Division,
Institute for Theoretical Physics, Copenhagen
on leave of absence from
Groningen University.

References.

1) E. C. Kemble, The Fundamental Principles of Quantum Mechanics (New York 1937).
2) R. P. Feynman (1948), Rev. Mod. Phys. **20**, 367.
3) H. Bremmer (1949), Physica **15**, 593; Terrestrial Radio Waves (Amsterdam 1949).
4) R. Landauer (1951), Phys. Rev. **82**, 80.
5) L. Brillouin (1926), C. R. **183**, 24; J. de Phys. **7**, 353.
6) G. Wentzel (1926), Zs. f. Phys. **38**, 518.
7) H. A. Kramers (1926), Zs. f. Phys. **39**, 828.
8) H. Jeffreys (1953), Proc. Camb. Phil. Soc. **49**, 601; (1924) Proc. Lond. Math. Soc. **23**, 428.
9) S. C. Miller and R. H. Good Jr. (1953), Phys. Rev. **91**, 174.
10) V. A. Bailey (1954), Phys. Rev. **96**, 865.
11) H. Weyl (1927), Zs. f. Phys. **46**, 1; Gruppentheorie und Quantenmechanik (Leipzig 1928).
12) H. J. Groenewold (1946), Physica **12**, 405.
13) P. A. M. Dirac, The Principles of Quantum Mechanics (Oxford 1947).
14) L. de Broglie (1951), C. R. **233**, 641.
15) D. Bohm (1952), Phys. Rev. **85**, 166; 180.
16) W. Glaser, Grundlagen der Elektronenoptik (Wien 1952).
17) I. I. Gol'dman and A. B. Migdal (1955), Sov. Phys. JETP **1**, 304.
18) R. P. Feynmann (1949), Phys. Rev. **76**, 749.
19) Ph. Choquard (1955), Helv. Phys. Acta **28**, 89.
20) Cécile Morette (1951), Phys. Rev. **81**, 848.
21) W. Pauli, Ausgewählte Kapitel aus der Feldquantisierung (Zürich 1951).
22) B. Davison (1954), Proc. Roy. Soc. A **225**, 252.
23) T. Takabayasi (1954), Progr. Theor. Phys. **11**, 341.
24) J. E. Moyal (1949), Proc. Camb. Phil. Soc. **45**, 99.
25) J. Bass (1948), Rev. Sci. **86**, 643.
26) J. von Neumann, Mathematische Grundlagen der Quantenmechanik (Berlin 1932, New York 1943).
27) E. Wigner (1932), Phys. Rev. **40**, 749.
28) G. P. Dishkant (1955), Sov. Phys. JETP **1**, 166.

29) I. R. Senitzsky (1954), Phys. Rev. **95**, 1115.
30) C. A. Coulson and G. S. Rushbrooke (1946), Proc. Camb. Phil. Soc. **42**, 286.
31) G. Breit and P. B. Daitch, to be published.
32) R. F. Christy (1955), Bul. Am. Phys. Soc. **30** nr. 1, ZA 7.
33) P. O. Fröman (1957) Mat. Fys. Skr. Dan. Vid. Selsk. **1**, no. 3.

Indleveret til selskabet den 6. april 1956.
Færdig fra trykkeriet den 23. november 1956

Matematisk-fysiske Meddelelser
udgivet af
Det Kongelige Danske Videnskabernes Selskab
Bind **30**, no. 20

Mat. Fys. Medd. Dan. Vid. Selsk. **30**, no. 20 (1956)

ON THE COUPLING CONSTANTS IN β-DECAY

BY

O. KOFOED-HANSEN AND A. WINTHER

København 1956
i kommission hos Ejnar Munksgaard

Synopsis.

Recent experimental data on superallowed β-transitions are used in a redetermination of the β-decay coupling constants. It is suggested that the β-decay interaction may contain an admixture of vector coupling besides the usually adopted scalar and tensor interactions.

Printed in Denmark.
Bianco Lunos Bogtrykkeri A/S.

1. Introduction.

The improved accuracy in the experimental data on superallowed β-transitions as well as the determination of several new ft-values for superallowed $0 \rightarrow 0$ transitions permit a higher accuracy in the determination of the coupling constants in β-decay.

We shall follow the same procedure as applied earlier[1]). In the first section, we assume that no cross terms are present, which, according to recent recoil investigations[2]), means that the β-interaction is a mixture of scalar and tensor coupling only. In the second part, we consider the evidence on the possible admixture of axial vector and, especially, vector interaction.

2. Vanishing Cross Terms.

In Table I, we have collected the experimental data which we shall use. Only recent references which have not yet appeared in isotope tables are included. For the evaluation of the ft-values, the recent tables of Fermi integrals[3]) were used whenever possible; in other cases numerical integrations were performed.

Besides the mirror transitions between nuclei with closed

[1]) O. KOFOED-HANSEN and A. WINTHER, Phys. Rev. **86**, 428 (1952).
A. WINTHER and O. KOFOED-HANSEN, Mat. Fys. Medd. Dan. Vid. Selsk. **27**, no. 14 (1953).

[2]) J. M. ROBSON, Phys. Rev. **100**, 933 (1955).
MAXSON, ALLEN, and JENTSCHKE, Phys. Rev. **97**, 109 (1955).
W. P. ALFORD and D. R. HAMILTON, Phys. Rev. **95**, 1351 (1954).
B. M. RUSTAD and S. L. RUBY, Phys. Rev. **89**, 880 (1953) and **97**, 991 (1955).
J. S. ALLEN and W. K. JENTSCHKE, Phys. Rev. **89**, 902 (1953).

[3]) S. A. MOSZKOWSKI and K. M. JANTZEN, UCLA Technical Report, no. 10—26—55.

TABLE 1. Data for transitions used in B,x diagrams.

Decay	$E_{\text{Mev}}^{\max}$	t	ft	$\lvert\int 1\rvert^2$	$\lvert\int \vec{\sigma}\rvert^2$ Single particle	$\lvert\int \vec{\sigma}\rvert^2$ μ corrected	(Weight)$^{-1}$
$O^{14} \rightarrow N^{14}$	1.835 ± 8 [4]	$72^{s}.1 \pm 4$ [4] 99.4 pct.	3300 ± 75	2	0		75
$Al^{26} \rightarrow Mg^{26}$	3.202 ± 10 [5]	$6^{s}.54 \pm 10$ [6]	3080 ± 80	2	0		80
$Cl^{34} \rightarrow S^{34}$	4.50 ± 3 [7]	$1^{s}.53 \pm 2$ [8]	3110 ± 120	2	0		120
$K^{38} \rightarrow A^{38}$	5.06 ± 11 [9]	$0^{s}.935 \pm 25$ [8]	3140 ± 400	2	0		400
$n \rightarrow p$	$.782 \pm 1$	$12^{m}.2 \pm 1.5$ [10]	1220 ± 150	1	3		300
$H^3 \rightarrow He^3$	$.0183 \pm 2$	$12^{y}.262 \pm 4$ [11]	1060 ± 40	1	3	3.51 [12] 3.72 [13] 3.62 [14]	370
$O^{15} \rightarrow N^{15}$	1.735 ± 8 [15]	$123^{s} \pm 2$ [8]	4400 ± 100	1	1/3	0.350	100
$F^{17} \rightarrow O^{17}$	1.746 ± 6 [16]	$65^{s} \pm 2$ [17]	2330 ± 80	1	7/5	1.373	100
$Ca^{39} \rightarrow K^{39}$	5.58 ± 8 [18]	$0^{s}.90 \pm 1$ [8]	4650 ± 300	1	3/5	0.390	650
$Se^{41} \rightarrow Ca^{41}$	4.94 ± 5 [19]	$0^{s}.87 \pm 5$	2560 ± 160	1	9/7		430 [20]

[4]) R. SHERR and J. B. GERHART, Phys. Rev. **91**, 909 (1953).
J. B. GERHART, Phys. Rev. **95**, 288 (1954).
SHERR, GERHART, HORIE, and HORNYAK, Phys. Rev. **100**, 945 (1955).
[5]) KINGTON, BAIR, COHN, and WILLARD, Phys. Rev. **99**, 1393 (1955).
ENDT, KLUYVER, and VAN DER LEUN, Physica **20**, 1299 (1954), and Phys. Rev. **94**, 1795 (1954).
ELBEK, MADSEN, and NATHAN, Phil. Mag. **46**, 663 (1955).
T. H. HANDLEY and W. S. LYON, Phys. Rev. **99**, 755 (1955).
KAVANAGH, MILLS, and SHERR, Phys. Rev. **97**, 248 (1955).
[6]) HASLAM, ROBERTS, and ROBB, Can. J. Phys. **32**, 361 (1954).
GREEN, HARRIS, and COOPER, Phys. Rev. **96**, 817 (1954).
[7]) W. ARBER and P. STÄHELIN, Helv. Phys. Acta **26**, 433 (1953).
P. STÄHELIN, Helv. Phys. Acta **26**, 691 (1953).
D. GREEN and J. R. RICHARDSON, Phys. Rev. **96**, 858 (1954).
[8]) R. M. KLINE and D. J. ZAFFARANO, Phys. Rev. **96**, 1620 (1954).
[9]) W. A. HUNT, Thesis, Iowa State College, 1954.
P. STÄHELIN, Helv. Phys. Acta **26**, 691 (1953).
[10]) SPIVAC, SOSNOVSKY, PROKOFIEV, and SOKOLOV, Geneva Conference. A/CONF 8/P/650 (1955).
[11]) W. M. JONES, Phys. Rev. **100**, 124 (1955).
[12]) From H^3 magnetic moment.
[13]) From He^3 magnetic moment.
[14]) Average value.
[15]) KINGTON, BAIR, COHN, and WILLARD, Phys. Rev. **99**, 1393 (1955).
[16]) C. WONG, Phys. Rev. **95**, 765 (1954).
[17]) WARREN, LAURIE, JAMES, and ERDMAN, Can. J. Phys. **32**, 563 (1954), L. KOESTER, Zeit. f. Naturf. **9a**, 104 (1954).
[18]) D. J. ZAFFARANO, priv. comm.
[19]) H. S. PLENDL and F. E. STEIGERT, Phys. Rev. **98**, 1538 (1955).
[20]) Matrix element uncertainty equated to uncertainty for Ca^{39}.

shells $\pm$ one nucleon, we have included the transitions of type $0 \rightarrow 0$, $\Delta T = 0$ (no). The Fermi matrix element, $|\int 1|^2$, for all the transitions can be determined from the assumption of charge independence of nuclear forces only[21]). Coulomb corrections are expected to be small for the light nuclei in question and will be neglected. While the Gamow-Teller matrix elements vanish for the $0 \rightarrow 0$ transitions, the matrix elements for the other transitions in Table I are expected to be given in a good approximation by the single-particle value quoted in column 6. This is supported by the fact that in most cases also the magnetic moment of these nuclei deviates only slightly from the single-particle value. A semi-empirical value for the Gamow-Teller matrix element obtained from the magnetic moment, μ, is given by[1])

$$|\int \vec{\sigma}|^2 = 4 \frac{J+1}{J} \left(\frac{\mu - g_l J}{g_s - g_l} \right)^2, \tag{1}$$

where J is the nuclear spin, and g_l and g_s are the gyromagnetic ratios for orbital angular momentum and spin of the odd particle, respectively. In the following, we adopt the matrix element values of eq. (1) for the closed shell $\pm$ one nucleon transition. However, in the weight which we attribute to the transition (column 8), we include the deviation of eq. (1) from the single-particle value as an additional uncertainty besides the experimental.

We find for each β-transition a B,x line defined by

$$B = ft \{ (1-x) |\int 1|^2 + x |\int \vec{\sigma}|^2 \} \tag{2}$$

with

$$B = \frac{2 \pi^3 \hbar^7 \ln 2}{(g_S^2 + g_T^2)\, m^5 c^4} \tag{3}$$

and

$$x = g_T^2/(g_S^2 + g_T^2), \tag{4}$$

[21]) E. WIGNER and E. FEENBERG, Rep. Prog. Phys. **8**, 274 (1941).

where g_S and g_T are the scalar and tensor coupling constants, respectively. We use the conventional units where f is measured in units $m = c = 1$, and t in seconds.

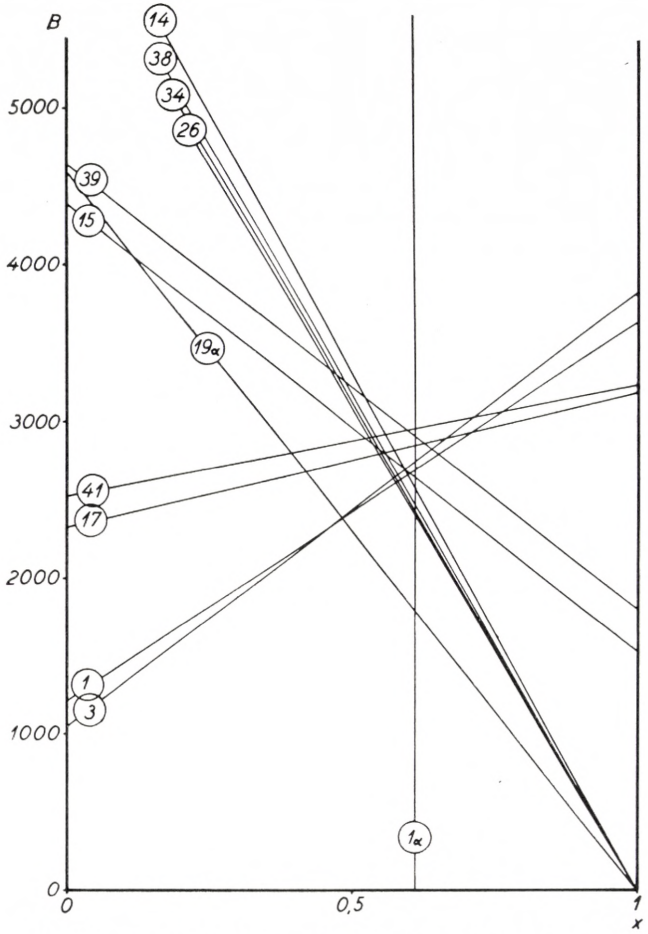

Fig. 1. The B,x diagram under the assumption of vanishing cross terms. The mass numbers of the transitions are indicated.

The B,x plot obtained from eq. (2) by means of the data in Table I is shown in Fig. 1. In this diagram, we have also included the recent correlation data from the neutron decay and Ne^{19}. For the neutron $|\int 1|^2$ and $|\int \vec{\sigma}|^2$ are known and we may therefore write for the angular correlation parameter

$$\alpha = \frac{-g_S^2 \left| \int 1 \right|^2 + \frac{1}{3} g_T^2 \left| \int \vec{\sigma} \right|^2}{g_S^2 \left| \int 1 \right|^2 + g_T^2 \left| \int \vec{\sigma} \right|^2} \tag{5}$$

$$= \frac{-(1-x) + x}{(1-x) + 3x} \tag{6}$$

which together with the value $\alpha = 0.089 \pm 0.108$, found by ROBSON[2]), gives

$$x = \frac{1}{2} \frac{1+\alpha}{1-\alpha} = 0.60 \pm 0.13. \tag{7}$$

This leads to the vertical line marked 1_α in Fig. 1.

For Ne^{19} we may combine the *ft*-value with the angular correlation parameter $\alpha = -0.21 \pm 0.08$ found by MAXSON *et al.*[2]) and with the $\left| \int 1 \right|^2$ value found from charge independence[21]). We may then solve eq. (5) with respect to B and x and find

$$\left.\begin{aligned} B &= ft \left| \int 1 \right|^2 (4/(1-3\alpha))\,(1-x) \\ &= (4600 \pm 900)\,(1-x), \end{aligned}\right\} \tag{8}$$

which is a B,x line of exactly the same type as those for the $0 \rightarrow 0$ transition, but numerically slightly inconsistent with these. This line is marked 19_α in Fig. 1.

Using the method of least squares and applying the weights given in Table I, we obtain the value

$$\left.\begin{aligned} B &= 2787 \pm 70 \\ x &= 0.560 \pm .012 \end{aligned}\right\} \tag{9}$$

for the common intersection point. The errors quoted are twice the standard error as obtained from internal consistency of the data. It should be noted that the B,x plot is not internally consistent inside the experimental errors quoted in Table I (cf. O^{14} and Al^{26}).

It is evident that systematic errors involved in the evaluation of the matrix elements may add to the errors given in eq.s (9).

The Coulomb corrections, although small, are errors of this type[22]). However, the sign is such that the inconsistency between O^{14} and Al^{26} is enlarged. Another source of systematic errors is the possible existence of cross terms.

3. Non-vanishing Cross Terms.

The limits available on the cross terms are derived from three sources: the shapes of β-spectra, the K-capture to positron ratios, and the consistency of the B,x diagram, whereas the recoil correlations are indeed very insensitive to such effects[1, 23]).

The limits obtained from β-spectrum shapes have been summarized by MAHMOUD and KONOPINSKI[24]) and by DAVIDSON and PEASLEE[25]). Also recent He^6 spectrum measurements should be taken into account[26]) as wsll as measurements of the spectra of C^{11} and F^{17} [27]). The limits in the GAMOW-TELLER interference term is quite well established in this way with the result $|g_A/g_T| < 0.05$ based especially on the He^6 spectrum. Here, g_A is the axial vector coupling constant. Information about the Fermi interference term was based solely on the N^{13} spectrum and the statements made on the vector coupling constant g_V are therefore somewhat more uncertain. KONOPINSKI and MAHMOUD conclude that $|g_V/g_S| < 0.20$. The spectra of C^{11} and F^{17} do not permit to narrow this limit (cf. Fig. 4).

The K capture to positron emission ratio for Na^{22} studied by SHERR and MILLER[28]) leads to the estimate $g_A/g_T = -0.01 \pm 0.02$.

These limits for the Fierz terms are, in Fig. 2, expressed as limits on the interference term constant b_F and b_{GT} given by

$$b_F = \frac{2\gamma g_S g_V}{g_S^2 + g_V^2}, \tag{10}$$

[22]) W. M. MCDONALD, Princeton thesis 1955.
[23]) O. KOFOED-HANSEN and A. WINTHER, Phys. Rev. **89**, 526 (1953).
[24]) H. M. MAHMOUD and E. J. KONOPINSKI, Phys. Rev. **88**, 1266 (1952).
[25]) J. P. DAVIDSON and D. C. PEASLEE, Phys. Rev. **91**, 1232 (1953).
[26]) A. SCHWARZCHILD, priv. com.
[27]) C. WONG, Phys. Rev. **95**, 765 (1954).
[28]) R. SHERR and R. H. MILLER, Phys. Rev. **93**, 1076 (1954).

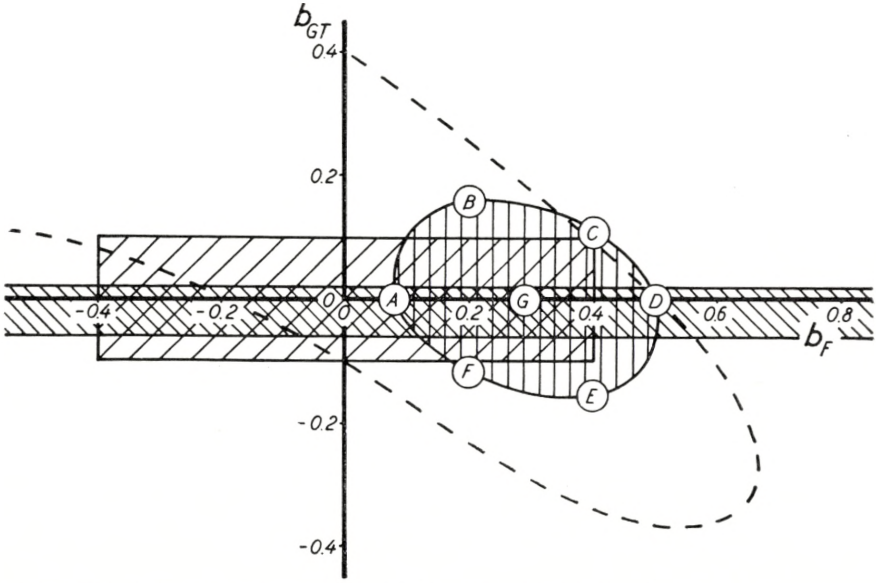

Fig. 2. The areas in the b_F, b_{GT} plane which are consistent with experimental data. B,x values in the points A to G are given in Table II.

limits from K capture to positron ratio of Na^{22}.

limits from spectral shapes.

limits from consistency of (1953) B,x plot.

limits from consistency of (1956) B,x plot.

and

$$b_{GT} = \frac{2\gamma\, g_A\, g_T}{g_A^2 + g_T^2}, \tag{11}$$

where

$$\gamma = \sqrt{1 - (\alpha Z)^2}. \tag{12}$$

In this figure, we also show the older limits on possible b_F, b_{GT} values as derived from internal consistency of the B,x diagram[1]). In using the B,x diagram for such investigation we redefine

$$\left.\begin{aligned} B = ft\{ &(1-x)\,(1 \pm b_F \langle 1/W\rangle_{AV})\,\left|\int 1\right|^2 \\ &+ x\,(1 \pm b_{GT}\langle 1/W\rangle_{AV})\,\left|\int \vec{\sigma}\right|^2\} \end{aligned}\right\} \tag{13}$$

and

$$x = \frac{g_T^2 + g_A^2}{g_S^2 + g_V^2 + g_A^2 + g_T^2}, \tag{14}$$

where the + sign in (13) applies to β^- decay and the — sign to β^+ decay.

With the new ft-values of Table I, one obtains a much narrower region which is also given in Fig. 2. The limits correspond to twice the standard deviation as observed from internal consistency of the B, x diagram and coincide very closely with the points where one or more of the experimental lines show a definite inconsistency with the common B, x point in question inside the experimental errors. It is noted that inside the region the $0 \to 0$ transitions show consistent ft-values contrary to the case of no interference terms discussed above. Also no inconsistency with the neutron recoil correlation occurs, and the Ne^{19} correlation is in no worse agreement here than in the case of absence of Fierz terms.

TABLE II. B, x values at the b_F, b_{GT} points indicated in Fig. 2 and at $b_F = b_{GT} = 0$.

b_F, b_{GT} point	B	x
A	2750	0.553
B	2640	0.552
C	2550	0.535
D	2510	0.522
E	2630	0.518
F	2720	0.539
G	2620	0.537
0,0	2787	0.560

Of course, B and x are now functions of b_F, b_{GT} and we have given, in Table II, a sequence of values in the center and at the border of the region of consistency. It is seen that the variations of B and x are much larger than the uncertainties found for fixed values of b_F and b_{GT} (cf. eq.s (9)). In Fig. 3, we give the B, x plot corresponding to the most probable value of $(b_F, b_{GT}) = (0.29,0)$ and, in Fig. 4, we show the Fierz plots of the spectra of C^{11} and F^{17} derived under the assumption that $b_F = 0.29$ and using the matrix element obtained from charge independence and the B, x point of Fig. 3.

If one includes the Coulomb correction as recently calcu-

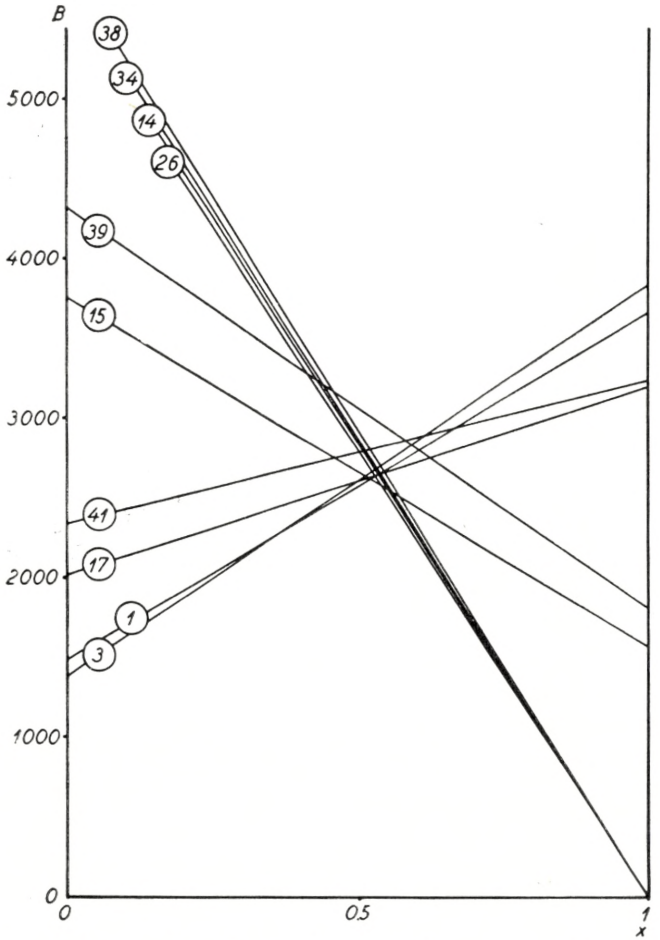

Fig. 3. The B, x diagram for the best fit obtained at $b_F = 0.29$ and $b_{GT} = 0$.

lated[22]) in the cross term investigation, this correction tends to lower B and x and to make b_F larger.

It is seen that the available material is consistent with the assumption of the presence of a small amount of vector coupling, but it should be remembered that the conclusion from the B, x plots is on the limits of the uncertainties in the experimental data as well as on the theoretical evaluation of the matrix elements.

It is interesting to note that recent experiments[29]) indicate a small difference between the spectra of Al^{25} and Al^{26}

[29]) Elbek, Madsen, and Nathan, Phil. Mag. **46**, 663 (1955).

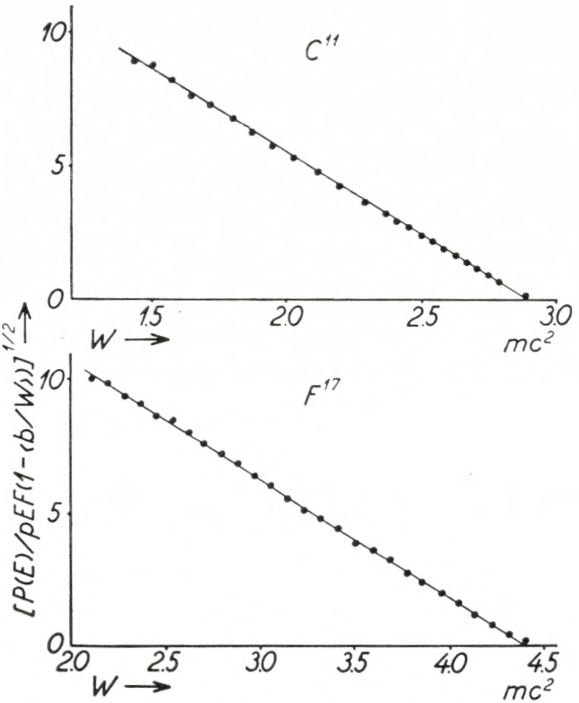

Fig. 4. Fierz plots of the C^{11} and F^{17} spectra observed by WONG[27]) using $b_F = 0.29$ and $b_{GT} = 0$.

measured under identical conditions. This could be ascribed to the above amount of cross terms even allowing for the branching in the Al^{25} decay. However, the accuracy in the spectra hardly permits definite conclusions. Thus it is to be hoped that further comparisons of β-spectra of neighbouring $0 \rightarrow 0$ and mirror transitions will be carried out. Such transitions show nearly the same maximum energy, and difference spectra might therefore be independent of scattering troubles which usually prevent accurate information about cross terms.

Institute for Theoretical Physics
University of Copenhagen, Denmark.

Indleveret til selskabet den 4. juni 1956.
Færdig fra trykkeriet den 26. oktober 1956.

Matematisk-fysiske Meddelelser
udgivet af
Det Kongelige Danske Videnskabernes Selskab
Bind **30,** no. 21

Mat. Fys. Medd. Dan. Vid. Selsk. **30,** no. 21 (1956)

QUANTUM MECHANICS IN GENERALIZED HILBERT SPACE

BY

VACHASPATI

København 1956
i kommission hos Ejnar Munksgaard

CONTENTS

Synopsis.

An attempt is made to generalize the Hilbert space of quantum mechanics in analogy with the development of the general relativity theory from the theory of special relativity. The state vectors, ψ, $\overline{\psi}$, of quantum mechanics are found to be analogous to the four-velocity, v^μ, of relativity and therefore coordinates, χ, $\overline{\chi}$, are introduced, corresponding to the coordinates x^μ of a particle, such that the time derivatives of χ and $\overline{\chi}$ equal ψ and $\overline{\psi}$. The metric η, used in constructing the probability density, is supposed to be a function of χ and $\overline{\chi}$. The unitary transformations of the usual theory are replaced by quite general transformations χ and $\overline{\chi}$. A tensor calculus for this generalized Hilbert space is developed and equations of motion for the states and the dynamical variables are postulated as generalizations of the usual Heisenberg equations when the ordinary time differentiation is replaced by invariant time differentiation. In this way a non-linear theory is obtained. However, the expectation values of the dynamical variables are found to be the same in the new theory as in the old, showing that this theory cannot give any physical results different from those of the usual theory.

Printed in Denmark
Bianco Lunos Bogtrykkeri A-S

1. Introduction.

The present-day quantum mechanics has been successful in explaining a large number of phenomena, particularly those involving electrons and electromagnetic radiation. It has, however, not been so successful in dealing with other particles. The discovery of several new particles in recent years seems to indicate that the basis of the present theory ought to be broadened. In an ideal theory, one should be able to describe the various particles as possible states of one system. It is probable that this can be achieved by constructing a non-linear theory in which the principle of superposition of states is valid only as a first approximation.

Some attempts in this direction have recently been made, notably by SCHIFF (1951 a, b, 1952), by THIRRING (1952), by HEISENBERG (1953, 1954) and by HEISENBERG, KORTEL and MITTER (1955), who introduced non-linear terms into the wave equations. The addition of such terms is, however, an entirely arbitrary procedure and therefore unsatisfactory. These attempts can therefore be considered only as phenomenological until they have some acceptable principles as their basis.

A well-known example of a non-linear theory in classical physics is the theory of general relativity. The special relativity theory allows only linear transformations of the coordinates; the general theory abandons this restriction and takes quite general coordinate transformations into account. This leads in a fairly natural way to the explanation of the gravitational phenomena. But gravitation plays only a very minor role in atomic and nuclear phenomena and therefore the theory of general relativity in itself is not of much interest to the atomic physicist. However, one can

still learn a great deal from it. Its methods may, for instance, be applied to the construction of a more general Hilbert space in which the unitary transformations of the usual theory can be abandoned in favour of more general transformations. This paper deals with exploring this possibility. It is shown here that such a generalization is possible and leads, as expected, to non-linear wave equations in quantum mechanics.

The development outlined below is similar to that of the general relativity theory. However, it is hoped that this paper can be understood, at least in its main line of arguments, without previous familiarity with general relativity or Riemannian geometry.

2. Analogy between Relativity Theory and Quantum Mechanics.

We here start by discussing a Hilbert space of finite dimensions, N. A system in quantum mechanics is completely specified when the components, ψ^m, of its state vector are known in all the N mutually orthogonal directions in Hilbert space. The state ψ is usually normalized to unity, which means that

$$\sum_{m=1}^{N} \overline{\psi}^m \psi^m = 1 . \tag{2.1}$$

Here $\overline{\psi}^m$ is the complex conjugate of ψ^m. One could, if one wished, choose a different normalization for ψ, but normalization to unity is most convenient. The unitary transformations are such that they leave (2.1) invariant. Indicating the transformed variables by primes, we have

$$\sum_m \overline{\psi}^{m'} \psi^{m'} = \sum_m \overline{\psi}^m \psi^m = 1 . \tag{2.2}$$

If we define

$$\psi_m = \overline{\psi}^m \tag{2.3}$$

we can write (2.1) as

$$\sum_m \psi_m \psi^m = 1 . \tag{2.4}$$

Let us denote a general dynamical variable by A with components $A_{\overline{m}n}$. When ψ goes over to ψ' by means of a unitary

transformation, A goes over to A' such that the expression $\sum_{m,\,n} \bar{\psi}^m A_{\bar{m}n} \psi^n$ remains invariant:

$$\sum_{m,\,n} \bar{\psi}^{m'} A'_{\bar{m}n} \psi^{n'} = \sum_{m,\,n} \bar{\psi}^m A_{\bar{m}n} \psi^n. \tag{2.5}$$

The reason why we have put a bar over m in $A_{\bar{m}n}$ is that this suffix is contracted with $\bar{\psi}^m$ while the other suffix, n, which is without a bar, is contracted with ψ^n.

With the help of the above notation for the components of a dynamical variable, we can write (2.3) as

$$\psi_m = \sum_n \bar{\psi}^n \eta_{\bar{n}m}, \tag{2.6}$$

where $\eta_{\bar{n}m}$ is the unit matrix.

In special relativity we meet an analogous situation. If v^μ denotes the four-velocity, $\dfrac{dx^\mu}{d\tau}$, of a particle (τ is the proper time, $c = 1$), we have

$$v_\mu v^\mu = 1. \tag{2.7}$$

Here the covariant components, v_μ, are related to the contravariant vector v^μ by means of the metric $g_{\nu\mu}$:

$$v_\mu = \sum_\nu v^\nu g_{\nu\mu}, \tag{2.8}$$

where

$$\left.\begin{aligned} g_{00} = 1, \quad g_{11} = g_{22} = g_{33} = -1, \\ g_{\mu\nu} = 0 \text{ for } \mu \neq \nu. \end{aligned}\right\} \tag{2.9}$$

If one expressed x^μ as functions of some other parameter s, one would get another factor instead of 1 on the right-hand side of (2.7). However, it is most convenient to have the normalization 1 by choosing the independent variable as τ.

We now notice a formal similarity between the equations (2.4) and (2.6) of the quantum theory, on the one hand, and the equations (2.7) and (2.8) of relativity, on the other. The analogue of the equation (2.5) in relativity would merely specify the transformation properties of a second rank tensor.

Because of this formal similarity between the relativity and the quantum theories, we can say that the quantum state ψ with components ψ^m corresponds to the relativistic velocity $\vec{v}$ with components v^μ.

3. Coordinates in Hilbert Space and Generalization of η.

The fact that ψ^m corresponds to the velocity v^μ suggests that we introduce coordinates χ^m such that, by definition,

$$\psi^m = \frac{d\chi^m}{dt}. \tag{3.1}$$

This relation is analogous to the definition

$$v^\mu = \frac{dx^\mu}{d\tau}.$$

The χ^m's do not form a vector, just as x^μ does not constitute a vector in relativity. The upper position of the index m in χ^m is inserted only for convenience and does not imply that it is a vector.

From (2.4) and (3.1) it follows that

$$d\chi_m \, d\chi^m = dt^2, \tag{3.2}$$

where, according to (2.6),

$$d\chi_m = \sum_n d\bar{\chi}^n \, \eta_{\bar{n}m}. \tag{3.3}$$

(3.2) can also be written as

$$\sum_{m,\,n} \eta_{\bar{m}n} \, d\bar{\chi}^m \, d\chi^n = dt^2 \tag{3.4}$$

which is analogous to the relativity relation

$$\sum_{\mu,\,\nu} g_{\mu\nu} \, dx^\mu \, dx^\nu = d\tau^2. \tag{3.5}$$

In special relativity the $g_{\mu\nu}$'s are constants given by (2.9). The transition from this theory to the theory of general relativity

consists in abandoning the constancy of $g_{\mu\nu}$ and allowing them to be functions of the coordinates x^μ. In view of the formal similarity between the equations (3.4) and (3.5), it now suggests itself that in quantum theory we regard $\eta_{\overline{m}n}$ as functions of χ and $\overline{\chi}$:

$$\eta_{\overline{m}n} = \eta_{\overline{m}n}(\chi, \overline{\chi}). \tag{3.6}$$

4. Definitions of Vectors and Tensors.

We now assume that quite general transformations of χ and $\overline{\chi}$ are possible such that the transformed coordinates $\chi^{m'}$ depend on $\chi^1, \chi^2, \chi^3, \ldots\ldots\ldots \chi^N$ and similarly $\overline{\chi}^{m'}$ depend on $\overline{\chi}^1, \overline{\chi}^2, \overline{\chi}^3, \ldots\ldots\ldots \overline{\chi}^N$:

$$\left.\begin{aligned} \chi^{m'} &= \chi^{m'}(\chi^1, \chi^2, \chi^3, \ldots \chi^N) \\ \overline{\chi}^{m'} &= \overline{\chi}^{m'}(\overline{\chi}^1, \overline{\chi}^2, \overline{\chi}^3, \ldots \overline{\chi}^N) \\ & \qquad\qquad m = 1 \ldots N. \end{aligned}\right\} \tag{4.1}$$

Note that $\chi^{m'}$ does not depend on $\overline{\chi}^r$, nor does $\overline{\chi}^{m'}$ depend on χ^r.

From (4.1) it follows that

$$d\chi^{m'} = \frac{\partial \chi^{m'}}{\partial \chi^n} d\chi^n \tag{4.2 a}$$

and

$$d\overline{\chi}^{m'} = \frac{\partial \overline{\chi}^{m'}}{\partial \overline{\chi}^n} d\overline{\chi}^n. \tag{4.2 b}$$

We now follow the usual convention that, unless otherwise stated, when a suffix occurs once below and once above, summation over it will be understood.

We define a 'contravariant vector' as one whose components transform like $d\chi^m$ and a 'conjugate contravariant vector' as one whose components transform as $d\overline{\chi}^m$. Sometimes, we distinguish vectors of the kind $d\chi^m$ by calling them 'ordinary' as contrasted with conjugate vectors. Thus, an ordinary contravariant vector, A^m, transforms as

$$A^{m'} = \frac{\partial \chi^{m'}}{\partial \chi^n} A^n \tag{4.3 a}$$

and a conjugate contravariant vector, $A^{\overline{m}}$, as

$$A^{\overline{m}'} = \frac{\partial \overline{\chi}^{m'}}{\partial \overline{\chi}^{n}} A^{\overline{n}}. \tag{4.3 b}$$

We put a bar over the suffix which transforms as a conjugate vector, while the suffixes which transform as ordinary vectors will be left unbarred.

From (4.2 a, b) and (3.1) it follows that ψ is an ordinary and $\overline{\psi}$ a conjugate contravariant vector.

Besides contravariant vectors, we also have covariant vectors. An ordinary covariant vector, A_m, is defined to transform as

$$A'_m = \frac{\partial \chi^n}{\partial \chi^{m'}} A_n. \tag{4.4 a}$$

The conjugate covariant vectors transform as

$$A'_{\overline{m}} = \frac{\partial \overline{\chi}^{n}}{\partial \overline{\chi}^{m'}} A^{\overline{n}}. \tag{4.4 b}$$

These definitions are arranged so that, by contracting the indices of a covariant vector and a contravariant vector of the same kind, we get an invariant result:

$$A'_m B^{m'} = A_m B^m \tag{4.5 a}$$

$$A'_{\overline{m}} B^{\overline{m}'} = A_{\overline{m}} B^{\overline{m}}. \tag{4.5 b}$$

Tensors of higher ranks can be defined in exactly the same way as in the ordinary tensor analysis. Thus, a second rank tensor $A^m{}_n$ transforms as

$$A^{m}{}_{n}{}' = \frac{\partial \chi^{m'}}{\partial \chi^{a}} \frac{\partial \chi^{b}}{\partial \chi^{n'}} A^{\overline{a}}{}_{b} \tag{4.6 a}$$

and a tensor $A^{\overline{m}}{}_n$ transforms as

$$A^{\overline{m}}{}_{n}{}' = \frac{\partial \overline{\chi}^{m'}}{\partial \overline{\chi}^{a}} \frac{\partial \chi^{b}}{\partial \chi^{n'}} A^{\overline{a}}{}_{b}, \tag{4.6 b}$$

etc.

From (3.4) and (4.2 a, b), it is clear that, if we have

$$\eta'_{\overline{m}n} = \frac{\partial \overline{\chi}^a}{\partial \overline{\chi}^{m'}} \frac{\partial \chi^b}{\partial \chi^{n'}} \eta_{\overline{a}b}, \tag{4.7}$$

the expression (3.4) will be invariant. We can say that η is a covariant tensor of the mixed kind. It is easy to see that $A_{\overline{m}n}$ in (2.5) is also a covariant tensor, of the mixed kind.

Besides being a tensor, the equation (3.4) shows that η is a Hermitian matrix, i. e.,

$$\overline{\eta}_{\overline{m}n} = \eta_{\overline{n}m}. \tag{4.8}$$

5. Covariant Differentiation.

If φ is a scalar, i. e., if

$$\varphi' = \varphi,$$

it follows that

$$\frac{\partial \varphi'}{\partial \chi^{m'}} = \frac{\partial \varphi}{\partial \chi^a} \frac{\partial \chi^a}{\partial \chi^{m'}}. \tag{5.1}$$

Comparing (5.1) with (4.4 a) we see that the gradient, $\frac{\partial \varphi}{\partial \chi^m}$, is a covariant vector. Similarly one can see that $\frac{\partial \varphi}{\partial \overline{\chi}^m}$ is a conjugate covariant vector.

Let us now consider the gradient of a vector A^m. We have, on using (4.3 a),

$$\left.\begin{aligned} \frac{\partial A^{m'}}{\partial \chi^{n'}} &= \frac{\partial}{\partial \chi^{n'}} \left[\frac{\partial \chi^{m'}}{\partial \chi^a} A^a \right] \\ &= \frac{\partial \chi^b}{\partial \chi^{n'}} \frac{\partial}{\partial \chi^b} \left[\frac{\partial \chi^{m'}}{\partial \chi^a} A^a \right] \\ &= \frac{\partial \chi^{m'}}{\partial \chi^a} \frac{\partial \chi^b}{\partial \chi^{n'}} \frac{\partial A^a}{\partial \chi^b} + \frac{\partial \chi^b}{\partial \chi^{n'}} \frac{\partial^2 \chi^{m'}}{\partial \chi^b \partial \chi^a} A^a. \end{aligned}\right\} \tag{5.2}$$

Comparing (5.2) with (4.6 a) we see that $\frac{\partial A^m}{\partial \chi^n}$ would have been a tensor if the last term in (5.2) were absent. Because of its pre-

sence, $\dfrac{\partial A^m}{\partial \chi^n}$ is no longer a tensor. As in general relativity, we therefore introduce an 'affinity' Γ^m_{rn} such that, by definition,

$$A^m_{;\,n} = \frac{\partial A^m}{\partial \chi^n} + A^r \, \Gamma^m_{rn} \tag{5.3}$$

is a tensor. We call $A^m_{;\,n}$ the covariant derivative of A^m and denote it by a semi-colon. It is evident that Γ^m_{rn} cannot be a tensor. We shall find its transformation properties presently.

Since $A^m_{;\,n}$ is by definition a tensor, we have, on using (4.6 a),

$$A^{m\,\prime}_{;\,n'} = \frac{\partial \chi^{m'}}{\partial \chi^a} \frac{\partial \chi^b}{\partial \chi^{n'}} A^a_{\;;\,b}.$$

When we substitute the definition (5.3) of $A^m_{;\,n}$ and express $A^{m'}$ in terms of A^r by using (4.3 a), we get

$$\Gamma^{m\,\prime}_{nr} = \frac{\partial \chi^{m'}}{\partial \chi^a} \frac{\partial \chi^b}{\partial \chi^{n'}} \frac{\partial \chi^c}{\partial \chi^{r'}} \Gamma^a_{bc} + \frac{\partial \chi^{m'}}{\partial \chi^a} \frac{\partial^2 \chi^a}{\partial \chi^{n'} \partial \chi^{r'}}. \tag{5.4}$$

This is precisely the transformation law for Γ^m_{nr} in general relativity. Note that, because of the second term in the right-hand side of (5.4), Γ^m_{nr} is not a tensor.

It is easy to see that, since the last term in (5.4) is symmetric in n and r, Γ^m_{nr} will remain symmetric in all coordinate frames if it is chosen symmetric in one. This, of course, does not *prove* that Γ^m_{nr} is symmetric. In this paper we shall take it to be symmetric for the sake of simplicity.

We have seen that the gradient of a scalar is a vector. We can therefore say that the covariant derivative of a scalar is the same as the ordinary derivative

$$\varphi_{\,;\,r} = \frac{\partial \varphi}{\partial \chi^r}. \tag{5.5}$$

Assume now that the usual product rule for differentiation holds also for covariant differentiation

$$(fg)_{;\,n} = f_{;\,n}\, g + f g_{;\,n} \tag{5.6}$$

so that, in particular,

$$(A^m B_m)_{;\,n} = A^m_{;\,n} B_m + A^m B_{m;\,n}. \tag{5.7}$$

Since $A^m B_m$ is a scalar, we get from (5.5)

$$(A^m B_m)_{;\,n} = \frac{\partial A^m}{\partial \chi^n} B_m + A^m \frac{\partial B^m}{\partial \chi^n}.$$

When we substitute this and (5.3) in (5.7), we find that

$$A_{m;\,n} = \frac{\partial B_m}{\partial \chi^n} - B_a \Gamma^a_{mn}. \tag{5.8}$$

This provides the rule for differentiation of covariant vectors.

The rules for differentiating conjugate vectors with regard to $\bar{\chi}^n$ are similar. One has there to use an affinity which is the complex conjugate of Γ^m_{nr}.

$$B^{\overline{m}}_{;\,\overline{n}} = \frac{\partial A^{\overline{m}}}{\partial \bar{\chi}^n} + A^{\overline{a}} \Gamma^{\overline{m}}_{\overline{a}\,\overline{n}} \tag{5.9}$$

$$B_{\overline{m};\,\overline{n}} = \frac{\partial B_{\overline{m}}}{\partial \bar{\chi}^n} - B_{\overline{a}} \Gamma^{\overline{a}}_{\overline{m}\,\overline{n}}, \tag{5.10}$$

where

$$\Gamma^{\overline{m}}_{\overline{r}\,\overline{n}} = \overline{\Gamma^m_{rn}}. \tag{5.11}$$

So far the discussion has been quite analogous to that of the usual tensor analysis. Let us now consider the differential coefficient of a conjugate vector with respect to χ^n. We have

$$\left.\begin{aligned} \frac{\partial A^{\overline{m}'}}{\partial \chi^{n'}} &= \frac{\partial}{\partial \chi^{n'}} \left[\frac{\partial \bar{\chi}^{m'}}{\partial \bar{\chi}^a} A^{\overline{a}} \right] \\ &= \frac{\partial \chi^b}{\partial \chi^{n'}} \frac{\partial}{\partial \chi^b} \left[\frac{\partial \bar{\chi}^{m'}}{\partial \bar{\chi}^a} A^{\overline{a}} \right] \\ &= \frac{\partial \chi^b}{\partial \chi^{n'}} \frac{\partial \bar{\chi}^{m'}}{\partial \bar{\chi}^a} \frac{\partial A^{\overline{a}}}{\partial \chi^b}. \end{aligned}\right\} \tag{5.12}$$

In getting the last step we have made use of the fact, stated in the equation (4.1), that $\bar{\chi}^{m'}$ does not depend on χ^a so that

$$\frac{\partial}{\partial \chi^b}\left[\frac{\partial \bar{\chi}^{m'}}{\partial \bar{\chi}^a}\right] = 0. \tag{5.13}$$

From (5.12) we see that $\dfrac{\partial A^{\overline{m}}}{\partial \chi^n}$ is a tensor and thus there is no need of introducing any affinity here. Alternatively, we can say that the covariant derivative of $A^{\overline{m}}$ with respect to χ^n is the same as the ordinary derivative

$$A^{\overline{m}}_{;\,n} = \frac{\partial A^{\overline{m}}}{\partial \chi^n}. \tag{5.14}$$

We summarize here the rules for covariant differentiation:

$$\left.\begin{aligned}
\varphi_{;\,n} &= \frac{\partial \varphi}{\partial \chi^n} & \varphi_{;\,\bar{n}} &= \frac{\partial \varphi}{\partial \bar{\chi}^n} \\
A^m_{;\,n} &= \frac{\partial A^m}{\partial \chi^n} + A^a \Gamma^m_{an} & A^m_{;\,\bar{n}} &= \frac{\partial A^m}{\partial \bar{\chi}^n} \\
A_{m;\,n} &= \frac{\partial A_m}{\partial \chi^n} - A_a \Gamma^a_{mn} & A_{m;\,\bar{n}} &= \frac{\partial A_m}{\partial \bar{\chi}^n} \\
A^{\overline{m}}_{;\,n} &= \frac{\partial A^{\overline{m}}}{\partial \chi^n} & A^{\overline{m}}_{;\,\bar{n}} &= \frac{\partial A^{\overline{m}}}{\partial \bar{\chi}^n} + A^{\bar{a}} \Gamma^{\overline{m}}_{\bar{a}n} \\
A_{\overline{m};\,n} &= \frac{\partial A_{\overline{m}}}{\partial \chi^n} & A_{\overline{m};\,\bar{n}} &= \frac{\partial A_{\overline{m}}}{\partial \bar{\chi}^n} - A_{\bar{a}} \Gamma^{\bar{a}}_{\overline{m}n} \\
& & \Gamma^{\overline{m}}_{\overline{n}\,r} &= \overline{\Gamma^m_{nr}}
\end{aligned}\right\} \tag{5.15}$$

The differentiation rules for tensors can be obtained from (5.15) and (5.6). A tensor like A_{mn} transforms like the product of two vectors B_m and C_n. Therefore its differentiation law ought to be the same as for the product $B_m C_n$. This gives

$$A_{mn;\,r} = \frac{\partial A_{mn}}{\partial \chi^r} - A_{an}\,\Gamma^a_{mr} - A_{ma}\,\Gamma^a_{nr}.$$

Similarly,

$$\left.\begin{aligned}
A^{mn}_{\;;r} &= \frac{\partial A^{mn}}{\partial \chi^r} + A^{an}\,\Gamma^m_{ar} + A^{ma}\,\Gamma^n_{ar} \\
A_{\overline{m}n;\,r} &= \frac{\partial A_{\overline{m}n}}{\partial \chi^r} - A_{\overline{m}a}\,\Gamma^a_{nr} \\
A^{\overline{m}}{}_{n;\,r} &= \frac{\partial A^{\overline{m}}_{n}}{\partial \chi^r} - A^{\overline{m}}{}_{a}\,\Gamma^a_{nr} \\
A^{\overline{m}n}_{\;;r} &= \frac{\partial A^{\overline{m}n}}{\partial \chi^r} + A^{\overline{m}a}\,\Gamma^n_{ar} \\
A_{\overline{m}}{}^{n}{}_{;\,r} &= \frac{\partial A^{n}_{\overline{m}}}{\partial \chi^r} + A_{\overline{m}}{}^{a}\,\Gamma^n_{ar}.
\end{aligned}\right\} \qquad (5.16)$$

The rules for differentiating with regard to $\bar{\chi}^r$ are quite similar. One can easily write down the differentiation rules for tensors of higher ranks.

6. Lowering and Raising of Suffixes; Relation between the Affinity and the Metric.

We use the metric $\eta_{\overline{m}n}$ to lower the indices of tensors in the following way:

$$A_n = A^{\overline{m}}\,\eta_{\overline{m}n} \qquad (6.1\,\text{a})$$

and

$$A_{\overline{m}} = \eta_{\overline{m}n}\,A^n. \qquad (6.1\,\text{b})$$

From (6.1 a) it follows that

$$A_{n;\,r}\,A^{\overline{m}}_{\;;r}\,\eta_{\overline{m}n} + A^{\overline{m}}\,\eta_{\overline{m}n;\,r}. \qquad (6.2)$$

We now assume that

$$\eta_{\overline{m}n;\,\mathrm{r}} = 0\,. \qquad (6.3)$$

As one can see from (6.2), this enables us to perform the operation of lowering the suffixes inside the differentiation sign, viz.,

$$A_{n;\,r} = A^{\overline{m}}_{;\,r}\,\eta_{\overline{m}n}.$$

From (5.16) it follows that the equation (6.3) means

$$\frac{\partial \eta_{\overline{m}n}}{\partial \chi^r} - \eta_{\overline{m}a}\,\Gamma^a_{nr} = 0. \tag{6.4}$$

Let us now introduce the inverse of $\eta_{\overline{m}n}$. We denote it by $\eta^{m\overline{n}}$:

$$\eta_{\overline{m}a}\,\eta^{a\overline{n}} = I^{\overline{n}}_{\overline{m}} \tag{6.5 a}$$

$$\eta^{m\overline{a}}\,\eta_{\overline{a}n} = I^m_n, \tag{6.5 b}$$

where I is the unit matrix so that I^m_n equals 1 if $m = n$ and is zero otherwise. One can easily establish the tensor character of $\eta^{m\overline{n}}$ and of I^m_n. The matrix $\eta^{m\overline{n}}$ can be used to raise the suffixes of covariant vectors and tensors in a way analogous to (6.1 a, b).

If we multiply (6.4) by $\eta^{s\overline{m}}$, we get

$$\eta^{s\overline{m}}\,\frac{\partial \eta_{\overline{m}n}}{\partial \chi^r} - I^s_a\,\Gamma^a_{nr} = 0$$

or

$$\Gamma^s_{nr} = \eta^{s\overline{m}}\,\frac{\partial \eta_{\overline{m}n}}{\partial \chi^r}. \tag{6.6}$$

We have thus expressed the affinity in terms of the fundamental metric $\eta_{\overline{m}n}$. Note that the right-hand side of (6.6) is not, in general, symmetric in n and r. If we want Γ^s_{nr} to be symmetric, we must impose some restrictions on the metric; namely, the metric has to satisfy

$$\frac{\partial \eta_{\overline{m}n}}{\partial \chi^r} = \frac{\partial \eta_{\overline{m}r}}{\partial \chi^n}. \tag{6.7 a}$$

By taking the complex conjugate of (6.7 a) and using the fact that $\eta_{\overline{m}n}$ is a Hermitian matrix [see (4.8)], we also get

$$\frac{\partial \eta_{\overline{n}m}}{\partial \overline{\chi}^r} = \frac{\partial \eta_{\overline{r}m}}{\partial \overline{\chi}^n}. \tag{6.7 b}$$

The equations (6.7 a, b) show that we can write

$$\eta_{\overline{m}n} = \frac{\partial^2 \varphi}{\partial \overline{\chi}^m \, \partial \chi^n} \tag{6.8}$$

where φ is a real local scalar.

Taking the complex conjugate of (6.6) and using (5.11) and (4.8), we find

$$I^{\overline{s}}_{\overline{n}\,\overline{r}} = \frac{\partial \eta_{\overline{n}m}}{\partial \overline{\chi}^r} \, \eta_{m\overline{s}}. \tag{6.9}$$

7. Curvature Tensor.

The expression (6.6) looks very different from the usual expression for affinity in relativity theory. However, it will be shown that, by using a suitable notation, we can put it in a form similar to that in relativity theory.

Let us define

$$\overline{\chi^m} = \chi^{N+m}. \tag{7.1}$$

In general, let us write $N+m$ instead of $\overline{m}$ wherever the latter occurs. Thus, in our new notation,

$$\left.\begin{aligned} A^{\overline{m}} &= A^{N+m} \\ \text{and} \qquad \eta_{\overline{m}n} &= \eta_{(N+m)\,n}. \end{aligned}\right\} \tag{7.2}$$

We also define

$$\eta_{\mu\nu} = \left\{\begin{aligned} &\eta_{\overline{(\mu-N)}\nu} \text{ when } \mu > N,\ \nu \leq N \\ &0 \qquad\qquad \text{in all other cases} \end{aligned}\right\} \tag{7.3}$$

where, in this section, the Greek indices take the values $1,2 \ldots 2N$.

The invariant line element (3.4) becomes

$$\sum_{\mu,\nu} d\chi^\mu \, \eta_{\mu\nu} \, d\chi^\nu = dl^2 \tag{7.4}$$

which is similar to the expression (3.5) of the relativity theory. One can easily verify that the expressions (6.6) and (6.9) for the affinity can now be written together as

$$\left.\begin{aligned} \Gamma^{\mu}_{\nu\sigma} = \frac{1}{2}\,\eta^{\mu\alpha}\left[\frac{\partial \eta_{\alpha\nu}}{\partial \chi^{\sigma}} + \frac{\partial \eta_{\alpha\sigma}}{\partial \chi^{\nu}} - \frac{\partial \eta_{\nu\sigma}}{\partial \chi^{\alpha}}\right] \\ + \frac{1}{2}\left[\frac{\partial \eta_{\nu\alpha}}{\partial \chi^{\sigma}} + \frac{\partial \eta_{\sigma\alpha}}{\partial \chi^{\nu}} - \frac{\partial \eta_{\sigma\nu}}{\partial \chi^{\alpha}}\right]\eta^{\alpha\mu}. \end{aligned}\right\} \tag{7.5}$$

(7.5) is quite similar to the usual expression in real space. The inverse matrix $\eta^{\mu\nu}$ is here defined as

$$\eta^{\mu\nu} = \left\{\begin{array}{ll} \eta^{\mu\,\overline{(N-\nu)}} & \text{when } \mu \leq N,\ \nu > N \\ 0 & \text{in all other cases.} \end{array}\right\} \tag{7.6}$$

As in the tensor analysis of real space, the expression (7.5) gives rise to the curvature tensor

$$B^{\mu}{}_{\nu\varrho\sigma} = -\frac{\partial \Gamma^{\mu}_{\nu\varrho}}{\partial \chi^{\sigma}} + \frac{\partial \Gamma^{\mu}_{\nu\sigma}}{\partial \chi^{\varrho}} + \Gamma^{\mu}_{\alpha\varrho}\,\Gamma^{\alpha}_{\nu\sigma} - \Gamma^{\mu}_{\alpha\sigma}\,\Gamma^{\alpha}_{\nu\varrho}. \tag{7.7}$$

If we write (7.7) in our previous notation, using barred and unbarred suffixes, we find

$$\left.\begin{aligned} &B^{m}{}_{nrs} = 0, \quad B^{m}{}_{\bar{n}rs} = 0, \quad B^{m}{}_{n\bar{r}\bar{s}} = 0, \quad B^{m}{}_{\bar{n}\bar{r}s} = 0, \\ &B^{m}{}_{\bar{n}r\bar{s}} = 0, \quad B^{m}{}_{\bar{n}\bar{r}s} = 0; \end{aligned}\right\} \tag{7.8}$$

$$B^{m}{}_{nr\bar{s}} = -B^{m}{}_{n\bar{s}r} = -\frac{\partial \Gamma^{m}_{nr}}{\partial \bar{\chi}^{s}}. \tag{7.9}$$

The complex conjugates of (7.8) and (7.9) also hold.

Thus $B^{m}{}_{nr\bar{s}}$ is essentially the curvature tensor in this theory[1].

8. Condition for Flat Space.

One can easily show that the affinity can be made zero at any *one* given point, say at the origin, by a suitable choice of the coordinate system. In fact, not only the affinity Γ^{m}_{nr}, but also its

[1] I am thankful to Professor C. Møller for first pointing this out to me. The expression (7.9) can also be found directly from the previous formalism (without introducing the notations (7.1)–(7.3)) by extending the idea of parallel displacements to the complex space. (Private communication).

See appendix for the contracted forms of the curvature tensor.

gradient $\dfrac{\partial \Gamma^m_{nr}}{\partial \chi^s}$ can be made to vanish at any *one* point. This can be explicitly verified by carrying out the transformation

$$\chi^m = \chi^{m'} + \frac{1}{2}\alpha^m_{nr}\,\chi^{n'}\,\chi^{r'} + \frac{1}{6}\beta^m_{nrs}\,\chi^{n'}\,\chi^{r'}\,\chi^{s'}, \tag{8.1}$$

where

$$\alpha^m_{nr} = -(\Gamma^m_{nr})_0 \tag{8.2 a}$$

and

$$\left.\begin{aligned}\beta^m_{nrs} &= \left[\Gamma^m_{na}\,\Gamma^a_{sr} + \Gamma^m_{ar}\,\Gamma^a_{sn} - \frac{\partial \Gamma^m_{nr}}{\partial \chi^s}\right]_0 \\ &= \left[\Gamma^m_{as}\,\Gamma^a_{nr} + \Gamma^m_{an}\,\Gamma^a_{sr} + \Gamma^m_{ar}\,\Gamma^a_{sn} - \eta^{m\bar{a}}\frac{\partial^2 \eta_{\bar{a}n}}{\partial \chi^r\,\partial \chi^s}\right]_0 .\end{aligned}\right\} \tag{8.2 b}$$

Note that, due to the relation (6.7 a), the right-hand side in (8.2 b) is symmetric in n, r and s, as it should be because (8.1) shows that $B^m{}_{nrs}$ is symmetric in these suffixes.

However, the affinity and its gradient vanish at one point only; they do not vanish even at a neighbouring point unless the curvature tensor (7.9) vanishes. To see this, we have merely to expand Γ^m_{nr} in a Taylor series about the origin:

$$\left.\begin{aligned}\Gamma^m_{nr}(d\chi, d\bar{\chi}) &= (\Gamma^m_{nr})_0 + \left[\frac{\partial \Gamma^m_{nr}}{\partial \chi^s}\right] d\chi^s + \left[\frac{\partial \Gamma^m_{nr}}{\partial \bar{\chi}^s}\right]_0 d\bar{\chi}^s + \ldots \\ &= -\left[B^m{}_{nr\bar{s}}\right]_0 d\bar{\chi}^s + \ldots\end{aligned}\right\} \tag{8.3}$$

Hence, it is a necessary condition for the vanishing of the affinity that the curvature tensor must vanish:

$$B^m{}_{nr\bar{s}} = 0. \tag{8.4}$$

As the form (7.7) closely resembles the expression for the curvature tensor in real space, it is not difficult to see that (8.4) is also a sufficient condition for the vanishing of the affinity in some coordinate system.

From (6.6) and (6.9) we see that, if the affinity vanishes, $\eta_{\bar{m}n}$ are constants independent of χ, $\bar{\chi}$. In other words, the space is then flat and we can take, by correspondence with the usual quantum theory,

$$\eta_{\bar{m}n} = I_{\bar{m}n}, \tag{8.5}$$

where I is the unit matrix, i. e.,

$$I_{\bar{m}n} \begin{cases} 1 & \text{if} \quad m = n \\ 0 & \text{if} \quad m \neq n. \end{cases} \tag{8.6}$$

From the above discussion it follows that, if our theory is to be essentially different from the usual quantum theory, we must have a curvature tensor which is not zero.

9. Equations of Motion.

In general relativity theory, the equations of motion of a particle in a gravitational field can be obtained by the variation of the Lagrangian

$$\mathfrak{L} = \int \left[g_{\mu\nu} \frac{dx^\mu}{d\tau} \frac{dx^\nu}{d\tau} \right]^{1/2} d\tau$$

with respect to $x^\mu(\tau)$. We assume that we can obtain the equations of motion for $\chi(t)$ in our quantum theory by a similar variational principle. As the Lagrangian we take

$$\left.\begin{aligned} \mathfrak{L} &= \int_{t_0}^{t_1} L \, dt \\ L &= \left[\eta_{\bar{m}n}(\chi, \bar{\chi}) \frac{d\bar{\chi}^m}{dt} \frac{d\chi^n}{dt} \right]^{1/2} \end{aligned}\right\} \tag{9.1}$$

and make in χ and $\bar{\chi}$ independent variations that vanish at the end points t_0 and t_1.

In this way we easily obtain

$$\frac{D\psi^m}{dt} = 0 \tag{9.2 a}$$

and

$$\frac{D\bar{\psi}^m}{dt} = 0, \tag{9.2 b}$$

where

$$\left.\begin{aligned} \frac{D\psi^m}{dt} &= \psi^m_{;\,r}\,\frac{d\chi^r}{dt} + \psi^m_{;\,\overline{r}}\,\frac{d\overline{\chi}^r}{dt} \\ &= \left[\frac{\partial\psi^m}{\partial\chi^r} + \psi^a\,\Gamma^m_{ar}\right]\frac{d\chi^r}{dt} + \frac{\partial\psi^m}{\partial\overline{\chi}^r}\,\frac{d\overline{\chi}^r}{dt} \\ &\quad [\text{see (5.15)}] \\ &= \frac{d\psi^m}{dt} + \Gamma^m_{ab}\,\psi^a\,\psi^b, \end{aligned}\right\} \tag{9.3 a}$$

and similarly

$$\frac{D\overline{\psi}^m}{dt} = \frac{d\overline{\psi}^m}{dt} + \Gamma^{\overline{m}}_{\overline{a}\,\overline{b}}\,\overline{\psi}^a\,\overline{\psi}^b. \tag{9.3 b}$$

The equations (9.2 a, b) now replace the equations

$$\frac{d\varphi_m}{dt} = 0 \tag{9.4 a}$$

and

$$\frac{d\overline{\varphi}_m}{dt} = 0 \tag{9.4 b}$$

of the usual quantum theory in the Heisenberg representation. [To denote the states of the usual theory we have here used φ_m, $\overline{\varphi}_m$ to distinguish them from ψ, $\overline{\psi}$ of the present work.]

Besides (9.4 a, b), we have also equations for the dynamical variables, F:

$$\frac{dF_{mn}}{dt} = \frac{i}{\hbar}[H, F]_{mn}, \tag{9.5}$$

where the square bracket stands for the commutator. We replace these equations by the covariant ones

$$\frac{D\boldsymbol{F}^m{}_n}{dt} = \frac{i}{\hbar}[\boldsymbol{H}, \boldsymbol{F}]^m{}_n. \tag{9.6}$$

Here

$$\left.\begin{aligned} \frac{D\boldsymbol{F}^m{}_n}{dt} &= \boldsymbol{F}^m{}_{n;\,r}\frac{d\chi^r}{dt} + \boldsymbol{F}^m{}_{n;\,\bar{r}}\frac{d\bar{\chi}^r}{dt} \\ &= \left[\frac{\partial \boldsymbol{F}^m{}_n}{\partial \chi^r} + \boldsymbol{F}^a{}_n\,\Gamma^m_{ar} - \boldsymbol{F}^m{}_a\,\Gamma^a_{nr}\right]\frac{d\chi_r}{dt} + \frac{\partial \boldsymbol{F}^m{}_n}{\partial \bar{\chi}^r}\frac{d\bar{\chi}^r}{dt} \quad [\text{see (5.16)}] \\ &\quad - \frac{d\boldsymbol{F}^m{}_n}{dt} + [\Gamma^m_{ar}\boldsymbol{F}^a{}_n - \boldsymbol{F}^m{}_a\,\Gamma^a_{nr}]\,\psi^r . \end{aligned}\right\} \quad (9.7)$$

It will be shown below that the Hamiltonian $\boldsymbol{H}$ of the new theory is, in general, different from the Hamiltonian H of the old theory. This is the reason why the two Hamiltonians have been written in different ways in (9.5) and (9.6).

It may be remarked that, when the space is flat so that the affinity vanishes, the equations (9.2 a, b) and (9.6) of the new theory reduce to the equations (9.4 a, b) and (9.5) of the old theory.

10. Relation between the Old and the New Hamiltonians.

If we replace $\boldsymbol{F}$ by $\boldsymbol{H}$ in (9.6), we get

$$\frac{D\boldsymbol{H}^m{}_n}{dt} = 0 \quad (10.1)$$

or

$$\frac{d\boldsymbol{H}^m{}_n}{dt} = (\boldsymbol{H}^m{}_a\,\Gamma^a_{nr} - \Gamma^m_{ar}\,\boldsymbol{H}^a{}_n)\,\psi^r \quad (10.2)$$

[see (9.7)]

or

$$\boldsymbol{H}^m{}_n(t) = \boldsymbol{H}^m{}_n(0) + \int_0^t (\boldsymbol{H}^m{}_a\,\Gamma^a_{nr} - \Gamma^m_{ar}\,\boldsymbol{H}^a{}_n)\,\psi^r\,dt . \quad (10.3)$$

Let us understand by 0 the instant at which the geodesic coordinates are introduced such that

$$\Gamma^m_{nr}(0) = 0, \quad \frac{\partial \Gamma^m_{nr}}{\partial \chi^s}(0) = 0 \quad (10.4)$$

[see section 8]. At this instant the equations (9.6) and (9.2 a, b) of our theory go over into the equations (9.5) and (9.4 a, b) of the old theory. We can therefore put

$$\boldsymbol{H}^{m}{}_{n}\,(0) = H^{m}{}_{n}, \tag{10.5}$$

where $H^{m}{}_{n}$ is the old Hamiltonian. Then (10.3) becomes

$$\boldsymbol{H}^{m}{}_{n} = H^{m}{}_{n} + \int_{0}^{t} (H^{m}{}_{a}\, \Gamma^{a}_{nr} - \Gamma^{m}_{ar}\, \boldsymbol{H}^{a}{}_{n})\, \psi^{r}\, dt. \tag{10.6}$$

This shows that, as the affinity does not vanish everywhere on the track, the Hamiltonian $\boldsymbol{H}$ is, in general, different from the Hamiltonian H.

11. Expectation Values and Equivalence of the Old and the New Theories.

The expectation value of an observable $\boldsymbol{F}$ in this theory is given by

$$<\boldsymbol{F}> = \psi_{m}\, \boldsymbol{F}^{m}{}_{n}\, \psi^{n}. \tag{11.1}$$

We shall now show that this is the same as the expectation value

$$<F>_{u} = \bar{\varphi}_{m}\, F_{mn}\, \varphi_{n}, \tag{11.2}$$

where φ_{m} denotes the states of the usual theory [cf. (9.4 a, b), (9.5)] and the suffix 'u' denotes the 'usual' theory to distinguish (11.2) from (11.1). To show this, we first remark that, in general, the expectation values (11.1) and (11.2) depend on time. At the instant 0 at which we introduce the geodesic coordinates [cf. sections 9 and 10], we can take both of them to be equal:

$$<\boldsymbol{F}>(0) = <F>_{u}(0). \tag{11.3}$$

To get the expectation value at any later instant t, we make the Taylor expansion

$$\left.\begin{aligned} <\boldsymbol{F}>(t) &= <\boldsymbol{F}>(0) + t\left[\frac{d<\boldsymbol{F}>}{dt}\right]_{0} \\ &\quad + \frac{1}{2!}\, t^{2}\left[\frac{d^{2}<\boldsymbol{F}>}{dt^{2}}\right]_{0} + \cdots \\ &= \sum_{\nu=0}^{\infty} \frac{t^{\nu}}{\nu!}\left[\frac{d^{\nu}<\boldsymbol{F}>}{dt^{\nu}}\right]_{0}. \end{aligned}\right\} \tag{11.4}$$

Now

$$\frac{d<\boldsymbol{F}>}{dt} = \frac{D<\boldsymbol{F}>}{dt} \text{ [because } <\boldsymbol{F}> \text{ is a scalar]}$$

$$= \psi_m \frac{D\boldsymbol{F}^m{}_n}{dt} \psi^n \text{ [using (9.2 a, b)]}$$

$$= \frac{i}{\hbar} \psi_m [\boldsymbol{H}, \boldsymbol{F}]^m{}_n \psi^n \text{ [using (9.6)]}.$$

At the instant 0, all the variables of the new theory go over into those of the old theory, giving

$$\left[\frac{d<\boldsymbol{F}>}{dt}\right]_0 = \frac{i}{\hbar} \bar{\varphi}_m [H, F]_{mn} \varphi_n,$$

Similarly, one can easily see on using (9.2 a, b), (9.6), and (10.1), that

$$\left[\frac{d^\nu<\boldsymbol{F}>}{dt^\nu}\right]_0 = \left(\frac{i}{\hbar}\right)^\nu \bar{\varphi}_m [H, F]^{(\nu)}_{mn} \varphi_n, \tag{11.5}$$

where

$$[H, F]^{(\nu)} = \underbrace{[H, [H, \ldots\ldots [H, F]] \ldots]}_{\nu \text{ terms}}. \tag{11.6}$$

Thus (11.4) becomes

$$<\boldsymbol{F}>(t) = \sum_{\nu=0}^{\infty} \left(\frac{i}{\hbar}\right)^\nu \frac{t^\nu}{\nu!} \bar{\varphi}_m H, F]^{(\nu)}_{mn} \varphi_n. \tag{11.7}$$

This, however, is precisely the expression that one would obtain also from (11.2). Hence

$$<\boldsymbol{F}>(t) = <\boldsymbol{F}>_u(t).$$

Thus, the expectation values of all dynamical variables will be the same in the new theory as in the old[1]. Note that this result does not depend on the curvature tensor.

[1] I am thankful to Professor C. Møller for pointing out in a letter to me this equivalence of the old and the new theories.

12. Conclusion and Outlook.

We have tried to make a generalization of the Hilbert space by introducing the variables χ, $\overline{\chi}$, and admitting quite general transformations of these 'coordinates'. It was hoped that this might lead to a more general theory than the present quantum mechanics which allows only linear transformations of states. The result of the last section, however, shows that, irrespective of whether the space is curved or not, the physical results of the new theory will be the same as those obtained from the old theory. We therefore conclude that no essential generalization of quantum mechanics can be obtained, at least in the framework of the present formalism, by introducing a curved Hilbert space.

There are, however, a number of questions that need clarification and may provide further insight into the theory. The most important of them is whether we can assign any physical significance to the variables χ, $\overline{\chi}$. It would be interesting also to understand the significance of the relation (3.4) in which the arc-length in χ-space is identified with the physical time, t. Besides these questions of interpretation, there are also some mathematical points that need examination. In section 9, the equations (9.2 a, b) for the time-variation of the state vectors were derived by means of a variational principle, (9.1). However, the equation of motion, (9.6), for the dynamical variables was simply postulated as a generalization from the usual quantum theory. It would be of interest to investigate whether we can arrive at (9.6) also by means of a variational procedure. This equation is primarily responsible for the equivalence of physical results in the old and the new theories, and, therefore, an alteration here is likely to affect the conclusion that we have reached above. If, for example, there is a term containing the gradient of the Hamiltonian in (9.6), the latter will still be a possible generalization of (9.5), but the equivalence of the old and the new theories will no longer hold. Again, we have confined ourselves to the case of a symmetric affinity in this work. But, from section 6 it will be clear that a symmetric affinity does not appear to be the most natural thing to have in the complex space. It would therefore be worthwhile to investigate whether a non-symmetric affinity can lead to any new results. Finally, we have treated the case of a Hilbert

space of finite dimensions. In quantum mechanics, however, we have to work in an infinite dimensional space. A generalization of this work to the latter case will be of interest, at least to the mathematician, and perhaps also to the physicist.

Acknowledgments.

I am grateful to Professor C. MØLLER, Institute for Theoretical Physics, University of Copenhagen, for some very useful comments on this paper. I am also indebted to Professor M. A. PRESTON for extending to me hospitality at the McMaster University, and to the Canadian National Research Council for the award of a fellowship which enabled me to visit Canada.

Appendix.

Contracted Forms of the Curvature Tensor.

From the curvature tensor (7.9) we can, apparently, obtain two tensors of the second rank, viz.,

$$R_{\bar{s}r} \equiv B^{m}{}_{mr\bar{s}} \tag{A. 1}$$

and

$$S^{m}{}_{n} \equiv \eta^{r\bar{s}}\, B^{m}{}_{nr\bar{s}}. \tag{A. 2}$$

We here obtain explicit expressions for these tensors in terms of the metric η and show that they are essentially the same.

We first consider $R^{\bar{s}r}$.

From (6.5 b) we note that

$$\frac{\partial \eta^{m\bar{a}}}{\partial \bar{\chi}^{s}}\, \eta_{\bar{a}n} + \eta^{m\bar{a}}\, \frac{\partial \eta_{\bar{a}n}}{\partial \bar{\chi}^{s}} = 0$$

or

$$\frac{\partial \eta^{m\bar{r}}}{\partial \bar{\chi}^{s}} = -\eta^{n\bar{r}}\, \eta^{m\bar{a}}\, \frac{\partial \eta^{\bar{a}n}}{\partial \bar{\chi}^{s}}. \tag{A. 3}$$

Now

$$\left.\begin{aligned}
R_{\bar{s}r} &= -\frac{\partial \Gamma^{m}_{mr}}{\partial \bar{\chi}^{s}} \text{ [from (7.9) and (A. 1)]} \\
&= -\frac{\partial}{\partial \bar{\chi}^{s}}\left[\eta_{m\bar{a}}\, \frac{\partial \eta_{\bar{a}m}}{\partial \chi^{r}}\right] \text{ [using (6.6)]} \\
&= -\frac{\partial \eta^{m\bar{a}}}{d\bar{\chi}^{s}}\, \frac{\partial \eta_{\bar{a}m}}{\partial \chi^{r}} - \eta^{m\bar{a}}\, \frac{\partial^{2} \eta_{\bar{a}m}}{\partial \bar{\chi}^{s}\, \partial \chi^{r}} \\
&= \eta^{n\bar{a}}\, \eta^{m\bar{b}}\, \frac{\partial \eta_{\bar{b}n}}{\partial \bar{\chi}^{s}}\, \frac{\partial \eta_{\bar{a}m}}{\partial \chi^{r}} - \eta^{m\bar{a}}\, \frac{\partial^{2} \eta_{\bar{s}r}}{\partial \bar{\chi}^{a}\, \partial \chi^{m}} \\
&\quad \text{[using (A. 3) in the first (6.7 a, b) in the second]} \\
&= \eta^{n\bar{a}}\, \eta^{m\bar{b}}\, \frac{\partial \eta_{\bar{s}n}}{\partial \bar{\chi}^{b}}\, \frac{\partial \eta_{\bar{a}r}}{\partial \chi^{m}} - A\eta_{\bar{s}r},
\end{aligned}\right\} \tag{A. 3}$$

where

$$\Delta = \eta^{a\bar{b}} \frac{\partial^2}{\partial \bar{\chi}^b \partial \chi^a}. \tag{A.5}$$

We can also derive an alternative expression for $R_{\bar{s}r}$ if we use

$$\eta^{\bar{m}n} = \frac{M^{\bar{n}m}}{|\eta|}, \tag{A.6}$$

where $M^{\bar{n}m}$ is the cofactor of $\eta_{\bar{n}m}$ in the determinant $|\eta_{\bar{a}b}| = |\eta|$. We first note that

$$\left.\begin{aligned} \frac{\partial |\eta|}{\partial \chi^r} &= \frac{\partial |\eta|}{\partial \eta_{\bar{a}b}} \frac{\partial \eta_{\bar{a}b}}{\partial \chi^r} \\ &= M^{\bar{a}b} \frac{\partial \eta_{\bar{a}b}}{\partial \chi^r} \\ &= |\eta| \eta^{b\bar{a}} \frac{\partial \eta_{\bar{a}b}}{\partial \chi^r}. \end{aligned}\right\} \tag{A.7}$$

Now, from (6.6) we notice that

$$\eta^{b\bar{a}} \frac{\partial \eta_{\bar{a}b}}{\partial \chi^r} = \Gamma^a_{ar}.$$

Substituting this in (9.13) we find

$$\Gamma^a_{ar} = \frac{1}{|\eta|} \frac{\partial |\eta|}{\partial \chi^r} = \frac{\partial}{\partial \chi^r} [\log |\eta|]. \tag{A.8}$$

Hence

$$\left.\begin{aligned} R_{\bar{s}r} &= -\frac{\partial \Gamma^m_{mr}}{\partial \bar{\chi}^s} \\ &= -\frac{\partial^2}{\partial \chi^r \partial \bar{\chi}^s} [\log |\eta|]. \end{aligned}\right\} \tag{A.9}$$

If we contract (A.9) again, we get

$$R = \eta^{r\bar{s}} R_{\bar{s}r} = -\Delta [\log |\eta|]. \tag{A.10}$$

Let us now look at (A. 2). We get

$$\eta^{r\bar{s}} B^{m}_{nr\bar{s}} = -\eta^{r\bar{s}} \frac{\partial \Gamma^{m}_{nr}}{\partial \bar{\chi}}$$

$$= -\eta^{r\bar{s}} \frac{\partial}{\partial \bar{\chi}^{s}} \left[\eta^{m\bar{a}} \frac{\partial \eta_{\bar{a}n}}{\partial \chi^{r}} \right] \text{ [using (6.6)]}$$

$$= -\eta^{r\bar{s}} \left[\frac{\partial \eta^{m\bar{a}}}{\partial \bar{\chi}^{s}} \frac{\partial \eta_{\bar{a}n}}{\partial \chi^{r}} + \eta^{m\bar{a}} \frac{\partial^{2} \eta_{an}}{\partial \bar{\chi}^{s} \partial \chi^{r}} \right]$$

$$= -\eta^{r\bar{s}} \left[-\eta^{b\bar{a}} \eta^{m\bar{c}} \frac{\partial \eta_{\bar{c}b}}{\partial \bar{\chi}^{s}} \frac{\partial \eta_{\bar{a}n}}{\partial \chi^{r}} + \eta^{m\bar{a}} \frac{\partial^{2} \eta_{\bar{a}n}}{\partial \bar{\chi}^{s} \partial \chi^{r}} \right].$$

[using (A.3)]

Therefore

$$\eta_{\bar{k}m} \eta^{r\bar{s}} B^{m}_{nr\bar{s}} = -\eta^{r\bar{s}} \left[-\eta^{b\bar{a}} \frac{\partial \eta_{\bar{k}m}}{\partial \bar{\chi}^{s}} \frac{\partial \eta_{\bar{a}n}}{\partial \chi^{r}} + \frac{\partial^{2} \eta_{\bar{k}n}}{\partial \bar{\chi}^{s} \partial \chi^{r}} \right]$$

$$= \eta^{b\bar{a}} \eta^{r\bar{s}} \frac{\partial \eta_{\bar{k}b}}{\partial \bar{\chi}^{s}} \frac{\partial \eta_{\bar{a}n}}{\partial \chi^{r}} - \Delta \eta_{\bar{k}n}$$

which is precisely the expression (A.4) when we replace k by s and n by r and use suitable dummy indices. Thus

$$R_{\bar{s}r} = \eta_{\bar{s}m} S^{m}{}_{r}$$

and hence the curvature tensor $B^{m}_{nr\bar{s}}$ gives rise to only one tensor of the second rank.

Physics Department, McMaster University,
Hamilton, Ontario, Canada.

References.

HEISENBERG, W. (1953) Nachr. Göttinger Akad. Wiss., p. 111.
HEISENBERG, W. (1954) Z. Naturforschg. **9 a,** 292.
HEISENBERG, W., KORTEL F., and MITTER, H. (1955) Z. Naturforschg. **10 a,** 425.
SCHIFF, L. I. (1951 a) Phys. Rev. **84,** 1.
SCHIFF, L. I. (1951 b) Phys. Rev. **84,** 10.
SCHIFF, L. I. (1952) Phys. Rev. **86,** 856.
THIRRING, W. E. (1952) Z. Naturforschg. **7 a,** 63.

Indleveret til selskabet den 11. juli 1956.
Færdig fra trykkeriet den 6. november 1956.

Matematisk-fysiske Meddelelser
udgivet af
Det Kongelige Danske Videnskabernes Selskab
Bind **30,** no. 22

Mat. Fys. Medd. Dan. Vid. Selsk. **30,** no. 22 (1956)

VARIATION OF THE PARAMETERS OF ELECTROSTATIC INTERACTION F_k DERIVED FROM ABSORPTION SPECTRA OF LANTHANIDE COMPLEXES

BY

CHR. KLIXBÜLL JØRGENSEN

København 1956
i kommission hos Ejnar Munksgaard

Synopsis.

The narrow f^n-absorption bands of *Pr* (III), *Nd* (III), *Sm* (III), and *Gd* (III) are shown to be shifted $\sim 1\,\%$ towards lower wave numbers in anion complexes, compared to the aquo ions. This effect is interpreted as a decrease of the parameters F^k of electrostatic interaction between electrons in a partly filled shell. The ratios $F^2 : F^4$ and $F^4 : F^6$ are not freely adjustable, but slightly depend on the radial wave function. It is possible to extrapolate from the values of F^k to the average radius r_0 of the partly filled shell, which is somewhat smaller than the ionic radii of trivalent lanthanides. The decrease of F^k is shown to be caused by partly covalent bonding. The broad $4f \rightarrow 5d$ transitions of *Ce* (III), which occur at lower wave number in the aquo ion than in gaseous Ce^{+3} is further shifted in anion complexes where the crystal field also gives varying splittings of $5d$. A weak band of the *Ce* (III) aquo ion possibly originates from a rare geometrical configuration. The absorption spectra of $CeCl_3$ in C_2H_5OH and HCl are reported, and the complex equilibria discussed.

Printed in Denmark
Bianco Lunos Bogtrykkeri A-S

The absorption spectra of transition group complexes with partly filled d-shells can be described by crystal fields of different strength and symmetry, acting on the terms of the gaseous ion, known from atomic spectroscopy.[50] TANABE and SUGANO,[88] OWEN,[67] and ORGEL[66] introduced the idea that the term differences are smaller in complexes than in the gaseous ions. This is equivalent to a decrease of the parameters of electrostatic interaction F_k as defined by CONDON and SHORTLEY.[9] SCHÄFFER[77] and the present author[48, 50] found that F_k decreases more in anion complexes such as tris-oxalato or hexa-chloro complexes than in complexes with neutral ligands such as water and amines. Representative values of the decrease of F_k are 8—12 % in manganese (II), 15—30 % in nickel (II), 20—50 % in chromium (III), and even more in cobalt (III) and rhodium (III) complexes. There is a rough correlation between the decrease of F_k and the crystal field strength $(E_1 - E_2)$ in octahedral complexes,[49] —about 2 % for each 1000 K.* The present paper is a report on investigations into the much smaller decrease of F_k in complexes with partly filled f-shells and the behaviour of $[Xe]\, 4f \rightarrow [Xe]\, 5d$ transitions in cerium (III) complexes. Absorption spectra of complexes in solution at room temperature are measured.

Praseodymium (III) Complexes.

The four visible band groups[32] of Pr (III) are caused by transitions from $^3H_4$ to $^1D_2$, $^3P_0$, $^3P_1$, and $^3P_2$, respectively. The first group is rather broad in solution, while the three other groups in the blue are each represented by a single maximum of the

* The unit of wave number cm^{-1} will be called K (= Kayser) in this paper in accordance with the proposal made by the Joint Committee for Spectroscopy, 1952.

TABLE 1: The shift of absorption bands of Praseodymium (III) complexes.

Excited level:	$^3P_0$		$^3P_1$		$^3P_2$		Average shift	Ref. no.
Aquo ion	4822 Å	20740 K	4675 Å	21390 K	4430 Å	22570 K	0.0 %	
Acetate	4830	— 35	4695	— 90	4446	— 80	0.3	
Ethylenediaminetetraacetate	4878	— 240	4730	— 250	4478	— 245	1.2	
Nitrogentriacetate	4855	— 145	4720	— 205	4455	— 130		
	(4895)	— 310	(4770)	— 430	(4510)	— 410	1.2	
Tartrate	4854	— 140	4724	— 220	4463	— 170	0.8	
Citrate	4830	— 35	(4648)	+ 120	(4410)	+ 100		
	4861	— 170	4712	— 170	4475	— 230	1.1	
	4890	— 290	4732	— 260				
Pr^{+++} in 10 M HCl	4835	— 55	4687	— 55	4444	— 70	0.3	
PrF_3	4803	+ 80	4680	— 20	4425	+ 25	0.1	13
$PrCl_3$	4898	— 315	4755	— 360	4503	— 370	1.6	13
$PrBr_3$	4930	— 450	4788	— 510	4532	— 510	2.2	13
PrJ_3	4959	— 570	4821	— 650	4565	— 680	2.9	13
$PrCl_3$, 7 H_2O	4828	— 25	4727	— 240	4462	— 160	0.4	13
$PrCl_3$, 8 NH_3	4867	— 190	4732	— 260	4480	— 250	1.1	12
$PrBr_3$, 6 H_2O	4845	— 95	4718	— 195	4462	— 160	0.3	13
PrJ_3, 6 H_2O	4855	— 140	4737	— 280	4484	— 270	1.1	13
PrJ_3, 9 H_2O	4845	— 95	4708	— 150	4452	— 110	0.5	13
$Pr_2(CO_3)_3$	4840	— 75	4720	— 200	4445	— 75	0.6	14
$Pr(NO_3)_3$, 6 H_2O	4841	— 80	4705	— 135	4445	— 75	0.4	14
$(NH_4)_2Pr(NO_3)_5$, 4 H_2O	4810	+ 50	4640	+ 160	4390	+ 205	— 0.6	14
$Pr(OH)_3$	4849	— 110	4749	— 340	4460	— 150	1.0	14
	4882	— 250						
Pr_2O_3, ignited 550° C	4960	— 570	4850	— 770	4585	— 670	3.1	15
Pr_2O_3, ignited 900° C	5120	— 1300	4948	— 1170	4790	— 1220	5.7	15
$Pr(JO_3)_3$, 4 H_2O	4847	— 110	4720	— 200	4475	— 230	0.9	16
$Pr\ aca_3$	4850	— 120	4737	— 280	4450	— 100	0.8	16

aquo ion. These bands are shifted $\sim 1\ ^0/_0$ towards lower wave numbers in the anion complexes in solution as seen from Table 1. The absorption bands of the nitrogentriacetate and citrate complexes are split into several components (but it is not certain that

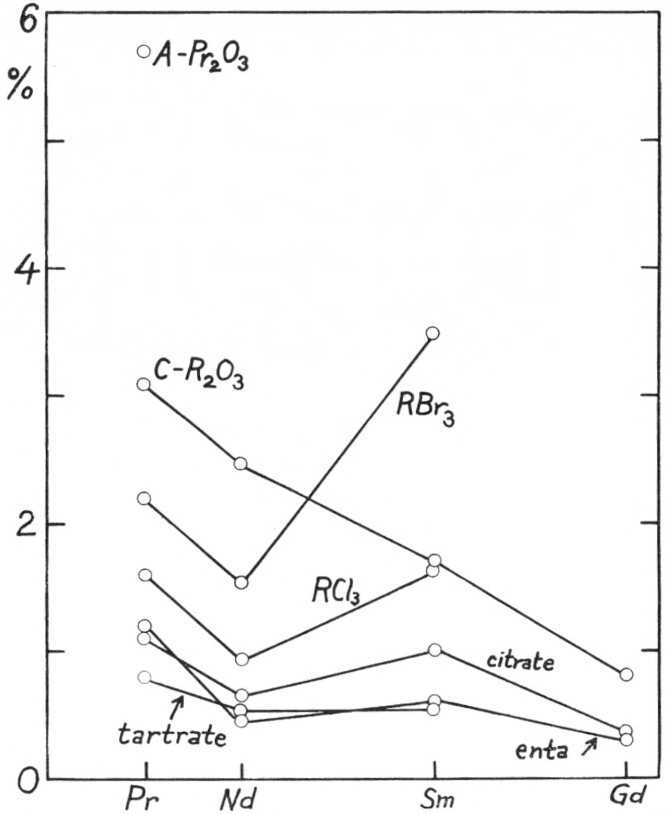

Figure 1. Decrease of the term distances in lanthanide complexes, relative to the aquo ions. The percentage decrease is given as a function of the atomic number for A-Pr_2O_3, the C-oxides, anhydrous bromides and chlorides, and the solutions of citrates, tartrates, and ethylenediaminetetraacetates studied here.

these spectra correspond to a single complex, with a definite geometrical configuration, even though the spectra are independent of the concentration of the ligand, when it is present in a large excess). However, average shifts $\sim 1\ ^0/_0$ can also be estimated in these complexes. BIRMINGHAM and WILKINSON[4] found a larger shift, $\sim 3\ ^0/_0$, relative to the aquo ion in the strongly split band groups of praseodymium (III) tris (cyclopentadienide). Figure 1 illustrates the relative decrease of this red shift of the

absorption bands of several compounds with increasing atomic number in the series *Pr*(III), *Nd*(III), *Sm*(III), and *Gd*(III). EPHRAIM and BLOCH[12–15] studied the absorption spectra of solid praseodymium (III) salts and found in the anhydrous halides a red shift, amounting to $\sim 2\ ^0/_0$ of the wave number, while the solid hydrates and ammoniacates exhibited much smaller red shifts. In only one case, the ammonium double nitrate, the shift was found towards higher wave numbers (and the percentage is then reckoned as negative in Table 1). Most other praseodymium (III) salts with oxy-anions exhibit moderate shifts towards the red. An extreme case is represented by Pr_2O_3, where the shift can exceed $5\ ^0/_0$. BOULANGER[7] later studied *Pr*(III) and found a similar large shift in some forms of $Pr_2(MoO_4)_3$. The existence of more crystal forms of Pr_2O_3 (*A*-type stable at high temperatures, *C*-type at low) was established by GOLDSCHMIDT.[26] Since the local environment of oxygen atoms around a praseodymium (III) ion in *C*-Pr_2O_3 consists of two types of defect cubes[97] (two of the eight places are empty) and in *A*-Pr_2O_3 consists of seven irregularly arranged oxygen atoms,[97] the low co-ordination numbers 6 and 7 can be said empirically to produce decreased term differences, relative to the ordinary 9-co-ordinated lanthanide complexes.[34,36,68] As discussed by ZACHARIASEN,[81] the ionic distances increase by 0.11 Å for the co-ordination number $N = 9$ and by 0.19 Å for $N = 12$, as compared with cations with $N = 6$. The values given by ZACHARIASEN for the ionic radii of 6-co-ordinated lanthanides (see Table 8) perhaps deviate from those given by GOLDSCHMIDT due to this effect.

EPHRAIM explained the shift in wave number as a contraction of the lanthanide ion, when influenced by many ligand atoms, as found in solvates and in solution. In partly covalent compounds, such as Pr_2O_3, PrJ_3, $PrBr_3$, and $PrCl_3$, the $4f$-shell was assumed to have a larger radius, corresponding to lower wave numbers. It is interesting that the acetylacetonate $Pr\ aca_3$ is not very covalent according to this criterion (Table 1). As discussed below, Ephraim's hypothesis is qualitatively correct, if restricted to the dilatation in covalent compounds. The high wave numbers found of the absorption bands of aquo ions and double nitrates do not in the author's opinion depict an active

influence of the environment; rather the conditions of the free, gaseous ion with the highest wave numbers are approached.

Even before the crystal field theory of BETHE,[30] BRUNETTI[8] assumed the observed band shifts of praseodymium(III) salts to be due to the strong intermolecular electrostatic fields. However, while the sub-levels of each level have different energy caused by this Stark-effect, the levels can only be moved by variation of the central field, as shown below from the theory of perturbations.

The shifts found at room temperature are composed of changes in the energy differences between the levels $^{2S+1}L_J$ and changes of the sub-levels of the excited levels and the ground level, due to the influence of crystal fields. The sub-levels of a given level are usually distributed over a range $\sim 200\ K$. The absorption spectra of solids cooled to low temperatures (e. g. in liquid helium) are caused by transitions from the lowest sub-level of the ground-level, since other sub-levels are not sufficiently populated in the Boltzmann distributions. Even though the lowest sub-level was situated some $50\ K$ lower in the anion complexes relative to the aquo ion, it could not explain the observed red shifts between 100 and 1000 K.

Neodymium (III) Complexes.

The excited level $^2P_{1/2}$, which cannot split into sub-levels due to the Kramers degeneracy, corresponds to a very narrow band in $Nd(\mathrm{III}) \sim 23400\ K$[44]. The shift observed of this band is given in Table 2a, while the shift of some other band groups are shown for a few anion complexes in Table 2b. The results are scattered around 1 % shift and seem to be smaller than in the corresponding praseodymium(III) complexes (cf. Fig. 1).

LIVELING[55] discovered that the absorption bands of $NdCl_3$ and $Nd(NO_3)_3$ are shifted towards lower wave numbers for organic solvents than for aqueous solutions. JONES et al.[39, 40, 41] thoroughly investigated these effects and especially the intermediate spectra of solutions with a few volume % water. The exchange process of water, alcohols, and anions will be discussed below in a separate section. SCHÄFFER[78] and UZUMASA[91, 92] also studied

TABLE 2 a. The shift of absorption bands of Neodymium (III) complexes.

a: The excited level	$^2P_{1/2}$		Shift	Ref. no.
Aquo ion	4273 Å	23400 K	0.00 %	
Ethylenediaminetetraacetate	4292	— 105	0.44	
Nitrogentriacetate	4293	— 110	0.47	
Tartrate	4296	— 125	0.54	
Citrate	4301	— 150	0.65	
Nd^{+++} in 12 M HCl	4330	— 310	1.33	82
	4297	— 130	0.56	
	4271	+ 10	— 0.05	
	4328	— 285	1.24	
	4291	— 100	0.41	
	4272	+ 5	— 0.02	
$NdCl_3$ in CH_3OH	4295	— 120	0.52	6,39
$Nd(NO_3)_3$ in CH_3OH	4280	— 40	0.16	39
3 M $Nd(NO_3)_3$ in H_2O	4280	— 40	0.16	41,82
Didymium glass	4312	— 210	0.94	
$Nd\ aca_3$, anhydrous	4305	— 170	0.75	21
$Nd\ aca_3$, $2H_2O$	4301	— 150	0.65	21
$Nd\ aca_3$ in C_6H_6, CCl_4, CS_2, or C_2H_5J	4310	— 200	0.87	73
	4303	— 160	0.70	
	4297	— 130	0.56	
$Nd\ aca_3$ in CH_3OH	4302	— 160	0.68	73
$Nd(BrO_3)_3$, 9 H_2O	4273.8	— 5	0.02	11
$Nd(C_2H_5SO_4)_3$, 9 H_2O	4279.7	— 36	0.14	11
$NdCl_3$, 6 H_2O (in La-salt)	4283.6	— 58	0.23	11
NdF_3	4265	+ 45	— 0.11	17
$NdCl_3$	4313	— 215	0.94	17
$NdBr_3$	4334	— 330	1.53	17
$Nd_2(C_2O_4)_3$, 10 H_2O	4299	— 140	0.61	17
$(NH_4)_2\ Nd(NO_3)_5$, 4 H_2O	4261	+ 65	— 0.28	17
Nd_2O_3	4378	— 560	2.46	17,96

this phenomenon and HARTMANN and LORENZ[28] $NdCl_3$ in mixtures of water and formamide.

The acetylacetonate $Nd\ aca_3$ has been studied in a solid state[21] and in many different solvents.[73] Since the dihydrate is rather stable,[21] and since $Nd\ aca_3$ seems* to dimerize[38] in CCl_4 and CS_2,

* Note added in Proof: However, MOELLER and ULRICH[61a] detected no dimerization by cryoscopy. These authors compare the solvent effects on acetylacetonates thoroughly and find much higher intensity of some bands of $Nd\ aca_3$, $Ho\ aca_3$, and $Er\ aca_3$ than of the corresponding aquo ion bands, while other bands of these complexes, and all bands of $Pr\ aca_3$, do not exhibit increazed intensities.

TABLE 2 b. The shift of absorption bands of Neodymium (III) complexes.

The excited levels:	Aquo ion		Ethylenediamine-tetraacetate		Nitrogentriacetate		Tartrate		Citrate	
Two sub-levels of $^4F_{7/2}$	7422 Å	13470 K	7470 Å	— 85 K			7450 Å	— 50 K	7475 Å	— 95
	7340	13620	7370	— 55			7370	— 55	7385	— 85
Sub-levels of $^4G_{9/2}$ (?)	5220	19160	5265	— 170	5260 Å	— 140 K	5252	— 130	5255	— 135
	5215	19180	5250	— 120	5250	— 120				
	5125	19510	5145	— 125	5160	— 130	5130	— 70	5135	— 90
	5100	19610			5130	— 110				
Three levels of ^4D ...	3539	28260	3576	— 295	3568	— 230	3569	— 240	3576	— 295
			3551	— 95						
	3507	28530	3536	— 235	3533	— 210	3539	— 255	3531	— 190
	3468	28830	3496	— 235	3493	— 210	3496	— 235	3501	— 280
Average shift.....		0.0 %		0.7 %		0.7 %		0.7 %		0.8 %

there seems to be a considerable rest affinity in the 6-co-ordinated *Nd aca*$_3$.

Recently, ethylenediaminetetraacetate and nitrogentriacetate have been discussed by MOELLER and BRANTLEY[60] and VICKERY[94] as a mean for splitting of the absorption bands of lanthanides. The low symmetry of the crystal field produces $2J + 1$ distinct sub-levels from each level in the case of an even number of $4f$-electrons and $J + \frac{1}{2}$ sub-levels for an odd number of $4f$-electrons. However, in many cases, such as *Pr enta*$^-$ and *Gd enta*$^-$ studied here, the absorption bands are not conspicuously more split than for the aquo ions. Actually, the red shift is the most prominent difference between the spectra of *Nd*(III) anion complexes (such as $Nd(SO_3)_3^{---}$) and the aquo ion.[95]

If δ denotes the distance from a maximum with the molar extinction coefficient ε_n to the wave number σ, where $\varepsilon = \frac{\varepsilon_n}{2}$, δ is only 16 K for the $^2P_{1/2}$ of the neodymium(III) aquo ion, exemplifying the sharpness of transitions between two single sub-levels (cf. Fig. 4). The somewhat broader band at 23090 K cannot be re-found in the other complexes and is perhaps caused by an excited sub-level at 320 K over the ground-level.

SATTEN[75] found the five sub-levels of the ground-level $^4I_{9/2}$ at 0,115,184,363, and 384 K in $Nd(BrO_3)_3$, $9H_2O$, while SATTEN and YOUNG[76] found the sub-levels at 0,76,226,263, and 301 K in $Nd_2(SO_4)_3$, $8H_2O$.

Samarium (III) Complexes.

Only the band slightly below 25000 K has been measured here. It is presumably[44] due to a transition from $^6H_{5/2}$ to a level of ^6P. In the aquo ion, the band is symmetrical with $\delta = 100$ K, while it develops a shoulder towards the red in some of the anion complexes. The shifts are somewhat smaller than found for the soluble complexes of *Nd*(III), while the anhydrous solid compounds[17] such as $SmCl_3$ and $SmBr_3$ exhibit a rather large shift towards lower wave numbers (cf. Fig. 1).

TABLE 3. The shift of an absorption band of Samarium (III) complexes.

				Shift	Ref.
Aquo ion	4012 Å	24920 K		0.0 %	
Ethylenediaminetetra-acetate	4036	24780	— 140 K	0.6	
	(4060)	24630	— 290		
Nitrogentriacetate	4036	24780	— 140	0.6	
Tartrate	4034	24790	— 130	0.55	
Citrate	4051	24690	— 230	1.0	
Sm^{+++} in 12 M HCl	4017	24890	— 30	0.1	
$SmCl_3$	4080	24510	— 410	1.7	17
$SmCl_3$, 8 NH_3	4037	24770	— 150	0.6	17
$SmBr_3$	4156	24050	— 870	3.5	17
Sm_2O_3	4082	24500	— 420	1.7	17

Gadolinium (III) Complexes.

The Gd(III) aquo ion exhibits a rather complicated spectrum in the ultraviolet[61, 87] consisting of bands with $\delta \sim 10$—15 K. The band groups are assumed[44] to have the multiplets ^6P and ^6I as the excited levels. The spin-forbidden character of the transition from $^8S_{7/2}$ is not evident in the four intense bands. As appears from Table 4 and Figure 2, these bands are regularly shifted in the ethylenediaminetetraacetate and citrate, while the fine structure is somewhat blurred out. NUTTING and SPEDDING[64] investigated many solid gadolinium(III) salts and found a series of increasing wave numbers of the band groups:

$$Gd(C_2H_5COO)_3, 3H_2O < GdCl_3, 6H_2O < Gd_2(SO_4)_3,$$
$$8H_2O < Gd(C_2H_5SO_4)_3, 9H_2O.$$

BERTON and BOULANGER[3] found the band groups of Gd_2O_3 shifted much more (0.8 %) towards lower wave numbers than the other anion complexes ($\sim$ 0.3 %) as seen from Table 4 and Fig. 1. Thus, the general trend of strongest red shift of the oxides is common to all the lighter lanthanides.

Erbium (III) Complexes.

SELWOOD[82] found that for strong nitrate solutions, the bands of Nd(III) are shifted towards lower wave numbers, but of Ho(III) and Er(III) towards higher wave numbers. Thus, the

TABLE 4. The shift of absorption bands of Gadolinium (III) complexes.

Group no.	Aquo ion		Ethylenediaminetetraacetate			Citrate			Gd_2O_3 (ref. 3)		
					Shift			Shift			Shift
1.....	3118 Å	32030 K	—	—	—	3130 Å	31950 K	— 80 K	3140 Å	31850 K	— 180 K
2.....	3060	32680	—	—	—	—	—	—	3082	32450	— 230
3.....	2792	35820	2800 Å	35710 K	— 110 K	2804	35660	— 160	—	—	—
	2789	35860	2798	35740	— 120	2799	35730	— 130	—	—	—
4.....	2765	36170	2772	36070	— 100	2777	36010	— 150	2789	35850	— 320
	2760	36230	2767	36140	— 100	2769	36120	— 110	2784	35920	— 320
	2759	36240				2766	36150	— 120			
	2757	36270									
5.....	2744	36450	2751	36350	— 120	2756	36280	— 170	2769	36110	— 370
	2740	36500				2750	36360	— 140			
6.....	2735	36560	2740	36500	— 100	2742	36470	— 90	2759	36240	— 320
	(2734)	36580				2740	36500	— 100	2755	36300	— 300
	2732	36600				2737	36550	— 90	2751	36350	— 290
	(2729)	36640									
7.....	2522	39650	2530	39530	— 120	2532	39500	— 150	—	—	—
8.....	2461	40630	(2470)	40490	— 140	—	—	—	—	—	—
Average shift....		0.00 %			0.30 %			0.36 %			0.8 %

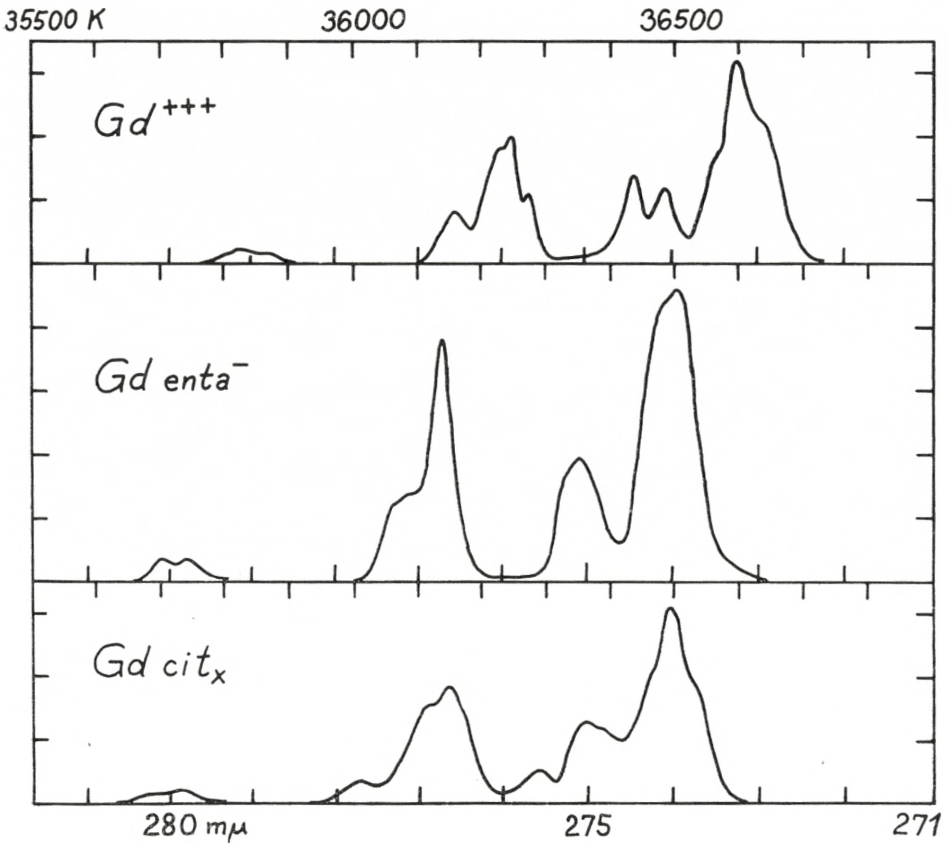

Figure 2. The absorption spectra of Gadolinium (III) complexes. The aquo ion, the ethylenediaminetetraacetate and the citrate are measured as described in the experimental section. The unit of the molar extinction coefficient scale is 1.

decreasing red shift in anion complexes with increasing atomic number seems to be reversed in this case. EPHRAIM, JANTSCH, and ZAPATA[18] still observed a small red shift in the anhydrous halides of holmium (III) and erbium (III). VICKERY[94] did not detect any systematic trend in the wave numbers of *Er enta*$^-$ and $Er(H_2O)_N^{+++}$. Table 5 gives some of the strongest bands of these two complexes. BIRMINGHAM and WILKINSON[4] did not observe a shift in erbium (III) tris(cyclopentadienide) either.

A similar result is found by HELLWEGE et al.[31,33] for $EuCl_3$, $6\,H_2O$ and $Eu_2Zn_3(NO_3)_{12}$, $24\,H_2O$, where the centres of gravity of $^5D_0$, $^5D_1$, and $^5D_2$ only deviate 0.012, 0.014, and 0.017 % respectively.

TABLE 5. The strongest absorption bands of Erbium (III) complexes.

Group no.	Aquo ion		Ethylenediaminetetraacetate	
1.....	6650 Å	15040 K	6560 Å	15240 K
	6520	15340	6540	15290
			6505	15370
2.....	5230	19120	5210	19190
	(5210)	19190	5195	19250
			5185	19290
3.....	4915	20350	4885	20470
	4875	20510		
	(4855)	20600		
4.....	4535	22050	4505	22200
	4500	22220		
5.....	4070	24570	4075	24540
	4055	24660	4055	24660
6.....	3795	26350	(3804)	26290
			3788	26400
			3780	26460
			3776	26480
7.....	3645	27440	3664	27290
	(3640)	27470	3653	27380
			3607	27720

Ytterbium (III) Complexes.

Since there is only one hole in the $4f$-shell, only one term exists of $[Xe]4f^{13}$, and the parameters of electrostatic interaction F_k cannot be determined. The band group[60] with maxima at 10,250 K ($\varepsilon = 1.7$) and 10,620 K ($\varepsilon = 0.6$) of the aquo ion is therefore caused by the spin-reversing transition $^2F_{7/2} \rightarrow {}^2F_{5/2}$. The ethylenediaminetetraacetate is not very different with maxima at 10,220 K ($\varepsilon = 1.8$) and 10,640 K ($\varepsilon = 0.9$). All four bands have $\delta = 150$ K.

FREED and MESIROW[20] reported broad bands of Yb(III) in the ultraviolet. Even though the bands were weaker than those of Ce(III), they were believed to be $[Xe]\,4f^{13} \rightarrow [Xe]\,4f^{12}\,5d$ transitions. However, the solution of ytterbium(III) perchlorate measured here does not show any sign of these bands, and ε is below 0.1 in the range 25,000—40,000 K. Probably, traces of

iron (III) or organic materials are responsible for the frequent observation of broad ultraviolet absorption bands of lanthanides with higher atomic number than cerium.

Actinide Complexes.

The anion effect seems to be somewhat larger and more varying in the actinides than in the lanthanides. The present author[43] reported the bands of the uranium (IV) tetraoxalate ion with $\sim 2\,\%$ lower wave numbers than of the aquo ion. Similar results have been obtained from the solutions in strong hydrochloric acid, while the effect is negligible in the ethylenediaminetetraacetate. The spreading of the sub-levels of U (IV) is rather large as evident from GRUEN's study of fluorides.[27] In the chloride and nitrate complexes of plutonium (III) and plutonium (IV), the bands are shifted towards higher wave numbers.[81] In a note in Acta Chem. Scand., it will be discussed, how the absorption spectrum of grey U (III) in $HClO_4$ or 2–6 $MHCl$ is changed in 11 $MHCl$, corresponding to the dark red colour.[44]

Cerium (III) Complexes.

FREED[19] discovered three high and broad bands of Ce (III) in the ultraviolet, which by cooling of $Ce(C_2H_5SO_4)_3$, $9\,H_2O$ from $300^0\,K$ to $20^0\,K$ were shifted only $400\,K$ towards higher wave numbers. Besides these bands, $CeCl_3$, $6H_2O$ was found to exhibit a weak band at 33,100 K at room temperature only.

LANG[54] found the energy levels of gaseous Ce^{+++}:

$$\begin{aligned}
[Xe]\,4f\text{:}\ & {}^2F_{5/2} && 0\ K\\
& {}^2F_{7/2} && 2253\\
[Xe]\,5d\text{:}\ & {}^2D_{3/2} && 49737\\
& {}^2D_{5/2} && 52226\\
[Xe]\,6s\text{:}\ & {}^2S_{1/2} && 86602.
\end{aligned}$$

The internal ^2F-transition has not yet been identified in cerium (III) complexes, even though the reflection spectrum of an anhydrous compound such as CeF_3 probably would show it. KRÖYER and BAKKER[53] estimate the splitting of the doublet as 1900 K from the emission spectrum of fluorescent cerium (III) compounds.

The strong bands have as excited levels the term ^2D, split by the crystal field. Due to KRAMERS' degeneracy, no more than five levels are possible for any symmetry of the complex. Five bands are known of the aquo ion, according to STEWART[87] and HEIDT and BERESTECKI[29] (see Table 6 and Fig. 3). It is evident that the centre of gravity of these levels are situated some thousand K below 51,230 K from the gaseous ion.

Table 6 demonstrates that the anion effect in Ce(III) complexes is composed of two phenomena: the average distance between the electron configurations $[Xe]\,4f$ and $[Xe]\,5d$ is decreased, and the crystal field splitting of $[Xe]\,5d$ is changed with resulting variation of the relative positions of the strong absorption bands.

The two strongest absorption bands of the cerium(III) aquo ion are shifted $\sim$ 4000 K towards lower wave numbers in the case of ethylenediaminetetraacetate, nitrogentriacetate, and acetate complexes (Table 6). Thus, in the latter complexes, the distance between the electron configurations $[Xe]\,4f$ and $[Xe]\,5d$ is roughly 72 % of the distance in the gaseous ion, while in the aquo ion the value is 83.5 %, if the band at 39,500 K is assumed to be doubly degenerate, and the small band at 33,700 K is not reckoned, as rationalized below.

FRIED and HINDMAN[22] found a close analogy between the absorption spectra of protactinium(IV) and cerium(III), implying the ground state $[Em]\,5f$ of the former ion. Thus, the two aquo ions have probably the same co-ordination number, 8 or 9. There does not seem to be a small band of Pa(IV) at a lower wave number than the strong bands, which are situated[22] at 36,300 K, 39,200 K, and 44,800 K with $\varepsilon_n \sim$ 1500, 1000, and 400, respectively. Thus, the spreading of the three bands in Pa(IV) is 8600 K, while the analogous distance in Ce(III) is 5600 K. This increase in the crystal field strength, amounting to 54 % from $5d$- to $6d$-electrons, can be compared with the crystal field strength, denoted by $(E_1 - E_2)$ in octahedral d^n-complexes, which have the ratios 1.00:1.45:1.75 for $3d$-, $4d$-, and $5d$-electrons, respectively.[47,50] The absolute value of the crystal field splitting of $[Xe]\,5d$ in Ce(III) and of $[Em]\,6d$ in Pa(IV) is rather low, as compared with $(E_1 - E_2) \sim$ 20,000 K of titanium(III) and other trivalent hexaaquo ions. The small values found for cerium(III) may be explained by three causes: the symmetry

TABLE 6. The shift of absorption bands of Cerium (III) complexes. Wave length λ_n, wave number σ_n, and molar extinction coefficient ε_n of the band maxima.

	λ_1	σ_1	ε_1	λ_2	σ_2	ε_2	λ_3	σ_3	ε_3	λ_4	σ_4	ε_4	λ_5	σ_5	ε_5
Aquo ion*	2970 Å	32700 K	16	2525 Å	39600 K	710	2395 Å	41700 K	600	2215 Å	45100 K	380	2110 Å	47400 K	270
$CeCl_3$ in 6 M HCl	3005	33300	32	2525	39600	680	2405	41600	560	2225	44900	380			
$CeCl_3$ in 12 M HCl	3090	32400	430	2555	39100	570	(2445)	40900	—						
$CeCl_3$ in conc. HCl, ref. 10	3100	32300	—	2585	38700	—	2480	40300	—	2415	41400	—			
$CeCl_3$ in C_2H_5OH:															
C_{Ce} C_{H_2O}															
0.0004 M 0.3 M	3090	32400	700	2505	39900	580									
0.0004 2.0	3000	33300	210	2505	39900	760									
0.002 1.0	3055	32700	480	2505	39900	450	(2250)	44400	—						
0.002 1.6	3025	33100	360	2505	39900	600	(2410)	41500	550	(2220)	45000	700	(2110)	47400	—
0.002 3.5	2995	33400	160	2520	39700	710	2400	41700	660	2225	44900	560	2115	47300	660
0.002 5.0	2990	33400	100	2530	39500	760	2400	41700	690	2225	44900	560	2120	47200	660
0.002,1 M HCl, 7 M H_2O	2985	33500	100	2525	39600	720	2400	41700	670	2230	44800	540	2115	47300	610
Ce^{+++} in 0.1 M Na_2SO_4	2965	33700	33	2545	39300	650	2410	41500	600	2230	44800	400	2110	47400	400
0.1 M $Ce_2(SO_4)_3$, ref. 74	2960	33800	36	2540	39400	740	2400	41700	630						
Acetate				2740	36500	600									
Tartrate	(3330)	30000	—	2810	35600	—									
Citrate	3260	30700	150	2785	35900	600									
Ethylenediaminetetra-acetate				2810	35600	480	2610	38300	450						
Nitrogentriacetate				2960	33800	550	2750	36400	450						

* 0,002 M $CeCl_3$ in H_2O, 1 M, 3 M, and 5 M aqueous HCl give identical values for λ_2, λ_3, λ_4, ε_2, ε_3, and ε_4 within the experimental uncertainty (10 Å and ~ 10 in ε).

of the crystal field may produce a low over-all splitting (especially, if it approximates spherical symmetry); and ions with no crystal field stabilization of the ground state usually have comparatively small values of the crystal field strength. This may be ascribed to the decreased distances to the ligands in the stabilized complexes and perhaps also to partly covalent bonding, i. e. intermixing of molecular orbitals. Thus, the d^5-systems with $S = \frac{5}{2}$ are not stabilized, and $(E_1 - E_2)$ is only 7800 K for manganese (II) and 13,700 K for iron (III) hexaaquo ions.[50] Finally, the ionic radius of Ce(III) is considerably larger than that of most other trivalent ions with partly filled shells.

The Possibility of an Equilibrium between Cerium (III) Aquo Ions with Different Co-Ordination Number, and the Absorption Spectra of Lanthanide Chlorides in Aqueous and Alcoholic Solutions.

The band at 33,700 K of cerium (III) aquo ions has only an intensity $\sim$ 3 % of the other bands. It may be caused by a comparatively rare geometrical configuration in equilibrium with the other Ce(III) complexes. J. Bjerrum[5] suggested that aquo ions with different co-ordination number N can be in equilibrium in solution, e. g. zinc (II) with four or six water molecules. Analogously, the common form of cerium (III) aquo ions might have $N = 9$ (as found[34] in $Nd(BrO_3)_3, 9H_2O$) and the rare form might be octahedral with $N = 6$. Heidt and Berestecki[29] studied the spectra of $Ce(ClO_4)_3$ in solutions of $HClO_4$ and $NaClO_4$. ε_1 of the small band at 33,700 K is further diminished, and the presence of an isosbestic point supports the formation of only one complex $Ce(ClO_4)(H_2O)_x^{++}$. However, a surprising effect was reported: ε_1 of the aquo ion is raised from 18 to 26 by warming the solution from 16° C. to 54° C., while the intensity of the strong bands is not noticeably changed. The present author has found a similar result for 0.03 M $CeCl_3$ in H_2O.

If the oscillator strength of the small band does not vanish for accidental reasons such as a selection rule for transitions in the crystal field,[30] the temperature effect is almost a proof of the existence of an equilibrium, where the complex giving the small

band is formed under absorption of heat, probably with a lower co-ordination number than the common form. SPEDDING et al.[84,85,86] assume that the lighter lanthanides may have a higher co-ordination number in solutions than the heavier lanthanides, since the ionic conductances and thermodynamic functions are not monotonous functions of the atomic number, and since[36] La^{+++} in $La_2(SO_4)_3$, $9\,H_2O$ has partly $N = 9$, partly $N = 12$.

The small band of $CeCl_3$ in $6\,M$ HCl is ~ 2 times higher than the band of the aquo ion, analogously to the result of NEWTON and ARCAND[63] for $CeSO_4^+$. In $12\,M$ HCl, the small band has increased to be as intense as the other bands, and it is shifted 1300 K towards lower wave numbers (Figure 3 and Table 6). Since the second band has had no large tendency to move, the chloro complexes in strong HCl can be assumed to have the low co-ordination number. $0.002\,M$ $CeCl_3$ in ethanolic solutions exhibit a similar development when the water content is removed. Thus 10 volume % water produces $\varepsilon_1 = 100$, rather independently of the chloride concentration, if added in excess, while the absorption spectrum of $0.002\,M$ $CeCl_3$ in 2 % H_2O* much resembles the spectrum of $CeCl_3$ in aqueous $12\,M$ HCl. It might seem reasonable to ascribe the variations of absorption spectrum of ethanolic $CeCl_3$ by addition of small quantities of water to the exchange of C_2H_5OH and H_2O in the first co-ordination sphere without the interference of chloride ions. However, since $Ce(ClO_4)_3$ exhibits a much smaller band at 33,400 K in 98 % C_2H_5OH, the ethanol solvate of $CeCl_3$ must be assumed to contain at least one chloride ion.

KATZIN[51,52] discovered anion complexes (in organic solvents) the formation of which is much more dependent on the absence of water than on the presence of a considerable excess of the free anion. The system $CeCl_3$, C_2H_5OH, H_2O is a new member of this class. Thus, $0.0004\,M$ $CeCl_3$ in 99.5 % C_2H_5OH is seen from Table 6 to form the chloride-ethanol complex to a high extent, while in aqueous $0.6\,M$ HCl, the formation constant[57] of $CeCl^{++}$ is only 3.

The situation cannot be described only on the assumption that the order of bonding to metal ions is

* This is the explanation of the new band reported of $PrCl_3$ in absolute ethanol.[39]

alcohol < anion < water,

since alcohol distinctly is not 1000 times more weakly bound to metal ions than water, but only ~ 10 times more weakly bound

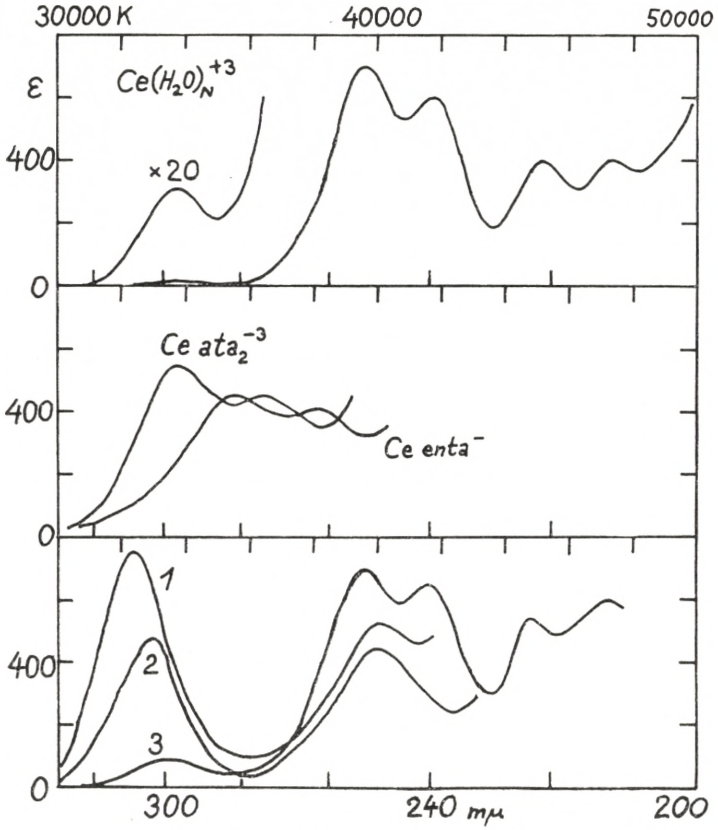

Figure 3. The absorption spectra of Cerium (III) complexes. The first part gives the spectrum of the aquo ion, the second part the nitrogentriacetate and the ethylenediaminetetraacetate. The third part gives the spectra of the following solutions in aqueous ethanol:

Curve 1: 0.0004 *M* $CeCl_3$, 0.3 *M* H_2O
- 2: 0.002 *M* $CeCl_3$, 1 *M* H_2O
- 3: 0.002 *M* $CeCl_3$, 5 *M* H_2O.

per molecule.[6,45,51] Rather, the formation of anion complexes serves as indicator for the ethanol solvation, since the pure ethanol solvate is much more unstable towards uptake of anions, relative to the aquo ion. In the case of cerium (III) the high coordination number (nine?) cannot be obtained with ethanol

molecules alone. The characteristic property of water as an ionizing solvent is its ability to replace all the anions in the first co-ordination sphere of a metal ion in solution or in salt hydrates, rather independently of the dielectric constant.

In the case of $NdCl_3$ in alcohols with a small content of water[6,39,40,41] it cannot be excluded that the anhydrous form is actually a mixed chloride-alcohol complex. Thus, the behaviour of $Nd(NO_3)_3$ and $NdCl_3$ in ethanol highly resembles the solutions in concentrated HNO_3 and HCl, respectively. Thus, QUILL and SELWOOD[71] found a shift 30 K and broadening of the $^2P_{1/2}$ band of Nd(III) in 16 M HNO_3, while three bands with a larger distance are exhibited in 12 M HCl (Table 2 and Figure 4).

The somewhat narrower band of the Nd(III) aquo ion is not changed in 6 M HCl, while the effect of nitrate is observed in much more dilute solutions. It is rather surprising that the neodymium(III) spectrum is not changed until two or three chloride ions are taken up, as extrapolated from the equilibrium constant for $CeCl^{++}$ (if the latter does not refer to some association of chloride ions* in the second co-ordination sphere). Thus, the spectral change may very well be connected with a dehydration, leading to a lower co-ordination number. The third band of $NdCl_3$ in 12 M HCl, which has a wave number even 80 K below the band of anhydrous $NdCl_3$, can of course belong to an excited sub-level of the ground-level. Figure 4 gives the absorption bands of Nd(III) in aqueous hydrochloric acid of varying concentration.

The reflection spectra[2] of $Na_2Ce(NO_3)_5$ and $Mg_3Ce_2(NO_3)_{12}$, 24 H_2O exhibit absorption edge at 27,000 K, while the edge in the corresponding lanthanum(III) compounds is situated at 33,000 K. Even though the nitrate ion has a band at the latter position, there seems to be a specific cerium(III) nitrate absorption band. A similar case is encountered[2] in the oxalate $Ce_2(C_2O_4)_3$, 9 H_2O with the edge 27,200 K, while the other lanthanide oxalates have edges above 37,000 K.

* as suggested by the fact (Table 6) that the high Ce(III) bands are identical in aqueous 0 – 5 M hydrochloric acid.

Red Shifts of Emission Bands of Fluorescent Cerium (III) and other Lanthanide Compounds.

ORGEL[66] explained the shift of emission bands of fluorescent and phosphorescent manganese(II) compounds to lower wave numbers than those of the absorption bands by means of the FRANCK-CONDON principle. The excited levels have another equilibrium distance of the ligands than the ground level, if the two levels have a different crystal field stabilization, and therefore the transition by emission from the excited level corresponds to an energy difference $\sim 2000\ K$ too small.

GOBRECHT[25] and MUKHERJEE[62] observed fluorescence of cerium(III) in crystals and in solutions. The emission band is rather broad, with the maximum at 28,000 K. If the corresponding absorption band is the small band discussed above, the red shift is $\sim 5000\ K$. KRÖYER and BAKKER[53] investigated the fluorescence of many other cerium(III) compounds and found two exciting wave number ranges.

Also the other $[Xe]\,4f^{n-1}\,5d$ states of the lanthanides can decay with emission of light, which is shifted towards lower wave numbers. PRZIBRAM[69,70] recognized these excited electron configurations in divalent lanthanides, which occur as traces in fluorite. Thus, Sm^{++} gives an emission maximum at 15,900 K, Eu^{++} at 23,800 K, and Yb^{++} at 17,500 K. This is in all cases $\sim 6000\ K$ below the corresponding absorption maxima.

On the other hand, the fluorescence of gadolinium(III) salts[3,89] occurs at almost the same wave number as the absorption, because neither the ground state nor the excited level is stabilized by the crystal field. In the case of Sm^{+++}, Eu^{+++}, and Dy^{+++}, the emission ends with excited multiplets of the configuration $[Xe]\,4f^n$.

The Integrals of Electrostatic Interaction between Electrons.

In the theory of SLATER, CONDON, and SHORTLEY[9] the distances between the centres of gravity of the different terms (with a definite S and L) of a given electron configuration can be expressed as multiples of the integrals F^k, which can be written for equivalent electrons:[9]

$$F^k = e^2 \int_0^\infty \left[\int_0^{r_2} \frac{r_1^k}{r_2^{k+1}} R^2 \, dr_1 + \int_{r_2}^\infty \frac{r_2^k}{r_1^{k+1}} R^2 \, dr_1 \right] R^2 \, dr_2 . \qquad (1)$$

e is the electronic charge and R is the radial wave function. For the energy differences of f^n-systems, the integrals with $k = 2$, 4, and 6 are of consequence.

For isomorphous radial wave functions, which can be transformed to each other by change of the unit of distance r, the ratios between $F^2 : F^4 : F^6$ will be identical, and the integrals F^k will be inversely proportional to a characteristic radius, e. g. r_{max} with the maximum value of R^2.

If the electron was concentrated on the surface of a sphere with radius r_0, the integrals F^k would all be identical and equal to the integral

$$W = e^2 \int_0^\infty \frac{R^2}{r} dr ; \text{ in casu } W = \frac{e^2}{r_0} . \qquad (2)$$

For all other radial functions R, a set of inequalities will be valid:

$$W > F^0 > F^2 > F^4 > F^6 > \ldots \qquad (3)$$

However, for reasonable functions R, the decrease of F^k with k will not be very great. Therefore, the present author[44] and JUDD[42] emphasized that the ratios $F^2 : F^4$ and $F^4 : F^6$ are only semi-adjustable parameters; it is objectionable to admit $F^2 \simeq F^4 \simeq 10 \, F^6$ as maintained for the configuration $[Xe] \, 4f^2$ of La^+, which must be strongly perturbed by electron configuration interactions.[9] TREFFTZ[90] calculated for hydrogen-like $4f$-wave functions

$$F^2 = 0.45 \, W ; \; F^4 = 0.30 \, W ; \text{ and } F^6 = 0.22 \, W. \qquad (4)$$

As shown below, this slow decrease of F^k with increasing k is present for most radial functions R rather independently of the shape. Thus, the observed values of F^k can be translated to characteristic values of radii $r_0 = \frac{e^2}{W}$ by extrapolation to W.

We consider the "rectangular" function

$$R^2 = \frac{1}{n-1} \text{ for } 1 \leq r \leq n, \text{ and elsewhere } R^2 = 0 . \qquad (5)$$

The integrals F^k are then for $k > 0$:

$$\left.\begin{aligned} F^k &= \frac{1}{(n-1)^2}\int_1^n\left[\int_1^{r_2}\frac{r_1^k}{r_2^{k+1}}\,dr_1 + \int_{r_2}^n\frac{r_2^k}{r_1^{k+1}}\,dr_1\right]dr_2 \\ &= \frac{1}{(n-1)^2}\int_1^n\left[\frac{1}{k+1} - \frac{1}{r_2^{k+1}(k+1)} + \frac{1}{k} - \frac{r_2^k}{k\cdot n^k}\right]dr_2 \\ &= \frac{1}{(n-1)^2}\left[\frac{2n}{k+1} - \frac{2}{k} + \frac{2}{n^k\,k\,(k+1)}\right], \end{aligned}\right\} \qquad (6)$$

while for $k = 0$

$$F^0 = \frac{2}{(n-1)^2}(n - 1 - ln\ n) \qquad (7)$$

and

$$W = \frac{ln\ n}{n-1}. \qquad (8)$$

For the limiting case, R^2 a delta function as discussed above, n can be set $= 1 + \delta$. Then the series, valid also for $k = 0$, is:

$$F^k = 1 - \frac{k+2}{3}\delta + \frac{(k+2)(k+3)}{3\cdot 4}\delta^2 - \ldots \qquad (9)$$

Table 7 gives the numerical results for $n = 2$, 3, 5, and 10 for several of these integrals. It is seen from Table 7 that the decrease, represented by the inequality signs in eq. 3 is more prominent, the higher n, i. e. the broader the wave function. The values in eq. 4 for hydrogen-like $4f$-wave functions correspond rather closely to a value of $n = 3.1$ for the „rectangular" approximation of eq. 5, while hydrogen-like $3d$-wave functions with $F^2 = 0.41\ W$ and $F^4 = 0.27\ W$ (see ref. 4) correspond to $n = 4$. For hydrogen-like l-wave functions, the integrals F^k diverge for $k \geq 2l + 2$, while F^k is defined for all k in eq. 6. However, this does not seem to be of consequence for the allowed ratios between F^k. If the radial wave function has maxima for two or more values of r, the decrease of F^k relative to W will generally be more pronounced. This case is realized[46] for $4d$-, $5d$-, ... $5f$-, ... electrons, since the number of maxima of a hydrogen-like (nl)-wave function is $n - l$; and for covalent bonding, where the linear combination of atomic orbitals have

TABLE 7. Numerical values of the integrals F^k and W, derived in eqs. 6, 7, and 8 for the rectangular wave function, defined in eq. 5.

n =	2	3	5	10
W	0.6932	0.5493	0.4024	0.2558
F^0	0.6137	0.4507	0.2988	0.1654
F^2	0.4167	0.2593	0.1467	0.0700
F^4	0.3062	0.1753	0.0938	0.0432
F^6	0.2388	0.1310	0.0686	0.0312
F^8	0.1945	0.1042	0.0538	0.0243
F^{10}	0.1637	0.0864	0.0433	0.0200
F^2/W	0.602	0.472	0.366	0.274
F^4/W	0.442	0.320	0.234	0.169
F^6/W	0.345	0.238	0.171	0.122

maxima both in the central ion and in the ligands. If the square of the radial function R^2 is distributed on several peaks with the areas A_n, arranged according to increasing values of r_n, an approximate expression will be:

$$F^k = \sum_n \frac{A_n^2}{r_n}\left[1 - \frac{k+2}{3}\,\delta_n + \ldots\right] + \sum_{m>n} \frac{2\,A_n A_m r_n^k}{r_m^{k+1}}. \qquad (10)$$

The first part of eq. 10 is derived from the series in eq. 9 for a peak with width δ_n, while the second part can make the further approximation of assigning the width $\delta_n = 0$ to the individual peaks A_n.

CONDON and SHORTLEY[9] divide the integrals F^k by denominators D^k in order to get integral values of the multiples of the new integrals $F_k = \dfrac{F^k}{D^k}$. Thus, these authors define for f-electrons

$$F^2 = 225\,F_2;\ F^4 = 1089\,F_4;\ \text{and}\ F^6 = 7361{,}64\,F_6\,, \qquad (11)$$

while for d-electrons

$$F^2 = 49\,F_2 \ \text{and}\ F^4 = 441\,F_4. \qquad (12)$$

The Decrease of F^k in Complexes.

According to eq. 1, the observation of different values of F^k in various complexes of the same central ion can easily be interpreted as a variation of the average radius of the electron cloud. This can either be caused by a general expansion of the electron cloud, conforming to some sort of „electroneutrality" principle,[50] or to a transport of a certain amount of the wave function into the region of the ligands.[67]

Actually, some kind of covalent bonding is present if defined as more negative charge being present between the nucleus of the central ion and the electron considered than in the corresponding gaseous ion. This follows from the theory of perturbation: The electrostatic potential U from a spherical surface with radius r_0 and charge e is constant inside the sphere, and continuously approaching zero outside the sphere:

$$U = \frac{e}{r_0} \text{ for } r < r_0 \text{ and } U = \frac{e}{r} \text{ for } r > r_0. \qquad (13)$$

Thus, if any wave function is totally imbedded in the sphere, i. e. $R = 0$ for $r > r_0$, the perturbation energy delivered by the potential of eq. 13 will be a constant. Only if the wave function slightly penetrates into the volume with $r > r_0$, the perturbation energy will decrease, if the charge e is negative.

Schläfer[79] observed that the term differences in the spectra of manganese(II) chloride solutions decrease for increasing chloride concentrations. The present author[49] maintains that these phenomena can rather be ascribed to formation of complexes $Mn(H_2O)_5Cl^+$ and $Mn(H_2O)_4Cl_2$ than to a physical salt effect. However, Schläfer[79] investigates an electrostatic model for this variation of the term differences, which is quite interesting. For numerical calculations, he uses the *ns*-levels of a hydrogen atom. This choice is provoked by the results, valid for crystal fields which have no spherical symmetry: The crystal field from a distribution of electrical charges is generally expanded in a series[37]: G_0, representing the action on a charged sphere, G_2, and G_4. The first contribution is very large, but not measurable,

because it appears identically in the energy of any level of the central ion. The parameters G_2 and G_4 have the weighted average contribution zero for the levels, split by the crystal field. Thus, G_2 and G_4 are of no consequence for the *ns*-levels, which cannot be split.

The result of SCHLÄFER that a Debye-Hückel potential of the type

$$U = -a \cdot \frac{1 - e^{-br}}{r} = -a\left[b - \frac{b^2 r}{2} + \ldots\right] \qquad (14)$$

and a crystal lattice with the anions nearest to the central ion both decrease the energies of the excited hydrogen levels, and most for the highly excited levels, is a paraphrase of the action of negative charge between the nucleus and the electron. The Debye-Hückel potential of eq. 14 can only be created by a charge distribution, which partly presents also small values of r, cf. eq. 13.

Now, the observed decrease of F^k can be formulated in two ways: either the electron considered is partly present in the domain of the ligands, or electrons from the ligands have partly invaded the central ion.

The first possibility has been discussed as formation of molecular orbitals γ_3 by linear combination of *d*-orbitals from the central ion and some distinct orbitals from the ligands.[67, 88, 93] If the intermixing of *d*-orbitals is so great that the part x of the anti-bonding orbital occurs in the ligands and the part $(1 - x)$ in the central ion, then F^k will to a first approximation be multiplied by $(1 - x)^2$, according to eq. 10, since r_m is much larger than r_1. Thus, the most complete intermixing with $x = 0.5$ (when the unperturbed orbitals have the same energy) will imply F^k slightly over 25 % of the value, found in the gaseous ion. These conditions hardly prevail even in $Co(CN)_6^{---}$ or $RhCl_6^{---}$. The latter arguments are not changed much[49] by the consideration of the large overlap integrals 0.4—0.7, which occur between the *d*-electron and the orbitals of the ligands, if the Pauling case is approached.

The second possibility does not necessitate that the covalent bonding occurs in the γ_3-orbitals in the case of *d*-electrons. Any other kind of bonding, e. g. of even γ_1 and odd γ_4-orbitals, forming the *s*- and p^3-parts of Pauling's sp^3d^2-hybridization,[47] can

increase the electron density, producing the central field in the theory of CONDON and SHORTLEY.[9] ORGEL[65] compared the screening effects of s-electrons in the electron configurations of gaseous ions $[A]\ 3d^n\ 4s$ and $[A]\ 3d^n\ 4s^2$ relative to $[A]\ 3d^n$ with the analogous effect of covalent bonding. Thus, the small decrease of F^k in $[Xe]\ 4f^n$-complexes do not necessarily imply the beginning presence of $4f$-electrons out in the ligands, but can as well be ascribed to the effective charge of the central ion being diminished by more conventional forms of covalent bonding. Since F^k is roughly proportional in the lanthanides to Z_0, the external charge plus one,[46] a decrease in F^k amounting to 1 % corresponds to an effective charge 2.96. It would be interesting to extrapolate to the value of F^k in the gaseous ions of the lanthanides from the observed differences for aquo ions and anion complexes. It would not be expected from the d^n-systems that the shift gaseous ion → aquo ion would be more than three times as large as the shift aquo ion → anion complex. The diminished term differences between $[Xe]\ 5d$ and $[Xe]\ 4f$ in cerium(III) complexes reported above disclose a similar effect.

In the theory of absorption spectra of the transition group complexes, the interest has been concentrated much more on the energy levels than on the wave functions. However, in the discussion of covalent bonding, evidence from paramagnetic resonance and its hyperfine structure*, due to the ligands' nuclei, can be very valuable.[67] A very interesting discovery was made by SHULL, STRAUSSER and WOLLAN,[83] who found the $3d$-wave function of manganese(II) compounds from the neutron diffraction of these paramagnetic materials. The wave function has $r_{max} = 0.6$ Å and vanishes more rapidly for large values of r than HARTREE's self-consistent $3d$-wave function.

Actual Values of F^k in the Lanthanides.

The absorption spectra of trivalent lanthanides[44, 75] have provided values of F^k for the $[Xe]\ 4f^n$-systems, which according to eq. 4 and Table 7 can give information about the average radius (or rather the average reciprocal distances) of the f-shell. The distances between the terms with the maximum value of S,

* cf. the recent study[88a] of *Mn (II)*, *Fe (II)*, *Co (II)*, and *Cr (III)*, imbedded in ZnF_2.

TABLE 8. Observed values of F^k and crystallographic radii of the trivalent lanthanide ions. The average radius of the $4f$-shell r_0 derived from eq. 2 and the assumption $W = 2F^2$.

	F^2	r_0	Ionic radius	
			ZACHARIASEN[81]	GOLDSCHMIDT[26]
f^2 La^+	21000 K	2.8 Å	1.6 Å extrapolated from Cs^+	
f^2 Pr^{+++}	69000	0.84	1.00 Å	1.16 Å
f^3 Nd^{+++}	72000	0.80	0.99	1.15
f^5 Sm^{+++}	72000	0.80	0.97	1.13
f^7 Gd^{+++}	76000	0.76	0.94	1.11
f^9 Dy^{+++}	78000	0.74	0.91	1.07
f^{12} Tm^{+++}	98000	0.59	0.86	1.04

giving the strongest absorption bands, are multiples[72,80] of $5F_2 + 6F_4 - 91F_6$. However, there is no doubt[44] that the single parameters can reliably be isolated by assuming eq. 4 or slightly higher values of $F_6:F_2$. Thus, the terms with lower S in praseodymium(III) and neodymium(III) can then be explained, and the sextet terms in gadolinium(III) also imply a value of F_2, which agrees with the neighbouring lanthanides.[42,44] Table 8 gives the values of F^2, which probably are not 10 % in error. It is remarkable that F^k does not increase much in the range from *Pr*(III) to *Dy*(III). If W is assumed to equal $2F^2$, values of r_0 can be inferred as given in Table 8. The value of $r_0 \sim 0.8$ Å is somewhat smaller than the crystallographic radii, as given in Table 8. Thus, the f-electron can be said to be mainly incorporated in the kernel,[46] while[4] La^+ with $F^2 = 21{,}000$ K under the same assumptions corresponds[1] to $r_0 = 2.8$ Å. GOEPPERT MAYER[56] predicts a rather drastic change of the screening conditions for $4f$-electrons at the beginning of the lanthanide group. The position calculated of the "inner" f-electron at 0.22 Å in *La* and 0.17 Å in *Nd* is undoubtedly too small. The values observed of F^k are not compatible with a smaller r_0 than 0.5 Å in the trivalent lanthanides. Since the $4f$-wave functions in complexes cannot be as broad as the hydrogen-like ones, where R^2 has half the maximum value for $r = 1.5\, r_{max}$, lower values of n from Table 7

[1] A hydrogen-like $4f$-electron with $Z_0 = 2$ has $r_0 = 4.23$ Å.

are suggested for the complexes supporting this conclusion. In the first transition group F^2 and F^4 are approximately proportional[9] to Z_0, the external charge plus one, in the d^2-systems from Sc^+ to Ni^{+8}. The values observed are $F^2 = Z_0 \cdot 17{,}000\ K$ and $F^4 = Z_0 \cdot 13{,}500\ K$, while a hydrogen-like $3d$-electron has $F^2 = Z_0 \cdot 9950\ K$, $F^4 = Z_0 . 6490\ K$, and $W = Z_0 . 24{,}390\ K$. In gaseous ions such as Cr^{+++} or Ni^{++}, the value of F^2 is $\sim 70{,}000\ K$. If W is assumed to be 150,000 K, the effective radius r_0 will be $116{,}000/150{,}000 = 0.77\ Å$. Since F^2 is decreased in nickel(II) and chromium(III) complexes, the corresponding values of $r_0 \gtrsim 1\ Å$ are definitely larger than the crystallographic radii, suggesting a partly covalent bonding of the type described by eq. 10.

Experimental.

Cerium (III) solutions. $CeCl_3, 6\ H_2O$ was recrystallized by saturation of the solution with hydrogen chloride gas at 0° C. This removes iron(III) efficiently, while considerable amounts of other lanthanides were present in the crystals. However, the latter do not influence the spectrum in the ultraviolet. Solutions of tartrates and citrates in aqueous ammonia are rapidly oxidized to yellow cerium (IV) complexes, while ethylenediaminetetraacetates and nitrogentriacetates (made from 0.2 M Na_4 *enta* and 0.2 M Na_3*ata*, both of "Komplexon" quality) are much more slowly oxidized. The acetate complex was measured in 2 M CH_3COONH_4, 2 M CH_3COOH.

The consecutive formation constants of the cerium(III) sulphate complexes[23] in 1 M $NaClO_4$ are: $CeSO_4^+$: 43, $Ce(SO_4)_2^-$: 5, and $Ce(SO_4)_3^{-3}$: 6, while in dilute solutions the first formation constant[86] is 2600. The consecutive formation constants of acetate complexes[24] are 48, 10, 3.2, and 2.

Since the neutral cerium(III) citrate is feebly soluble, the easily soluble complex in alkaline solution probably contains two citrate groups.[1] Boulanger[7] demonstrated the formation of lanthanide complexes with two nitrogentriacetate groups, while the ethylenediaminetetraacetates do not seem to react with excess of the reagent.[59]

Praseodymium (III) solutions. Pr_6O_{11} was supplied by Thorium Ltd., London. From the absorption bands at 7400 and 2540 Å

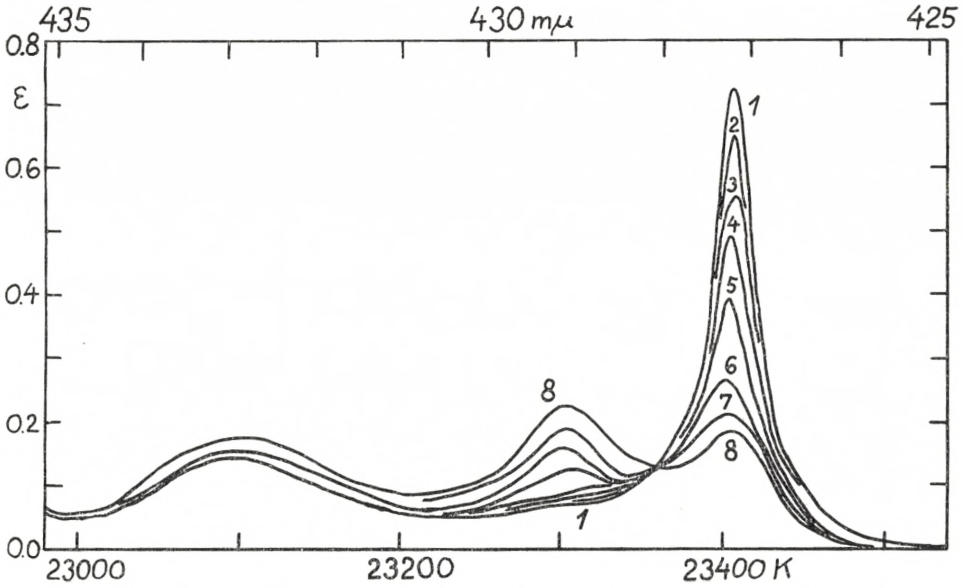

Figure 4. The absorption spectra of Neodymium (III) in hydrochloric acid. 0.38 *M* didymium chloride, as described in the experimental section, dissolved in the following solutions:

Curve	1	H_2O	Curve	5	9.5 *M HCl*
-	2	6.2 *M HCl*	-	6	10.3 *M* -
-	3	7.4 *M* -	-	7	11.0 *M* -
-	4	8.9 *M* -	-	8	11.3 *M* -

1.9 *M* didymium chloride in H_2O gives in 2 cm cells a spectrum identical with Curve 1, which was measured as the other curves on the figure of solutions in 10 cm cells. The neodymium content is 54 % of the didymium mixture.

it was found to contain less than 0.7 % *Nd* and 0.015 % *Ce*. The double band in the far ultraviolet, reported by STEWART,[87] was observed as a single band at 2148 Å. A solution was prepared, 0.2 *M* $Pr(ClO_4)_3$, 0.4 *M* $HClO_4$, and added to solutions of organic acids in NH_3 and Na_2CO_3, as described above.

Neodymium (III) solutions. Technical Didymium Oxide B, as supplied by Thorium Ltd., London, was used for most measurements, because the *Nd*(III) bands studied are free from interference with bands of the other lanthanides. The lanthanide composition is 1 % *Ce*, 10 % *Pr*, 54 % *Nd*, and 11 % *Sm*, as estimated from spectrophotometry. The rest is mainly *La*. The absorption spectrum of the ethylenediaminetetraacetate was shown to be independent of addition of aqueous ammonia, when *pH* was higher than 8. But the solid salts, which can be crystal-

lized and which dissolve in water, giving $pH \sim 5$, show a different spectrum with more lines, which is changed on addition of base. Probably, the latter solution contains a mixture of complexes, i. e. some carboxyl groups are not co-ordinatively bound and have taken up protons.

BERZELIUS observed that didymium tartrate, dissolved in aqueous ammonia, by evaporation of the highly viscose solution at room temperature forms a transparent, glassy material. If the latter is dissolved in some water, it gives the same absorption spectrum of a mixed solution of $DiCl_3$, NH_3, and ammonium tartrate.

Solid $Diaca_3$ was precipitated from the stoichiometric amounts of acetylacetone, didymium chloride and aqueous ammonia in 90 volume % ethanol. It was observed that the oscillator strength of the peak at 5710 Å and the broad band ~ 5800 Å is roughly 10 times that of the band group ~ 5750 Å of the aquo ion. Else, the oscillator strengths*, i. e. the areas of the bands, do not vary much for various neodymium(III) complexes.

Two crystals of the size $3 \times 3 \times 2$ cm^3, of $(NH_4)_2\ Di(NO_3)_5$, $x\ H_2O$ were measured in the spectrophotometer. They both confirmed the blue shift of the 4265 and 4255 Å band group.[17] However, some other band groups were different in the two crystals. Thus, bands were found at 7310 and 7440 Å; and 7310 and 7470 Å, respectively.

The bathochromic effect of the decreased F^k in Nd_2O_3 is clearly demonstrated by the bright blue colour[96] in contrast to the other pink neodymium(III) complexes.

Samarium (III) solutions. 99 % Sm_2O_3 from Thorium Ltd., London, and a fraction from re-crystallization of magnesium double nitrates (Miss MERETE WICHFELD assisted in its preparation) were used for some measurements. However, for the study of the strong band at 4020 Å the didymium solutions mentioned above were sufficient, because the other lanthanides do not disturb this band.

Gadolinium (III) solutions. 200 mg Gd_2O_3 (from Universitetets Institut for teoretisk Fysik) was disolved in 2.5 ml 2 M $HClO_4$ and diluted to 3.1 ml in the absorption cell. The ethylenediamine-

* MERZ[58] reports that the oscillator strength of the bands of $Mg_3Pr_2(NO_3)_{12}$, 24 H_2O is ~ 20 times smaller than of $Pr_2(SO_4)_3$, 8 H_2O, and $Pr(C_2H_5SO_4)_3$, 9 H_2O. Cf. the foot-note p. 8.

tetraacetate was prepared by neutralization of a part with NH_3 and addition of a slight excess of Na_4enta, while another part was added to aqueous ammonia and citrate. It was not possible to dissolve $Gd(OH)_3$ to a large extent in NH_3 and tartrate.

Erbium (III) solutions. A sample of Er_2O_3, Y_2O_3 etc. from S. M. JØRGENSEN, and some fractions prepared by Miss KAREN JENSEN (now Mrs. KÜMMEL) from gadolinite supplied by Konservator K. KRISTOFFERSEN, Norges mineralogiske Museum, were used for the measurements.

Ytterbium (III) solutions. 200 mg Yb_2O_3 (from Universitetets Institut for teoretisk Fysik) was boiled with 3 ml 2 M $HClO_4$ for several minutes, until it suddenly passed into a clear solution. It was diluted to 3.1 ml in the absorption cell and later also measured as $Yb\ enta^-$.

The spectrophotometer was the Cary recording model 11 MS-50. For standardization of the wave-length scale, the $^2P_{1/2}$ band of the neodymium(III) ion was assumed to be situated at 4273 Å in general agreement with the literature. In the ultraviolet, mercury vapour (in a 10 cm cell at room temperature) was found to give the 2536.5 Å line very sharply. The measurements of the narrow bands were made with the lowest possible scanning speed and recorded with the tungsten lamp 8000—3250 Å (12.5 Å per division = 0.83 cm of paper) and with the hydrogen lamp 4000—2050 Å (5 Å per division). The slit control was set at 10. The relative shifts of the narrow bands can be measured with an uncertainty ~ 1 Å. The shift 23 Å of the narrowest band of neodymium(III) tartrate was also found with a Beckman DU spectrophotometer. The latter instrument was used for the measurement of Yb(III) in the infra-red.

Acknowledgments.

I am much indebted to Professor JANNIK BJERRUM for his kind interest in the work. Furthermore, I thank Professor BØGGILD, Universitetets Institut for teoretisk Fysik, for the samples of gadolinium and ytterbium oxides, and Professor F. H. SPEDDING, Iowa State College, Ames, for later supply of the pure heavy lanthanide oxides.

Summary

The narrow bands caused by internal f^n-transitions in Pr(III), Nd(III), Sm(III), and Gd(III) are shown to be shifted $\sim 1\,\%$ towards lower wave numbers in complexes with ligands such as ethylenediaminetetraacetate, nitrogentriacetate, tartrate, and citrate, relative to the aquo ions. Ephraim et al. have previously demonstrated even larger shifts in the reflection spectra of oxides and anhydrous halides. Even though the sub-levels of the ground levels can be distributed in a different way for the complexes, the main part of the red shift is due to a decrease of term differences. These can be interpreted as multiples of the parameters of electrostatic interaction between electrons, F^k, as defined by Slater, Condon, and Shortley.

The high and broad absorption bands of cerium(III) complexes, due to $4f \rightarrow 5d$ transitions, are shifted much more in anion complexes. One of these bands is comparatively low, and its change with temperature suggests the presence of a Ce(III) aquo ion with a low co-ordination number in equilibrium with the more common form. $CeCl_3$ in anhydrous ethanol develops a new band, which disappears by addition of water. Since $Ce(ClO_4)_3$ exhibits another behaviour, the new band is presumably due to a complex with chloride and ethanol whose formation is much more sensitive to addition of water to the solvent than to the chloride concentration. (Thus, the absorption spectrum of 0.0004 M $CeCl_3$ in ethanol resembles that of Ce(III) in 12 M HCl).

It is further shown that the fluorescence of excited $[Xe]\,4f^{n-1}\,5d$ levels in the lanthanides exhibits the red shift discussed by Orgel in the case of manganese(II) complexes.

The F^k integrals are shown to decrease smoothly with increasing k, rather independently of the wave function assumed for the electron in the partly filled shell. Thus, the ratios $F^2:F^4$ and $F^4:F^6$ are only semiadjustable parameters, as previously maintained. From the observed values of F^k in transition group complexes, the average radius of the wave function can be estimated. In trivalent lanthanides this radius varies slowly around 0.8 Å in the series from Pr(III) to Dy(III), approaching 0.6 Å in Tm(III). This is somewhat less than the crystallographic

radii of trivalent lanthanides, indicating no large screening. In La^+, the $4f$-electrons with radius = 2.8 Å are distinctly external electrons. Since the ionic radii are particularly small in Pr_2O_3, Nd_2O_3, Sm_2O_3, and Gd_2O_3 with the low co-ordination number, this may explain the large decrease of F^k in these solids. In all cases, the decrease of F^k is most conspicuous in Pr(III), where the two $4f$-electrons are least shielded.

The increased effective radii of the d-shell in d^n-complexes due to covalent bonding do not necessarily imply the intermixing of the d-electrons with the electrons of the ligands, since the central field can be changed by filling of bonding molecular orbitals of other symmetries. However, the values of F^k are so small, even in the gaseous ions, that the d-shell must penetrate into the domain of the ligands, thus forming partly covalent bonds.

Chemistry Department A,
Technical University of Denmark, Copenhagen.

References.

1. Bertin-Batsch, C., Ann. Chim. [12] **7** (1952) 481.
2. Berton, A., Compt. rend. **213** (1941) 653 and 1001.
3. Berton, A. and Boulanger, F., Compt. rend. **224** (1947) 1153.
4. Birmingham, J. M. and Wilkinson, G., J. Am. Chem. Soc. **78** (1956) 42.
5. Bjerrum, J., Metal Ammine Formation . . . Thesis. Copenhagen 1941.
6. Bjerrum, J. and Jørgensen, C. Klixbüll, Acta Chem. Scand. **7** (1953) 951.
7. Boulanger, F., Ann. Chim. [12] **7** (1952) 732.
8. Brunetti, R., Nuovo Cimento **5** (1928) 391 and **6** (1929) 347.
9. Condon, E. U. and Shortley, G. H., Theory of Atomic Spectra. Cambridge 1953.
10. Datta, S. and Deb, M., Indian J. Phys. **10** (1936) 163.
11. Dieke, G. H. and Heroux, L., Johns Hopkins University, Baltimore, NYO — 3977. 1955.
12. Ephraim, F. and Bloch, R., Ber. **59** (1926) 2692.
13. Ephraim, F. and Bloch, R., Ber. **61** (1928) 65.

14. Ephraim, F. and Bloch, R., Ber. **61** (1928) 72.
15. Ephraim, F., Ber. **61** (1928) 80.
16. Ephraim, F. and Rây, P., Ber. **62** (1929) 1509.
17. Ephraim, F. and Rây, P., Ber. **62** (1929) 1520 and 1639.
18. Ephraim, F., Jantsch, G. and Zapata, Cl., Helv. Chim. Acta **16** (1933) 261.
19. Freed, S., Phys. Rev. **38** (1931) 2122.
20. Freed, S. and Mesirow, R. J., J. Chem. Phys. **5** (1937) 22.
21. Freymann, M. and Freymann, R., Compt. rend. **211** (1940) 785.
22. Fried, S. and Hindman, J. C., J. Am. Chem. Soc. **76** (1954) 4863.
23. Fronæus, S., Svensk Kem. Tidskr. **64** (1952) 317.
24. Fronæus, S., Svensk Kem. Tidskr. **65** (1953) 19.
25. Gobrecht, H., Ann. Physik [5] **31** (1938) 181.
26. Goldschmidt, W. M. et al., Geochemische Verteilungsgesetze der Elemente, IV, V and VII, Oslo 1925 and 1926.
27. Gruen, D. M. and Fred, M., J. Am. Chem. Soc. **76** (1954) 3850.
28. Hartmann, H. and Lorenz, E., Z. Elektrochem. **54** (1950) 341.
29. Heidt, L. J. and Berestecki, J., J. Am. Chem. Soc. **77** (1955) 2049.
30. Hellwege, K. H., Ann. Physik [6] **4** (1948) 95, 127, 136, 143, 150, and 357.
31. Hellwege, K. H. and Kahle, H. G., Z. Physik **129** (1951) 62.
32. Hellwege, A. M. and Hellwege, K. H., Z. Physik **130** (1951) 549.
33. Hellwege, K. H. and Shröck-Vietor, W., Z. Physik **138** (1954) 449.
34. Helmholz, L., J. Am. Chem. Soc. **61** (1939) 1544.
35. Hoffmann, K. A. and Höschele, K., Ber. **47** (1919) 240.
36. Hunt, E. B., Rundle, R. E. and Stosick, A. J., Acta Cryst. **7** (1954) 106.
37. Ilse, F. E. and Hartmann, H., Z. Physik. Chem. **197** (1951) 239.
38. Jantsch, G. and Meyer, E., Ber. **53** (1920) 1577.
39. Jones, H. C. and Anderson, J. A., Carnegie Inst. Publ. No. 110. Washington 1909.
40. Jones, H. C. and Strong, W. W., Carnegie Inst. Publ. No. 130, Washington 1910.
41. Jones, H. C. and Strong, W. W., Carnegie Inst. Publ. No. 160, Washington 1911.
42. Judd, R. B., Proc. Roy. Soc. (London) **A 228** (1955) 120.
43. Jørgensen, C. Klixbüll, Mat. Fys. Medd. Dan. Vid. Selsk. **29**, (1955) no. 7.
44. Jørgensen, C. Klixbüll, Mat. Fys. Medd. Dan. Vid. Selsk. **29**, (1955) no. 11.
45. Jørgensen, C. Klixbüll, Acta Chem. Scand. **8** (1954) 175.
46. Jørgensen, C. Klixbüll, J. Inorg. Nucl. Chem. **1** (1955) 301.
47. Jørgensen, C. Klixbüll, Acta Chem. Scand. **10** (1956) 500, 518.
48. Jørgensen, C. Klixbüll, Acta Chem. Scand. **9** (1955) 1362 and **10** (1956) 887.

49. Jørgensen, C. Klixbüll, Acta Chem. Scand. **10** (1956)
50. Jørgensen, C. Klixbüll, Reports of X'th Solvay Conference, Bruxelles May 1956.
51. Jørgensen, C. Klixbüll and Bjerrum, J., Nature **175** (1955) 426.
52. Katzin, L. I. and Gebert, E., J. Am. Chem. Soc. **72** (1950) 4557.
53. Kröyer, F. A. and Bakker, J., Physica **8** (1941) 628.
54. Lang, R. J., Can. J. Res. **14 A** (1936) 127.
55. Liveling, G. D., Cambr. Phil. Soc. Trans. **1899** 255, Collected Papers on Spectroscopy. Cambridge University 1915.
56. Mayer, M. Goeppert, Phys. Rev. **60** (1941) 184.
57. Mayer, S. W. and Schwarz, S. D., J. Am. Chem. Soc. **73** (1951) 222.
58. Merz, A., Ann. Physik [5] **28** (1937) 569.
59. Moeller, Th. and Brantley, J. C., J. Am. Chem. Soc. **72** (1950) 5447.
60. Moeller, Th. and Brantley, J. C., Anal. Chem. **22** (1950) 433.
61. Moeller, Th. and Moss, F. A. J., J. Am. Chem. Soc. **73** (1951) 3149.
61a. Moeller, Th. and Ulrich. W. F. J. Inorg. Nucl. Chem. **2** (1956) 164.
62. Mukherjee, P. C., Z. Physik **109** (1938) 573.
63. Newton, T. W. and Arcand, G. M., J. Am. Chem. Soc. **75** (1953) 2449.
64. Nutting, G. C. and Spedding, F. H., J. Chem. Phys. **5** (1937) 33.
65. Orgel, L. E., J. Chem. Phys. **23** (1955) 1004 and 1824.
66. Orgel, L. E., J. Chem. Phys. **23** (1955) 1958.
67. Owen, J., Proc. Roy. Soc. (London) **A 227** (1955) 183.
68. Pabst, A., J. Chem. Phys. **11** (1943) 145.
69. Przibram, K., Z. Physik **102** (1936) 331 and **107** (1937) 709.
70. Przibram, K., Sitz. ber. Wien Akad. Mat. nat Kl. II a **147** (1938) 260.
71. Quill, L. L., Selwood, P. W. and Hopkins, B. S., J. Am. Chem. Soc. **50** (1928) 2929.
72. Racah, G., Phys. Rev. **76** (1949) 1352.
73. Radoitchitch, M., Ann. Chim. [11] **13** (1940) 5.
74. Roberts, R. W., Wallace, L. A. and Pierce, I. T., Phil. Mag. **17** (1934) 934.
75. Satten, R. A., J. Chem. Phys. **21** (1953) 637.
76. Satten, R. A. and Young, D. J., J. Chem. Phys. **23** (1955) 404.
77. Schäffer, C. E., Acta Chem. Scand.
78. Schäffer, H., Phys. Z. **7** (1906) 822.
79. Schläfer, H. L., Z. Physik. Chem. **6** (1956) 201.
80. Schuurmans, Ph., Physica **11** (1946) 475.
81. Seaborg, G. T. and Katz, J. J., The Actinide Elements. Nat. Nucl. Energy Ser. Vol. 14 A. 1954.
82. Selwood, P. W., J. Am. Chem. Soc. **52** (1930) 3112 and 4308.
83. Shull, C. G., Strausser, W. A. and Wollan, E. O., Phys. Rev. **83** (1951) 333.

84. Spedding, F. H., Porter, P. E. and Wright, J. M., J. Am. Chem. Soc. **74** (1952) 2055.
85. Spedding, F. H. and Yaffe, I. S., J. Am. Chem. Soc. **74** (1952) 4751.
86. Spedding, F. H. and Jaffe, S., J. Am. Chem. Soc. **76** (1954) 882.
87. Stewart, D. C., Light Absorption . . . I, AECD — 2389.
88. Tanabe, Y. and Sugano, S., J. Phys. Soc. Japan **9** (1954) 753 and 766.
88a. Tinkham, M. Proc. Roy. Soc. (London) **A 236** (1956) 535 and 549.
89. Tomaschek, R. and Mehnert, E., Ann. Physik [5] **29** (1937) 306.
90. Trefftz, E., Z. Physik. **130** (1951) 561.
91. Uzumasa, Y. and Okuno, H., Bull. Chem. Soc. Japan **6** (1931) 147
92. Uzumasa, Y., Bull. Chem. Soc. Japan **7** (1932) 85.
93. Van Vleck, J. H., J. Chem. Phys. **3** (1935) 803 and 807.
94. Vickery, R. C., J. Chem. Soc. **1952** 421.
95. Vickery, R. C., J. Chem. Soc. **1955** 2360.
96. Waegner, A., Z. anorg. Chem. **42** (1904) 118.
97. Strukturbericht Band I (1931) 744 and Band II (1937) 38.

Indleveret til selskabet den 4. maj 1956.
Færdig fra trykkeriet den 24. november 1956.

MATEMATISK-FYSISKE
MEDDELELSER

UDGIVET AF

DET KGL. DANSKE VIDENSKABERNES SELSKAB

BIND 30

KØBENHAVN

I KOMMISSION HOS EJNAR MUNKSGAARD

1955—56

INDHOLD